Mechanistic investigations of ruthenium-mediated reactions *via* vinylidene intermediates

Lucy Margaret Milner

Doctor of Philosophy

University of York

Chemistry

July 2016

Abstract

Experimental and computational mechanistic studies are reported for several ruthenium-promoted processes, including the anti-Markovnikov hydration of terminal alkynes, the alkenylation of pyridine and electrophilic fluorination. The synergy between experimental and theoretical results revealed new insights into the previously reported hydration and alkenylation processes of alkynes and allowed the elucidation of a novel outer-sphere electrophilic fluorination mechanism, 'OSEF'.

The mechanism of the anti-Markovnikov hydration of phenylacetylene by $[Ru(\eta^5\text{-}C_5H_5)(NCMe)(6\text{-DPPAP})(3\text{-DPICon})]^+$ (where 3-DPICon = 3-diphenylphosphinoisoquinolone and 6-DPPAP = 6-(diphenylphosphino)-N-pivaloyl-2-aminopyridine) was investigated using density functional theory. The proposed mechanism involves three ligand-assisted processes; alkyne-to-vinylidene tautomerism, attack of water at the vinylidene electrophilic α-carbon and tautomerisation from a hydroxyvinyl to acyl species. A catalyst deactivation product was identified experimentally and a potential mechanism of formation has been explored.

The reactivity of $[Ru(\eta^5\text{-}C_5H_5)(PR_3)(L)_2]PF_6$ (where PR_3 = triphenylphosphine, 2-(1,1-dimethylpropyl)-6-(diphenylphosphino)pyridine or diphenyl-2-pyridylphosphine, L = pyridine) in pyridine alkenylation was trialed in order to optimise a previously reported catalytic procedure and eliminate the solvent dependence of the reaction. The synthesis and reactivity of these complexes in both stoichiometric and catalytic reactions have been investigated.

A new electrophilic fluorination methodology is reported for the formation of carbon-fluorine bonds in the coordination sphere of ruthenium. A ruthenium-pyridylidene complex, synthesised from non-activated substrates, was observed to undergo rapid and selective monofluorination or deprotio-difluorination under mild reaction conditions. The procedure was then extended to allow the facile preparation of the first mononuclear fluorovinylidene complexes. Retention of the ligands allowed for subsequent investigation of metal-mediated reactivity and revealed unusual carbon-fluorine bond cleavage and migration processes. Experimental and computational mechanistic data suggested that fluorination was taking place *via* an unprecedented mechanism without metal-fluoride intermediates.

Table of Contents

List of Tables

List of Figures

List of Schemes

List of Accompanying Material

A compact disk is attached at the back of this thesis, which contains:

- CIF files for X-ray crystallography data
- Raw NMR data for each novel complex presented
- Further computational information, including tabulated energetic data, results of NBO calculations, details of structural isomers, naming systems, SCF energies, xyz coordinates and vibrational frequencies
- An electronic copy of this thesis

Acknowledgements

So this is it, the final few pages left to write and I don't know where to start! There have been some ups and downs over the years, but I consider myself extraordinarily lucky to have met such wonderful people during my time at York, some of whom have been by my side every step of the way. It is these very special people who I would like to thank here.

Firstly, a massive thank you to my two fantastic supervisors, Jason Lynam and John Slattery. Thank you for the opportunity to do this PhD and for the never-ending advice, support and enthusiasm. I've learned a lot from both of you and not all of it was chemistry ... in particular, Jason has taught me that it's <u>definitely</u> 'wicket keeper' and not 'back-stop', and John has repeatedly proven that seafood doesn't just have to be savoury. I wish you both all the best for the future. I would also like to thank Duncan Bruce who was my undergraduate supervisor and continues to offer his encouragement and guidance in whatever I choose to do. Finally, thanks to Paul Walton who always makes time for a chat when I need it most; your kindness has truly made a massive difference.

Thanks also to the wider chemistry community: Heather and Pedro for your skills and patience with NMR data collection; Adrian, Natalie and Sam for your hours spent solving disorder (and trying to teach me to do the same); Abby for the hundreds of NMR tubes you've made (and repaired, sorry!); Graeme for the countless samples I submitted to achieve successful elemental analyses; Steve and Mike for making every trip to fetch a cylinder into a social event rather than a chore, and Karl for all of your mass spec know-how. A big thank you is also well deserved for Naser, Iman and Charlotte who take care of E114 and for Rachel, Sharon and Alice in the graduate office who keep us all organised and can answer even our most obscure questions! Without each of you, the department could not function and I'm very grateful for the help you have always willingly and expertly provided.

Equally, I was very fortunate to have worked with an exceptional group of SLUGS, both past and present, and I would like to mention just a few in particular. DFT Dave - in our tiny old office in C-block, with the patience of a saint and the hair of a champion, you taught me everything I needed to know about running calculations. Rich and Neets - you introduced me to Schlenk lines, gloveboxes AND Zumba, an unusual combination! And Lizzie - thank you for making sure that the lab ran like clockwork, always having time for a chat and for helping me out when we went to Italy, even if it meant you got next to no sleep! The lab hasn't been the

same without you. In the current group, a big thanks to Lewis as my ally in Team Fluorine - may all of your NMRs be clean and your reactions catalytic. You're a wonderful friend and I have a lot of fun working alongside you every day. We've also been lucky enough to have some very talented MChem, BSc and summer students in our lab - Lucy B and Fran continue to be much valued friends and I hope to see you both soon! Finally, the rest of E114 have been a fab team of people to work with; grazie mille to Jess and Tom for all the peach cakes and Italian lessons, and congratulations to Josh, Alan, Lyndsay, and George - we started out together and we've all made it through!

Every day at half twelve, the lunch-group-group assemble and head to Derwent: Dan, AKDK team captain, always full of fun and ready to help (turns out that a difference of 41 m/z is acetonitrile); Ellis, who makes amazing cakes, and Tom ... who eats them all - only kidding, Tom (!); Ben and Claire who provide warm hospitality, freshly baked bread and access to Monty; Andy, who is quite simply one of the kindest men I have ever met; Esther and Martin, who allowed me to share their office for several weeks and who are both fantastic at bridge; Chris, who gives great hugs, and Linda, Sindhu and the Robs who make chemistry such a cheerful place to be. Special thanks to Danielle, who has been a great friend from our first year, and to Natalie, who completes this unstoppable duo. I know I can always count on you to provide wise advice and loyal friendship, and I look forward to seeing you soon in Bristol! Jo - we met in the very first week and even though we don't see each other all the time, when we do meet up it's always like we've never been apart. I'm very lucky to have you as my friend. Finally, thank you to Dr Luisa 'Charlie' Ciano, who is not only my unofficial 'third supervisor' but more importantly is my partner in crime … if one of us is doing something silly, chances are that the other is doing it with them. So for everything from introducing me to Nutella to welcoming me wholeheartedly into *Team Italy* - thank you for always being there for me.

Last but not least, I would like to acknowledge my brilliant family. My Grandma and Grandad, who are still proud of the crystals that I (accidentally) made in second year teaching labs; Jayne, Dave, Beckie and Carl, who always take an interest in my chemistry and put up with my constant 'singing' (sorry Bex), and Auntie Mary and Marg, who have been two of my 'biggest fans' from the start. Mum and Dad – the biggest thanks of all goes to you. For your unconditional love, unwavering support and always putting me first, I couldn't ask for more wonderful parents.

Author's Declaration

I declare that the research presented in this thesis is, to the best of my knowledge, original and was carried out under the supervision of Dr Jason Lynam and Dr John Slattery in the Chemistry Department of the University of York between October 2012 and May 2016. I am the sole author and none of this work has been submitted previously for examination at this, or any other, university. Contributions from other authors and co-workers are listed below, and referenced in the appropriate chapters throughout this thesis.

- MS experiments were performed by Mr Karl Heaton or Miss Helen Robinson;
- X-ray crystallography data was collected by, or with the assistance of, Dr Natalie Pridmore, Dr Adrian Whitwood or Mr Sam Hart;
- Elemental analyses were performed by Dr Graeme McAllister;
- Spectra from the 700 MHz NMR spectrometer were collected by Dr Pedro Aguiar;
- The ligands in Chapter 2, 6-DPPAP and 3-DPICon, were prepared by Dr Urs Gellrich at Albert-Ludwigs-Universität in Freiburg, Germany;
- Preliminary DFT calculations on some complexes reported in Chapter 2 were performed by Mr Timothy Li as part of an MChem project;
- Several results from the catalytic testing of complex **[7c]PF$_6$**, reported in Chapter 3, were previously reported in my MChem report in 2012 and contribute towards a publication in *Dalton Transactions* as listed below;
- DFT calculations on the fluorination of complex **[16^{CF3}]** *via* a radical mechanism, reported in Chapter 4, were performed by Dr John Slattery;
- DFT calculations on the reactivity of complex **[27^{Ph}]$^+$** with pyridine, reported in Chapter 5, were performed by Dr Jason Lynam;
- Halogenated ruthenium vinylidene complexes (**[39]BF$_4$, [40]BF$_4$, [41]Br$_3$** and **[42]I$_3$** in Chapter 5) were synthesized by Mr Matthew Skeats as part of a summer project.

The results presented herein have contributed towards the following publications:

- The computational and experimental results presented in Chapter 2 were published in:

  Mechanistic insight into the ruthenium-catalysed anti-Markovnikov hydration of alkynes using a self-assembled complex: a crucial role for ligand-assisted proton shuttle processes; B. Breit, U. Gellrich, T. Li, J. M. Lynam, **L. M. Milner**, N. E. Pridmore, J. M. Slattery and A. C. Whitwood, *Dalton Trans.*, **2014**, *43*, 11277

- The results of the catalytic testing of complex **[7c]PF$_6$** presented in Chapter 3 were published in:

  [Ru(η^5-C$_5$H$_5$)(η^6-C$_{10}$H$_8$)]PF$_6$ as a catalyst precursor for the one-pot direct C–H alkenylation of nitrogen heterocycles; J. M. Lynam, **L. M. Milner**, N. S. Mistry, J. M. Slattery, S. R. Warrington and A. C. Whitwood, *Dalton Trans*., **2014**, *43*, 4565

- The computational and experimental results presented in Chapter 4 were published in:

  Outer-Sphere Electrophilic Fluorination of Organometallic Complexes; **L. M. Milner**, N. E. Pridmore, A.C. Whitwood, J. M. Lynam and J. M. Slattery, *J. Am. Chem. Soc.*, **2015**, *137*, 10753

- The computational and experimental results presented in Chapter 5 were published in:

  *Access to novel fluorovinylidene ligands **via** exploitation of outer-sphere electrophilic fluorination: new insights into C–F bond formation and activation*; **L. M. Milner**, L. M. Hall, N. E. Pridmore, M. K. Skeats, A. C. Whitwood, J. M. Lynam and J. M. Slattery, *Dalton Trans.*, **2016**, 45, 1717

- The research on outer-sphere electrophilic fluorination presented in Chapters 4 and 5 also formed the basis of a patent application:

  Metal-Mediated Outer-Sphere Electrophilic Fluorination, Patent Application Number PCT/GB2015/053732; L. M. Hall, J. M. Lynam, **L. M. Milner**, J. M. Slattery, Filing date 4/12/2015

- Experimental results not presented in this thesis have also contributed to a publication:

  Dispersion, solvent and metal effects in the binding of gold cations to alkynyl ligands: implications for Au(I) catalysis, L. Ciano, N. Fey. C. J. V. Halliday, J. M. Lynam, **L. M. Milner**, N. Mistry, N. E. Pridmore, N. S. Townsend, A. C. Whitwood, *Chem. Commun.*, **2015**, 47, 9702

Thesis Numbering System

(1) All compounds reported in the literature, for example those in Chapter 1 and in each chapter introduction will be labelled as '**n-*a***', '**n-*b***' … '**n-*aa***', '**n-*ab***' etc where '**n**' indicates the thesis chapter in which the compound is first encountered. If a literature complex has been used as part of this study, this will be noted in the caption.

(2) All metal complexes which have been experimentally observed or isolated will be labelled with a **bold** number in square brackets, and for cationic complexes either the charge or counter ion will be stated, for example, **[2]PF$_6$** or **[2]$^+$**.

If more than one derivative of a complex or compound has been synthesised, superscript will be used to indicate the substituent of the structural analogue, for example **[5^R]$^+$**. **R** indicates the identity of the alkyne used in the synthesis and will be one of the following:

R	alkyne
Ph	phenylacetylene
CF3	4-ethynyl-α,α,α-trifluorotoluene
OMe	4-ethynylanisole
tBu	4-*tert*-butylphenylacetylene

(3) In Chapter 3, a series of analogous complexes have been synthesised which contain different phosphine ligands. The phosphine will be indicated using a lower case letter ('**a**', '**b**', or '**c**') after the complex number, for example **[6a]$^+$**. Phosphines **b** and **c** are used exclusively in Chapter 3; if the complex (**[6]$^+$**, in this case) is encountered in another chapter it will be as the triphenylphosphine derivative and the letter **a** will be omitted.

letter	phosphine
a	triphenylphosphine
b	2-(1,1-dimethyl)-6-(diphenylphosphino)pyridine
c	diphenyl-2-pyridylphosphine

Ph₃P

Ph₂P

Ph₂P

triphenylphosphine

2-(1,1-dimethylpropyl)-6-(diphenylphosphino)pyridine

diphenyl-2-pyridylphosphine

a

b

c
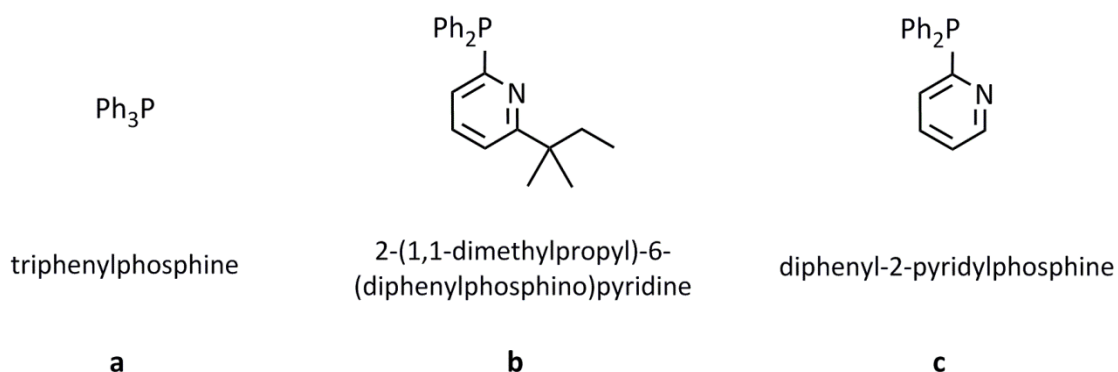
(4) Organic compounds will be labelled with a **bold** number.

(5) All compounds which have been modelled only as part of computational studies and not experimentally isolated or observed will be labelled with a **bold** capital letter in square brackets, for example, '**[A]**', '**[B]**⁺'. All complexes in computational studies have been modelled in the absence of an anion.

In most computational studies in this thesis, only one conformational isomer of the intermediates and transition states are presented in the text. Alternative conformational isomers which have been calculated are listed in Chapter 6. However, in Chapter 5, the *E*- and *Z*- stereochemistry of the intermediates was an important consideration and this has been highlighted in the compound label, for example **[Y-*E*]⁺ or [Y-*Z*]⁺.**

(6) Complexes which have been experimentally observed or isolated and also form part of a computational study will retain their original complex number allocated in (2).

(7) All transition states will be labelled as '**TS$_{[A][B]}$**', where the first complex in the name corresponds to the species preceding the transition state, and the second complex indicates the species being formed.

Chapter 1

Introduction

1 Introduction

1.1 Organometallic complexes in synthesis

Organometallic complexes are ubiquitous in many aspects of chemistry; in catalysis, nature, medicine and functional materials.[1-2] At one time, transition-metal catalysed reactions were the last resort for the synthetic chemist; instead, these reactions are now used preferentially and routinely for the synthesis of many categories of organic molecule.[2] The development of transition metal-catalysed reactions stems from the discovery of elementary reactions that can take place at metal-heteroatom bonds and by the increased understanding of factors that control this reactivity.[2] Upon coordination to a metal centre, an organic molecule often displays markedly different reactivity which can allow novel and useful transformations to be performed.[3] Furthermore, elucidation of stoichiometric reaction mechanisms allows the development of a catalytic system as a route to synthesise new carbon-carbon or carbon-heteroatom bonds with high selectivity, high atom efficiency and lower energy reaction conditions. These findings have allowed the development of an organometallic 'tool kit' which is likely to be integral to future advances in synthetic chemistry.

The utility and application of a mechanism-driven approach as applied to the advancement of organometallic reactivity was exemplified in 2005 by the award of a Nobel Prize to Yves Chauvin, Robert H. Grubbs and Richard R. Schrock 'for the development of the metathesis method in organic synthesis'.[4] The exposition of the Chauvin [2+2] cycloaddition mechanism allowed the development of highly efficient and active ruthenium-based catalysts for organic chemistry and polymerisation. In 2010, the Nobel prize was again awarded for developments in organometallic chemistry, to Richard F. Heck, Ei-ichi Negishi and Akira Suzuki for 'palladium-catalysed cross couplings in organic synthesis'.[5] Palladium cross-coupling reactions are highly selective, functional-group tolerant and efficient even with extremely low catalyst loadings.[6]

This thesis introduction will provide a discussion of the literature surrounding the development and utilisation of organometallic complexes in a range of applications – in synthesis, catalysis and as pharmaceutical agents. Particular attention is given to ruthenium half-sandwich complexes and their ligands, including the generation, characterisation and reactivity of vinylidene and pyridylidene species which form the basis of the studies presented herein.

1.2 Phosphine ligands and substituent effects

The coordination of ligands to a metal centre is of great importance in controlling and modifying the reactivity of organometallic catalysts. The coordination sphere of the metal dictates the electronic and steric environment available to interact with incoming substrates, and therefore the choice of ligands and their substituents strongly affects the ability of a metal complex to carry out a specific transformation.[7] Therefore, a detailed understanding of ligand binding is crucial in order to design an effective catalyst with the desired properties.

1.2.1 Mono- and bidentate phosphine ligands

Phosphorus (III) ligands are considered to interact with a metal centre *via* synergic bonding; the phosphorus atom donates electron density to an empty metal d-orbital by σ-donation from the lone pair of electrons that reside in an occupied σ orbital, and accepts electron density from an occupied metal d-orbital through π-donation into a P-C σ* orbital, shown in Figure 1.1.[8] The balance of these two interactions is influenced by both the electron density of the metal centre to which the ligands are bound and the properties of the phosphine ligand substituents. The energy of the σ* orbitals is lower for phosphine ligands with electronegative substituents and therefore they participate more strongly in π-backbonding, whereas the opposite effect is observed for phosphine ligands with electron-donating substituents.

Metal empty   Phosphine full
d orbital   σ-orbital

Metal full   Phosphine empty
d orbital   σ* orbital
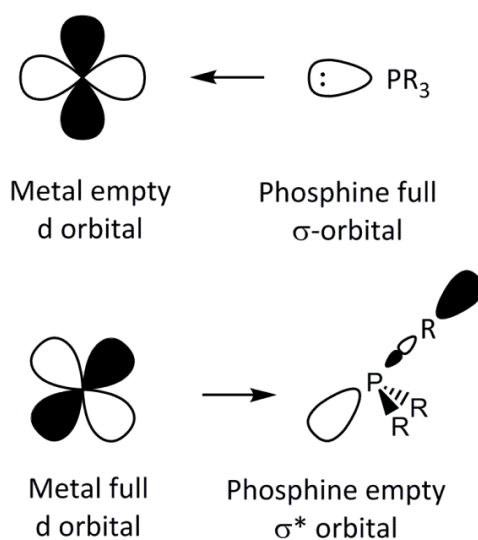
Figure 1.1 Bonding diagram of a phosphorus (III) ligand to a metal centre (R = alkyl, aryl etc)

Phosphine ligands are of broad utility in organometallic catalysis due to their highly tuneable electronic and steric properties, which are controlled by varying the substituents at the

phosphorus atom. These properties are intimately connected and cannot be modified independently; a change in phosphine ligand substituent changes both the steric and electronic effects because the group that is varied is directly bonded to the donor atom.[9] However, a practical and useful distinction can be made between them by consideration of the Tolman steric and electronic parameters, shown schematically in Figure 1.2.[10]
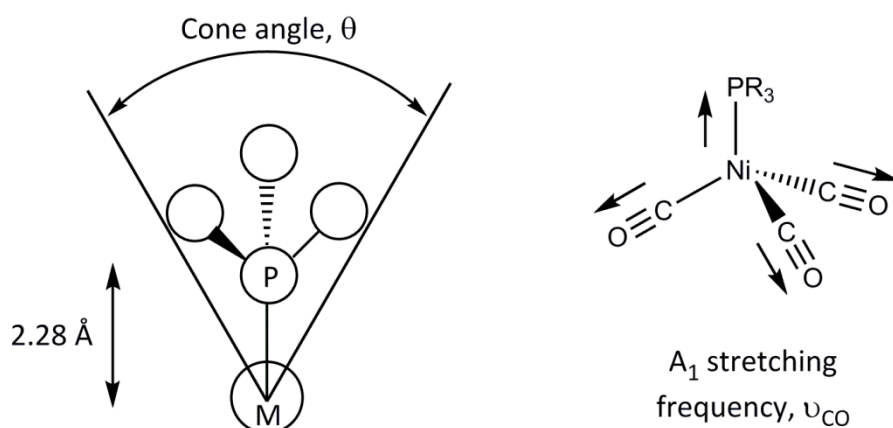
Figure 1.2 Schematic description of the Tolman electronic and steric parameters

In order to calculate the electronic parameter of a phosphine ligand, the frequency of the A_1 carbonyl mode was recorded by IR spectroscopy on complexation of the phosphorus (III) ligand, L, to $Ni(CO)_4$ to form $Ni(CO)_3L$. The trend indicated that more electron-donating groups at the phosphorus atom led to lower values of v_{CO}. This can be explained by considering that a more electron rich phosphorus atom in a phosphine ligand donates more electron density to the metal centre. This increased electron density at the metal results in increased back bonding to the CO ligands, a reduction in bond order of the CO, and therefore a weaker CO bond.[10] The electronic properties of phosphine ligands were also studied by Gusev using computational and experimental approaches.[11]

The steric parameter can be considered as a 'cone angle' – in its most simple form (when all substituents are equivalent), the parameter is defined as the angle of a cylindrical cone whose apex is 2.28 Å from the centre of the phosphorus atom and whose edges touch the van der Waals radii of the outermost atoms.[10] Consideration of both the electronic and steric parameters allows the selection of a phosphine ligand to optimise the catalytic properties of a complex.

In this thesis, a range of phosphine ligands were used. The most commonly used monodentate spectator phosphine ligand was triphenylphosphine, PPh_3. However, in

Chapter 5, the two triphenylphosphine ligands in the $[Ru(\eta^5\text{-}C_5H_5)(PPh_3)_2]^+$ fragment were exchanged for a 1,2-bis(diphenylphosphino)ethane ligand, abbreviated to dppe. Dppe is a bidentate phosphorus ligand and contains two donor atoms linked by an ethylene chain which allows chelation at the ruthenium centre. It is well known that the use of bidentate ligands forms complexes with much higher thermodynamic stability than their monodentate counterparts due to their higher binding constants.[12] This higher stability is predominantly attributed to entropic effects; less entropy of disorder is lost on the formation of complexes containing a single multidentate ligand in comparison to a structural analogue which contains multiple monodentate donors. An alternative view is to consider ligand dissociation from a metal complex. If a monodentate ligand is displaced, it becomes part of the bulk solution. If one donor atom of a bidentate ligand dissociates, the ligand remains in the coordination sphere of the metal which allows the rapid reattachment of the dissociated arm. This phenomenon is known as the 'chelate effect'.[13]

Despite the advantages offered by chelating phosphines, the use of bidentate phosphines in catalysis was slow to develop. Although the synthesis of dppe was reported as early as 1959,[14] the first paper to describe specific results for diphosphine ligands was only published in 1966 by Iwamoto and Yuguchi, who studied a series of iron catalysts with a range of bidentate phosphine ligands for the codimerisation of ethane and butadiene.[15] The slow development of these ligands is unsurprising, as in many catalytic systems the rate of reaction is significantly slowed by the use of bidentate phosphine donors.[14] For example, one of the first commonly used phosphine complexes in catalysis was Wilkinson's hydrogenation catalyst, $[RhCl(PPh_3)_3]$ and as this catalyst relies on phosphine dissociation, the replacement of triphenylphosphine with a bidentate phosphine actually inhibited its activity.[14] Therefore, further mechanistic investigations were needed before the use of chelating diphosphine complexes became prevalent in catalysis.[14]

However, bidentate ligands are now recognised to be advantageous in many cases. Alongside increased catalyst stability which reduces degradation, bidentate phosphine containing catalysts tend to produce higher levels of both regio- and enantioselectivity due to a more rigid microenvironment surrounding the metal atom. This leads to a higher energy variation between competing mechanisms, and so one pathway is more strongly favoured than the rest.[16]

1.2.2   Chemically non-innocent phosphine ligands

In addition to the use of phosphorus-based spectator ligands such as PPh$_3$ and dppe, the work described in Chapters 2 and 3 of this thesis relies on the incorporation of chemically 'non-innocent' or 'cooperative' phosphine ligands into the coordination spheres of ruthenium half-sandwich complexes. Cooperative ligands are those which either participate directly in bond activation and undergo a reversible chemical transformation, or engage in intramolecular interactions in order to promote a reaction.[17]

1.2.2.1   Bifunctional catalysis in nature

Most synthetic catalysts rely primarily on the reactivity of the metal centre to enable substrate transformations, whereas nature's metalloenzymes employ the reactivity of the metal centre in combination with functional groups on the protein backbone to facilitate catalytic reactions.[18] One such example is the amide hydrolysis catalyst carboxypeptidase, shown in Figure 1.3.[19]
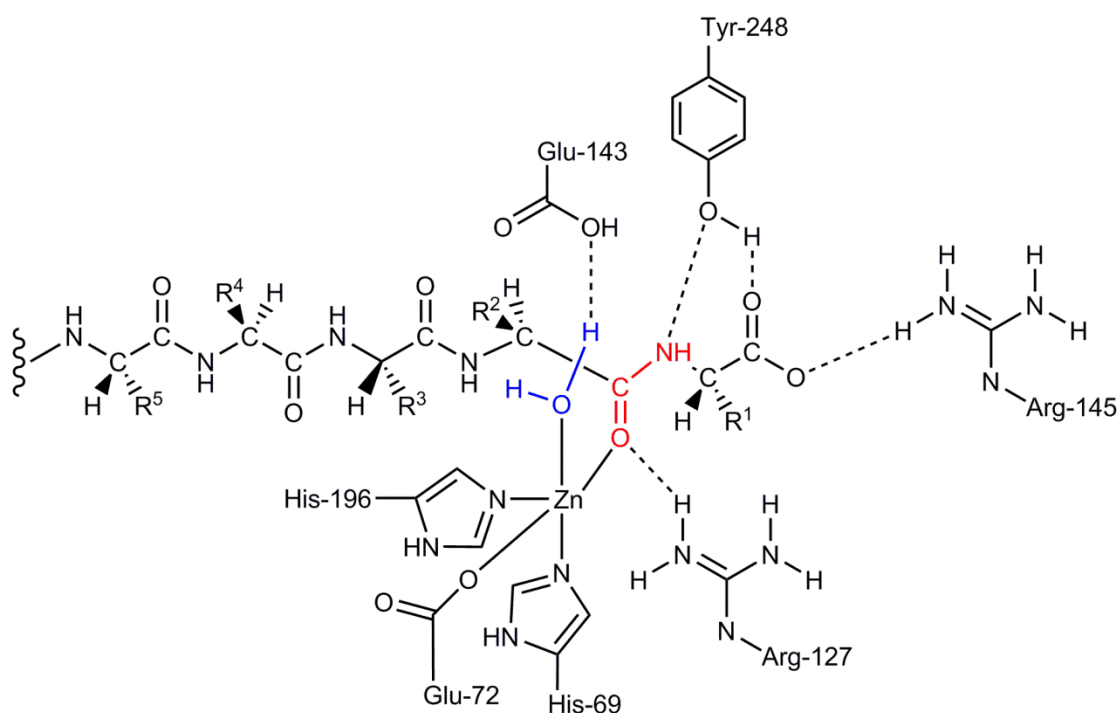
Figure 1.3 Active site of amine-hydrolysis catalyst carboxypeptidase

The Zn(II) is coordinated in the enzyme active site by the carboxylate group of a glutamine residue (Glu-72) and the imidazole groups of two histidine residues (His-69 and His-196). The free coordination sites allow the Zn(II) centre to act as a Lewis acid towards the water molecule which will perform the hydrolysis (blue) and the amide carbonyl group to be

hydrolysed (red). Hydrogen bonding interactions from the tyrosine (Tyr-248) and arginine (Arg-127) residues are believed to assist binding of the substrate, and a glutamine residue (Glu-143) activates water for nucleophilic attack, also by a hydrogen bond. In the absence of a catalyst, amide-bond hydrolysis has a half-life of 350 − 500 years (at pH 7 and 25 °C), whereas a carboxypeptidase enzyme can complete the same reaction in seconds giving a rate enhancement of 4 x 10^{11}.[20-21] This example from nature highlights the remarkable enhancements to catalysis offered by cooperative metal-ligand effects. Organometallic chemists can mimic the synergistic effects between metal centres and their ligands to improve both the selectivities and activities of synthetic complexes by using 'bio-inspired' approaches to catalyst design.

1.2.2.2 Bifunctional catalysis in organometallic complexes

As in biological systems, the synergy between metal centres and chemically non-innocent ligands can be very powerful, and ligand functionality has been shown to assist both stoichiometric and catalytic transformations. In enzymatic catalysis, hydrogen bonding and proton transfer are the most common secondary interactions and this also seems to be true for synthetic organometallic catalysts. For example, either stoichiometric or catalytic ligand assisted C-H activation is reported in ambiphilic metal-ligand activation (AMLA), concerted metalation-deprotonation (CMD), ligand-assisted proton shuttle (LAPS) and ligand-to-ligand hydrogen transfer (LLHT) mechanisms, shown in Scheme 1.1.[17,22-24]
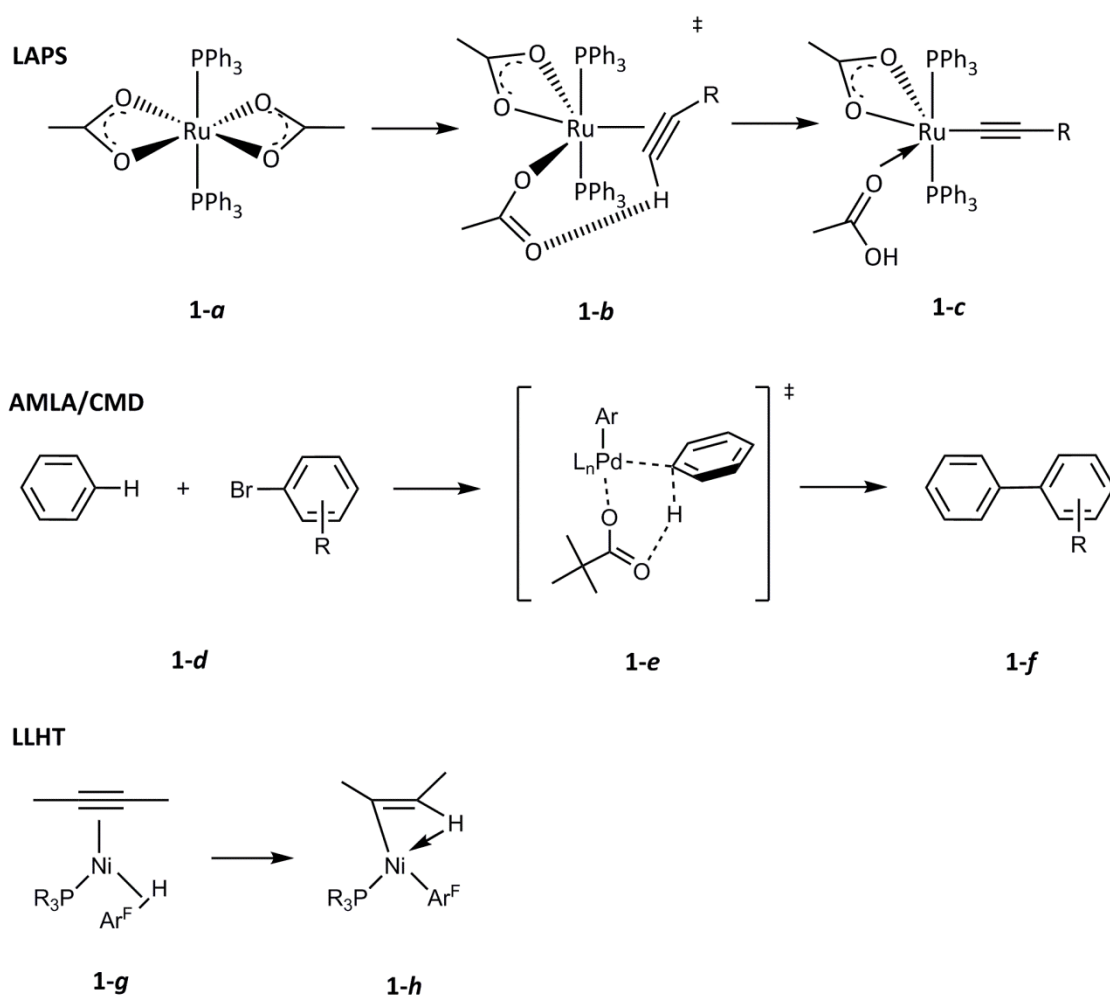
Scheme 1.1 Ligand-assisted processes in organometallic catalysts (LAPS, ligand-assisted proton shuttle[24]; AMLA/CMD, carbon-carbon bond formation *via* ambiphilic metal-ligand activation or concerted metalation-deprotonation[25]; LLHT, ligand-to-ligand hydrogen transfer[26])

In the LAPS mechanism, the hemilabile acetate group can alter coordination mode from bidentate to monodentate in order to allow the alkyne substrate to bind, **1-b**. The acetate

group can then act as an intramolecular base to form the acetylide complex **1-c**. In the AMLA or CMD mechanism, during transition state **1-e**, the pivaloyl group again acts to assist in the deprotonation of the aryl substrate concomitantly with metal-carbon bond formation. In the LLHT system, cleavage of the aryl carbon-hydrogen bond in complex **1-g** is facilitated by proton transfer to a second ligand in the metal coordination sphere. Each of these processes exemplifies bifunctional catalysis in which a coordinated ligand plays an important role in the transformation between intermediates.

In this thesis, all chemically non-innocent ligands employed are monodentate phosphines comprising two phenyl groups and a single aromatic substituent with more complex functionality, which is able to engage in interactions with incoming substrates or other ligands in the coordination sphere. Pyridyl- and imidazolyl-functionalised phosphine ligands have previously been reported in the literature to engage in a variety of bifunctional catalytic processes. One example of this is Grotjahn's catalyst for alkene isomerisation shown in Figure 1.4.[27-28] Complex **1-i** can isomerise a range of heterofunctionalised alkene derivatives with high selectivity for the *E*-isomer, using moderate catalyst loadings of between 2 - 5 mol% and temperatures between 25 - 70 °C.[27-28]

1-i
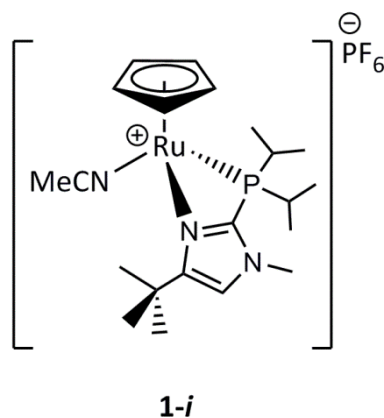
Figure 1.4 Grotjahn's catalyst for alkene isomerisation[27]

The hemilabile imidazolyl-substituted phosphine can engage in bidentate coordination with the ruthenium centre as shown above, however, the imidazolyl group is able to dissociate in order to act as an intramolecular proton-shuttle during the isomerisation reaction. The reaction mechanism is shown in Scheme 1.2.[27]

E-isomer formation

Z-isomer formation
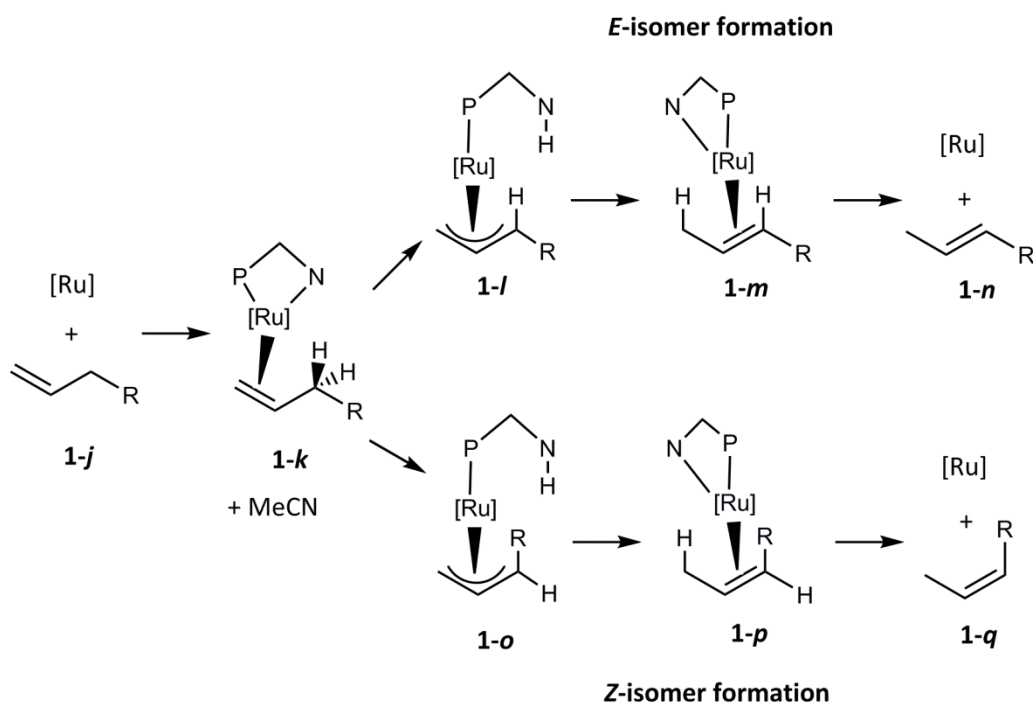
Scheme 1.2 Mechanism of alkene isomerisation using Grotjahn's catalyst to form either the *Z*-or *E*-isomer ([Ru] = 1-*i* in Figure 1.4, with imidazolyl-phosphine partly shown)

Upon addition of substrate, the labile acetonitrile ligand in **1-*j*** can dissociate in order to allow the alkyne molecule to coordinate, **1-*k***. The imidazolyl-substituent of the phosphine can then act firstly as an intramolecular base to deprotonate the alkene and form an allyl intermediate (**1-*l*** or **1-*o***), before protonation at the opposite end of the allyl group to isomerise the alkene (**1-*m*** or **1-*p***). The high levels of selectivity observed exclusively for the *E*-isomer of the alkene arise from the high energy transition states (for example, **1-*o*** to **1-*p***) or intermediates (**1-*o*** or **1-*p***) involved in formation of the *Z*-isomer due to unfavourable steric interactions between the alkene substituent and the phosphine ligand. Compelling evidence for the role of the heterocyclic phosphine can be obtained by replacement of the imidazolyl group with a phenyl substituent, which reduces the rate of reaction with 1-pentene by 330 times.[27] This study demonstrates the enhancements that can be gained from bifunctional catalysis, and the influence that chemically non-innocent ligands can have on the rate of reaction.

In Chapter 2, an experimental and computational study is described for anti-Markovnikov terminal alkyne hydration, and in Chapter 3, pyridyl-phosphine complexes are examined for potential benefits in a pyridine alkenylation process. The role and reactivity of pyridyl- and imidazolyl-functionalised phosphine complexes in the context of alkyne hydration is explored further in the introduction to Chapter 2.

1.3 Classical Fischer-type, Schrock-type and *N*-heterocyclic carbenes

1.3.1 Classical Fischer- and Schrock-type carbenes

Carbenes are neutral compounds which feature a divalent carbon atom with six electrons in its valence shell.[29] The combination of a carbene ligand and an organometallic fragment yields a carbene complex, which can be classified as either Fischer- or Schrock-type.[30] The complexes are often distinguished based on several criteria; the structure of the carbene ligand, the oxidation state of the metal centre, and their subsequent reactivity with electrophiles and nucleophiles.[31] However, it must be noted that in some cases, complexes can have characteristic features from each of the classes which makes their assignment difficult and arbitrary. In osmium complex [(PPh$_3$)$_2$Cl(NO)OsCH$_2$], the absence of a stabilising-heteroatom in the carbene ligand and the reactivity of the carbene-carbon atom with a range of electrophilic reagents indicates a Schrock-type complex. Conversely, the low oxidation state of the metal centre (as osmium(II)) is typical of a Fischer-type carbene complex.[32]

The binding of Fischer and Schrock carbenes to metal centres is dictated by their ground state multiplicity, as shown in Figure 1.5.[31,33]

singlet carbene

triplet carbene

occupied metal
d-orbital

empty
p-orbital

interactions of triplet
state metal and triplet
carbene

empty metal
d-orbital

full σ-orbital
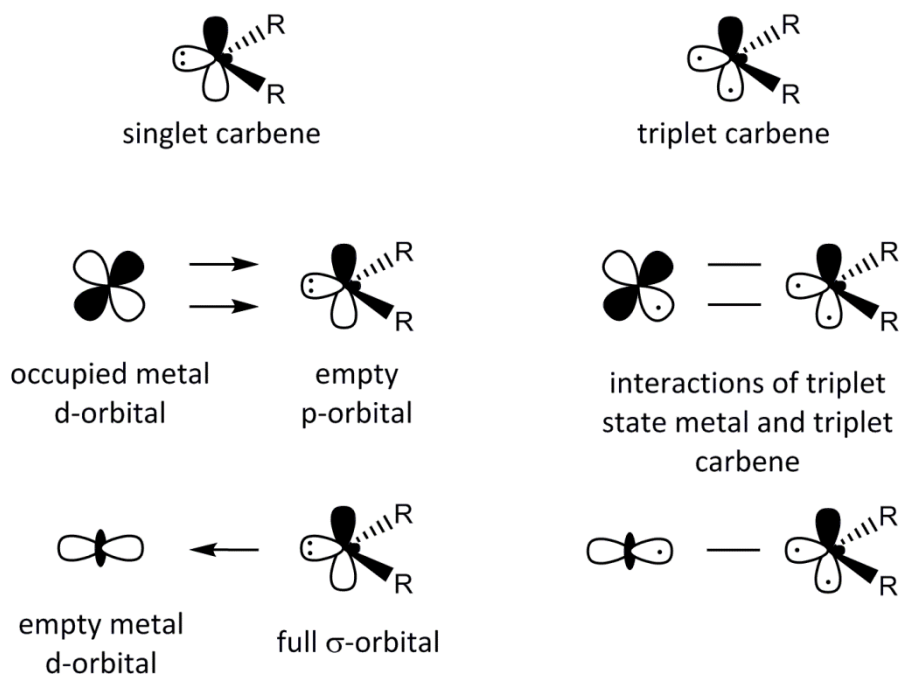
Figure 1.5 Ground state multiplicities of singlet and triplet carbenes and their interactions with metal centres

Carbenes can exist either in the singlet state, in which both valence electrons reside in the same sp^2-hybrid orbital, or in the triplet state, in which one electron is localised in the sp^2-hybrid orbital and the other electron in a carbene-carbon *p*-orbital (Figure 1.5). The relative stabilities of each form are affected by a range of factors, including the steric bulk of the substituents and their inductive and mesomeric effects towards the carbene-carbon atom, summarised in Figure 1.6.[29-31]

a

π-donors can donate electron
density to unoccupied carbene
p-orbital of a singlet carbene
(e.g. nitrogen, oxygen, phosphorus,
sulfur)

π-acceptors can accept electron
density from occupied
carbene σ-orbital of a
singlet carbene (e.g. boron)

b
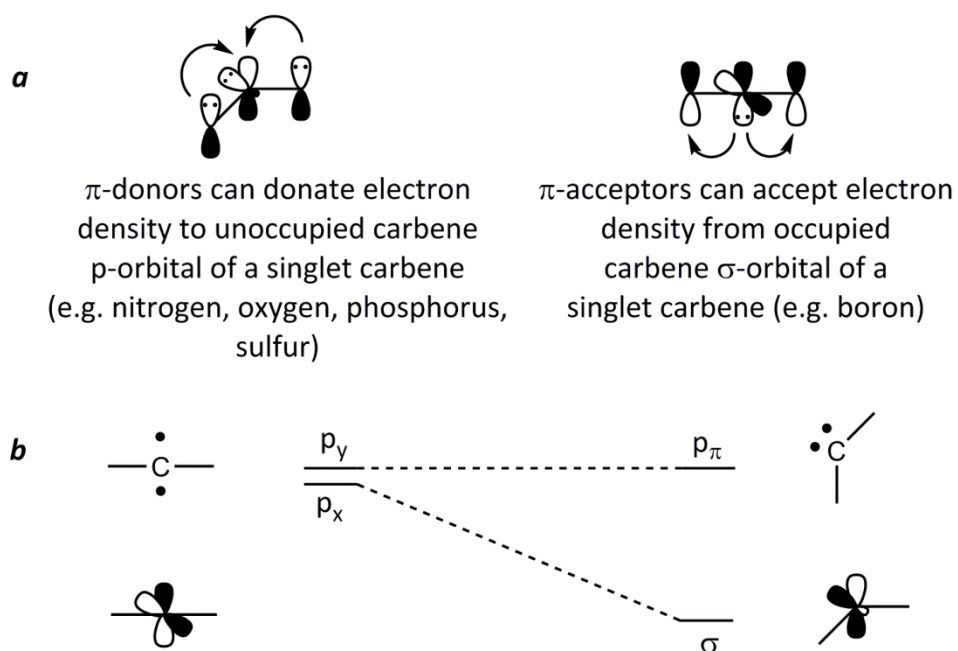
Large substituents: large dihedral angle due to steric interactions,
triplet state favoured
Small substituents: small dihedral angle, singlet state favoured

Figure 1.6 Factors affecting the relative stabilities of singlet and triplet carbenes (a, mesomeric electronic effects and b, steric interactions of the carbene α-substituents)

Part *a* of Figure 1.6 demonstrates the mesomeric electronic effects of the carbene α-substituents on the ground state multiplicity.[34] Both π-electron donors and π-electron acceptors can stabilise the singlet carbene due to donation of electron density to the unoccupied carbene p-orbital and acceptance of electron density from the occupied σ-orbital respectively.[29,34] Mesomeric electronic effects tend to play the most dominant role in the determination of the ground state multiplicity; however, inductive affects of the substituents can also have an influence.[29,35] σ-electron-withdrawing substituents stabilise the singlet

ground state by induction. The s character of the σ-non-bonding orbital is increased, whereas the p_π-orbital energy remains unchanged. This widens the energy difference between the carbene frontier orbitals and therefore the singlet state is favoured. In contrast, σ-electron-donating substituents induce a smaller energy difference and preferentially favour the triplet state.[35]

Large carbene α-substituents kinetically stabilise both singlet and triplet carbenes by providing the carbene-carbon atom with steric protection.[29] However, as shown in part **b** of Figure 1.6, the triplet state is most favourable with a large carbene dihedral angle due to the degeneracy of the carbene frontier orbitals.[29,36] Increasing the steric bulk of the carbene substituents favours this linear geometry and therefore favours the triplet state. Smaller substituents allow for a smaller dihedral angle – this leads to loss of orbital degeneracy and a preference for the singlet state.

Fischer-type carbene complexes typically comprise of well-stabilised, heteroatom-containing carbene ligands, often with alkoxy- or amino- α-substituents, coordinated to low oxidation state metal centres.[30] Fischer carbene ligands engage in synergic bonding to metal centres, comprised of carbene to metal σ-donation and metal to carbene π-back donation, which affords partial double bond character to the metal-carbene bond, **a** in Figure 1.5.[33] The double bond character decreases on stabilisation of the carbene-carbon atom by its α-substituents due to decreased π-back donation from the metal.[37] The π-electron density is polarised towards the metal centre, and the carbene-carbon atom is susceptible to nucleophilic attack.[37]

Schrock-type carbene complexes contain non-stabilised carbene ligands, often with alkyl α-substituents. They are considered to engage in covalent bonding with the metal centre, with the π-electrons equally distributed between the metal and the ligand to create a true double bond between them, as shown in Figure 1.5.[33] A Schrock carbene-carbon atom reacts with electrophiles.[31]

1.3.2 Conventional *N*-heterocyclic carbenes

Conventional *N*-heterocyclic carbene ligands (NHCs) have made a significant impact to the development of organometallic catalysis and now have numerous applications in commercially important processes.[38] They are defined as heterocyclic species containing a carbene carbon and at least one nitrogen atom within the structure of the ring. The first reported crystalline NHC ligand was reported by Arduengo *et al.* in 1991, *a* in Figure 1.7, and demonstrates the electronic and structural features that explain the general properties of this ligand class.[39] Figure 1.7 part *b* demonstrates the electronic effects of the nitrogen heteroatoms which help to stabilise the reactive carbene carbon.[40]
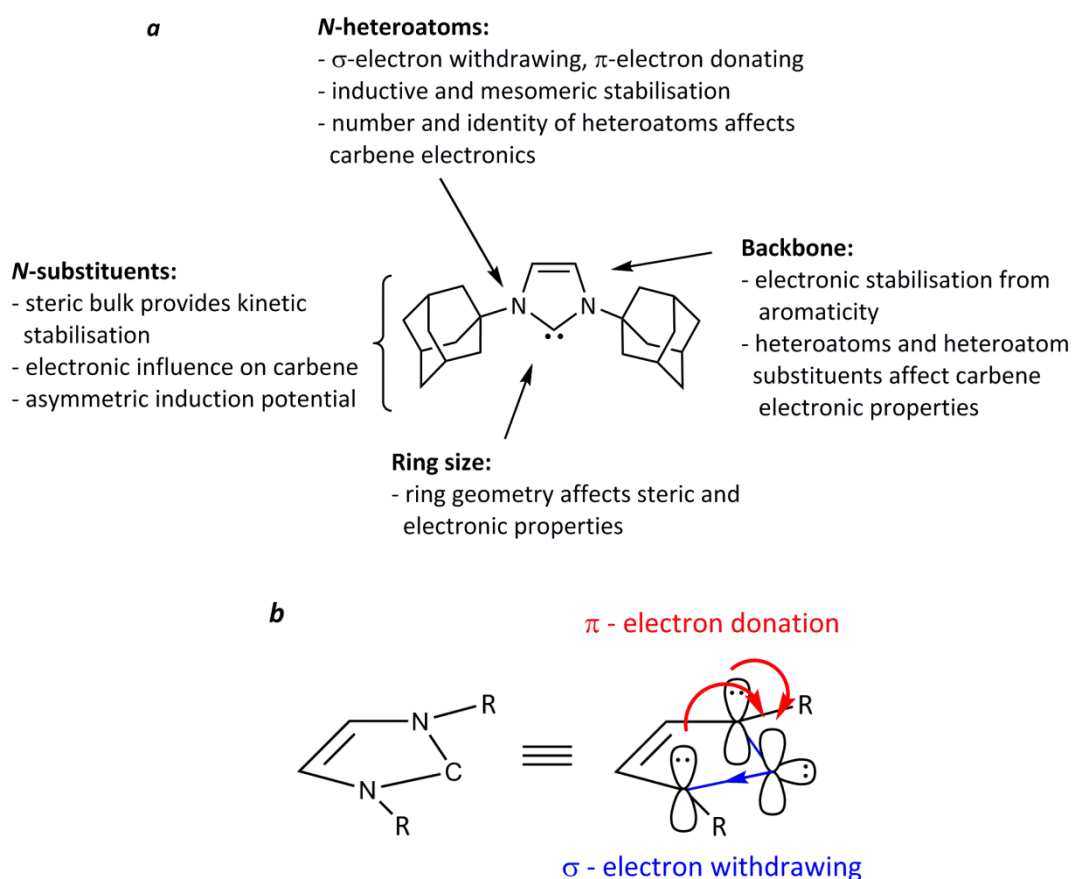
Figure 1.7 The structure of adamantyl-substituted NHC *a* highlights the key structural features of an NHC ligand, *b* indicates the electronic properties of the nitrogen heteroatoms in carbene stabilisation

The diversity of synthetic approaches for the formation of NHCs allows exploration of the effects of the substituents, heterocyclic backbone and other structural features which permits the selection of an NHC structure which is optimised for its role.[40] The strong σ-donor and weak π-acceptor properties of NHC ligands allow their comparison with

phosphines; however, there are important differences between the two ligand classes. NHCs are more strongly σ-donating which leads to stronger and shorter metal to ligand bonds. Therefore, NHC complexes tend to exhibit higher thermal and oxidative stability than their phosphine analogues. The shape of an NHC ligand is also markedly different to that of a phosphine – if phosphines are considered to be 'cone-shaped', NHCs instead are 'umbrella-shaped' with the *N*-substituents oriented towards the metal centre. As a result, NHCs tend to be more sterically demanding and alternation of the *N*-substituents impacts more strongly at the metal centre. NHC ligands are also highly anisotropic (in contrast to phosphine groups) and can rotate around the metal - carbene bond in order to minimise steric clashing with other bulky ligands.

Upon coordination to transition metals, organometallic complexes of NHCs have many different applications.[41-42] The most famous NHC-metal complex is Grubbs' second generation olefin metathesis catalyst, complex **1-s** in Scheme 1.3.[43]
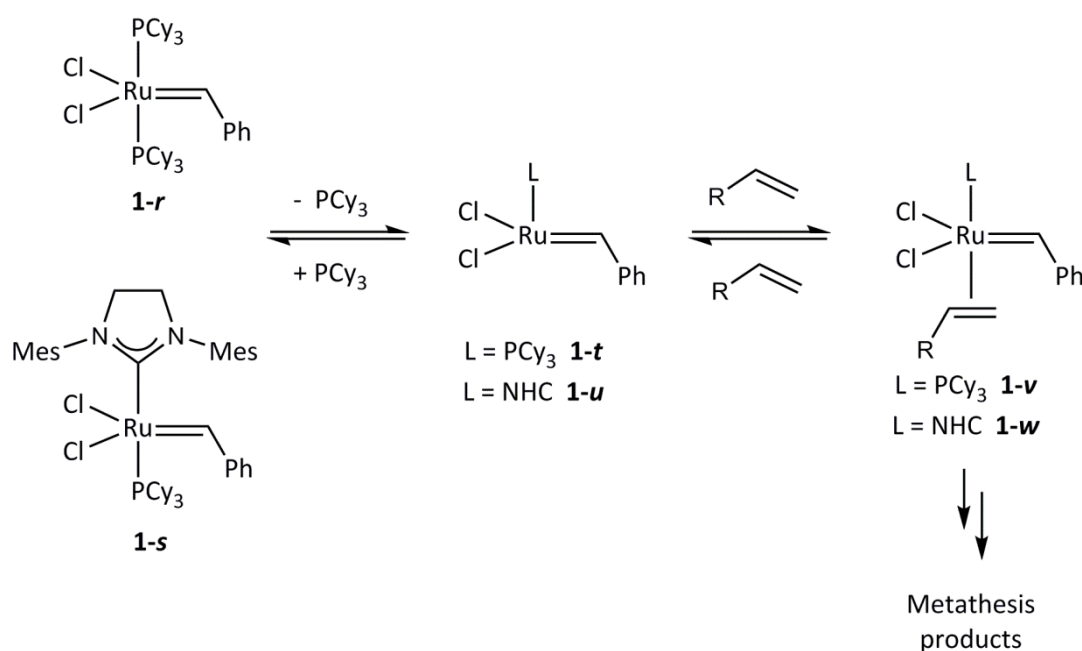
Scheme 1.3 NHCs as ligands in ruthenium-catalysed alkene metathesis

Replacement of a tricyclohexylphosphine ligand from the first generation catalyst, complex **1-r**, with an NHC ligand (SIMes) yielded complex **1-s** with greater thermal stability, a wider substrate scope and high catalytic activity at lower catalyst loadings. This increased activity was due to more favourable alkene binding by the NHC-stabilised catalytically-active species, **1-u**, compared to the phosphine-stabilised analogue, **1-t**, to form **1-w** or **1-v** respectively.

1.3.3 Non-conventional *N*-heterocyclic carbenes

The importance of NHCs in transition metal complexes is well established and conventional NHCs, or Arduengo's-type NHCs, have been exploited as ligands for many transition metal catalysed processes. However, carbene compounds based on nitrogen-containing heterocycles can also be synthesised, which can offer superior electron-donating properties in comparison to classical NHCs. For example, pyridylidene ligands are both effective σ-donors and effective π-acceptors on coordination to transition metals, Figure 1.8.[44]

2-pyridylidene   3-pyridylidene   4-pyridylidene
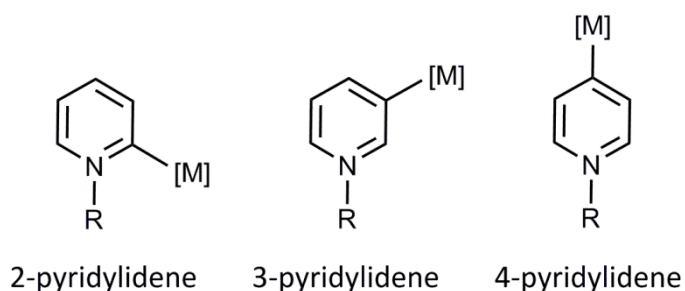
Figure 1.8 2-, 3- and 4-pyridylidene complexes

Pyridylidene is a high energy tautomer of pyridine, formed by a formal hydrogen migration from the carbon-hydrogen bond in the 2-position, to reveal an unsaturated carbene.[45] As in the case of alkyne to vinylidene tautomerisation, pyridine to pyridylidene tautomerisation can often be facilitated by a transition metal complex. Examples of such complexes include the *tris*-pyrazolylborate iridium fragment, which can tautomerise 2-substituted pyridine derivatives to their pyridylidene forms.[46] The relief of steric strain on removing the substituent in the 2-position further from the metal centre is a secondary driving force for this process (again, a similar factor is often important in alkyne to vinylidene tautomerisation). The number of complexes able to tautomerise unsubstituted pyridine to the parent pyridylidene is very limited.[45,47]

The tautomeric forms of pyridine were first accessed in the 1930's[48] and since then, a wide range of synthetic routes to prepare pyridylidenes have been reported. These include the *N*-functionalisation of pyridyl derivatives, oxidative addition of halide-functionalised pyridine starting materials to transition metal complexes, deprotonation of a carbon-hydrogen bond of a pyridinium salt, transmetallation, decarboxylation of pyridinium carboxylates and the tautomerisation of pyridine by transition metal complexes.[30,44] Pyridine tautomerisation,

shown in Figure 1.9, can be considered as an analogous process to alkyne-vinylidene tautomerisation discussed in Section 1.4.
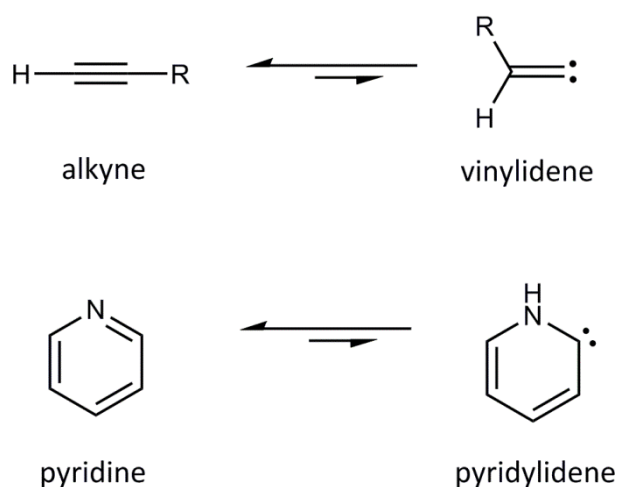
Figure 1.9 Alkyne to vinylidene and pyridine to pyridylidene tautomerisation

The formation of a pyridylidene complex, synthesised directly from non-activated pyridine under mild conditions, was reported by Lynam and Slattery in 2013.[45] The complex was proposed to be a key intermediate in the formation of *E*-styryl pyridines from pyridine and terminal alkynes, promoted by half-sandwich complex $[Ru(\eta^5\text{-}C_5H_5)(PPh_3)(NC_5H_5)_2]PF_6$. In the presence of excess pyridine in the reaction mixture, *E*-styryl pyridines could be formed catalytically. However, in the absence of pyridine, the major organometallic product was pyridylidene complex **1-y**, which could undergo reversible deprotonation to form **1-z**, Scheme 1.4.
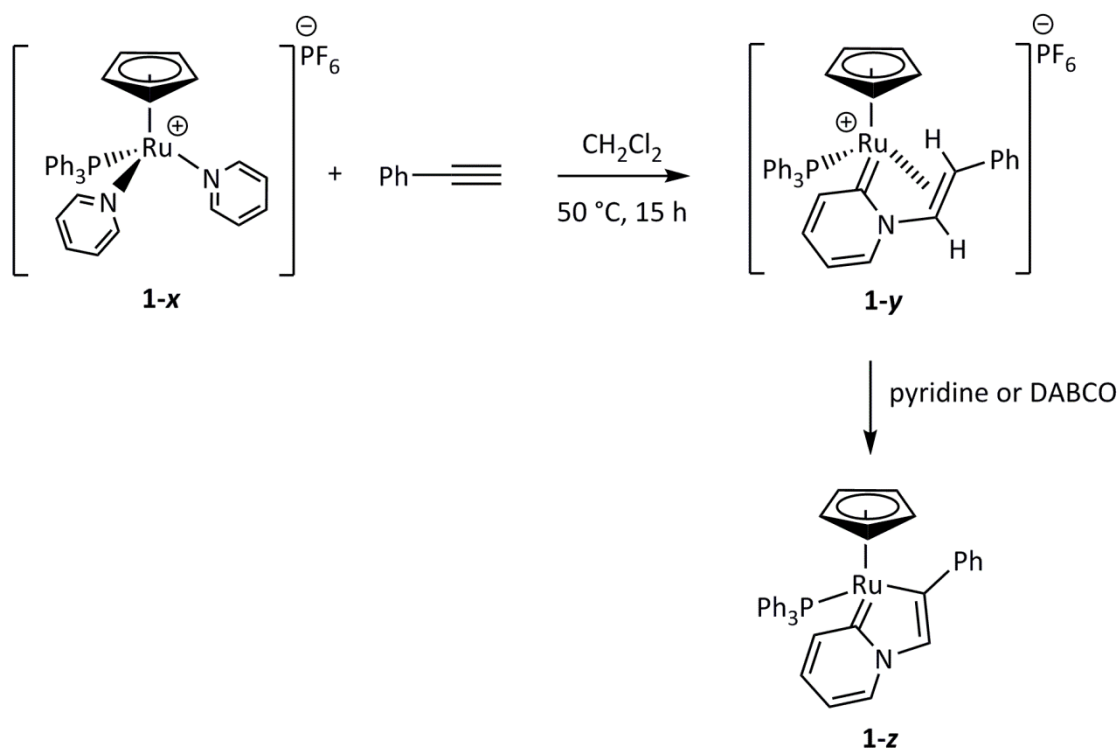
Scheme 1.4 Formation of ruthenium pyridylidene complexes 1-*y* and 1-*z* (1-*x* later referred to as [7]PF$_6$, 1-*y* as [13]PF$_6$ and 1-*z* as [16])

The in-depth computational and experimental findings suggested a pyridylidene intermediate was a 'branching point' from which the productive pathway could proceed under the optimised catalytic conditions, but also a state from which catalyst deactivation could occur (complexes **1-*y*** and **1-*z*** in Scheme 1.4 represent catalyst deactivation products, see Chapter 3 for further details). The project also highlighted the potential for pyridylidene intermediates as synthetically relevant species from which to activate nitrogen-containing heterocycles in useful and efficient catalytic reactions.

Pyridylidene complex **1-*z*** forms the starting material for the electrophilic fluorination reactions reported in Chapter 4, and attempts to optimise the pyridine activation reaction to form *E*-styryl pyridines using chemically non-innocent ligands are reported in Chapter 3. Therefore, further information on the formation, properties and reactivity of this complex are reported in each of these Chapters.

1.4   Vinylidene Ligands

1.4.1   Organic vinylidenes

The tautomerisation of an alkyne molecule produces a high energy, unsaturated carbene species known as a vinylidene ($R_2C=C:$). The simplest vinylidene is formed on tautomerisation of ethyne *via* a 1,2-hydrogen shift, Figure 1.10.[49]
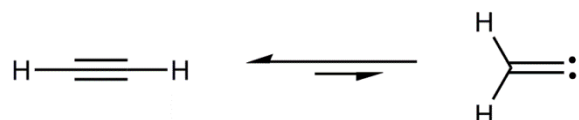
Figure 1.10 Tautomerisation of ethyne by a 1,2-hydogen shift to form a vinylidene

In the free state, the two tautomers are in equilibrium; however, the vinylidene form has a very short lifetime of just 10^{-10} s^{-1} due to the presence of six valence electrons at the terminal carbon.[49] The lone pair on this carbon atom makes vinylidenes highly reactive species, but as with other transient species (including phosphalkynes and carbyne moieties) they can be stabilised on coordination to a metal centre.[49-52] A range of metals can be utilised, but complexes of vinylidene ligands are often based on ruthenium or osmium centres (electron rich, d^6 metals).[49] Other common complexes include iridium, cobalt, tungsten, iron and manganese.[49-50] The stability of a vinylidene complex increases with increasing electron density at the metal centre.[49,53]

In the absence of metal coordination, harsh reaction conditions are often required to promote the formation of vinylidene intermediates. This is exemplified in the total synthesis of ($\pm$)−isoptychanolide, during which the alkyne was heated in the gas phase to 620 K to form the postulated intermediate **1-ab**, Scheme 1.5.[54] These conditions are highly energy intensive and allow little control over the reaction. Therefore, a more accessible route may be found by the introduction of a metal complex to stabilise the vinylidene.
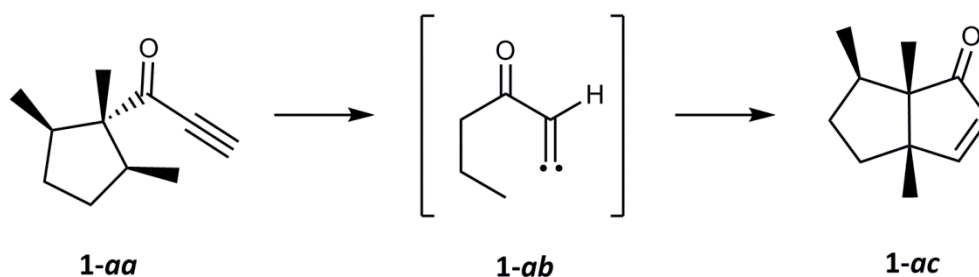
Scheme 1.5 Vinylidene intermediate 1-ab in the synthesis of the ($\pm$)-isoptychanolide

1.4.2 Metal-stabilised vinylidenes

On coordination to a transition metal complex, an alkyne can undergo metal-promoted tautomerisation to the vinylidene form; retention of the vinylidene moiety at the metal centre affords enhanced stabilisation and an increased vinylidene lifetime. The ability to isolate metal vinylidene complexes has allowed for these ligands to be characterised and their reactivity to be explored. A vinylidene ligand displays marked reactivity from the parent alkyne from which it is derived, Figure 1.11.[24,49,55] This principle is explored in a mechanistic study of ruthenium-catalysed terminal alkyne hydration, reported in Chapter 2.[56]
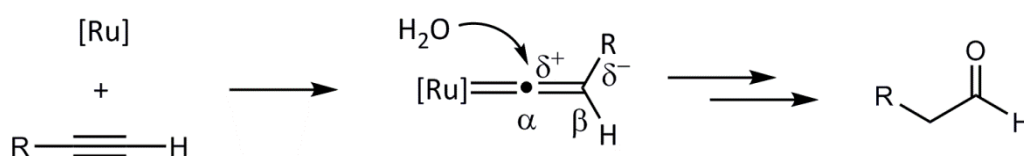
Figure 1.11 Polarisation of a Fisher-type vinylidene complex and reactivity with nucleophiles

The metal-bound α-carbon is electron poor and therefore is electrophilic in nature, whereas the opposite polarisation and reactivity is observed for the β-carbon. Vinylidene ligands also exhibit metal-carbene character across the metal-α-carbon double bond. These characteristic properties influence many of the stoichiometric and catalytic reaction mechanisms for those pathways which encompass vinylidene intermediates; for ruthenium vinylidene complexes, the most common processes are usually the addition of nucleophiles at the α-carbon; alkyl, alkenyl or alkynyl migration from the metal to the α-carbon or [2+2] cycloaddition of alkenes and alkynes across the metal-carbon double bond.[55]

1.4.2.1 Electronic structure and molecular orbital diagram of Fisher vinylidene complexes

As is common with metal-carbene complexes, metal-vinylidene complexes can be classified into two main groups – Fischer or Schrock-type complexes – based on the π-electron density between the metal and the metal-bound α-carbon, Figure 1.12.[49]

Figure 1.12 Fisher and Schrock-type vinylidene complexes

Schrock-type vinylidene complexes arise from coordination to an early transition metal centre and display a nucleophilic metal-bound α-carbon. However, the most commonly isolated vinylidene complexes are of the Fisher-type, which are generated from later transition-metal centres (Groups 6 – 10) in low oxidation states.[49] These species are electrophilic at the α-carbon, and nucleophilic with respect to the metal and β-carbon positions (as discussed in section 1.4.2).

The molecular orbital (MO) diagram of a Fisher-type vinylidene is displayed in Figure 1.13.[49]
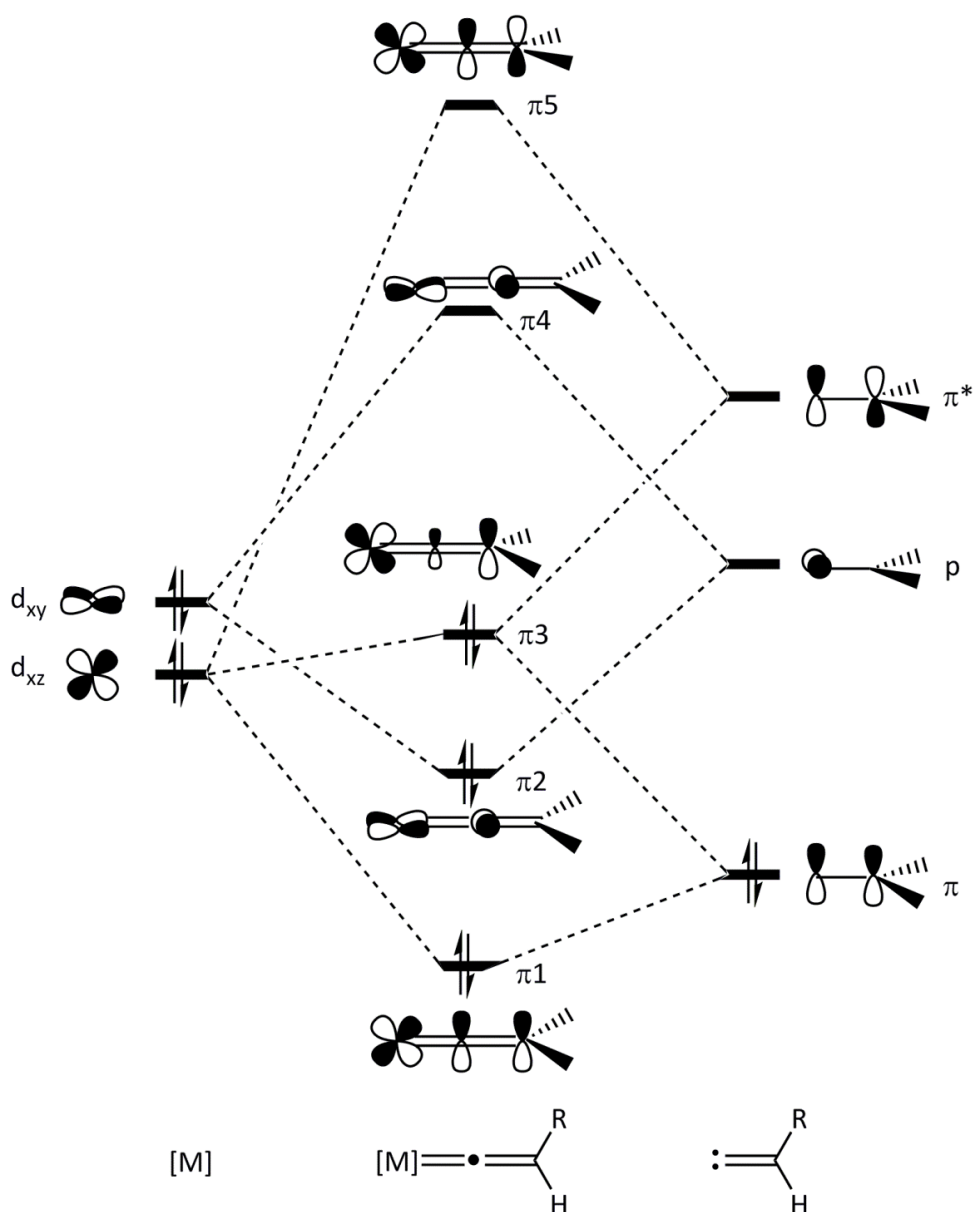
Figure 1.13 Schematic molecular orbital diagram of a Fisher type vinylidene fragment, [M] = Ru (II), Mn (I) etc

The MO diagram can be used to explain the polarisation across a vinylidene moiety in terms of orbital interactions and hence the subsequent reactivity that they exhibit. To form the lowest unoccupied molecular orbital (the LUMO, π4), the highest orbital contribution is received from the empty p_π orbital of the α-carbon of the vinylidene component. This explains the electrophilic character at this position and therefore why it can undergo nucleophilic attack. The highest occupied molecular orbital (the HOMO, π3), is antibonding in nature and formed from an interaction between a C=C π-bonding orbital of the vinylidene moiety and a symmetry-adapted metal d_π-orbital. Therefore, the regions of highest electron density are located at the vinylidene β-carbon and the transition metal centre, allowing electrophilic attack at either of these positions.

Due to this well-understood reactivity profile, transition-metal vinylidene complexes can be used to selectively synthesise new carbon-carbon or carbon-heteroatom bonds, often with high atom economy and relatively mild reaction conditions.[57] The stabilisation achieved on coordination to a metal centre also allows for mechanistic study of the reaction pathway, and additional stabilisation can be achieved by modification of the other ligands in the coordination sphere. Phosphine ligands are a popular choice to create electron rich complexes (see Section 1.2.1) and their tuneable properties can modify reactivity through the variation of both steric and electronic effects. For example, a triphenylphosphine ligand (PPh$_3$) would slow the rate of approach of an incoming nucleo- or electrophile more effectively than a smaller trimethylphosphine ligand (PMe$_3$) which would allow a more accessible metal centre.

1.4.2.2 Characterisation of metal vinylidene complexes

The characterisation of novel metal-vinylidene complexes represents a large contribution to this thesis, especially in Chapter 5, in which the first examples of fluorinated vinylidene complexes have been prepared and thoroughly characterised with reference to their non-fluorinated analogues.

Typically, the vinylidene moieties of transition metal vinylidene complexes are characterised by multinuclear NMR spectroscopy, IR spectroscopy and X-ray crystallography.[50,58-60] In the ^{13}C{^{1}H} NMR spectra, the two carbon atoms of the vinylidene ligand backbone resonate at very different chemical shifts due to their opposite polarisations. On coordination to ruthenium half-sandwich complexes, the metal-bound α-carbon is very deshielded and

typically resonates between 350 and 390 ppm, whereas the β-carbon resonates between 90 and 100 ppm.[50] On variation of the metal centre, the chemical shifts are modified but the principle remains the same. The ^{1}H NMR resonance of any proton substituents on the β-carbon are heavily affected by the nature of the metal centre and other substituents on the vinylidene ligand and the chemical shifts tend to vary between 2 and 5 ppm.[52] Therefore the ^{1}H NMR is a less useful diagnostic tool to identify the presence of a vinylidene ligand (unless other similar complexes are available for comparison). The C=C bond has a typical stretching frequency of 1650 to 1600 cm^{-1} in the IR spectrum.[50]

Vinylidene complexes are commonly isolated and crystallised in order to allow structural determination by single-crystal X-ray crystallography. For structures which form single crystals, X-ray crystallography allows in-depth examination of the bond lengths, bond angles and 3-D structure in the solid state. In all cases, vinylidene ligands tend towards linearity with bond angles of between 161° and 180°.[50] The bond lengths suggest bond orders in the range of two for the metal - α-carbon linkage and between two and three for the α-carbon-β-carbon bond. As vinylidenes are electron withdrawing ligands, the short metal-α-carbon bond arises from a strong synergic bonding interaction, and the short α-carbon-β-carbon bond is explicable by the partial sp character of the β-carbon.

It is worth noting that other characterisation techniques can be utilised in order to study transition-metal vinylidene complexes (including mass spectrometry and UV-visible spectroscopy). Multinuclear NMR spectroscopy can also be used to study other ligands in the complex coordination sphere; of particular relevance in this thesis is the use of ^{31}P{^{1}H} NMR spectroscopy for the observation and study of phosphine ligands. However in most cases, these approaches provide additional information about the nature of the entire complex rather than the vinylidene moiety specifically, and so they have not been included here. Large compilations of spectroscopic data for vinylidene complexes have been reported in reviews by Michael Bruce[50] and Lynam and Fey.[61]

1.4.2.3   Synthesis of ruthenium vinylidene complexes

There are several preparative methods to produce vinylidene ligands within the coordination sphere of a metal; these include 1,2-hydrogen migration of terminal alkynes at a transition-metal centre,[62] electrophilic attack of a metal acetylide complex[63-65] and deprotonation of a metal alkynyl ligand,[66] to name but a few.[49]

The most common route to a vinylidene ligand involves the coordination of a terminal alkyne to a metal centre, in replacement of either a neutral or anionic ligand, to respectively produce a neutral or cationic complex. This practical and efficient method of vinylidene formation was first reported by Bruce and Wallis in 1979.[62] The ruthenium half-sandwich complex **1-*ad*** was reacted with a terminal alkyne and a halide scavenger with a counter-ion (NH_4PF_6) and briefly heated in methanol (to avoid methanol behaving as a nucleophile towards the vinylidene product). This procedure produced an eighteen-electron species with a full coordination sphere, **1-*ae***, Scheme 1.6.
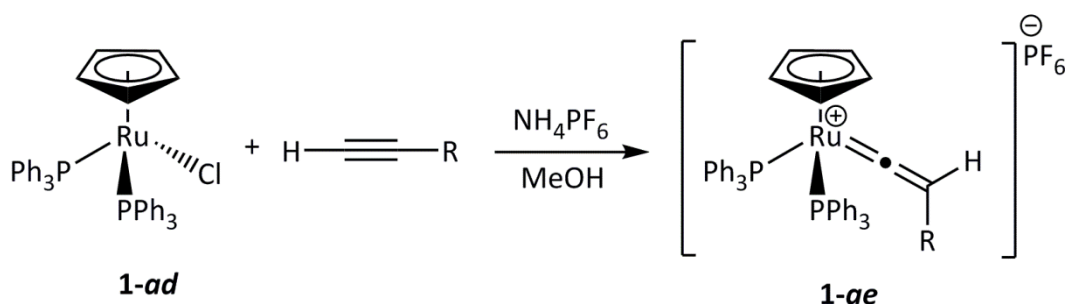
Scheme 1.6 Synthesis of a vinylidene moiety by coordination to a metal centre

Terminal alkynes are used most commonly in these syntheses, but in some cases the migration of other groups is possible, including Group 14 substituents such as $-SiMe_3$ and $-SnPh_3$.[58] These groups can then be replaced by hydrogen *in situ* using conventional treatments such as $[NBu_4]F$.[49] One such example of this methodology was provided by the reaction of $[RhCl(PiPr_3)_2]_n$ and $RC\equiv CSiMe_3$ (where R = $-CH_3$, $-C_6H_5$, $-CO_2Et$, $-CH_2OH$, $-COCHPh_2$ or $-CO_2SiMe_3$) to produce the corresponding $[RhCl(=C\{SiMe_3\}R)(PiPr_3)_2]$ complex.[67] 1,2-halogen shifts of iodine have also been reported at tungsten and manganese.[49,68]

More recently, the migration of carbon-containing functional groups has been reported. In 2007, Shaw and co-workers presented the first example of η^1-vinylidene complex formation from carbon-carbon migration of an internal alkyne. They observed that the addition of $PhC\equiv CCOPh$ to $[Ru(\eta^5-C_5H_5)(PPh_3)_2Cl]$ in the presence of a halide scavenger such as $AgPF_6$

resulted in the formation of $[Ru(\eta^5\text{-}C_5H_5)(PPh_3)_2C=C\{COPh\}Ph)]PF_6$ over 18 hours at 25 °C.[69] A second cationic complex, thought to be an intermediate of vinylidene formation, was also observed during the reaction, in which the $[Ru(\eta^5\text{-}C_5H_5)(PPh_3)_2Cl]$ precursor had lost a chloride ligand and instead contained an $\eta^1(O)$-bound PhC≡CCOPh moiety.

More recently, the research group of Ishii (and others) have reported the conversion of unfunctionalised internal alkynes to their vinylidene tautomers, promoted by iridium, ruthenium and iron centres.[70-72] In the first reported example, ruthenium complex **1-af** was shown to react with a range of internal alkynes with reaction times of between three hours (PhC≡CC₆H₄-4-OMe) to three days (PhC≡CC₆H₄-4-CO₂Et), Scheme 1.7.[72] In the presence of ester-substituted alkynes, η^2-alkyne complexes could be isolated as intermediates and converted to the corresponding vinylidene ligands by heating or irradiation with UV light.[72]
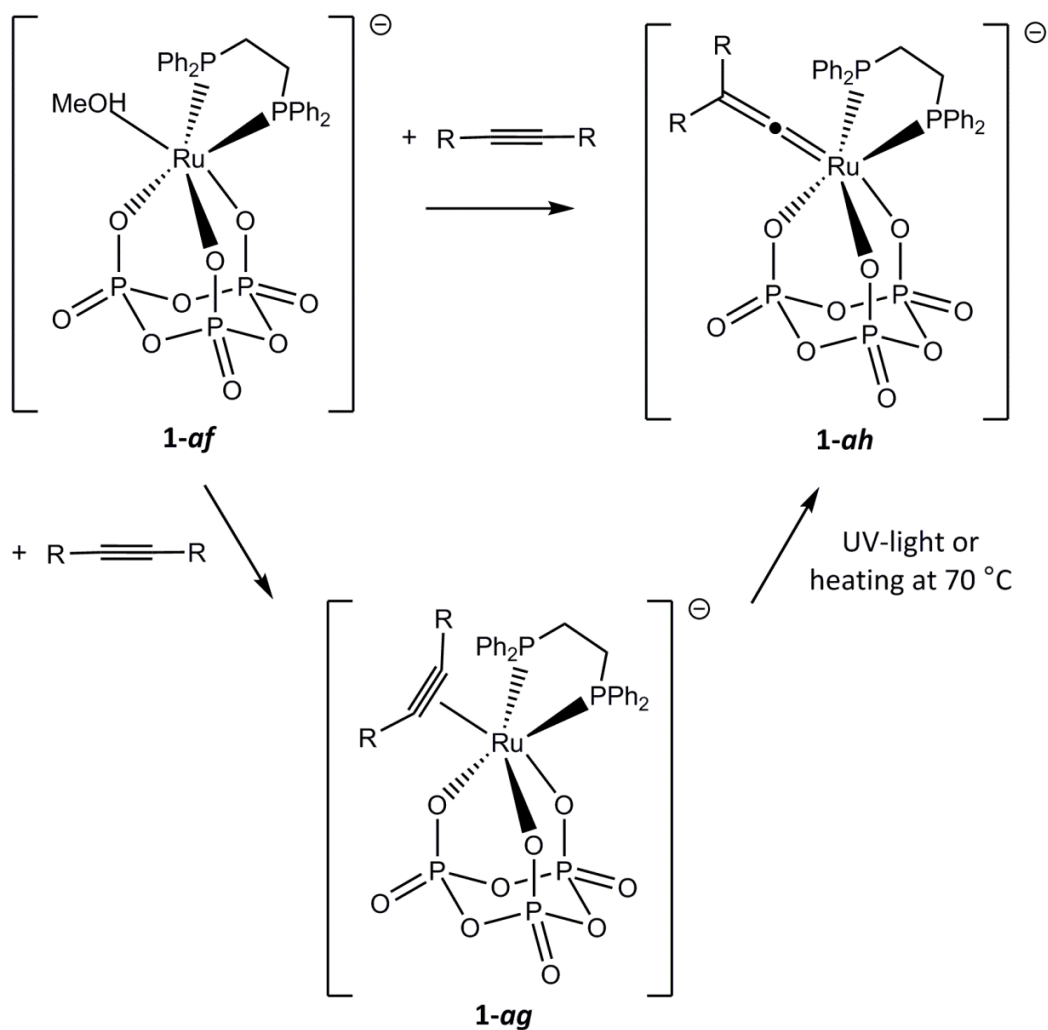
Scheme 1.7 Internal alkyne to vinylidene tautomerisation mediated by complex 1-*af*

Studies on the conversion of the η^2-complex **1-*ag***, $[Ru(P_3O_9)(dppe)(\eta^2\text{-}EtC\equiv CCO_2Et)]^-$, into vinylidene complex **1-*ah***, $[Ru(P_3O_9)(dppe)(C=C\{CO_2Et\}Et)]^-$, demonstrated that the reaction followed first-order kinetics, and was believed to undergo an intramolecular 1,2-alkyl/aryl shift rather than *via* an oxidative addition route.[72] Repetition of the reaction with a range of alkyne substrates indicated that alkynes with electron-withdrawing groups exhibited the highest migratory ability. However, the rate of formation of the vinylidene complexes showed the opposite trend. Therefore it can be concluded that the rate of vinylidene complex formation depends on the stability of the intermediate η^2-alkyne complex rather than the migratory aptitude of the substituents.

Alternatively, vinylidene complexes can be accessed from acetylide precursors, in which the acetylide ligand can undergo electrophilic attack at the β-carbon (in the presence of a counter ion) to form a cationic complex. For example, it was demonstrated by Bruce that reaction of $[Ru(\eta^5\text{-}C_5H_5)(PPh_3)_2(C\equiv CR)]$ with HBF_4 or HPF_6 yielded the respective protio-vinylidene complexes.[62] The complexes can undergo several cycles of quantitative deprotonation and reprotonation by the addition of appropriate acids and bases.

The protonation of metal-acetylide ligands allows access to the complexes formed by H-migration from the corresponding terminal alkyne, whereas reaction of such acetylide precursors with other electrophiles can provide a convenient route to disubstituted vinylidene ligands. For example, the acetylide β-carbon of $[Ru(\eta^5\text{-}C_5H_5)(PPh_3)_2(C\equiv CR)]$ is sufficiently nucleophilic to react with a range of electrophiles including halogens Cl_2, Br_2 and I_2.[64] This methodology is directly relevant to some of the work described in this thesis and will be explored in more detail in Chapter 5. In place of protonation or halogenation, alternative electrophiles include haloalkanes (often iodoalkanes), triflates (alkyl, benzyl, cyclopropyl), azoarenes ($[ArN_2]^+$) and halides XCH_2R (R = -CN, $-C_6H_5$, $-C_6F_5$, $-C_6H_4\text{-}4\text{-}CN$, $-C_6H_4\text{-}4\text{-}CF_3$ and $-CO_2Me$).[49]

1.4.2.4 Mechanistic pathways for vinylidene formation

The tautomerisation of an alkyne to a vinylidene at a metal centre can proceed *via* a range of mechanisms; commonly by either a 1,2-hydrogen migration (pathway **A**), or a formal oxidative addition with subsequent 1,3-hydride shift (pathway **B**).[73] Other less common pathways are highlighted as pathways **C** and **D**, Scheme 1.8.[24,56,73]

Pathway A

Pathway B
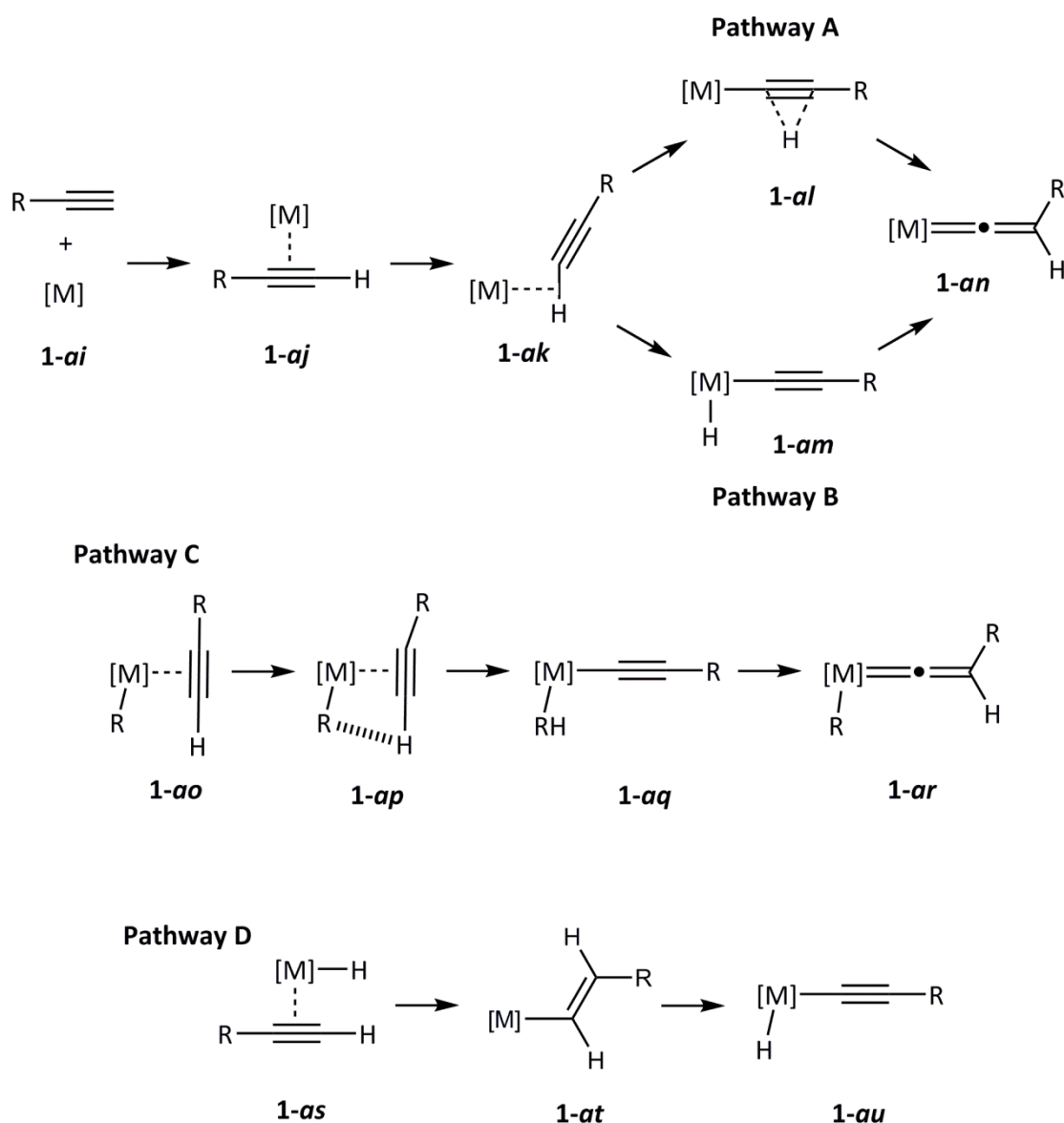
Pathway C

Pathway D

Scheme 1.8 Potential mechanisms of vinylidene formation

In each of the mechanisms above (**A** to **D**), the metal complex must have or create a vacant coordination site in order to allow initial η^2-binding of the alkyne (**1-aj**, **1-ao**, **1-as**). In pathways **A** and **B**, the next step is slippage of the coordinated alkyne to coordination by the terminal carbon-hydrogen bond, **1-ak**. The formation of σ-complex **1-ak** is important to weaken the C-H bond and allow more facile bond activation or migration. At this point, the pathways diverge and the alkyne can either undergo 1,2-hydrogen migration (**A**) or formal oxidative addition across the carbon-hydrogen bond (**B**). Pathway **A** is most common for electron-poor complexes, which includes the majority of ruthenium species, and has been studied computationally in great detail by Silvestre and Hoffmann (for [Mn(η^5-C$_5$H$_5$)(CO)$_2$],

isolobal with $[Ru(\eta^5\text{-}C_5H_5)(PR_3)_2]^+)$ and confirmed the necessity of complexes **1-*ak*** and **1-*al*** in the alkyne to vinylidene tautomerisation process.[74] Direct 1,2-hydrogen migration from η^2-alkyne complex **1-*aj*** was calculated to have a transition state energy barrier of 230 kJ mol^{-1} which was reduced to 121 kJ mol^{-1} *via* intermediates **1-*ak*** and **1-*al***. Examination of the MO diagrams also indicated the increased stability on conversion of the η^2-alkyne complex **1-*aj*** (with an antibonding high energy HOMO) to the vinylidene **1-*an*** complex (with a lower energy HOMO due to significant non-bonding character).

Pathway **B** is more common for electron rich complexes, including those of rhodium and iridium. The work of Silvestre and Hoffmann suggested that the energy barrier for the 1,3-hydride shift was much higher for their model complex compared to the 1,2-hydrogen migration and so unlikely to proceed.[74] Both Wakatsuki and De Angelis confirmed that the 1,3-hydride shift was unlikely for a d^6 metal centre, and Wakatsuki reported that it was thermodynamically unfavourable for the metal to access a d^4 configuration.[53,75] The formation of the hydrido-acetylide complex is observed but rarely for ruthenium complexes, but becomes more favourable on increasing electron density at the metal centre.[76] Pathways **A** and **B** are highly system dependent and by changing the conditions or coordination sphere at the metal centre, the two mechanisms become interchangeable.[77]

In order to take advantage of the catalytic properties of vinylidene complexes, facile access to the vinylidene ligand is essential to allow the use of mild reaction conditions. Pathway **C** in Scheme 1.8 represents the incorporation of chemically non-innocent ligands into the coordination sphere of the metal in order to assist in the alkyne to vinylidene tautomerisation. In **1-*ap***, the ligand acts as an intramolecular base in the deprotonation of the vinylidene ligand to form the acetylide, **1-*aq***, and then delivers the proton to the β-carbon to form the vinylidene, **1-*ar***. This intramolecular 'proton shuttle' process forms an important contribution to this thesis in Chapters 2 and 3. An experimental and computational study by the groups of Lynam and Slattery observed that the rate of vinylidene formation was significantly enhanced by the use of ruthenium complex $[Ru(\kappa^2\text{-}OAc)_2(PPh_3)_2]$ in comparison to the chloride analogue $[RuCl_2(PPh_3)_2]$, due to the involvement of the acetate groups as 'proton shuttles'.[24] Pyridyl-functionalised phosphine ligands have also successfully been utilised in these transformations using rhodium and ruthenium mediated systems.[56,78]

1.4.3 Reactivity of ruthenium-vinylidene complexes

Although the synthesis and reactivity of vinylidene complexes represents an active and dynamic area of current research, the promotion of alkyne to vinylidene tautomerisation is a well-established ability of many transition metals.[49-50] The subsequent stabilisation of the vinylidene ligand at the metal centre has allowed their reactivity to be explored in a wealth of stoichiometric and catalytic reactions. Furthermore, their straightforward synthesis by tautomerisation of a terminal alkyne has given them a privileged position in catalysis as they can easily be regenerated *in situ* under appropriate reaction conditions.[45,56,79]

As discussed previously, the facile synthesis and characteristic reactivity of vinylidene ligands renders them useful in a range of catalytic processes, and there are multiple reviews that explore the exploitation of these transition metal complexes in many different reactions.[49,55,57,80] The importance of vinylidene intermediates in both the anti-Markovnikov terminal alkyne hydration mechanism and in the alkenylation of pyridine is discussed in detail in Chapters 2 and 3 of this thesis, and the reactivity of fluorinated vinylidene ligands is explored in Chapter 5. These studies exemplify the reactivity of ruthenium vinylidene complexes with nucleophiles (water, pyridine) and the use of vinylidene intermediates in carbon-carbon bond forming reactions. Therefore, this section will provide a brief overview of the general reactivity of vinylidene complexes and their applications in alkyne dimerisation.

The variety of reactivities exhibited by vinylidene complexes can be rationalised by consideration of their properties; an electrophilic metal-bound α-carbon, a nucleophilic metal centre and β-carbon, and a highly unsaturated backbone (the metal-α-carbon bond retains carbene-like character). General reactions are shown in Figure 1.14.[55]
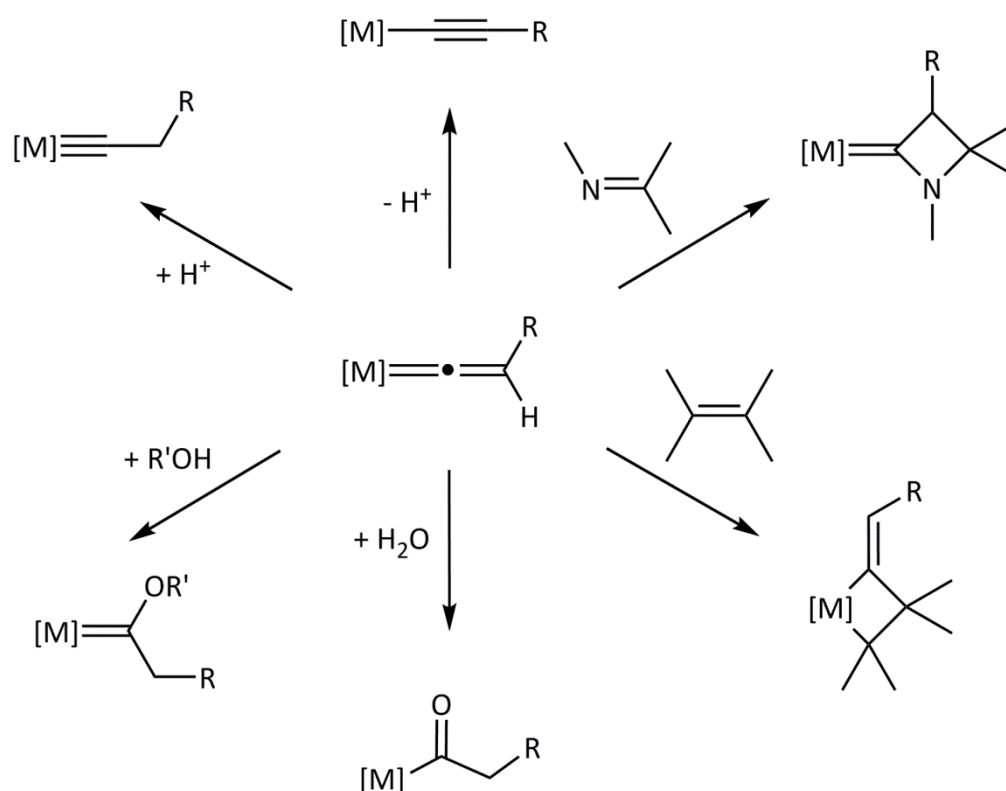
Figure 1.14 Reaction patterns of Fischer vinylidene complexes

1.4.3.1   Vinylidene complexes in terminal alkyne dimerisation

Transition-metal catalysed terminal alkyne dimerisation is a convenient route to construct highly unsaturated four carbon structures which can subsequently be used as active components in light-emitting and conductive polymers and as building blocks for organic synthesis.[81] The head-to-head dimerisation of terminal alkynes to form enynes requires the coordination of two alkyne molecules at the metal centre. Mechanistic investigations, and the isolation of ruthenium enynyl intermediates, has confirmed that the pathway involves the migration of an alkynyl ligand to the metal bound α-carbon of the vinylidene ligand, as shown in Scheme 1.9.[55] On protonation of the metal-carbon bond, the enyne organic products are released (red reaction pathway, Scheme 1.9). Alternatively, the enynyl ruthenium can instead rearrange to form a cumulenyl ruthenium complex from which protonolysis yields a butatriene compound (blue reaction pathway).[55]

Scheme 1.9 Mechanism of formation of enyne and butatriene compounds (red and blue pathways respectively)

The equilibrium position between the formation butatrienes or enynes is strongly influenced by the steric bulk of the alkyne substrate and the coordination sphere of the metal centre.[57] For the formation of enyne organic products, the most effective ruthenium complexes for this transformation often incorporate sterically bulky and electron-donating polydentate ligands, including polydentate nitrogen ligands (for example, tris(pyrazolyl)borate ligands), polypodal phosphorus ligands (for example, $P(CH_2CH_2PPh_2)_3$) and pentamethylcyclopentadienyl ligands, Cp*.[57,82-83] Remarkable selectivity has been observed for the dimerisation of phenylacetylene using $[RuH_3(\eta^5-C_5Me_5)(PR_3)]$ type complexes. In the presence of $[RuH_3(\eta^5-C_5Me_5)(PCy_3)]$, **1-*av***, the reaction is selective for the *Z*-butenyne (*Z:E* = 90:10). However, replacement of the PCy_3 ligand for the less sterically demanding PMe_3 in **1-*aw*** forms the *E*-isomer selectively. These observations can be rationalised by consideration of steric interactions between the phenyl groups and the phosphine ligands, Scheme 1.10.[82]

Scheme 1.10 Formation of *E*- and *Z*-butenynes catalysed by [RuH$_3$(η^5-C$_5$Me$_5$)(L)]

The formation of butatrienes is favoured with bulky alkynes such as *tert*-butylacetylene or benzylacetylene in the presence of ruthenium catalyst precursors including [RuH$_2$(CO)(PPh$_3$)$_2$], [Ru(cod)(cot)] (cot = cyclooctatriene) or [RuH$_3$(η^5-C$_5$H$_5$)(PCy$_3$)].[55] Although 1,2,3-butatriene derivatives are thermodynamically less stable than butenynes, Wakatsuki has developed a highly selective dimerisation of *tert*-butylacetylene to (Z)-*t*-BuCH=C=CH(*t*-Bu) using [RuH$_2$(CO)(PPh$_3$)$_2$] as a catalyst. This selectivity arises from unfavourable steric interactions (between a *tert*-butyl group of the coordinated butenynyl moiety and the triphenylphosphine ligand) in the reaction intermediate that would form the more stable butenyne isomer of the organic product.[84]

1.5 Versatility of ruthenium(II) half-sandwich complexes

Ruthenium(II) half-sandwich complexes, including those with cyclopentadienyl ligands, exhibit versatile chemistry and as such have found applications as potential pharmaceutical agents, as organometallic catalysts and in the preparation of synthetic molecular cages.[85] Coordination cages have many uses, for example, they can be used as sensors,[86] as nanoreactors for chemical transformations,[87] as delivery agents for anticancer compounds,[88] for the stabilization of highly reactive guest molecules,[85] and as catalysts for important catalytic organic transformations including ring opening metathesis polymerisation,[89] transfer hydrogenation[90] and terminal alkyne hydration.[91]

This section will examine some of the uses of ruthenium half-sandwich complexes with a particular focus on $[Ru(\eta^5\text{-}C_5H_5)]^+$ which is a fragment encountered frequently throughout this thesis.

1.5.1 Ruthenium half-sandwich complexes as pharmaceutical agents

In the last fifteen years, interest in the medicinal properties of ruthenium(II) half-sandwich compounds has grown significantly.[92] Since the landmark discovery of cisplatin, the development of organometallic pharmaceutical compounds has been an important focus for organometallic compounds with notable interest centred on the evaluation of Group 8 compounds. The first medicinal application of a ruthenium(II) half-sandwich compound was reported in 1992[92] and further studies have highlighted valuable pharmacological properties of complexes based on this sub-unit. These properties may be summarised as follows:[92]

- The ruthenium(II) metal ion is a viable ion for medicinal applications upon coordination to an arene ligand. The stability of the ruthenium-arene bond allows for the systematic modification of the complex in order to introduce functionality, most importantly to introduce biologically active groups, *via* facile procedures.

- It was postulated that ruthenium(III) complexes are prodrugs, activated only on reduction to ruthenium(II) in cancer cells, and hence ruthenium(II) complexes administered directly would display systematic toxicity towards all cells. However, this does not seem to be the case.

- The aromatic ligand provides a polyaromatic, hydrophobic surface to promote interaction of the complex with biomolecular targets such as DNA *via* non-covalent

interactions. However, it should be noted that this increase in cytotoxicity does not necessarily improve selectivity (e.g. for cancer cells in preference to healthy cells).

- Hydrolysis of a ruthenium-chloride bond allows the direct coordination of a toxic heavy metal to a biomolecular target. Other labile ligands can be used in place of chloride to modify the rate of reaction.

- Supporting ligands can be easily modified to control the pharmacological properties of the ruthenium(II) half-sandwich compounds.

The range of structural modifications of ruthenium(II) half-sandwich compounds are highlighted in Figure 1.15.[92]
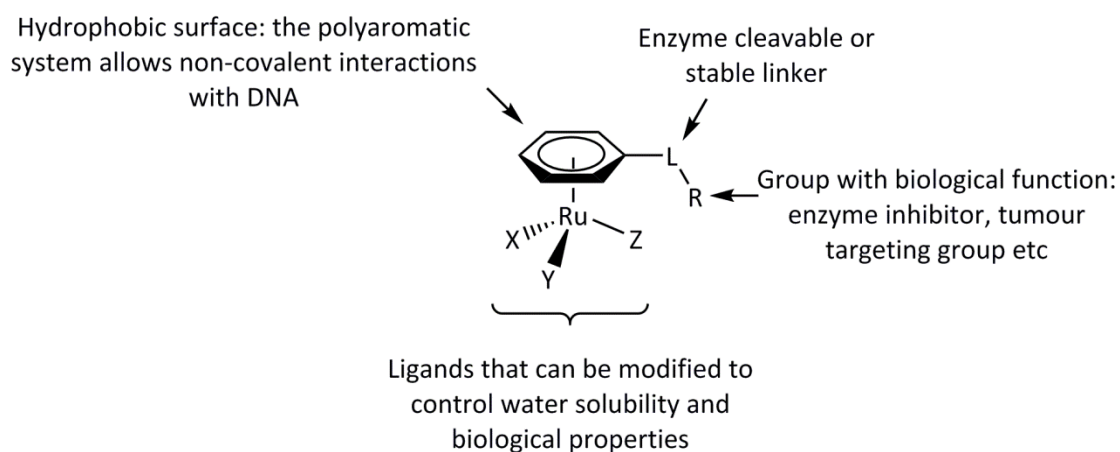
Figure 1.15 Possible adaptations of ruthenium(II) half-sandwich pharmaceutical compounds

These types of modifications can also be applied to other families of metal complexes including osmium(II)-arene and ruthenium(II)-, rhodium(II)- and iridium(III)-cyclopentadienyl compounds.[92] Due to the ease of functionalisation and the ability to prepare a range of derivative complexes, the ruthenium(II) half-sandwich unit has emerged as a useful synthon for the preparation of a number of compounds that can be evaluated for cytotoxicity in cancer cells.

A specific family of ruthenium-based cytotoxic compounds with cyclopentadienyl ligands are summarised in Figure 1.16.[93-95] Both compounds **1-*ax*** and **1-*ay*** caused a significant effect in the cell viability of human colon adenocarcinoma (LoVo) and pancreatic (Mia-PaCa) in the nanomolar range, with **1-*ay*** decreasing cell survival rates by as much as 90 % at 500 nm in both cell lines.[95] For both compounds, the IC_{50} values are amongst the lowest reported for ruthenium half-sandwich structures. The mechanism of action was thought to be *via*

interaction with the plasmid pBR322 DNA, either by intercalation between the DNA base pairs (for **1-ax**) or covalent bond formation to the purine base (for **1-ay**).[95]

1-ax	PP = dppe, L = triazine
1-ay	PP = 2 PPh$_3$, L = pyridazine
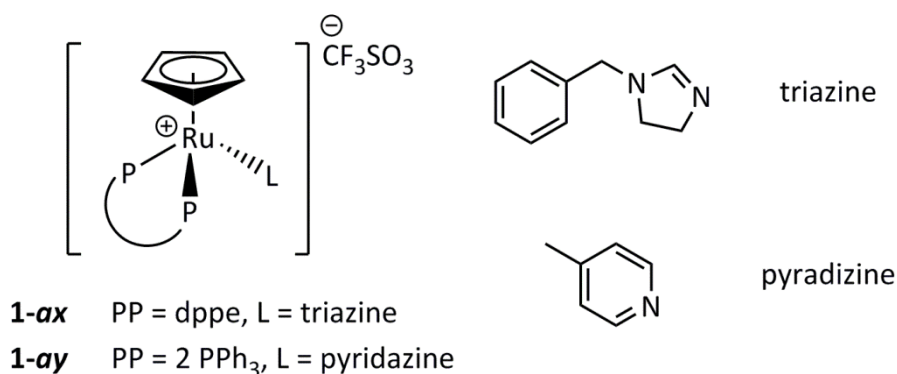
Figure 1.16 Ruthenium-cyclopentadienyl complexes with cytotoxic activity

In conclusion, ruthenium(II) compounds represent a viable approach to the development of new pharmaceutical products, particularly anti-cancer agents, due to their low general toxicity, stronger affinity for cancer tissue over healthy tissue and their ability to mimic iron binding to biomolecules such as transferrin and albumin.[96] Therefore, it is hoped that this strongly emerging field of research will lead to several ruthenium-based clinical treatments.

1.5.2 Ruthenium half-sandwich complexes in organic transformations

The versatile coordination chemistry of ruthenium(II) half-sandwich compounds has yielded them as useful catalysts for a range of organic transformations. A particular benefit of the ruthenium(II) half-sandwich complexes is their 'chiral-at-metal' potential.[97] During chemical transformations, chiral metal complexes can direct the attack of substrates and therefore influence the enantiomeric selectivity of the reaction products. In order to induce chirality, a chiral ligand is often coordinated to the metal centre.[97] However, by analogy of a ruthenium half-sandwich complex to a 'piano-stool' structure, on coordination of an arene moiety and three different monodentate ligands (or one monodentate and an asymmetric bidentate ligand) to the metal centre, the asymmetric metal centre becomes analogous to an asymmetric carbon atom.[97] Their unique properties (synthesis under mild reaction conditions, often soluble and stable in a range of solvents, wide structural diversity) have allowed them to occupy an important position as catalysts.

Transfer hydrogenation reactions, that involve the transfer of hydrogen from one organic molecule to another, are an important class of transformations in organic chemistry in order to avoid the use of molecular hydrogen. For example, the synthesis of secondary alcohols

with high enantiomeric purity is a critical reaction for the formation of numerous pharmaceuticals, and can be achieved by catalytic asymmetric reduction of prochiral ketones. The bimetallic ruthenium catalyst by Shvo, **1-az** in Scheme 1.11, behaves as a very effective ketone and aldehyde transfer hydrogenation catalyst with yields of between 92 and 100 %, turnover numbers of up to 8000 and low catalyst loadings of 0.013-0.03 mol% (reaction **a**, Scheme 1.11). This catalyst is also capable of transfer hydrogenation to 1,3-diones to prepare 1,3-diols (reaction **b**, Scheme 1.11)[98] and in the oxidation of secondary alcohols.[99]

1-az

Shvo's hydrogenation catalyst

a

R_1 = alkyl, aryl
R_2 = alkyl, aryl, H

0.013 - 0.03 mol% **1-az**

100 °C

92 - 100 %

b

n = 0, 1, 2
R = H, Me

1-az

isopropanol,
120 °C

n = 0, 1, 2
73 - 93 %
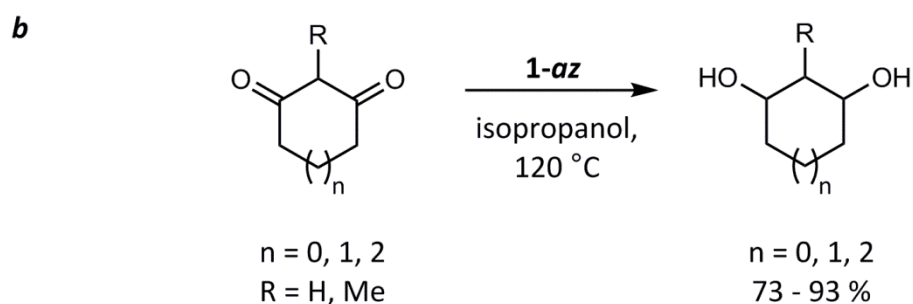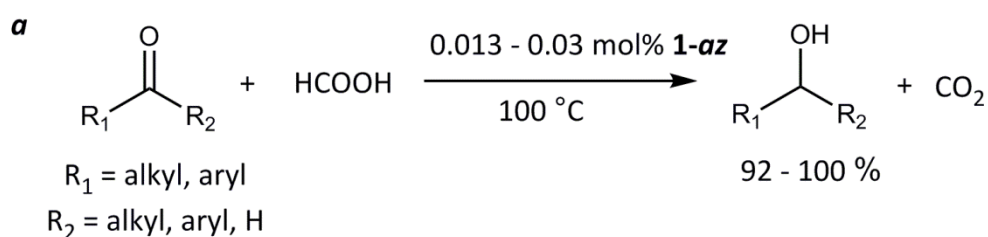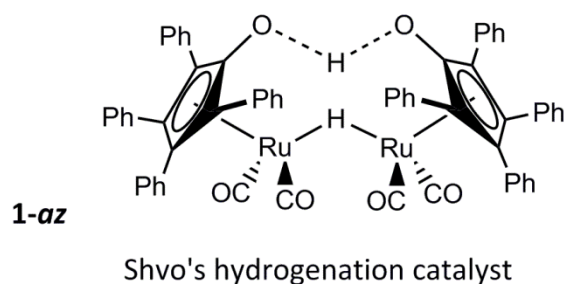
Scheme 1.11 Shvo's hydrogenation catalyst (1-az) for transfer hydrogenation of ketones (a) and 1,3-diones (b)

1.5.3 Functionalisation of [Ru(η^5-C$_5$H$_5$)(NCMe)$_3$]PF$_6$[100]

The lability of the acetonitrile ligands in [Ru(η^5-C$_5$H$_5$)(NCMe)$_3$]PF$_6$ means that this complex is a precursor of choice for many catalysts and complexes containing the [Ru(η^5-C$_5$H$_5$)] fragment.[100] For example, [Ru(η^5-C$_5$H$_5$)(NCMe)$_3$]PF$_6$ can react with arenes to provide facile access to a new family of cationic [Ru(η^5-C$_5$H$_5$)(arene)]$^+$ sandwich complexes.[101] On coordination, the arene becomes activated towards nucleophilic addition and substitution reactions. This methodology is exemplified below in the formation of a biaryl ether during the synthesis of Ristocetin A, a structurally similar compound to the Vancomycin family of antibiotics, Scheme 1.12.[102] The ligand can be complexed to ruthenium under very mild conditions, undergo esterification with the avoidance of racemisation and subsequently be demetallated by photolysis. The complexation with ruthenium activates the precursor compound to aromatic nucleophilic substitution.
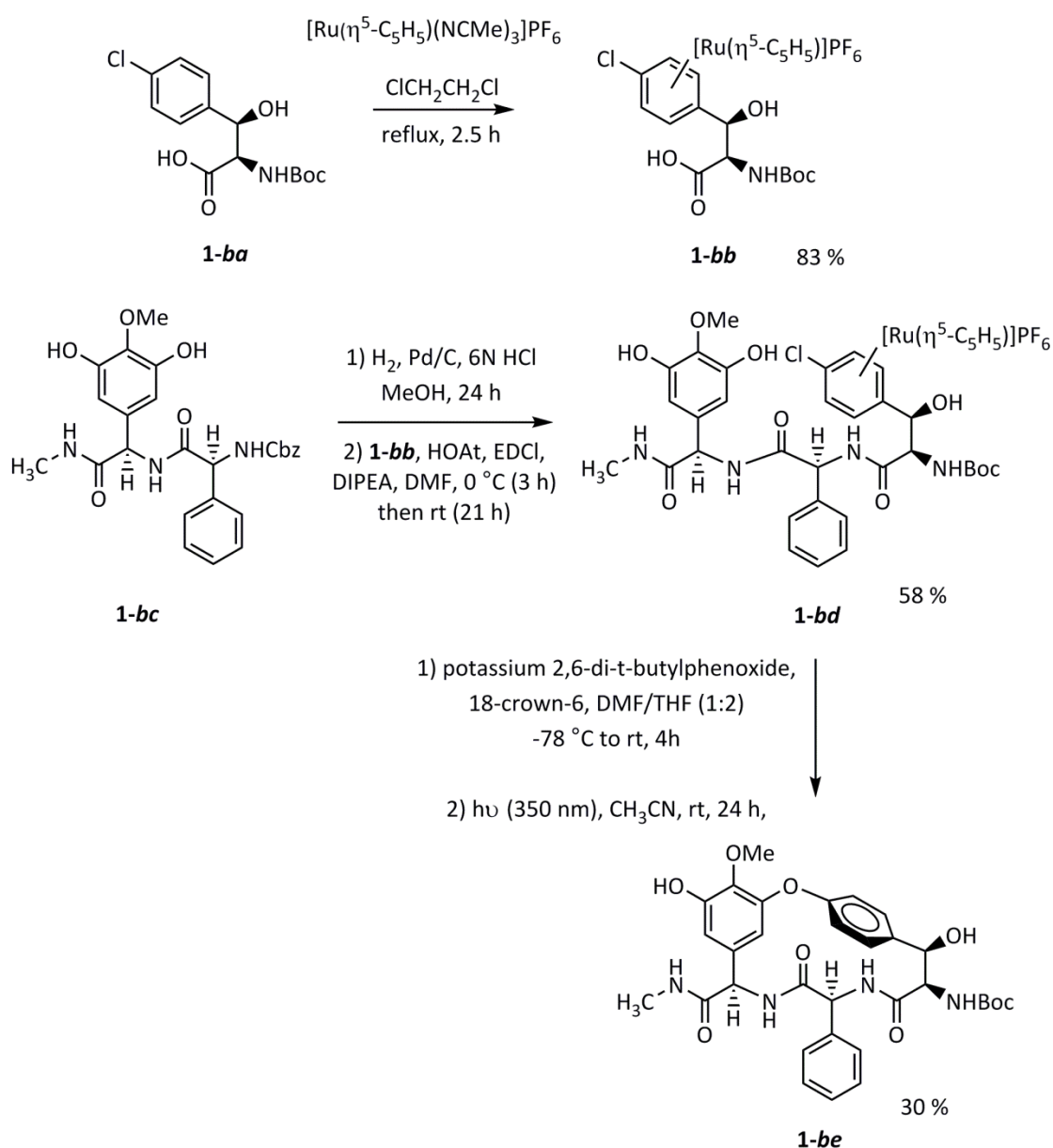
Scheme 1.12 Nucleophilic aromatic substitution promoted by complexation to ruthenium

Furthermore, other monodentate ligands can coordinate to the metal centre in place of the acetonitrile groups in order to create more structurally complex ruthenium half-sandwich complexes. This principle was important in the formation of $[Ru(\eta^5\text{-}C_5H_5)(PPh_3)(NC_5H_5)_2]PF_6$ which can be used as a pyridine alkenylation catalyst (see Chapter 3) and in the formation of Grotjahn's alkene isomerisation catalyst shown in Figure 1.4.[27]

The majority of complexes described in Chapters 2, 3 and 5 of this thesis were originally synthesised from $[Ru(\eta^5\text{-}C_5H_5)(NCMe)_3]PF_6$.

1.6 Aims and objectives

Chapter 1 provides a general introduction to the chemistry which is relevant to each of the studies presented in this thesis; however, specific literature is reviewed in each chapter introduction in order to provide a comprehensive preface to the presented findings. With these case studies and chemical principles in mind, the objective of this PhD project was to investigate a range of ruthenium-mediated and catalysed reactions. This thesis is comprised of four interlinked projects, each of which aims to either optimise or elucidate known catalytic methodologies, or develop new ruthenium-mediated strategies for the synthesis of fluorinated ligands and fluorinated organic molecules.

The aim of Chapter 2 was to investigate a self-assembled ruthenium catalyst, in order to elucidate the mechanism of catalytic anti-Markovnikov terminal alkyne hydration and understand the role of the highly functionalised, chemically non-innocent ligand system. The initial objective was to use DFT calculations in order to determine if ligand-assisted processes provided a lower energy catalytic process compared to the non-ligand-assisted pathway. The computational findings were complemented by experimental studies, with the objective of isolating chemically-relevant intermediates.

The objective of Chapter 3 was to further investigate the principles of ligand-assistance in an attempt to optimise the direct carbon-hydrogen bond activation of pyridine for the catalytic production of *E*-styryl pyridine organic products. The aim of this study was to investigate a range of pyridyl-functionalised ligands in both stoichiometric and catalytic reactions in order to incorporate an intramolecular base into the coordination sphere of ruthenium, and therefore remove the necessity for excess base in the reaction mixtures.

In Chapter 4, the main aim was to investigate a pyridylidene complex (the 'catalyst deactivation product' from the studies in Chapter 3) as a precursor to electrophilic fluorination. The initial objective was to explore the reactivity of this complex with electrophilic fluorinating agents, and the indication of a novel mechanism prompted further experimental studies of reactivity and supporting computational calculations in order to gain important insights into carbon-fluorine bond formation and activation.

The target of the studies presented in Chapter 5 was to apply electrophilic fluorination methodology to the synthesis of fluorovinylidene complexes from ruthenium-acetylide precursors. The fluorovinylidene ligands were then investigated in a range of stoichiometric

reactions, with the long-term goal of incorporating these complexes in catalytic fluorination processes.

Chapter 2

Mechanistic insight into anti-Markovnikov terminal alkyne hydration using a self-assembled ruthenium catalyst

2 Mechanistic insight into anti-Markovnikov terminal alkyne hydration using a self-assembled ruthenium catalyst

2.1 Introduction

Terminal alkynes are privileged starting materials in a range of chemical transformations, and thousands of terminal alkynes are commercially available or can be readily synthesised.[103-106] They often display inert behaviour towards oxidative, reductive, acidic and basic reagents, yet are readily activated in the presence of a metal by either π-complexation or vinylidene formation, Scheme 2.1.[106] As illustrated in Scheme 2.1, the metal-alkyne intermediate (**2-a** or **2-b**) affects the subsequent reactivity with nucleophiles (and electrophiles) and therefore dictates the final products (**2-c** and **2-d**). This unique reactivity with metal complexes under mild conditions can allow selective transformation even in the presence of other complex functionality.[106]
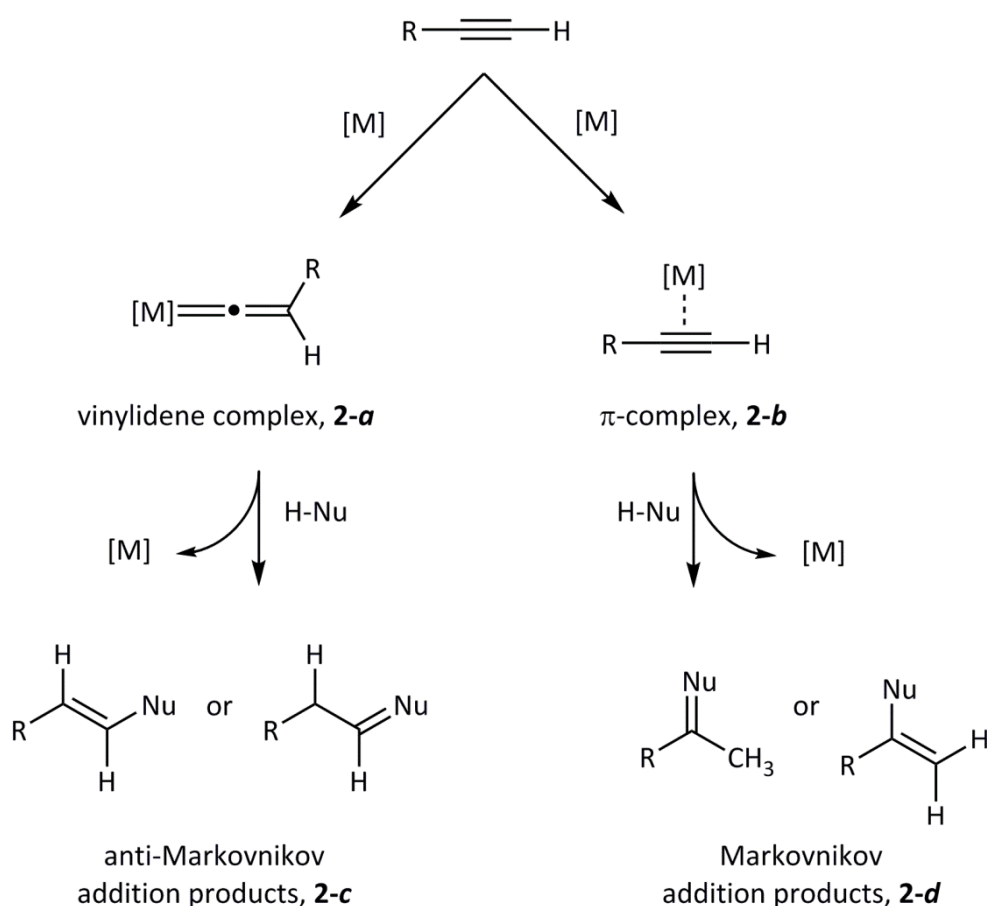
Scheme 2.1 Common routes of alkyne activation mediated by metal complexes under mild conditions

The hydration of terminal alkynes can produce two possible carbonyl-containing compounds; the Markovnikov (branched) product of a ketone or the anti-Markovnikov (linear) product of an aldehyde as shown in Scheme 2.2.[106-107]
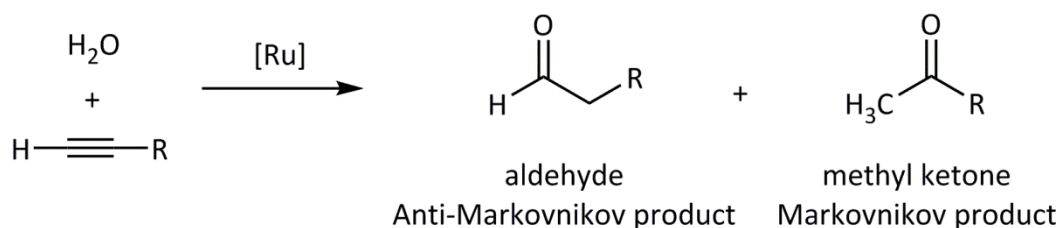
Scheme 2.2 General scheme of terminal alkyne hydration catalysed by ruthenium

Traditionally, alkyne hydration methods have involved the use of either strong acid catalysts and Hg(II), or stoichiometric transition metal salts.[108-110] These non-environmentally friendly techniques also exclusively produced the Markovnikov product of a methyl ketone. Until fairly recently, anti-Markovnikov alkyne hydration, used to install aldehyde functionality, was only possible through stoichiometric hydroboration or hydrosilylation, followed by oxidation.[111]

However, metal-catalysed methods for the direct anti-Markovnikov addition have now been developed which can impart highly efficient and selective alkyne to aldehyde transformations.[18] The propensity of ruthenium, in particular, to promote alkyne to vinylidene tautomerisation (commonly believed to be the first step in metal-catalysed routes, intermediate **2-a** in Scheme 2.1) has lead to a surge of new ruthenium-based complexes which have become very efficient catalysts to effect this reaction. This introduction will explore the development of such ruthenium species, and the commonly accepted mechanistic similarities which are important in their operation.

2.1.1 Development of ruthenium-catalysed alkyne hydration

Regioselective functionalisation is fundamental for effective organic synthesis to allow functional-group installation into basic carbon frameworks. Transition metal catalysis is a popular approach to promote substrate functionalisation, however, methods were slow to develop for the direct anti-Markovnikov hydration of alkyne substrates.[106] Despite this, the chronological development of these complexes is fascinating, and demonstrates a logical, informed and stepwise approach to catalyst optimisation. Therefore, a brief history of the advances in these systems will be presented, in order to understand each of the key

structural features which have been carefully selected to promote the selective alkyne to aldehyde transformation.

In 1998, the first example of ruthenium-catalysed anti-Markovnikov terminal alkyne hydration was reported by Tokunaga and Wakatsuki using complexes **2-e** and **2-f**, Scheme 2.3.[112] By modifying the phosphine ligand, this methodology could be tuned towards either the aldehyde or methyl ketone product, and was tolerant to a range of alkyne substrates. However, there were several drawbacks to this catalytic system; the necessity of extra added phosphine led to a high catalyst loading (over 0.5 grams of catalyst per gram of octanal produced) and some alkynes could not be used due to steric limitations of the catalytic system.
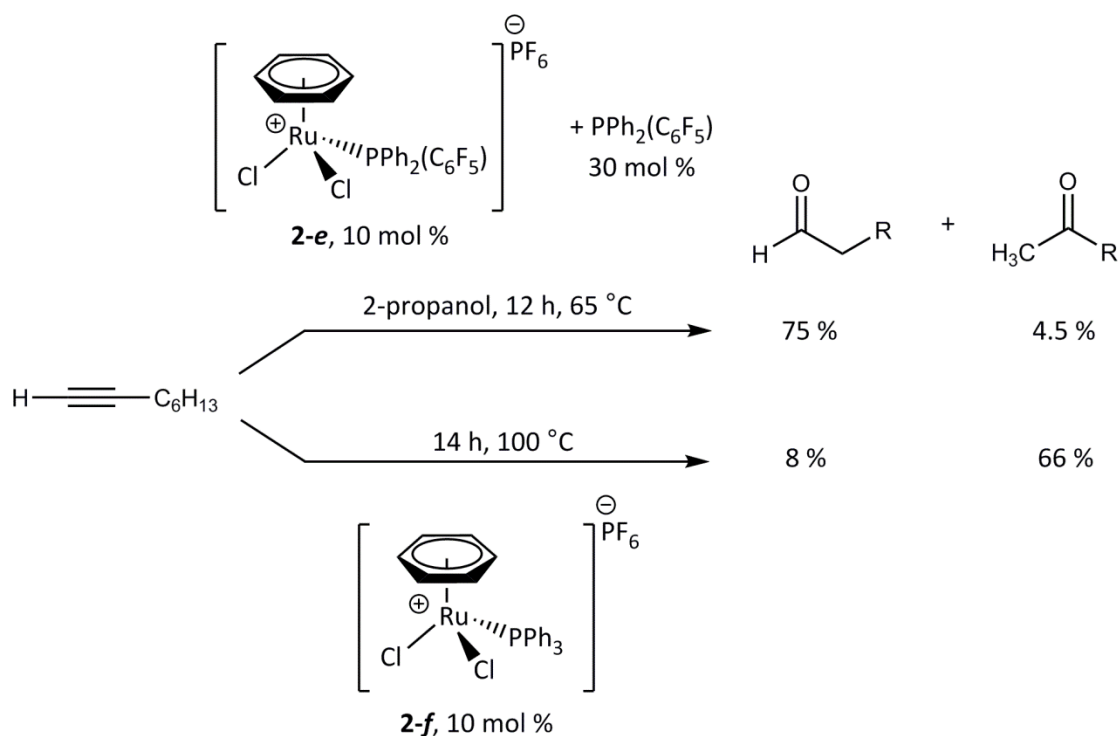
Scheme 2.3 Ruthenium-catalysed hydration of octyne using complexes 2-*e* and 2-*f*

Tokunaga and Wakatsuki proposed that the major problem with these catalysts was the dissociation of benzene from the ruthenium centre, which led to the proposal by Grotjahn that an anionic Cp (η^5-C_5H_5, cyclopentadienyl) ligand would allow a more robust catalyst structure. In fact, the η^5-cyclopentadienyl ruthenium fragment has emerged as a common substructure in almost all anti-Markovnikov hydration catalysts.[18] Further investigation

showed that a more electron rich or sterically crowded metal centre could cause the loss of a phosphine ligand and promote alkyl migration to form an alkane and a carbonyl complex, whereas an electron deficiency or decreased steric bulk would disfavour alkyne-vinylidene tautomerism.[107] [Ru(Cp)(*bis*-phosphine)] species had previously been shown to assist in the tautomerisation of terminal alkynes to vinylidenes,[113] which have from the start been considered to be key intermediates in almost all proposed alkyne hydration mechanisms. However, early attempts by Grotjahn produced ruthenium carbonyl complexes rather than the desired aldehydes.[18] In 2001, the Suzuki group (including Tokunaga and Wakatsuki) had moderate success, Scheme 2.4, but again with high catalyst loadings, low selectivity and significant catalyst degradation to a carbonyl species, **2-k**.[114]
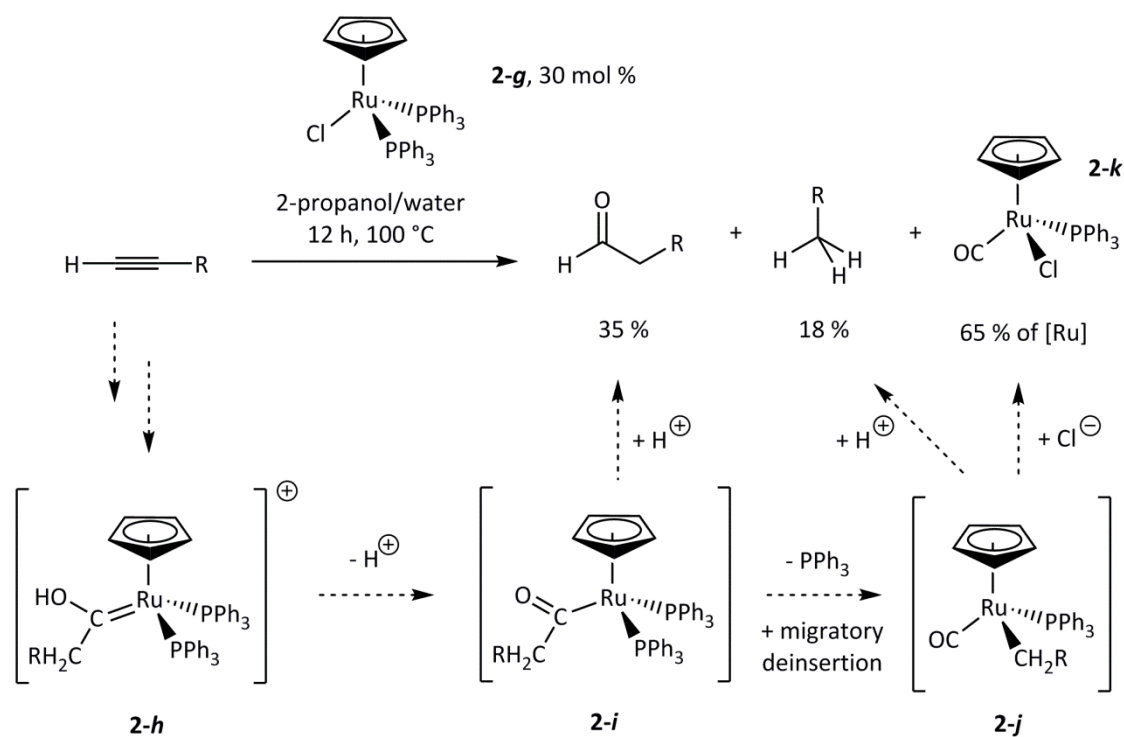
Scheme 2.4 Degradation of catalyst *a via* loss of a triphenylphosphine ligand to form carbonyl complex 2-*k*, R = alkyl or aryl group

As degradation was caused by phosphine loss from the metal, strategies employed to overcome this weakness included the use of smaller but more electron-donating, or chelating phosphine ligands. Alkyne hydration reactions catalysed by **2-*l***, Scheme 2.5, were both high-yielding and selective, but bulkier substrates required high catalyst loadings (~ 10 mol %) and high temperatures.[114]
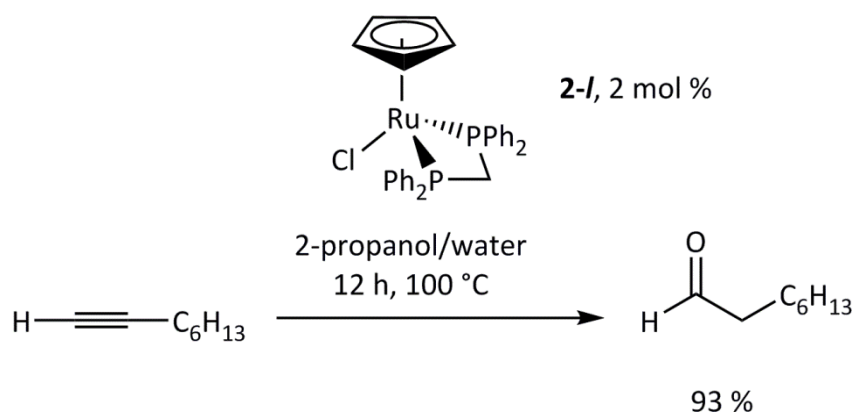
Scheme 2.5 Terminal alkyne hydration catalysed by complex 2-*l* with a bidentate dppm ligand

The introduction of a 'pendant base' into the ruthenium coordination sphere guided the next significant advancement in the field of alkyne hydration. It was suggested by Grotjahn that an intramolecular base in close vicinity to the vinylidene moiety may act to activate water and therefore assist in nucleophilic attack.[18] Bulky substituents were necessary to avoid the addition of the nucleophilic ligand directly with the vinylidene, **2-*m***, Figure 2.1.[18] Secondly, although a crystal structure of complex **2-*n***, Figure 2.1, could be obtained showing a promising water 'binding pocket' between the imidazolyl-functionalised phosphine ligands, the water was held too tightly and inhibited efficient catalysis.[115] Replacement of the imidazolyl-functionalised phosphine ligands with less basic pyridyl-functionality, complex **2-*o***, produced a highly efficient alkyne hydration catalyst.[107] For the first time, alkyl-, aryl- and electron-rich alkynes could be hydrated effectively with only a 2 mol % catalyst loading. With a 5 mol % catalyst loading, alkylacetylenes could also undergo alkyne to aldehyde transformations at room temperature over a two day period.
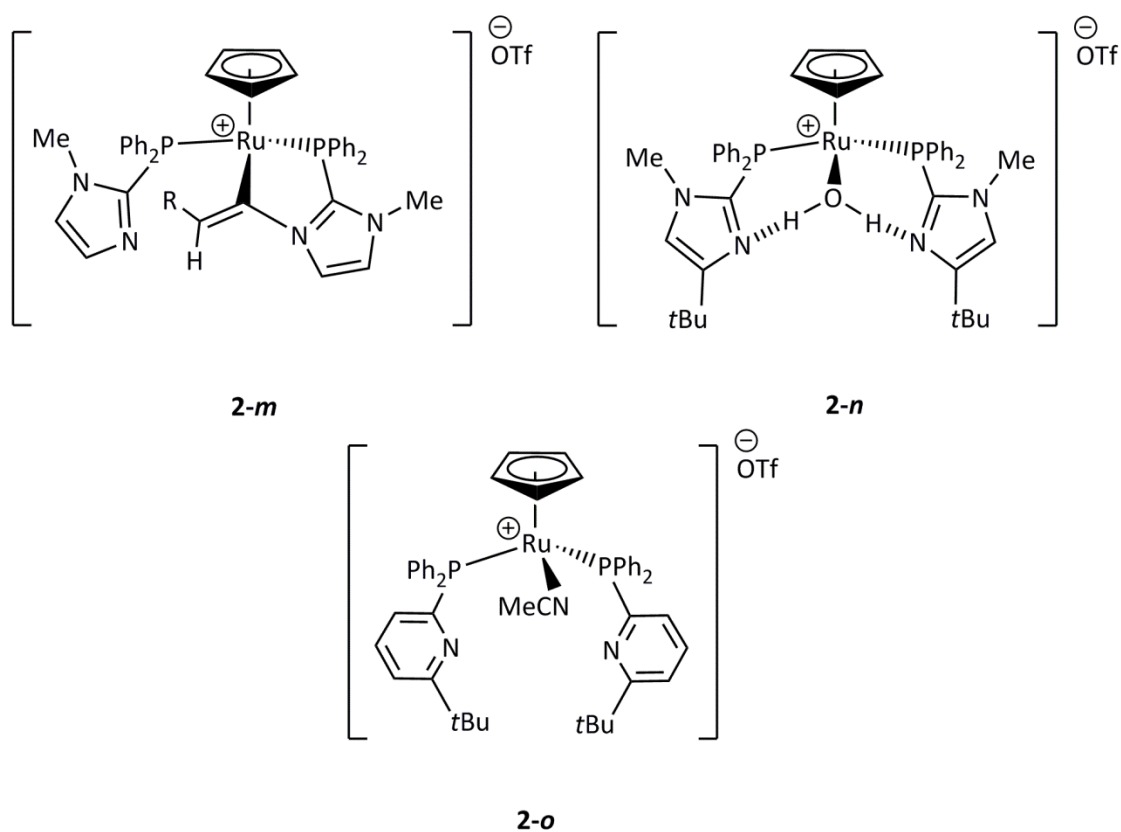
Figure 2.1 Development of terminal alkyne hydration catalysts with non-innocent ligand systems

Most synthetic organometallic catalysts rely mainly on the metal centre to facilitate substrate transformations, whereas the complexes in Figure 2.1 may use the reactivity of the metal centre in synergy with ligand functionality to enable catalytic reactions. This behaviour is analogous to that of nature's metalloenzymes, which also use metals in conjunction with functional groups on the protein backbone to promote substrate transformation.[107,115] In recent years, a range of bio-inspired organometallic complexes have been developed which can catalyse both stoichiometric and catalytic transformations; these include ligand-assisted proton shuttle (LAPS), ambiphilic metal to ligand activation (AMLA) and ligand to ligand proton transfer processes (as discussed in Chapter 1).[17,22-23] Common functionality for these non-innocent ligand systems includes pyridyl- and imidazolyl-functionalised phosphine ligands and acetate moieties.[115-116] Due to this similarity in mechanism, complexes such as those illustrated in Figure 2.1 can be considered to act in an 'enzyme-like' way and arguably, the catalytic efficiencies of such complexes can also rival the performance of an enzyme.[18,107]

2.1.2   Ligand self-assembly in alkyne hydration catalysts

One of the most recent developments in the field of anti-Markovnikov terminal alkyne hydration is the introduction of self-assembling ligands.[117] This concept is illustrated in Figure 2.2.
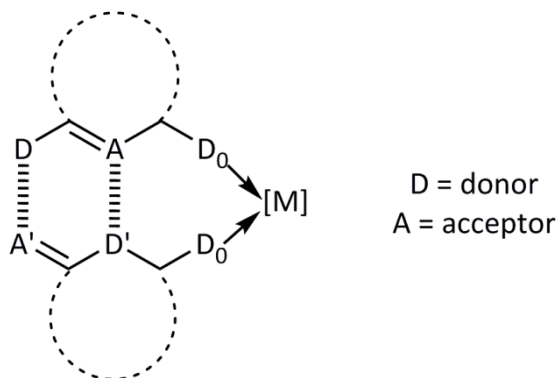
Figure 2.2 A self-assembling ligand structure can create a pseudo-bidentate ligand

Although each ligand is monodentate, through intermolecular interactions they can create a pseudo-bidentate structure. This approach was originally intended as a simple way to build combinatorial ligand libraries of pseudo-bidentate ligands, as the use of a bidentate ligand has considerable benefits compared to a monodentate counterpart.[12,118] The catalytic reactions in which bidentate ligands are implicated tend to produce higher levels of both regio- and enantioselectivity, due to a more rigid micro-environment around the metal atom.[119] This leads to a larger energy variation between competing reaction mechanisms, and so one pathway is favoured above the rest. Secondly, a bidentate phosphine can make use of the chelate effect, to avoid ligand loss and subsequent catalyst degradation.[12] However, the synthetic difficulties and costs of synthesising complex bidentate ligands with the correct electronic and steric properties can often overshadow the potential benefits. Therefore a pseudo-bidentate ligand, made of two simpler ligands which can interact, could offer significant promise.[118]

To use this phenomenon in alkyne hydration catalysts was first suggested in a publication by Breit and Chevallier in 2006.[117] Previous work had shown that a related rhodium catalyst was successful in terminal alkene hydroformylation, and they noted that the features deemed necessary for effective alkyne hydration were offered by the self-assembled ligand structures. These factors include the presence of bidentate phosphines, often phosphinopyridine ligands, which promote the coordination of water through hydrogen

bonding.[107,114-115] The strong hydrogen-bonding interactions between the two complementary phosphines allow emulation of a bidentate ligand, and ensure that even upon dissociation of one phosphorus atom the ligand is not necessarily lost from the coordination sphere.[117]

A range of self-assembled ligand combinations were trialled and the best catalyst identified as the heterodimeric structure **[1]PF$_6$**, which gave 'outstanding activity and perfect regioselectivity' (with 1-nonyne), shown in Figure 2.3.[118]
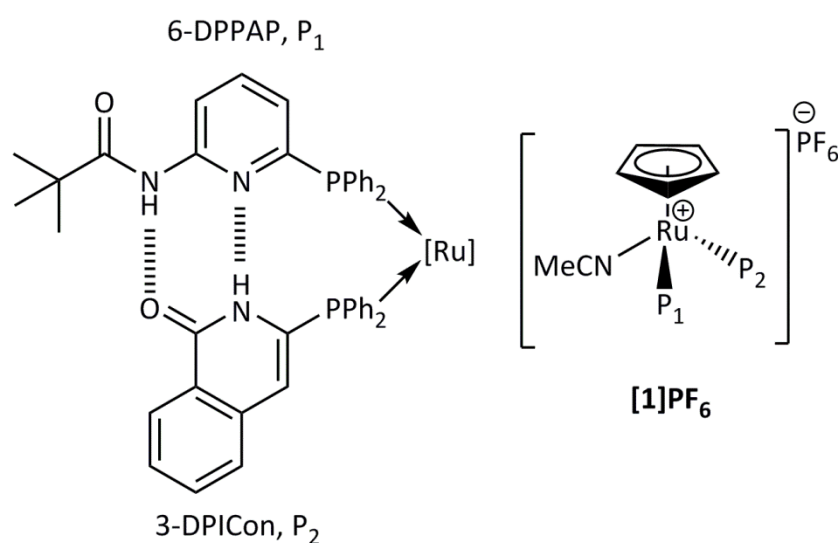
Figure 2.3 Structure of self-assembled terminal alkyne hydration catalyst, [1]PF$_6$

Complex **[1]PF$_6$** offers significant advantages over other related alkyne hydration catalysts. Firstly, the self-assembly process means that **[1]PF$_6$** is reported to form on simple combination of a stoichiometric amount of each ligand and $[Ru(\eta^5\text{-}C_5H_5)(MeCN)_3]PF_6$, affording facile synthesis.[118] More importantly, the catalytic results using 2-10 mol % of **[1]PF$_6$** produced a range of aldehydes in good yields.[118] With many substrates, the regioselectivity of aldehyde:ketone was above 99:1, and the catalyst could cope with a range of alkynes, the most complex of these being a steroid ring system.

2.1.3 Mechanisms of ruthenium-catalysed terminal alkyne hydration

Several key structural features are shared by the most successful ruthenium-based terminal alkyne hydration catalysts:[18]

- An $[Ru(\eta^5\text{-}C_5H_5)]^+$ core − this unit has optimal electronic and steric properties to promote alkyne to vinylidene tautomerism, but is small enough to prevent phosphine loss and alkyl migration

- Bidentate phosphine ligands − to prevent phosphine dissociation. The bidentate structure can be mimicked by self-assembly of complementary monodentate phosphines

- Coordination of water to the ligands by hydrogen bonding − suggested to activate water to be a superior nucleophile

- Nitrogen-containing, heterocyclic (often phosphinopyridine) ligands − believed to aid conversions between intermediates in the catalytic cycle

Various research groups have proposed mechanisms for anti-Markovnikov alkyne hydration, many of which contain very similar features.[78,112,114] A common attribute to almost all mechanisms is the concept of alkyne to vinylidene tautomerism, in order to explain the anti-Markovnikov selectivity. Indeed, the first report in 1998 of Tokunaga and Wakatsuki suggested that a vinylidene intermediate was crucial in order to obtain the correct regioisomeric product, Scheme 2.6.[112]
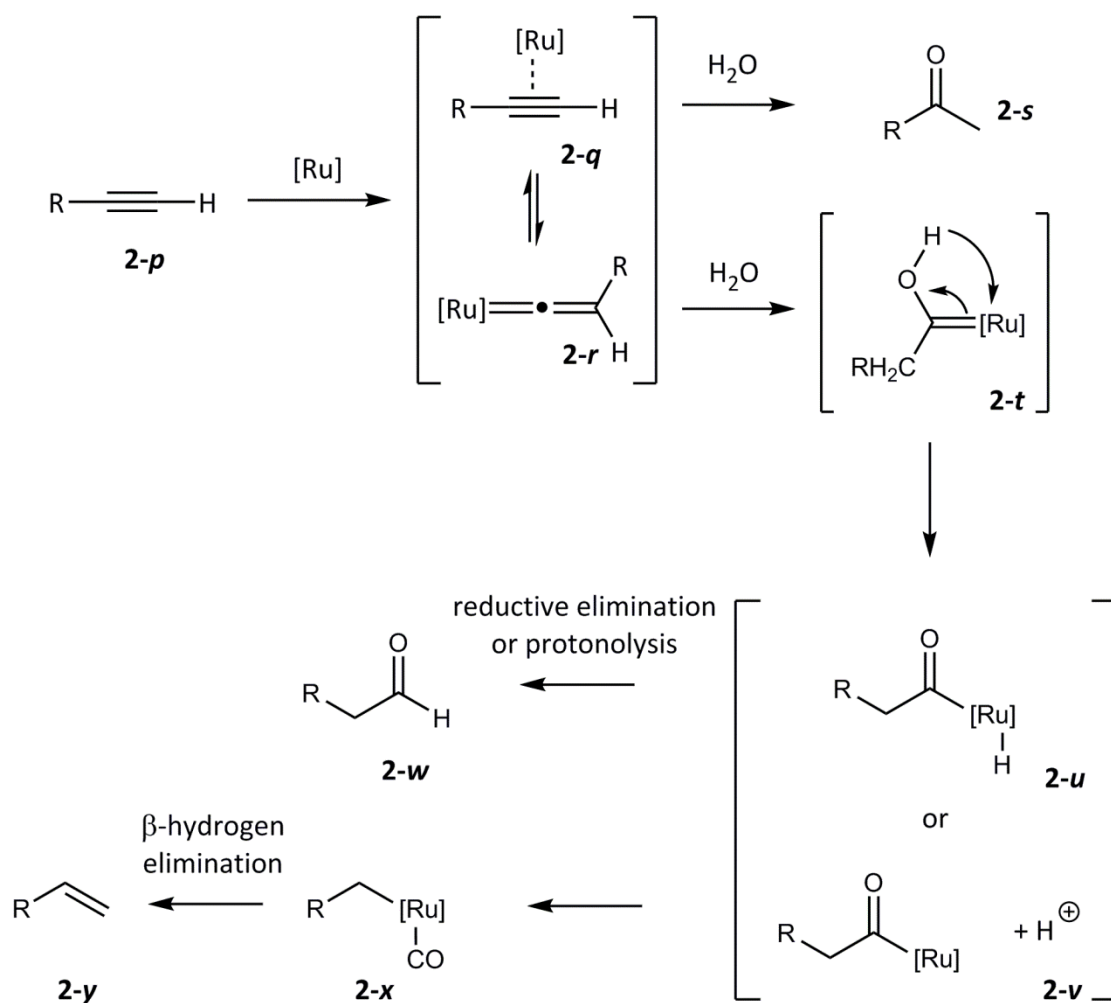
Scheme 2.6 The Tokunaga-Wakatsuki mechanism of alkyne hydration, [Ru] = [RuCl$_2$(C$_6$H$_6$)(phosphine)], R = alkyl or aryl group

The pathway begins with the coordination of the terminal alkyne in an η^2-binding mode, **2-q**, which can undergo a subsequent tautomerisation to ruthenium (II) vinylidene complex **2-r**. Reaction of water with η^2-alkyne complex **2-q** produces the Markovnikov product, ketone **2-s**. Instead, attack of water at the vinylidene α-carbon leads to formation of hydroxycarbene complex **2-t** which can either rearrange to a hydride complex, **2-u**, or liberate H$^+$ to form **2-v**. From hydride **2-u**, reductive elimination or protonolysis can lead to the desired aldehyde, compound **2-w**. However, a decarbonylation process can also occur simultaneously which leads to the formation of an alkene, **2-y**, and a ruthenium carbonyl species. Scheme 2.6 illustrates the importance of the ruthenium (II) vinylidene intermediate which templates the attack of water and therefore produces the aldehyde selectively over the ketone.

An alternative interpretation of the alkyne hydration mechanism was provided by the same group in 2001, when they contradicted their initial proposal to suggest the pathway shown in Scheme 2.7.[120]
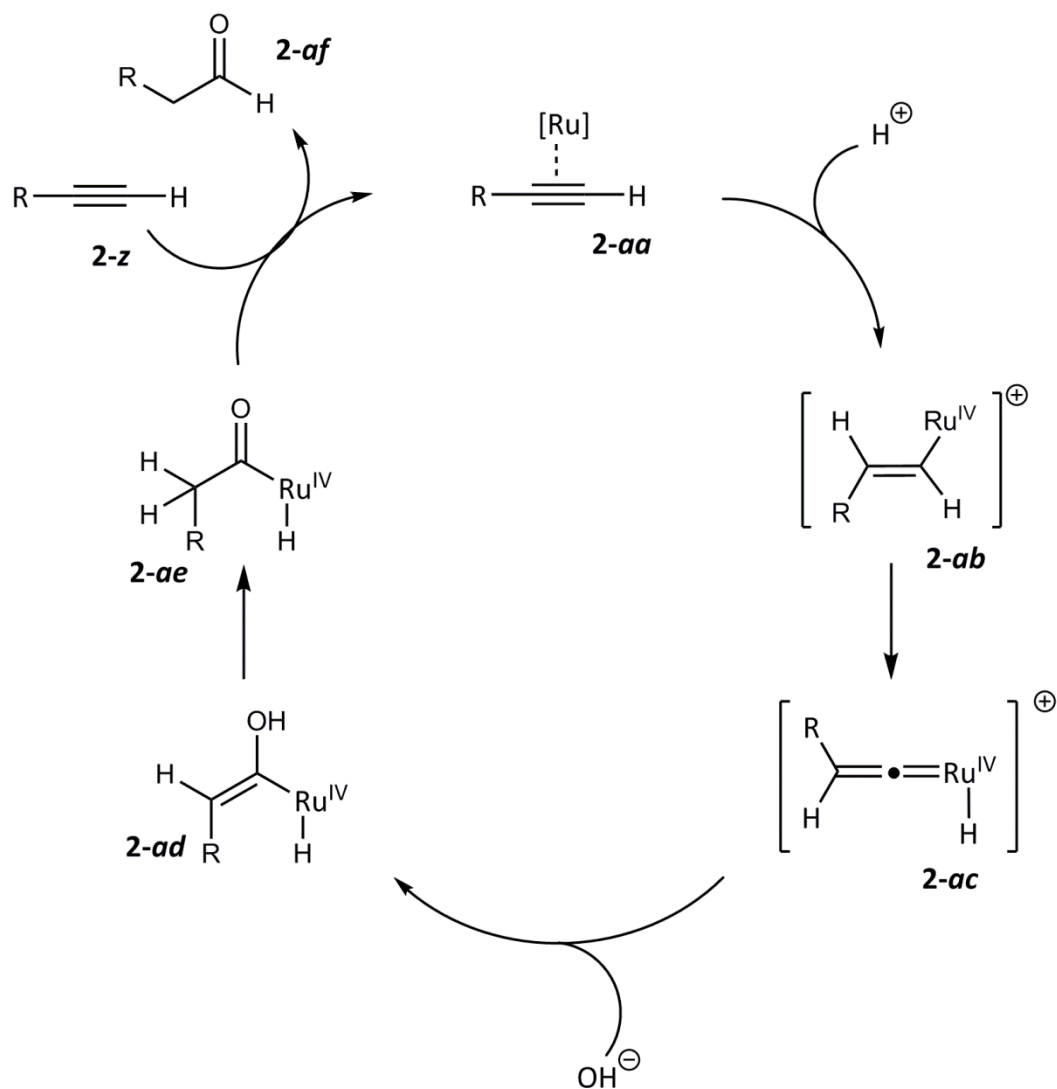
Scheme 2.7 Alternative mechanism suggested by Tokunaga and Wakatsuki, [Ru] = [Ru(η^5-C$_5$H$_5$)(dppm)], R = alkyl or aryl group

From combined theoretical and experimental studies, it was suggested that rather than initial alkyne to vinylidene tautomerism to form a Ru (II) intermediate, attack of water at the most substituted carbon atom of η^2-alkyne complex **2-aa** forms vinyl complex **2-ab**. The α-hydrogen of the Ru (IV) vinyl complex **2-ab** then migrates to the ruthenium centre to form a ruthenium (IV) vinylidene complex **2-ac**. Attack of hydroxide at the α-carbon of the Ru (IV) vinylidene forms hydroxycarbene, **2-ad**, which subsequently tautomerises to acyl complex **2-ae** and reductively eliminates the aldehyde, **2-af**. Both experimental and computational

evidence seemed to support this conclusion; primarily, the hydration of terminally-deuterated alkyne, RC≡CD led almost exclusively to RCH_2CDO, and the Ru (II) acetylide and vinylidene complexes $[Ru(\eta^5\text{-}C_5H_5)(dppm)(\text{-}C≡CR)]^+$ and $[Ru(\eta^5\text{-}C_5H_5)(dppm)(C=CR)]$ failed to react under catalytic conditions (whereas the precursor $[Ru(\eta^5\text{-}C_5H_5)Cl(dppm)]$ initiates effective hydration). Furthermore, the calculated energy barriers for the mechanism in Scheme 2.7 seemed to match the experimentally observed reactivity.

A later mechanism was then suggested by Grotjahn, Scheme 2.8,[78,106] which supported the earlier proposals of Tokunaga and Wakatsuki shown in Scheme 2.6.[112] This reaction pathway also found a ruthenium (II) vinylidene complex, **2-ai**, to be a key intermediate. A major difference was that Grotjahn's intermediates were stabilised by a hydrogen-bonding network between the pyridyl-functionalised phosphine ligands; these ligands were proposed to assist the alkyne to vinylidene tautomerisation, activate the water nucleophile, aid the hydroxycarbene to acyl conversion and assist in protonolysis in the final step to liberate the aldehyde.
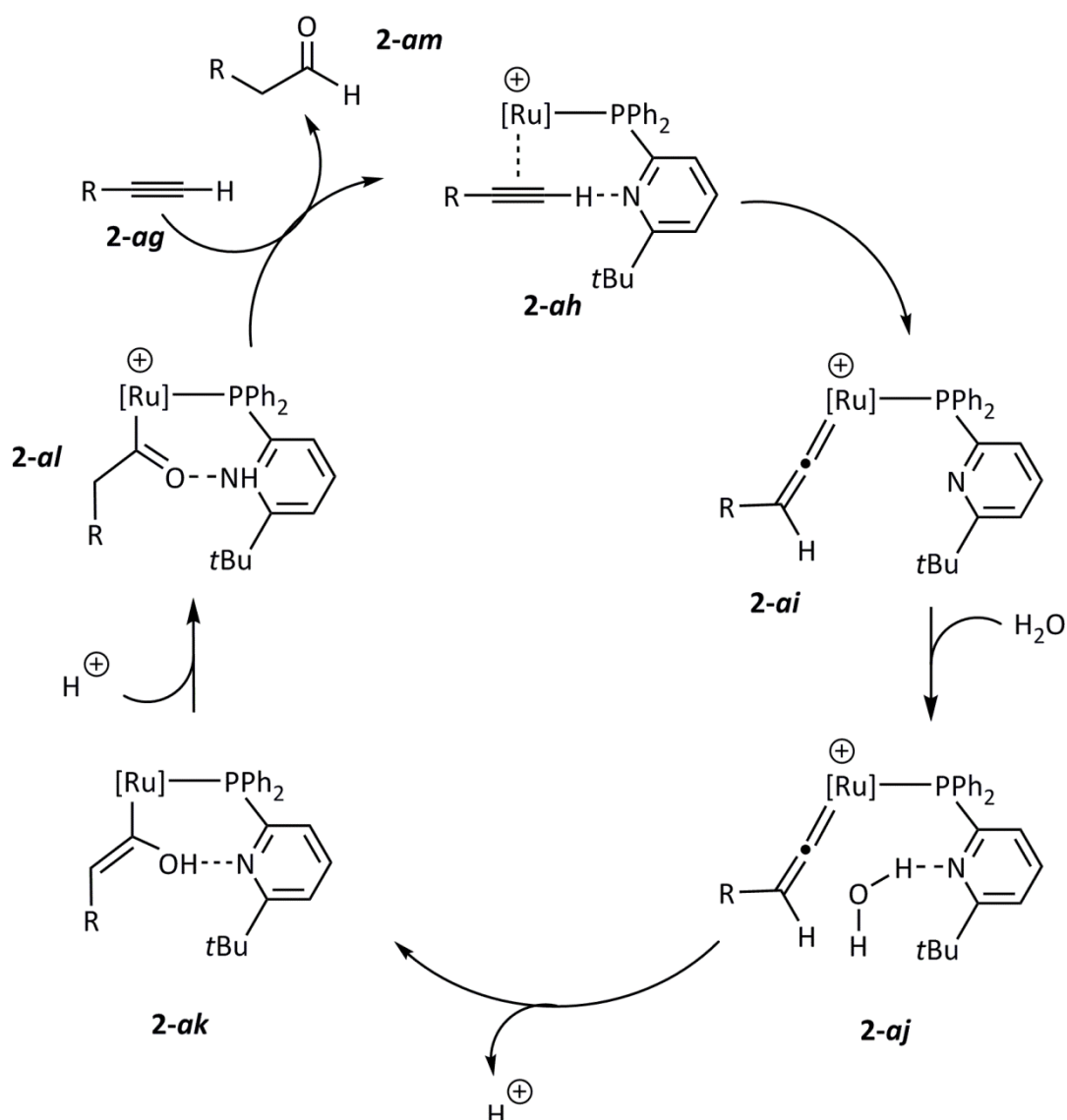
Scheme 2.8 The Grotjahn mechanism for alkyne hydration, [Ru] = [Ru(η^5-C$_5$H$_5$)(P(6-tBu-2-pyridyl)Ph$_2$)], R = alkyl or aryl group

Several spectroscopically detectable intermediates have been identified, Figure 2.4, providing credence to the proposed mechanism of action of the catalyst.[116] These include complex **2-an** (showing the water 'binding pocket'), vinylidene complex **2-ao** and acyl intermediate **2-ap**. These complexes indicate both some important intermediates in alkyne hydration and also the roles of the heterocyclic ligands. For example, in **2-ap**, the proton coordinated to the pyridyl-phosphine ligand indicates that this moiety could be involved in the deprotonation of the hydroxycarbene intermediate; it could also be involved in intramolecular protonolysis to liberate the aldehyde product (although there was no conclusive evidence for these processes).
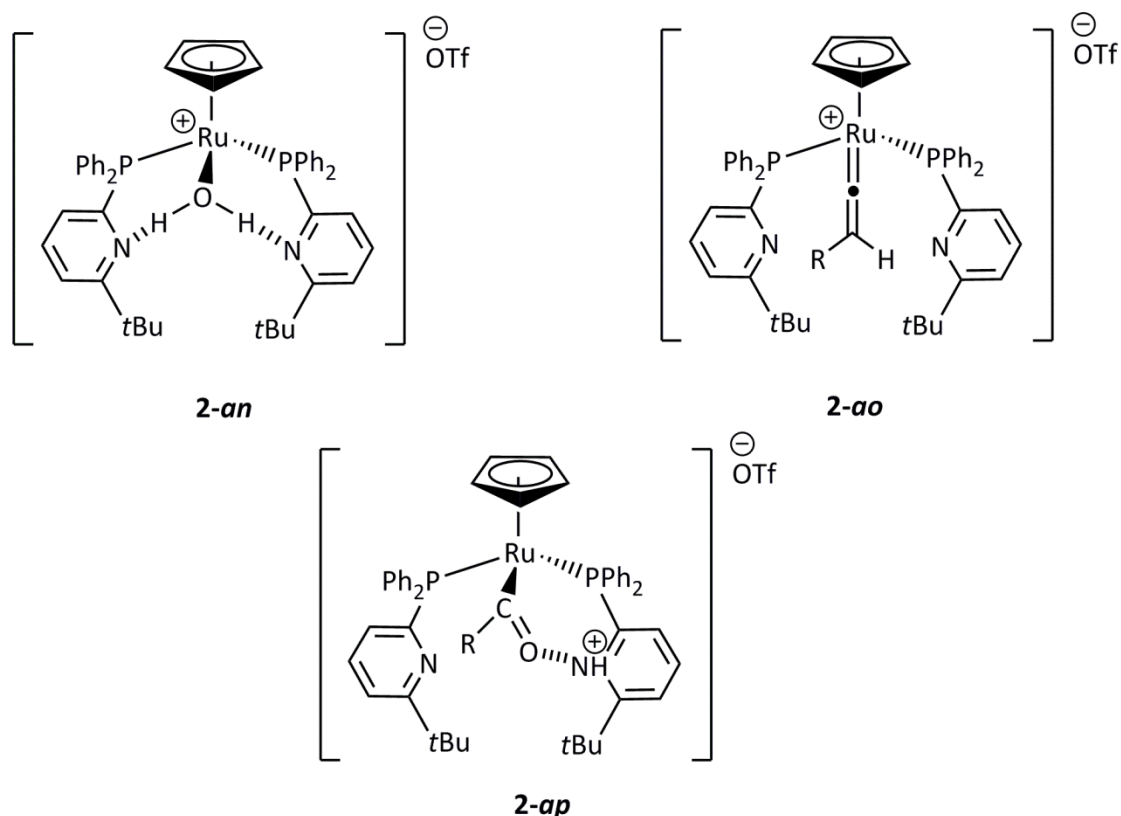
Figure 2.4 Experimentally observed intermediates in alkyne hydration catalysed by [Ru(η^5-C$_5$H$_5$)(P(6-tBu-2-pyridyl)Ph$_2$)$_2$(NCMe)]OTf

Concurrently with our investigation, the complete mechanism of a related ruthenium catalyst comprising heterocyclic ligands, [Ru(η^5-C$_5$H$_5$)(PMe$_2$Im')$_2$]$^+$ (where Im' = 1,4-dimethylimidazol-2-yl) was proposed based on DFT studies by Cooksy *et* al, Scheme 2.9.[78] In this study, the calculations were able to predict qualitative features of the reaction pathway, including the roles of the heterocyclic ligands in reducing the major transition state energies, and the low energy intermediates with high subsequent energy barriers which could be observed spectroscopically (complexes **2-aq**, **2-ar**, **2-at** and **2-ax**). Similarly to the Grotjahn mechanism in Scheme 2.8, vinylidene intermediates **2-at** and **2-au** in Scheme 2.9, are thought to be crucial to obtain the anti-Markovnikov selectivity, and intramolecular ligand assistance (*via* ligand-assisted proton shuttling, LAPS) allows a lower energy alkyne to vinylidene tautomerisation process (between intermediates **2-ar** and **2-at**). A second LAPS process acts to stabilise the transition state on the nucleophilic attack of water at the vinylidene α-carbon (between **2-au** and **2-av**), and at several subsequent stages the ligands can aid the interconversion between intermediates to form the final aldehyde, **2-ay**, and regenerate the

active catalyst. Due to the strong similarities between the Cooksy system and ours, the key features will be highlighted throughout the chapter.
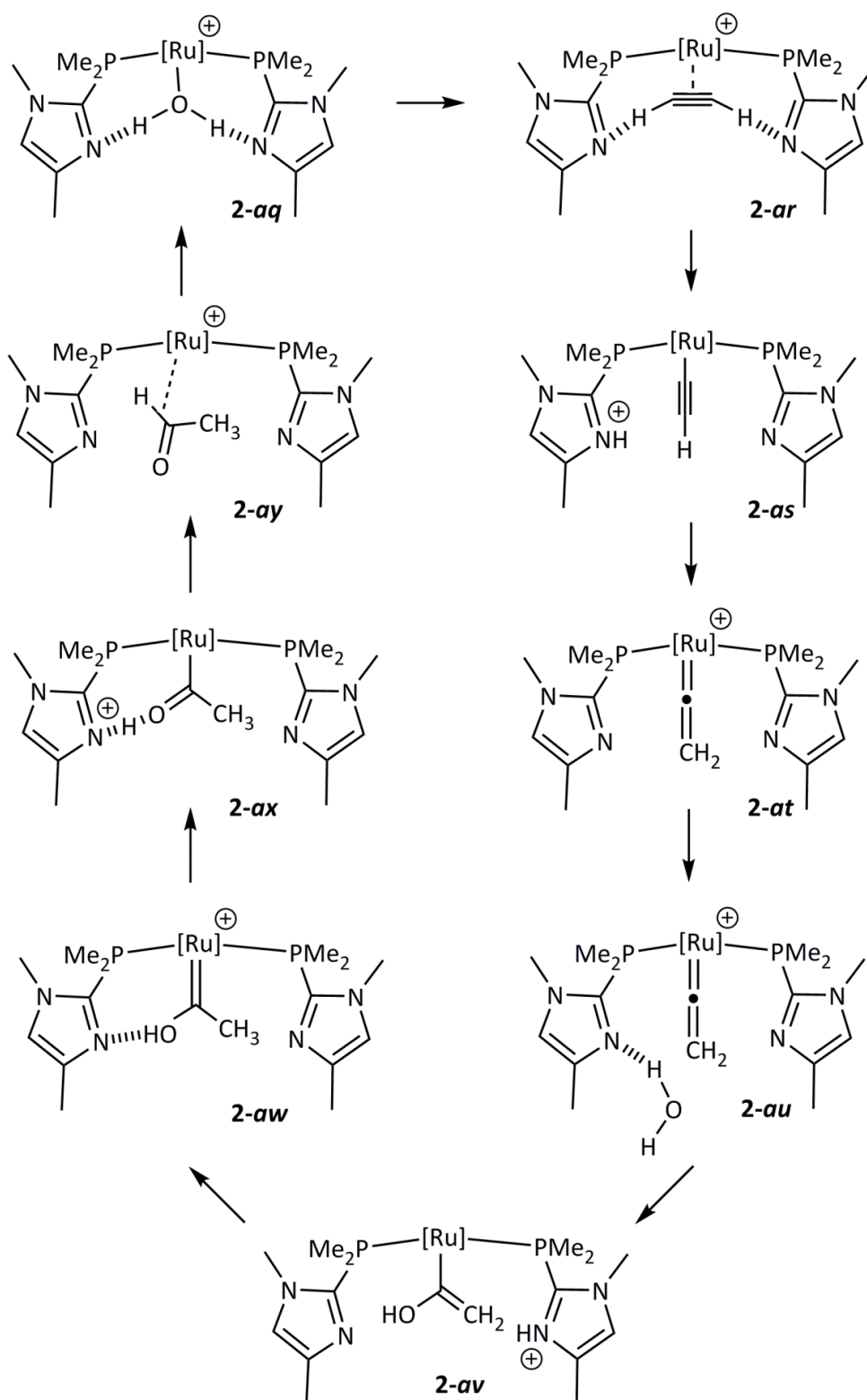
Scheme 2.9 The Cooksy mechanism of acetylene hydration, [Ru] = [Ru (η⁵-C₅H₅)][78]

2.1.4 Aims

This chapter describes a combined experimental and computational mechanistic study of the catalytic hydration of terminal alkynes (using phenylacetylene as the alkyne) by $[Ru(\eta^5\text{-}C_5H_5)(NCMe)(6\text{-}DPPAP)(3\text{-}DPICon)]PF_6$, **[1]PF$_6$**, Figure 2.5.[118]
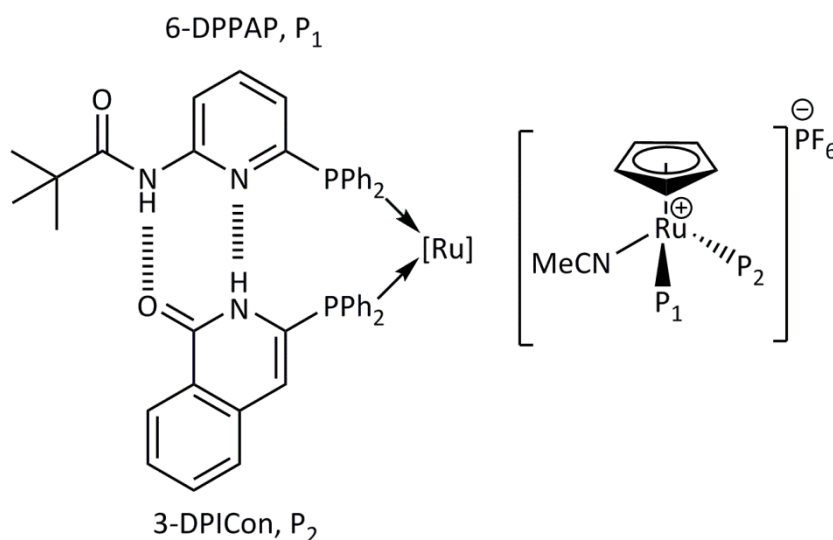
Figure 2.5 Structure of alkyne hydration catalyst, [1]PF$_6$

As shown in Figure 2.5, complex **[1]PF$_6$** comprises two monodentate phosphine ligands, 6-DPPAP and 3-DPICon, which interact through a hydrogen bonding network. The significance of this is two-fold; not only do these interactions serve to create a pseudo-bidentate ligand and therefore increase catalyst stability, the ligands can also interact with incoming substrates to stabilise catalytic intermediates and assist in their interconversion along the catalytic pathway. Additionally, experimental evidence for a catalyst deactivation pathway is presented, and a mechanism for the formation of the observed catalyst deactivation product has been proposed.[18,107,115-116,121-122]

2.2   Mechanistic proposal and methodology

The mechanism of terminal alkyne hydration catalysed by $[Ru(\eta^5\text{-}C_5H_5)(NCMe)(6\text{-}DPPAP)(3\text{-}DPICon)]PF_6$, **[1]PF_6**, comprises a series of discrete stages;

i.   Displacement of acetonitrile from complex **[1]**$^+$ and initial vinylidene formation, **[D]**$^+$, *via* η^2-alkyne complex **[A]**$^+$:

[1]$^+$ **[A]**$^+$ **[D]**$^+$
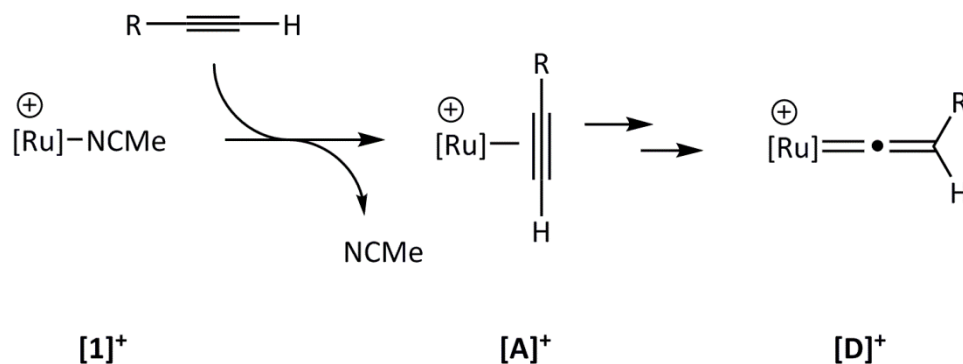
Scheme 2.10 Displacement of acetonitrile and alkyne-vinylidene tautomerisation, [Ru] = $[Ru(\eta^5\text{-}C_5H_5)(6\text{-}DPPAP)(3\text{-}DPICon)]$

ii.   Attack of H_2O at **[D]**$^+$ and tautomerisation from hydroxyvinyl complex **[F]**$^+$ to protonated acyl complex **[G]**$^+$:

[E]$^+$ **[F]**$^+$ **[G]**$^+$
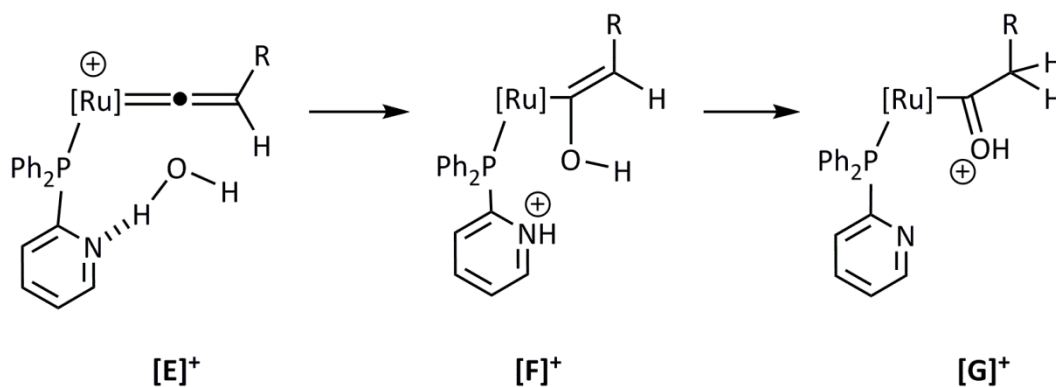
Scheme 2.11 Water incorporation and vinyl-acyl tautomerisation, [Ru] = $[Ru(\eta^5\text{-}C_5H_5)(6\text{-}DPPAP)(3\text{-}DPICon)]$ (6-DPPAP partly shown)

iii.   Rearrangement of complex **[G]**$^+$ to form aldehyde complex **[K]**$^+$:
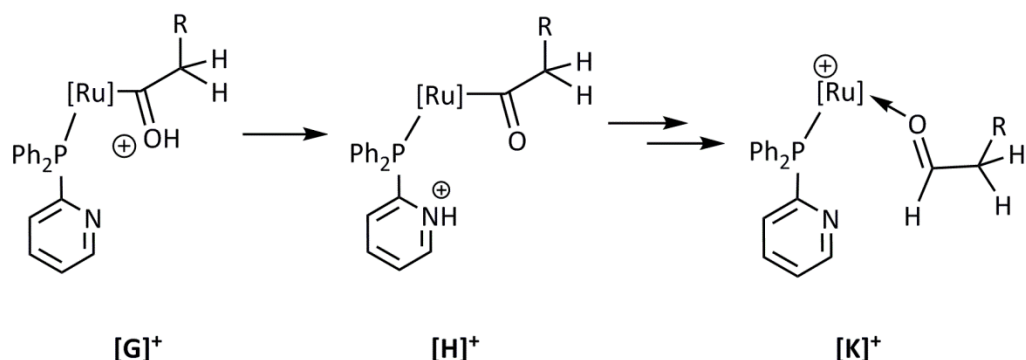
Scheme 2.12 Rearrangement of protonated acyl complex [G]$^+$ to aldehyde complex [K]$^+$, [Ru] = [Ru(η^5-C$_5$H$_5$)(6-DPPAP)(3-DPICon)] (6-DPPAP partly shown)

For each of i – iii, there are a number of mechanistic possibilities, each of which have been evaluated by DFT calculations. At each stage, results will be compared to similar studies in the literature, in particular, a detailed computational study of alkyne hydration by Cooksy which uses a similar imidazolyl phosphine system, Section 2.1.3.

Due to changes in molecularity during the proposed reaction pathway, there are significant differences between the Gibbs energies and the zero-point-energy-corrected electronic energies ($E_{SCF+ZPE}$). This discrepancy arises from the limitation that solution-phase entropy changes (more specifically, translational entropy changes[123]) on ligand binding are often significantly overestimated.[123-125] In fact, a recent publication by Grimme stated that it must be accepted that theoretical estimates of free binding energies have an uncertainty of approximately 30 kJ mol^{-1} for systems of this size.[125] The estimation of entropy is a difficult and controversial problem, and primarily concerns two issues: the amount of translational and rotational entropy that a ligand has in solution, and how much of this entropy is retained on formation of a complex.[124] The zero-point-energy-corrected electronic energies will be discussed, although Gibbs energies at 298.15 K are also presented on the potential energy surfaces (PES). The reference point for the calculations was chosen as complex **2** and H$_2$O, and so all other energies are given relative to these components (which have been set to 0 kJ mol^{-1}). Single point DFT-D3 corrections have been applied using Grimme's DFT-D3 v3.0 Rev 2 programme.[126-127] (The reason for this correction is explained in the Supporting Information for Chapter 2 (attached CD)).

2.3 Computational studies of catalysis

2.3.1 Formation of vinylidene complex, [D]$^+$

The reaction mechanism comprises a series of discrete stages; the first of which is the coordination of phenylacetylene to the metal in place of the labile acetonitrile ligand and subsequent alkyne-vinylidene tautomerisation. From the η^2-alkyne complex [Ru(η^5-C$_5$H$_5$)(HCCPh)(6-DPPAP)(3-DPICon)]$^+$, **[A]$^+$**, the first step is slippage of the alkyne to allow coordination *via* the C-H σ-bond, Scheme **2.13**.
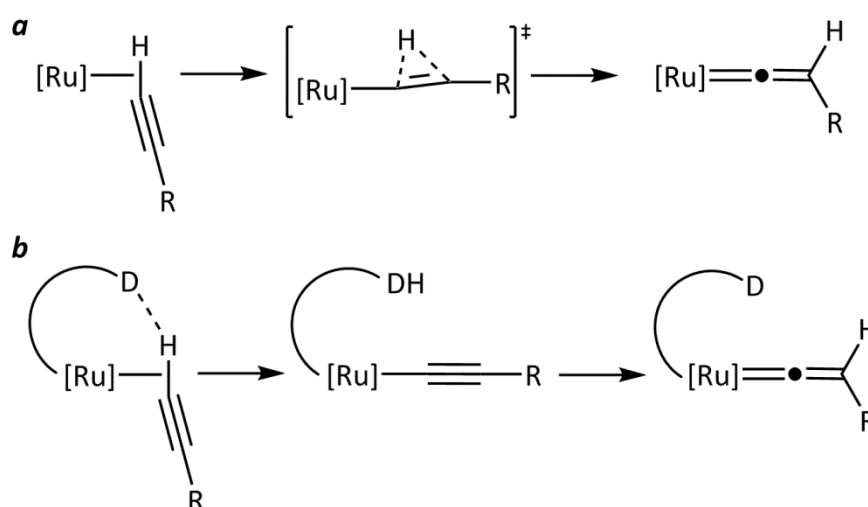
Scheme 2.13 The two alkyne-vinylidene tautomerisation mechanisms considered here: *a*) direct 1,2-hydrogen migration and *b*) ligand-assisted proton shuttle (LAPS) mechanism; where D is a Lewis basic group close to the metal centre (e.g. the oxygen atom in an acetate or carboxylate ligand or the basic nitrogen of the 6-DPPAP ligand). In this study, [Ru] = [Ru(η^5-C$_5$H$_5$)(6-DPPAP)(3-DPICon)] (6-DPPAP shown schematically in *b*)

From here, two potential pathways can then be proposed. Like other electron-poor complexes, many ruthenium species undergo alkyne-vinylidene tautomerisation *via* a 1,2-hydrogen migration mechanism from the C-H σ-complex directly to the vinylidene, pathway *a*, Scheme 2.13.[49] However in this case, tautomerisation can also occur *via* a ligand-assisted proton shuttle (LAPS) mechanism, pathway *b*,[128] Scheme 2.13, which has been demonstrated to occur in a ruthenium-acetate system. In this study, [Ru(κ^2-OAc)$_2$(PPh$_3$)$_2$] reacts with phenylacetylene to form [Ru(κ^1-OAc)(κ^2-OAc)(C=C{H}Ph)(PPh$_3$)$_2$] and the acetate ligand plays a key non-innocent role in the alkyne-vinylidene tautomerisation. The C-H activation process to form the acetylide intermediate in the acetate system is displayed in pathway *a*, Scheme 2.15.

The alternative possibility for vinylidene formation, oxidative addition of the C-H bond and 1,3-migration of the hydride, has not been considered in this study. Preliminary calculations by MChem student, Timothy Li, on a simplified model system showed that this pathway was considerably higher in energy. This is unsurprising as this route is more common for electron rich (rhodium and iridium) complexes, as noted in Chapter 1.

In the case at hand the basic pyridyl nitrogen atom of the aminopyridine moiety of 6-DPPAP can deprotonate σ-complex [B]$^+$ to form acetylide complex [C]$^+$. The protonated 6-DPPAP ligand can then reprotonate the β-carbon of the acetylide to form vinylidene [D]$^+$, Scheme 2.14.
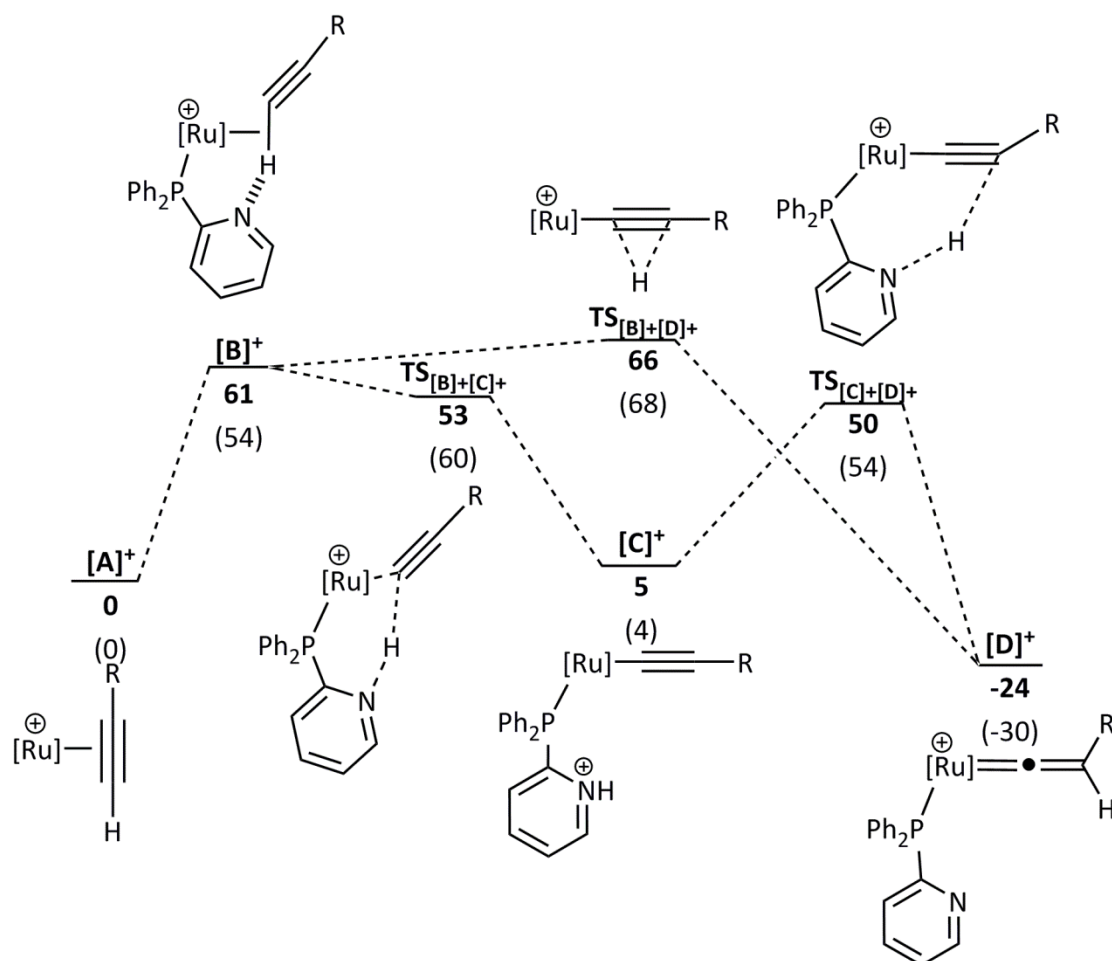
Scheme 2.14 Potential Energy Surface (PES) for the formation of vinylidene complex [D]$^+$ from the η^2-alkyne complex [A]$^+$, [Ru] = [Ru(η^5-C$_5$H$_5$)(3-DPICon)(6-DPPAP)], R = Ph. Where appropriate, 6-DPPAP is partly shown. $E_{SCF+ZPE}$ energies (top, in bold) and relative Gibbs free energies (bottom, in parentheses) at 298.15 K, both in acetone (COSMO solvation model), are shown in kJ mol^{-1}. Calculations are at the (RI-)PBE0-D3/def2-TZVPP//(RI-)BP86/SV(P) level of theory.

Scheme 2.14 illustrates the potential energy surface (PES) for each of these processes. $E_{SCF+ZPE}$ energies in acetone solution will be used in the discussion. The energy barrier for 1,2-hydrogen migration (*via* transition state **TS$_{[B]+[D]+}$**) is 66 kJ mol^{-1} and the barrier to the LAPS mechanism ($\Delta E_{SCF+ZPE}$ between intermediates **[A]$^+$** and **[B]$^+$**) is marginally lower at 61 kJ mol^{-1}. At this level of theory, these barriers are very similar in energy but it does appear that ligand assistance from the 6-DPPAP ligand could facilitate both deprotonation of the alkyne in **[B]$^+$** *via* **TS$_{[B]+[C]+}$** and reprotonation of acetylide **[C]$^+$** *via* **TS$_{[C]+[D]+}$**. In related [Ru(κ^2-OAc)$_2$(PPh$_3$)$_2$] and Cooksy's [Ru(η^5-C$_5$H$_5$)(PMe$_2$Im')$_2$]$^+$ (where Im' = 1,4-dimethylimidazol-2-yl) systems, the LAPS mechanism involves Gibbs energies of C-H bond activation of 32 and 86 kJ mol^{-1} respectively, suggesting that the structure and nature of the ligand system can have a significant effect on activation barriers, Scheme 2.15.[78,128]
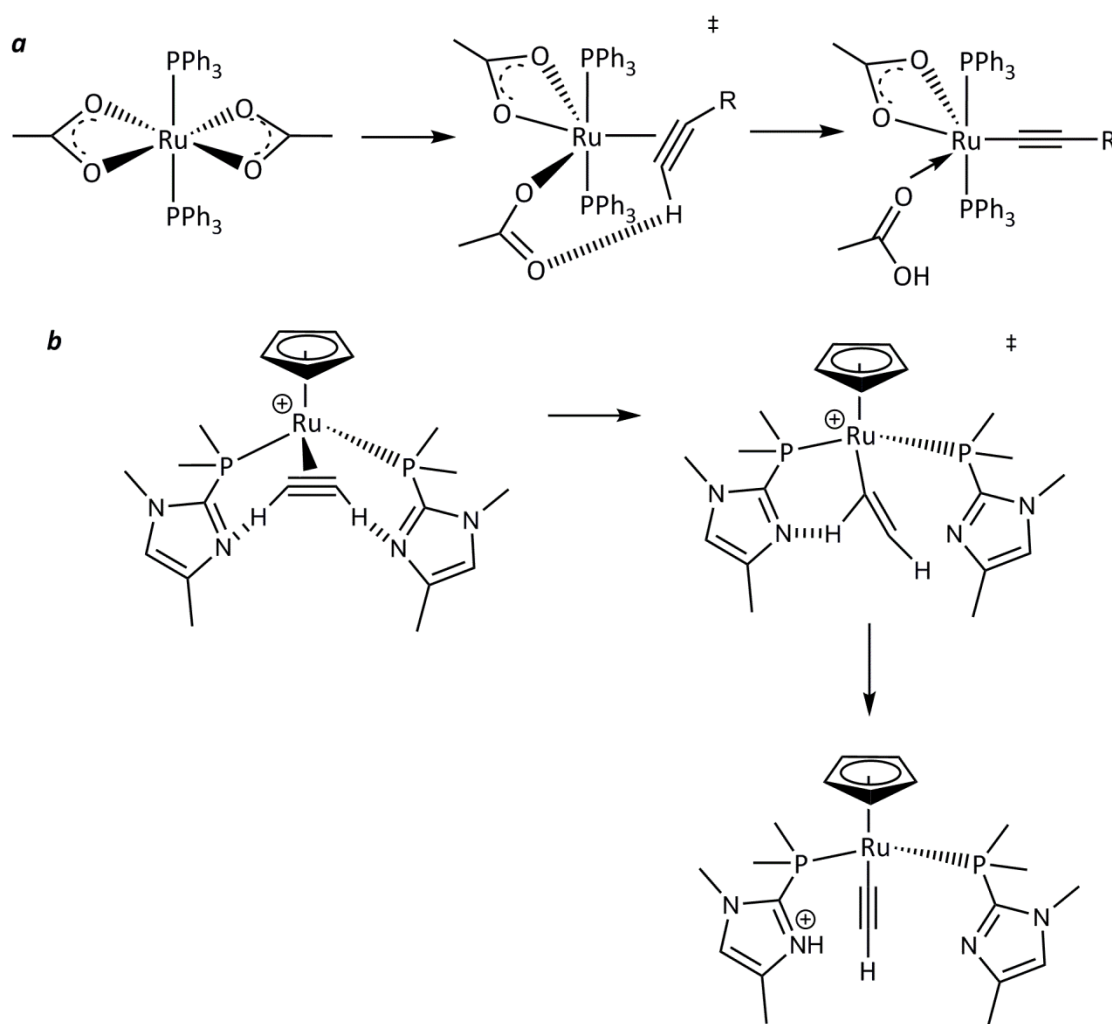
Scheme 2.15 Ligand-assisted C-H bond activation by [Ru(κ^2-OAc)$_2$(PPh$_3$)$_2$] (a, above, trans-phosphine isomer shown) and [Ru(η^5-C$_5$H$_5$)(H$_2$O)(PMe$_2$Im')$_2$]$^+$ (b, below)

2.3.2 Approach of H$_2$O to vinylidene complex [D]$^+$

A molecule of water can approach the vinylidene ligand in **[D]**$^+$ and bind between one hydrogen bond of the phosphine ligands to form complex **[E]**$^+$. In this way, the ligand set provides a water-binding pocket close to the metal centre that is important for catalysis. The calculated structure of intermediate **[E]**$^+$ shows the water binding pocket in the structure, Figure 2.6.
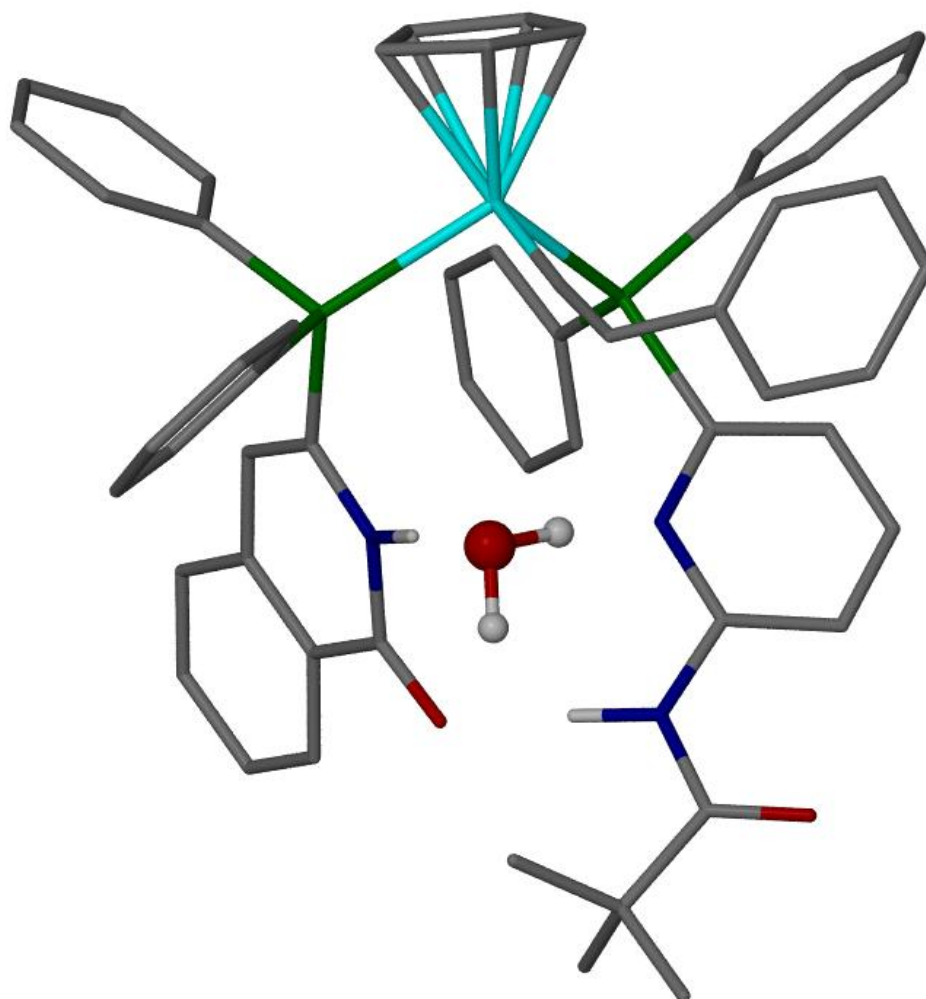
Figure 2.6 DFT-optimised structure of intermediate [E]$^+$, highlighting the water pocket within the ligand system of the vinylidene system

The water-binding pocket within **[E]**$^+$ has a dual purpose – it both activates water such that it behaves as a better nucleophile, and holds it in close proximity and with the correct orientation for attack at the α-carbon of the vinylidene ligand. The binding of water at a

metal centre by heterocyclic ligands has also been observed experimentally in both imidazolyl and pyridyl phosphine complexes, Section 2.1.3.[115-116]

Binding of water into this pocket has an energy cost of 26 kJ mol^{-1}, suggesting that the formation of the two new hydrogen bonds (**D3** and **D4**, Figure 2.7) within the structure do not compensate for the loss of hydrogen bond **D1** and the increased steric bulk around the ruthenium centre. This process also involves a decrease in entropy that will disfavour water binding, which is not incorporated in the $E_{SCF+ZPE}$ energies (as entropy changes in solution are difficult to assess from gas phase calculations and so entropy corrections are not included here).[129-131]

One hydrogen bond is retained during water incorporation (**D2** and **D5**) maintaining the pseudo-bidentate nature of the ligand system.
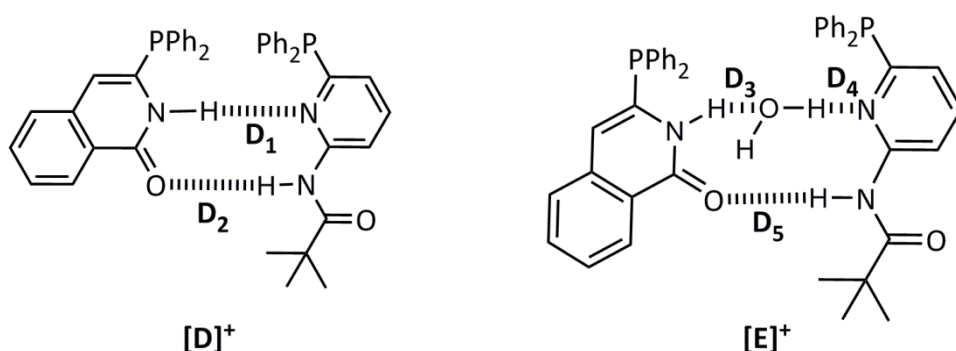
Figure 2.7 Hydrogen bond networks in intermediates [D]$^+$ and [E]$^+$. Ru and the other ligands are omitted for clarity.

Hydrogen Bond	Length / Å
D1	1.87
D2	1.77
D3	1.68
D4	1.81
D5	1.81

Table 2.1 Hydrogen bond lengths in [D]$^+$ and [E]$^+$

The binding of water in between one hydrogen bond of the self-assembled ligand system without interruption of the other demonstrates the versatility of these ligands in hosting incoming substrates at the metal centre. This flexibility can be seen at various points along

the reaction coordinate, as during all LAPS processes – the formation of vinylidene **[D]**$^+$ from alkyne **[A]**$^+$, addition of water to the vinylidene, and protonation of the ruthenium-carbon bond to form the aldehyde product through acyl complex **[H]**$^+$ – only one hydrogen bond is broken (**D$_1$** in Figure 2.7) and the other (**D$_2$** or **D$_5$**) is retained to maintain the pseudo-bidentate ligand structure. Although hydrogen bond **D$_1$** is broken, the hydrogen bond donor and acceptor sites become involved in bonding to substrate O or OH groups along the reaction coordinate (in a similar manner to that observed in **[E]**$^+$).

2.3.3 Incorporation of water into vinylidene complex [D]$^+$ and tautomerisation to protonated acyl complex [G]$^+$

The PES for the conversion of vinylidene complex **[D]**$^+$ to protonated acyl complex **[G]**$^+$ is shown in Scheme 2.16. The aminopyridine moiety of 6-DPPAP acts as an intramolecular base for the deprotonation of water promoting attack at the vinylidene *via* **TS$_{[E]+[F]+}$**, to form hydroxyvinyl complex **[F]**$^+$ with an energy barrier of 44 kJ mol^{-1}. Complex **[F]**$^+$ is stabilised by a hydrogen bond between the protonated 6-DPPAP and the oxygen atom of the hydroxyvinyl group. The N-H proton is then transferred to the β-carbon of the hydroxyvinyl group *via* **TS$_{[F]+[G]+}$** with an energy barrier of 45 kJ mol^{-1} to form complex **[G]**$^+$, Scheme 2.16. This deprotonation and reprotonation process represents a second LAPS process in the mechanism, where the aminopyridine moiety plays an important role as a proton shuttle.
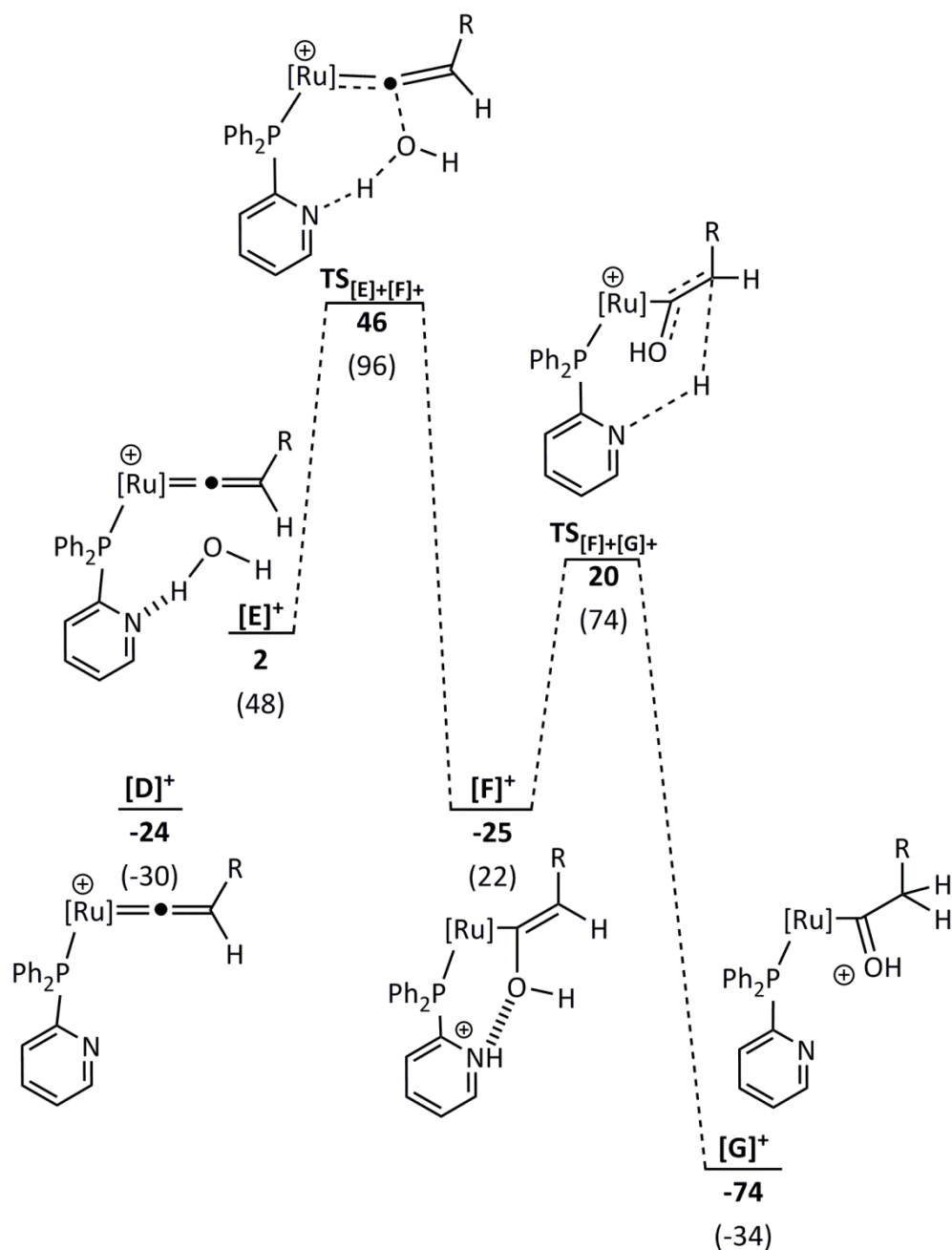
Scheme 2.16 Potential Energy Surface (PES) for the formation of protonated acyl complex [G]$^+$ from vinylidene complex [D]$^+$, [Ru] = [Ru(η^5-C$_5$H$_5$)(3-DPICon)], R = Ph, 6-DPPAP is partly shown. $E_{SCF+ZPE}$ **(top, in bold) and relative Gibbs free energies (bottom, in parentheses) at 298.15 K both in acetone (COSMO solvation model) are shown in kJ mol^{-1}. Calculations are at the (RI-)PBE0-D3/def2-TZVPP//(RI-)BP86/SV(P) level of theory.**

2.3.4   Rearrangement of complex [G]⁺ to form aldehyde complex [K]⁺

The PES for the rearrangement of complex **[G]**⁺ to form the phenylacetaldehyde complex **[K]**⁺ is shown in Scheme 2.17. Complex **[G]**⁺ can be considered as either a protonated acyl or as a hydroxycarbene species. Analysis of the bond metrics of **[G]**⁺ suggest a contribution from both resonance forms, with a Ru-C bond length of 1.943 Å and a C-O distance of 1.335 Å. Subsequent calculations suggest that the reactivity of **[G]**⁺ is biased towards the protonated acyl structure, as all attempts to optimise a structure in which the O-H group points towards the aminopyridine nitrogen led to deprotonation by the basic nitrogen of 6-DPPAP to form complex **[H]**⁺. This indicates a negligible barrier to proton transfer consistent with a strongly Brønsted acidic O-H group and a basic 6-DPPAP pyridyl nitrogen atom.

There are two possible pathways from complex **[G]**⁺ to form aldehyde complex **[K]**⁺. The complex can isomerise to form ruthenium (IV) hydride intermediate **[I]**⁺ (*via* a protonation of the metal centre by protonated acyl **[G]**⁺), from which reductive elimination forms the coordinated aldehyde in complex **[J]**⁺. A subsequent rearrangement can then form complex **[K]**⁺ – a lower energy isomer of **[J]**⁺ in which the aldehyde is coordinated through the oxygen atom rather than the aldehyde C-H bond in an agostic interaction. Alternatively, the nitrogen atom of the 6-DPPAP ligand can deprotonate the protonated acyl group in **[G]**⁺ to form complex **[H]**⁺ – this is presumably a negligible energy barrier as discussed above. The protonated nitrogen of the ligand can then deliver the proton to the α-carbon of the acyl ligand via **TS$_{[H]+[J]+}$** to form the same aldehyde complex **[J]**⁺.
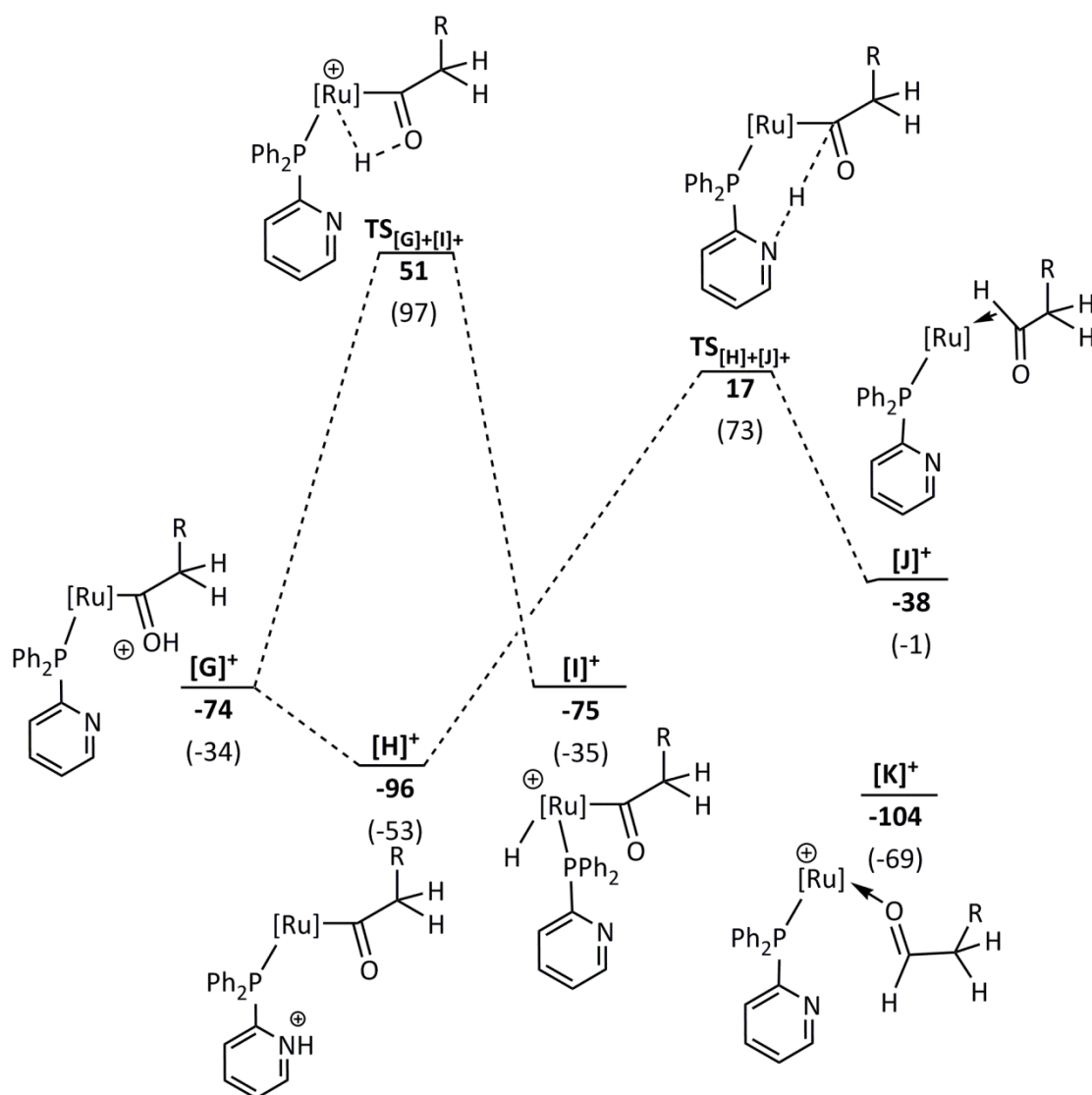
Scheme 2.17 Potential Energy Surface (PES) for the formation of complex [K]⁺ from protonated acyl complex [G]⁺, [Ru] = [Ru(η⁵-C₅H₅)(3-DPICon)], R = Ph, 6-DPPAP is partly shown. $E_{SCF+ZPE}$ **(top, in bold) and relative Gibbs free energies (bottom, in parentheses) at 298.15 K, both in acetone (COSMO solvation model) are shown in kJ mol⁻¹. Calculations are at the (RI-)PBE0-D3/def2-TZVPP//(RI-)BP86/SV(P) level of theory. The free aldehyde product and starting complex lie at -142 (-104) kJ mol⁻¹ relative to the reference point.**

On examination of the PES for these processes, the viability of the two pathways can be assessed. Hydride formation from complex **[G]⁺** has an energy barrier of 125 kJ mol⁻¹, but due to the facile deprotonation of complex **[G]⁺** by the basic nitrogen atom of the 6-DPPAP ligand, all energy barriers should be assessed from complex **[H]⁺**. This increases the energetic span for hydride migration to 147 kJ mol⁻¹. A transition state for proton transfer from the protonated acyl in **[G]⁺** to 6-DPPAP could not be located. However, this is expected to be a low energy process, due to the high Brønsted acidity of the protonated acyl and high basicity

of the aminopyridine group in 6-DPPAP. Unfortunately, a transition state for reductive elimination from **[I]$^+$** to **[J]$^+$** could also not be located.

Protonation of the acyl carbon in complex **[H]$^+$** by the protonated 6-DPPAP ligand is also a high energy process with an energy barrier of 113 kJ mol^{-1}. Although a substantial barrier, this option is more feasible than hydride formation, **[I]$^+$**. The high energy barrier can be rationalised by the formation of a very sterically hindered transition state, and the unfavourable protonation of the electron poor α-carbon of the acyl ligand in **[H]$^+$**. In this pathway, the 6-DPPAP ligand has again acted as a proton shuttle to perform the third LAPS process of the mechanism.

2.3.5 Summary of DFT calculations

Using the energetic span model of Kozuch and Shaik (ES model[132] - the basis of which is described in Appendix 1) the energetic span for the formation of complex **[J]$^+$** (and concomitantly the production of the aldehyde organic product) can be calculated. The ES model is a 'bridge' that links the outcome of experimental observations and computational catalysis. It allows for comparison between the pathways of productive catalysis and those of side reactions in order to ascertain the most probable mechanism of reaction.

If the turnover-determining intermediate, TDI, is taken to be complex **[H]$^+$** and the turnover-determining transition state, TDTS, taken to be **TS$_{[H]+[J]+}$** then the energetic span for the formation of complex **[J]$^+$** is 113 kJ mol^{-1}. This is consistent with the experimentally required conditions of heating at a temperature of 120 °C for 26 hours during the catalytic reaction. The alternative hydride-mediated pathway has a much higher energetic span of 147 kJ mol^{-1} (TDI = **[H]$^+$**, TDTS = **TS$_{[G]+[I]+}$**) which suggests that this mechanistic possibility is unlikely.

The related DFT study by Cooksy *et al* on an anti-Markovnikov alkyne hydration catalyst developed by the Grotjahn group, [Ru[(η^5-C$_5$H$_5$)(PMe$_2$Im')$_2$]$^+$ (where Im' = 1,4-dimethylimidazol-2-yl), finds that the energetic span is also 113 kJ mol^{-1} (considering the TDI to be the Ru-water pre-catalyst, and the TDTS to be deprotonation of a Ru η^2-alkyne complex by the basic nitrogen atom of an imidazolyl ligand to form a ruthenium-acetylide species).[78] On first inspection of the data, the TDTS appears to be the displacement of water in the pre-catalyst by the incoming alkyne molecule.

However, this is unlikely to be well modelled due to the wide range of alkyne approach angles relative to the water complex and the lack of an accurate solvent model to effectively compare the energies of the water-alkyne exchange. Therefore, as suggested by the authors, in reality this transition state is unlikely to be the actual TDTS.

It is also relevant to highlight the different turnover-determining states between Breit's 6-DPPAP/3-DPICon system studied in this chapter and the imidazolyl-based catalyst studied by the Cooksy group. In the 6-DPPAP/3-DPICon system, the deprotonation of the alkyne in complex **[A]$^+$** to form acetylide intermediate **[C]$^+$** is facile, and the final protonation of an acyl ligand in complex **[H]$^+$** is the highest-energy barrier to aldehyde formation. In Cooksy's imidazolyl system, alkyne deprotonation is a high energy process. This is potentially due to the disruption of two hydrogen bonds formed between the alkyne and the imidazolyl ligands that must be broken to form the alkyne-deprotonation transition state structure. Although protonation of the ruthenium-carbon bond of the acyl complex is still relatively high in energy (at 92 kJ mol^{-1}) it is considerably lower than the 6-DPPAP/3-DPICon system (at 113 kJ mol^{-1}). These subtle differences in reactivity highlight that modification of these highly functionalised ligand systems offers an effective approach for reaction optimisation.

2.4 Experimental studies

In combination with DFT calculations, the reactivity of complex **[1]PF$_6$** with terminal alkynes was also explored experimentally, using both stoichiometric studies and catalytic conditions. Stoichiometric studies are often crucial in mechanistic investigations as they can allow the observation, or even isolation, of important reaction intermediates which cannot be characterised under the catalytic reaction conditions.[45,133] The observation of intermediates experimentally has two important consequences. Firstly, the observation of a catalytically relevant complex can provide crucial insight into the reactivity of a particular system, and therefore provide an important starting point or give direction to the calculations. Secondly, experimental evidence of species postulated by DFT calculations gives credence and support to the proposed mechanism.

2.4.1 Formation of catalyst, [1]PF$_6$

Preparation of [Ru(η^5-C$_5$H$_5$)(NCMe)(6-DPPAP)(3-DPICon)]PF$_6$, **[1]PF$_6$,** initially proved more challenging than expected. The hydrogen bonding network between the ligands was reported to allow ligand self-assembly to form complex **[1]PF$_6$** in high yield. However, addition of 6-DPPAP and 3-DPICon simultaneously to [Ru(η^5-C$_5$H$_5$)(NCMe)$_3$]PF$_6$, **[2]PF$_6$,** in acetone led to a range of organometallic species. Independent syntheses confirmed these to be the homoleptic *bis*-phosphine complexes containing either two 6-DPPAP or two 3-DPICon ligands - [Ru(η^5-C$_5$H$_5$)(6-DPPAP)$_2$]PF$_6$, **[3]PF$_6$,** and [Ru(η^5-C$_5$H$_5$)(NCMe)(3-DPICon)$_2$]PF$_6$, **[4]PF$_6$.** Complex **[3]PF$_6$** appeared as a doublet at -16.6 ppm ($^2J_{PP}$ of 36.6 Hz) and a broad singlet at 48.8 ppm, and **[4]PF$_6$** appeared as a singlet at 50.4 ppm the ^{31}P{^{1}H} NMR spectra.

The position of the doublet at -16.6 ppm for complex **[3]PF$_6$** is an unusual upfield chemical shift for *bis*-phosphine complexes of this type and suggests a chelating binding mode for one of the 6-DPPAP ligands. The proposed structure of **[3]PF$_6$** is shown in Figure 2.8.
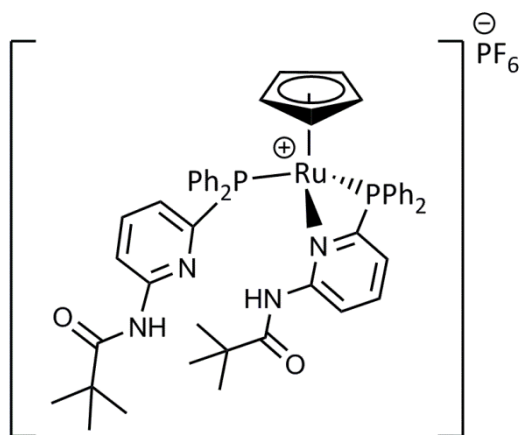
Figure 2.8 Proposed structure of [Ru(η^5-C$_5$H$_5$)(6-DPPAP)$_2$]PF$_6$, [3]PF$_6$. Both the phosphorus and nitrogen atoms of one 6-DPPAP ligand are coordinated to the metal centre.

Chelation by ligands of this type, which contain both phosphorus and nitrogen atoms, is not unusual and has been observed in the literature by Grotjahn and others for pyridyl- and imidazolyl- phosphine ligands[121]; the participation of the pyridyl moiety in diphenyl-2-pyridylphosphine has also been observed for similar ruthenium complexes, **[9c]PF$_6$** and **[10c]PF$_6$**, reported in Chapter 3.

Heating reaction mixtures containing **[3]PF$_6$** and **[4]PF$_6$** did not affect the product distribution and allow conversion to desired complex **[1]PF$_6$**. Monitoring the reaction by NMR spectroscopy indicated the formation of additional unidentified resonances in the ^{31}P{^{1}H} NMR spectrum, presumably due to complex degradation.

A pure sample of **[1]PF$_6$** was obtained through dissolution of [Ru(η^5-C$_5$H$_5$)(NCMe)$_3$]PF$_6$, **[2]PF$_6$**, in dichloromethane and dropwise stoichiometric addition of one equivalent of 3-DPICon as a dilute dichloromethane solution, followed by subsequent addition of one equivalent of 6-DPPAP in the same manner. Slow addition of the phosphine ligands avoided the formation of the homoleptic species observed previously. The analytical data for **[1]PF$_6$** synthesised by this method matches that in the literature; the ^{31}P{^{1}H} NMR spectrum shows two doublets at 54.2 and 46.0 ppm with a $^2J_{PP}$ of 36.1 Hz.[117-118]

2.4.2 Reaction between complex [1]PF$_6$ and alkynes

On addition of stoichiometric alkyne to complex **[1]PF$_6$**, the observation of acetylide complex **[C]$^+$** or vinylidene complex **[D]$^+$** was expected, according to Scheme 2.14. DFT calculations suggest these intermediates to be minima with moderate energy barriers to formation. However, no reaction was observed between **[1]PF$_6$** and a range of alkynes (phenylacetylene,

4-ethynyl-α,α,α-trifluorotoluene, 1-nonyne) at room temperature, even after stirring for 24 hours in dichloromethane. This may be due to a higher barrier to acetonitrile-alkyne exchange rather than alkyne-vinylidene tautomerisation, which prevents alkyne binding under these conditions. This acetonitrile-alkyne ligand exchange has not been modelled due to the limitations of effectively determining the energetic profile of this process (predominantly the role of the solvent and entropic effects). Cooksy also noted a high barrier to initial water-alkyne exchange as the preliminary process in the $[Ru[(\eta^5\text{-}C_5H_5)(PMe_2Im')_2]^+$ system, and noted that although in his study the energy was calculated, it was unlikely to be accurate for similar reasons to those listed here.[78] The reverse process of acetonitrile-alkyne exchange has been studied in some detail in a related system, Scheme 2.18.[134]
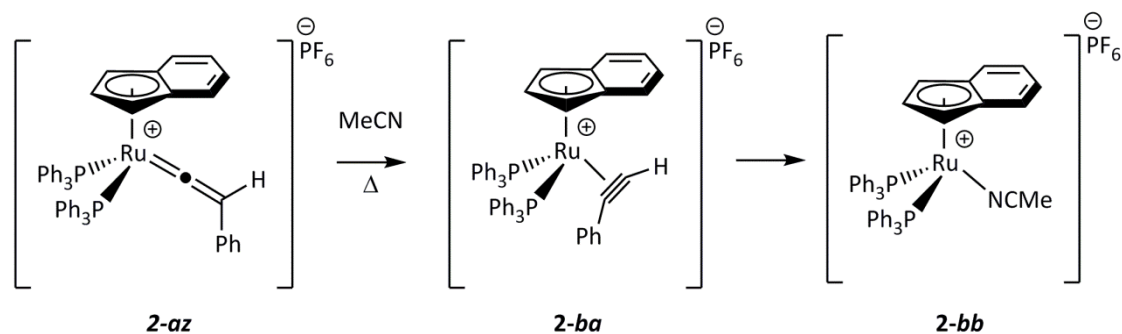
Scheme 2.18 Release of phenylacetylene from ruthenium-vinylidene complex 2-*az* to form acetonitrile complex 2-bb *via* an η²-alkyne complex 2-*ba*

Ruthenium complex **2-*az***, Scheme 2.18, can promote the reverse tautomerisation from vinylidene to η²-alkyne complex **2-*ba***, from which the acetonitrile can displace the alkyne to form complex **2-*bb*** and free alkyne. This process has an energy barrier of 100 (±4) kJ mol^{-1} which corresponds to proton migration from C_β to C_α to yield the alkyne C-H agostic complex. The entropy of activation is close to zero which also supports a unimolecular process (in this case, proton migration) as the rate determining step. This vinylidene-alkyne demetallation has been exploited in order to prepare a range of terminal γ-ketoalkynes, 1,-diynes, 1,3-, 1,5- and 1,6-enynes. No energy barrier was stated for the formation of **2-*bb*** from **2-*ba*** (alkyne-acetonitrile exchange).

Heating a stoichiometric mixture of **[1]PF$_6$** and phenylacetylene in a dichloromethane solution at 50 °C led to clean conversion to a new organometallic complex, observed by $^{31}P\{^1H\}$ NMR as two new resonances – a doublet at 65.4 ppm with a $^2J_{PP}$ of 32.4 Hz and a

broad signal at 40.3 ppm. The ^{1}H NMR spectrum indicated that the characteristic downfield resonances, representing the hydrogen bonding network in **[1]**[+], had been lost during the transformation and a singlet resonance was observed in the cyclopentadienyl region at 5.00 ppm. However, neither acetylide complex **[C]**[+] nor vinylidene complex **[D]**[+] was observed. The absence of the vinylidene ligand was confirmed by repetition of the reaction with ^{13}C-labelled phenylacetylene, which did not display the characteristic downfield resonance in the ^{13}C{^{1}H} NMR spectrum at ~ 350 ppm for the vinylidene α-carbon. Curiously though, high resolution ESI-MS indicated an organometallic species with an exact mass of vinylidene complex **[D]**[+]. The product was in fact **[5**[Ph]**]PF$_6$**, as shown in Scheme 2.19.
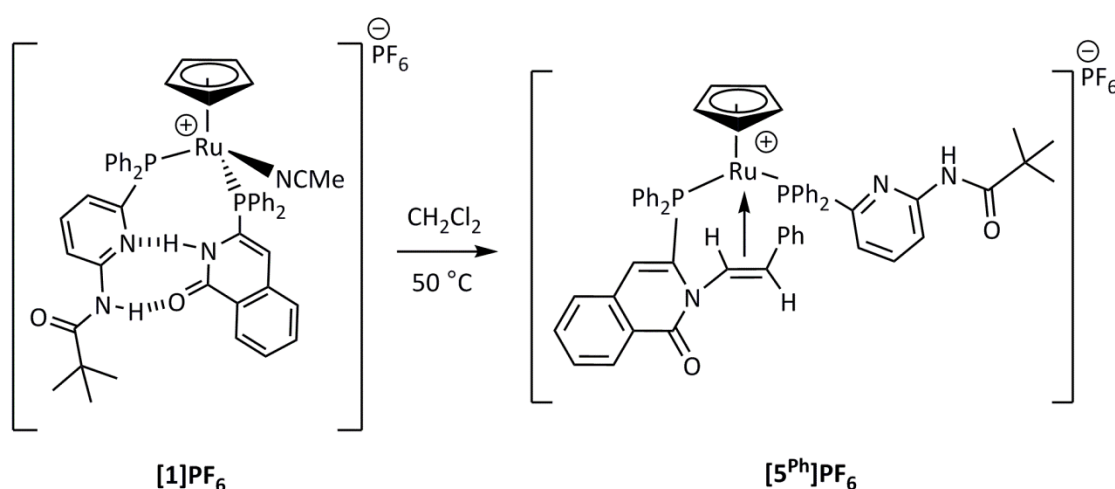
Scheme 2.19 Conversion of complex [1]PF$_6$ to complex [5[Ph]**]PF$_6$**

A single crystal X-ray structure of an analogous reaction between **[1]PF$_6$** and 4-ethynyl-α,α,α-trifluorotoluene confirmed the structure to be complex **[5]PF$_6$**, the formation of which occurs from a formal insertion of the alkyne into the N-H bond in the isoquinolone moiety of the 3-DPICon ligand. The ^{13}C{^{1}H} NMR spectrum supported the identification of complex **[5**[Ph]**]PF$_6$** by the presence of resonances at 62.3 ppm (s, C_{15}) and 76.4 ppm (d, $^2J_{PC}$ = 6.7 Hz, C_{16}) for the alkene carbon atoms, Figure 2.9.
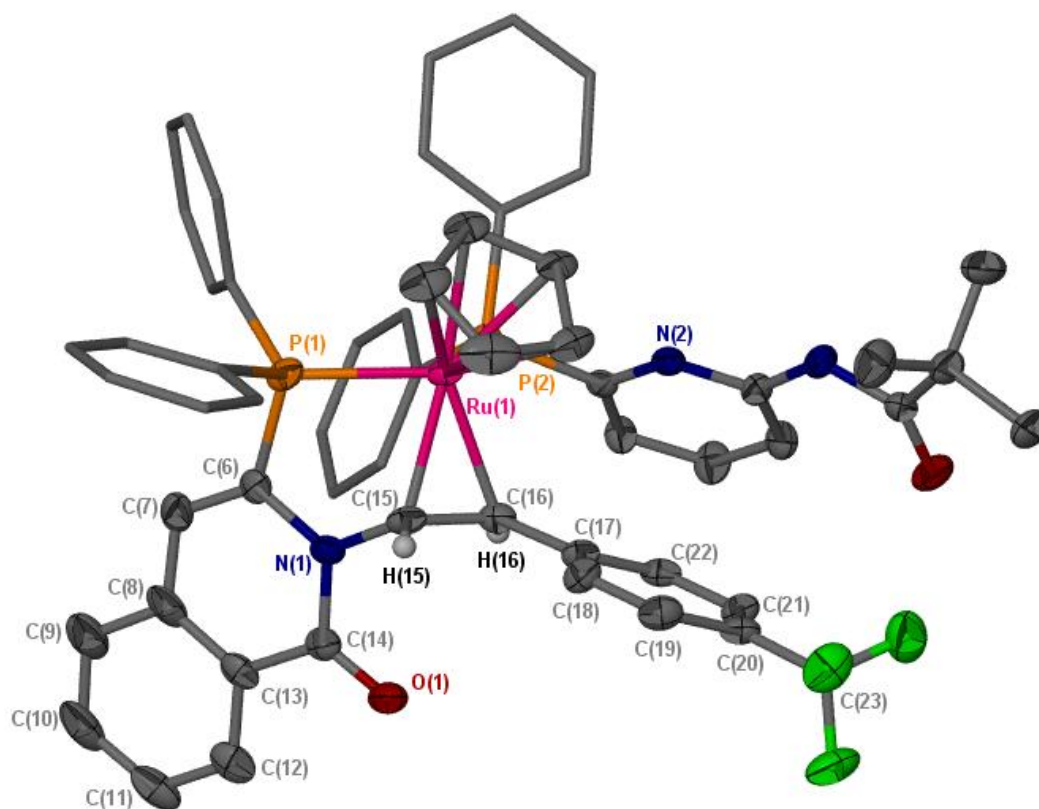
Figure 2.9 X-Seed diagram of the cation from complex [5^{CF3}]PF$_6$. Most hydrogen atoms, a PF$_6^-$ anion and a dichloromethane and diethyl ether of crystallisation have been omitted for clarity, and where shown the thermal ellipsoids are at a 50 % probability level.

The crystal structure of **[5^{CF3}]$^+$** indicates significant differences to that of complex **[1]$^+$**, the initial parent complex from which **[5^{CF3}]$^+$** is derived. Alkyne insertion into the N-H bond of the isoquinolone moiety of the 3-DPICon ligand has caused a complete loss of the hydrogen bonding network between the 3-DPICon and 6-DPPAP ligands - this leads to structural changes both in terms of conformation and bond lengths. The pyridyl-nitrogen of the 6-DPPAP ligand cannot engage in hydrogen bonding with the 3-DPICon ligand amide moiety and so orients towards the cyclopentadienyl ring in order to minimise steric congestion. Differences in the bond lengths of the isoquinolone moiety are also observed – a lengthening of the C(14)-N(1) bond and a contraction of the C(14)-O(1) bonds is consistent with the loss of the hydrogen bonding network.

[5^{CF3}]$^+$ also shows notable similarities to previously reported related ruthenium pyridylidene complex **[13^{CF3}]$^+$** in Chapter 4 and Figure 2.10.[45,79] Although it must be noted that **[5^{CF3}]$^+$** does not have a pyridylidene backbone and is instead based on a pyridyl phosphine, similar bond lengths are observed between N(1)-C(15), C(15)-C(16) and Ru(1)-C(15). The considerably

longer Ru(1)-C(15) bond length of [5^{CF3}]$^+$ may be due to the larger ring size of [5^{CF3}]$^+$ compared to [13^{CF3}]$^+$. An isomer of [13^{CF3}]$^+$ has also been studied by single-crystal X-ray crystallography, complex **2-*bc***, and the data show that each of these ruthenium d^6 complexes shows similar alkene binding to the metal centre. This indicates a similar electronic environment at the metal atom in all cases.
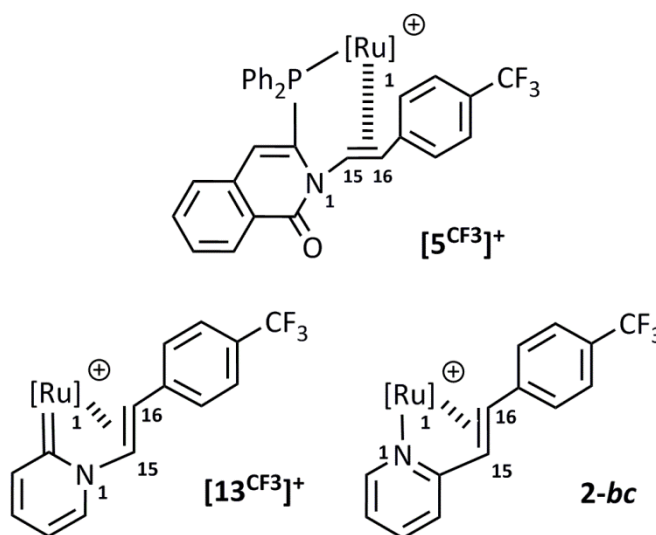
		Structure		
		[5^{CF3}]$^+$	[13^{CF3}]$^+$	**2-*bc***
Bond Lengths / Å	C(15)-C(16)	1.405(6)	1.406(4)	1.404(4)
	N(1)-C(15)	1.469(6)	1.459(4)	-
	Ru(1)-C(15)	2.181(4)	2.127(3)	2.188(3)
	Ru(1)-C(16)	2.248(4)	2.245(3)	2.274(3)

Figure 2.10 Single crystal X-ray crystallography data for [5^{CF3}]$^+$ and a series of related ruthenium complexes

Complex [5^{CF3}]PF$_6$ was investigated for catalytic activity, but under standard catalytic conditions, no formation of aldehyde was detected. (Standard catalytic conditions are: 2 mol% [Ru], 1 mmol alkyne and 5 mmol water in 1.6 ml deoxygenated acetone, with heating at 120 °C under nitrogen for 26 hours in a sealed tube). However, monitoring a standard catalytic reaction (using [1]PF$_6$ as the catalyst under identical conditions) reveals a significant

amount of **[5]PF$_6$** in the final reaction mixture, which indicates that **[5]PF$_6$** is a catalyst deactivation product.

Factors which may influence the balance between the successful formation of phenylacetaldehyde complex **[K]$^+$** and catalyst deactivation to form **[5]PF$_6$** are discussed in Section 2.5. A potential mechanism for the formation of **[5]$^+$** is also investigated.

2.5 Catalyst deactivation

A potential mechanism for the formation of complex **[5^{Ph}]$^+$** is shown in Scheme 2.20. COSMO solvation corrections are shown for dichloromethane, the solvent used in these experimental studies, rather than for acetone, the solvent of catalysis.

On the formation of complex **[L]$^+$**, the lactim nitrogen atom can perform an intramolecular nucleophilic attack at the vinylidene α-carbon to form 5-membered metallocyclic intermediate **[M]$^+$** *via* low energy transition state **TS$_{[L]+[M]+}$** with an energy barrier of only 2 kJ mol^{-1}. This low energy barrier can be explained by the close proximity of the nitrogen atom to the electrophilic vinylidene α-carbon, and the relatively small structural changes needed to allow nucleophilic attack. The lactim tautomer of the 3-DPICon ligand is also significantly higher in energy (by 61 kJ mol^{-1}) compared to the lactam form, and gains significant stabilisation on attack of the vinylidene to form **[M]$^+$**. Lactam to lactim tautomerisation is discussed at length in Section 0. From **[M]$^+$**, a proton can be transferred from the hydroxyl group of 3-DPICon to the aminopyridine nitrogen of 6-DPPAP *via* **TS$_{[M]+[N]+}$** which can then protonate the ruthenium carbon bond to form the bound alkenyl ligand in complex **[5^{Ph}]$^+$**. Therefore the Lewis basic nitrogen atom of 6-DPPAP is implicated in yet another LAPS process, transferring a proton from the 3-DPICon ligand to the metal-bound carbon atom of intermediate **[N]$^+$**. The largest energy barrier for the formation of **[5^{Ph}]$^+$** is at 91 kJ mol^{-1} and corresponds to intramolecular proton transfer between the phosphine ligands in **TS$_{[M]+[N]+}$**.
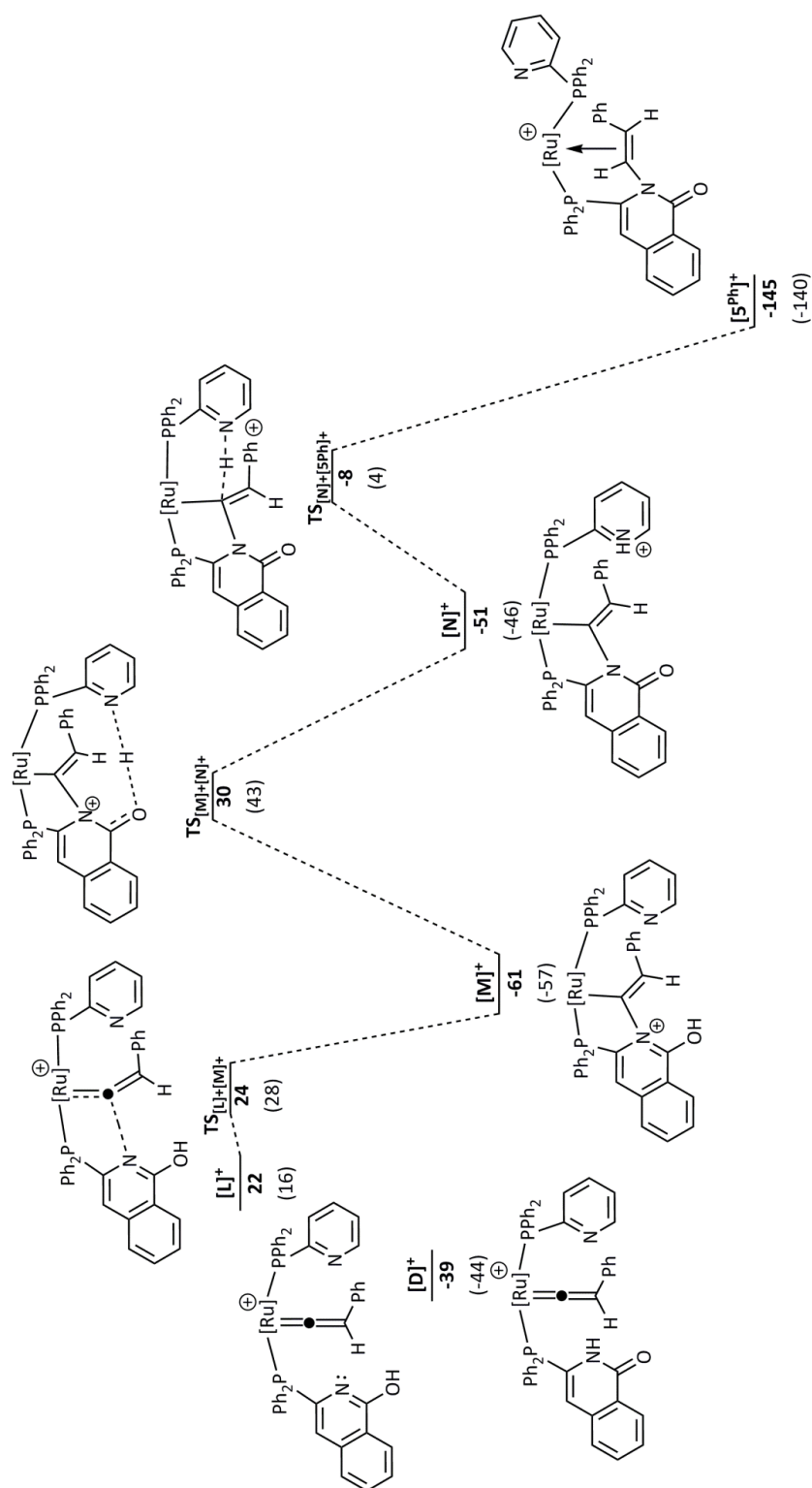
Scheme 2.20 Potential Energy Surface (PES) for the formation of catalyst deactivation product [5^{Ph}]$^+$ from vinylidene complex [D]$^+$, [Ru] = [Ru(η^5-C$_5$H$_5$)], R = Ph, 6-DPPAP is partly shown. $E_{SCF+ZPE}$ (top, in bold) and relative Gibbs free energies at 298.15 K (bottom, in parentheses) both in dichloromethane (COSMO solvation model) are shown in kJ mol^{-1}. Calculations are at the (RI-)PBE0-D3/def2-TZVPP//(RI-)BP86/SV(P) level of theory.

2.5.1 Lactam to lactim tautomerisation of 3-DPICon

The potential energy surface for the formation of **[5^{Ph}]⁺** begins from vinylidene complex **[D]⁺** – this can therefore be considered as a 'branching point' from which either productive catalysis to form the aldehyde or catalyst deactivation can occur. From vinylidene complex **[D]⁺**, lactam to lactim tautomerisation of the isoquinolone moiety in the 3-DPICon ligand reveals a nucleophilic lone pair of electrons on the nitrogen atom *via* a hydroxyisoquinolone motif, **[L]⁺**. Unfortunately, a transition state could not be located for this process but it is well documented in the literature and could occur by an intramolecular, an intermolecular or a solvent-mediated pathway.[56]

The lactam-lactim tautomerisation for 1-hydroxyisoquinoline is shown in Scheme 2.21.

lactam, **2-*bd***   lactim, **2-*be***

2-*bf*
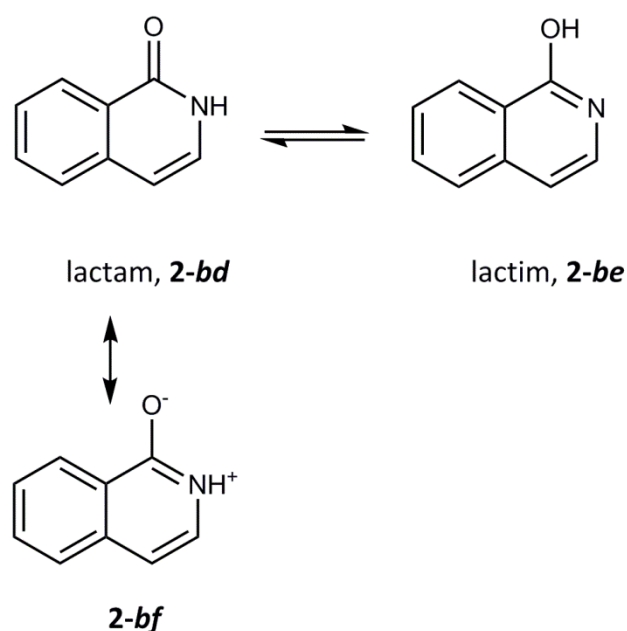
Scheme 2.21 Lactam to lactim (2-*bd* to 2-*be*) tautomerisation of 1-hydroxyisoquinoline and the 6 pi-electron lactam resonance form (2-*bf*)

This tautomerisation has been studied extensively as at the molecular level, proton-transfer tautomerisation has been proposed as a mechanism for errors during DNA replication, leading to DNA mutation.[135] Theoretical calculations (at the G3/B3LYP level of theory) suggest that the lactam form of 1-hydroxyisoquinoline is considerably more stable by 18.7 kJ mol^{-1} – from free energy values at 298 K, the ratio of lactim to lactam was calculated to be 5.3 x 10^{-4}.[136] This is unsurprising considering typical bond energies, as these would predict the carbonyl-containing tautomer (lactam) to be more stable than the lactim forms. Additionally,

compounds with a 2-hydroxypyridine motif are stabilised by 6 pi-electron resonance in their lactam form, **2-*bf***, Scheme 2.21. Conversely, other isomers of hydroxypyridines (for example, 5-hydroxyisoquinoline) or phenols, exist primarily in the lactim form due to loss of aromatisation in the keto form.[136]

However, the lactim forms of these moieties can be accessed and tautomerisation can be mediated by the solvent, or inter- or intramolecular proton transfer processes.[56] It has been shown that tautomerisation (from 2-pyridone to 2-hydroxypyridine motifs) can also be promoted by conjugated dual hydrogen-bonding (CDHB), which is defined as 'dual hydrogen bonding in which both proton donating and accepting sites can be induced resonantly'.[135] This concept is demonstrated in the formation of complex **2-*bg*** in Scheme 2.22, which contains a 2-pyridone/2-hydroxypyridine tautomer system. On coordination to a metal centre such as Pt(II) or Rh(II), the 6-DPPon ligand can self- assemble to form a pseudo-bidentate ligand – in this case the resulting rhodium complex can catalyse the regioselective hydroformylation of terminal alkenes.[16]
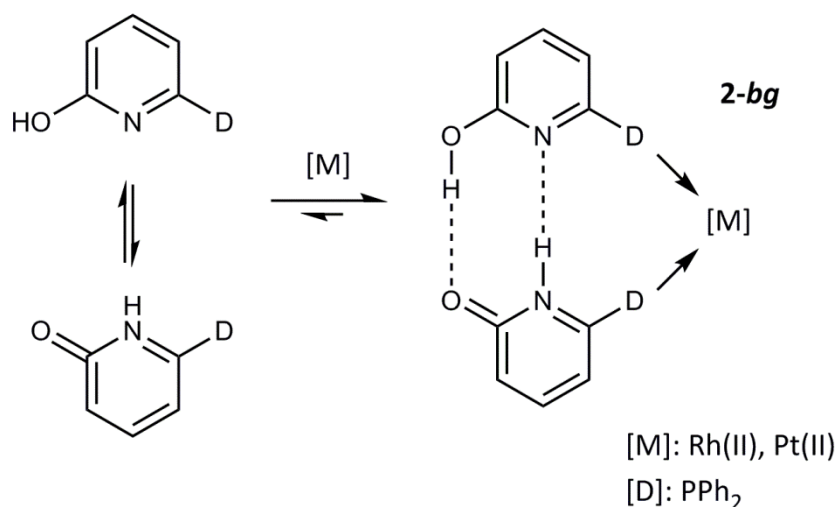
Scheme 2.22 Self-assembled rhodium or platinum complexes with the general structure of 2-*bg*, containing the 2-pyridone/2-hydroxypyridine tautomer system

In complex **[D]$^+$** it is possible that the aminopyridine moiety of the 6-DPPAP ligand can assist in the tautomerisation of 3-DPICon from the lactam to the lactim resonance form through a LAPS style process. Under these conditions (dichloromethane, 50 °C, in the absence of water) complex **[1]PF$_6$** is transformed selectively into complex **[5]PF$_6$** which suggests that lactam-lactim formation is favoured compared to under catalytic conditions (acetone, 120 °C, excess water). It remains uncertain as to why this is the case. Although high temperatures promote

lactam-lactim tautomerisation, both the presence of water and the use of a high polarity solvent are reported to promote the lactam tautomer.[137] Therefore it seems that the more polar acetone solvent and presence of water in the catalytic reaction mixture may inhibit the lactam to lactim tautomerisation that leads to the formation of complex **[L]**$^+$ and hence inhibit catalyst deactivation.

2.5.2 Summary of DFT calculations

Using again the energetic span model of Kozuch and Shaik,[132] considering the TDI to be **[M]**$^+$ and the TDTS to be **TS$_{[M]+[N]+}$**, the energetic span for the formation of complex **[5^{Ph}]**$^+$ in dichloromethane is 91 kJ mol^{-1}, which is consistent with full conversion to **[5^{Ph}]PF$_6$** upon heating catalyst **[1]PF$_6$** and alkyne at 50 °C in dichloromethane over a number of days.

On comparison with the productive catalytic pathway to form complex **[J]**$^+$, which has an energetic span of 113 kJ mol^{-1} in acetone, it seems that **[5^{Ph}]**$^+$ is the kinetic product in this catalytic system. **[5^{Ph}]**$^+$ is also similarly stable to the formation of the aldehyde product *via* the productive catalytic pathway (**[5^{Ph}]**$^+$ = -145 kJ mol^{-1} compared to -142 kJ mol^{-1} for the production of aldehyde and regeneration of catalyst **[1]**$^+$). The high stability of **[5^{Ph}]**$^+$ results from the high energy barrier of the backward reaction to form vinylidene **[D]**$^+$, the intermediate from which successful catalysis could occur. The energetic span of aldehyde production from deactivation product **[5^{Ph}]**$^+$ is 175 kJ mol^{-1},, considering the TDI to be **[5^{Ph}]**$^+$ and the TDTS to be **TS$_{[M]+[N]+}$**. This supports the experimental findings that complex **[5^{Ph}]**$^+$ is unable to act as a catalyst for the production of aldehyde and so **[5^{Ph}]**$^+$ can be considered as a catalyst deactivation product. There are similarities between this catalyst deactivation mechanism and one reported recently for pyridine alkenylation (discussed in Chapter 3).[45]

In summary, the DFT calculations suggest that catalyst deactivation product **[5^{Ph}]**$^+$ is both the kinetic and thermodynamic product of this system when compared to formation of the aldehyde organic product and regeneration of the catalyst. **[5^{Ph}]**$^+$ has a lower energetic span of formation (91 kJ mol^{-1} versus 113 kJ mol^{-1} for aldehyde production) and a lower thermodynamic energy (-145 kJ mol^{-1} versus -142 kJ mol^{-1} for the aldehyde and regenerated catalyst). Therefore, the calculations do not accurately predict the experimental results in this case. Based on the DFT calculated energies, the formation of **[5^{Ph}]**$^+$ should be favoured over productive catalysis.

In reality, although the rate of catalyst deactivation is not enough to prevent aldehyde formation, a significant amount of **[5^{Ph}]PF$_6$** is in fact observed in the reaction mixture with a characteristic ^{31}P{^{1}H} signature as a doublet at 65.5 ppm with a $^2J_{PP}$ of 32.4 Hz and as a broad singlet at 40.3 ppm. However, it should be taken into account that catalyst deactivation described above occurs under notably different conditions to the catalytic conditions – in dichloromethane rather than acetone, at a lower temperature of 50 °C rather than 120 °C and in the absence of water. Therefore, the catalyst deactivation pathway has also been modelled with dichloromethane solvation but yields an identical energetic span of 91 kJ mol^{-1}, highlighting that in this instance implicit solvation cannot help to explain the differences. As yet, the origin of this effect has not been understood but it could be that under active catalytic conditions, the binding of water to one or more intermediates along the reaction coordinate may alter the energy barriers enough to promote productive catalysis and inhibit catalyst deactivation.

2.6 Conclusions

On the basis of a thorough mechanistic study using DFT calculations, coupled with experimental evidence from analogous systems and a complementary computational study on a related catalyst species by Cooksy *et al*,[78] a potential mechanism for anti-Markovnikov terminal alkyne hydration using the self assembled phosphine complex [Ru(η^5-C$_5$H$_5$)(NCMe)(6-DPPAP)(3-DPICon)]PF$_6$, **[1]PF$_6$** has been proposed.

The mechanism includes three ligand-assisted proton shuttle (LAPS) processes - initial vinylidene formation, nucleophilic attack of water at the vinylidene α-carbon and tautomerisation from a hydroxyvinyl to acyl species - all of which provide lower energy routes to aldehyde formation than the non-ligand assisted alternatives. The high level of functionality in the phosphine ligands, 6-DPPAP and 3-DPICon, allow these transformations to take place, and the synergy between the metal centre and the non-innocent ligand system, both playing active roles in catalysis, allows comparison of catalyst **[1]PF$_6$** with one of nature's metalloenzymes.[18]

The stoichiometric experimental studies have discovered a catalyst deactivation species, **[5]PF$_6$**, which could also be observed in reaction mixtures after standard catalytic conditions. **[5]PF$_6$** has been identified using multinuclear NMR spectroscopy, high resolution ESI-MS and single crystal X-ray crystallography. A potential mechanistic pathway to **[5^{Ph}]$^+$** has been explored and also involves a LAPS process, mediated by the phosphine ligands *via* initial lactam to lactim tautomerisation of the isoquinolone moiety of the 3-DPICon ligand. At least in dichloromethane, **[5^{Ph}]$^+$** is a kinetic (and potentially thermodynamic) product in this system and represents a catalyst deactivation product. **[5^{CF3}]PF$_6$** was isolated and tested in catalysis, showing no activity under standard operating conditions.

Chapter 3

Investigation of pyridyl-substituted phosphine ligands in catalysis

3 Investigation of pyridyl-substituted phosphine ligands in catalysis

3.1 Introduction

Pyridine motifs are among the most important heterocyclic substructures, widely found in natural products, pharmaceuticals, as organometallic ligands, and in functional materials.[138] More than 100 currently marketed human medicines contain this privileged unit,[139] and specific examples of pyridine-based pharmaceutical agents include Loratidine (marketed as Claritin) for the treatment of allergies, Esomprazole (marketed as Nexium) for the treatment of acid reflux and stomach ulcers and Crizotinib (marketed as Xalkori) for the treatment of lung cancers, Figure 3.1.

Loratidine
(Claritin, Bayer)

Crizotinib
(Xalkori, Pfizer)

Esomeprazole
(Nexium, Astra Zeneca)
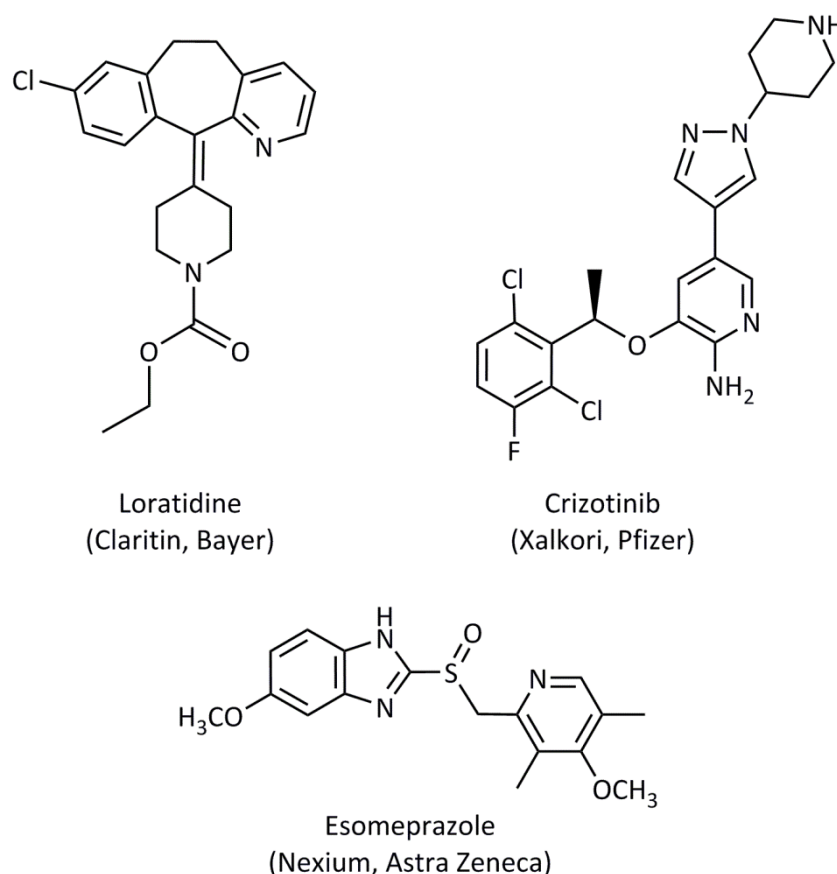
Figure 3.1 Pyridine motifs in pharmaceutical agents – labelled with generic name with brand name and primary manufacturer (in brackets)

Therefore, efficient, selective and atom-economical routes to these structures continue to be highly sought after.[138]

3.1.1 Functionalisation of pyridine

Due to the electronegativity of the nitrogen atom in the pyridine ring, the aromatic system is regarded as electron-deficient and therefore, in comparison to benzene, is less susceptible to functionalisation *via* electrophilic aromatic substitution (abbreviated hereafter as EAS) such as the Friedel-Crafts reaction. This presents a significant challenge for the organic chemist. In EAS, the most reactive position is *meta-* to the nitrogen atom, and this selectivity can be further enhanced by the formation of a pyridinium ion.

To force EAS reactions at the *ortho-* and *para-* positions requires the use of activated pyridine substrates or condensation and cycloaddition reactions.[140] Alternatively, pyridine can be activated at the *ortho-* and *para-* positions by conversion to pyridine *N*-oxide, as a lone pair of electrons from oxygen can stabilise the positive charges in the corresponding Wheland intermediates. In 2008, Nakao *et al.* reported the alkenylation of pyridine *N*-oxides at the *ortho-* position with high levels of regio- and stereoselectivity using $Ni(COD)_2$ (COD = cyclooctadiene) and a phosphorus (III) ligand additive.[141] The conditions were later modified to allow pyridine activation *in situ* by cooperative catalysis between the nickel complex, a phosphorus additive and a Lewis acid (LA).[142] Furthermore, the choice of LA could influence the reaction outcome; the use of diorganozinc compounds allowed the isolation of monoalkenylated products, **3-*f*** in Scheme 3.1, whereas the use of $AlMe_3$ afforded *ortho-* dienylated products, **3-*g***, from the double insertion of alkynes into the C-H bond. The postulated mechanism for this process is shown in Scheme 3.1. The first step is coordination of the LA to the pyridine nitrogen atom and coordination of the alkyne in an η^2-binding mode to the nickel centre, **3-*a***. Metallation of the *ortho-* C-H bond of pyridine leads to **3-*b***, and migration of the hydride ligand forms **3-*c***. At this point, the two ligands can couple to form product **3-*f***; alternatively, insertion of a second alkyne molecule can form product **3-*g***.

The methodology was then optimised further to allow selective reaction at the *para-* position by the use of a sterically bulky NHC ligand, 1,3-(2,6-diisopropylphenyl)imidazol-2-ylidene, rather than a phosphine ligand.[143]
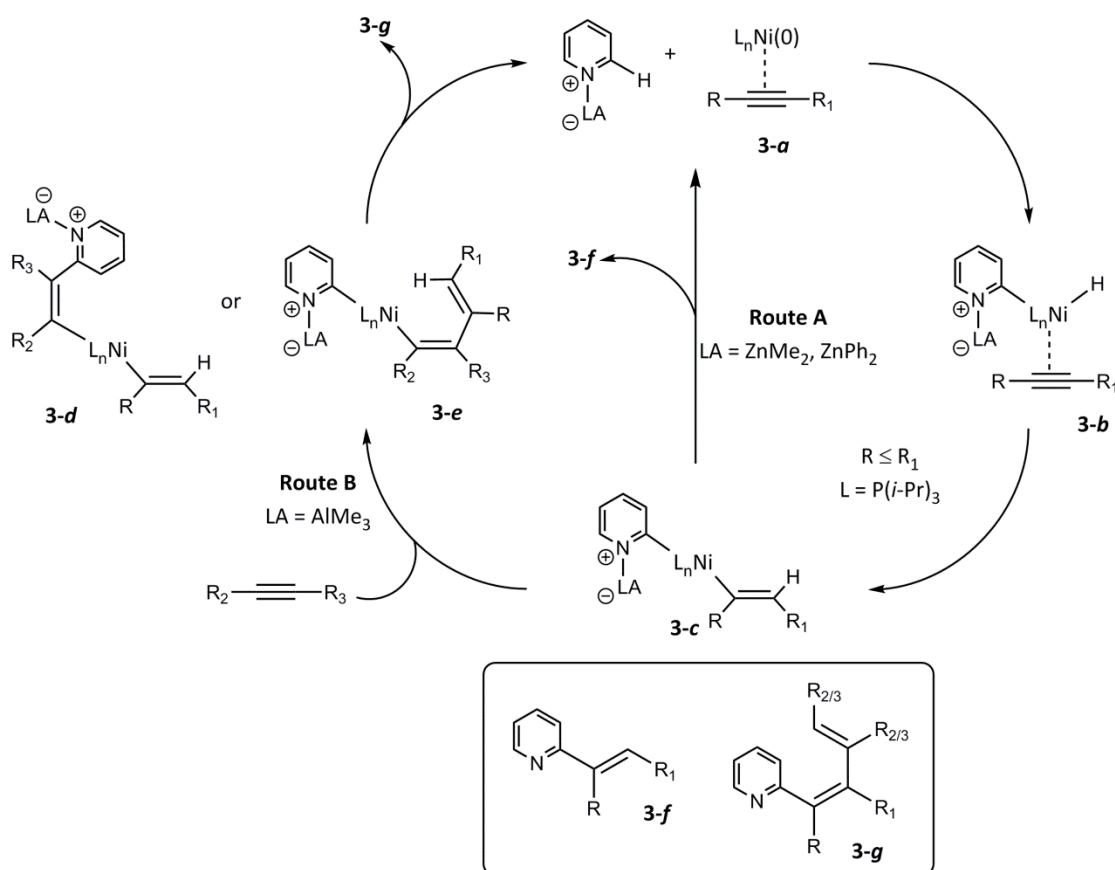
Scheme 3.1 Alkenylation of pyridine at the *ortho*- position catalysed by Ni(COD)$_2$ and a Lewis acid

3.1.2 Synthetic routes to *E*-2-styryl pyridine

The focus of the work described in this chapter is to optimise a recently reported synthetic procedure to *E*-2-styryl pyridine and derivatives, described in Section 3.1.3.2. Therefore, some other synthetic routes to these compounds are described here.

Common preparation methods for *E*-2-styrylpyridine involve transition metal catalysis, in particular, palladium cross-coupling approaches. Both the Mizoroki-Heck (coupling between an aryl halide and an alkene) and the Suzuki-Miyaura (coupling of an aryl halide with an organoboronic acid) have been utilised with varying degrees of success. However, each of these strategies requires pre-functionalisation of one or both reagents respectively and often also demands several of the following conditions; long reaction times (of approximately 20 hours),[144] complex catalyst preparations (up to five synthetic steps),[145] anhydrous conditions or high reaction temperatures (up to 140 °C).[144,146] Although some palladium cross-coupling systems have been reported which operate at lower temperatures, for example the coupling of aryl trimethoxysilanes and vinyl groups reported by Ye *et al.*, this method requires the

addition of three equivalents of silver fluoride. This costly additive is thought to both regenerate the Pd (II) species and activate the aryl trimethoxysilane.[147]

Other metals can catalyse the formation of *E*-2-styrylpyridine, including rhodium, iron, and copper,[148-150] and even rare earth metals such as a scandium half-sandwich complexes which can form derivatives of *E*-2-styryl pyridine by coupling to allenes.[138] Both the iron and copper catalysed routes initially seem attractive due to the obvious advantage of using readily available, inexpensive metal complexes; however, they are not necessarily more atom efficient. For example in the copper case, the pyridine moiety is activated by conversion to an *N*-iminopyridinium ylide, **3-h**, and coupled with a vinyl iodide, Scheme 3.2.
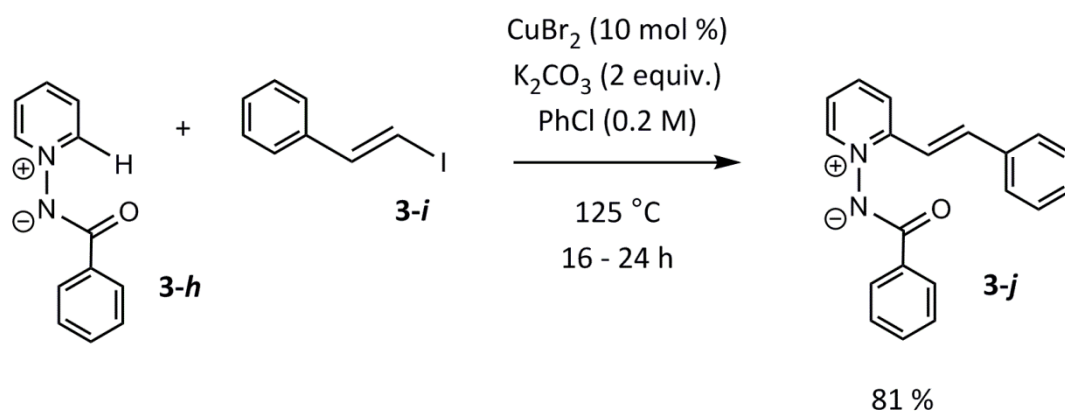
Scheme 3.2 Copper-catalysed synthesis of *E*-2-styrylpyridine

Several completely metal-free routes have also been presented, but the substrates must be pre-functionalised in order to achieve regioselectivity.[151-152]

3.1.3 Synthetic routes to *E*-2-styryl pyridine *via* direct C-H activation

Studies on the synthesis of alkenylated pyridine derivatives by direct C-H activation (without pre-functionalisation of either substrate) have remained limited, despite the significant benefits that these approaches can offer.[138] The avoidance of halogenated substrates allows the number of synthetic steps to be reduced, leading to higher atom efficiencies and the elimination of salt-based by-products, which allows facile isolation of the organic product and recovery of the catalyst. Several methods to achieve direct C-H functionalisation of organic substrates are reported in the literature.[153-154] The use of directing groups, such as heteroatoms or unsaturated moieties, can template substrate coordination to the metal centre and therefore facilitate reactivity and impart regio-selectivity to the transformation.[45]

The C-H activation step can also be assisted by an intramolecular base, such as an acetate group, which promotes substrate deprotonation.[24]

An alternative pathway to promote the functionalisation of heterocyclic substrates, **3-k**, is to take advantage of their carbene tautomers.[155] In the case of pyridine, conversion to the pyridylidene tautomer by a formal hydrogen migration reveals an unsaturated carbene moiety, which can be stabilised on coordination to a metal centre, **3-n**. The metal-bound carbon atom is then susceptible to further reaction, for example, coupling to unsaturated substrates and aromatic halides, Scheme 3.3. [156-158]
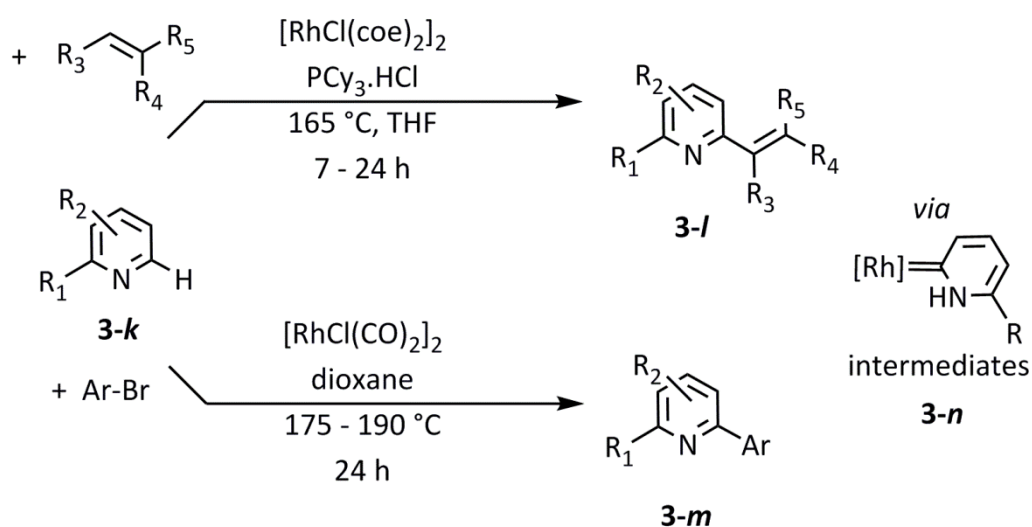
Scheme 3.3 Rhodium-catalysed pyridine functionalisation *via* pyridylidene intermediates, Ar-Br = various aryl bromides, R$_{1-5}$ = aromatic, aliphatic, *N*-heterocyclic groups

For a comprehensive introduction to pyridylidene complexes, see Chapter 1, Section 1.3.2.

3.1.3.1 Alkenylation of pyridine: Murakami and Hori

In 2003, Murakami and Hori presented a catalytic system for the formation of *E*-2-styryl pyridine from pyridine (which acts as both the substrate and the reaction solvent) and a trimethylsilyl-protected alkyne.[159] The TMS-protection of the alkyne was necessary in order to avoid alkyne dimerisation under the catalytic conditions. The reaction scheme and proposed mechanism is shown in Scheme 3.4.
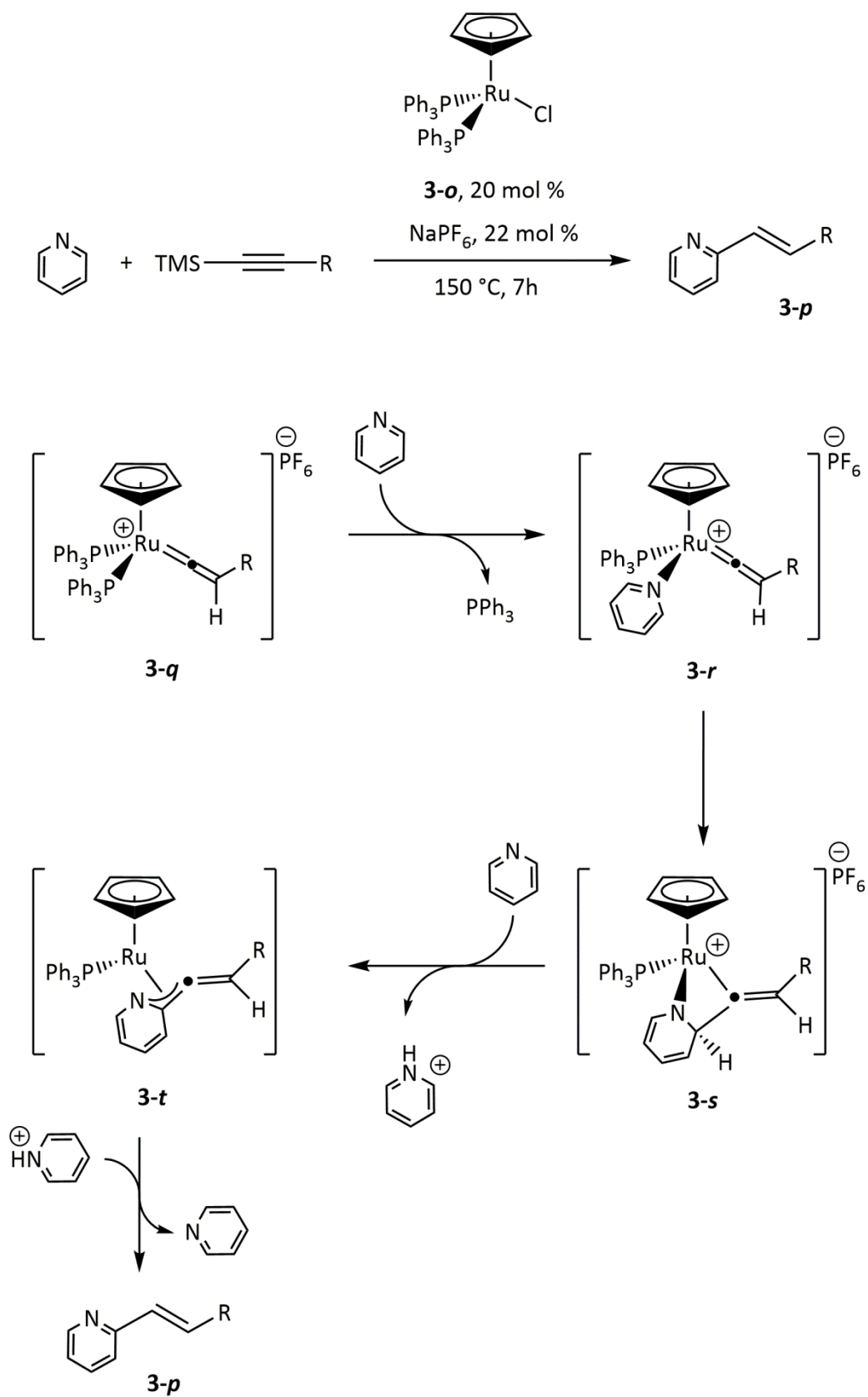
Scheme 3.4 Pyridine alkenylation mechanism proposed by Murakami and Hori, R = aromatic or alkyl substituent (3-o later referred to as [25], 3-p as 14, 3-q as [28^R]PF$_6$ and 3-r as [11]PF$_6$)

The first step of the mechanism was proposed to be formation of vinylidene complex **3-q**, followed by replacement of a triphenylphosphine ligand at the ruthenium centre to form complex **3-r**. An intramolecular [2+2] cycloaddition between coordinated pyridine and the vinylidene ligand could then occur to form **3-s**, and proton migration *via* π-azaallyl complex **3-t** (assisted by excess pyridine) could yield the final organic molecule **3-p** and regenerate an active catalytic species.

The reaction offers some extremely attractive features; it exhibits both high regio- and stereoselectivity, as pyridine reacts exclusively at the *ortho-* position to produce only the *E-* isomer of the alkene, and is relatively atom-efficient for transformations of this type. However, the high reaction temperatures (150 °C), high catalyst loading of **3-o** (20 mol %) and the need for a TMS protected alkyne are considerable weaknesses. Therefore, the Lynam and Slattery groups employed a mechanistic approach using combined experimental and theoretical studies in order to investigate and optimise the catalysis.

3.1.3.2 Alkenylation of pyridine: Lynam and Slattery

The combined experimental and computational studies of the Lynam and Slattery groups discovered several key mechanistic steps in the ruthenium-catalysed pyridine alkenylation process of Murakami and Hori, which allowed significant optimisation of the previously required catalytic conditions.[45]

Firstly, dissolution of $[Ru(\eta^5\text{-}C_5H_5)(PPh_3)_2(C=C\{H\}Ph)]PF_6$, **3-q** (observed as an intermediate in the Murakami and Hori mechanism, Scheme 3.4) in pyridine, coupled with subsequent reactivity studies indicated that the active catalytic species was in fact $[Ru(\eta^5\text{-}C_5H_5)(PPh_3)(NC_5H_5)_2]PF_6$, **3-v**, in Scheme 3.5. The stoichiometric addition of either phenylacetylene or 4-ethynyl-α,α,α-trifluorotoluene to a pyridine solution of independently prepared **3-v** resulted in quantitative conversion to **3-p** (however, on subsequent additions of phenylacetylene to the complex, the NMR spectra indicated the slow conversion of the ruthenium catalyst to complex **3-w**, Scheme 3.6).
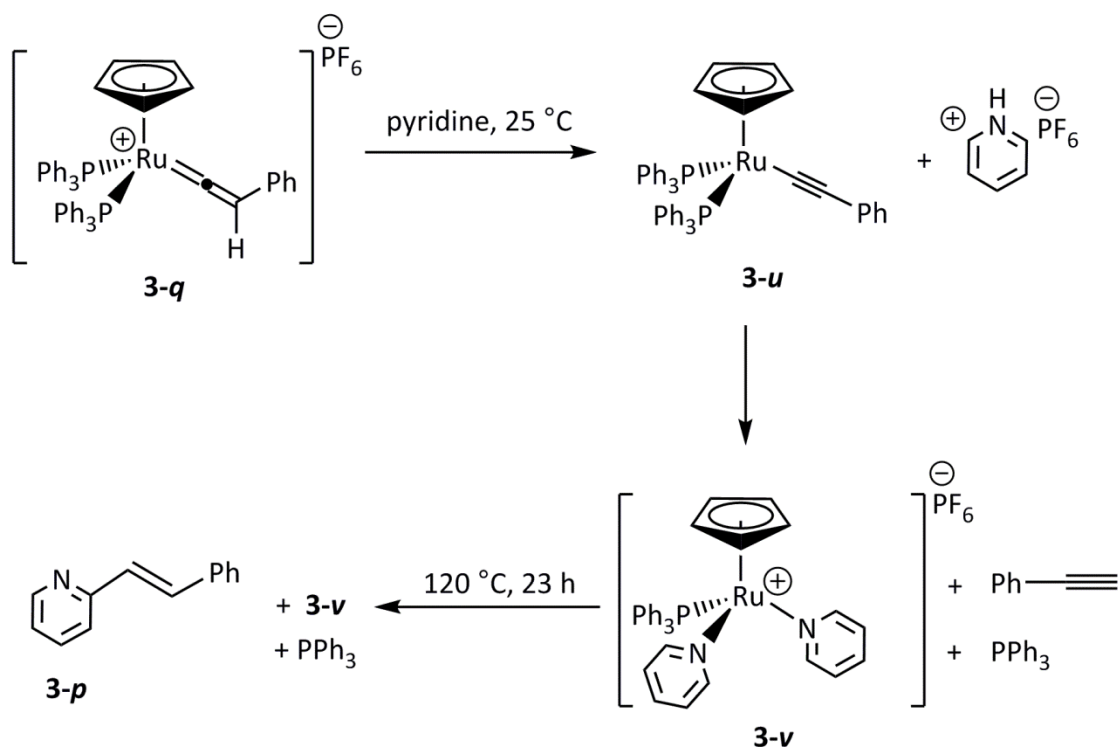
Scheme 3.5 The addition of pyridine to vinylidene complex 3-*q* and subsequent reactivity with phenylacetylene (3-*q* later referred to as [28^{Ph}]PF$_6$, 3-*u* as [26^{Ph}], 3-*v* as [7]PF$_6$ and 3-*p* as 14)

This finding allowed the reaction to be conducted at a lower temperature of 50 °C, which was not only beneficial in terms of energy requirements but also inhibited the dimerisation of terminal alkynes under catalytic conditions. Therefore it was no longer necessary to employ TMS-protected alkynes in the reaction, affording 100 % atom efficiency.

The experimental investigations also revealed that the reaction between complex **3-*v*** and terminal alkynes exhibited a marked solvent dependence. In contrast to the analogous reaction in pyridine solution, on addition of a terminal alkyne to a solution of the complex in dichloromethane and heating at 50 °C for 16 hours, no conversion was observed to the organic product. Instead, the major organometallic product was shown to be **3-*w***, Scheme 3.6.
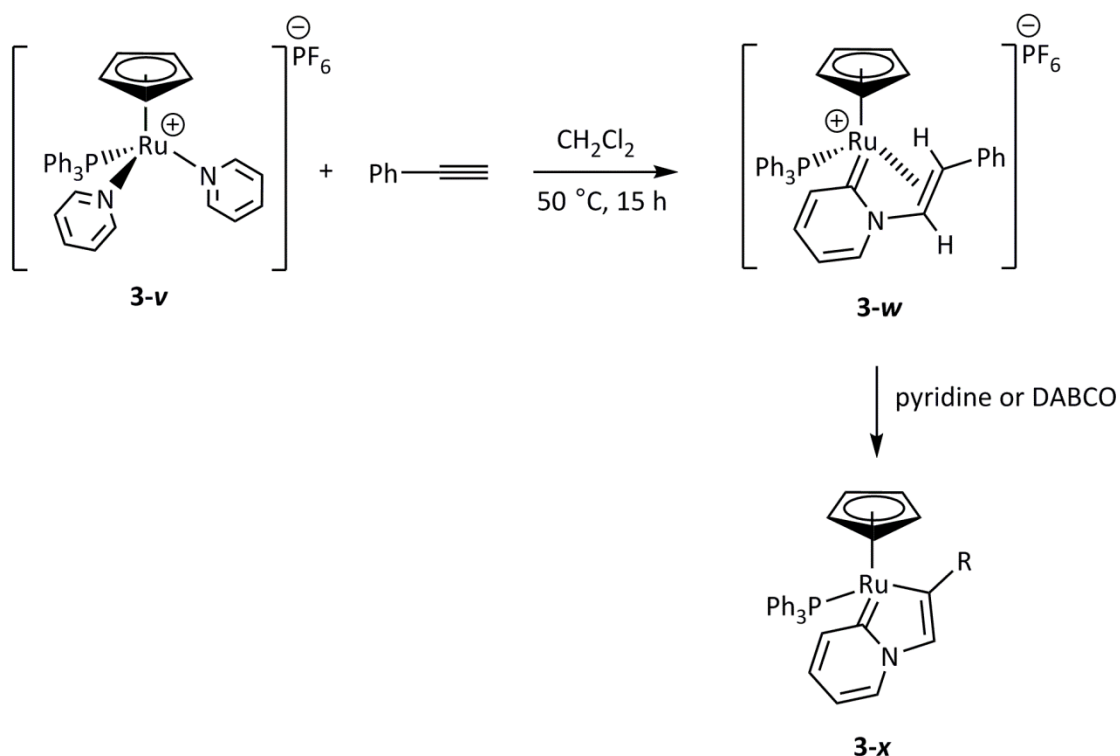
Scheme 3.6 Reactivity of 3-*v* with phenylacetylene in dichloromethane (3-*v* later referred to as [7]PF$_6$, 3-*w* as [13]PF$_6$ and 3-*x* as [16])

This result can be explained by examination of several of the key steps in the reaction mechanism, Scheme 3.7.[45] In this mechanism, the addition of a terminal alkyne to complex **3-*v*** affords vinylidene complex **3-*r*** The pyridine substrate can then attack at the vinylidene α-carbon to form vinyl complex **3-*y*** A subsequent loss of pyridine from the ruthenium centre and activation of the *ortho-* C-H bond of the pyridyl group on the vinyl ligand forms pyridylidene-hydride complex **3-*z*** Complex **3-*z*** is a catalyst 'branching point', from which successful catalysis can proceed or the catalyst is subject to deactivation. In the presence of pyridine, hydride intermediate **3-*z*** can be deprotonated and the reaction continues through a series of intermediates to produce the organic product, **3-*p*** and regenerate the active catalyst **3-*v*.** In the absence of pyridine, the deprotonation of pyridylidene-hydride **3-*z*** is thought to be very slow, the complex instead undergoes a hydride migration to form **3-*w*** and the catalyst is deactivated. DFT studies suggest that **3-*w*** is the kinetic product, and experimental studies confirm that harsh reaction conditions are required to liberate **3-*p*** after **3-*w*** is detected. However, although complexes **3-*w*** (and **3-*x***) are deactivation products for this particular catalytic system, they are important examples of pyridylidene-containing

species formed from non-activated starting materials of pyridine and phenylacetylene (discussed further in Chapters 1 and 4).
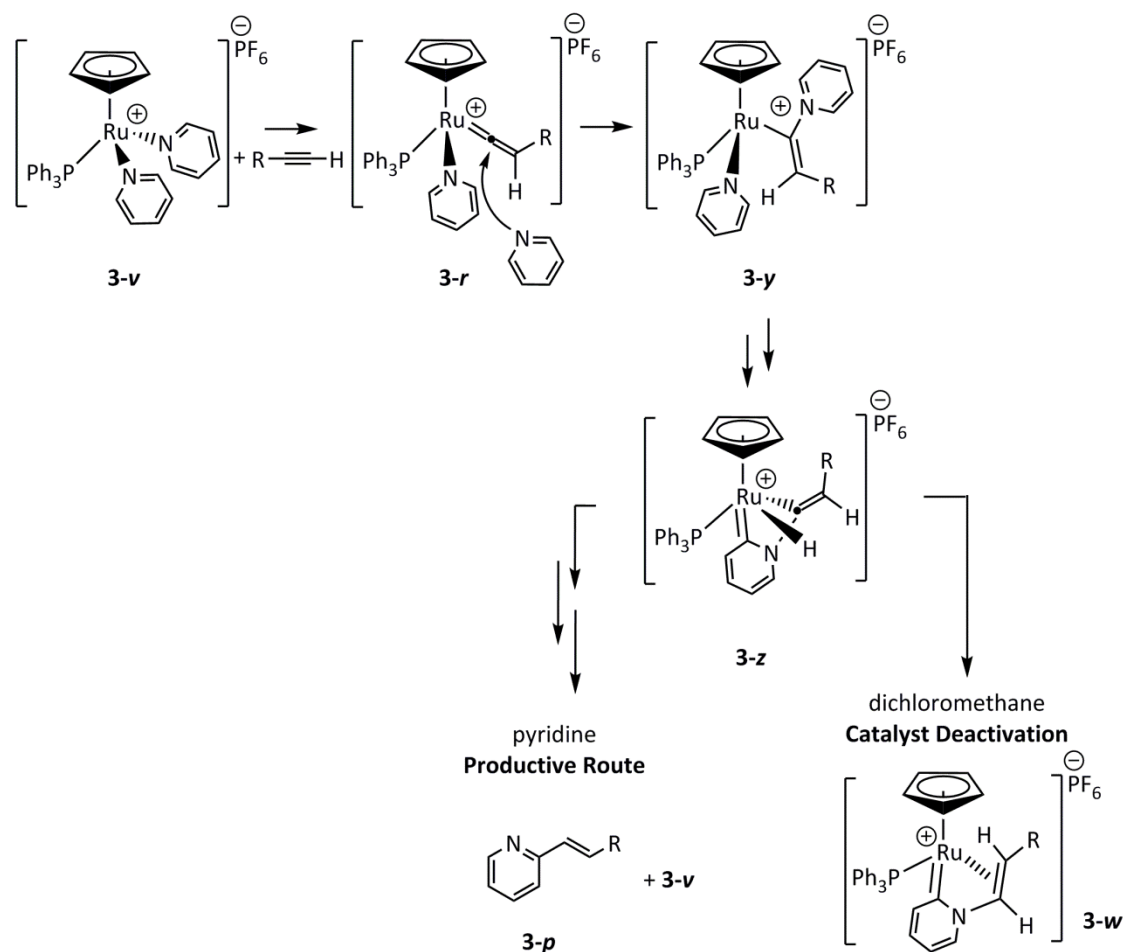
Scheme 3.7 Pyridine alkenylation mechanism proposed by Lynam and Slattery (3-*v* later referred to as [7]PF$_6$, 3-*r* as [11]PF$_6$, 3-*w* as [13]PF$_6$ and 3-*p* as 14)

Consequently, the mechanism given in Scheme 3.7 shows how the presence of excess pyridine is crucial for successful catalysis; pyridine must act as the substrate, reaction solvent and intermolecular proton transfer medium. However, to extend the substrate scope to a range of *N*-containing heterocycles, an alternative source of base is necessary. This could either be an external source of base, or the incorporation of an intramolecular base into the coordination sphere of the metal. If successful, this would retain the complete atom efficiency of the reaction and allow the heterocycle to act only as the substrate, hence increasing the scope of the reaction. An intramolecular base could also decrease the potential for side reactions and the formation of by-products.

3.1.4   Aims

In Chapter 2, the role of non-innocent phosphine ligands in anti-Markovnikov terminal alkyne hydration was examined by a combined experimental and computational study. Through intramolecular ligand-assistance *via* proton shuttle processes, lower energy barriers were observed for key steps in the reaction mechanism and therefore catalysis could operate under milder conditions.[56,118] A review of pyridyl- and imidazolyl- functionalised phosphine ligands in catalysis is provided in Chapter 2.

The work in this chapter describes the synthesis and reactivity of half-sandwich complexes containing pyridyl-functionalised phosphine ligands, and examines their influence in pyridine alkenylation mechanisms. The primary aim of using a pyridyl-functionalised ligand was to achieve intramolecular deprotonation of hydride complex **3-z**, Scheme 3.7, and hence prevent catalyst deactivation by the formation of complex **3-w**. If deprotonation of **3-z** could be achieved by the phosphine ligand, the necessity of excess base would be removed and therefore the catalyst could operate in solvents other than pyridine.

The work began with preliminary stoichiometric studies in order to understand the reactivity of the new ruthenium complexes with terminal alkynes (phenylacetylene and 2-ethynyl-α,α,α-trifluorotoluene) in the presence and absence of pyridine. The complexes were then trialled under catalytic conditions in order to observe any effect of the pyridyl-functionalised phosphine ligands in the catalytic alkenylation of pyridine.

3.2   Preparation of [Ru(η^5-C$_5$H$_5$)(PPh$_2$R)(NC$_5$H$_5$)$_2$]PF$_6$, [7]PF$_6$

3.2.1   Choice of phosphine ligands

Two phosphine ligands were selected for study as alternatives to PPh$_3$: 2-(1,1-dimethylpropyl)-6-(diphenylphosphino)pyridine (**b**) and diphenyl-2-pyridylphosphine (**c**).

Ph$_3$P   Ph$_2$P   Ph$_2$P

triphenylphosphine	2-(1,1-dimethylpropyl)-6-(diphenylphosphino)pyridine	diphenyl-2-pyridylphosphine
a	**b**	**c**
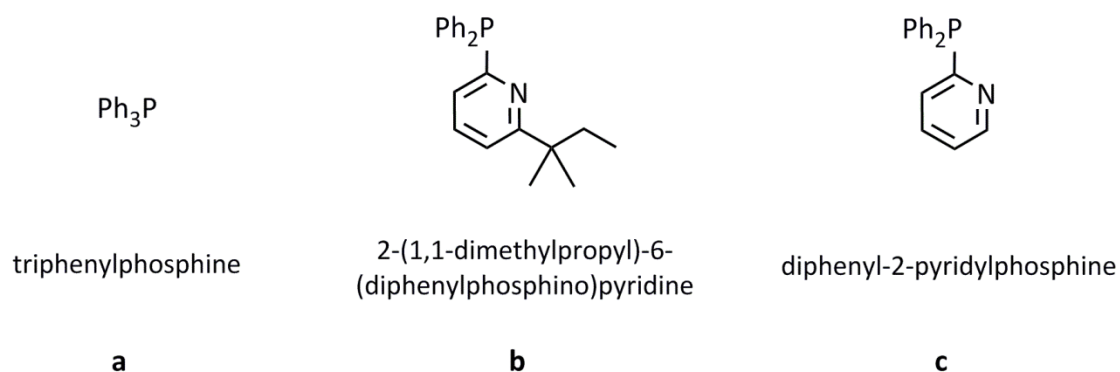
Figure 3.2 Structure of phosphine ligands a - c

The incorporation of ligands **b** and **c** into the complex [Ru(η^5-C$_5$H$_5$)(PPh$_2$R)(NC$_5$H$_5$)$_2$]PF$_6$, **[7]PF$_6$**, places an intramolecular base into the coordination sphere. Ligands of this type have been shown to play a non-innocent role in a range of catalytic processes and transformations (more detailed information can be found in the introduction to Chapter 2). Both **b** and **c** have similar electronic properties, but the increased steric bulk of **b** may lead to different reactivity and participation in catalysis compared with both **a** and **c**.

3.2.2   Synthesis of complexes [6]PF$_6$ and [7]PF$_6$

Complexes **[7]PF$_6$** were synthesised by modified literature methods.[45] The catalyst precursor complex **[2]PF$_6$**, [Ru(η^5-C$_5$H$_5$)(NCMe)$_3$]PF$_6$, contains three labile acetonitrile ligands that can be replaced under mild reaction conditions by the addition of stronger ligands, notably phosphorus- and nitrogen-containing donors. Therefore, on the addition of one equivalent of triphenylphosphine (**a**) and subsequent introduction of excess pyridine to complex **[2]PF$_6$**, the acetonitrile ligands can be substituted to create the active catalytic species **[7a]PF$_6$**, [Ru(η^5-C$_5$H$_5$)(**a**)(NC$_5$H$_5$)$_2$]PF$_6$. The generation of complexes **[7b]PF$_6$** and **[7c]PF$_6$** can be achieved by the replacement of triphenylphosphine, **a**, in this reaction scheme with the pyridyl-functionalised phosphine ligands, **b** and **c**, Scheme 3.8.
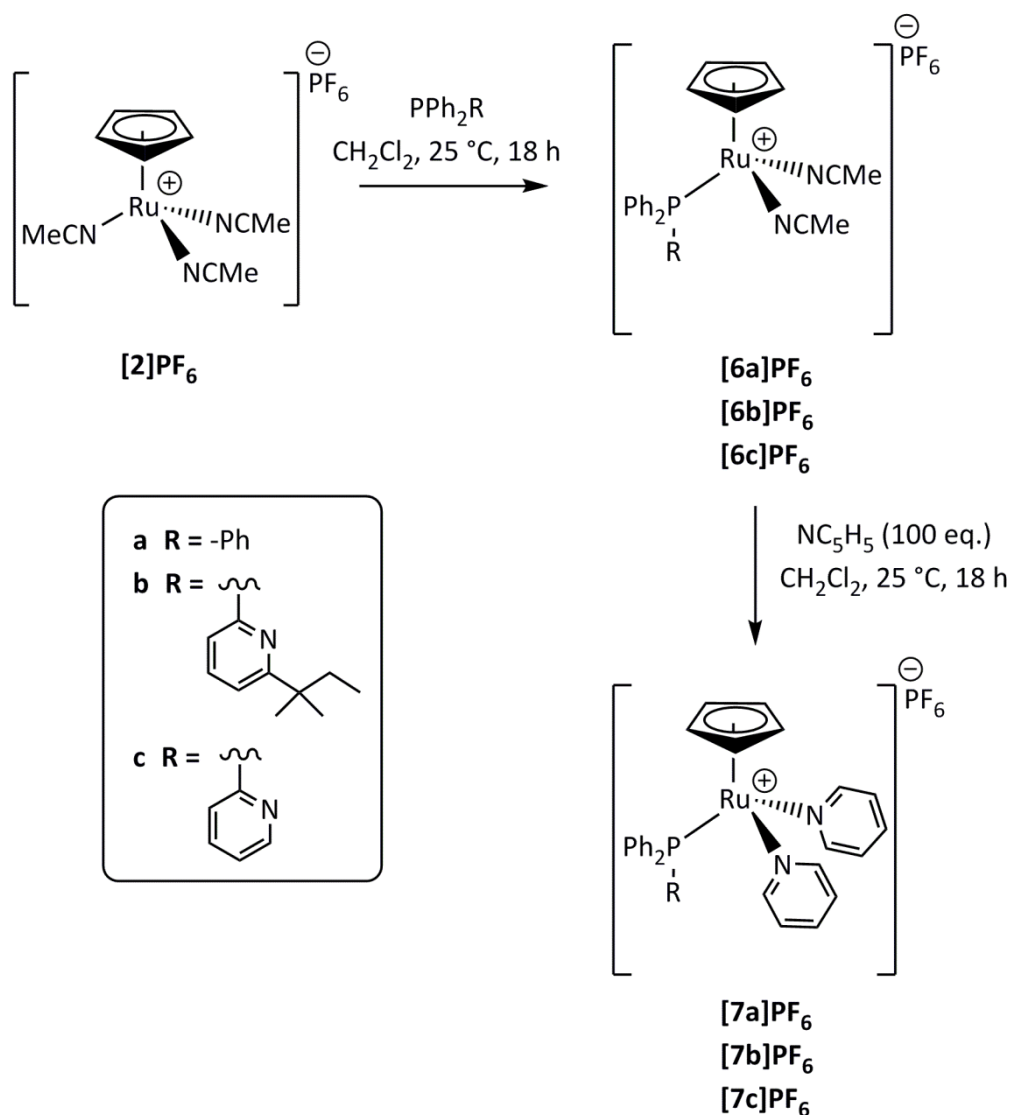
Scheme 3.8 Synthesis of complexes [6]PF$_6$ and [7]PF$_6$

Treatment of complex **[2]PF$_6$** with stoichiometric quantities of **a**, **b** and **c** resulted in a rapid reaction to generate **[6a]PF$_6$**, **[6b]PF$_6$** and **[6c]PF$_6$** in quantitative spectroscopic yields under mild conditions (25 °C, dichloromethane, 18 hours, Scheme 3.8). Careful control of phosphine stoichiometry was required in order to avoid the formation of *bis*-phosphine complexes [Ru(η^5-C$_5$H$_5$)(PPh$_2$R)$_2$(NCMe)]PF$_6$. The ^{31}P{^{1}H} NMR spectra for **[6a]PF$_6$**, **[6b]PF$_6$** and **[6c]PF$_6$** all exhibit signals for the PF$_6^-$ anion at -143.0 ppm which appears as a septet with a $^1J_{PF}$ of 711 Hz, and singlet resonances for the coordinated phosphine ligands at 50.2, 51.4 and 52.3 ppm respectively. In the ^{1}H NMR spectra, each complex shows a resonance for the cyclopentadienyl moiety with an integration of 5 protons at ~4.4 ppm and one resonance for the acetonitrile ligands that integrates to 6 protons at ~ 2.1 ppm. These data demonstrate the

coordination of two acetonitrile ligands per molecule and the similar ^{31}P{^{1}H} chemical shifts indicate similar structural and electronic properties. Both the ^{1}H and ^{31}P{^{1}H} spectra of complexes **[6c]PF$_6$** and **[7c]PF$_6$** were complicated by additional resonances (see Section 3.2.2.1).

The two remaining acetonitrile ligands within the coordination sphere of **[6]PF$_6$** may be replaced by the addition of excess pyridine (25 °C, 100 eq. pyridine, dichloromethane, 18 hours) to produce complexes **[7]PF$_6$** in high isolated yields, Scheme 3.8. On coordination of pyridine, the ^{31}P{^{1}H} resonances shift by less than 1 ppm in all cases and the resonances for the acetonitrile ligands in the ^{1}H NMR spectrum are replaced by those for coordinated pyridine. The most characteristic and easily distinguishable signals for **[7]PF$_6$** are for the pyridine *ortho*-protons which are the most downfield signals at ~ 8.5 ppm with an integration of 4 protons relative to the cyclopentadienyl ligand. The pure complexes can be isolated as orange crystals *via* the slow diffusion of pentane into dichloromethane solutions of **[7]PF$_6$**. The complexes were air sensitive and stored under a nitrogen atmosphere.

The synthesis can also be attempted with other *N*-containing heterocycles. Reaction of **[6a]PF$_6$** and **[6b]PF$_6$** with 2-methylpyridine leads to monosubstitution of an acetonitrile ligand to give complexes [Ru(η^5-C$_5$H$_5$)(PPh$_2$R)(NC$_6$H$_7$)(NCMe]PF$_6$, **[8a]PF$_6$** and **[8b]PF$_6$**. The lack of disubstitution is presumably due to steric overcrowding at the metal centre due to the position of the methyl group in the *ortho*- position of the pyridine ring.[160]

3.2.2.1 Bidentate coordination of c

The syntheses of complexes **[6c]PF$_6$** and **[7c]PF$_6$** are complicated by the presence of two products as shown by ^{1}H and ^{31}P{^{1}H} NMR spectroscopy. The ^{31}P{^{1}H} NMR spectra show two singlet resonances, indicating two phosphorus-containing organometallic species (**[6c]PF$_6$** and **[9c]PF$_6$**: 52.3, 1.6 ppm; **[7c]PF$_6$** and **[10c]PF$_6$**: 52.0, 2.8 ppm). The unusual upfield chemical shifts indicate a bidentate chelation mode *via* both the phosphorus and the nitrogen atom of the phosphine ligand, which has been previously observed in studies of similar complexes by the Grotjahn group and in complex **[3]PF$_6$** in Chapter 2.[18] The ^{1}H NMR spectrum containing **[6c]PF$_6$** and **[9c]PF$_6$** also shows the presence of two resonances in the cyclopentadienyl- region at 4.46 and 4.54 ppm which integrate with a ratio of 5:6 protons and 5:3 protons respectively relative to the bound acetonitrile protons. This indicates the

presence of two complexes with either two or one bound acetonitrile ligands, (**[6c]PF$_6$** and **[9c]PF$_6$** respectively, Figure 3.3).
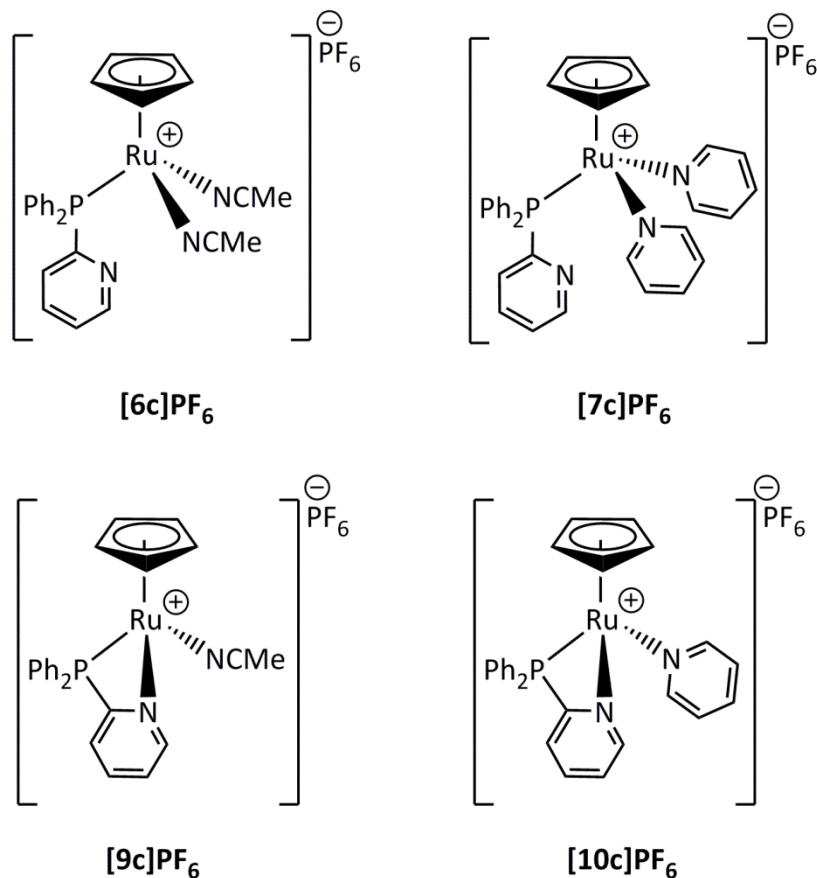
Figure 3.3 Monodentate and bidentate complexes [6c]PF$_6$, [7c]PF$_6$, [9c]PF$_6$ and [10c]PF$_6$

In order to obtain pure samples of complexes **[9c]PF$_6$** and **[10c]PF$_6$,** samples were placed under high vacuum conditions for 8 hours in order to eliminate an acetonitrile or pyridine ligand respectively. The procedure was successful for the conversion of **[6c]PF$_6$** to **[9c]PF$_6$** but not for the conversion of **[7c]PF$_6$** to **[10c]PF$_6$** demonstrating the superior lability of acetonitrile. On the addition of excess pyridine to an NMR sample of **[7c]PF$_6$** and **[10c]PF$_6$,** complete conversion to **[7c]PF$_6$** was achieved.

3.2.3   X-ray crystallography studies of complexes [7]PF$_6$

Crystals suitable for study by X-ray crystallography have previously been reported for [7a]PF$_6$,[45] and orange crystals of [7b]PF$_6$ and [7c]PF$_6$ could be obtained under similar crystallisation conditions by the slow diffusion of pentane into a dichloromethane solution of the complexes. The resulting structural determinations are shown in Figure 3.4 and Figure 3.5.
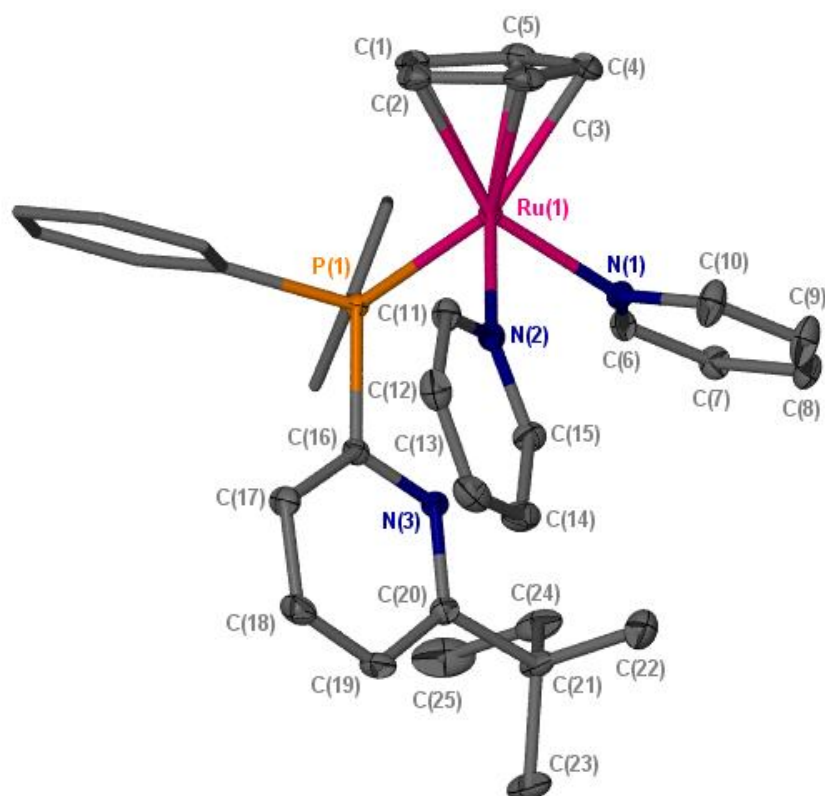
Figure 3.4 X-Seed diagram of the cation from complex [7b]PF$_6$. Hydrogen atoms and a PF$_6^-$ anion have been omitted for clarity, and where shown the thermal ellipsoids are at a 50 % probability level.
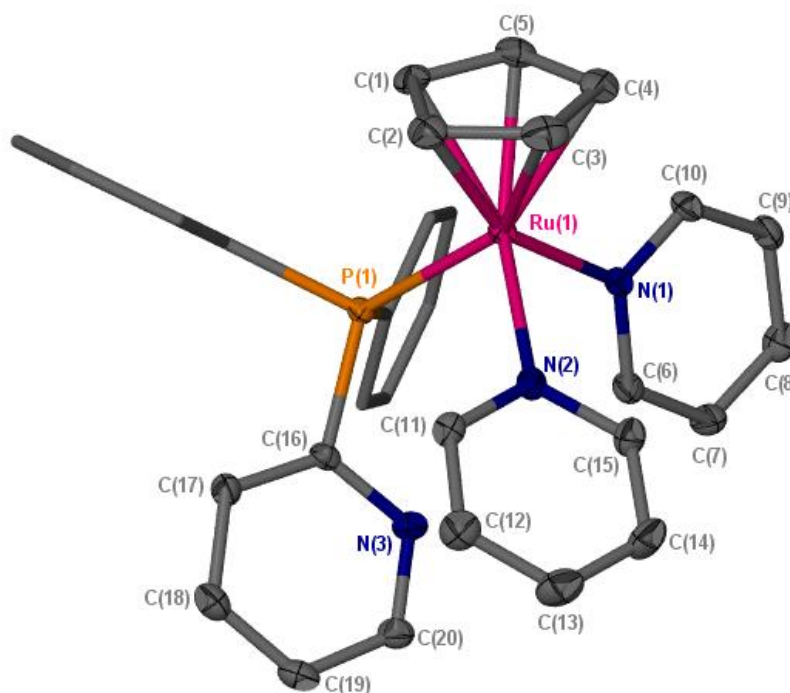
Figure 3.5 X-Seed diagram of the cation from complex [7c]PF$_6$. Hydrogen atoms and a PF$_6^-$ anion have been omitted for clarity, and where shown the thermal ellipsoids are at a 50 % probability level.

As has been noted previously from **[7a]$^+$**, the higher trans influence of the phosphine ligand in each of the complexes (in comparison to the pyridine ligands) leads to longer C(3)-Ru(1) and C(4)-Ru(1) bond lengths than the C(2)-Ru(1) and C(5)-Ru(1) distances, Table 3.1.

Surprisingly, **[7b]$^+$** and **[7c]$^+$** exhibit statistically identical Ru(1)-P(1) bond lengths which are both shorter than in **[7a]$^+$**. On first inspection, it may be expected that complex **[7b]$^+$** would have the longest Ru(1)-P(1) bond length due to the increased steric bulk of the phosphine ligand **b**. However, on examination of the structure of **[7b]$^+$** it can be observed that the bulky alkyl 1,1-dimethylpropyl chain of the phosphine is orientated away from the metal centre and therefore does not restrict the approach of the phosphorus atom to the metal.

In both **[7b]$^+$** and **[7c]$^+$**, the nitrogen atoms incorporated into the phosphine are orientated towards the centre of the complex. In **[7c]$^+$**, this can be justified by invoking the presence of a hydrogen bond between the pyridyl nitrogen N(3) and a C-H bond of a coordinated pyridine moiety (C(6)-H(6)). In **[7b]$^+$** there is no obvious hydrogen bonding interaction observable and so the orientation of the phosphine is less easily explained – one possible reason could be improved crystal packing with the phosphine in this position.

	Bond Lengths / Å		
	[7a]+	[7b]+	[7c]+
C(1) - Ru(1)	2.220(2)	2.168(2)	2.151(3)
C(2) - Ru(1)	2.182(2)	2.189(2)	2.171(4)
C(3) - Ru(1)	2.221(2)	2.216(2)	2.209(3)
C(4) - Ru(1)	2.220(2)	2.215(2)	2.215(4)
C(5) - Ru(1)	2.188(2)	2.179(2)	2.173(3)
N(1) - Ru(1)	2.1530(18)	2.1341(16)	2.156(3)
N(2) - Ru(1)	2.1293(19)	2.1570(17)	2.130(3)
P(1) - Ru(1)	2.3181(6)	2.3095(5)	2.311(8)
C(6) - N(1)	1.342(3)	1.341(2)	1.348(5)
C(10) - N(1)	1.351(3)	1.344(3)	1.349(4)
C(11) - N(2)	1.347(3)	1.352(3)	1.351(4)
C(15) - N(2)	1.351(3)	1.354(3)	1.343(4)
C(16) - N(3)	-	1.344(2)	1.342(4)
C(20) - N(3)	-	1.346(3)	1.340(4)

Table 3.1 Selected bond lengths for complexes [7]+

All three complexes show distorted octahedral geometries, evidenced by the deviation of N(2)-Ru(1)-N(1), N(1)-Ru(1)-P(1) and N(2)-Ru(1)-P(1) from 90 ° due to the higher steric bulk of the phosphine ligands **a-c** in relation to the pyridine groups, Table 3.2.

	Bond Angles / °		
	[7a]+	[7b]+	[7c]+
N(2) – Ru(1) – N(1)	88.12(7)	87.94(6)	89.64(11)
N(1) – Ru(1) – P(1)	91.04(5)	89.25(4)	89.29(8)
N(2) – Ru(1) – P(1)	97.35(5)	96.35(5)	91.63(8)

Table 3.2 Selected bond angles for complexes [7]+

3.3   Reactivity studies of complex [7]PF$_6$ with alkynes

The reactivity of complex **[7a]PF$_6$** has been studied extensively due to the use of this species as a successful pyridine alkenylation catalyst.[45] A detailed knowledge of the behaviour of **[7a]PF$_6$** with a range of alkynes and *N*-containing heterocycles allowed for rational optimisation of the catalytic conditions. Similar reactivity studies are explored in this chapter to investigate the influence of the pyridyl-functionalised phosphines **b** and **c**, and to see how the presence of the intramolecular base affects the reaction. Results will be compared to analogous reactions of **[7a]PF$_6$**.

3.3.1   General reaction conditions

A range of conditions were employed to explore the reaction between **[7b]PF$_6$** and **[7c]PF$_6$** with terminal alkynes. These include:

i.   Stoichiometric addition of phenylacetylene to complexes **[7]PF$_6$**

ii.   Stoichiometric addition of 4-ethynyl-α,α,α-trifluorotoluene to complexes **[7]PF$_6$**

iii. Stoichiometric addition of phenylacetylene to complexes **[7]PF$_6$** in the presence of two equivalents of pyridine

iv.   Stoichiometric addition of 4-ethynyl-α,α,α-trifluorotoluene to complexes **[7]PF$_6$** in the presence of two equivalents of pyridine

v.   Addition of two equivalents of alkyne to complexes **[7]PF$_6$**

vi.   Catalytic testing of **[7]PF$_6$** under pyridine alkenylation conditions

Reactions were all initially performed on an NMR scale (~ 20 mg of ruthenium complex). Reactions performed in the presence of additional pyridine tended to be slower presumably due to increased competition for coordination at the metal centre.

3.3.2   Reaction between complex [7b]PF$_6$ and phenylacetylene

Addition of one equivalent of phenylacetylene to **[7b]PF$_6$** in dichloromethane at room temperature resulted in an almost immediate colour change from yellow to red which indicated a rapid initial reaction, Scheme 3.9.
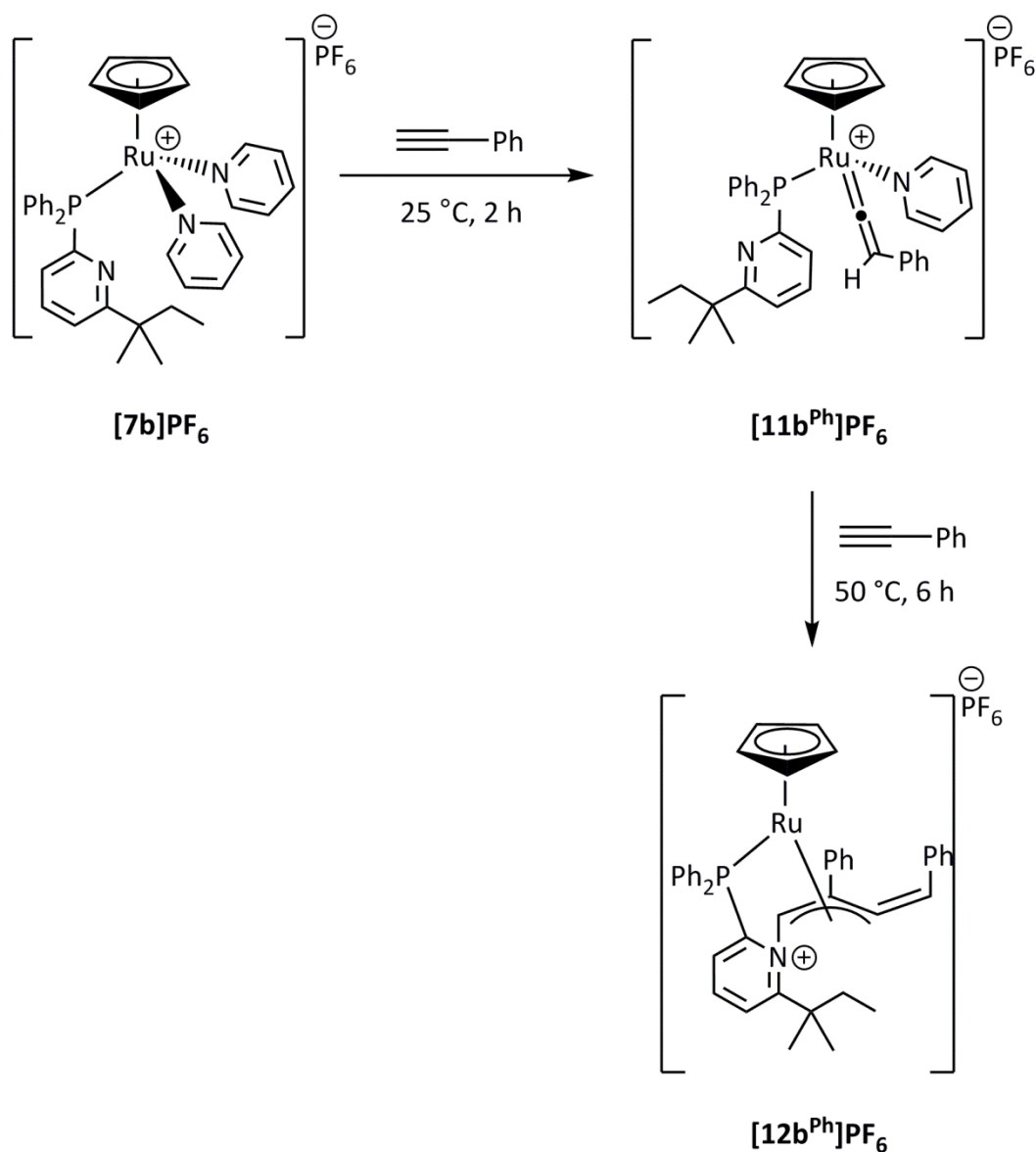
Scheme 3.9 Synthesis of complex [12b^{Ph}]PF$_6$

After one hour, ^{31}P{^{1}H} NMR spectroscopy showed the presence of unreacted **[7b]PF$_6$** and a new singlet resonance at 51.4 ppm. This was postulated to be vinylidene complex [Ru(η^5-C$_5$H$_5$)(**b**)(NC$_5$H$_5$)(C=C{H}Ph]PF$_6$,   **[11b^{Ph}]PF$_6$**,   based   on   comparison   with [Ru(η^5-C$_5$H$_5$)(**a**)(NC$_5$H$_5$)(C=C{H}Ph]PF$_6$, **[11a^{Ph}]PF$_6$**, which has a chemical shift of 51.8 ppm.

When the reaction was repeated with ^{13}C-labelled phenylacetylene, H^{13}C≡CPh, a change in multiplicity of the resonances was observed. The singlet at 51.4 ppm in the ^{31}P{^{1}H} NMR spectrum became a doublet with a $^2J_{PC}$ of 16.7 Hz. This coupling constant matched that of the enhanced ^{13}C{^{1}H} signal at 353.1 ppm – this chemical shift is characteristic of a vinylidene metal-bound carbon atom (the α-carbon).[50]

The NMR tube containing the reaction mixture was heated at 50 °C for three hours and the spectra recorded again. The ^{31}P{^{1}H} NMR spectrum still indicated the presence of **[7b]PF$_6$** and **[11b^{Ph}]PF$_6$** with a new singlet signal observed at 86.0 ppm due to **[12b^{Ph}]PF$_6$**. On the addition of a second equivalent of phenylacetylene and further heating for three hours at 50 °C, the reaction reached completion with the loss of resonances for **[7b]PF$_6$** and **[11b^{Ph}]PF$_6$** and the signal at 86.0 ppm becoming dominant. In the absence of pyridine in the reaction mixture, the reaction was very selective with small amounts of other unidentified products being formed. In the presence of two pyridine equivalents, the reaction was much less selective and produced a range of unidentified species.

In order to identify the new species at 86.0 ppm in the ^{31}P{^{1}H} NMR spectrum, **[12b^{Ph}]PF$_6$**, the reaction was repeated again with H^{13}C≡CPh. On the incorporation of the ^{13}C label, the signal at 86.0 ppm became a doublet of doublets with coupling constants of 14.7 and 7.2 Hz. This indicated that two ^{13}C-labelled phenylacetylene molecules had been incorporated into the complex. This was confirmed by high resolution ESI-MS of the reaction mixture which showed m/z values of 785.2543 ([Ru(η^5-C$_5$H$_5$)(**b**)(NC$_5$H$_5$)(H^{13}C≡CPh)$_2$]$^+$) and 706.2077 ([Ru(η^5-C$_5$H$_5$)(**b**)(NC$_5$H$_5$)(H^{13}C≡CPh)]$^+$).

Crystals of **[12b^{Ph}]PF$_6$** suitable for study by X-ray diffraction were obtained by the slow diffusion of pentane into a dichloromethane solution of the reaction mixture. The results of the structure determination are shown in Figure 3.6.
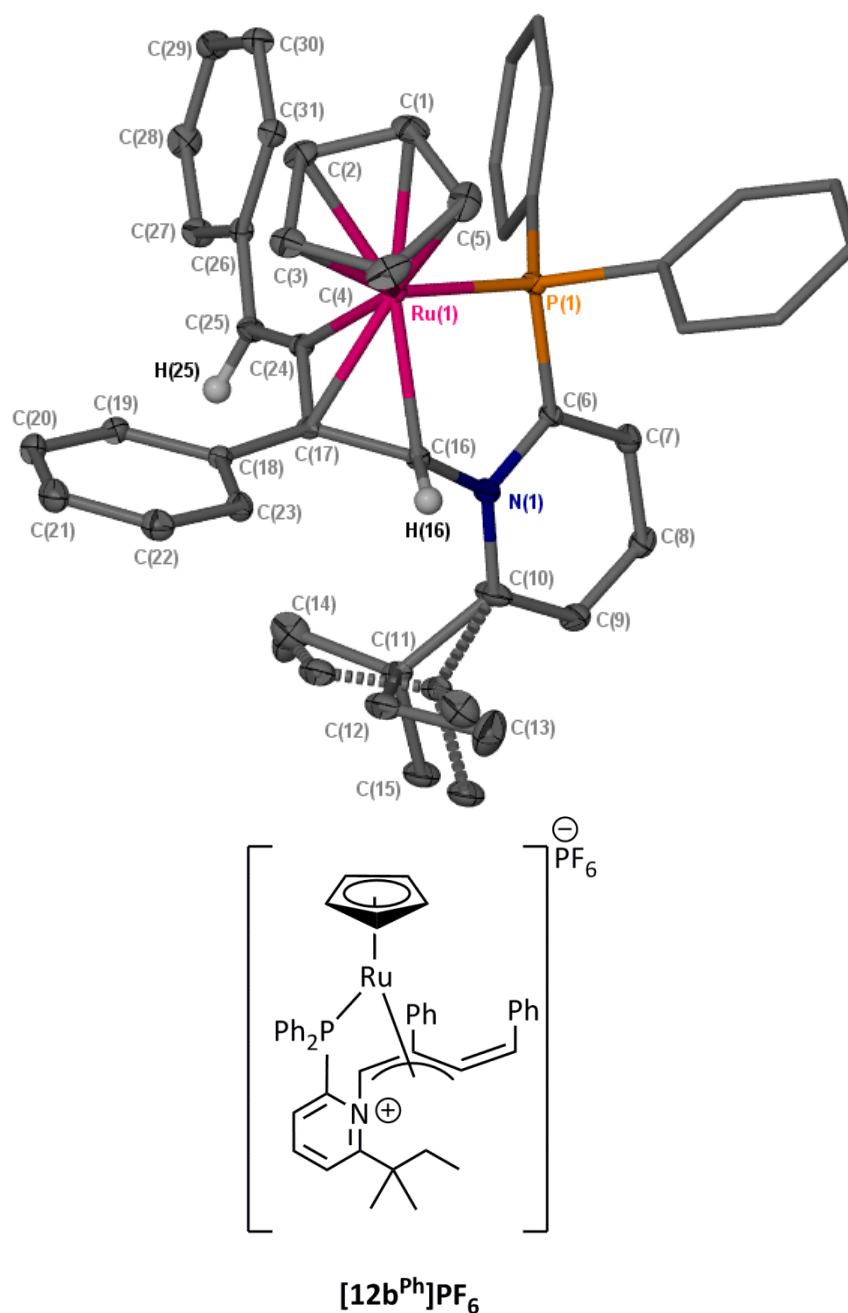
Figure 3.6 X-Seed diagram of the cation from complex [12b^{Ph}]PF$_6$. Most hydrogen atoms and a PF$_6^-$ anion have been omitted for clarity, and where shown the thermal ellipsoids are at a 50 % probability level.

This structure is directly comparable to an η^3-butadienyl complex reported previously by the Lynam and Slattery groups, complex **3-aa**, Figure 3.7.[45] The formation can be explained as a condensation reaction between two phenylacetylene and one pyridine molecule to form the coordinated η^3-butadienyl moiety. In the case of **[12b^{Ph}]PF$_6$**, an analogous reaction has occurred, only now the pyridine group is part of the coordinated phosphine ligand **b**.
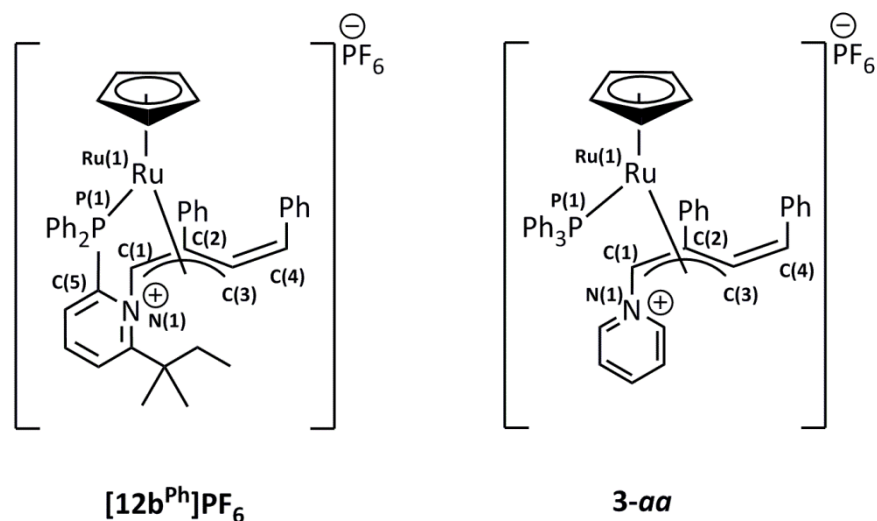
Figure 3.7 Comparison of complex [12b^{Ph}]PF$_6$ and structurally similar complex 3-*aa*

In both cases (**[12b^{Ph}]PF$_6$** and **3-*aa***, Figure 3.7) the pyridinium butadienyl fragment consists of an allyl moiety bound asymmetrically to the ruthenium centre though three carbon-ruthenium interactions in an η^3-binding mode. Both complexes contain an exo-vinyl group which is oriented away from the metal centre, allowing negligible interaction between Ru(1) and the vinylic carbon atom, C(4).

As has been noted previously for a range of η^3-butadienyl complexes, the ruthenium-carbon bond lengths vary across the allyl group. The Ru(1)-C(3) bond lengths in both **[12b^{Ph}]$^+$** and **3-*aa*** are significantly shorter than Ru(1)-C(1) and Ru(1)-C(2), Table 3.3. This trend has been reported by Bruce *et al* who found that this behaviour is most evident for complexes where the substituent on C(4) is strongly electron withdrawing, which would be accompanied by an elongation of C(3)-C(4).[161] Conjugation of the η^3-cyclobutadienyl moieties of both **[12b^{Ph}]$^+$** and **3-*aa*** are highlighted by the similar C(1)-C(2) and C(2)-C(3) bond lengths, which supports the delocalisation of the pi-electrons across the allyl groups.[161-162] The asymmetrical bonding of the η^3-cyclobutadienyl fragment to the metal indicates partial carbenoid character in the Ru(1)-C(3) bond and therefore a contribution from a zwitterionic form, Scheme 3.10.
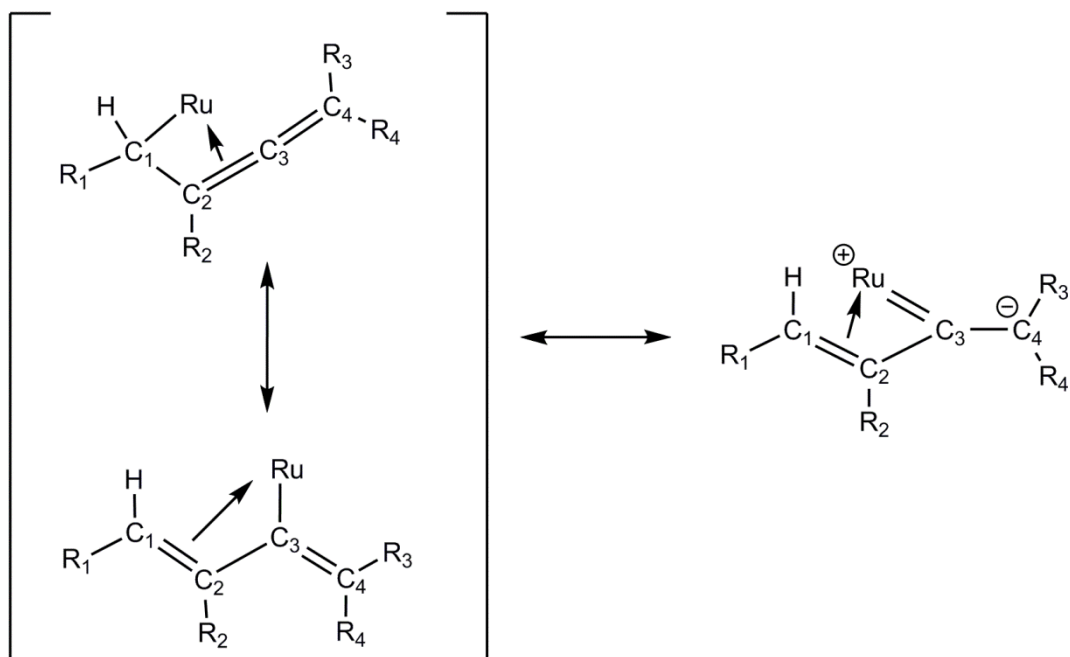
Scheme 3.10 Zwitterionic form of ruthenium η^3-cyclobutadienyl complexes (right)

However, both the bond length and the orientation of the vinyl group, -C(3)=C(4)H{C$_6$H$_5$}, suggests that this moiety is not involved in conjugation with the η^3-cyclobutadienyl ligand – the C(3)-C(4) bond length is shorter than the carbon-carbon bonds of the allyl group, consistent with a higher degree of double bond character, and the vinyl moiety is also bent out of the plane of the allylic group, Table 3.3. This suggests that the pi orbitals of the vinylic system are not in resonance with the pi orbitals of the allyl group. These observations are consistent with those of Brisdon and Walton on a range of similar 1,2,3-butadienyl complexes,[163] and with their DFT calculations[164] which concluded that the presence of two independent pi-systems in these complexes led to higher stability than full conjugation.

	Bond Lengths / Å			Bond Angles / °	
	3-*aa*	**[12b^Ph]+**		**3-*aa***	**[12b^Ph]+**
C(1) – C(2)	1.427(10)	1.444(2)	**C(1) – Ru(1) – P(1)**	97.87(18)	80.90(4)
C(2) – C(3)	1.432(9)	1.432(2)	**C(3) – Ru(1 – P(1)**	94.03(18)	90.09(4)
C(3) – C(4)	1.344(9)	1.337(2)	**N(1) – C(1) – C(2)**	119.8(6)	118.95(12)
Ru(1) – C(1)	2.141(9)	2.1436(15)	**C1 – C(2) – C(3)**	116.1(6)	112.13(13)
Ru(1) – C(2)	2.142(7)	2.1068(15)	**C(2) – C(3) – C(4)**	134.3(6)	137.20(15)
Ru(1) – C(3)	2.086(7)	2.0754(14)	**Ru(1) – P(1) – C(5)**	-	106.02(5)
N(1) – C(1)	1.495(9)	1.514(2)	**P(1) – C(5) – N(1)**	-	115.65(11)
Ru(1) – P(1)	2.3535(18)	2.2241(4)	**C(5) – N(1) – C(1)**	-	116.21(13)
P(1) – C(5)	-	1.8156 (14)			
C(5) – N(1)	-	1.362(2)			

Table 3.3 Selected bond lengths and angles for complex [12b^Ph]PF$_6$ and 3-*aa* (atom labelling shown corresponds to Figure 3.7)

3.3.3 Reaction between complex [7b]PF$_6$ and 4-ethynyl-α,α,α-trifluorotoluene

The reaction between **[7b]PF$_6$** and alkyne was repeated with 4-ethynyl-α,α,α-trifluorotoluene as an alternative alkyne to phenylacetylene. The presence of the trifluoromethyl group on the aromatic ring promotes a strongly electron withdrawing influence by induction (Hammett parameter for a *para-* trifluoromethyl group = +0.54 compared to only +0.06 for a *para-*fluorine substituent). Therefore a change in reactivity is possible between the two alkynes.

On the addition of one equivalent of 4-ethynyl-α,α,α-trifluorotoluene to complex **[7b]PF$_6$**, after heating at 50 °C for 2 hours the ^{31}P{^{1}H} NMR spectrum showed two signals – a singlet resonance for **[7b]PF$_6$** at 52.2 ppm and a new singlet resonance at 50.4 ppm; this was believed to be a vinylidene intermediate **[11b^CF3]PF$_6$**, Scheme 3.11. The ^{1}H NMR spectrum showed a major new resonance at 4.98 ppm for the cyclopentadienyl proton. The analogous vinylidene complex with triphenylphosphine, [Ru(η^5-C$_5$H$_5$)(**a**)(NC$_5$H$_5$)(C=C{H}C$_6$H$_4$-4-CF$_3$]PF$_6$ (**[11a^CF3]PF$_6$**), exhibits a broad ^{31}P{^{1}H} NMR signal at 51.0 ppm and characteristic resonances in the ^{1}H NMR spectrum - the cyclopentadienyl resonance appears at 5.53 ppm and the vinylidene proton as a broad signal at 5.17 ppm with a relative integration of 5:1 protons. The broadness of these peaks could be attributed to the reversible protonation and

deprotonation of the vinylidene proton to form the corresponding acetylide complex $[Ru(\eta^5\text{-}C_5H_5)(a)(NC_5H_5)(\text{-}C{\equiv}C\text{-}C_6H_4\text{-}4\text{-}CF_3)]$.

After further heating for twelve hours, both of these signals were no longer observed and replaced with a single peak at 52.0 ppm. The ^1H NMR spectrum indicated only one organometallic species was present as only one signal in the cyclopentadienyl region at 4.98 ppm was observed.
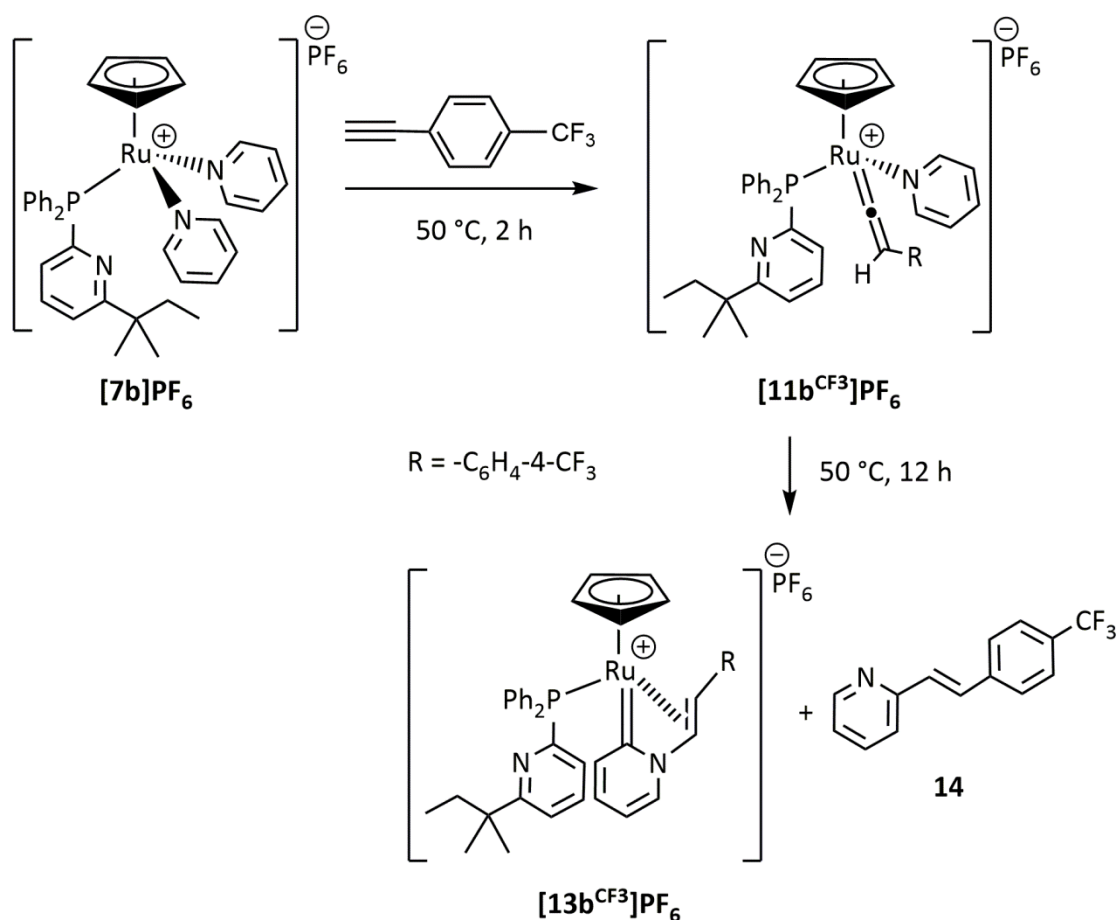
Scheme 3.11 Synthesis of complex [13b^{CF3}]PF$_6$

A high resolution ESI-MS of the reaction mixture showed only one peak for a ruthenium-containing species with an *m/z* of 749.1843, and a second ion at *m/z* of 250.0858 which corresponded to the mass of the protonated organic product of pyridine mono-alkenylation, **14**. Single crystals of the organometallic product were grown by layering the reaction mixture in dichloromethane with pentane. The structural determination showed that the pyridylidene complex **[13b^{CF3}]PF$_6$** had been formed – analogous to the deactivation product

reported previously in the reaction with **[7a]PF$_6$**. The NMR signals are also consistent with the PPh$_3$ analogue, **[13a^{CF3}]PF$_6$**.
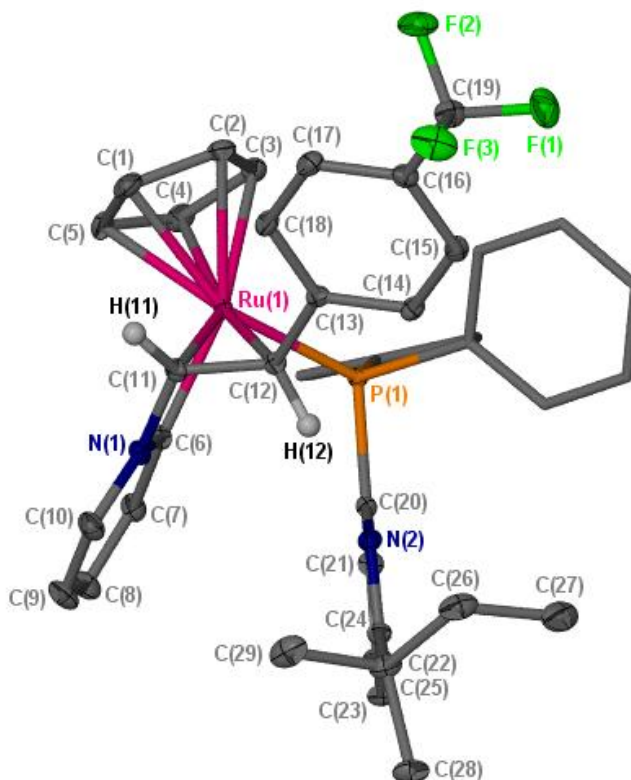
Figure 3.8 X-Seed diagram of the cation from complex [13b^{CF3}]PF$_6$. Most hydrogen atoms and a PF$_6^-$ anion have been omitted for clarity, and where shown the thermal ellipsoids are at a 50 % probability level.

	Bond Lengths / Å
Ru(1) – C(6)	2.0337(15)
Ru(1) – C(11)	2.1467(15)
Ru(1) – C(12)	2.2628(14)
Ru(1) – P(1)	2.3159(4)
C(11) – C(12)	1.408(2)
H(12) – N(2)	2.348*

Table 3.4 Selected bond lengths for [13b^{CF3}]$^+$

Selected bond lengths for **[13b^CF3]^+** are displayed in Table 3.4. The Ru(1) - C(6) bond length of 2.0337(15) Å is consistent with a pyridylidene complex, and the structure is directly comparable to the PPh$_3$ analogues with both phenylacetylene and 4-ethynyl-α,α,α-trifluorotoluene (**[13a^Ph]^+** and **[13a^CF3]^+** respectively) published in earlier work by the Lynam and Slattery groups.[45] The Ru(1) − C(6) bond length is shorter than related ruthenium cyclopentadienyl complexes with coordinated phenyl groups; in these cases, metal-carbon bond lengths range between 2.06 and 2.10 Å.[45] NBO (natural bond order calculations, explained in Appendix 2) analysis of **[13a^Ph]^+** also indicated metal-carbon double bond character, and as this structure is very similar to that of **[13a^Ph]^+**, this would be a valid conjecture for Ru(1) - C(6). The C(11) - C(12) bond length of 1.408(2) is consistent with the length of the aromatic bonds in the ligand, suggesting double bond character and involvement in the conjugated system. Hydrogen atoms were placed using a 'riding model', and so an exact bond length between H(12) and N(2) was not obtainable but it was estimated to be approximately 2.348 Å. This indicates a hydrogen-bonding interaction between these atoms, which also explains the unusual chemical shift of this proton in the ^{1}H NMR spectrum (Section 3.3.3.1).

The structure of **[13b^CF3]^+** contains a *trans*-alkene moiety between C(11) and C(12). Three-bond coupling constants between *trans*-alkene protons typically fall between 12 and 16 Hz, and so the observed $^3J_{HH}$ between H(11) and H(12) of only 8.0 Hz is lower than expected. This can be explained by metal-to-ligand back bonding, with electron density donated from a full metal d-orbital to the empty π* orbital of the coordinated alkene moiety. This weakens the bonding between the carbon atoms and reduces the level of hybridisation from sp^2 to sp^3, leading to poorer orbital overlap and hence a lower coupling constant between the protons. This can also be evidenced by the C(11) − C(12) bond lengths. A typical carbon sp^2-sp^2 bond length is around 1.34 Å.[165] In **[13b^CF3]^+**, the C=C bond length is considerably longer at 1.408(2) Å. The increased bond length in **[13b^CF3]^+** indicates the synergic interaction of the alkene moiety and the metal centre − both donation of electron density from the full alkene pi-bonding orbital to an empty metal d-orbital, and acceptance of electron density from a metal d-orbital into the alkene pi-antibonding orbital leads to reduced interaction of the orbitals and therefore the lower coupling constant. The C=C bond in **[13a^CF3]^+** is statistically identical at 1.411(4) Å and protons H(11) and H(12) also show a lower than expected *trans*-alkene coupling of 7.9 Hz.

3.3.3.1 Low temperature NMR study of complex [13b^{CF3}]PF$_6$

Crystals of **[13b^{CF3}]PF$_6$** were isolated and NMR spectra recorded. The spectra showed notable differences to those of **[13a^{Ph}]PF$_6$** and **[13a^{CF3}]PF$_6$**. At room temperature, no clear characteristic alkene proton signal corresponding to H(12) could be observed, Figure 3.9.
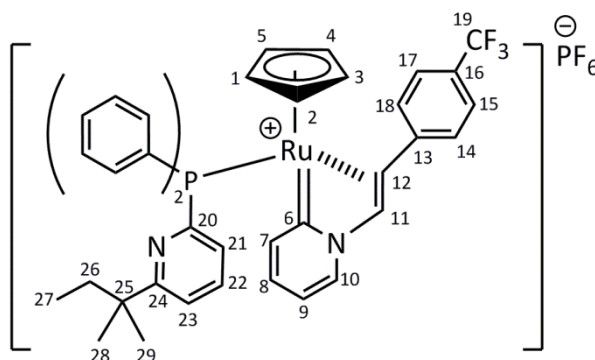
Figure 3.9 Structure of complex [13b^{CF3}]PF$_6$

In order to observe the resonance for proton H(12), the sample was subjected to low VT NMR to 215 K, decreasing the temperature in 20 K intervals as shown in Figure 3.10.
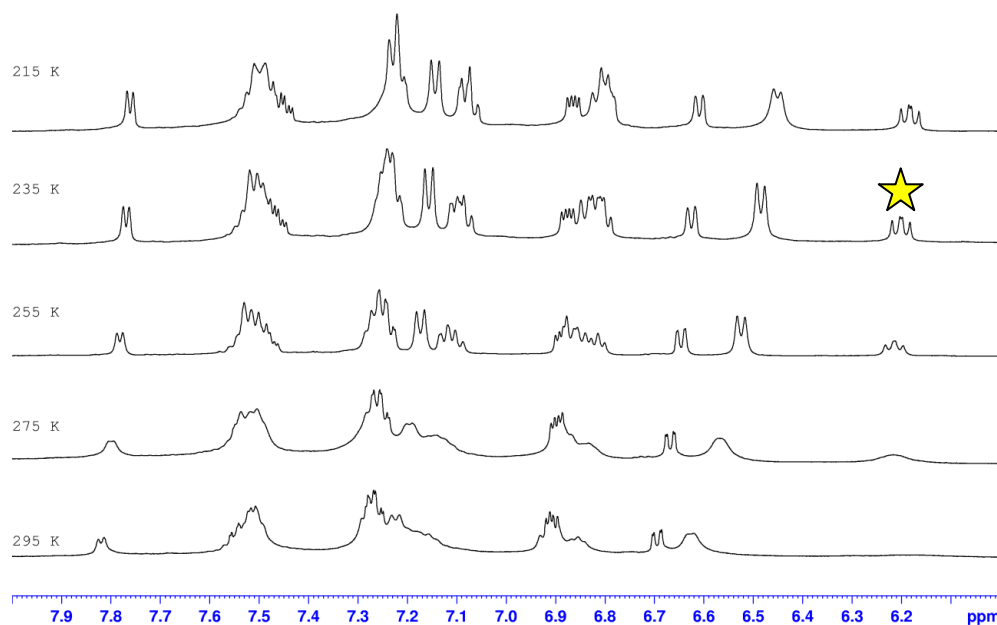
Figure 3.10 Low VT ^{1}H NMR spectra of complex [13b^{CF3}]PF$_6$ (aromatic region only)

At the lowest temperature of 215 K, the proton corresponding to H(12) became visible at 6.20 as a doublet of doublets (coupling constants of $^3J_{HP}$ = 10.3 Hz and $^3J_{HH}$ = 8.0 Hz). Through a 2D ^{1}H-^{1}H COSY experiment, this signal coupled to a doublet with the same coupling

constant at 6.63 ppm; this was therefore assigned as H(11). As H(12) could only be observed at low temperature, this suggests fluxionality within the complex. This is possibly due to the hydrogen bond between H(12) and N(2); at low temperatures, the motion of the phosphine ligand is reduced sufficiently to allow this hydrogen bonding proton to be detected.

The chemical shift of H(12) was very different to that of the analogous triphenylphosphine complexes, **[13a^{Ph}]PF$_6$** and **[13a^{CF3}]PF$_6$**, which appear at 3.60 and 3.65 ppm respectively (although with very similar coupling constants of $^3J_{HP}$ = 11.4 Hz and $^3J_{HH}$ = 7.9 Hz for **[13a^{CF3}]PF$_6$**). On closer inspection of the crystal structure (Figure 3.8), this could be explained by the presence of a hydrogen bond between the nitrogen of the phosphine and H(12) in **[13b^{CF3}]PF$_6$** which has altered the position of this signal in the NMR.

The reaction of **[7b]PF$_6$** with stoichiometric 4-ethynyl-α,α,α-trifluorotoluene and no extra pyridine equivalents also generated **[13b^{CF3}]PF$_6$** as the major product, but this was produced less cleanly, with a wider range of unidentified side products in the ^{31}P{^{1}H} NMR spectrum, at higher concentrations. By comparison of ^{31}P{^{1}H} chemical shifts, a small singlet resonance with a chemical shift of 84.7 ppm may correspond to **[12b^{CF3}]PF$_6$**.

3.3.4 Reaction between complex [7c]PF$_6$ with phenylacetylene or 4-ethynyl-α,α,α-trifluorotoluene

On the addition of either phenylacetylene or 4-ethynyl-α,α,α-trifluorotoluene to complex **[7c]PF$_6$**, an immediate colour change was observed from bright yellow to dark green indicating initial rapid reactions were occurring. In the presence of two equivalents of pyridine the reactions were slightly slower as would be expected due to extra competition with the alkyne for coordination at the metal centre, but in all cases reactions reached completion at room temperature within three to twelve hours. This was very different to reactions of **[7b]PF$_6$**, which in some cases required long periods of heating at 50 °C to reach completion.

In reactions of **[7c]PF$_6$** with either alkyne, high resolution ESI-MS indicated that analogous products were being formed. A single ruthenium containing ion with an *m/z* ratio which matched [Ru(η^5-C$_5$H$_5$)(**c**)(NC$_5$H$_5$)(alkyne)]$^+$ was observed. Therefore only one equivalent of alkyne was required for the reactions to reach completion. The reactions were also much more selective than with complex **[7b]PF$_6$**, and produced the new organometallic complex in high conversion, with only one signal observed by ^{31}P{^{1}H} NMR and one cyclopentadienyl

signal in the ^{1}H NMR spectra. In the ^{1}H NMR spectra, signals for the new cyclopentadienyl resonances could be observed at 4.58 and 4.62 ppm and ^{31}P{^{1}H} NMR spectra showed new resonances at 88.5 and 88.7 ppm for reactions with phenylacetylene and 4-ethynyl-α,α,α-trifluorotoluene respectively. The ^{31}P{^{1}H} NMR chemical shifts are very downfield with respect to the majority of ruthenium half-sandwich complexes discussed in this chapter but are reminiscent of those of **[12b^{Ph}]PF$_6$**, which immediately indicated a non-innocent role of phosphine **c** in the new complex.

In order to gain some insight into the complexes being formed, the reaction was repeated with ^{13}C-labelled phenylacetylene and a ^{13}C{^{1}H} NMR spectrum recorded in order to investigate which signal was enhanced. This experiment showed enhancement of a carbon signal at 190.5 ppm (d, $^2J_{CP}$ = 16.6 Hz). This downfield chemical shift and phosphorus-carbon coupling constant was indicative of a metal-bound carbon atom, and a ^{13}C-DEPT experiment showed that this signal was quaternary. The ^{31}P-^{13}C coupling constant suggested that this carbon atom was bound directly to the ruthenium, and X-ray diffraction studies confirmed the structure, **[15c^{Ph}]PF$_6$**, shown in Figure 3.11.
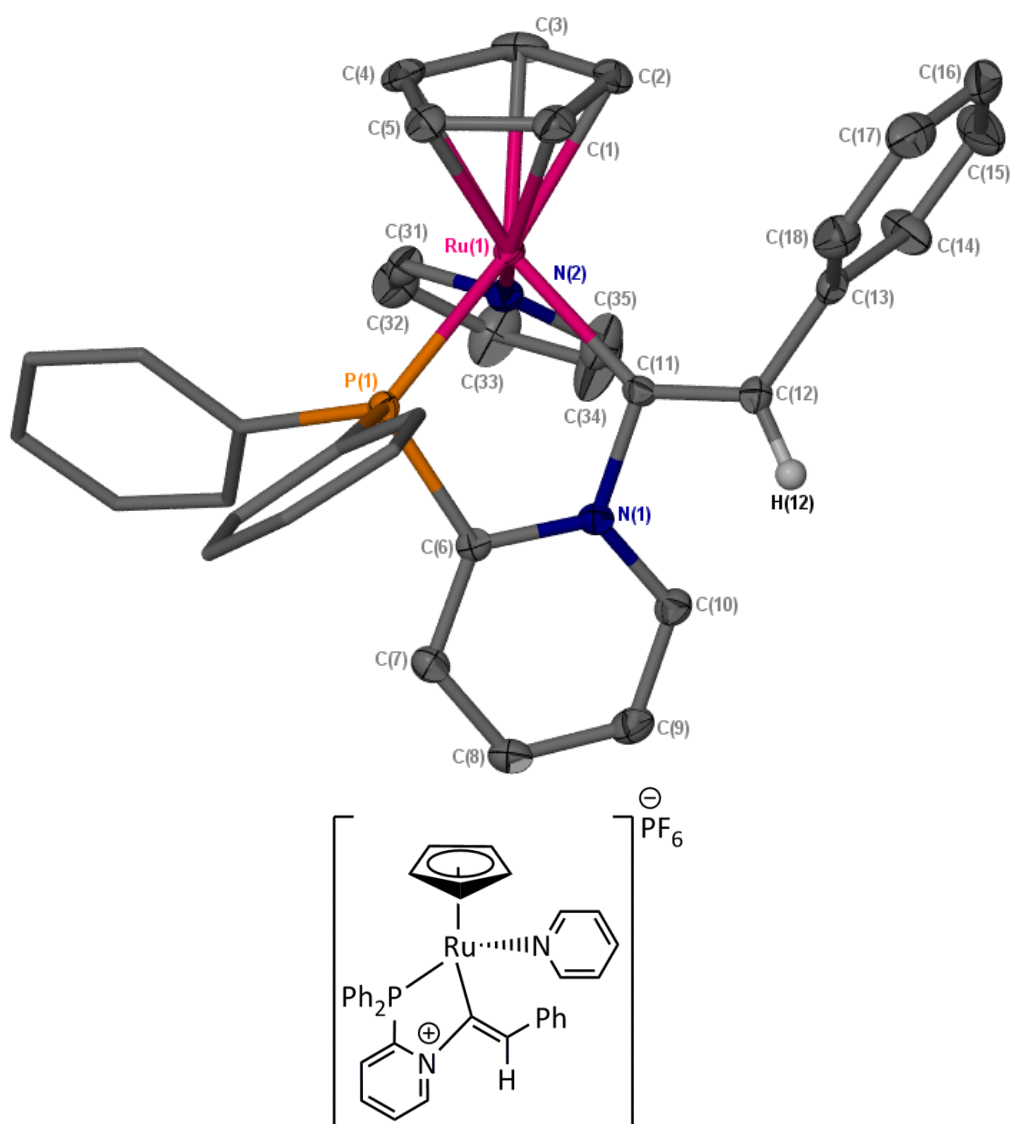
Figure 3.11 X-Seed diagram of the cation from complex [15c^{Ph}]PF$_6$. Most hydrogen atoms and a PF$_6^-$ anion have been omitted for clarity, and where shown the thermal ellipsoids are at a 50 % probability level.

The analogous structure with 4-ethynyl-α,α,α-trifluorotoluene is shown in Figure 3.12.
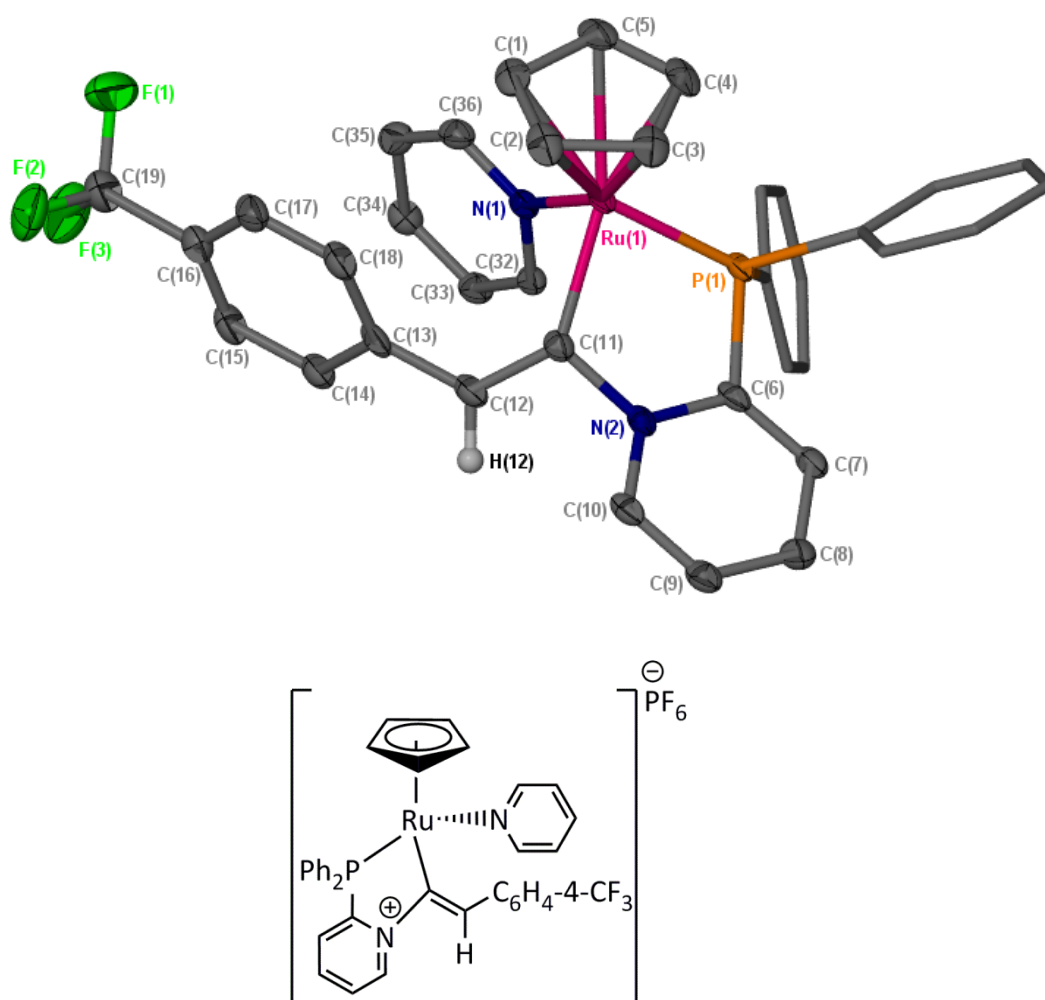
Figure 3.12 X-Seed diagram of the one of the cations from complex [15c^{CF3}]PF$_6$. The unit cell contains two statistically identical cations of [15c^{CF3}]$^+$ and only one has been displayed. Most hydrogen atoms, two PF$_6^-$ anions and two dichloromethane molecules of crystallisation have been omitted for clarity. Where shown the thermal ellipsoids are at a 50 % probability level.

It is interesting to note the differences between these two structures. In **[15c^{Ph}]PF$_6$**, both the pyridine ligand and phenyl group of the vinylidene are orientated in almost the same plane as the cyclopentadienyl ring. This means that the phenyl group of the vinylidene is not in conjugation with the pyridyl phosphine pyridine moiety. However, in **[15c^{CF3}]PF$_6$** both the pyridine ligand and the trifluorotoluene- ring of the vinylidene are twisted into the opposite plane to the cyclopentadienyl ligand. This increases the conjugation between the trifluorotoluene- ring with the pyridyl phosphine. The orientation of the phenyl groups on the pyridyl phosphine also differ between the two structures.

These structures support the mechanism of catalysis shown in Scheme 3.7. In Scheme 3.7, intermediate **3-y**, a pyridine molecule has attacked at the electrophilic α-carbon of the

vinylidene atom in **3-r**. In the postulated mechanism, there was no experimental evidence for this process and intermediate **3-y** was only supported by DFT studies. However, with the pyridine moiety incorporated into the structure of the phosphine, the α-carbon nucleophilic attack is intramolecular and as C-H activation cannot now proceed, **[15c]PF$_6$** may be isolated. (Other complexes which support the formation of **3-r** are **[44^{Ph}]BF$_4$** and **[45^{Ph}]NSI**, Chapter 5, in which fluorine incorporation at the vinylidene β-carbon allows isolation of the complexes after nucleophilic attack by pyridine).

Structures **[15c^{Ph}]PF$_6$** and **[15c^{CF3}]PF$_6$** can be compared to structures reported by Grotjahn, in which both pyridyl-and imidazolyl- phosphines were observed to undergo similar reactivities, and attack at the α-carbon of the vinylidene in *bis*-phosphine complexes, as shown in Figure 3.13.[18]
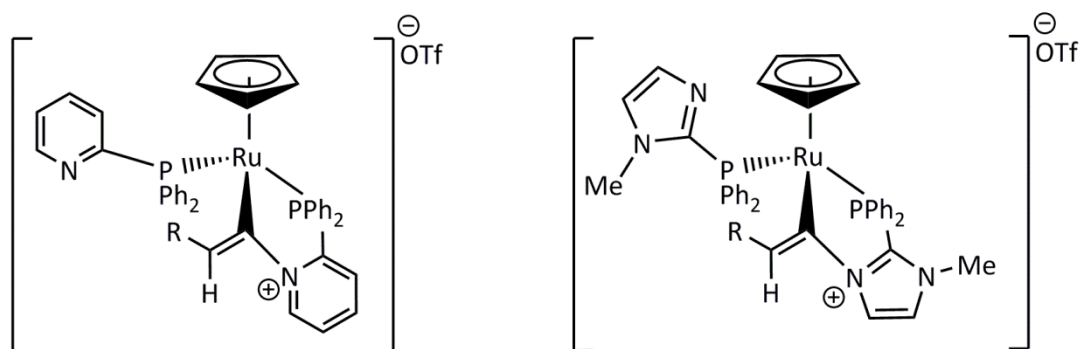
Figure 3.13 'Trapped' vinylidene structures with *bis* pyridyl- and imidazolyl- phosphines and 1-hexyne

3.4 Evaluation of complexes [7b]PF$_6$ and [7c]PF$_6$ as pyridine alkenylation catalysts

The primary purpose for the synthesis of complexes **[7b]PF$_6$** and **[7c]PF$_6$** was to provide alternatives to **[7a]PF$_6$** as catalysts for pyridine alkenylation. By incorporation of the pyridyl group into the structure of **[7]PF$_6$**, it was hoped that this would remove the need for excess base in the reaction mixture - the phosphine could act as an intramolecular base and disfavour formation of the catalyst deactivation product, **3-w** (Scheme 3.6). This would eliminate the use of pyridine as the reaction solvent and so increase the substrate scope of the system.

Using complex **[7a]PF$_6$** as a catalyst, the reported optimised conditions for pyridine mono-alkenylation were a 20 mol % catalyst loading of **[7a]PF$_6$** and one equivalent of alkyne with heating at 50 °C for 48 hours, which provided a 50 % yield of *E*-2-styryl pyridine, Scheme 3.12.

20 mol % **[7a]PF$_6$**

50 % yield of **14^R**
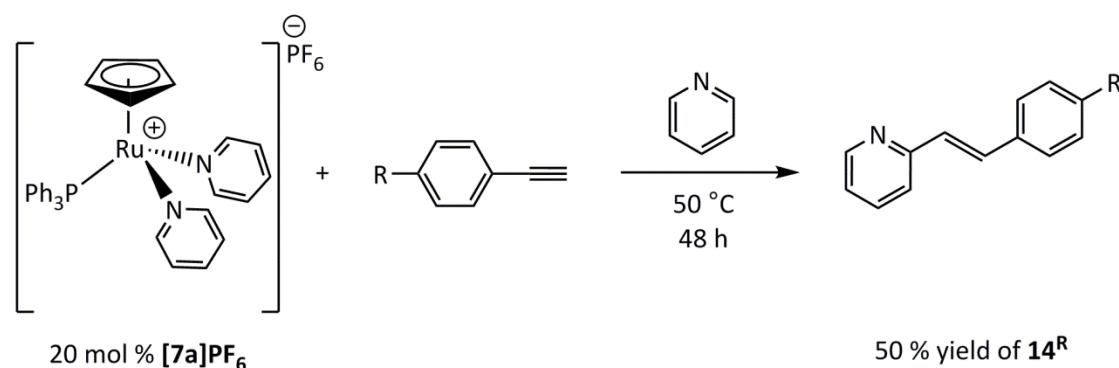
Scheme 3.12 Catalytic procedure for the formation of *E*-2-styryl pyridine and derivatives using complex [7a]PF$_6$

However, due to the intramolecular base incorporated into the structure of phosphines **b** and **c**, it was hypothesised that catalysts **[7b]PF$_6$** and **[7c]PF$_6$** should function in the absence of pyridine as the intermolecular proton transfer medium. Therefore, modified catalytic conditions were trialled in order to investigate this idea, Scheme 3.13, taken from a previous study of pyridine alkenylation.[159] Only twenty equivalents of pyridine were added to the reaction mixture – under these conditions, pyridine can primarily be considered as the substrate rather than the solvent of the reaction. 4-ethynyl-α,α,α-trifluorotoluene was selected as the alkyne substrate for the catalytic tests due to the facile determination of

conversion to **14^CF3** using ^{19}F NMR spectroscopy. Reactions were performed in a J. Young's NMR tube using CD_2Cl_2 as the solvent.
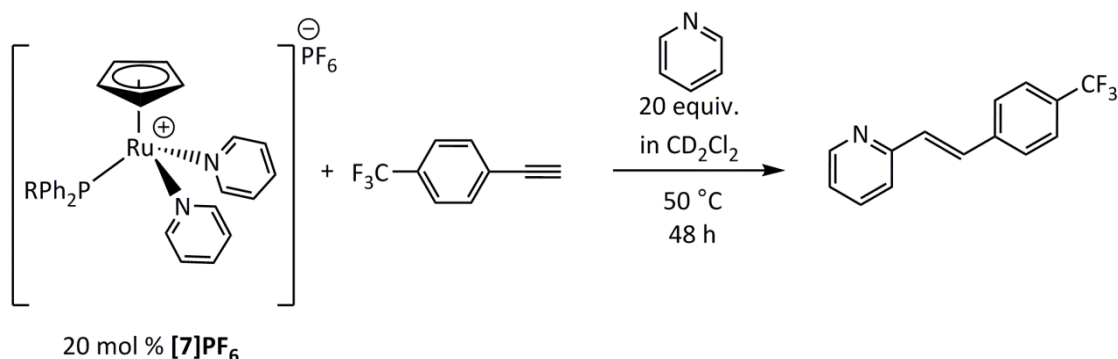
Scheme 3.13 Modified catalytic procedure for the testing of complexes [7b]PF$_6$ and [7c]PF$_6$

3.4.1   Catalytic testing of complex [7b]PF$_6$

Complex **[7b]PF$_6$** was investigated under the modified catalytic conditions shown in Scheme 3.13. The reaction mixture was heated at 50 °C for 12 hours, and NMR spectra recorded. The $^{31}P\{^1H\}$ NMR spectrum indicated two new broad resonances – a major signal at 51.7 ppm and a smaller signal at 62.1 ppm. This correlated well with the ^1H NMR spectrum which indicated two cyclopentadienyl signals at 4.99 ppm (major) and 4.77 ppm (minor). The majority of 4-ethynyl-α,α,α-trifluorotoluene remained unreacted, as evidenced by a singlet signal in the ^1H NMR spectrum at 3.48 ppm for the terminal alkyne proton.

The NMR tube was heated for a further three days at 50 °C, after which the reaction mixture still contained considerable quantities of unreacted alkyne. The original ^1H NMR signal for the cyclopentadienyl protons of **[7b]PF$_6$** could no longer be observed – this signal was replaced with the two new signals listed above. The $^{31}P\{^1H\}$ NMR spectrum also showed a mixture of the two phosphorus-containing species as detailed above. A high resolution ESI-MS of the reaction mixture showed a single peak corresponding to a ruthenium-containing species with a mass corresponding to $[Ru(\eta^5\text{-}C_5H_5)(\textbf{b})(NC_5H_5)(\text{alkyne})]^+$. By comparison of these data with independently synthesised material, the major product was assigned as **[13b^CF3]PF$_6$**, and the minor product as **[16b^CF3]**, Scheme 3.14. These complexes are analogous to previously reported pyridylidene compounds containing triphenylphosphine, which are used as fluorination precursors in Chapter 4.[45] The reversible protonation and deprotonation pathway that connects **[13b^CF3]PF$_6$** and **[16b^CF3]** is well established and understood for the

triphenylphosphine analogues. Complex [13b^{CF3}]PF$_6$ could be isolated purely and confirmed by elemental analysis.
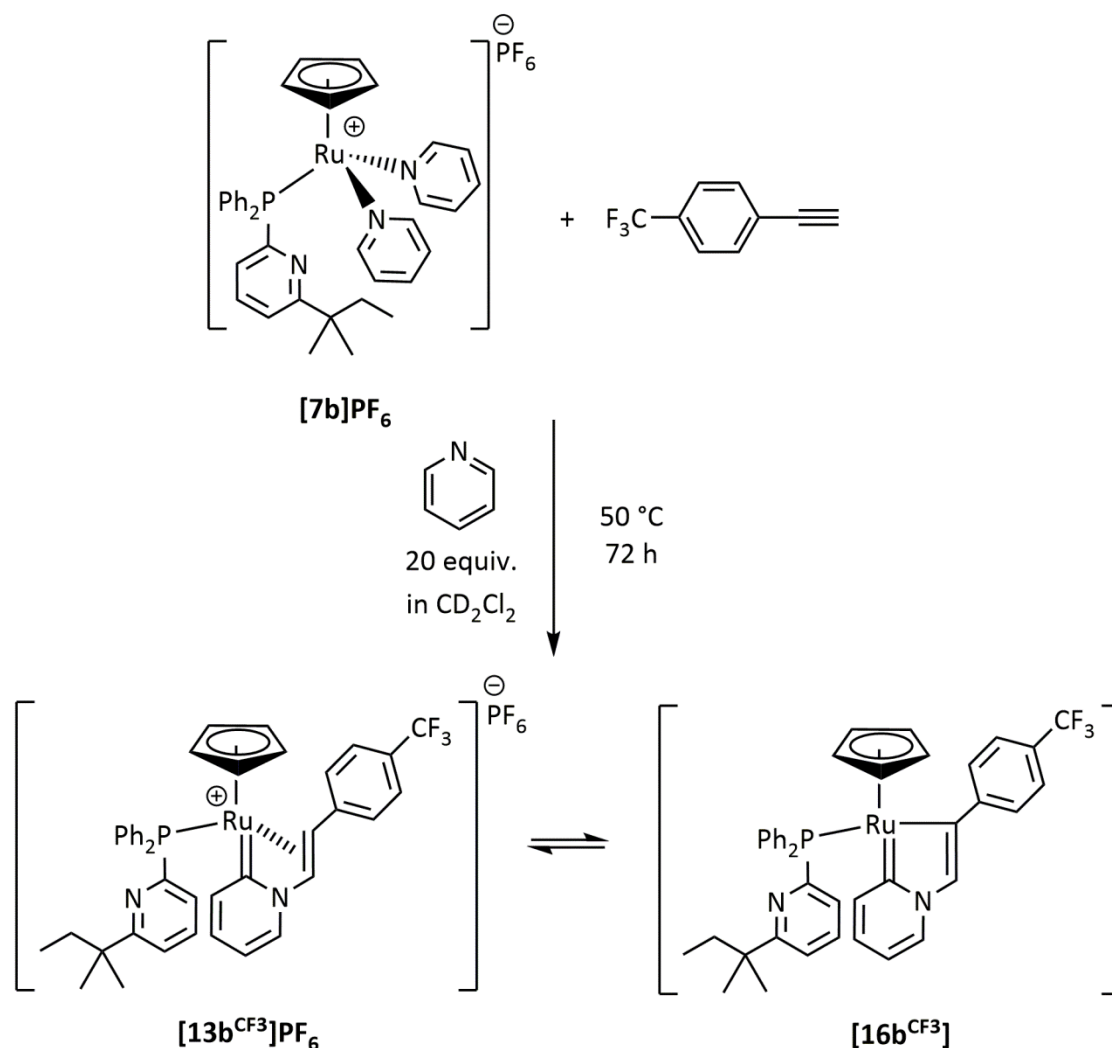
Scheme 3.14 Reactivity of complex [7b]PF$_6$ under standard catalytic conditions

3.4.2 Catalytic testing of complex [7c]PF$_6$

Complex **[7c]PF$_6$** was trialled for catalytic activity using the conditions detailed in Scheme 3.13. As **[7c]PF$_6$** could not be synthesised in the absence of **[10c]PF$_6$**, a mixture of these complexes was initially present. Previous studies (Section 3.2.2.1) indicated that on the addition of pyridine, **[10c]PF$_6$** is fully converted to complex **[7c]PF$_6$**. Therefore, under catalytic conditions it was hypothesised that all ruthenium should be in the form of **[7c]PF$_6$**. This was verified by recording a ^{31}P{^{1}H} NMR spectrum of the reaction mixture before heating, which showed a clean spectrum with a singlet corresponding to **[7c]PF$_6$** as the only phosphorus-containing species.

The reaction mixture was heated for 48 hours and monitored by NMR spectroscopy. The $^{31}P\{^1H\}$ NMR spectrum showed a mixture of organometallic products and integration of the spectrum allows for an approximate quantification of each complex. The major resonance was a singlet at 88.2 ppm and corresponds to $[15^{CF3}]PF_6$ (integration = 34 %). The presence of $[15^{CF3}]PF_6$ indicates that formation of vinylidene intermediate $[11c^{CF3}]$ is possible under catalytic conditions, but rather than acting as an intramolecular base, the pendant pyridyl group of phosphine **c** is instead behaving as a nucleophile and 'trapping' the vinylidene, therefore preventing productive catalysis. The next most intense resonance corresponds to unreacted (or regenerated) $[7c]PF_6$ (integration = 27 %). A singlet signal at 62.6 ppm (integration = 18 %) has tentatively been assigned as $[16c^{CF3}]$, by comparison of this chemical shift to the triphenylphosphine and 2-(1,1-dimethylpropyl)-6-(diphenylphosphino)pyridine analogues (61.2 and 61.5 ppm for $[16a^{CF3}]$ and $[11b^{CF3}]$ respectively). An additional four unidentified phosphorus-containing species were also present in the reaction mixture. The integration of these individual compounds was between 3 % and 8 % and so their identities were not investigated further, Scheme 3.15.
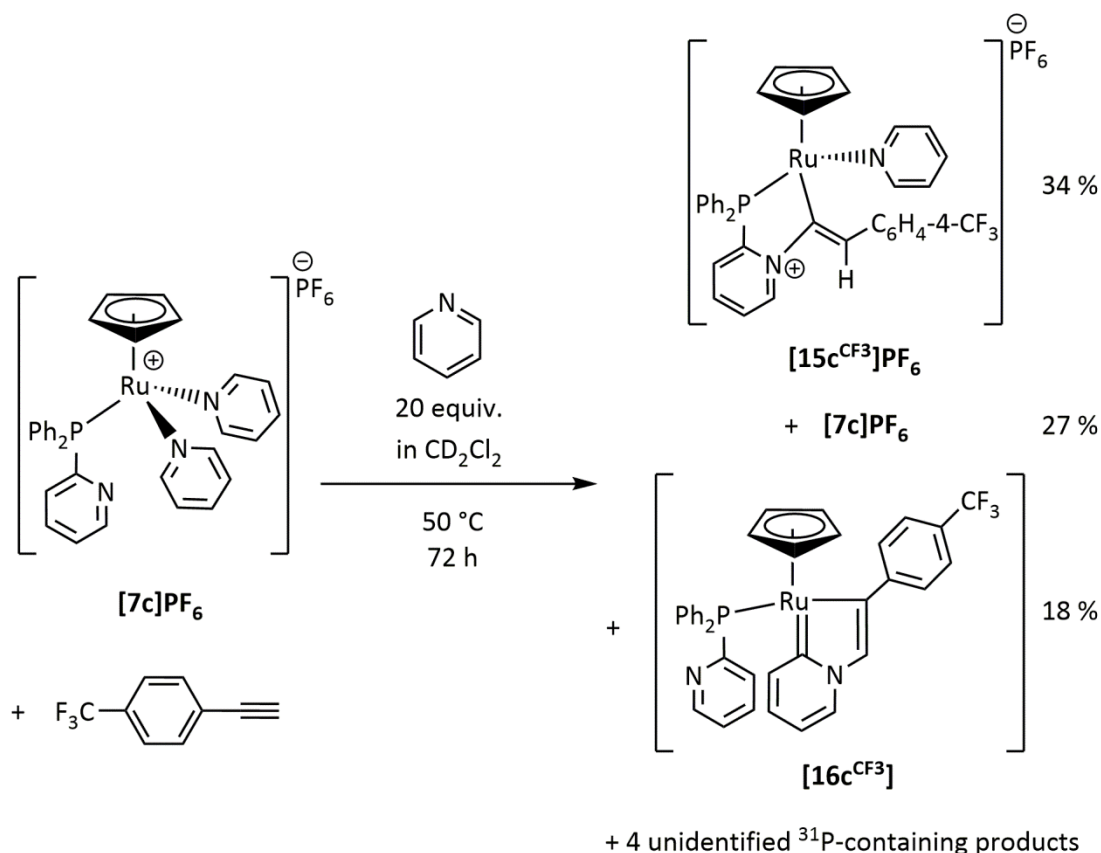
Scheme 3.15 Reactivity of complex [7c]PF₆ under standard catalytic conditions

A high resolution ESI-MS of the reaction mixture showed the presence of $[Ru(\eta^5\text{-}C_5H_5)(c)(NC_5H_5)(alkyne)]^+$, which supports the presence of both **[15c^{CF3}]$^+$** and **[16c^{CF3}]$^+$** and **14^{CF3}** at an *m/z* of 250.0818. Thin layer chromatography of the reaction mixture in a 3:1 solution of pentane and ethyl acetate against an authentic sample of **14^{CF3}** confirmed that this product had been formed. Therefore, a preparative TLC was performed in the same solvent system to isolate **14^{CF3}** in 26 % yield. This indicates that complex **[7c]PF$_6$** behaves as a poor pyridine alkenylation catalyst under these conditions.

Complex **[15c^{CF3}]PF$_6$** was also investigated under catalytic conditions, in order to understand whether it was a deactivation product or could participate in pyridine alkenylation. A pure sample of **[15c^{CF3}]PF$_6$** was isolated, and used under the conditions described in Scheme 3.13. After 16 hours of heating at 50 °C, NMR spectra were recorded. The ^{1}H NMR spectrum indicated the alkyne remained unreacted by the presence of a singlet at 3.36 ppm for the terminal alkyne proton. The ^{31}P{^{1}H} NMR spectrum showed little change – four small peaks were visible in the baseline at chemical shifts of 52.6, 74.0 and 132.1 ppm with integrations of 18 %, 4 % and 5 % respectively. The spectra were recorded again after 48 hours of heating. The ^{31}P{^{1}H} NMR spectrum contained ten phosphorus resonances in a chemical shift range between 20 and 130 ppm, some of which were broad. Presumably, these products were due to degradation of **[15c^{CF3}]PF$_6$**. By high resolution ESI-MS, only one organometallic species could be identified at an m/z of 679.1046 which corresponds to the mass of **[15c^{CF3}]$^+$**. However, some of the phosphorus-containing species in the ^{31}P{^{1}H} NMR spectrum may not appear in the mass spectrum, and others could be isomers of **[15c^{CF3}]$^+$** and so appear at the equivalent *m/z* value. Importantly, the ^{1}H NMR indicated that all of the 4-ethynyl-α,α,α-trifluorotoluene remained unreacted and so catalysis was unsuccessful. The sample was heated further to probe whether the spectrum would become cleaner on prolonged heating. This was not the case and the spectrum did not change after a further 24 hours.

Complex **[7c]PF$_6$** has also been involved in a wider catalytic study of pyridine alkenylation. These results formed a contribution to my MChem report, submitted in 2012, and a publication in *Dalton Transactions*.[79] In this investigation, half-sandwich ruthenium complexes were synthesised *in situ* and tested for catalytic activity. The formation of a range of different complexes without the necessity for isolation and purification allowed for a rapid screening of variables including the phosphine ligand, number of heterocycle equivalents, catalyst loading and other reaction conditions. The process is illustrated in Scheme 3.16.
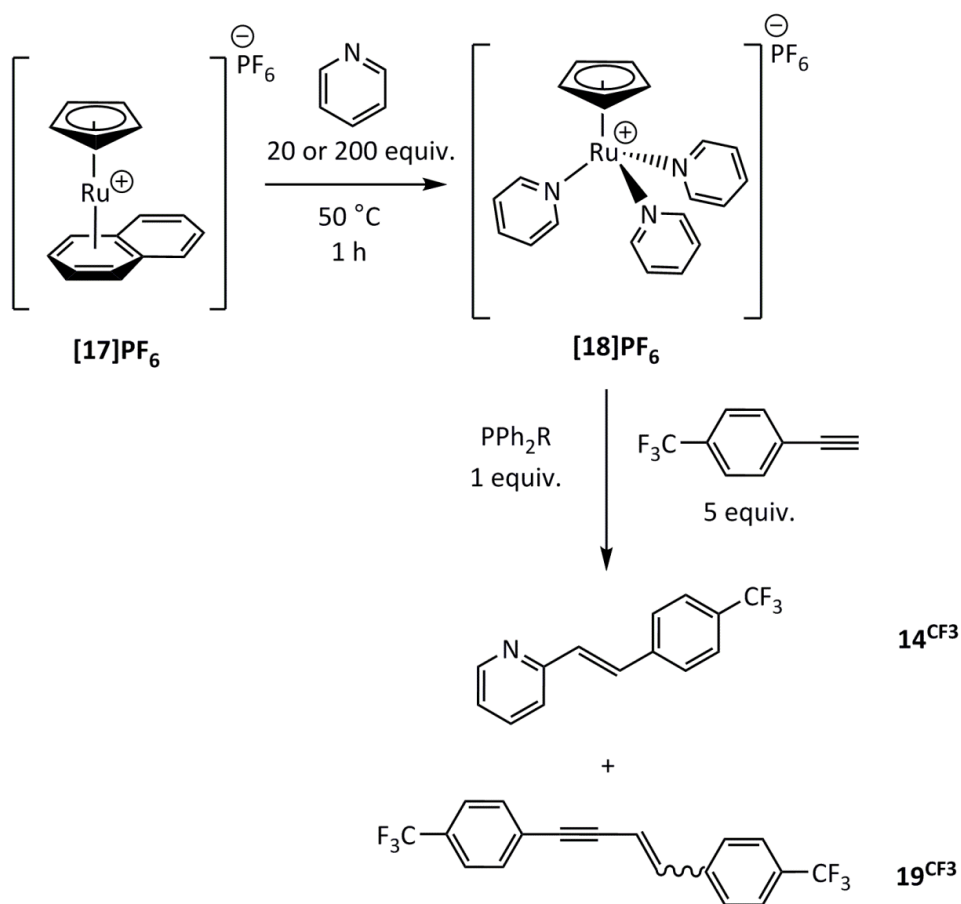
Scheme 3.16 Formation of ruthenium catalyst *in situ* and subsequent test of catalytic activity

Key results are summarised in Table 3.5.

Entry	Phosphine	Pyridine equivalents	Time	Conversion to 14^{CF3} / % (isolated)	Conversion to 19^{CF3} / %
1	a	20	16 h	trace (9)	-
2	c	20	20 min	Trace	-
3	c	20	40 min	8 (13)	-
4	a	200	40 min	trace (2)	-
5	c	200	40 min	42	17
6	PMe$_3$	200	40 min	68 (21)	14

Table 3.5 Key findings from the *in situ* catalytic study. All reactions were heated under nitrogen at 150 °C. All were performed in a microwave reactor (with the exception of Entry 1). Yields were calculated by ^{19}F NMR spectroscopy of the reaction mixtures.

Table 3.5 highlights the influence of the choice of phosphine ligand and catalytic conditions on the success of catalysis. Entries **1**, **2** and **3** each employ twenty equivalents of pyridine and all perform poorly in pyridine alkenylation. Entries **3** and **5** demonstrate that increasing the number of pyridine equivalents in the reaction can have a significant impact – on increasing from 20 to 200 equivalents of *N*-heterocycle the yield of **14^{CF3}** increased from 8 % to 42 %. However, the most important comparison that can be drawn from these results comes from entries **4**, **5** and **6**. These reactions are performed under identical conditions but with different phosphine ligands. Phosphine **c** shows a substantial increase in yield compared to **a**, but cannot match the most successful **PMe$_3$** catalyst analogue which provides a 68 % yield. The use of phosphine **c** also yields the highest quantity of the unwanted alkyne dimerisation product. Therefore from these limited results it seems that although phosphine **c** has limited success in catalysis, and in some respects can rival the original triphenylphosphine analogue, it does not appear to be the optimal choice for the progression of pyridine mono-alkenylation under these conditions. The incorporation of the intramolecular base does not provide considerable advantages in catalysis.

3.5 Conclusions

In this chapter, the synthesis of half-sandwich ruthenium complexes with the formula [Ru(η^5-C$_5$H$_5$)(PPh$_2$R)(L)$_2$]PF$_6$ (PPh$_2$R = 2-(1,1-dimethylpropyl)-6-(diphenylphosphino)pyridine or diphenyl-2-pyridylphosphine, L = nitrogen donor ligand) has been achieved. The reactivity of these species has then been investigated with both phenylacetylene and 4-ethynyl-α,α,α-trifluorotoluene, in the presence and absence of excess pyridine, and the results compared to the reactivity of the PPh$_3$ analogue, **[7a]PF$_6$**.

Complex **[7b]PF$_6$** containing the sterically encumbered 2-(1,1-dimethylpropyl)-6-(diphenylphosphino)pyridine ligand reacted differently with each of the alkynes. In the presence of phenylacetylene, the reaction required two equivalents of alkyne to perform a reaction in which **[7b]PF$_6$** catalysed a condensation reaction between two phenylacetylene molecules to form a η^3-butadienyl ligand, **[12b^{Ph}]PF$_6$**. This was attached at one end by the pyridyl moiety of the phosphine. A similar structure has been reported with triphenylphosphine complex **[7a]PF$_6$**; in the latter reaction, inter- rather than intramolecular attack of pyridine had occurred.[45]

In the presence of 4-ethynyl-α,α,α-trifluorotoluene, complex **[7b]PF$_6$** displayed different reactivity. After heating the reaction at 50 °C for several hours, complete conversion was observed to pyridylidene complex **[13b^{CF3}]PF$_6$**. The formation of an analogous pyridylidene complex has also been observed from the PPh$_3$ analogue, **[7a]PF$_6$**, but limited examples of pyridylidene formation from non-activated substrates such as pyridine and terminal alkynes have been reported in the literature. However, the formation of the pyridylidene complex **[13b^{CF3}]PF$_6$** in this reaction signified the formation of a catalyst deactivation product from which successful catalysis could not occur. The pyridyl-nitrogen incorporated into the phosphine could not act as an efficient base which the reaction requires to follow the productive pyridine alkenylation pathway.

In the presence of either phenylacetylene or 4-ethynyl-α,α,α-trifluorotoluene, complex **[7c]PF$_6$** reacted immediately and selectively to produce complexes **[15c^{Ph}]PF$_6$** and **[15c^{CF3}]PF$_6$**. The mechanism of formation is postulated to be initial vinylidene formation followed by rapid nucleophilic attack at the α-carbon to form the 'trapped vinylidene' product. This result is arguably the most significant from this chapter. In the previously suggested mechanism of pyridine alkenylation, Scheme 3.7, a crucial step in the pathway is intermolecular attack of a pyridine molecule at the vinylidene α-carbon, shown by intermediates **3-*r*** and **3-*y***. However, due to the kinetic profile of this reaction, the intermediate was short-lived and no experimental evidence could be acquired. Instead, the species could only be modelled by DFT calculations. However, as the pyridine moiety is incorporated into the phosphine, attack is now intramolecular and produces an isolatable species that can be fully characterised and which adds credence to the reaction mechanism.

In conclusion, the presence of a pyridyl-functionalised phosphine ligand cannot, in the case of complexes **[7b]PF$_6$** and **[7c]PF$_6$**, act as an intramolecular base to afford access to **14^{CF3}** and avoid catalyst deactivation. However, the reactivity studies have instead provided both valuable supporting experimental evidence for proposed mechanism of pyridine mono-alkenylation *via* 'trapped vinylidene' complexes **[15c]PF$_6$**, and also allowed access to further examples of novel pyridylidene complexes formed from non-activated substrates in the form of complexes **[13b^{CF3}]PF$_6$** and **[16b^{CF3}]**.

Chapter 4

Outer-sphere electrophilic fluorination of a ruthenium metallocycle: a study of mechanism and reactivity

4 Outer-sphere electrophilic fluorination of a ruthenium metallocycle: a study of mechanism and reactivity

4.1 Introduction

4.1.1 Importance of fluorination

Carbon-fluorine bond formation is a vital process for the production of a range of commercially important compounds including pharmaceuticals,[166] agrochemicals,[167] ^{18}F-labelled tracers for positron emission tomography,[168] and in materials with novel properties such as Teflon (polytetrafluoroethylene).[169] Due to the distinctive properties of fluorine, primarily its high electronegativity and small size, the introduction of this unique halogen into a molecule can have a dramatic impact on its properties.[170] These qualities are exploited particularly in the development of molecules with biologically-relevant applications.

Following fluorine incorporation, pharmaceutical-candidate molecules frequently exhibit higher bioavailabilities and increased membrane penetration, due to modulation of the pK_a values of surrounding functional groups such as the reduction of amine basicity.[171-172] Fluorinated molecules also often demonstrate higher metabolic stabilities (through reduced susceptibility to P450 oxidation enzymes)[170] and show stronger interactions with their target proteins, likely due to attractive polar interactions which are enhanced by the highly polarised carbon-fluorine bond.[170] These higher metabolic, thermal and oxidative stabilities, and the increased lipophilicities of fluorinated organic compounds,[170] lead to enhanced efficacies for both pharmaceuticals and agrochemicals. For this reason, fluorine is commonly used as an isostere for hydrogen in the development of biologically-relevant molecules[170] (despite the similarity of van der Waals radii being closer to oxygen (fluorine, 1.47 Å; oxygen, 1.52 Å; hydrogen, 1.20 Å)).[170]

Currently, approximately twenty percent of all drugs and thirty percent of agrochemicals contain fluorine, which demonstrates the importance of selective and facile carbon-fluorine bond formation procedures.[166] Three out of five top-selling pharmaceutical products contain fluorine, for example, atorvastatin (Lipitor), which is used for the treatment of high cholesterol and for the prevention of strokes and heart attacks.[170] Trifluoromethylated drugs have also proven successful.[173] Selected examples of fluorine-containing blockbuster drugs are shown Figure 4.1.[166,173]
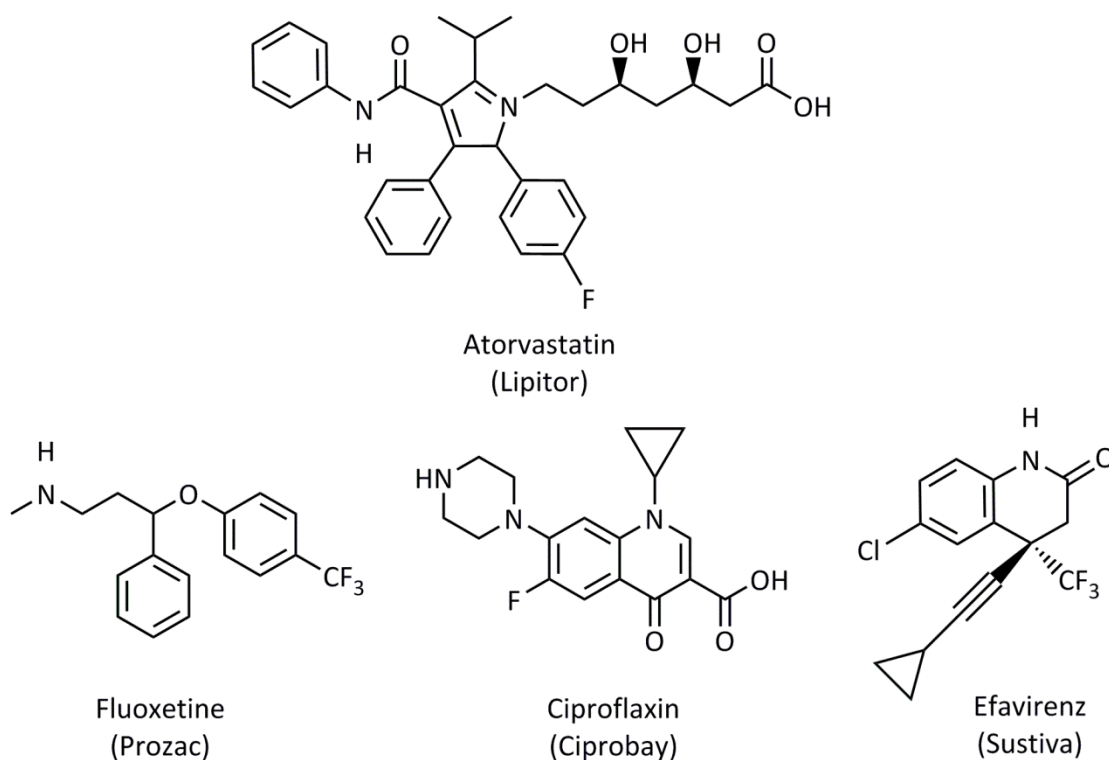
Figure 4.1 Selected examples of fluorine-containing blockbuster drugs. Fluoxetine, marketed as Prozac by Eli Lilly, is an antidepressant drug and Ciproflaxin, marketed as Ciprobay by Bayer, is used to treat bacterial infections. Efavirenz, a trifluoromethyl-containing drug marketed as Sustiva by Bristol-Myers Squibb, is used to treat and reduce the risk of HIV.

However, despite intensive research, the formation of carbon-fluorine bonds remains challenging.[170] Conventional fluorination techniques developed in the early 20th century are limited to simple molecular structures, and selective fluorination remains problematic. Even nature has not yet developed a wide range of fluorination reactions; despite fluorine being the thirteenth most abundant element in the Earth's crust, only 21 natural molecules are known from biosynthesis.[170,174] Following recent developments in the field, new procedures have been developed to allow more selective fluorination but there is still a need for more general and practical reaction conditions, as currently available methods are not cost efficient and often lack practicability.[170,175] Fluorination strategies which are regio- and stereoselective, avoid the pre-functionalisation of substrates and which can construct less common structural frameworks (alkenyl- or alkyl- carbon-fluorine bonds) are highly sought after.[170,175-176]

4.1.2 Challenges of carbon-fluorine bond formation

Fluorination reactions are particularly challenging due to the facts that fluorine is the most electronegative element (with a Pauling electronegativity of 4.0), it is the most oxidising element, and has a small ionic radius of 1.33 Å.[177] Therefore, fluoride ions form strong hydrogen bonds with water, alcohols, amines and amides and act as weak nucleophiles in the presence of hydrogen-bond donors.[170] This places limitations on the substrate scope for carbon-fluorine bond formation *via* nucleophilic substitution reactions. However, in rigorously dry solvents and in the absence of hydrogen-bond donors, fluoride is strongly basic and can promote undesired side reactions.[170]

Traditional nucleophilic aromatic substitutions such as the Balz-Schiemann reaction[170] (which transforms anilines into aryl fluorides) and the Halex process[178-179] (in which other halogens are replaced with fluorine atoms) are used currently on an industrial scale for the bulk synthesis of aryl fluoride compounds, as they allow some level of control over the regioselectivity of the products. Recent developments of the Halex process allow the fluorination of a range of arenes (electron-poor, chloro-, nitro- or trimethylammonium-functionalised aromatic compounds) at room temperature with yields of up to 95 %.[180] However, these reactions more commonly require harsh conditions and none of the procedures has a wide substrate scope or a wide range of functional group compatibility.[170] In the absence of catalysts, high temperatures or highly reactive intermediates or reagents have generally been the only methods to incorporate fluorine into arenes.[181] This is demonstrated in the reaction shown in Scheme 4.1, in which fluorination of naphthyl bromide occurs *via* fluoride trapping of highly reactive aryne intermediates which are generated *in situ* from bromide elimination by the strongly basic anhydrous fluoride. The nature of the aryne intermediates leads to a mixture of regio-isomers.[181]
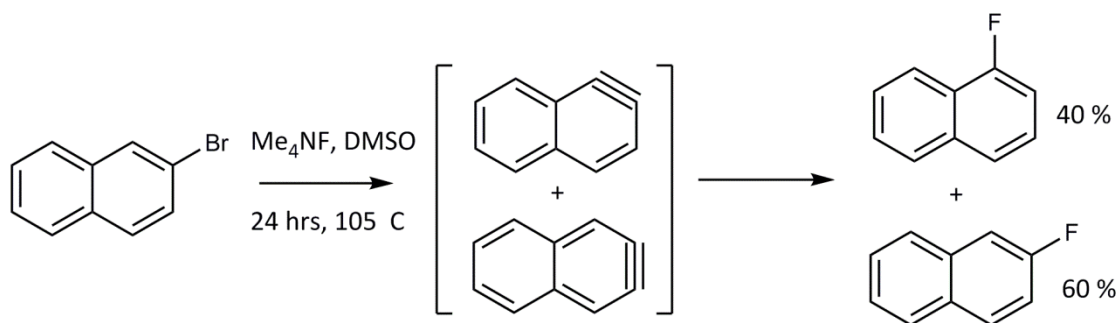
Scheme 4.1 Aryl fluorination *via* aryne intermediates

Reactions which are thermodynamically feasible but kinetically challenging can often be accessed by the use of an appropriate catalyst and, conceptually, this theory can be applied to carbon-fluorine bond formation.[175,182] A carbon-fluorine bond is the strongest single bond known between carbon and any other element;[175] therefore, the majority of carbon-fluorine bond formation reactions are thermodynamically favoured. However, the barrier to carbon-fluorine bond formation is difficult to overcome because metal-fluorine bonds are also very strong.[182] Traditional methods of metal-catalysed cross-coupling reactions, illustrated in Scheme 4.2, experience difficulties in carbon-fluorine bond formation.[182]
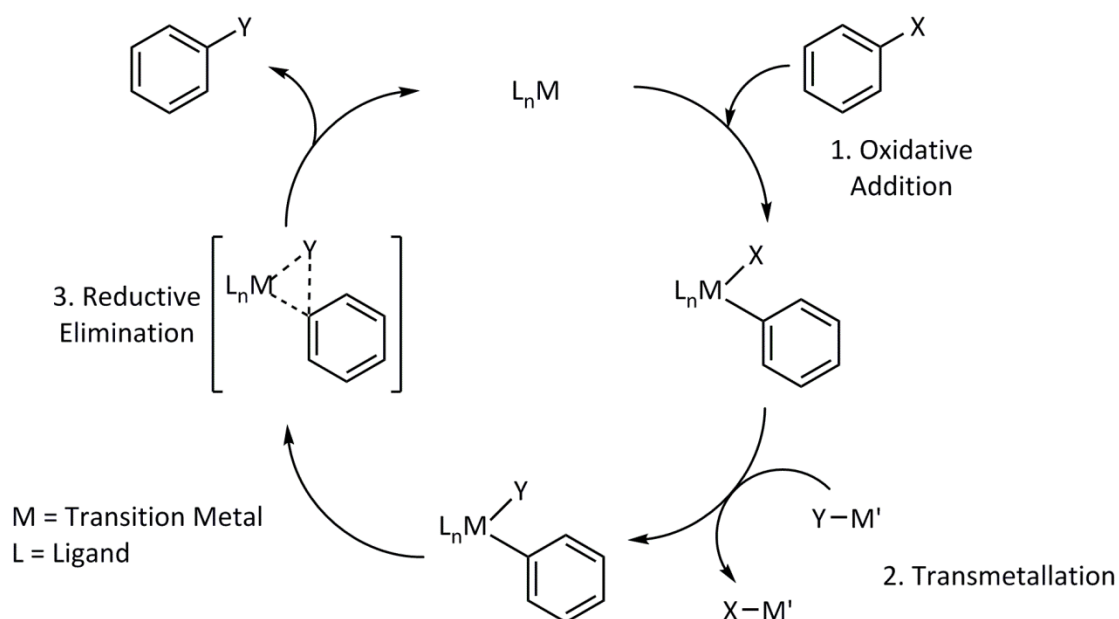
Scheme 4.2 Metal-catalysed cross-coupling general reaction scheme – the metal-fluoride bond can be formed by ligand exchange with nucleophilic fluoride or oxidative addition of an electrophilic fluorinating agent

The most problematic step for cross-coupling is the reductive elimination of the fluorinated product, Step 3 shown in Scheme 4.2.[183] Reductive elimination requires sufficient orbital overlap between both metal and ligand σ-orbitals.[176] However, strong polarisation of the metal-fluorine bond causes a lack of electron density in the region of carbon- fluorine bond formation, and additionally introduces a significant ionic character of the bond, leading to a higher metal-fluorine bond strength which is subsequently harder to break.[182] A further consideration is that reductive elimination must be faster than any other side reactions for this strategy to be successful. This concept as applied to carbon-fluorine bond formation was first reported in 2008[184], and will be discussed in detail in Section 4.1.5.2.

4.1.3   Methods of fluorination

The varied and essential applications of fluorine-containing compounds mean that the development of novel catalytic procedures for carbon-fluorine bond formation is highly valuable and many recent strategies have been reported, including organo-, photo- and enzymatic- catalytic methods.[170,185-191] Carbon-fluorine bond cleavage and hydrodefluorination of highly fluorinated substrates are alternative routes to introduce new functionality into pre-fluorinated materials.[192-193] It is beyond the scope of this thesis to report in more detail each of these fields, and so this introduction will focus on transition-metal mediated reactions for carbon-fluorine bond formation.

4.1.3.1   General features of transition-metal mediated fluorination reactions

Transition-metal promoted carbon-fluorine bond formation reactions offer significant potential for regio-, stereo- and enantioselective reactions with high atom- and step economy under mild conditions, and in the past decade, procedures have been developed which introduce carbon-fluorine (or carbon-trifluoromethyl) bonds into both aromatic and aliphatic moieties.[170,175] Transition metals can be used in conjunction with either electrophilic or nucleophilic sources of fluorine, and the choice of metal is dictated by the evaluation of metal-fluoride bond strengths. Early transition metals tend to form stronger bonds to fluorine, due to increased π-back bonding from fluorine to the empty metal d-orbitals and because the metal-fluorine bonds are more highly polarised. Therefore, carbon-fluorine bond formation catalysts tend to be based on late transition metals.[182]

Transition-metal mediated reactions allow the synthesis of organic molecules which were not previously accessible using traditional fluorination chemistry; however, significant challenges still remain.[170,175] These challenges will be highlighted throughout this introduction in order to assess and suggest the future directions of research in the field of fluorination, and the most cutting-edge methodologies will be presented.

4.1.4 Nucleophilic *versus* electrophilic fluorination

4.1.4.1 Nucleophilic fluorination

Conceptually, fluorination methodologies can be divided into two classes; either electrophilic or nucleophilic, depending on the nature of the fluorine source. The challenges of nucleophilic fluorination arise from the high electronegativity of fluorine as discussed in Section 4.1.2. In the presence of hydrogen-bond donors, fluoride is surrounded by a 'solvent cage' and behaves as a poor nucleophile, whereas rigorous exclusion of potential donors causes the highly charge-dense fluoride ion to behave as a strong base, and leads to unwanted side reactions.[170] In S_N2 reactions the choice of solvent is crucial to success, and dipolar aprotic solvents such as tertiary alcohols and DMSO tend to offer a good compromise between these properties.[194]

Common fluoride sources include alkali metal fluorides, such as LiF, KF and CsF.[170] The use of these reagents is desirable due to their low cost, especially in comparison to electrophilic sources of fluorine.[175,195] Within the alkali metal fluorides, LiF is the least reactive reagent due to the strongest ionic attraction (and hence the strongest lattice energy).[196] This decreases the solubility, and hence the reactivity, of the fluoride nucleophile in organic solvents. Crown ethers can be used to increase the solubility of these reagents.[197] An alternative class are tetra-alkyl ammonium fluorides, which have lower ionic bond strengths and higher solubilities. The most widespread reagents in this field include the tetrabutyl- and tetramethyl- derivatives.[170]

4.1.4.2 Electrophilic fluorination

Unlike nucleophilic fluoride sources, electrophilic fluorinating agents are generally utilisable in protic solvents. Although some reagents exhibit highly oxidising properties (fluorine gas, hypofluorites[198], xenon difluoride[199]), the development of crystalline, air- and moisture stable electrophilic fluorinating reagents allowed the expansion of selective and functional-group tolerant fluorination methodologies.[200] The four fluorinating agents used as part of the work in this thesis are illustrated in Figure 4.2.
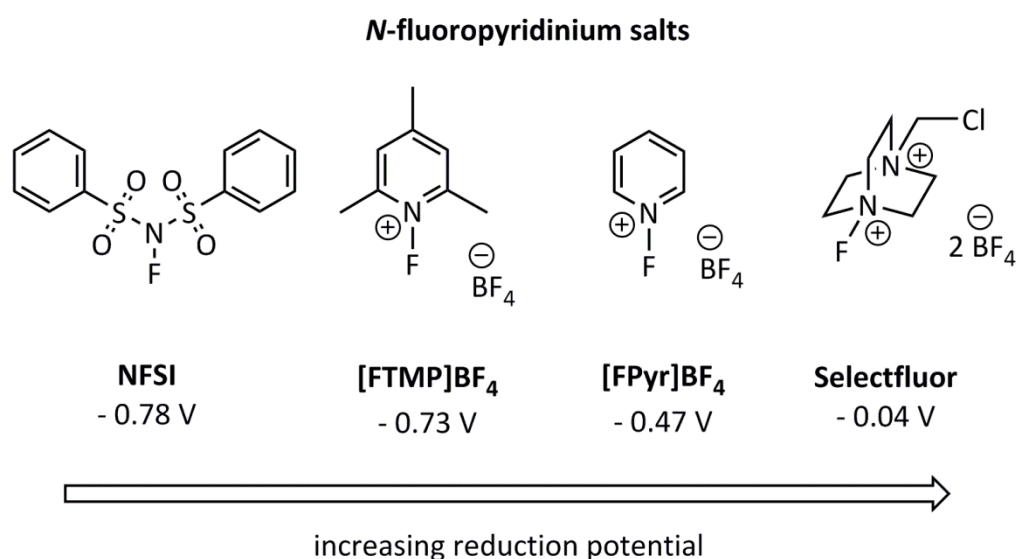
Figure 4.2 Air-stable, crystalline electrophilic fluorinating agents (reduction potentials in acetonitrile vs. SCE)[201]

N-fluoropyridinium salts, Figure 4.2, and have become an important source of electrophilic fluorine. They can be used with a wide range of substrates, and variation of the supporting structure can be used to control the reactivity.[170] Selectfluor is a more recent source of 'F^{+}', and is also a commercially available, stable reagent.[202-203] Although each reagent behaves as a source of 'F^{+}', the nitrogen-fluorine bonds are in fact polarised towards fluorine, which has a partial negative charge. Nucleophilic attack occurs at the fluorine atom due to the sterically inaccessible σ^*_{N-F} orbitals on the nitrogen atom.[204] Possibly due to the small orbital coefficient of the σ^*_{N-F} orbital on the fluorine atom and its low energy, other mechanistic pathways can compete; for example, single electron transfer (SET).[170,175,204] It is often very difficult to distinguish between these two mechanisms, and both SET and S_N2 pathways have been proposed to occur in electrophilic fluorination.[170,175] This will be discussed in more detail in the following sections.

4.1.5 Transition-metal-mediated aromatic carbon-fluorine bond formation

The direct conversion of arene carbon-hydrogen to carbon-fluorine bonds with predictable regioselectivity is a frontier in the field of fluorination, and therefore many recent publications have been based on the formation of aromatic carbon-fluorine bonds for the synthesis of aryl fluoride compounds.[175] However, despite these advances there remains a lack of practical and useful fluorination reactions that allow access to functionalised aryl fluorides. Industrial scale fluorination reactions often use harsh reaction conditions to create

structurally simple fluorinated building blocks, and similar approaches cannot be applied to structurally complex reaction intermediates which bear complex functionality.[175] Therefore, developments are required that allow the regio- and stereoselective syntheses of carbon-fluorine bonds in the presence of other functional groups. It is beyond the scope of this introduction to cover all the literature in this field, therefore selected examples will be discussed that illustrate a) important findings which have allowed increased understanding of fluorination methodologies, b) state-of-the-art techniques for aryl fluoride synthesis and c) different fluorination mechanisms that are in operation in various systems.

Unlike other halogenation procedures, the fluorination of arenes by electrophilic aromatic substitution is a challenging reaction as the high electronegativity of the fluorine substituent disfavours the formation of the necessary carbocationic intermediate. Aryl metal reagents[170] (including aryl-tin,[205] mercury[206], silicon[207] and boron[208] compounds) can react with strong electrophilic sources of fluorine (including fluorine gas, XeF_2 and hypofluorites) but these reactions are limited in terms of substrate scope due to the high reactivity of the reagents.[170] Alternatively, aryl nucleophiles can react with less reactive electrophilic fluorinating agents; the most reliable method being the fluorination of simple aryl Grignard reagents with N-fluorinated reagents, Scheme 4.3.[170,209-210] This reaction again is limited in terms of substrate scope, primarily due to the basicity and nucleophilicity of the aryl magnesium reagents.[209]
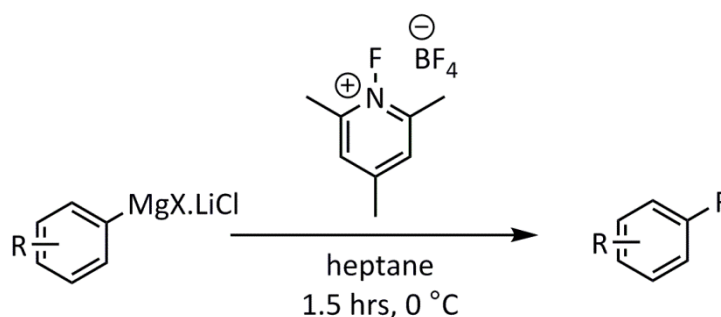
Scheme 4.3 The use of Grignard reagents in aryl-fluorine bond formation[209]

Transition-metal mediated and/or catalysed carbon-fluorine bond formation, using both electrophilic and nucleophilic sources of fluorine, has been investigated with a range of late-transition metals including platinum, palladium, nickel, copper and ruthenium and will be discussed in more detail below.

4.1.5.1 Electrophilic aromatic fluorination

The fluorination of aromatic compounds may be mediated- or catalysed by transition metal complexes, in order to allow functional group tolerant and selective fluorination procedures. Transition-metal mediated or catalysed processes using latent sources of 'F$^+$' can broadly be divided into two mechanistic classes, shown schematically in Figure 4.3.[63,170,175]
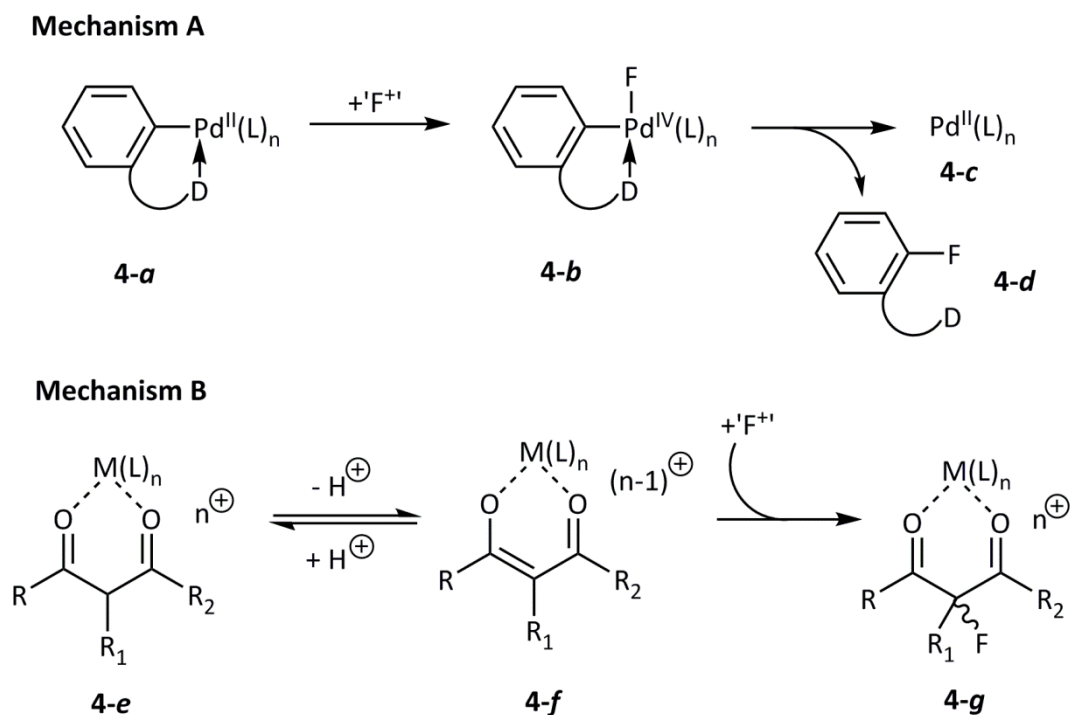
Figure 4.3 Schematic transition-metal mediated electrophilic fluorination mechanisms

In Mechanism A, the reaction of a redox active metal complex with an electrophilic fluorinating agent leads to the formation of an intermediate metal-fluoride complex with concomitant oxidation of the metal to form a high oxidation-state intermediate, **4-b**, followed by reductive elimination to form the new carbon-fluorine bond in **4-d**.[184,211-215] The high oxidation state of the metal can be supported by either ligand dissociation[184,211] or the formation of a multi-metallic species.[212] Alternatively, the redox-active metal may instead initiate SET processes that promote subsequent radical reactions.[215] Alternatively Mechanism B shows a Lewis-acid mediated route, in which the substrate is activated towards fluorination but the metal does not participate in any redox chemistry. The Lewis-acid acts to modify the pK$_a$ of the proton on the substrate, **4-e**, and stabilise the cationic intermediate, **4-f**. The fluorination of β-ketocarbonyl compounds has been promoted by a range of metal species,

including copper (II), nickel (II), zinc (II), titanium (IV), ruthenium (II) and palladium (II) complexes.[216]

These strategies are broadly utilised but have several limitations. For the formation of aromatic carbon-fluorine bonds, in some cases, the incorporation of directing groups into the substrate is necessary in order to ensure regioselectivity, whereas other strategies require substrate pre-activation (for example as an aryl stannane, silane or boronic acid).[170,175] In metal-mediated $C(sp^3)$-F bond formation, highly activated substrates are typically required (for example, β-ketocarbonyl compounds such as β-diketones, β-keto-esters or N-Boc protected amides).[170,175,216] Therefore, the development of new organometallic reactions which can eliminate the need for highly activated or pre-functionalised substrates is highly desirable.

4.1.5.2   Palladium-mediated and catalysed aryl fluoride synthesis

Aromatic fluorination reactions catalysed by transition metals were first reported in 2006.[217] Regioselective functionalisation was achieved by the reaction of substrates which contained ortho-directing groups, which place the selected carbon-hydrogen bond in close proximity to the metal centre, Scheme 4.4.[217-218]
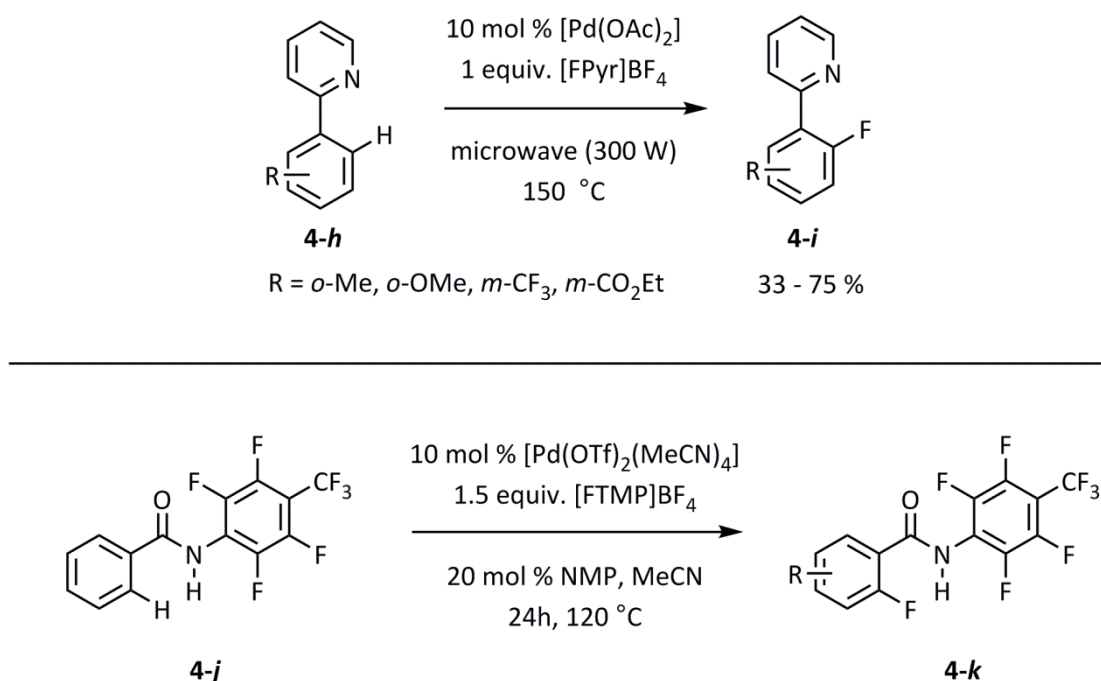
Scheme 4.4 Regioselective aromatic fluorination catalysed by transition metals

Although reasonable yields can be obtained, the necessity of a directing group limits the substrate scope and structural diversity of the products. The incorporation of a sterically bulky, weakly coordinating anionic *ortho*-directing *N*-perfluorotolylamide group in **4-h** and **4-i** addresses the problem of double fluorination, Scheme 4.4 (lower) as the monofluorinated product is rapidly displaced by the substrate.[219] The mechanisms of the reactions in Scheme 4.4 remain unknown – after cyclopalladation, fluorination may occur from a Pd(II) intermediate (similarly to the reaction with an aryl Grignard reagent) or by reductive elimination from a high oxidation state Pd(IV)-fluoride complex. The viability of multiple mechanisms for palladium catalysed aromatic fluorination has been demonstrated.

Carbon-fluorine reductive elimination from Pd(IV)

An early example of aryl fluoride synthesis by carbon-fluorine reductive elimination was demonstrated in 2008 by the Ritter group.[220] Using a stoichiometric palladium complex, **4-l**, and Selectfluor, arylboronic acids can be fluorinated *via* a two step process; slow transmetallation of the arene from boron to palladium to form **4-m**, followed by oxidation to release the fluorinated product, **4-n**, Scheme 4.5.
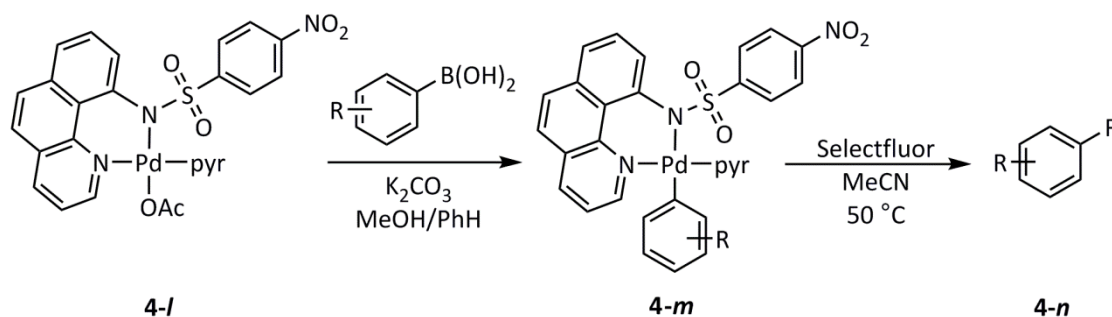
Scheme 4.5 Fluorination of arylboronic acids using palladium

Although the necessity of stoichiometric quantities of palladium and the incompatibility of the reaction conditions necessary for the transmetallation and fluorination steps prevented the application of this system in catalysis, the reaction provided a model system on which to conduct important mechanistic studies. The target was to elucidate the fluorination mechanism in order to rationally develop a new series of catalysts that overcome the often problematic barrier of reductive elimination. Through slight modification to the structure of the catalyst ligand system, the rate of reductive elimination was reduced sufficiently to allow experimental studies. Both experimental and DFT results support a mechanism of reductive

elimination from a palladium(IV)-fluoride, in which dissociation of an oxygen atom of the pyridylsulfonamide ligand in **4-o** affords a five coordinate complex, **4-p**, from which carbon-fluorine reductive elimination can readily occur to release **4-q**, Scheme 4.6.[184,211]

In this case, the pyridyl sulfonamide ligand is vital for stabilisation of the intermediates, made possible by the change in coordination mode from tridentate to bidentate during the conversion of **4-o** to **4-p**.[211] It was also shown, counter intuitively, that electron donating ancillary ligands at palladium increase the rate of carbon-fluorine bond formation. Although it would be expected that electron-withdrawing groups would enhance the rate of reduction elimination to form palladium (II), in fact it seems that the stabilisation of the palladium (IV) fluoride intermediate and the increased nucleophilicity of fluoride on attack of the electrophilic carbon are more influential factors, and so electron-donating ligands can enhance the process.[211]
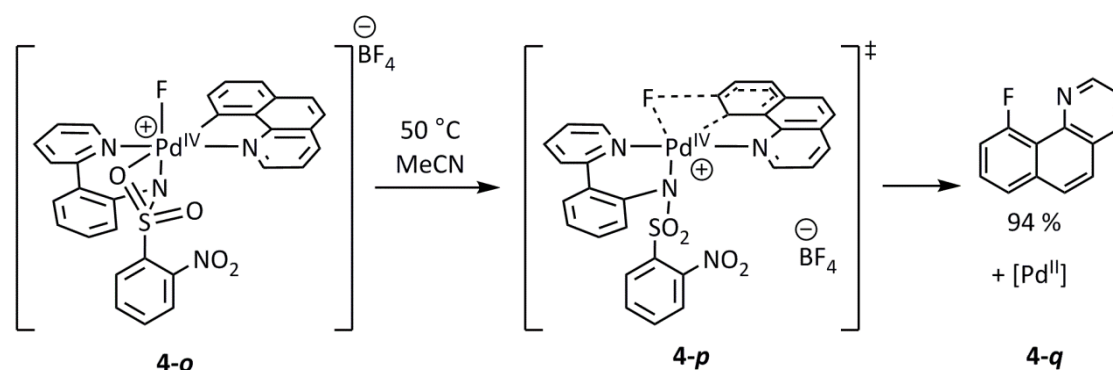
Scheme 4.6 Carbon-fluorine reductive elimination from a Pd(IV) fluoride complex

A further example of an isolated arylpalladium (IV) fluoride was reported by the Sanford group, synthesised by the addition of excess XeF_2 to arylpalladium (II) complex **4-r**, Scheme 4.7.[221]
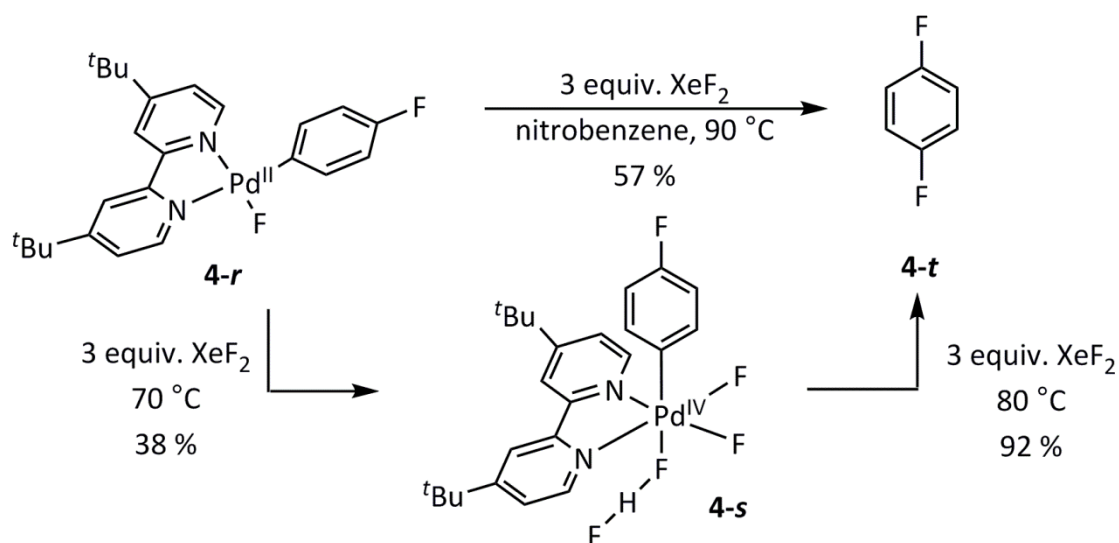
Scheme 4.7 Oxidatively-induced formation of a Pd(IV) bifluoride complex 4-*s* and subsequent formation of a new aromatic carbon-fluorine bond

The Pd(IV) species **4-*s*** was surprisingly unreactive on heating, and released the fluorinated aryl compound only after the addition of a further excess of XeF_2. The mechanism of carbon-fluorine bond formation remains unclear, and could be from either an electrophilic palladium-carbon bond cleavage or carbon-fluorine reductive elimination. Comparisons between the Sanford system (Scheme 4.7) with those of the Ritter group (Scheme 4.6) may provide some insight into the stability and reactivities of palladium (IV) intermediates. The presence of multiple fluoride ligands seems to contribute towards the higher thermal stabilities of palladium (IV) complexes, as both Sanford's **4-*s*** and a *bis*-fluoride analogue of Ritter's **4-*o*** exhibit high thermal stability.[184,221] These observations may indicate the requirement of a five coordinate palladium (IV) intermediate in order to promote carbon-fluorine reductive elimination, which is disfavoured in the presence of two anionic fluoride ligands that form very strong palladium-fluorine bonds. The fact that the two fluoride ligands are strongly electron-withdrawing also agrees with the findings of the Ritter group that carbon-fluorine bond formation is enhanced by the presence of electron-donating ancillary ligands.[211]

Single electron transfer (SET) mechanism via Pd(III)

Extensions to the aromatic fluorination methodology of arylboronic acid derivatives using palladium were reported in 2013, Scheme 4.8.[215] This system is simple to use in an open flask

and holds great promise as it is amenable to large, gram-scale syntheses. It can be performed in the presence of air and moisture, and protodeborylation side products are not observed.

$$2 \text{ mol\% } [(terpy)Pd(MeCN)][BF_4]_2$$
$$4 \text{ mol\% terpy}$$
$$1 \text{ equiv NaF}$$

R—⟨aryl⟩—BF$_3$K $\longrightarrow$ R—⟨aryl⟩—F

$$1 - 1.2 \text{ equiv Selectfluor}$$
$$\text{DMF or MeCN}$$
$$4 - 40 \text{ °C, 15 hours}$$
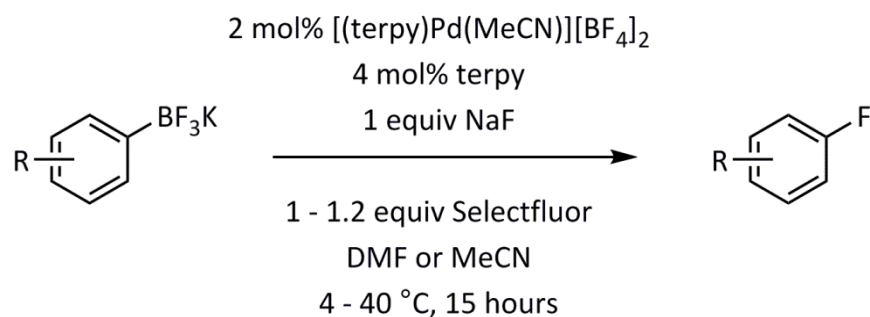
Scheme 4.8 Extended fluorination methodology of arylboronic acid derivatives

A much wider range of aryl trifluoroborates could be effectively fluorinated, including those which contain an electron-withdrawing or donating group, a sterically bulky substituent or protic functionality (alcohols, amides and carboxylic acids). However, the reaction is inappropriate for the fluorination of heterocycles, and some substrates with electron-withdrawing functionality gave constitutional isomers or difluorinated products. The necessary functionalisation of substrates to their arylboronic acid derivatives also introduces additional synthetic steps and lower atom economy.

As mentioned previously, transmetallation of arylboronic acid derivatives to palladium is slow under conditions which are also appropriate for fluorination.[220] In this system however, the experimental data suggests a SET mechanism in which a palladium (II) complex is oxidised to palladium (III) and carbon-fluorine bond formation occurs *via* a fluorine radical formed from the partial reduction of Selectfluor, Scheme 4.9.
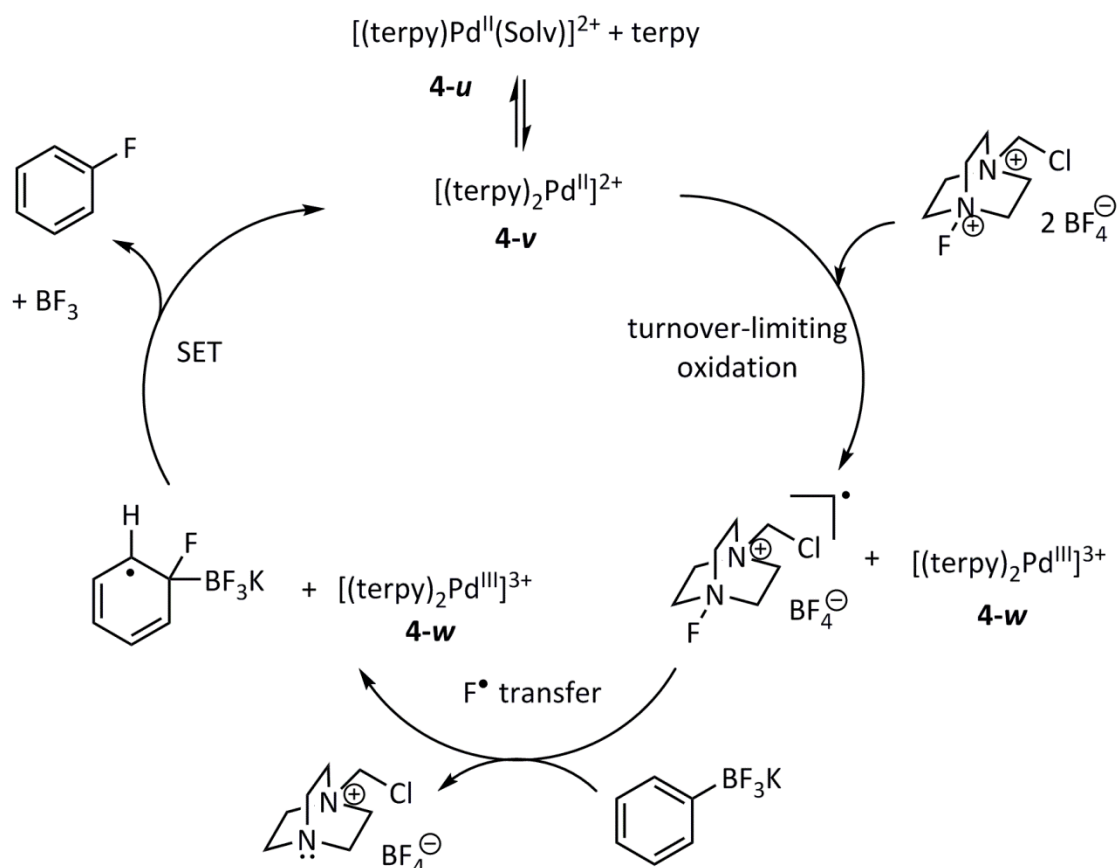
Scheme 4.9 Proposed SET mechanism for the palladium-catalysed fluorination of arylboronic acids

The first step of the mechanism is the turnover-limiting oxidation of **4-v** by Selectfluor to form palladium species **4-w** and a Selectfluor radical cation. The ability of Selectfluor to act as a single-electron oxidant has been previously documented in both experimental and theoretical studies.[170,204] The proposed palladium (III) intermediate could be synthesised under catalytically relevant conditions and characterised using EPR spectroscopy and X-ray crystallography. The EPR spectra indicated a d^7 electronic configuration with the unpaired electron centred on the palladium centre. Electrochemical measurements indicated that this oxidation occurred *via* an intermediate adduct between complex **4-v** and Selectfluor (potentially made possibly by the fluxional binding abilities of the terpy ligand (2,6-*bis*(2-pyridyl)pyridine) rather than by an outer-sphere SET; this is also consistent with the non-integer kinetic order measurement for Selectfluor of 1.4.

The subsequent carbon-fluorine bond formation could not be studied kinetically due to the preceding turnover-limiting oxidation step. There are two possibilities that must be considered: direct radical transfer of F to the arylboronic substrate, or a SET from the

arylboronic substrate to the Selectfluor radical cation, followed by nucleophilic attack of fluoride. In both cases, subsequent single-electron oxidation of the resulting organic radical would lead to the fluorinated aryl organic product and regeneration of complex **4-v** (palladium (II)). In order to further investigate the nature of the carbon-fluorine bond formation step, an isotopic labelling experiment was undertaken, shown in Scheme 4.10, in which the fluorination reaction was performed in the presence of [^{18}F]KF. If fluorination occurs *via* the nucleophilic attack of fluoride, some quantity of ^{18}F-labelled product should be observed. In fact this was not the case and, although the SET fluoride attack pathway *via* a tight solvent cage mechanism cannot be completely disregarded, the result supported the notion of fluorination by the radical pathway.
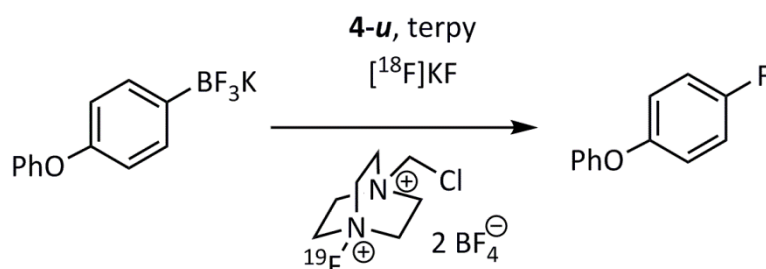
Scheme 4.10 Isotopic labelling experiment to investigate the nature of carbon-fluorine bond formation

This palladium catalysed fluorination reaction is highly unusual, in that it operates by a single electron transfer mechanism involving a well-defined palladium (III) intermediate, **4-w**. Therefore, in contrast to previously reported arene fluorination procedures which are presumed to operate *via* reductive elimination from metal-aryl fluoride complexes, this system instead proceeds in the absence of organopalladium intermediates yet still achieves high levels of selectivity. The reaction is practicable on a wide range of substrates under mild conditions on a multigram scale and in the presence of air and moisture, and therefore offers operational simplicity that lacked in previously reported aryl fluorination techniques. However, drawbacks of this reaction include the necessity of substrate prefunctionalisation, the inability to fluorinate heterocycles and the formation of isomers for some electron-poor substrates which then must be separated from the desired product.

4.1.5.3   Silver-mediated and catalysed aromatic fluorination

Silver-mediated fluorination methodology was first investigated by Tius[199,222] using XeF$_2$, and subsequent developments[223-225] in the field of fluorination using silver catalysts have lead to

the most functional group tolerant and versatile fluorination procedure reported to date.[212] (An alternative methodology for general access to functionalised aryl fluorides was reported by Buchwald in 2009 *via* a palladium-catalysed nucleophilic fluorination reaction, discussed in Section 4.1.5.5.[226]) Although the silver catalysis depends on the pre-functionalisation of substrates to toxic aryl stannanes, subsequent reactivity allows aromatic fluorination of nitrogen-containing heterocyclic nucleophiles and nucleophiles with electron-donating, electron-withdrawing, electrophilic and protic functional groups, including the structures of complex natural products. The general reaction and specific examples of fluorinated products are exemplified in Scheme 4.11.
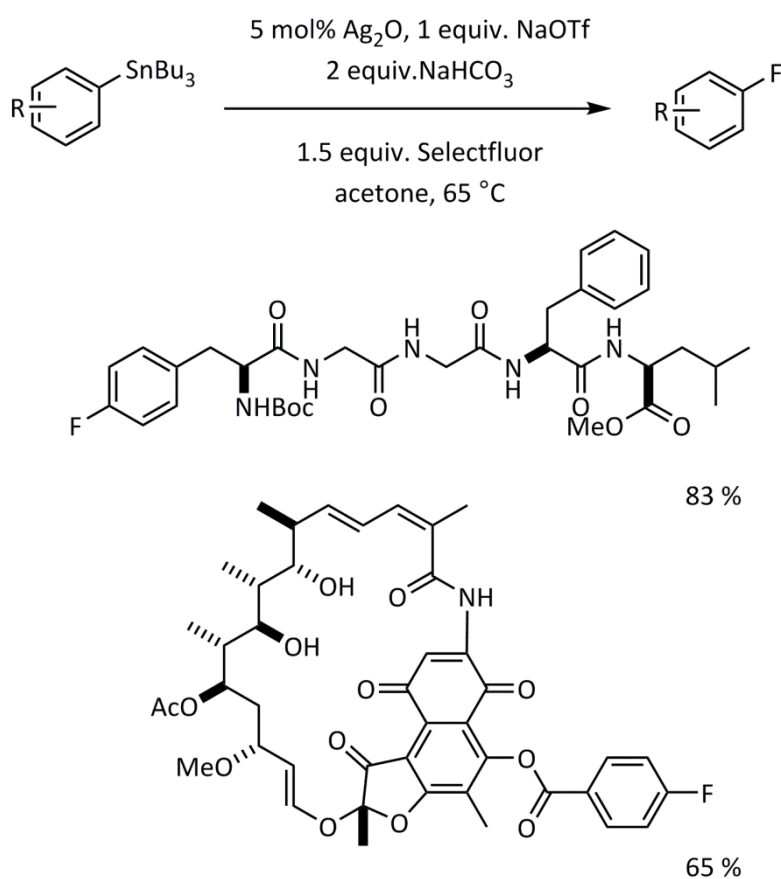
Scheme 4.11 Silver-catalysed aromatic fluorination of complex substrates

Silver catalysts are well established (as heterogenous oxidation catalysts in industry and as non-redox active Lewis acids in homogenous catalysis)[227], however, cross-coupling techniques tend to be based on transition metals such as palladium, whose two-electron redox pathways are well understood. Therefore, this study presented the first example of

silver (which participates in one electron redox processes) as a cross-coupling carbon-heteroatom catalyst.

The proposed mechanism of silver-catalysed aromatic fluorination *via* cross-coupling is shown in Scheme 4.12, and is distinct from conventional cross-coupling chemistry.
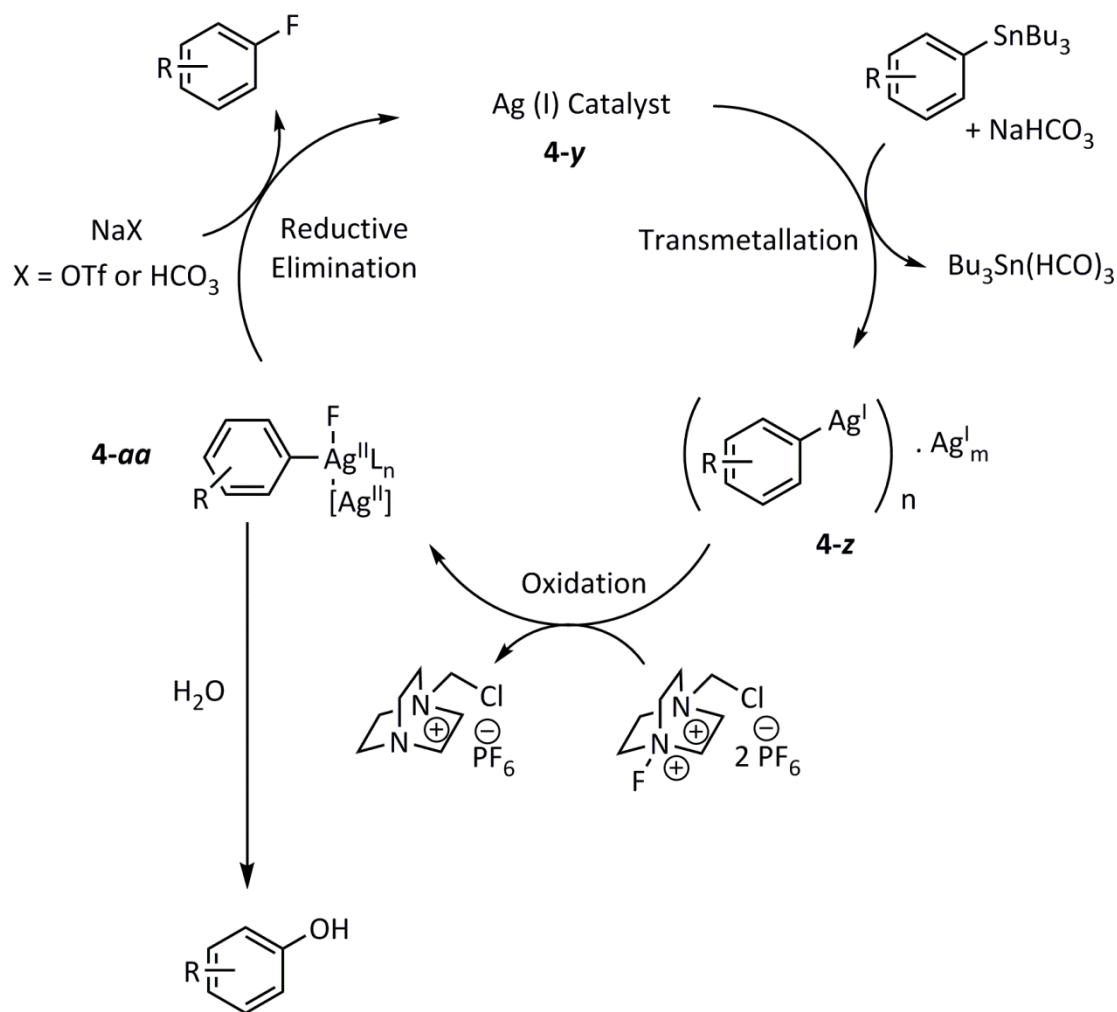
Scheme 4.12 Proposed mechanism of silver-catalysed aromatic fluorination using cross-coupling

Aryl transmetallation from tin to silver (I) produces arylsilver compounds such as **4-z**. Aggregation with additional silver (I) ions may occur under catalytic conditions, post-oxidation, to lead to dinuclear silver fluoride complex **4-aa**. The multinuclearity of **4-aa** is highly significant for this silver-catalysed cross-coupling scheme; silver participates in one-electron redox processes and therefore the presence of two ions may allow carbon-fluorine bond formation *via* metal-metal cooperation, in which more than one metal ion contributes to the redox activity. Indirect evidence for the involvement of a multinuclear silver

intermediate was obtained by an increased yield of aryl fluoride upon addition of two equivalents of silver catalyst to the reaction mixture rather than a stoichiometric amount. Reductive elimination of the carbon-fluorine bond leads to the aryl fluoride product and regeneration of the silver (I) catalyst, **4-y**.

This silver-catalysed fluorination procedure demonstrates a wide substrate scope and functional group compatibility which allows late-stage fluorination on complex precursor molecules such as strychnine under mild conditions, but still has several limitations; the preparation of toxic aryl stannanes adds an extra synthetic step, reduces atom economy and raises safety concerns, basic functional groups may interfere with Selectfluor to generate *N*-fluoro compounds which proceed to eliminate HF, and some protic functional groups which are deprotonated by $NaHCO_3$ (a component of the reaction mixture) proved problematic.

4.1.5.4   Copper-mediated fluorination

Despite the progression of aryl-fluorination reactions, the focus has centred on increasingly rare and expensive transition metal catalysed and mediated processes, with little attention paid to other possible mediators such as abundant first row metals. In 2013, independent publications by the Sanford and Hartwig groups highlighted the first example of fluorination mediated by copper, using arylboronic acid derivatives and $[FTMP]PF_6$, under mild reaction conditions and with a broad substrate scope, Scheme 4.13.[213,228] Sanford also reported a related fluorination of aryl stannanes.
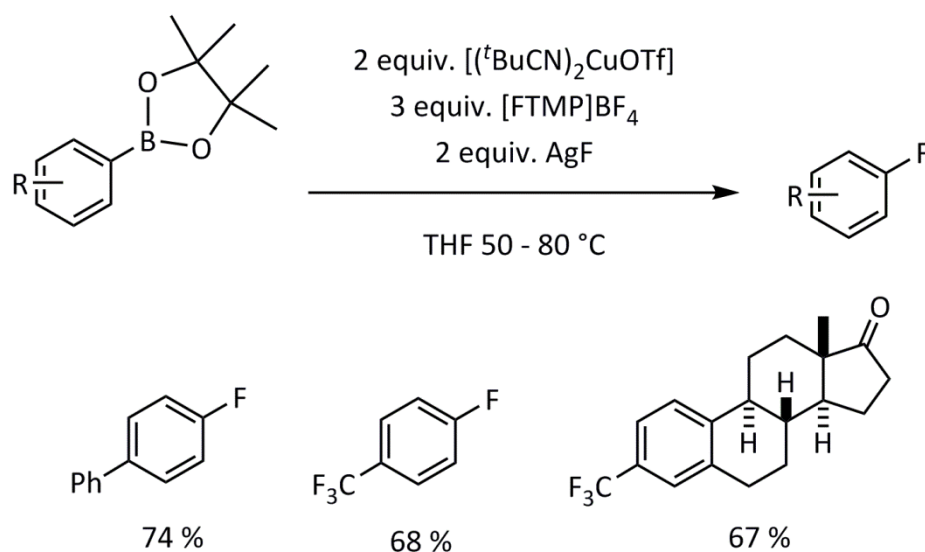
Scheme 4.13 Copper-mediated fluorination of arylboronic acid derivatives and selected examples of products. Yields obtained by ^{19}F NMR spectroscopy.

The methodology is applicable to aromatic substrates with either electron-donating or withdrawing substituents and with some heterocycles. However, the methodology is far from optimised – superstoichiometric amounts of both copper and oxidant are required and significant protodemetallation of the products is observed (primarily due to adventitious water).[228]

Mechanistic studies of copper-mediated fluorination suggest the reaction scheme illustrated in Scheme 4.14.[228]
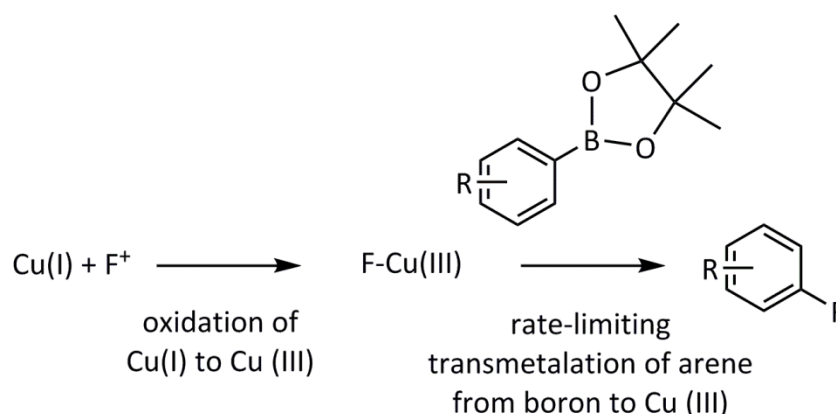
Scheme 4.14 Mechanism of copper-mediated aromatic fluorination

In this mechanism, the copper (I) is first oxidised to copper (III) by the [FTMP]PF$_6$ fluorinating agent, followed by slow transmetallation of the arene from boron to this high oxidation state Cu(III) intermediate. The nature of the fluorinating agent was important in terms of both the [TMP] and the PF$_6^-$ counter-ion – this is due to the identity of the copper (III)-fluoride intermediate in which both fragments are coordinated to the copper centre. Rapid reductive elimination from the copper (III)-fluoride forms the final carbon-fluorine bond. This reaction stands alone from that of the silver- and palladium-mediated routes reported previously, in that the transmetallation occurs at the high oxidation state metal centre.

4.1.5.5 Nucleophilic aromatic fluorination

Although the focus so far has focussed primarily on electrophilic fluorination, the inclusion of palladium-catalysed nucleophilic aromatic fluorination of aryl triflates as reported by Buchwald is necessary in order to provide a thorough introduction of transition-metal mediated routes to aryl fluoride compounds.[226,229] The Buchwald system provides general access to aryl fluorides with nucleophilic functional groups which are not often tolerated in electrophilic fluorination reactions due to competing side reactions. However, protic

functional groups are incompatible due to the strong basicity of the anhydrous fluoride source, and a mixture of constitutional isomers often forms due to the presence of aryne intermediates.[230] Reduction of the aryl triflate substrates to replace the carbon-fluorine bond with a carbon-hydrogen bond can also occur, which are subsequently difficult to separate.

Crucial to the success of this strategy was the choice of phosphine ligand, *t*BuBrettPhos, illustrated in Scheme 4.15. This ligand seemingly prevents the formation of a fluoride-bridged dimer of two palladium (II) centres; such species are subsequently unreactive to carbon-fluorine reductive elimination.[231] The bulky phosphine ligand also promotes carbon-fluorine reductive elimination from a three-coordinate, 'T-shaped' palladium (II) intermediate.[231]
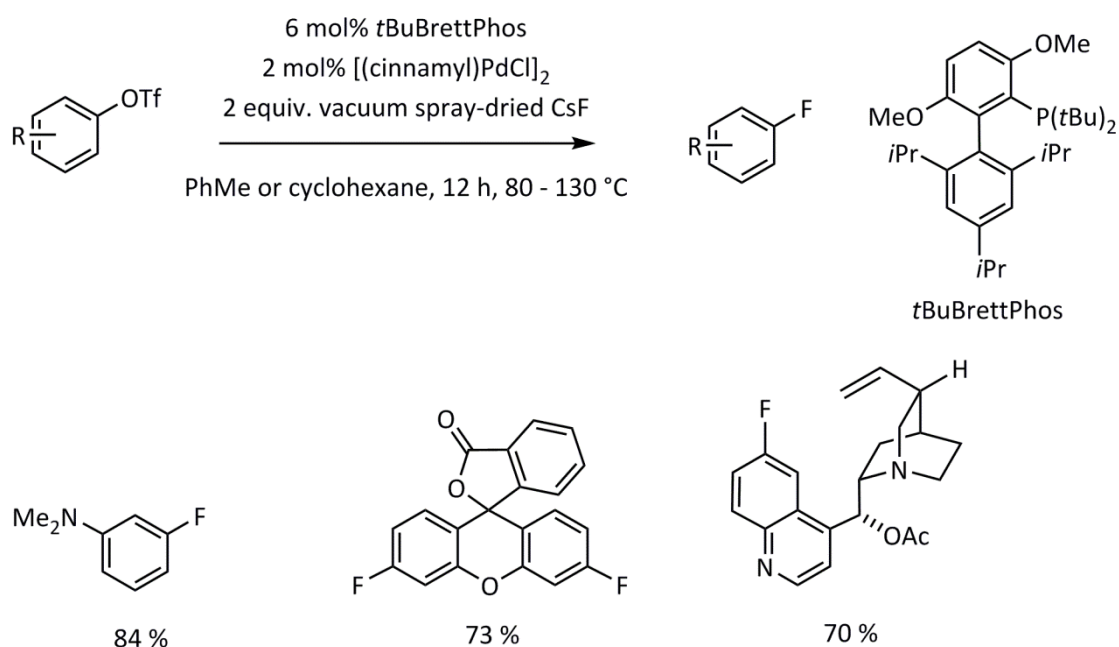
Scheme 4.15 Buchwald's palladium-catalysed nucleophilic aromatic fluorination[226]

Later developments by the Buchwald group uncovered a fluorination methodology for (hetero)aryl bromides and iodides with improved conditions to disfavour formation of the reduced arene side products, therefore allowing for more facile isolation of the aryl fluoride compounds.[232] However, the formation of constitutional isomers remains a problem for some substrates.

A facile and practical direct carbon-hydrogen to carbon-fluorine bond formation using AgF_2 has also been reported by the Hartwig group.[233] Using mild reaction conditions, 2-

fluoropyridine substrates with electron-donating and withdrawing groups, carbonyl functionality and base sensitive substituents can be synthesised, shown in Scheme 4.16.
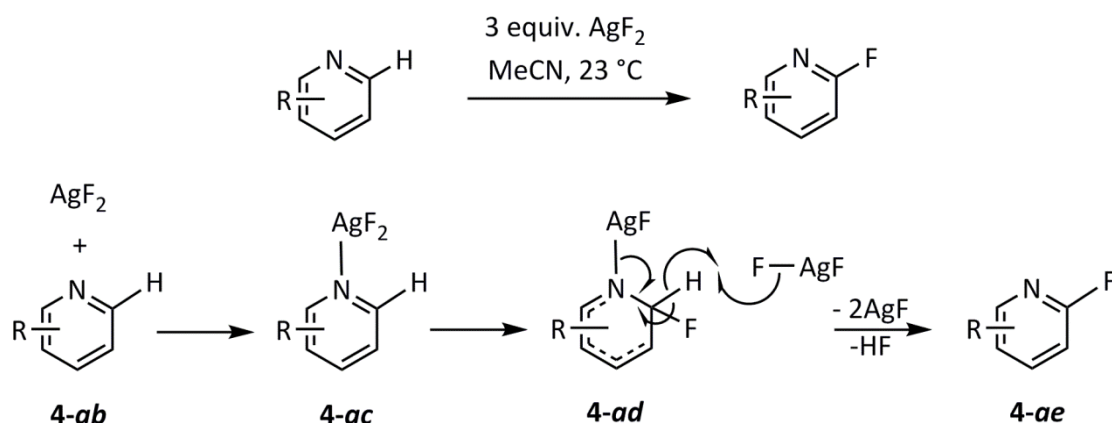
Scheme 4.16 Reaction scheme and proposed mechanism for the direct fluorination of *N*-heterocycles using AgF$_2$

The mechanism for this transformation is proposed to proceed *via* radical processes. The first step is coordination of the *N*-heterocycle to AgF$_2$ to form **4-*ac***. Addition of the silver-fluorine bond across the π-system of the pyridine yields an amido-silver(II)-fluoride complex, **4-*ad***, from which subsequent hydrogen atom abstraction affords the fluorinated organic product, **4-*ae***. This methodology can be used to prepare medicinally relevant compounds and the fluorinated products are easily separated from the protonated starting materials by column chromatography, due to a sufficient discrepancy between their basicities. AgF$_2$ is a readily available reagent, and the wide substrate scope and fast reaction times make this methodology an attractive choice for some applications. However, the *N*-heteroatom is essential to act as a directing group, and the reaction is intolerant to unprotected alcohols and amines.

Nucleophilic fluorination can also be mediated by copper complexes, as reported by several research groups including those of Ribas, Wang, Sanford and Hartwig, which are summarised in a recent review.[234]

4.1.5.6   Aromatic carbon-fluorine bond formation *via* oxidative fluorination

As described in Section 4.1.4, nucleophilic and electrophilic fluorination are complementary techniques which each possess key advantages and shortcomings. Fluoride salts are inexpensive and readily available, whereas reactions with sources of 'F$^+$' avoid unwanted side products due to problems of basicity.[170] The prospect of combining these two methodologies

by using fluoride anions and external oxidants is therefore highly desirable. Although this concept is very challenging, several groups have reported the first examples of oxidative fluorination for the preparation of both aliphatic and aromatic carbon-fluorine bonds.

Transition-metal free direct oxidative fluorination of aromatic carbon-hydrogen bonds is illustrated in Scheme 4.17.[235]
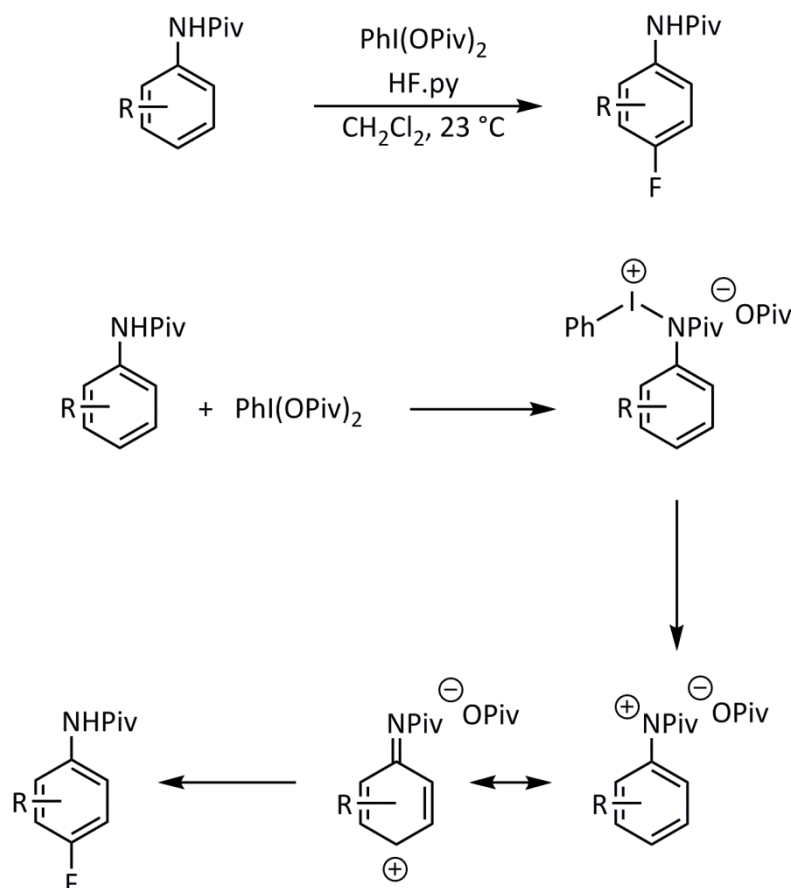
Scheme 4.17 Reaction scheme and proposed mechanism for the oxidative fluorination of anilide substrates

Although the substrate scope is limited to anilides, a range of substitution patterns are tolerated and fluorination occurs regioselectively to form the new carbon-fluorine bond in the *para*-position relative to the anilide functionality under mild conditions.

Copper-catalysed oxidative fluorination of benzoic acid derivatives was developed by the Daugulis group, Scheme 4.18.[236]
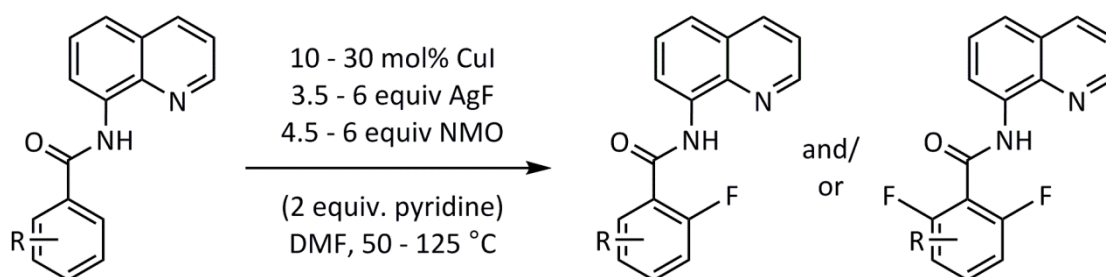
Scheme 4.18 Copper-catalysed oxidative fluorination of benzoic acid derivatives

The reaction requires a sterically bulky directing group derived from 8-aminoquinoline, with AgF as the source of fluoride and *N*-methylmorpholine *N*-oxide as the oxidant. Mono- or difluorination was observed in the aryl products.

In addition to direct oxidative fluorination, the methodology can also be applied to the fluorination of aryl metal complexes. In 2012, Ritter used aryl nickel (II) complexes for the regioselective synthesis of aryl fluorides, using a fluoride source of tetrabutylammonium triphenyldifluorosilicate (TBAT) and a hypervalent iodine oxidant **4-af**, Scheme 4.19.[237]
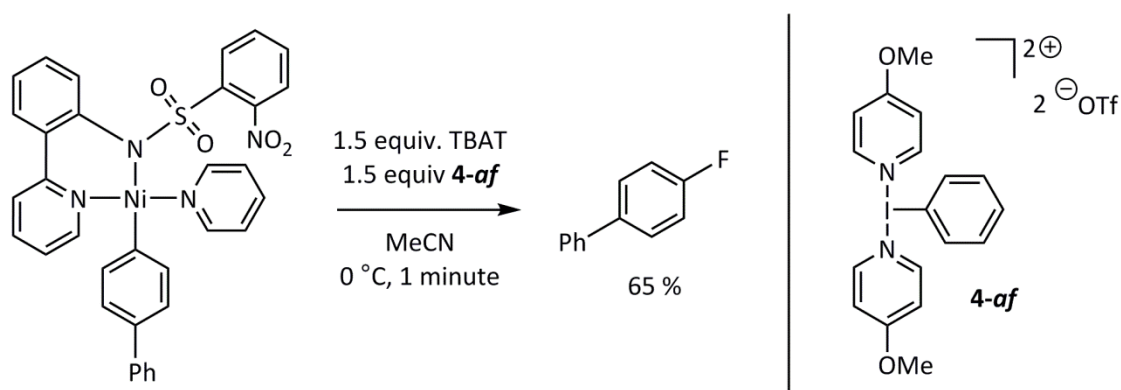
Scheme 4.19 Oxidative fluorination of aryl nickel complexes for the synthesis of ^{18}F-labelled tracers for PET

This process is extremely rapid and has hence been applied in the synthesis of ^{18}F-labelled aryl fluoride compounds to act as tracers in positron emission tomography.

The Sanford group reported that their previously published copper-mediated electrophilic fluorination reaction (Section 4.1.5.4) could alternatively be performed using oxidative fluorination techniques, by a simple replacement of the N-fluoropyridinium salt with KF and excess Cu(OTf)$_2$, Scheme 4.20.[238]
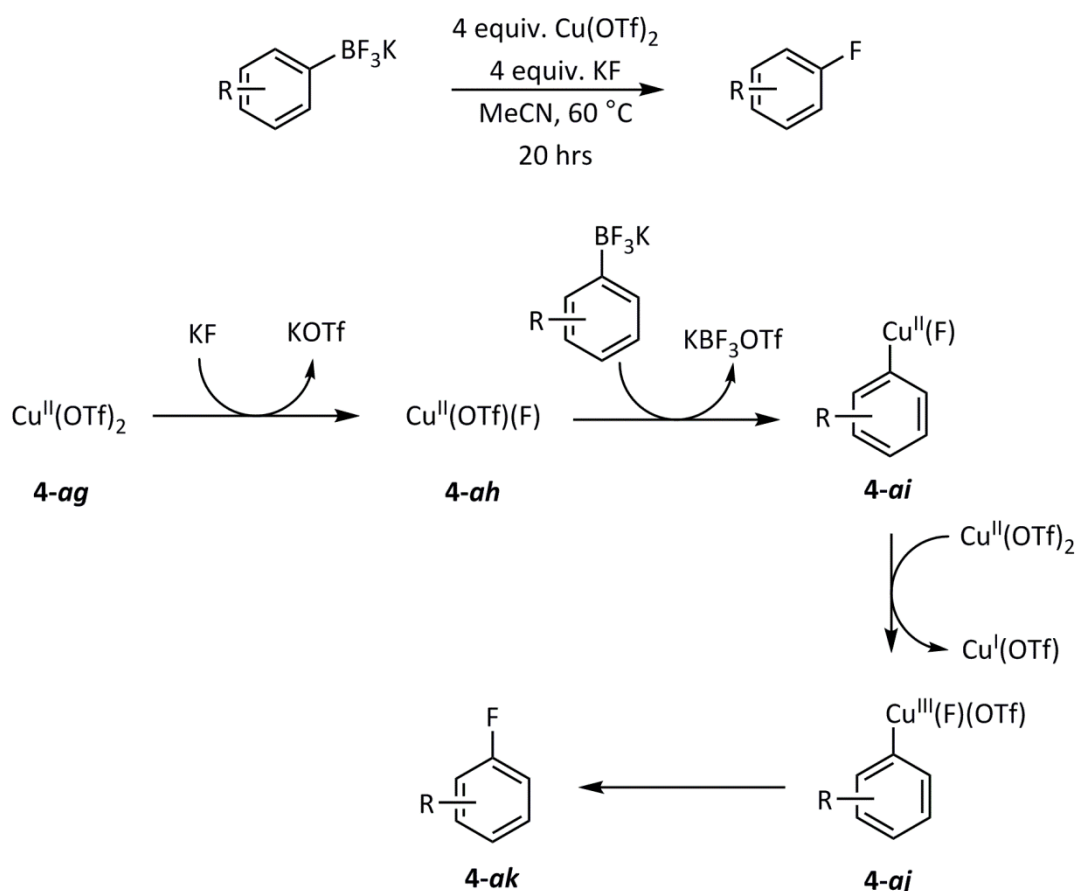
Scheme 4.20 Copper-mediated oxidative fluorination of aryl trifluoroborate substrates

The mild reaction conditions necessary for this transformation suggest that the activation barrier to carbon-fluorine coupling is low, and therefore the proposed mechanism includes a highly reactive copper (III) intermediate, **4-aj**. In Scheme 4.20, $Cu(OTf)_2$ plays a dual role; it acts both as the carbon-fluorine bond promoter and as a one-electron oxidant to form the copper (III)-aryl fluoride intermediate. Consistent with this role, the yield decreases dramatically on the use of less than two equivalents of $Cu(OTf)_2$ in the reaction mixture. The redox synergy of the two metal centres may help to lower the high kinetic barrier to carbon-fluorine reductive elimination, therefore allowing the use of milder reaction conditions.

The reaction has a wide substrate scope and is compatible with carbonyl functionality and heterocycles (although yields tend to decrease). However, many substrates give rise to small amounts of protodeboronated side products which in some cases are impossible to separate from the fluorinated species.

4.1.6 Transition-metal mediated sp³-carbon-fluorine bond formation

Aliphatic electrophilic fluorination reactions often employ stabilised carbanions as nucleophiles (such as β-keto carbonyl derivatives) in conjunction with fluorinating agents. An alternative approach involves the incorporation of fluorine across alkene moieties, which can be promoted by organocatalysts,[239] Lewis acids,[216] or phase transfer catalysis.[240]

Enantioselective variations of both of these types of reactions are known, and mechanisms with radical intermediates have been reported which opens these reactions to alternative substrate pools to those which operate through two-electron transfer processes.

Aliphatic nucleophilic fluorination reactions for the synthesis of sp³-carbon-fluorine bonds are also possible but are outside the scope of this chapter introduction. These methods are summarised in several reviews by Ritter *et al.*[170,202]

4.1.6.1 Electrophilic fluorination of carbonyl derivatives

The choice of strongly oxidising fluorination reagents, such as gaseous F_2 or XeF_2, used in conjunction with carbonyl and carbonyl-derived compounds often leads to α,α-difluorinated species.[241] Electrophilic fluorination agents however tend to be less reactive and more functional group tolerant, and so produce α-monofluorinated products.[242] Asymmetric α-fluorination has been achieved with both chiral fluorinating agents and chiral catalysts, which promote chiral enolate intermediates.[243-245]

To allow the enantioselective fluorination of dicarbonyls, the two point binding to Lewis acid complexes has been exploited. A vast range of catalysts have been developed, including titanium-, copper-, ruthenium- and scandium- based complexes,[216] but the most successful is a nickel complex, allowing the largest substrate scope with a modest 10 % catalyst loading, Scheme 4.21.[246]
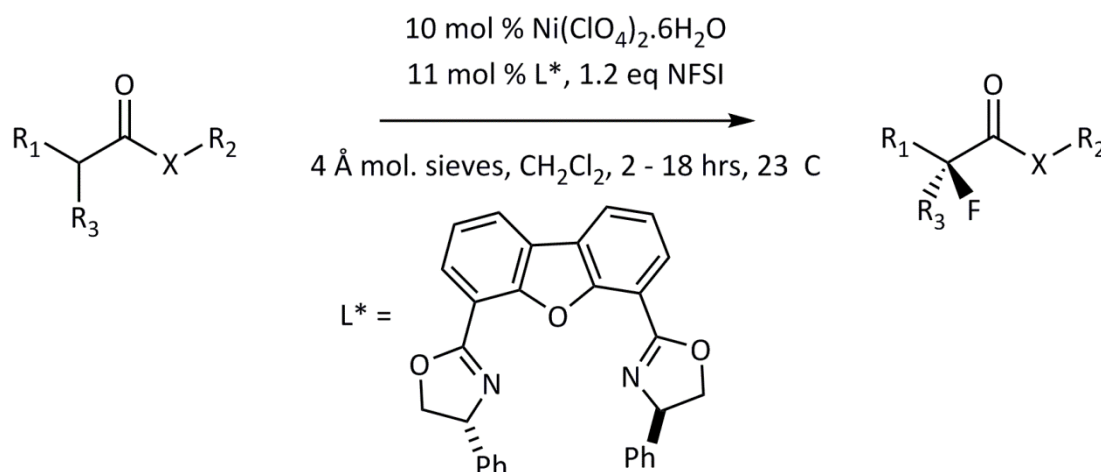
Scheme 4.21 Enantioselective nickel-catalysed fluorination of dicarbonyl-containing substrates. X and R_1 = oxygen, carbonyl, NBoc, aryl, R_2 = tBu, adamantly, benzyl and R_3 = aryl

This system produces yields and enantiomeric excesses of 71 – 93 and 83 – 99 % respectively, depending on the nature of the substrates. A high level of enantiomeric control is crucial in the formation of pharmaceutical and agrochemical products in which the identity of the enantiomer can have significant impacts on the biological effects. However, the necessity of highly activated substrates is a disadvantage of these approaches due to the limitations placed on the potential substrate scope. Notably, this mechanism is significantly different to those discussed in Section 4.1.5.1 as no redox activity of the metal is necessary.

Chiral palladium complexes can also be used for the enantioselective fluorination of dicarbonyl compounds, including β-keto esters as shown in Scheme 4.22.[247]
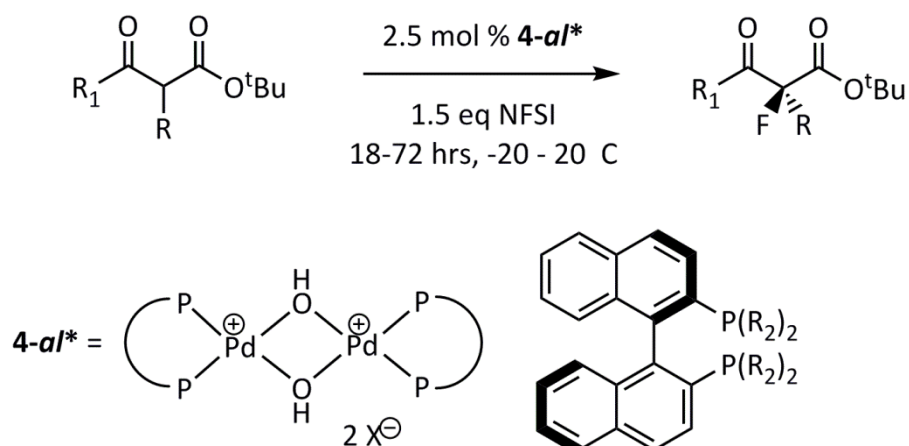
Scheme 4.22 Chiral palladium catalysis for the enantioselective fluorination of dicarbonyl-containing substrates. X = OTf or BF_4, R and R_1 = alkyl or aryl and R_2 = 3,5-dimethylphenyl

Organocatalysts are an alternative way to provide enantioinduction, by behaving as chiral fluorinating agents or generating chiral nucleophiles by reaction or coordination with the substrates.[175,239] An example of this principle is the reaction of substrates with cinchona alkaloids in the presence of achiral fluorinating agents.[248] Cinchona alkaloids impart chirality to the fluorinating agent rather than the substrate in order to control the enantioselectivity of the reaction. Despite the reduced substrate scope that is compatible with cinchona alkaloids in comparison to the scope available to Lewis-acid mediated strategies, the alkaloid approach has the advantage of being functional in the absence of a two-point binding site.

Additionally, phase-transfer catalysis can provide simple synthetic procedures for enantioselective fluorination reactions.[240] To ensure the formation and security of tight ion pairs (which cause the chirality), non-polar solvents are favoured. However, this approach is not always effective due to ion pair dissociation or other background reactions.

4.1.6.2 Electrophilic fluorination across double bonds

The fluorination of an alkene is an alternative method to synthesise fluorinated, sp^3-hybridised carbon centres. If an alkene is activated, such an enamine, then no catalyst is required and fluorination often occurs under mild conditions, Scheme 4.23.[249] In this example, the enamine undergoes electrophilic fluorination and the carbocation is trapped using cyanide.
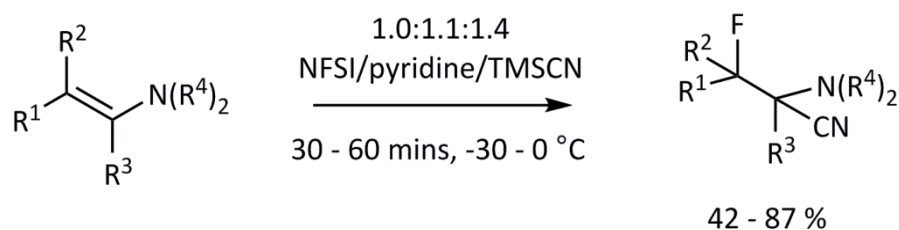
Scheme 4.23 Fluorocyanation of enamines

However, non-activated alkenes are less reactive and so require the presence of a catalyst. An example of this technique is shown in Scheme 4.24.[250]
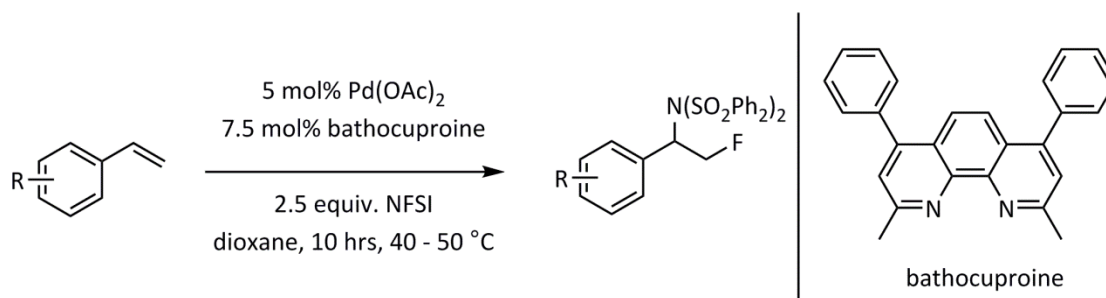
Scheme 4.24 Palladium-catalysed electrophilic aminofluorination

The mechanism for the aminofluorination reaction is thought to proceed by an initial fluoropalladation reaction involving the metal complex, fluorinating agent and substrate, followed by oxidation to a palladium (IV) species with subsequent reductive elimination of the carbon-nitrogen bond.

4.1.6.3 Electrophilic fluorination *via* carbon-fluorine reductive elimination

The first example of direct, palladium-catalysed carbon(sp^3)-fluorine bond formation was reported in 2006 by the Sanford group.[217] Under similar conditions to those reported in Section 4.1.5.2 for the fluorination of aryl pyridines, with [FTMP]BF$_4$ as the fluorine source and Pd(OAc)$_2$ as the catalyst, the fluorination of 8-methylquinoline derivatives can afford fluorinated quinolone products, Scheme 4.25.
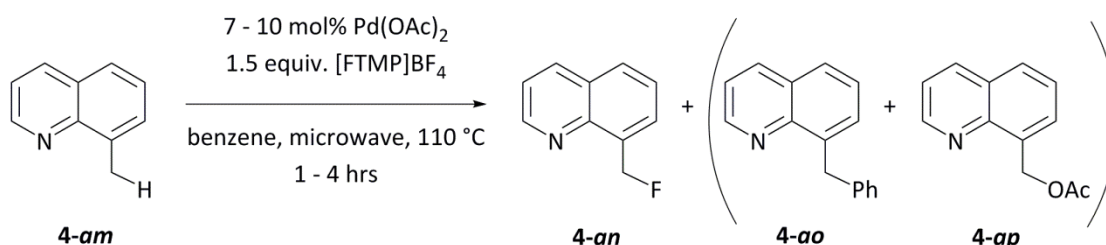
Scheme 4.25 The first example of palladium-catalysed carbon(sp^3)-fluorine bond formation

As in Section 4.1.5.2, the 8-methylquinolone substrate **4-am** was chosen as it contains a pyridyl moiety which directs carbon-hydrogen bond activation at palladium, and therefore imparts selectivity on the reaction. Two minor side products were obtained during the fluorination reaction of 8-methylquinoline derivatives – a phenylated product **4-ao** and an acetoxylated product **4-ap** – neither of which was observed during similar reactions with phenylpyridine. The reaction tolerates a range of functionality including aryl halides, ketones and esters, trifluoromethyl substituents and methyl ethers. The compatibility with aryl bromides is synthetically useful as these substrates readily undergo further reactions.

However, as with the direct carbon-fluorine aryl bond formation, the necessity of a directing group to template the reaction at palladium places limitations on the applicability of this approach in synthesis.

Until 2012, sp^3 carbon-fluorine bond formation was proposed to occur *via* transient and highly reactive palladium (IV)-fluoride intermediates, however, detailed understanding of the metal complexes involved in the key bond formation step was incomplete. Although several groups had proposed palladium (IV)-fluoride complexes as key intermediates,[251-252] such species had not been isolated. A seminal publication by the Sanford group reported air and moisture stable fluoride complexes, which reacted to afford clean reductive elimination at the alkyl ligand (in preference to the more commonly favoured aryl carbon groups).[214] The process of fluoride formation and subsequent carbon-fluorine bond formation is shown in Scheme 4.26.
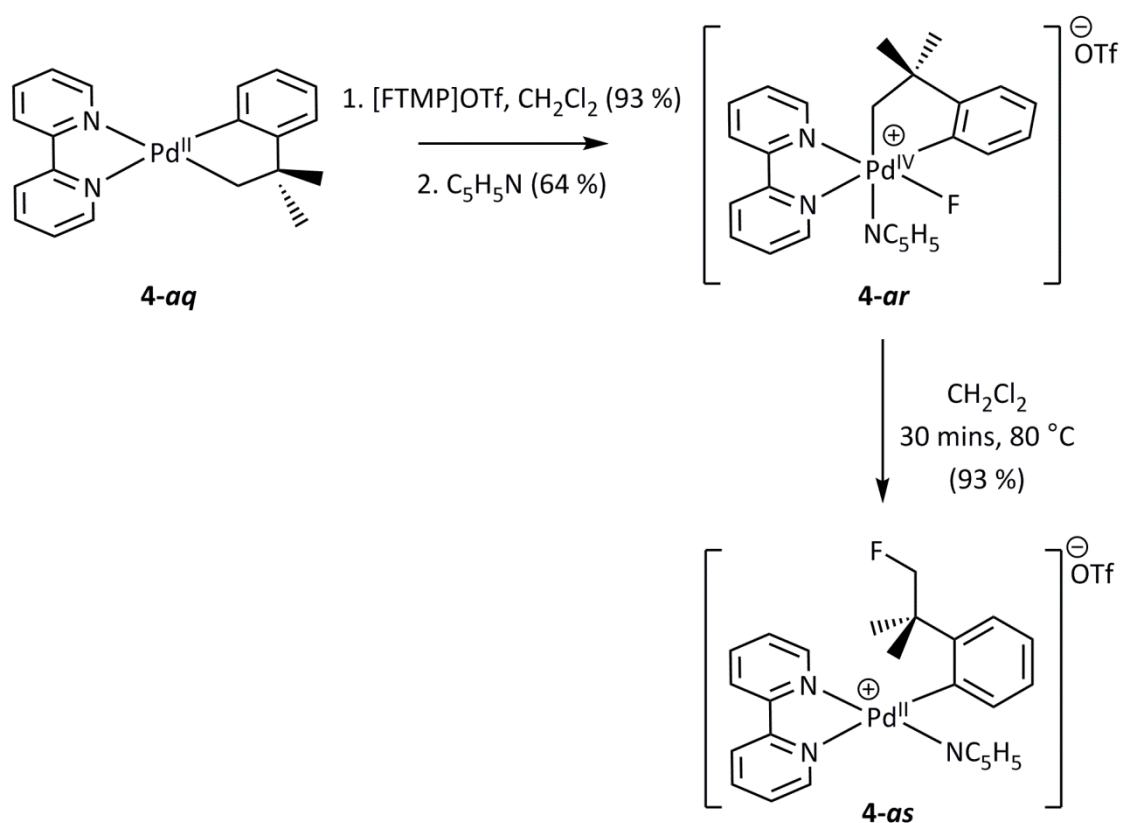
Scheme 4.26 Isolation and subsequent reactivity of a palladium (IV)-fluoride complex in carbon(sp^3)-bond formation

Mechanistic studies suggest that in the formation of **4-as** from **4-ar**, the first step is pyridine loss from the palladium centre, due to an inverse first-order dependence on pyridine

concentration. Following this, carbon-fluorine coupling could form either from direct reductive elimination or fluoride dissociation to form a palladium (IV) dication which could undergo nucleophilic attack. Direct reductive elimination is most probable as fluoride is a poor nucleophile in S_N2 reactions (especially at sterically protected positions), the generation of a dicationic intermediate is expected to be disfavoured, and the retention of stereochemistry at the β-carbon mimics analogous reactions from platinum (IV) and gold (III) complexes.[252-253] Computational studies showed a lower energy transition state for the formation of the alkyl-fluorine bond compared to the aryl-fluoride bond, suggesting that the selectivity is an 'inherent preference' of this palladium complex. No method to liberate the ligand from the metal centre was stated, and the fluorinated ligand is retained in the coordination sphere of the metal.

A further example of carbon(sp^3)-fluorine bond synthesis by reductive elimination from high valent complexes includes a gold-mediated system.[253] In this instance, stoichiometric gold (I) complexes are oxidised by XeF_2 to form gold (III)-fluoride intermediates, from which reductive elimination affords aliphatic fluorides. However, due to the strongly oxidising properties of XeF_2 and the propensity of gold complexes to undergo β-hydride elimination has restricted the substrate scope largely to β,β-disubstituted alkanes.[253]

4.1.6.4 Carbon(sp^3)-fluorine bond formation *via* oxidative fluorination

The first report of aliphatic carbon-fluorine bond formation *via* oxidative fluorination was published by the Sanford group in 2012.[254] Using a hypervalent iodine oxidant and silver fluoride, the fluorination of 8-methylquinolyl derivatives could be catalysed by $Pd(OAc)_2$, Scheme 4.27.
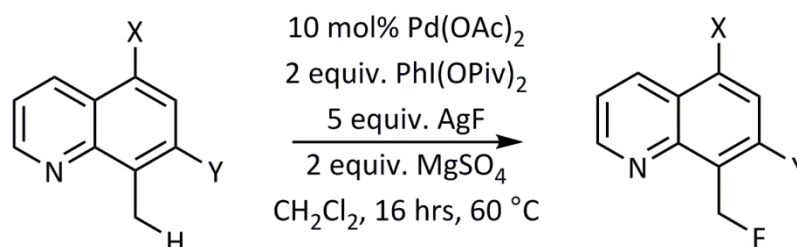
Scheme 4.27 Formation of carbon(sp^3)-fluorine bonds using palladium-mediated oxidative fluorination. X = H or Br, Y = H, NO_2, CN, CO_2Me, F, Br, I, OMe, Me or Ph

Oxidative fluorination can also be catalysed by a manganese porphyrin catalyst as shown in Scheme 4.28.[255]

6 - 8 mol% [Mn(TMP)Cl]
3 equiv. AgF, 0.3 equiv. TBAF.3H$_2$O
6 - 8 equiv. PhIO

MeCN/CH$_2$Cl$_2$ (3:1)
6 - 8 hrs, 50 °C

[Mn(TMP)Cl]
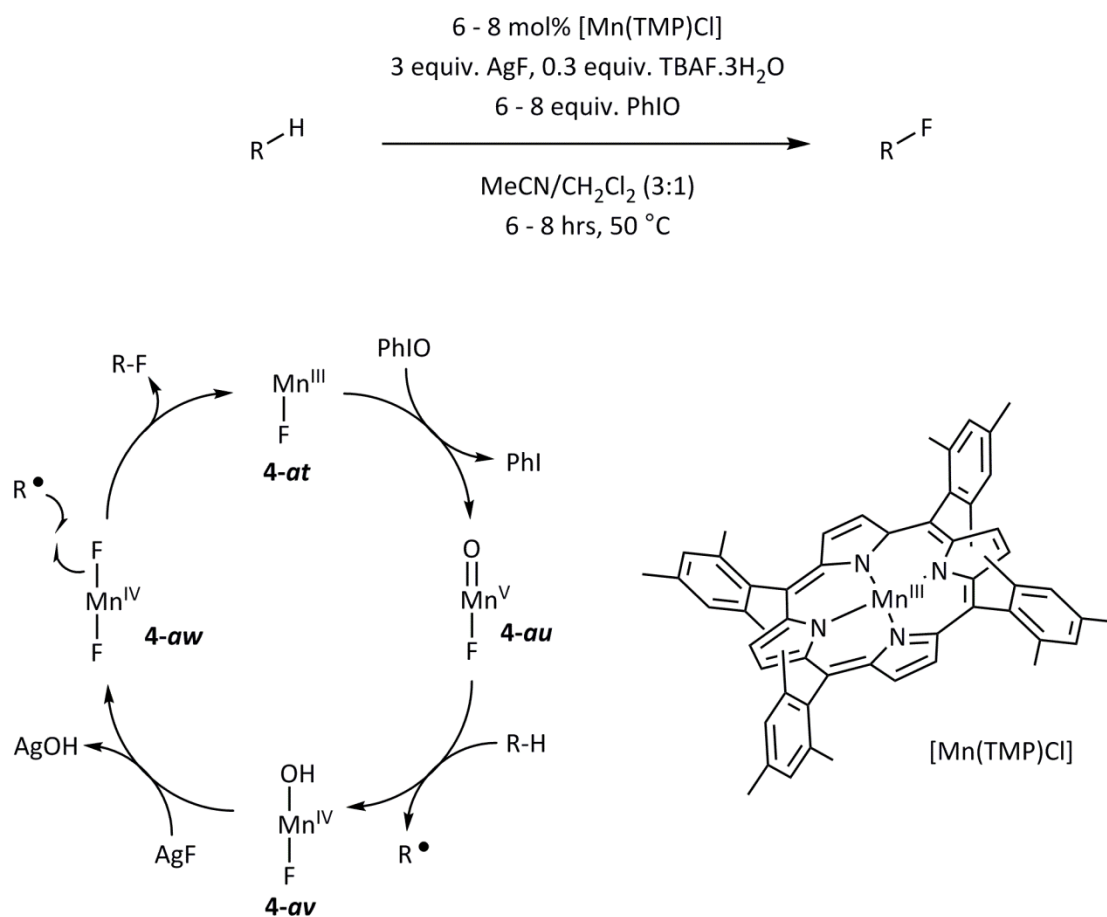
Scheme 4.28 Reaction scheme and projected mechanism of manganese-catalysed oxidative fluorination

The suggested catalytic cycle begins with oxidation of the resting state Mn (III) catalyst, **4-at**, using iodosylbenzene as the oxo-transfer agent to afford the oxomanganese (V) species **4-au**. **4-au** can then abstract a proton from the substrate to produce a carbon-centred radical and a Mn (IV)-hydroxy intermediate, **4-av**. Subsequent fluorination of **4-av** affords **4-aw**, from which a radical-mediated carbon-fluorine bond formation can occur to produce the fluorinated product and regenerate **4-at**. This system allows access to a range of fluorinated organic molecules containing complex functionality, including substituted cyclic molecules, terpenoids and steroid derivatives. Given that the source of fluorine is a fluoride ion, it is possible that this one-step one-pot protocol may be utilised for the production of ^{18}F labelled medical imaging agents in the future.

4.1.7   Summary and aims

The extensive current research in the field of carbon-fluorine bond formation, as highlighted in this review, indicates that fluorination chemistry is an active and important area of study, but one which presents significant synthetic challenges. Due to the use of fluorinated compounds in applications including pharmaceuticals, agrochemicals, liquid crystals and medical imaging agents, the development of fluorination methods to allow the selective formation of carbon-fluorine bonds is essential.[170] Despite momentous recent advances however, novel fluorination techniques are still required which provide stereo- and regioselectivity under practical reaction conditions from non-activated substrates, and which can provide access to less common structural frameworks including sp^2- and sp^3-hybridised carbon-fluorine bonds.[63]

In Chapter 3, modifications were attempted on a ruthenium catalyst for pyridine alkenylation, in order to prevent the formation of ruthenium metallocycle **[16$^{\text{CF3}}$]** which acted as a catalyst deactivation product. However, complex **[16$^{\text{CF3}}$]** presents an interesting organometallic complex; the structure contains a pyridylidene ligand which can be formed in high yield from non-activated substrates (pyridine and 4-ethynyl-α,α,α-trifluorotoluene). Therefore, the reactivity of **[16$^{\text{CF3}}$]** was studied in the presence of electrophilic fluorinating agents in an attempt to incorporate this complex into an alternative catalytic cycle.

Experimental studies revealed unpredicted reactivity and behaviour of **[16$^{\text{CF3}}$]** with sources of 'F$^+$' and therefore the mechanism of the fluorination reaction was investigated using detailed computational mechanistic studies in order to elucidate the reaction pathway.

4.2 Synthesis and characterisation of fluorinated ruthenium metallocycles

4.2.1 Synthesis and characterisation of complex [16^{CF3}]

As described in the previous chapter, access to ruthenium metallocycle **[16^{CF3}]** was revealed serendipitously during a mechanistic investigation of the mono-alkenylation of pyridine. In this catalytic system the complex was considered as a deactivation product, as further reaction to form the desired organic product, **14^{CF3}**, from **[16^{CF3}]** required high energy conditions.[45] However, complex **[16^{CF3}]** was of considerable interest due to its preparation from non-activated substrates (pyridine and 4-ethynyl-α,α,α-trifluorotoluene) under mild conditions; the number of examples in which unsubstituted pyridine is converted to the parent pyridylidene is limited. Therefore, we were interested in understanding the reactivity of **[16^{CF3}]** in order to incorporate this complex into a productive catalytic cycle. Electrophilic fluorination seemed to be a promising strategy in order to do this, and several possible products were considered, Scheme 4.29.

Related palladium-mediated fluorination chemistry would predict formation of a ruthenium-fluoride intermediate, **[O]$^{+}$**, which could potentially undergo reductive elimination to form a fluorinated pyridinium group, **[Q]$^{+}$**. Alternatively, a formal 'F^{+}' transfer, analogous to the known protonation of **[16^{CF3}]** would lead to the β-fluorovinyl pyridylidene complex, **[R]$^{+}$**.
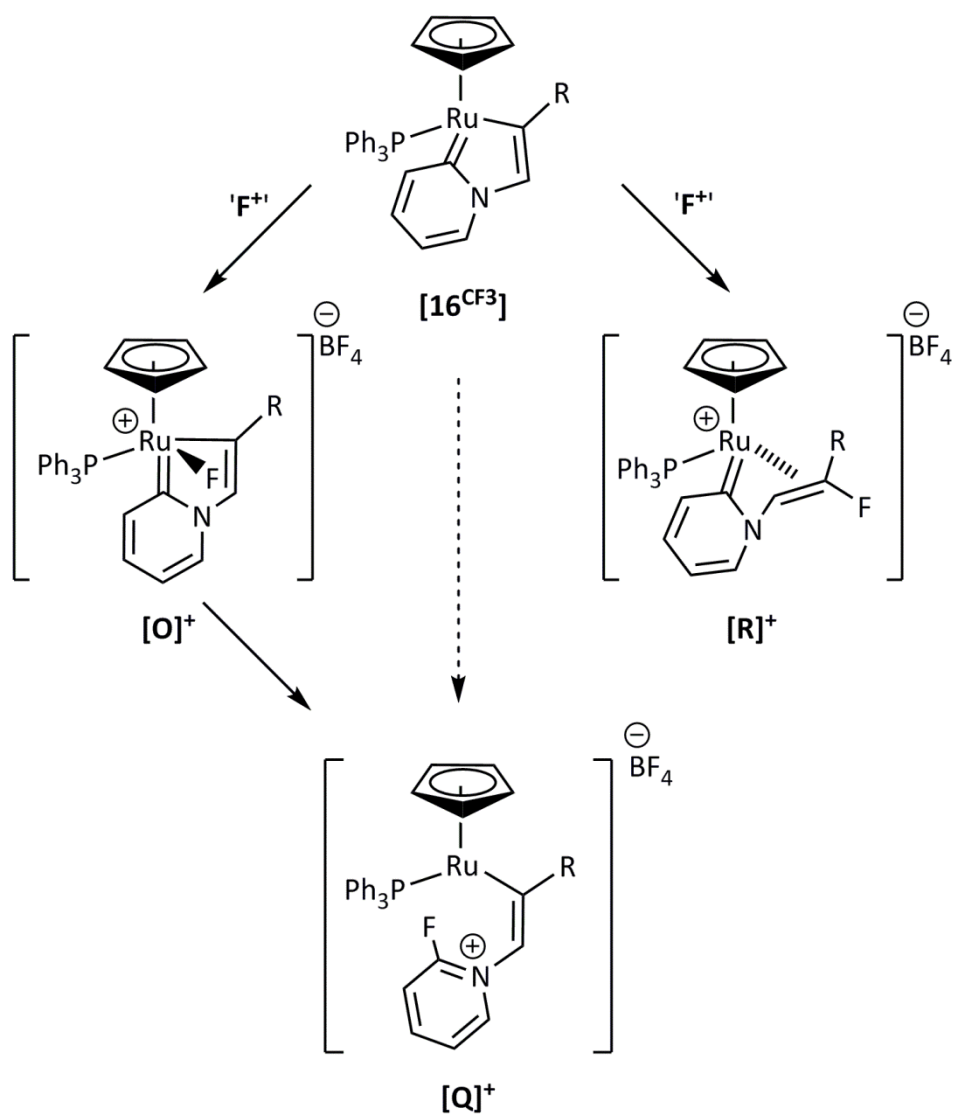
Scheme 4.29 Potential electrophilic fluorination products of [16^{CF3}]

The optimised synthetic procedure to form **[16^{CF3}]** is shown in Scheme 4.30.

Scheme 4.30 Optimised synthetic route to complex [16$^{\text{CF3}}$], R = -C$_6$H$_4$-4-CF$_3$

The isolated yields of **[16$^{\text{CF3}}$]** when synthesised by the literature procedure were low and the product was often obtained as a mixture of **[13$^{\text{CF3}}$]PF$_6$** and **[16$^{\text{CF3}}$]**.[45] Therefore, the synthesis underwent several optimisation steps.

By ^{31}P{^{1}H} NMR spectroscopy, conversion of **[7]PF$_6$** to **[13$^{\text{CF3}}$]PF$_6$** was observed to be 95 % however the isolated yield of **[13$^{\text{CF3}}$]PF$_6$** was reported to be only 48 % (after repeated crystallisations by the slow diffusion of pentane into a dichloromethane solution of the complex to obtain high purity).[45] Therefore, from complex **[7]PF$_6$**, the reaction to form **[16$^{\text{CF3}}$]** was instead carried out *in situ* without isolation of **[13$^{\text{CF3}}$]PF$_6$**. The impurities observed in the

spectra of complex [13^{CF3}]PF$_6$ could be removed during the work-up and purification of [16^{CF3}].

Secondly, the literature procedure for conversion of [13^{CF3}]PF$_6$ to [16^{CF3}] used two equivalents of DABCO to afford complete deprotonation of [13^{CF3}]PF$_6$, and after stirring for 18 hours the solvent was then completely removed *in vacuo*. The neutral ruthenium complex [16^{CF3}] was subsequently extracted from the dry residue by the addition of pentane and cannula filtration. However, this afforded a broad signal in the ^{31}P{^{1}H} NMR spectra, assumed to be a fluxional mixture of [13^{CF3}]PF$_6$ and [16^{CF3}]. In some cases, resonances for neutral DABCO could also be observed in the ^{1}H NMR spectra. In order to purify the samples, the volume of pentane could be reduced to allow crystallisation in the freezer but in our hands this was consistently unsuccessful. Therefore, this procedure was slightly modified and a sub-stoichiometric quantity (0.9 equivalents) of DABCO was used to deprotonate [13^{CF3}]PF$_6$. This allowed for complete removal of the protonated DABCO from ruthenium complex [16^{CF3}] with no contamination from residual neutral base. Furthermore, instead of evaporation of the dichloromethane solvent to dryness after stirring, the volume was reduced and complex [16^{CF3}] was precipitated by the addition of excess pentane. This could then be isolated by cannula filtration and produced higher yields of [16^{CF3}] which could be used without further purification.

4.2.2 Synthesis and characterisation of complex [20]BF$_4$

Treatment of [16^{CF3}] with a stoichiometric quantity of [FTMP]BF$_4$ resulted in quantitative and rapid conversion to [20]BF$_4$ (monitored by NMR spectroscopy). The ^{31}P{^{1}H} NMR spectrum showed a single resonance at 47.2 ppm with a $^4J_{PF}$ coupling of 7.7 Hz between the newly incorporated fluorine atom and the phosphorus atom of the triphenylphosphine ligand. The incorporation of fluorine could be confirmed by the ^{19}F NMR spectrum which displayed a resonance at −139.8 ppm with a corresponding coupling to coupling to triphenylphosphine, $^4J_{PF}$ of 7.7 Hz, and a $^2J_{HF}$ coupling constant of 52.0 Hz. This reciprocal coupling constant could be located in the ^{1}H NMR spectra as a resonance at 4.71 ppm with an integration of one proton (relative to the cyclopentadienyl resonance at 5.37 ppm). ESI-MS confirmed the incorporation of a single fluorine atom with a peak at m/z 696.1023 for a cationic molecular ion. The fluorination is also possible with alternative fluorinating agents including NFSI and Selectfluor.

As noted in Section 4.2.1, on the addition of stoichiometric 'F^{+}' several organometallic species were envisaged as potential products of electrophilic fluorination. The oxidative fluorination of **[16^{CF3}]** (as reported in related palladium chemistry) would form a ruthenium-fluoride containing species such as **[O]$^{+}$** in Scheme 4.31; however this product was inconsistent with the spectroscopic data. A metal-fluoride complex of this type would be expected to show an upfield chemical shift between -200 and -450 ppm in the ^{19}F NMR spectrum, and would not exhibit the $^{2}J_{HF}$ coupling constant of 52.0 Hz that was observed in both the ^{19}F and ^{1}H NMR spectra.[256-259] This coupling constant also disfavoured the presence of a fluorinated pyridinium group, **[Q]$^{+}$**, which would have formed from reductive elimination across the ruthenium-pyridylidene bond in complex **[O]$^{+}$**, Scheme 4.31. Similarly, a formal 'F^{+}' transfer (analogous to the known protonation of **[16^{CF3}]**) to form a β-fluorovinyl pyridylidene complex **[R]$^{+}$** was also implausible from the NMR spectra. In fact, single crystal X-ray diffraction confirmed incorporation of the fluorine atom at the 3-position of the 1-ruthanaindolizine ring leading to the unexpected formation of complex **[20]BF$_4$**, Scheme 4.31.
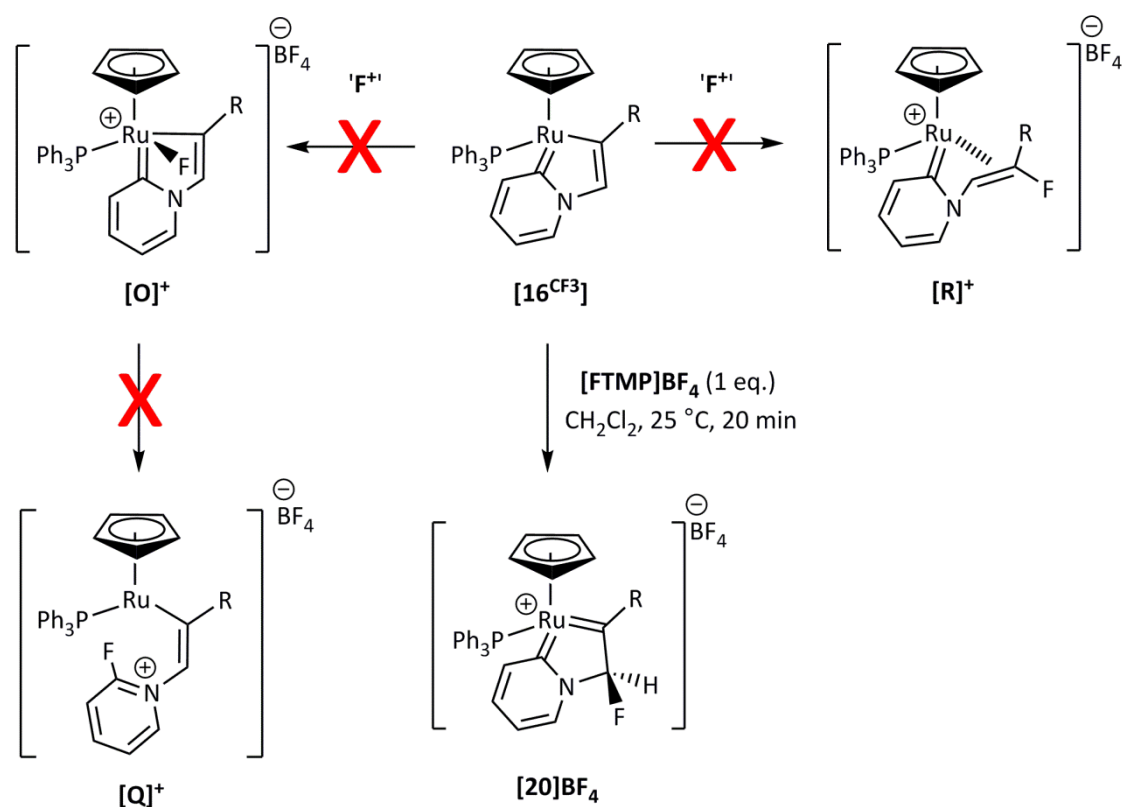
Scheme 4.31 Predicted ([O]$^{+}$, [Q]$^{+}$ and [R]$^{+}$) products and actual products ([20]BF$_4$) of electrophilic fluorination of complex [16^{CF3}]

There are two possible Lewis structures that can be drawn for complex [20]BF$_4$, Scheme 4.32.

[20]BF$_4$
pyridylidene form
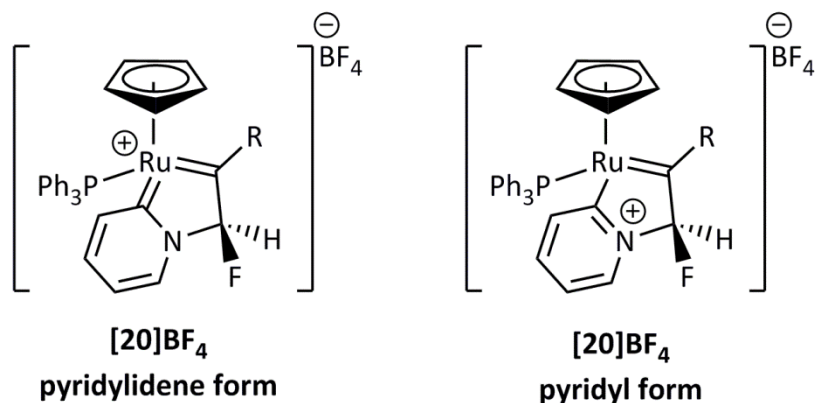
[20]BF$_4$
pyridyl form

Scheme 4.32 The pyridylidene- and pyridyl-based Lewis structures of [20]BF$_4$

Although each of these resonance forms may contribute to the overall structure, data from single crystal X-ray diffraction, NBO analysis and ^{13}C NMR studies suggest that the pyridylidene based Lewis structure most clearly represents the experimental data.

The solid-state structure of **[20]BF$_4$**, as determined by single crystal X-ray diffraction, is shown in Figure 4.4.
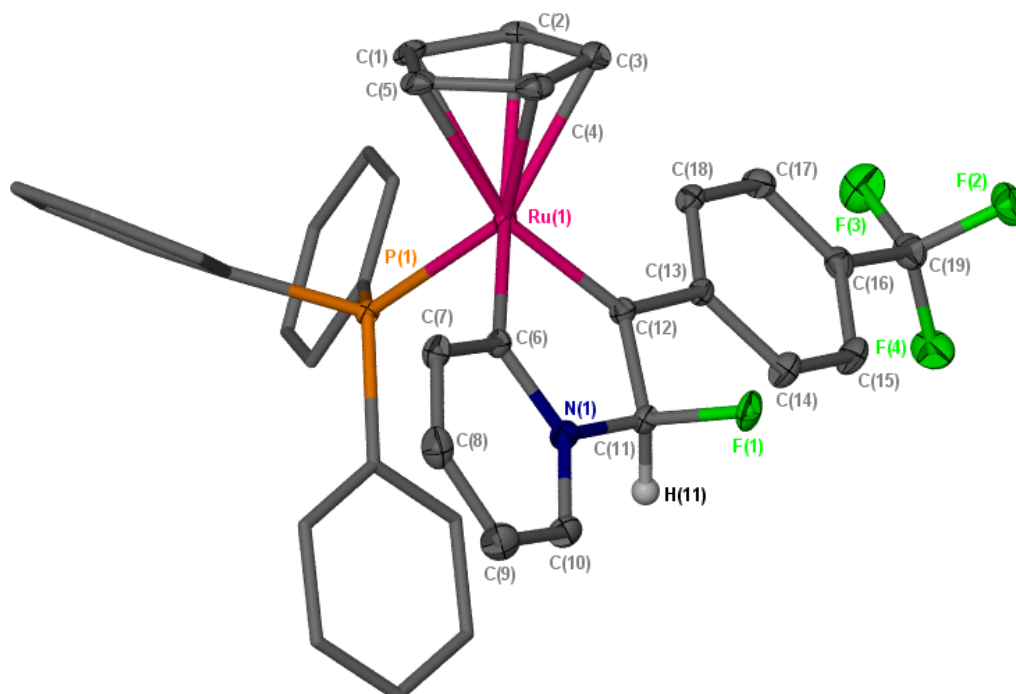
Figure 4.4 X-Seed diagram of the cation from complex [20]BF$_4$. Most hydrogen atoms, a BF$_4^-$ anion have been omitted for clarity, and where shown the thermal ellipsoids are at a 50 % probability level.

The X-ray diffraction studies indicate that **[20]BF$_4$** contains a metallocyclic ring system similar to that observed in **[16^{CF3}]** but with the formation of a new carbon-fluorine bond at C(11). The ruthenium-carbon bond lengths of the pyridylidene moieties (Ru(1) − C(6)) are similar across the two complexes (**[20]BF$_4$**, 1.990(2); **[16^{CF3}]**, 1.996(2) Å), whereas the ruthenium-carbon bond length Ru(1) − C(12) is significantly shorter in **[20]BF$_4$** (**[20]BF$_4$**, 1.916(2); **[16^{CF3}]**, 2.046(2) Å) consistent with an increase in double bond character upon fluorination. The C(11) − C(12) bond distance in **[20]BF$_4$** has lengthened compared to **[16^{CF3}]**; this is consistent with an increase in single bond character (**[20]BF$_4$**, 1.508(3); **[16^{CF3}]**, 1.339(2) Å). Therefore, the most appropriate Lewis structure for **[20]$^+$** is the one shown in Scheme 4.31, which displays pyridylidene character (rather than pyridyl) of the Ru(1) − C(6) bond and Schrock carbene character to Ru(1) − C(12). The geometry around C(11) shows slight distortions from tetrahedral geometry and the C(11) − F(1) bond is notably longer than expected for a typical sp^3-hybridised carbon-fluorine bond at 1.403(2) Å.

The X-ray diffraction studies also indicate that the fluorination of **[16^{CF3}]** to form **[20]BF$_4$** proceeds with complete diastereoselectivity to produce only the diastereomer in which the fluorine atom is oriented towards the cyclopentadienyl ring. This is supported by NOESY NMR experiments that show no cross-peak between H(11) and the cyclopentadienyl protons. The single-crystal X-ray structure of **[20]BF$_4$** is enantiopure, containing only the *RR* enantiomer. The diastereoselectivity can be explained by a consideration of the steric effects; delivery of '**F$^+$**' to the 'bottom' face of the metallocycle by **[FTMP]BF$_4$** is blocked by the three phenyl groups of the triphenylphosphine group, whereas approach of the fluorinating agent from the 'top' face is much less hindered. This effect is likely to be kinetic rather than thermodynamic, as the DFT-calculated energies suggest that the two isomers are essentially isoenergetic (-194 and -192 kJ mol^{-1} relative to **[16^{CF3}]** and **[FTMP]$^+$** for addition to the 'top' and 'bottom' faces respectively).

The Lewis structure obtained from the X-ray diffraction study is supported by NBO (natural bond order) calculations. Although the NBO reference structure of the cation **[20]$^+$** shows a single bond between Ru(1) − C(6), there is a significant amount of electron donation from the ruthenium centre to the C(6) − N(1) π* orbital which shows an occupation of 0.483 e$^-$ and a second order perturbation stabilisation energy of 83 kJ mol^{-1}; this affords considerable double bond character to the ruthenium-carbon bond. The Ru(1) − C(12) bond of **[20]$^+$** is instead described as a double bond in the NBO reference structure with a π-bond occupancy

of 1.815 e⁻ and a Wiberg bond index which is significantly higher than the analogous bond in **[16^CF3]** (**[20⁺]**, 1.067; **[16^CF3]**, 0.665) consistent with Ru(1) - C(12) double bond character.

Based on the Lewis structure, suggested by single crystal X-ray diffraction studies and supported by NBO analysis, the ruthenium complex **[20]BF₄** can be considered to have a formal oxidation state of +4, with one Fischer and one Schrock type carbene ligand. These assignments are further supported by the $^{13}C\{^1H\}$ NMR chemical shifts for these carbon atoms; C(6) resonates at 211.8 ppm and C(11) at 301.4 ppm. This is important because it indicates that the electrophilic fluorination of **[16^CF3]** is considerably different to that observed in previously reported electrophilic fluorination reactions (discussed in this chapter introduction). With regards to the metal, the reaction is oxidative and hence is similar to related palladium chemistry, but different to non-redox electrophilic fluorination reactions promoted by Lewis acidic metals such as titanium and nickel (Scheme 4.21).[216]

4.2.3   Synthesis of complex [21]BF₄

Remarkably, complex **[20]BF₄** is receptive to a second electrophilic fluorination reaction. On the addition of two equivalents of **[FTMP]BF₄** to **[16^CF3]** in dichloromethane solution, an initial and rapid reaction is observed to form **[20]BF₄** which then slowly but cleanly converts to a second complex, **[21]BF₄**, over a period of 24 hours. Identical reactivity is also observed on addition of stoichiometric **[FTMP]BF₄** to an isolated sample of **[20]BF₄**.

The NMR spectra show characteristic resonances for a difluorinated analogue of **[20]BF₄**. In the ^1H NMR spectrum, the characteristic signal with a geminal $^2J_{HF}$ coupling of 52.0 Hz at 4.71 ppm is lost, as is the ^{19}F NMR signal at -139.8 ppm with the corresponding coupling constant. Instead, the ^{19}F NMR spectrum exhibits two new ^{19}F resonances at -96.6 ppm and -78.0 ppm which are strongly mutually coupled with a coupling constant of 233.1 Hz. This is indicative of a $^2J_{FF}$ value, with both fluorine atoms on the same sp³-hybridised carbon atom. The resonance at -78.0 ppm is also coupled to the triphenylphosphine ligand with a $^4J_{PF}$ of 6.6 Hz. This coupling can be seen in the $^{31}P\{^1H\}$ NMR resonance which appears as a doublet at 46.1 ppm. ESI-MS shows a peak with an m/z of 714.0920, corresponding to a product of net deprotio-difluorination from **[16^CF3]**. Both the spectroscopic data and X-ray diffraction analysis indicated geminal difluorination at the 3-position of the 1-ruthanaindolizine ring of **[16^CF3]**. The reaction to form **[21]BF₄** from **[16^CF3]** is shown in Scheme 4.33.
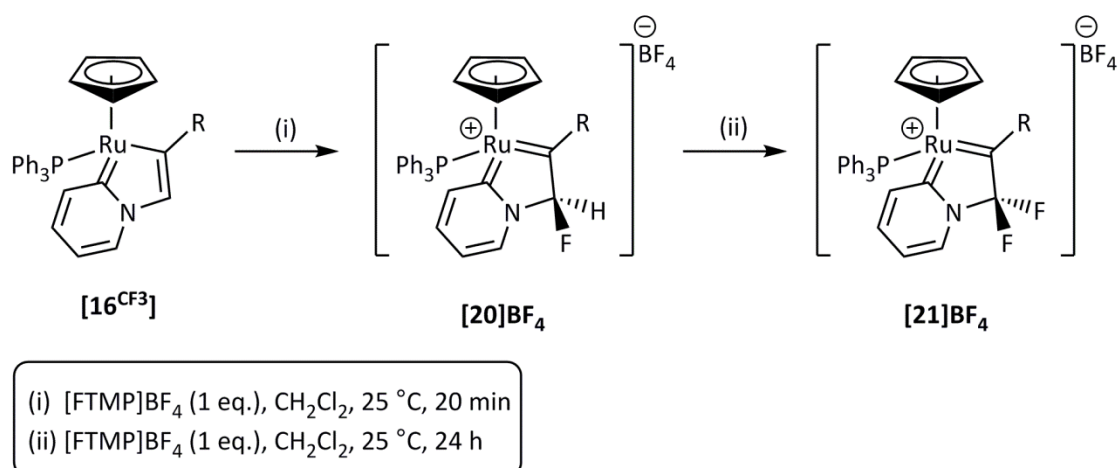
Scheme 4.33 Synthesis of complex [21]BF$_4$

The formation of **[21]BF$_4$** appears to occur *via* a two step process from **[16^{CF3}]**; formal addition of 'F^{+}' to C(11) to form **[20]BF$_4$**, followed by a subsequent C-H activation by deprotonation (presumably by free 2,4,6-trimethylpyridine, [TMP], in the **[FTMP]BF$_4$** fluorinating agent to form **[22]**) and fluorination to give **[21]BF$_4$**.

Crystals of **[21]BF$_4$** suitable for study by single crystal X-ray diffraction were obtained by the slow diffusion of pentane into a dichloromethane solution of the complex. The molecular structure is shown in Figure 4.5.
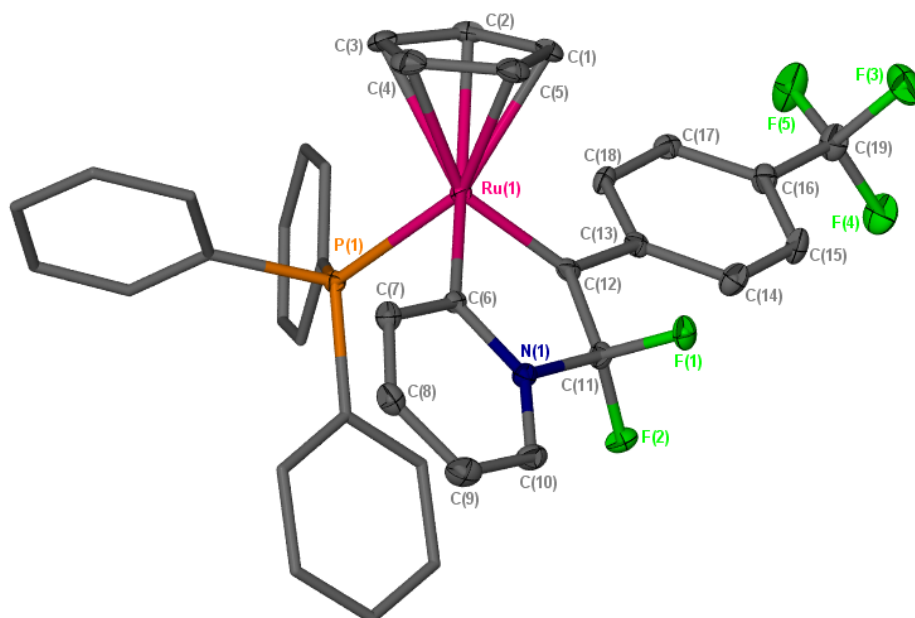
Figure 4.5 X-Seed diagram of the cation from complex [21]BF$_4$. Most hydrogen atoms, a BF$_4^-$ anion have been omitted for clarity, and where shown the thermal ellipsoids are at a 50 % probability level.

Similarly to **[20]BF₄**, the structure of **[21]BF₄** shows a shorter Ru(1) – C(12) bond (at 1.902(3) Å) and a longer C(11) – C(12) (at 1.516(4) Å) bond length compared to **[16^{CF3}]**. This again suggests pyridylidene character at C(12) and Schrock carbene character at C(6).

Compared to the carbon-fluorine bond in **[20]BF₄**, the carbon-fluorine bonds in **[21]BF₄** are significantly shorter (**[20]BF₄**, C(11) – F(1) 1.403(2) Å; **[21]BF₄**, C(11) – F(1) 1.374(2) Å, C(11) – F(2) 1.353(3) Å). This phenomenon can be explained by the progressive positive charge density on carbon, which increases linearly as additional fluorine atoms are incorporated.[260-262] In turn, this increases the ionic character of the carbon-fluorine bonds and therefore, they become shorter (and stronger) as the level of fluorination increases, as each of the electronegative fluorine atoms is attracted to an increasingly electropositive carbon centre.

The polarisation of the carbon-fluorine bonds also leads to a change in the geometry, which can be explained by the valence shell electron pair repulsion (VSEPR) theory.[263-264] The highly electronegative fluorine atoms pull electron density from the covalent bonds towards them, which allows relaxation between the fluorine substituents.[262] This can be observed in **[21]BF₄** as the F(1) – C(11) – F(2) bond angle is reduced to 105.10(19)°; considerably lower than the idealised sp³-hybridised carbon atom bond angle of 109°. However, compared to **[20]BF₄**, there is less distortion from an idealised tetrahedral geometry around C(11) and the carbon-fluorine bond lengths are more typical of those of an sp³-hybridised carbon atom.

4.3 Reactivity of complex [20]BF₄

The first step in the conversion of **[20]BF₄** to **[21]BF₄** is presumed to be deprotonation of the mono-fluorinated carbon atom by residual free TMP in the reaction mixture. The proposed 1-ruthana-3-fluoroindolizine complex, **[22]**, can be formed independently by the addition of 1,4-diazabicyclo[2.2.2]octane (DABCO) to a solution of **[20]BF₄** in dichloromethane at room temperature, Scheme 4.34. Complex **[22]** is a fluorinated analogue of the parent 1-ruthanaindolizine complex **[16^{CF3}]**. Deprotonation of **[20]BF₄** to form **[22]** results in a formal reduction of the metal from the +4 to +2 oxidation state. In the ^{31}P{^{1}H} NMR spectrum, the resonance for **[22]** appears as a singlet at 61.5 ppm, and in the ^{19}F NMR spectrum as a singlet -111.7 ppm (and -63.6 ppm for the trifluoromethyl moiety). The ^{31}P{^{1}H} NMR chemical shift is very similar to that of **[16^{CF3}]**, which appears as a singlet at 60.5 ppm.

Scheme 4.34 Deprotonation of complex [20]BF$_4$ with DABCO and resulting equilibrium between [22] and [23]BF$_4$ in the presence of [H.DABCO]BF$_4$

However, in the presence of [H.DABCO]BF$_4$ in dichloromethane, an equilibrium is established between **[22]** and **[23]BF$_4$** (a new α-fluorovinyl pyridylidene complex) and free DABCO, Scheme 4.34. Protonation at the 2-position of the 1-ruthanaindolizine ring has been observed previously on the addition of protons to complex **[16^{CF3}]**, and so it is unsurprising that the structurally analogous 1-ruthana-3-fluoroindolizine complex **[22]** exhibits similar reactivity.[45] Characteristic signals for complex **[23]BF$_4$** can be observed in the NMR spectra. In the ^{1}H NMR spectrum, the alkenyl-proton of **[23]BF$_4$** appears as a doublet of doublets at 3.09 ppm with a $^3J_{HP}$ of 11.6 Hz and a smaller $^3J_{HF}$ of 8.6 Hz. The ^{31}P{^{1}H} NMR spectrum exhibits a doublet signal at 49.7 ppm with a $^3J_{PF}$ of 3.4 Hz. These resonances were shown to be coupled by a ^{1}H-^{31}P 2D correlation experiment. The chemical shift of the ^{31}P{^{1}H} resonance of **[23]BF$_4$** is similar to the protio-analogue of the complex, **[13^{CF3}]PF$_6$** which appears as a singlet at 52.8 ppm. The alkenyl-fluorine atom of **[23]BF$_4$** appears as a doublet of doublets with corresponding values of $^3J_{HF}$ and $^3J_{PF}$. This equilibrium behaviour is rapid on the NMR timescale and cooling the reaction mixture to 195 K is not sufficient to fully resolve the resonances and make interconversion slow on the NMR timescale.

In order to prepare a sample of **[22]** which was free from dynamic behaviour, **[20]BF$_4$** was dissolved in d$_5$-pyridine which was able to act as both the base and the reaction solvent. The presence of excess base afforded total deprotonation of **[20]BF$_4$** to give a pure sample of **[22]** with no evidence of dynamic behaviour on the NMR timescale. The resonance for the triphenylphosphine ligand appears as a singlet at 61.5 ppm in ^{31}P{^{1}H} NMR spectrum (compared to a chemical shift of 61.2 ppm for the non-fluorinated complex analogue, **[16^{CF3}]**) and the fluorine atom of the mono-fluorinated carbon appears as a singlet in the ^{19}F NMR spectrum at -111.7 ppm.

4.4 Reactivity of complex [21]BF$_4$

The dissolution of **[20]BF$_4$** in pyridine resulted in deprotonation at the 3-position of the metallocycle to yield complex **[22]** – the fluorinated analogue of the initial metallocycle **[16^{CF3}]**. More surprisingly, dissolution of the difluorinated complex **[21]BF$_4$** in d$_5$-pyridine over the course of one week at room temperature also yielded **[22]** as the major product, Scheme 4.35.
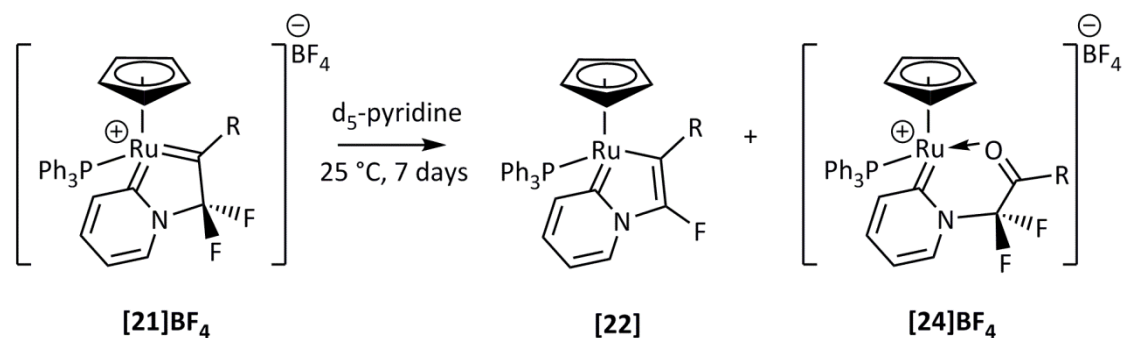
Scheme 4.35 Reactivity of complex [21]BF$_4$ on dissolution in pyridine

Formation of **[22]** is a most unusual observation and corresponds to a formal loss of 'F$^+$' from the -CF$_2$ group in **[21]BF$_4$** to form the 1-ruthana-3-fluoroindolizine metallocycle. However, the spectroscopic data do not suggest a simple transfer of 'F$^+$' from the complex to pyridine (in analogy to the deprotonation of **[20]BF$_4$**) as [F.pyridine]BF$_4$ could not be observed. Indeed, the cleavage of a carbon-fluorine bond to form a much weaker nitrogen-fluorine bond is thermodynamically unfavourable by approximately 200 kJ mol^{-1}.[265] This reactivity has instead been tentatively associated with the formation of a second organometallic species in the reaction mixture, **[24]BF$_4$**.

Although the structure of **[24]BF$_4$** cannot be unambiguously determined, the spectroscopic data strongly suggest the complex shown in Scheme 4.35. In the ^{19}F NMR spectra, complex **[24]BF$_4$** exhibits two strongly mutually coupled fluorine environments (at -78.7 ppm and -67.6 ppm with a $^2J_{FF}$ of 208.5 Hz) which suggests retention of the –CF$_2$ group within the structure. Similarly to **[21]BF$_4$**, the symmetry of **[24]BF$_4$** dictates that the two fluorine atoms are chemically inequivalent; however, in contrast to **[21]BF$_4$**, neither of the fluorine atoms in **[24]BF$_4$** show coupling to the phosphorus of the triphenylphosphine ligand. The mass spectrum of the reaction mixture indicates the presence of **[22]** and an additional ruthenium-containing species with an m/z of 730.0872 assigned as **[24]BF$_4$**. This peak corresponds to

incorporation of a single oxygen atom into the structure of **[21]⁺**. Two feasible structures could be proposed which match this spectroscopic data – oxygen incorporation could occur at either the pyridylidene carbon to form **4-ax**, Figure 4.6, or in the Schrock carbene position to form **[24]BF₄**.
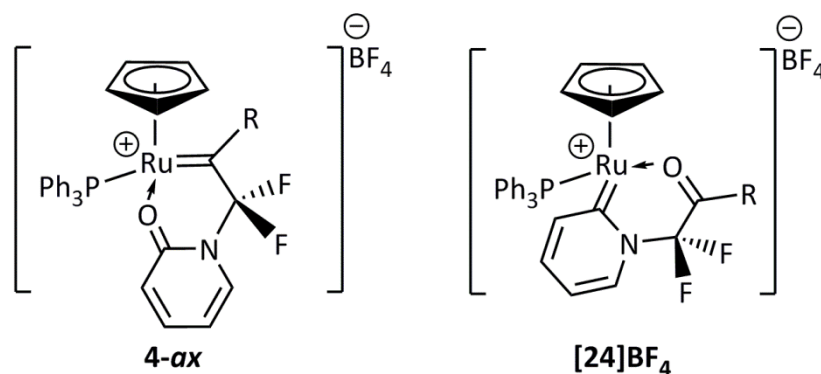
Figure 4.6 Potential structures of the unidentified product from the dissolution of [21]BF₄ in pyridine

Although in the ^{13}C{^{1}H} 1D NMR spectrum there is no signal observable in the carbonyl or pyridylidene region, in the ^{1}H-^{13}C HMBC 2D spectrum a clear signal at 203.7 ppm in the ^{13}C dimension can be observed which shows long-range coupling to a doublet in the ^{1}H NMR spectrum at 7.99 ppm with a $^{3}J_{HH}$ of 8.4 Hz. The resonances at 203.7 ppm and 7.99 ppm (in the ^{13}C{^{1}H} NMR and ^{1}H NMR spectra respectively) are reminiscent of those of the ruthenium-bound pyridylidene carbon atom and pyridylidene protons in related structures shown in Figure 4.7. This suggests retention of the pyridylidene moiety in **[21]BF₄** and therefore suggests that the new complex is **[24]BF₄**.
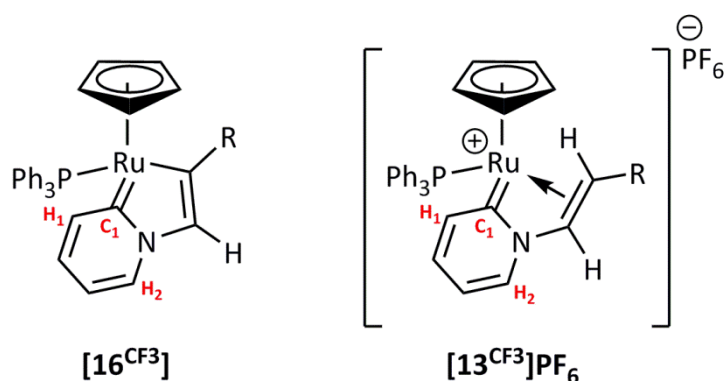
	[16^{CF3}]	[13^{CF3}]PF$_6$
C$_1$	219.3 ppm (br)	179.6 ppm (d, $^2J_{CF}$ = 19 Hz)
H$_1$	7.84 ppm (d, $^3J_{HH}$ = 6.4 Hz)	7.12 ppm (d, $^3J_{HH}$ = 7.9 Hz)
H$_2$	8.16 ppm (d, $^3J_{HH}$ = 8.3 Hz)	8.00 ppm (d, $^3J_{HH}$ = 6.1 Hz)

Figure 4.7 Key NMR spectroscopic data of related pyridylidene complexes [16^{CF3}] and [13^{CF3}]PF$_6$ to support the assignment of [24]BF$_4$

Combined with the knowledge that the Schrock carbene in complex **[22]** is probably more easily oxidised than the pyridylidene carbon atom, the collective spectroscopic data gives confidence in the structural assignment of the fluorinated ketone complex, **[24]BF$_4$**.

The signals for the complex assigned as **[24]BF$_4$** are observed to grow in the NMR spectra at a similar rate to those of **[22]** (in a ratio of 0.7:1 **[24]BF$_4$** to **[22]** based on the ^{19}F NMR integrations). Complex **[24]BF$_4$** may be formed by hydration of **[21]BF$_4$** by reaction with adventitious water in the d$_5$-pyridine solvent, with formal loss of H$_2$ during this process. It is unlikely that H$_2$ is lost in the gaseous state, and hydration may be coupled to the formal loss of 'F$^+$' from **[21]BF$_4$** to give the following balanced equation:

$$2 \text{ [21]BF}_4 + \text{pyridine} + \text{H}_2\text{O} \rightarrow \text{[22]} + \text{[24]BF}_4 + \text{[H.pyridine]BF}_4 + \text{HF}$$
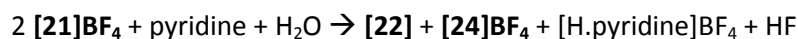
In support of this hypothesis, a broad N-H signal can be observed in the ^{1}H NMR spectrum at 9.1 ppm which is indicative of [H.pyridine]BF$_4$ in pyridine. The significant broadening of this signal can be attributed to dynamic proton exchange between **[22]** and **[23]BF$_4$** mediated by [H.pyridine]BF$_4$ (in analogy to the [H.DABCO]BF$_4$ mediated proton exchange observed previously). No evidence was observed for HF or related products; it is possible that the small amount of HF reacts with the glass reaction vessel and is not visible in solution.

4.5   Mechanistic considerations

Considering related palladium-mediated electrophilic fluorination reactions, it was surprising that **[16^{CF3}]** did not react with **[FTMP]BF$_4$** by oxidative fluorination of the metal to produce a ruthenium-fluoride complex such as **[O]$^+$**, or an aryl fluoride such as **[Q]$^+$** *via* reductive elimination from a ruthenium-fluoride intermediate, Scheme 4.31. The behaviour of **[16^{CF3}]** towards 'F^{+}' is also very different to the reactivity observed towards H$^+$. In the presence of H$^+$, reaction is observed at the 2-position of the 1-ruthanaindolizine (which leads to the regeneration of **[13^{CF3}]**, Scheme 4.30) whereas reactivity with 'F^{+}' occurs exclusively at the 3-position to form **[20]BF$_4$**. Reaction with 'F^{+}' at the 2-position would lead to the formation of a fluorovinyl pyridylidene complex such as **[R]$^+$**, Scheme 4.31, which was also not experimentally observed. These observations suggested that the electrophilic fluorination process in this system was controlled by a novel mechanism.

4.5.1   Low temperature NMR study of the fluorination of complex [16^{CF3}]

During both the monofluorination reaction to form **[20]BF$_4$** and the net deprotio-difluorination reaction to form **[21]BF$_4$**, no intermediates were observed spectroscopically at room temperature. The reactions seemed to proceed from complex **[16^{CF3}]** directly to **[20]BF$_4$**, followed by a slower conversion to complex **[21]BF$_4$** in the presence of two equivalents of **[FTMP]BF$_4$**. However, by comparison with reported palladium-mediated fluorination reactions, the pathway would be expected to proceed by a carbon-fluorine reductive elimination pathway *via* a ruthenium-fluoride intermediate complex. These species exhibit significantly upfield chemical shifts of around -200 to -450 ppm in the ^{19}F NMR spectra.[256-259] As no evidence of ruthenium-fluoride intermediates was observed at room temperature, the stoichiometric addition of **[FTMP]BF$_4$** to **[16^{CF3}]** to form **[20]BF$_4$** was probed using low temperature NMR spectroscopy. Conducting the reactions at lower temperature should afford a slower rate of reaction and potentially allow the observation of any short-lived intermediates.

In the NMR study, a stoichiometric quantity of **[FTMP]BF$_4$** was added to a CD$_2$Cl$_2$ solution of complex **[16^{CF3}]** in a Young's NMR tube which was frozen using liquid nitrogen. The NMR tube was allowed to thaw on the addition of the fluorinating agent, and was rapidly transferred to a pre-cooled NMR spectrometer at 195 K. ^{1}H, ^{19}F and ^{31}P{^{1}H} NMR spectra were recorded as the spectrometer was warmed to 295 K. No reaction was observed between **[16^{CF3}]** and

[FTMP]BF$_4$ at temperatures lower than 245 K but by 265 K the reaction was essentially complete, highlighting the fast kinetics even at low reaction temperatures. No potential reaction intermediates were observed in any of the NMR spectra at any temperature, suggesting that either fluorine is delivered directly to the site of fluorination or that only low-energy transition states connect any potential intermediates in the fluorination mechanism to form **[20]BF$_4$**.

4.5.2 Computational studies of fluorination

The mechanistic features of metal-mediated electrophilic fluorination involving 'F^{+}' sources such as **[FTMP]BF$_4$** or Selectfluor are the matter of some debate in the literature, as described in the introduction to this chapter. It is likely that the mechanism of operation varies between different systems; fluorination can proceed either by a single electron transfer (SET) process promoted by the strongly oxidising 'F^{+}' source followed by a rapid radical recombination, or by direct nucleophilic attack of the 'F^{+}' source by the metal complex. It is challenging to distinguish between these systems both experimentally and computationally due to the difficulties in correctly modelling the singlet diradical formed by a SET process. However, two alternative computational studies were conducted which suggest that a ruthenium-fluoride intermediate is not involved and that direct fluorination at the 3-position of the 1-ruthanaindolizine ring in complex **[16^{CF3}]** is likely to be a low-energy process.

4.5.2.1 Potential Energy Surface for fluorination of complex [16^{CF3}] *via* a ruthenium-fluoride intermediate

As stated previously, making the distinction between a SET-based mechanism and direct nucleophilic attack at the 'F^{+}' source is computationally challenging. Therefore, a PES was modelled of the 'post-fluorination' landscape for a potential mechanism which proceeds *via* a metal-fluoride intermediate. These calculations were undertaken in order to obtain the energies of potential ruthenium-fluoride intermediates, assess the likelihood of their involvement in the fluorination reaction of **[16^{CF3}]** and to provide insight into the observed but unexpected position of fluorination to form **[20]BF$_4$**. The PES is shown in Scheme 4.36.
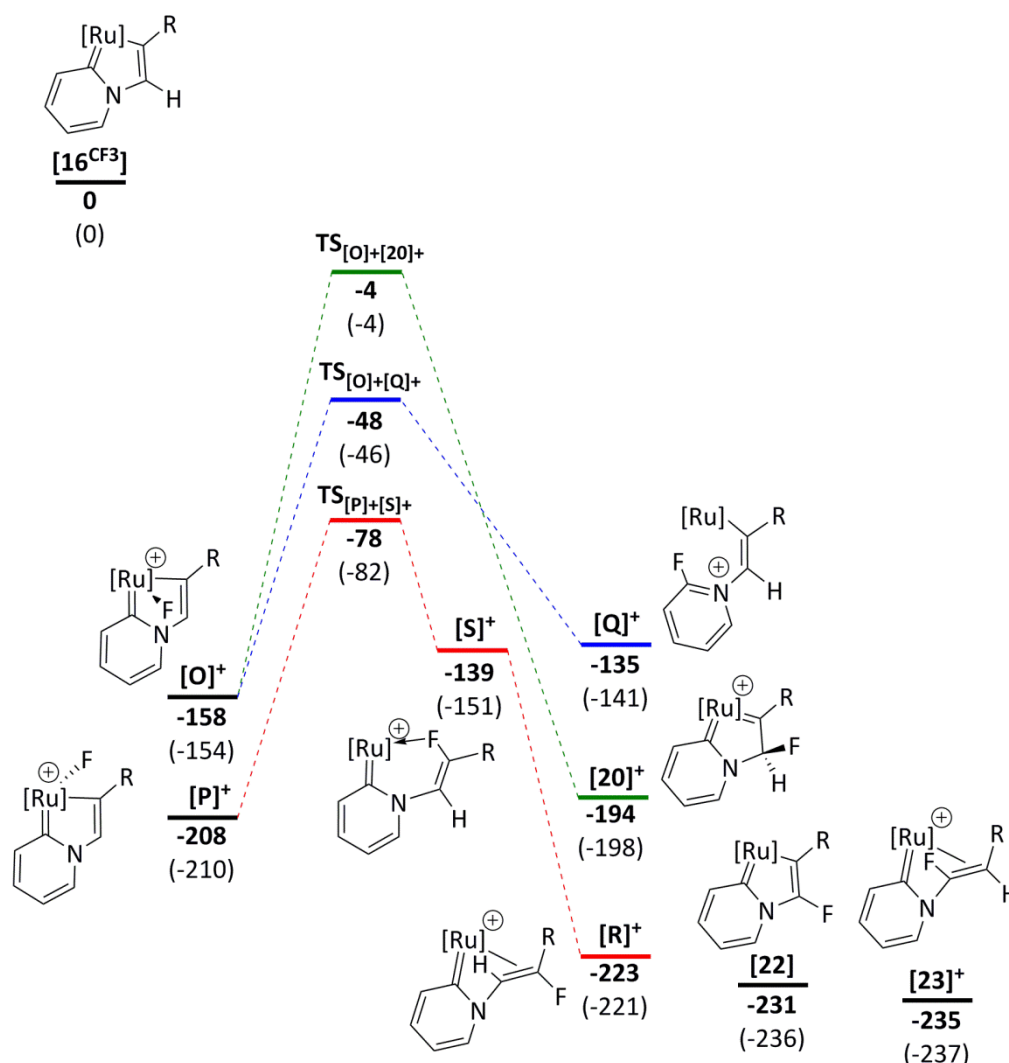
Scheme 4.36 Potential Energy Surface (PES) for the formation of complex [20]⁺ from [16^CF3] *via* a fluoride intermediate, [Ru] = [Ru(η⁵-C₅H₅)(PPh₃)], R = -C₆H₄-4-CF₃. $E_{SCF+ZPE}$ **energies (top, in bold) and relative Gibbs free energies (bottom, in parentheses) at 298.15 K, both in dichloromethane (COSMO solvation model), are shown in kJ mol⁻¹. Calculations are at the (RI-)PBE0-D3/def2-TZVPP//(RI-)BP86/SV(P) level of theory.**

Due to the difficulties of assessing solution phase entropy changes from gas phase calculations, the zero-point-energy-corrected electronic energies ($E_{SCF+ZPE}$) will be discussed rather than Gibbs energies, although both values are presented on the PES (and are very similar). The reference point for the calculations was chosen as the initial metallocycle **[16^CF3]** and one equivalent of **[FTMP]⁺** at 298 K, and so all other energies are presented relative to these components (which have been set to 0 kJ mol⁻¹).

On first inspection of the PES in Scheme 4.36, it can be noted that two potential isomers of a ruthenium-fluoride complex should be considered. The structure of complex **[O]⁺** contains the fluoride moiety above the plane of the metallocyclic ring, whereas in complex **[P]⁺** the

fluoride is nestled between the metallocycle and the triphenylphosphine ligand. Each of these isomers leads to alternative regioisomeric products. The formation of the ruthenium-fluoride complexes, **[O]**[+] and **[P]**[+], is thermodynamically favourable by 158 and 208 kJ mol^{-1} respectively; hence, the apparent absence of ruthenium-fluoride intermediates is likely to be attributable to kinetic effects and the inaccessibility of the ruthenium centre to the fluorinating agent. Assuming that both isomers of the complex are accessible and that the lowest energy isomer is populated, the transition state energy barriers to further reaction range between 130 kJ mol^{-1} and 204 kJ mol^{-1}. This is the first piece of evidence that ruthenium-fluoride intermediates are not involved in this system; if either ruthenium-fluoride complex was formed, it should have sufficient stability to be observable as an intermediate, especially in the low-temperature NMR study (Section 4.5.1). In addition, a transition state energy barrier of 204 kJ mol^{-1} is not consistent with the rapid formation of **[20]BF$_4$** observed at 265 K.

Secondly, the complex which is observed exclusively in this system is **[20]BF$_4$** with no traces of either the aryl fluoride complex **[Q]**[+] or the fluorovinyl pyridylidene complex **[R]**[+]. However, complex **[20]BF$_4$** is neither the kinetic nor the thermodynamic product of this system for a pathway which proceeds *via* a fluoride intermediate. Instead, fluorination would be expected (*via* fluoride **[P]**[+]) at the 2-position of the 1-ruthanaindolizine metallocycle to produce **[R]**[+]. Formation of **[R]**[+] proceeds through a closely related isomer, **[S]**[+], in which the alkenyl moiety is coordinated to the metal centre by an agostic interaction with the carbon-fluorine bond. This undergoes subsequent rearrangement in order to allow coordination through the alkenyl bond of the ligand, which is more stable by 84 kJ mol^{-1}.

In summary, the low thermodynamic energies of ruthenium-fluoride complexes **[O]**[+] and **[P]**[+] with respect to **[16^{CF3}]**, the subsequent high energy barriers from **[O]**[+] and **[P]**[+] to further reaction, and the fact that the experimentally observed product of monofluorination, **[20]BF$_4$**, is neither the kinetic nor thermodynamic product of a ruthenium-fluoride-mediated mechanism suggest that ruthenium-fluoride intermediates are not relevant in this system. The computational findings agree with the experimental results and the lack of observed ruthenium-fluoride intermediates in the low temperature NMR studies, and support the idea that this fluorination reaction operates *via* an unprecedented mechanism.

Each of the complexes **[20]**[+], **[22]** and **[23]**[+] have been observed experimentally. The addition of a base such as DABCO allows the deprotonation of complex **[20]**[+] to form **[22]**, which then undergoes dynamic protonation and deprotonation to form complex **[23]**[+]. The calculations suggest that **[22]** and **[23]**[+] are essentially isoenergetic, and their similar thermodynamic energies explain the presence of both of these species in solution with an approximately equal population of each complex. The rapid dynamic behaviour observed in the NMR spectra, even at 195 K, indicates a low energy transition state between the protonated and deprotonated forms.

The PES for the formation of **[21]BF$_4$** by deprotio-difluorination (Scheme 4.37) from a ruthenium-fluoride containing intermediate is very similar to that of monofluorination shown in Scheme 4.36 and suggests that this reaction also does not proceed through a ruthenium-fluoride complex.
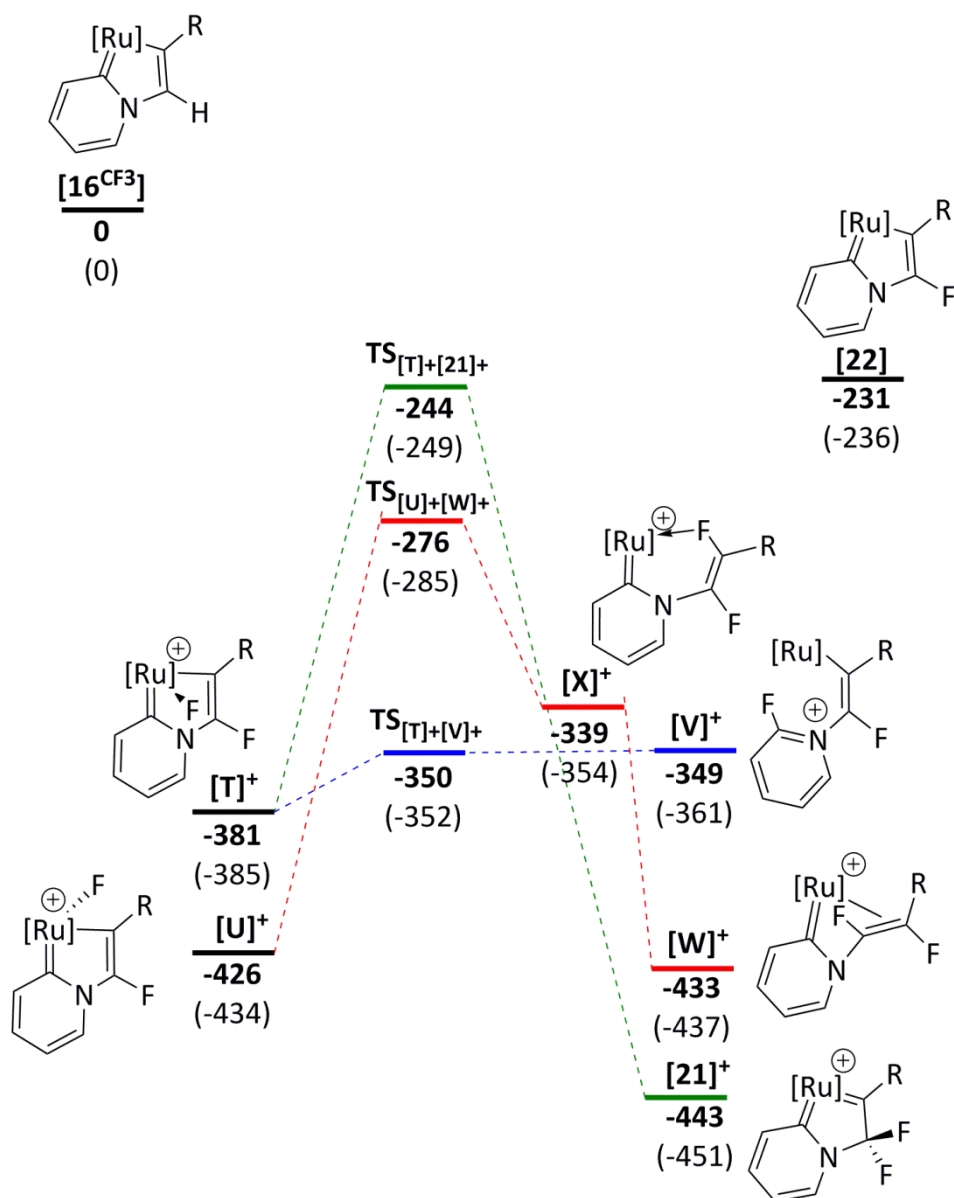
Scheme 4.37 Potential Energy Surface (PES) for the formation of complex [21]⁺ from [16^CF3] *via* **a fluoride intermediate, [Ru] = [Ru(η⁵-C₅H₅)(PPh₃)], R = -C₆H₄-4-CF₃.** $E_{SCF+ZPE}$ **energies (top, in bold) and relative Gibbs free energies (bottom, in parentheses) at 298.15 K, both in dichloromethane (COSMO solvation model), are shown in kJ mol⁻¹. Calculations are at the (RI-)PBE0-D3/def2-TZVPP//(RI-)BP86/SV(P) level of theory.**

The large energy barriers in both PES' and the fact that the complexes observed experimentally are not the isomers predicted by the DFT calculations suggest that another mechanism is in operation for the formation of **[20]BF₄** (and **[21]BF₄**). Direct outer-sphere electrophilic fluorination (OSEF) of the 3-position of the ruthanindolizine ring seems most probable in both cases.

4.5.2.2 Radical pathway for the fluorination of [16^{CF3}]

As the fluorination of **[16^{CF3}]** to form **[20]BF$_4$** *via* a fluoride intermediate seemed improbable, the mechanism of direct fluorination at the 3-position of the ruthanindolizine ring was investigated using relaxed PES scans for the closed-shell singlet, triplet and singlet diradical states. These calculations were performed by Dr John Slattery.

It was observed that BP86/SV(P) geometry optimisations, as used in the other computational studies discussed in this thesis, did not effectively model the geometry of the transition state in the singlet closed-shell potential energy surface; therefore, the PBE0 hybrid-functional was utilised for all of the geometry optimisations. In order to perform the calculations, an initial input structure was generated in which the metallocycle **[16^{CF3}]** and fluorinating agent **[FTMP]BF$_4$** were modelled in the same calculation, with a fixed distance of 4 Å between the fluorine atom and the carbon atom in the 3-position, which is believed to undergo the direct fluorination. A carbon-fluorine separation of 4 Å is sufficiently long to assume a negligible interaction between the two atoms. The carbon-fluorine bond length was then decreased from 4 Å to a minimum of 1.2 Å, in steps of 0.2 Å. In each calculation along the PES scan, the carbon-fluorine bond length was the sole constraint with all other atoms allowed to move freely in order to obtain the minima at each carbon-fluorine distance. The geometries of the constrained structures were subsequently optimised for the closed-shell singlet, closed-shell triplet and singlet diradical electronic states. The broken-symmetry diradical states were obtained from the optimised triplet geometries using the 'flip' function of the TURBOMOLE 'define' script. This allows the selection of a localised α-spin orbital of a particular atom (in this case, ruthenium) to become a β-orbital (or *vice versa*) to generate a broken symmetry (S=0) state. On attainment of appropriate molecular orbitals using this methodology, the geometries of the singlet diradical states could be optimised.

Mulliken population analyses were performed on the converged wave functions to confirm that singlet diradical character was retained during the optimisations. At carbon-fluorine distances of less than 2.2 Å, which corresponds to the approximate carbon-fluorine bond length of the transition state, the Mulliken population analyses indicate the loss of diradical character as the singlet diradical pathway slips onto the singlet closed-shell pathway. This would be expected, as the carbon-fluorine bond is being formed.

The results of the calculations are shown in Figure 4.8.
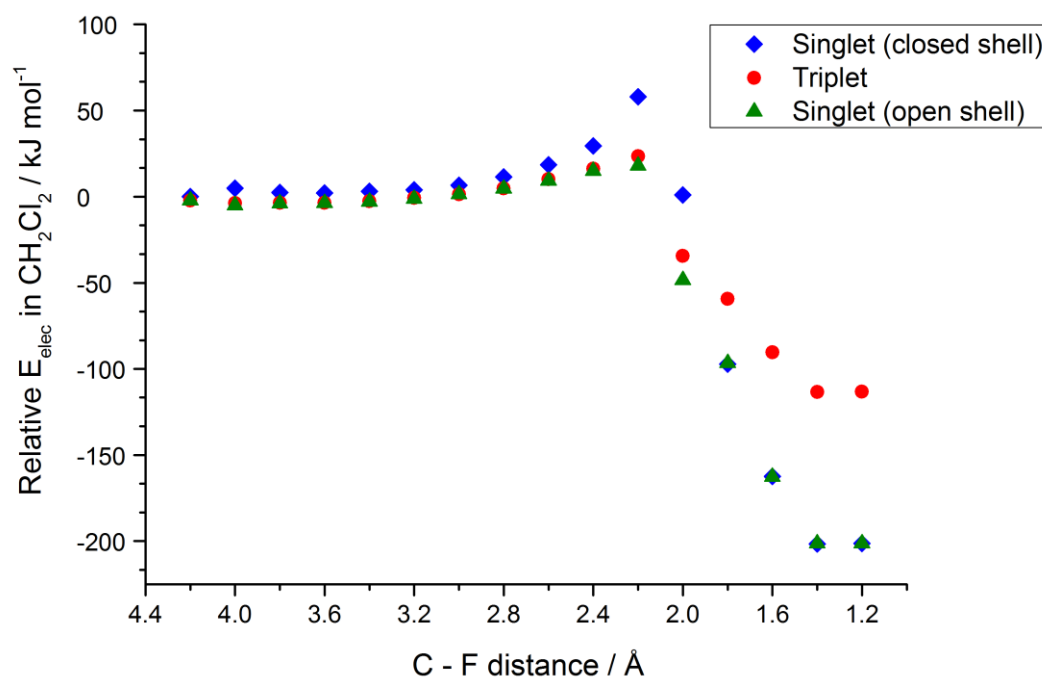
Figure 4.8 Electronic energies of the closed-shell singlet, closed-shell triplet and singlet diradical systems at carbon-fluorine distances between 4 Å and 1.2 Å

For each of the closed-shell singlet, closed-shell triplet and singlet diradical systems, the reaction pathways proceed through relatively low energy barriers (ΔE_{SCF} in dichloromethane of 58, 27 and 23 kJ mol^{-1} respectively) to form **[20]$^{+}$**. These barriers are consistent with the rapid rates of reaction and absence of experimentally-observed reaction intermediates. The low barriers to fluorination contrast markedly with those of carbon-fluorine bond formation *via* a metal-fluoride intermediate observed in Section 4.5.2.1 (of between 130 kJ mol^{-1} and 204 kJ mol^{-1}), supporting the notion that fluorination proceeds by an outer-sphere mechanism. Within the three routes of direct fluorination, the open-shell pathways are significantly lower in energy than the closed-shell, which suggests that a SET process may be feasible in this system. However, care must be taken with interpretation of the singlet diradical energies due to notable spin contamination.

The observed fluorination at the 3-position of the ruthanindolizine in complex **[16^{CF3}]** is consistent with a study conducted by Esteruelas et al, in which the kinetic site of protonation at -80 °C in a similar system was found also to be the 3-position. Subsequent hydrogen migration to the 2-position to access the thermodynamic product, **4-*az***, was observed on

allowing complex **4-*ay*** to warm to 20 °C.[266] Presumably, proton migration in Esteruelas' system is a more facile process than the fluorine migration in complex **[20]BF$_4$** and so isomerisation is not observed to form the thermodynamic product, **[R]$^+$**, under these experimental conditions.
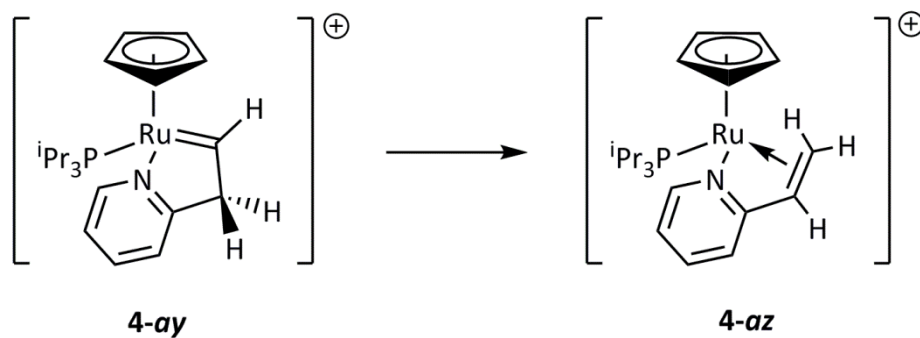
Scheme 4.38 Hydrogen migration from the 3-position to the 2-position as observed by Esteruaelas[266] which is not observed in the fluorinated system

4.6 Conclusions

The reaction of ruthenium pyridylidene complex **[16^{CF3}]** with a stoichiometric quantity of an electrophilic fluorinating agent, 'F$^+$', allows quantitative conversion to the mono-fluorinated metallocyclic complex **[20]BF$_4$**. The fluorination reaction proceeds rapidly under mild conditions and with complete regio- and stereoselectivity, reacting exclusively in the 3-position of the 1-ruthanaindolizine precursor, **[16^{CF3}]**, to form a carbon-fluorine bond on the 'top' face of the ligand. The addition of a second equivalent of 'F$^+$' allows the replacement of a hydrogen atom on the same carbon atom to produce a difluorinated product, **[21]BF$_4$**.

Due to the retention of the fluorinated ligands in **[20]BF$_4$** and **[21]BF$_4$**, their reactivity was explored under a range of different reaction conditions. On dissolution in pyridine, both complexes were found to lose 'H$^+$' or 'F$^+$' respectively to yield a fluorinated analogue of the precursor complex **[16^{CF3}]**. The origin of the carbon-fluorine bond cleavage in **[21]BF$_4$** has not been unambiguously determined, but is likely to be coupled to a hydration reaction of a second molecule of **[21]BF$_4$** and the formal loss of HF.

Mechanistic investigations, both from computational and experimental evidence, suggest that the fluorination reactions proceed *via* a brand new fluorination pathway termed outer-sphere electrophilic fluorination (OSEF), in which the fluorine atom is delivered directly to the ligand in the absence of any fluoride intermediates. Broken-symmetry DFT calculations suggest that this reaction may proceed through a single electron transfer pathway. This reactivity is distinct from previous fluorination methodologies in which either a high oxidation state metal-fluoride is formed and subsequent reductive elimination takes place to yield the new carbon bond, or non-redox active metals are utilised in order to create an activated, nucleophilic carbon centre. It is hoped that this novel fluorination methodology will be complementary to currently available techniques, in order to allow access to a range of new fluorinated structures which are presently either difficult or impossible to synthesise. The exploitation of the OSEF mechanism has already been applied in the synthesis of fluorovinylidene complexes, which will be discussed in Chapter 5.

Chapter 5

Synthesis and reactivity of novel fluorovinylidene ligands: an insight into carbon-fluorine bond formation and activation

5 Synthesis and reactivity of novel fluorovinylidene ligands: an insight into carbon-fluorine bond formation and activation

5.1 Introduction

5.1.1 Substituted vinylidene complexes

Metal vinylidene complexes are key intermediates in a range of stoichiometric transformations and catalytic processes, particularly in the formation of new carbon-carbon and carbon-heteroatom bonds. As such, many synthetic routes to prepare vinylidene complexes have been reported, such as 1,2-hydrogen migration of η^2-coordinated terminal alkynes, deprotonation of carbyne ligands and electrophilic attack of metal acetylide complexes.[49] (A more detailed introduction to the synthesis and reactivity of metal vinylidene complexes is given in Chapter 1.)

In 1987, Bruce and co-workers described a route to prepare a range of metal vinylidene complexes from readily-synthesised acetylide precursors.[64] For example, reaction of acetylide complex **5-a**$^{1-6}$ with a range of electrophiles leads to the formation of protio- or halogenated vinylidene complexes, **5-b**$^{1-6}$, Scheme 5.1.
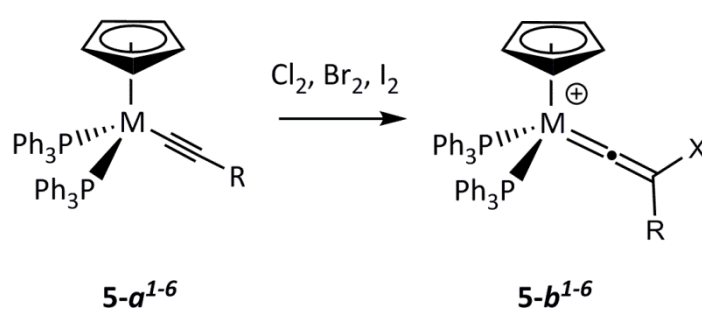
	X	R	M
1	I	Ph	Ru
2	I	Me	Ru
3	I	C_6F_5	Ru
4	I	Ph	Os
5	Br	C_6H_4-4-Br	Ru
6	Cl	Ph	Ru

Scheme 5.1 Synthesis of halogenated vinylidene complexes, 5-*b*¹⁻⁶, from metal-acetylide precursors, 5-*a*¹⁻⁶. These original halogenation methodologies by Bruce *et al* have been improved by the Lynam and Slattery groups (see Section 5.3.3.5).

This procedure has also been extended to the auration of acetylide complexes, Scheme 5.2.[267]
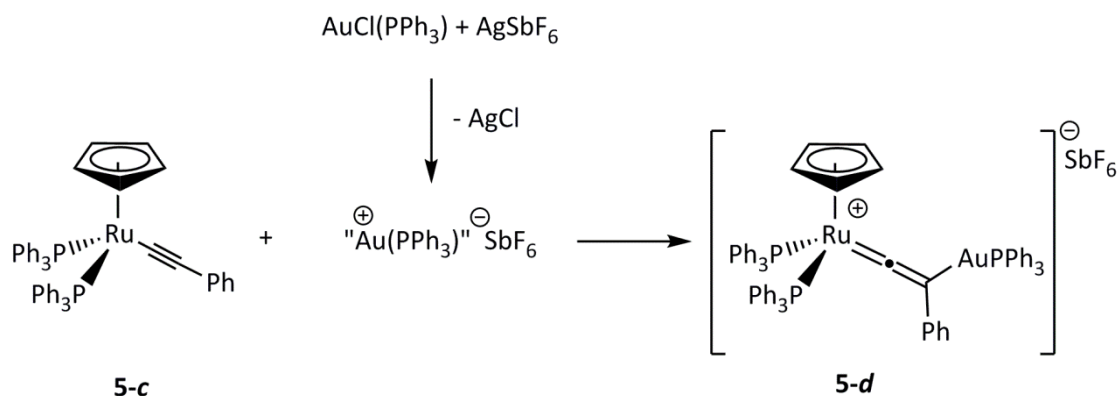
Scheme 5.2 Auration of ruthenium acetylide complex 5-*c*

On the basis of this methodology, the electrophilic fluorination of ruthenium acetylide complexes was investigated as a route to prepare fluorinated vinylidene ligands. Vinylidene complexes represent key catalytic intermediates in a plethora of reactions (Chapter 1, Section 1.4) and therefore the formation of fluorinated vinylidene complexes, coupled with subsequent reactivity, may provide access to novel fluorinated compounds that were previously impossible or very difficult to access. In particular, there is a lack of methodology to construct sp^2 and chiral sp^3 fluorinated functionality, and so developments in this area would be very advantageous. (Further information on fluorination and the uses of fluorinated molecules is provided in Chapter 4).

5.1.2 Fluorinated vinylidene complexes

Fluorovinylidene ligands have rarely been described - limited examples of dimeric iridium and iron species have been reported, formed *via* carbon-fluorine bond activation.[268-271]

The first example of a fluorinated vinylidene complex was reported by Schulze and Seppelt in 1988, Scheme 5.3.[272]
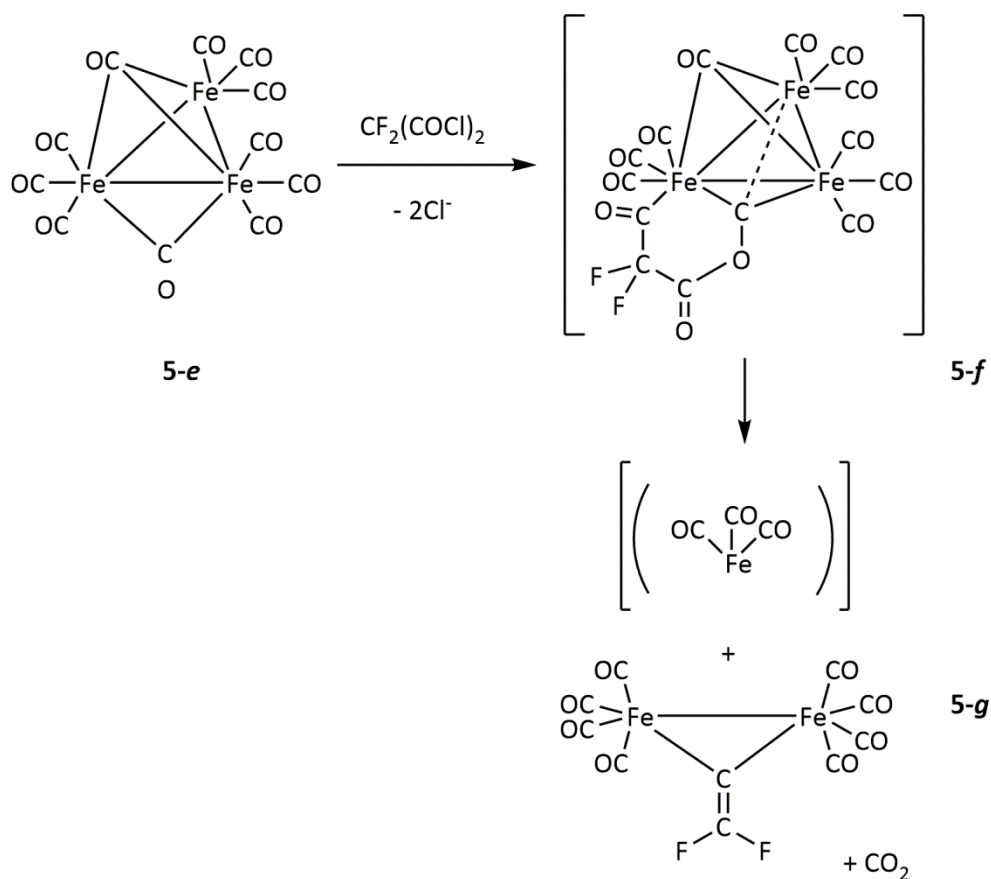
Scheme 5.3 Proposed synthetic pathway to the formation of [(CO)$_8$Fe$_2$(μ-C=CF$_2$)], 5-*g*

The reaction of difluoromalonyl dichloride with [Fe$_3$(CO)$_{11}$]$^{2-}$, **5-*e*** in Scheme 5.3, proved to be complex and no intermediates could be identified. However, a potential mechanism was postulated in which difluoromalonyl chloride attacks an oxygen atom of a bridging carbonyl moiety and an iron atom of **5-*e*** to form cyclic intermediate **5-*f***. This complex then undergoes loss of CO$_2$ and an iron carbonyl fragment to form the final difluorovinylidene complex **5-*g***. Crystal structure analysis of **5-*g*** showed a planar Fe$_2$C=CF$_2$ backbone and a geminal F-C-F angle of 106.2°. Reactivity studies have not been reported for complex **5-*g***.

In 2007, Cowie and co-workers reported the first example of a dimeric iridium fluorovinylidene complex, **5-l**, Scheme 5.4.[268]
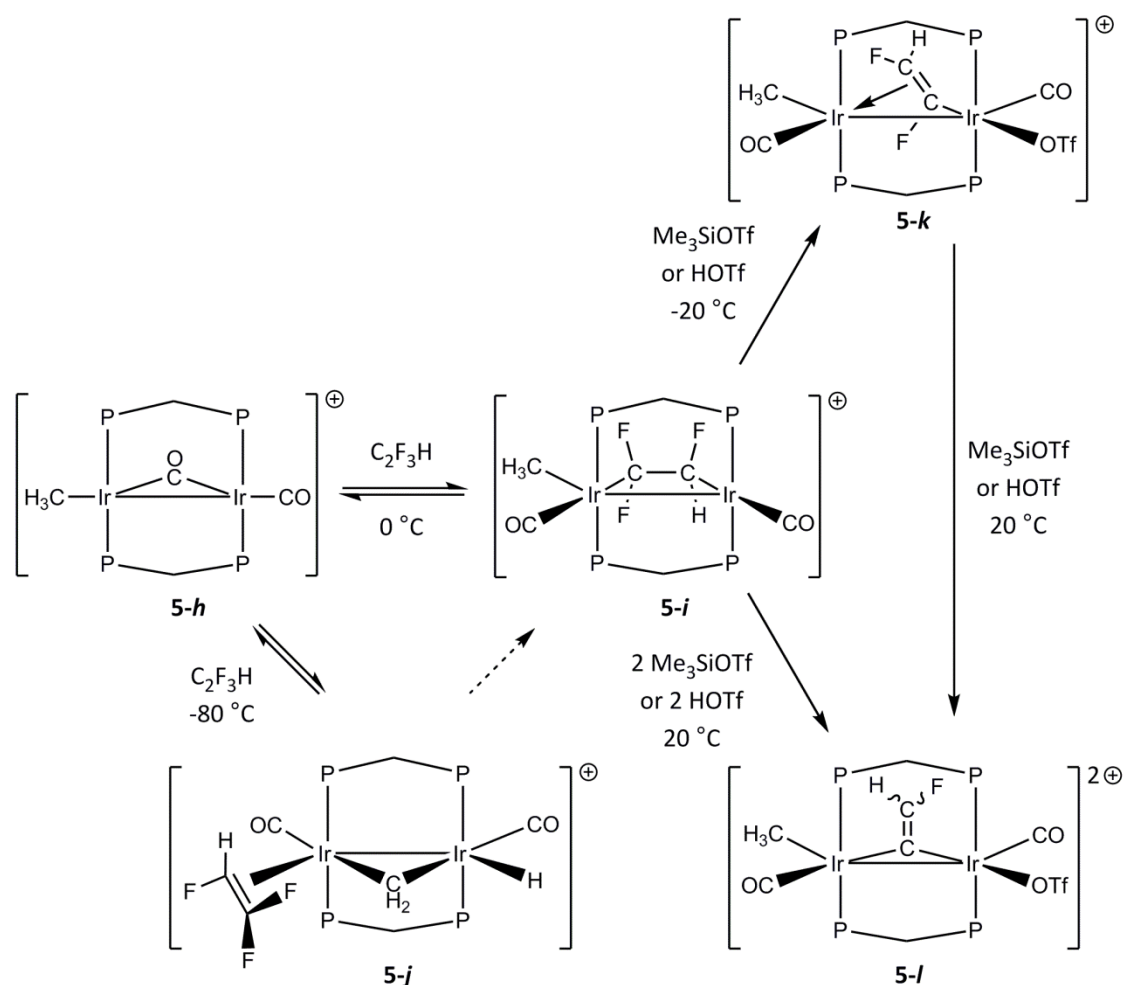
Scheme 5.4 Trifluoroethylene coordination to 5-*h* and fluoride ion abstractions to form vinylidene complex 5-*l*, P = PPh$_2$

Scheme 5.4 illustrates the synthesis of fluorinated vinylidene complex **5-l** *via* double carbon-fluorine bond activation of a fluorinated alkene precursor. The rationale for carbon-fluorine bond activation in trifluoroethylene using this methodology is that by coordination of the alkene in a bridging arrangement, **5-i**, the fluoroalkene can be considered as a 1,2-dimetallated fluoroalkane in which rehybridisation has occurred from sp^2 to sp^3. Each end of the alkene can therefore be viewed as a fluoroalkyl group and so is susceptible to fluoride ion abstraction as has been reported previously for late transition metal fluoroalkyl complexes.

The first step in fluorovinylidene formation is reversible coordination of trifluoroethylene to complex **5-h** to reversibly form either **5-i** or **5-j**. At -80 °C, the kinetic product, complex **5-j**, is

observed in approximately a 10 % yield and on warming to -60 °C, NMR resonances observed for complex **5-*j*** are replaced with those for complex **5-*i*** and unreacted **5-*h***. From this mixture, the quantitative formation of thermodynamic product **5-*i*** is slow and requires 1 hour at -20 °C. The conversion of **5-*j*** to **5-*i*** may occur directly or *via* **5-*h***.

Coordination of the fluoroalkene in the η^2-mode as observed in complex **5-*j*** is the usual kinetic product for fluorinated alkene substrates, but conversion to bridging complex **5-*i*** (and effective carbon rehybridisation from sp^2 to sp^3) is only observed for fluoroalkenes with at least one pair of geminal fluorine substituents. It seems that this is the only case in which the reorganisation required for the 'pyramidalisation' of the planar fluoroalkene is compensated - a consequence of the 'gem-difluoro effect'.[273] A second consequence of this effect is the orientation of the alkene in **5-*i***, which would not predicted on steric grounds but is the electronically favoured arrangement, with the more electron withdrawing alkene substituents adjacent to the more electron rich metal (due to the donor methyl group and assuming that the positive charge is localised on the other metal centre). This permits maximum electron donation to the carbon centre to allow 'pyramidalisation' and rehybridisation.

The resulting rehybridisation of the fluoroalkene in complex **5-*i*** to form fluoroalkyl-like functionality does indeed afford labilisation of the fluoride substituents and allows the removal of a fluoride ion to form complex **5-*k*** using a strong Lewis acid such as trimethylsilyl triflate, Me$_3$SiOTf, or triflic acid, HOTf. At -20 °C, quantitative conversion is achieved to the cis-difluorovinyl-bridged product, **5-*k***, which is stable at ambient temperature. The stereochemistry can be rationalised on the basis of hyperconjugation which makes the cis-difluorovinyl favoured over the trans-. From **5-*k***, an additional equivalent of Lewis acid yields the mono-fluorovinylidene-bridged product **5-*l*** by the removal of a fluoride ion on the α-carbon. Alternatively, this product can be formed directly from double carbon-fluorine bond activation of **5-*i*** using two equivalents of Lewis acid at ambient temperature. The second fluorine atom abstraction is a higher energy process due to only partial rehybridisation of the carbon centre compared to the complete rehybridisation achieved by fluoride removal from complex **5-*i***. The cis/trans stereochemistry of the vinylidene ligand could not be determined.

Further examples of dimeric iridium vinylidene complexes have since been reported by the Cowie group and are given in Scheme 5.5.[268-271]
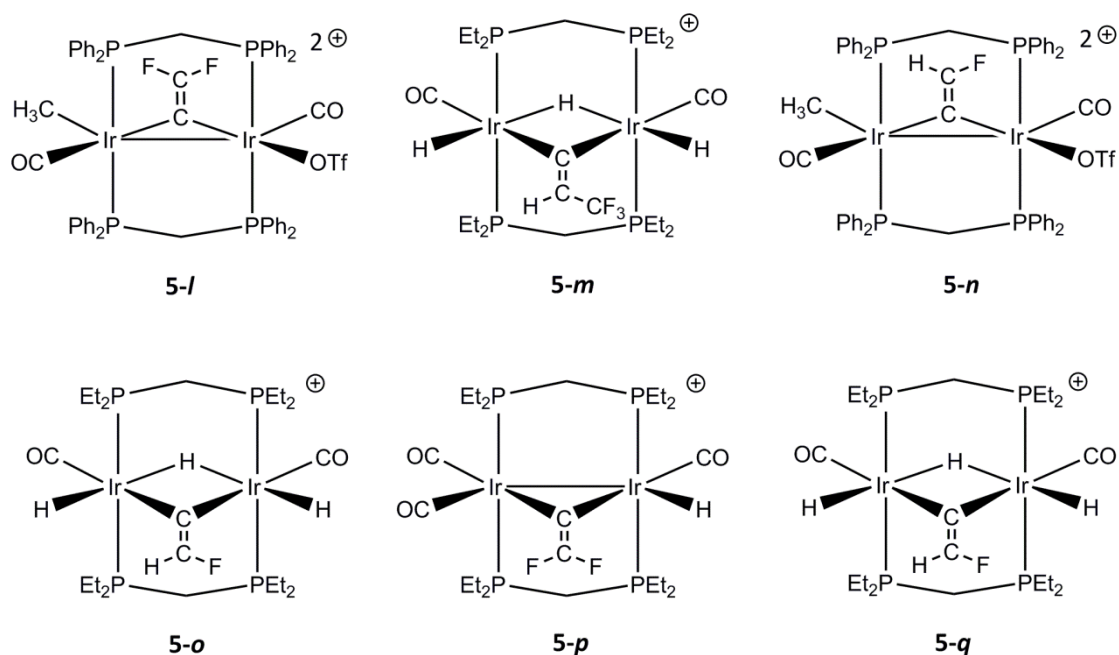
Scheme 5.5 Examples of dimeric iridium fluorovinylidene complexes

All examples, **5-l** to **5-q**, in Scheme 5.5, have been synthesised by carbon-fluorine or carbon-hydrogen bond activations, exploiting the bridging activation mode offered by the dimeric iridium backbone. Studies[268] have shown that interaction of a fluorovinyl group with a second metal centre (for example complex **5-k** in Scheme 5.4) allows a fluoride abstraction from the vinyl α-carbon whereas without this coordination, the complex remains unreactive to strong Lewis acids even at ambient temperature.

There have also been limited studies of reactivity on fluorinated complexes. Complex **5-l** was shown to be unreactive to the addition of CO,[269] and **5-m**, Scheme 5.5, reacted with CO only to replace the triflate group[268]. Complex **5-l** was also shown to be unreactive under a hydrogen atmosphere at ambient temperature.[269] This result was disappointing, as successful hydrogenolysis could allow selective conversion of the trifluoroethylene precursor to *cis*-difluoroethylene, 1,1-difluoroethylene or vinyl fluoride.[269]

In conclusion, although limited examples of fluorovinylidene complexes have been reported, the availability of these species with a range of substitution patterns is heavily restricted. Examples are limited to dimeric complexes, mainly based on iridium, which are synthesised by carbon-fluorine or carbon-hydrogen bond activation of pre-fluorinated alkene substrates using strong Lewis acids.[268-272] Although the methodology demonstrates selective and facile substrate activation promoted by unusual metal-metal cooperativity, this approach does not

represent a general method for the synthesis and exploitation of fluorovinylidene complexes and hence their reactivity is largely unexplored. This is despite their potential importance as catalytic intermediates, as highlighted by the prevalence of catalytic reactions that proceed *via* non-fluorinated vinylidene intermediates.[49]

This chapter describes the facile synthesis of fluorinated and trifluoromethyl-substituted mononuclear vinylidene complexes from readily-available, non-fluorinated alkyne substrates. The reactivity of these complexes with a range of nucleophiles and under a range of reaction conditions is presented.

5.2 Synthesis and characterisation of fluorinated vinylidene complexes

5.2.1 Synthesis of [Ru(η^5-C$_5$H$_5$)(PPh$_3$)$_2$(-C≡C{R})], [26^R]

Electrophilic addition reactions (of H$^+$, Cl$_2$, Br$_2$, I$_2$, Au(PPh$_3$)$^+$) to ruthenium acetylide complexes [Ru(η^5-C$_5$H$_5$)(PPh$_3$)$_2$(-C≡C{R})], **[26^R]**, allow access to a wide range of functionalised vinylidene complexes (see Section 5.1.1).[64] By analogy to these reactions, the preparation of fluorinated vinylidene ligands was attempted by electrophilic fluorination of the alkynyl moiety in **[26^R]**. Complexes **[26^R]** were selected as ideal precursors also due to ease of preparation from [Ru(η^5-C$_5$H$_5$)(PPh$_3$)$_2$Cl], **[25]**, with a variety of terminal alkynes.[274] This methodology allows **[26^R]** to be prepared with a range of **R** substituents which allows access to a range of fluorination-precursor complexes with differing electronic and steric properties.
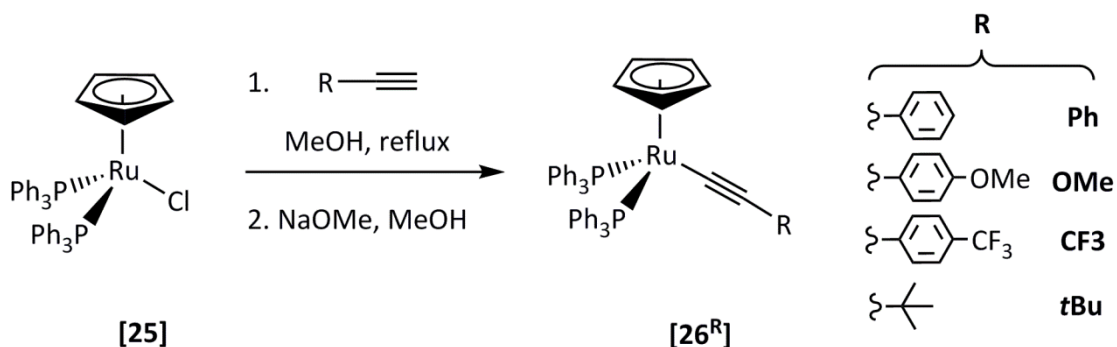
Scheme 5.6 Preparation of acetylide complexes [26^R]

Crystals of **[26^{CF3}]** were obtained by slow evaporation of the solvent from a dichloromethane solution. The structural determination is shown in Figure 5.1.
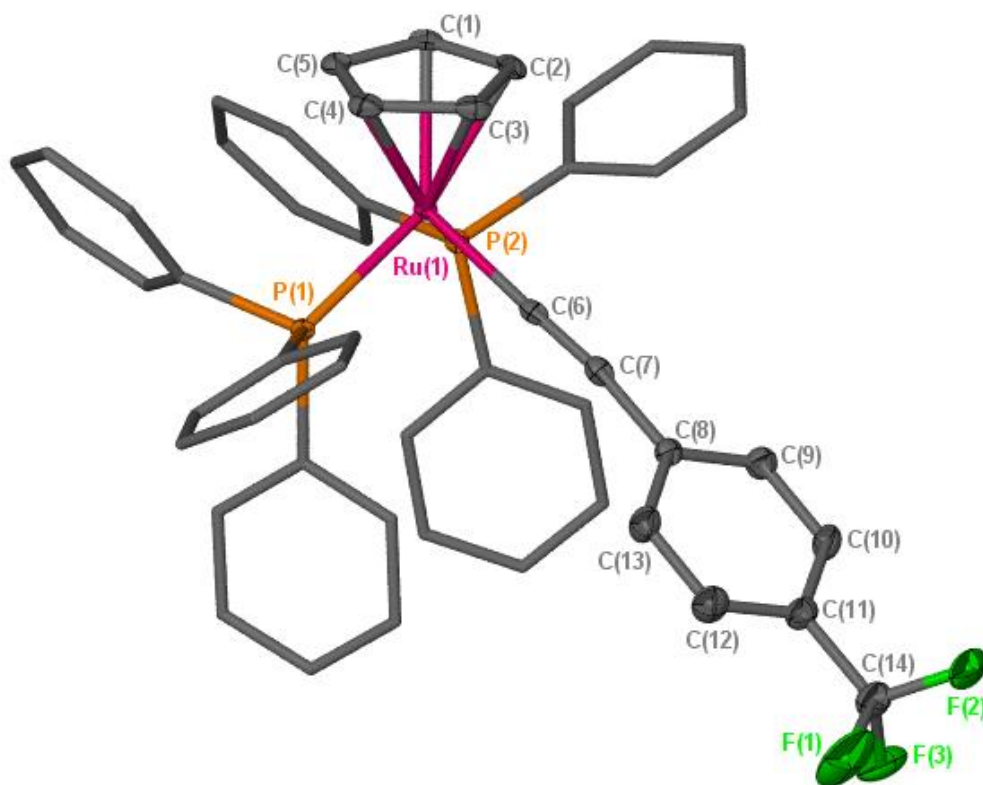
Figure 5.1 X-Seed diagram of complex [26^{CF3}]. Hydrogen atoms have been omitted for clarity, and where shown the thermal ellipsoids are at a 50 % probability level.

The bond lengths and angles of the acetylide ligand are similar to those reported for related [Ru(η^5-C$_5$H$_5$)(PPh$_3$)$_2$(-C≡C{R})], **[26^R]**, complexes.[275-277] The Ru(1)-C(6) bond distance of 2.0174(19) Å is a typical ruthenium-carbon single bond length in ligands of this type (**[26^{Ph}]**, 2.017(5) Å; **[26^{NO2}]**, R = -C$_6$H$_4$-4-NO$_2$, 1.994(5) Å; **[26^{Pyr}]**, R = -oC$_5$H$_4$N, 2.007(3) Å). The C(6)-C(7) triple bond (1.203(3) Å) is also comparable in length to that of **[26^{Ph}]** (1.214(7) Å), **[26^{NO2}]** (1.202(8) Å) and **[26^{Pyr}]** (1.216(4) Å).

5.2.2 Synthesis of [Ru(η^5-C$_5$H$_5$)(PPh$_3$)$_2$(C=C{F}Ph)]BF$_4$, [27^{Ph}]BF$_4$

On addition of stoichiometric 1-fluoro-2,4,6-trimethylpyridinium tetrafluoroborate, **[FTMP]BF$_4$**, to a dichloromethane solution of **[26^{Ph}]**, an immediate colour change was observed from yellow to dark green which indicated a rapid initial reaction. Multinuclear NMR spectroscopy recorded after ten minutes of addition of **[FTMP]BF$_4$** to the reaction mixture indicated quantitative conversion of **[26^{Ph}]** to a single new species. In the ^{31}P{^{1}H} NMR spectrum, the singlet resonance for the PPh$_3$ ligands of acetylide complex **[26^{Ph}]** at 50.9 ppm was replaced by a singlet resonance at 42.1 ppm, and in the ^{1}H NMR spectrum a new

cyclopentadienyl resonance was observed at 5.45 ppm which replaced that of **[26^{Ph}]** at 4.34 ppm. Most promisingly, the ^{19}F NMR spectrum exhibited two new signals – one corresponding to the BF$_4^-$ counter ion and a new singlet resonance at -208.7 ppm, indicating a single fluorine environment in the new species. High resolution ESI-MS showed the formation of a single species with an *m/z* of 811.1656 which was also consistent with the incorporation of a single fluorine atom into the structure of **[26^{Ph}]**. From this reaction mixture, **[27^{Ph}]BF$_4$** could be isolated in high yield, Scheme 5.7.
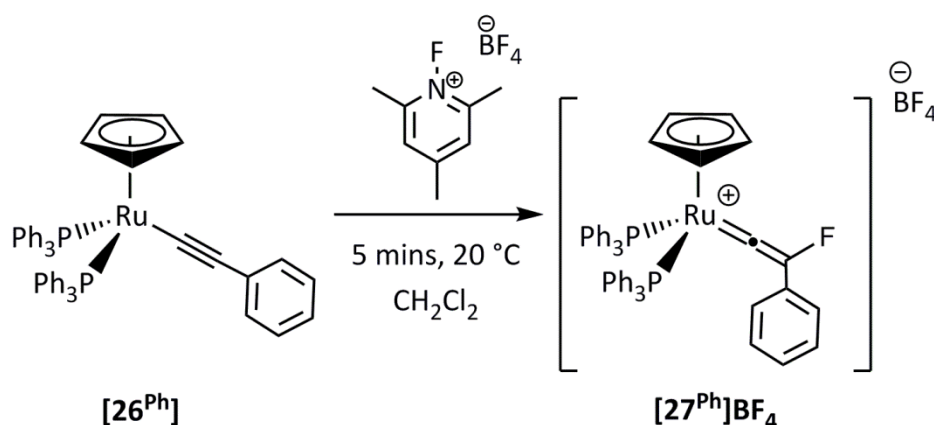
Scheme 5.7 Conversion of acetylide [26^{Ph}] to fluorovinylidene complex [27^{Ph}]BF$_4$

Complex **[27^{Ph}]BF$_4$** was characterised further by ^{13}C{^{1}H} NMR spectroscopy. Metal-vinylidene complexes are readily identified by downfield resonances for the α and β carbons due to extensive deshielding (see Chapter 1). In complex **[27^{Ph}]BF$_4$**, the α-carbon was observed as a doublet of triplets at 389.0 ppm with a $^2J_{CF}$ of 39.3 Hz and a $^2J_{CP}$ of 16.2 Hz, and the β-carbon appeared at 196.7 ppm as a doublet with a $^1J_{CF}$ of 222.1 Hz. With respect to the non-fluorinated analogue [Ru(η^5-C$_5$H$_5$)(PPh$_3$)$_2$(C=C{H}Ph)]PF$_6$, **[28]PF$_6$**, these chemical shifts were shifted downfield by approximately 30 and 70 ppm respectively, reflecting the incorporation of the strongly electron withdrawing fluorine substituent. Indeed, the metal bound α-carbon of **[27^{Ph}]BF$_4$** resonates at one of the lowest chemical shifts ever reported for a metal vinylidene complex.[50]

On cooling of complex **[27^{Ph}]BF$_4$** to 195 K in CD$_2$Cl$_2$ solution, the ^{1}H, ^{19}F and ^{31}P{^{1}H} NMR spectra showed no change, indicating a rapid rotation of the vinylidene complex on the NMR timescale. This behaviour is typical for ruthenium half-sandwich complexes with the general formula [Ru(η^5-C$_5$H$_5$)(P)$_2$(C=C{H}R')]$^+$ (P = phosphine ligand, R' = alkyl or aromatic substituent, and variable temperature NMR studies demonstrated a small barrier to rotation of

approximately 38 kJ mol^{-1} for complexes of this type.[278] The preferred geometry of these complexes in solution is the one in which the plane of the vinylidene ligand is perpendicular to that containing the vinylidene α-carbon, the metal atom and the centre of the cyclopentadienyl ring. In complex **[28]PF$_6$**, the rotational barrier was too low to be measured and the complex did not demonstrate any restricted rotation even when cooled to 195 K.[59] As this was also true for **[27^{Ph}]BF$_4$**, the incorporation of a fluorine atom into the structure of the vinylidene ligand does not appear to have affected this property.

Crystals suitable for study by X-ray diffraction were obtained and are discussed in detail in Section 5.3.1.

5.2.3   Extension of the fluorination methodology

Following the successful synthesis of **[27^{Ph}]BF$_4$**, the generality of the methodology was probed by reaction of a range of substituted acetylide complexes, **[26^R]**. Fluorination of **[26^R]** was successful with both electron withdrawing and electron donating substituents present on the acetylide ligand, which could either be aromatic or aliphatic, Scheme 5.8.

R		'F$^+$'	X
⌇─⟨◯⟩	Ph	[FTMP]BF$_4$	BF$_4$
⌇─⟨◯⟩─OMe	OMe	[FTMP]BF$_4$	BF$_4$
⌇─⟨◯⟩─CF$_3$	CF3	[FTMP]BF$_4$	BF$_4$
⌇─⟨	tBu	NFSI	NSI
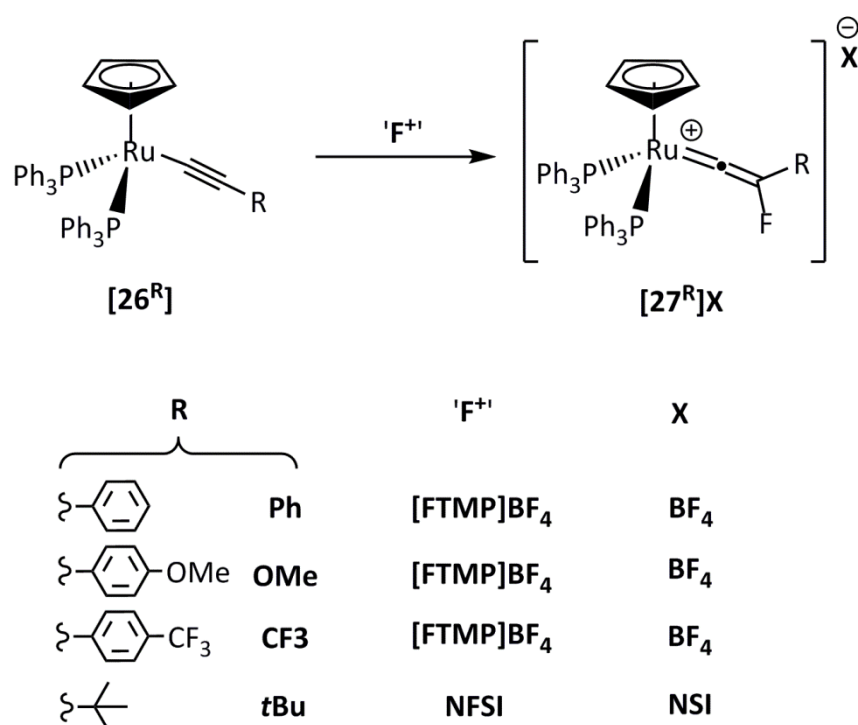
Scheme 5.8 Synthesis of complexes [27^R]X

Fluorination was also effective with a range of fluorinating agents including 1-fluoro-2,4,6-trimethylpyridinium tetrafluoroborate **[FTMP]BF$_4$**, N-fluorobenzene sulfonimide, **NFSI**, and 1-

chloromethyl-4-fluoror-1,4-diazoniabicyclo[2.2.2]octane *bis*(tetrafluoroborate), **Selectfluor** (also known as F-TEDA), Scheme 5.9. Fluorination of the 1,2-*bis*(diphenylphosphino)ethane (dppe)-substituted acetylide, **[29^{Ph}]**, is also possible using **NFSI**. The reactions of **[29^{Ph}]** with **[FTMP]BF$_4$** and **Selectfluor** have not yet been screened but would be expected to produce **[30^{Ph}]BF$_4$**.
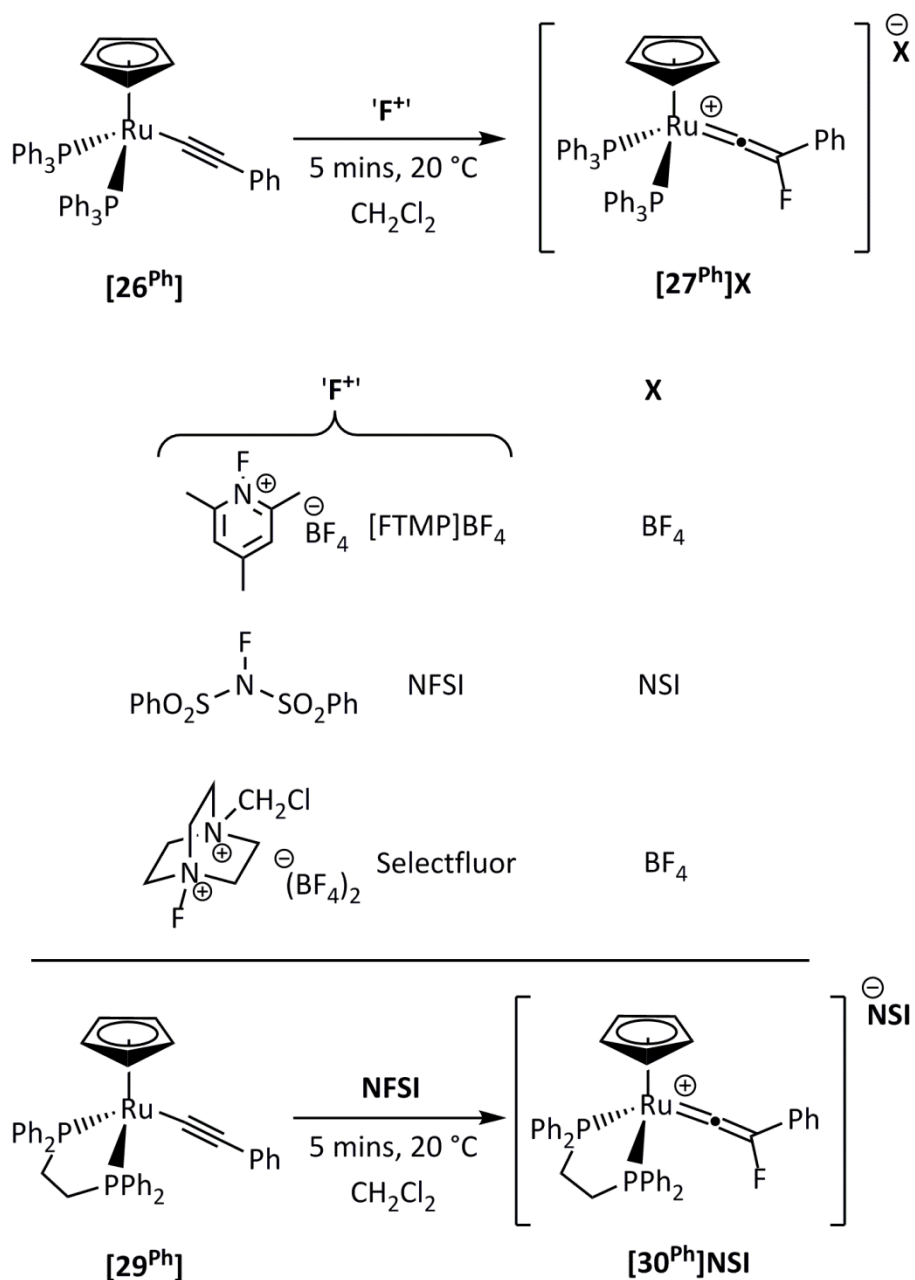
Scheme 5.9 Synthesis of complex [27^{Ph}]X using different fluorinating agents. The triphenylphosphine ligand in [26^{Ph}] can be replaced with dppe, [29^{Ph}], and fluorinated using NFSI under the same conditions to produce [30^{Ph}]NSI.

Crystals of **[30^{Ph}]PF$_6$** were obtained by salt metathesis (in order to exchange the NSI$^-$ counter-ion for PF$_6^-$) followed by the slow diffusion of pentane into a dichloromethane solution of the complex. The structural determination of **[30^{Ph}]$^+$** is shown in Figure 5.2.
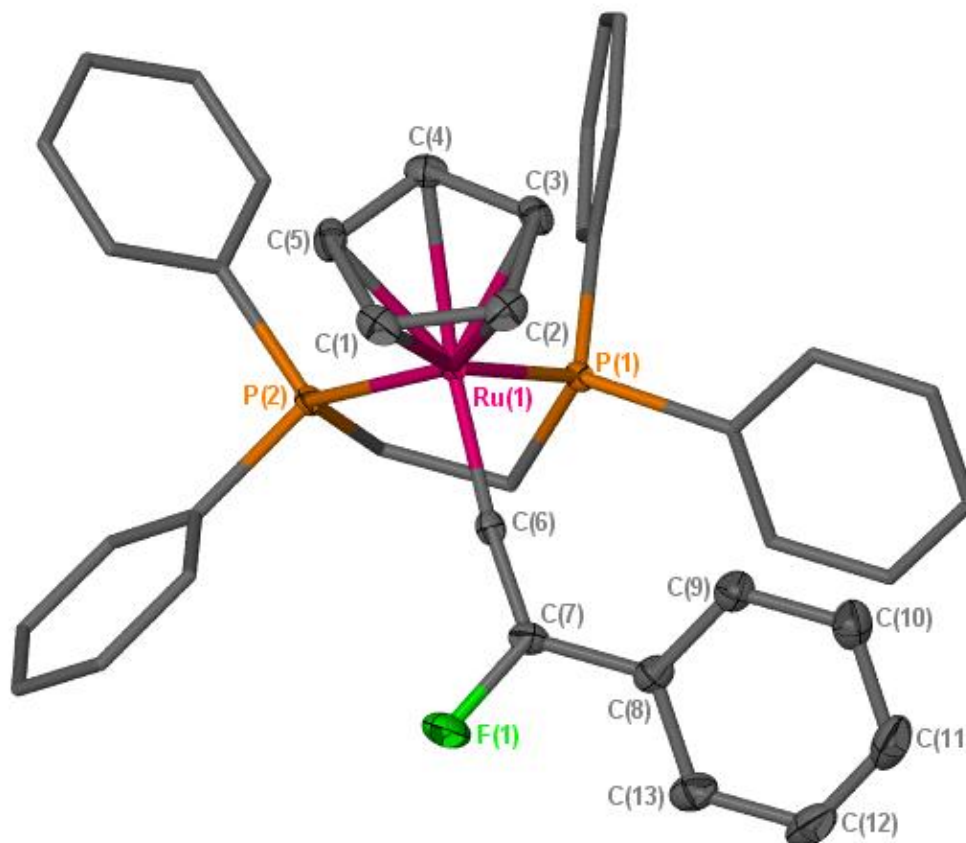
Figure 5.2 X-Seed diagram of the cation from complex [30^{Ph}]PF$_6$. Hydrogen atoms and a PF$_6^-$ anion have been omitted.

The phenyl group of the vinylidene ligand in **[30^{Ph}]$^+$** is in a plane perpendicular to that of the cyclopentadienyl ligand; this is similar to the orientation of the phenyl group observed in the green crystals of **[27^{Ph}]$^+$** (Section 5.3.1). In **[30^{Ph}]$^+$**, there appears to be a π-stacking interaction between the phenyl moiety of the vinylidene ligand and a phenyl group of the dppe, which could encourage the complex to adopt this configuration in the solid state by affording extra stabilisation. Despite the difference between the *bis*-triphenylphosphine ligands and the dppe functionality, the bond lengths are statistically identical between the fluorovinylidene moieties of **[27^{Ph}]$^+$** and **[30^{Ph}]$^+$**.

The success of these analogous reactions demonstrates the generality of this methodology and the compatibility of the procedure with different sources of '**F$^+$**' and different acetylide

substitution. Experiments performed by MChem student Lewis Hall showed that formation of **[27^Ph]BF_4** was also possible from the treatment of **[28]BF_4** with base *in situ* (to prepare the acetylide), followed by subsequent addition of **[FTMP]BF_4**. Furthermore, this synthesis was possible without the addition of base, although the rate was reduced and to reach completion the reaction required 30 minutes. Presumably, the source of base in the latter reaction is free 2,4,6-trimethylpyridine, **TMP**, present in the reaction mixture, and the slow rate may be explained by the low concentration of this species in solution. Hall has also performed studies on analogous 1,2,3,4,5-pentamethylcyclopentadienyl, Cp*, complexes and obtained evidence for the fluorinated vinylidene complexes, **[32^R]NSI** and **[34^R]NSI**, illustrated in Scheme 5.10. Summer-project students Daniella Cheang and James Pitts also demonstrated the successful fluorination of [*trans*-RuCl(-C≡C{Ph})(dppe)_2], **[35^Ph]** using NFSI to form the corresponding fluorovinylidene complex **[36^Ph]NSI**.[279]
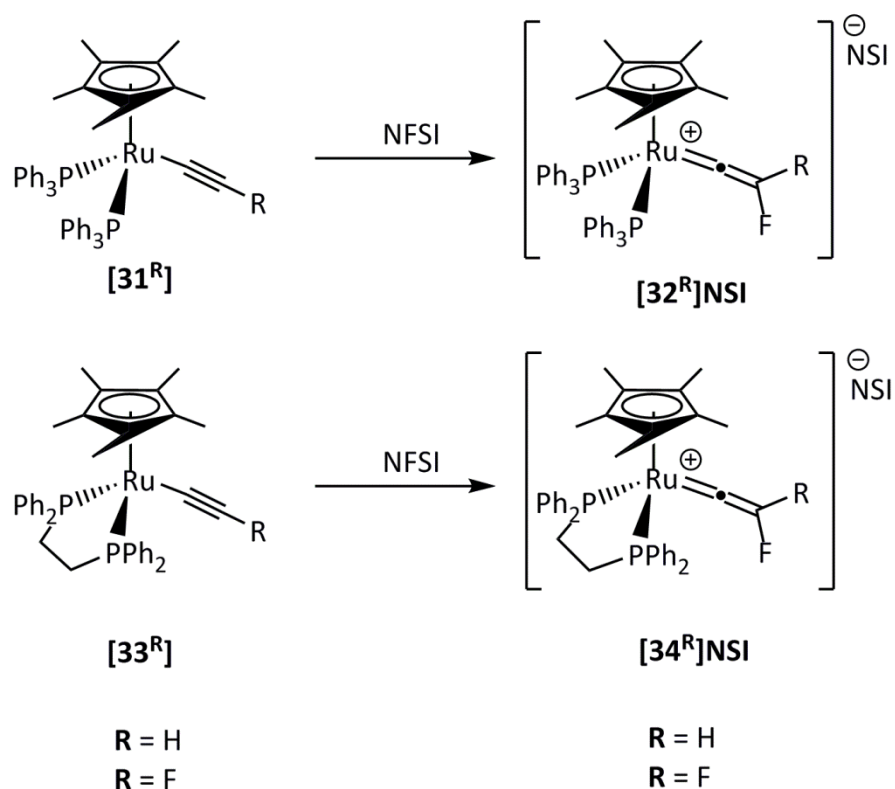
Scheme 5.10 Syntheses of Cp* substituted fluorovinylidene complexes [32^R]NSI and [34^R]NSI

5.2.4 Synthesis of complex [37^R]BF$_4$

The fluorination of acetylide complex **[26^R]** to form fluorovinylidene **[27^R]X** was tolerant to both changing the substitution of the acetylide ligand (R = -Ph, -C$_6$H$_4$-4-CF$_3$, -C$_6$H$_4$-4-OMe, *t*Bu) and the choice of fluorinating agent (**NFSI**, **Selectfluor**, **[FTMP]BF$_4$**) as illustrated in Scheme 5.8 and Scheme 5.9. However, reaction of **[26^{Ph}]** or **[26^{CF3}]** with 1-fluoropyridinium tetrafluoroborate, **[FPyr]BF$_4$** resulted in the formation of the corresponding disubstituted vinylidene complex **[37^R]BF$_4$**, Scheme 5.11.
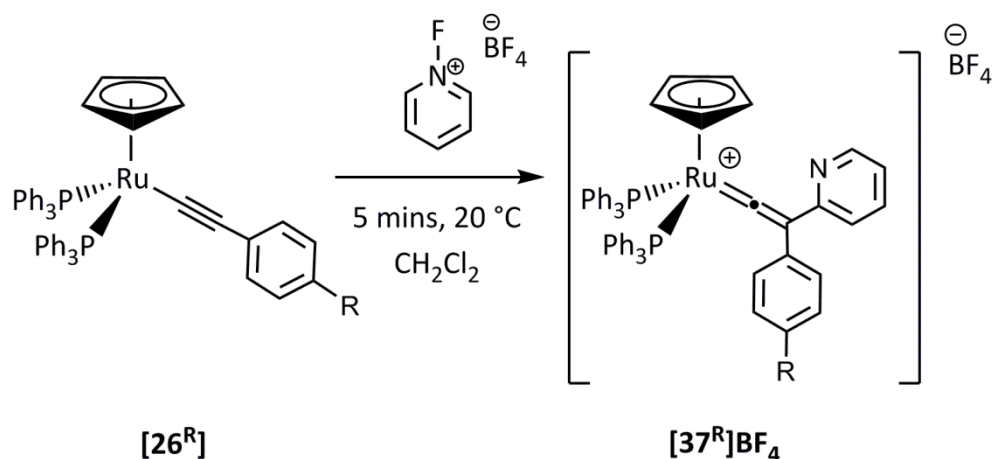
Scheme 5.11 Synthesis of complex [37^R]BF$_4$, R = H or CF$_3$

On addition of **[FPyr]BF$_4$** to a dichloromethane solution of **[26^{Ph}]**, an immediate colour change was observed from yellow to red, rather than to the characteristic dark green of the fluorovinylidene complexes synthesised previously. Multinuclear NMR spectroscopy recorded immediately after addition of **[FPyr]BF$_4$** indicated conversion primarily to one new organometallic complex (approx. 70 %). Other species in the reaction mixture could not be identified as the integration of each was never more than 7 %. The ^{1}H NMR could not be assigned completely in the aromatic region due to the presence of these impurities, but showed a new singlet resonance at 5.13 ppm for the cyclopentadienyl resonance and the ^{31}P{^{1}H} NMR spectrum showed a new singlet resonance at 41.5 ppm with no signals observed for residual **[26^{Ph}]**. High resolution ESI-MS indicated only one organometallic product with a peak corresponding to **[37^{Ph}]$^+$** at *m/z* 870.2024. Complex **[37^{Ph}]BF$_4$** appears to have been formed by formal nucleophilic aromatic substitution of **[FPyr]BF$_4$** by the acetylide moiety of **[26^{Ph}]**, concomitant with the loss of HF, which could not be observed in the NMR spectra. The proposed mechanism for this process is shown in Scheme 5.12. The formation of highly

reactive HF *in situ* may help to explain the formation of the other organometallic complexes present in the reaction mixture.
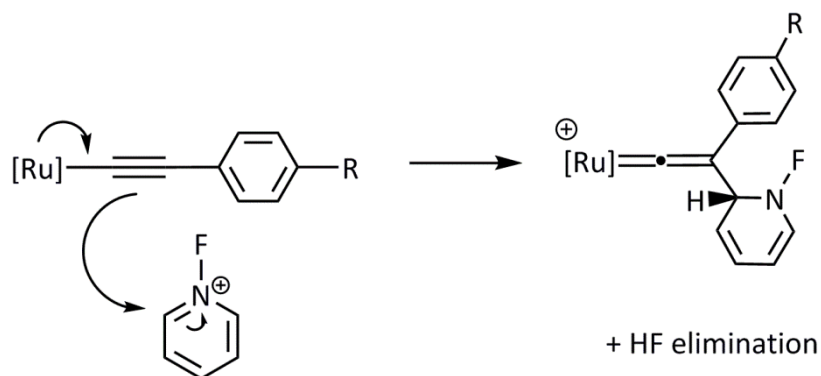
Scheme 5.12 Proposed mechanism for the formation of [37^R]BF$_4$

The analogous reaction with **[26^{CF3}]** produced **[37^{CF3}]BF$_4$** with fewer impurities than in the spectra of **[37^{Ph}]BF$_4$** which allowed full assignment of the ^{1}H and ^{13}C{^{1}H} NMR spectra. Red, needle-like crystals of **[37^{CF3}]BF$_4$** suitable for study by X-ray diffraction were obtained serendipitously from the pentane washings of the reaction mixture. The results of the structural determination are shown in Figure 5.3.
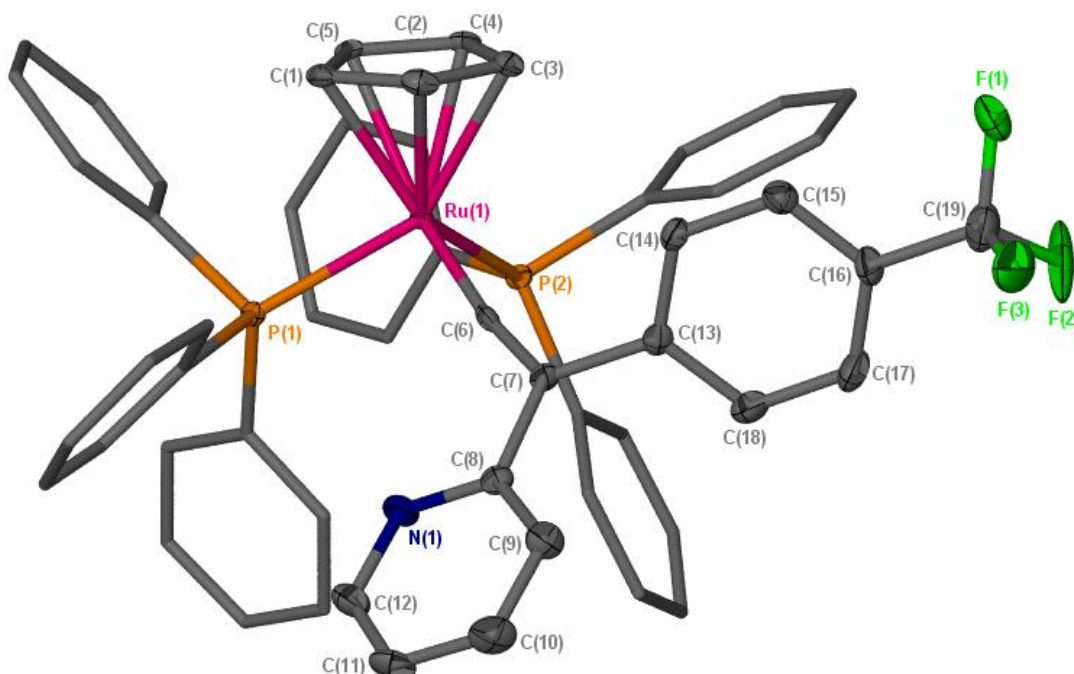
Figure 5.3 X-Seed diagram of the cation from complex [37^{CF3}]BF$_4$. Hydrogen atoms and a BF$_4^-$ anion have been omitted for clarity, and where shown the thermal ellipsoids are at a 50 % probability level.

In the literature, one example of a *ortho*-pyridyl-substituted acetylide complex has been reported, [Ru(η^5-C$_5$H$_5$)(PPh$_3$)$_2$(-C≡C{*o*-C$_5$H$_4$N})], **5-r**, which was synthesised from [Ru(η^5-C$_5$H$_5$)(PPh$_3$)$_2$Cl], **[25]**, and 2-ethynyl pyridine in a similar manner to that described in Scheme 5.6.[276] However, in the presence of methanol and in the absence of base, the intermediate vinylidene complex was intercepted by nucleophilic attack of methanol at the α-carbon leading to 2-picolyl methoxycarbene formation, [Ru(η^5-C$_5$H$_5$)(PPh$_3$)$_2$(=C{OMe}-CH$_2${*o*-C$_6$H$_4$N})], **5-s**, and so a mixed solvent system of CHCl$_3$/MeOH/NEt$_3$ was used at room temperature. The acetylide complex can be converted to the dicationic protio-vinylidene complex by the addition of excess HBF$_4$ in Et$_2$O, in which both the β-carbon and pyridyl-nitrogen atom accept a proton, but complexes **[37^R]BF$_4$** are believed to be the first examples of disubstituted *ortho*-pyridyl-vinylidene complexes.

5.2.5 Synthesis of complex [38]BF$_4$

In a similar manner to electrophilic fluorination, the incorporation of trifluoromethyl groups into the framework of vinylidene complexes, and ultimately into organic molecules, is highly desirable.[170] Trifluoromethyl groups are prevalent in the structure of many biologically active molecules that are used as pharmaceutical agents or agrochemicals (see Chapter 4).[173,280] A single example of a trifluoromethyl-substituted vinylidene complex has been reported by the Cowie group, complex **5-m**, Scheme 5.5, which exists as an iridium dimer synthesised *via* the activation of H$_2$C=CHCF$_3$. However, the reaction between **[26^{Ph}]** and Umemoto's reagent, 5-(trifluoromethyl)dibenzothiophenium tetrafluoroborate, results in the formation of a mononuclear trifluoromethylated vinylidene, **[38]BF$_4$**, Scheme 5.13.
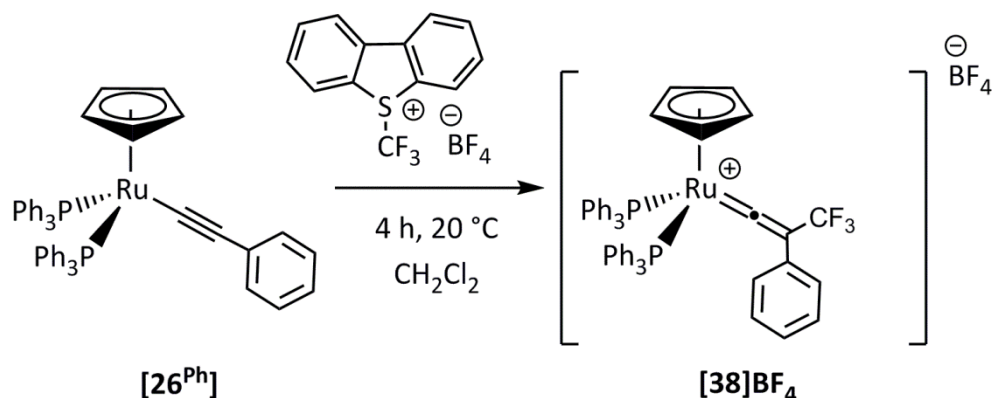
Scheme 5.13 Trifluoromethylation of complex [26^{Ph}] to form [38]BF$_4$

The ^{13}C{^{1}H} NMR spectrum of **[38]BF$_4$** shows characteristic signals for the vinylidene moiety. The α-carbon appears at 340.0 ppm as a triplet of quartets due to coupling with both the two equivalent triphenylphosphine ligands and the fluorine atoms of the trifluoromethyl group (15.2 Hz and 3.3 Hz respectively), and the β-carbon appears at 126.3 ppm as a quartet with a larger coupling to the trifluoromethyl group of 34.8 Hz. The high resolution ESI-MS shows a peak for a ruthenium-containing species at an *m/z* of 861.1611 which corresponds to protonated-**[38]$^+$**.

X-ray crystallography confirmed the incorporation of the trifluoromethyl group at the β-carbon of the ligand, Figure 5.4. The structure shows that the phenyl group of the vinylidene ligand is in a perpendicular plane to that of the cyclopentadienyl ligand; this is similar to the green crystals of **[27^{Ph}]$^+$**, but opposite to the orange crystals of **[27^{Ph}]$^+$** and the red crystals of **[28]$^+$** (see Section 5.3.1).
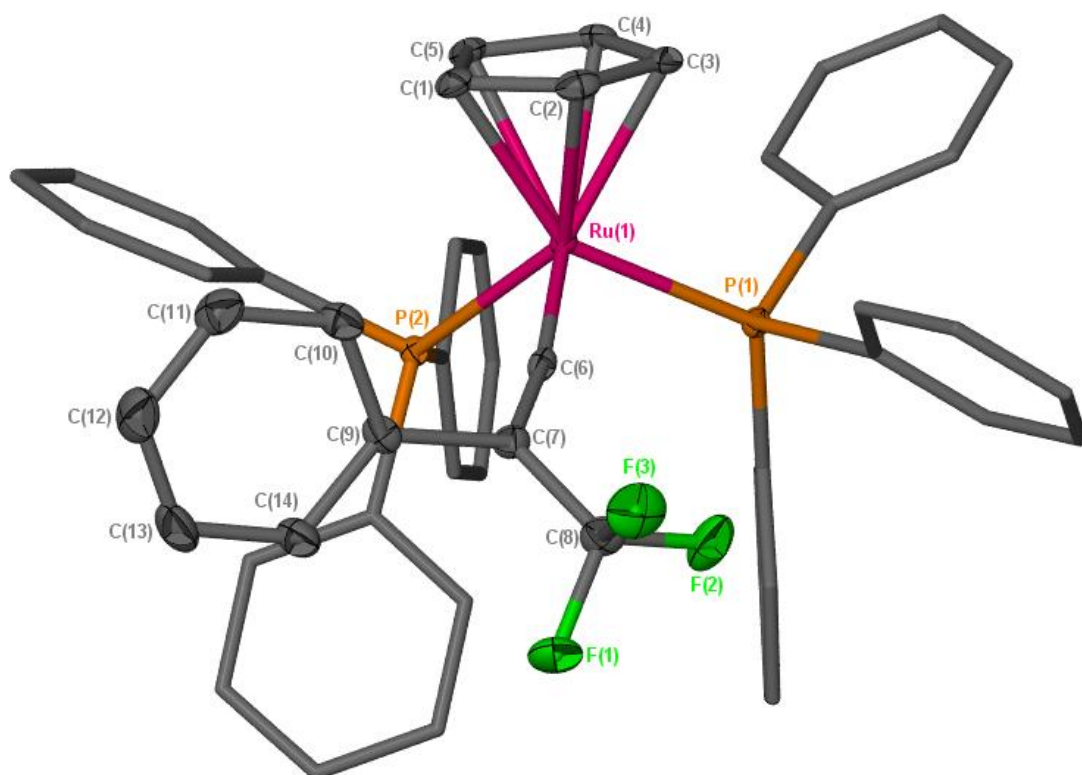
Figure 5.4 X-Seed diagram of the cation from complex [38]BF$_4$. Hydrogen atoms, a BF$_4^-$ anion and a dichloromethane of crystallisation have been omitted for clarity, and where shown the thermal ellipsoids are at a 50 % probability level.

5.3   Characterisation of fluorovinylidene complexes

As the new fluorinated ligands were retained in the coordination sphere of ruthenium, the effects of fluorine incorporation into the vinylidene moiety could be studied in terms of structural and electronic properties.

5.3.1   X-ray crystallography data for [Ru(η^5-C$_5$H$_5$)(PPh$_3$)$_2$(C=C{F}Ph]PF$_6$, [27^{Ph}]PF$_6$

In order to obtain crystals suitable for study by X-ray diffraction, **[27^{Ph}]PF$_6$** was synthesised by salt metathesis *via* the addition of 20 equivalents of NaPF$_6$ to a dichloromethane solution of **[27^{Ph}]BF$_4$**. The reaction mixture was allowed to stir for approximately one hour before removal of excess NaPF$_6$ (and the formed NaBF$_4$) by cannula filtration. Crystals were subsequently grown by the slow diffusion of pentane into a dichloromethane solution of the complex.

Two separate batches of crystalline **[27^{Ph}]PF$_6$** were obtained by slow diffusion of pentane into a dichloromethane solution of the complex – one green and the other orange in colour. Repeated crystallisation attempts on subsequent batches of the complex resulted in the formation of green crystals only. Analysis of each set of crystals indicated the presence of the **[27^{Ph}]$^+$** cation in both cases. However, the orientation of the vinylidene ligand, crystal packing and weak interionic interactions differed between the two sets. The two cations are shown in Figure 5.3. X-ray diffraction studies were also performed on the analogous, non-fluorinated structure **[28]PF$_6$**, in order to evaluate the influence of fluorine incorporation on the geometry and electronic properties of the vinylidene complex.
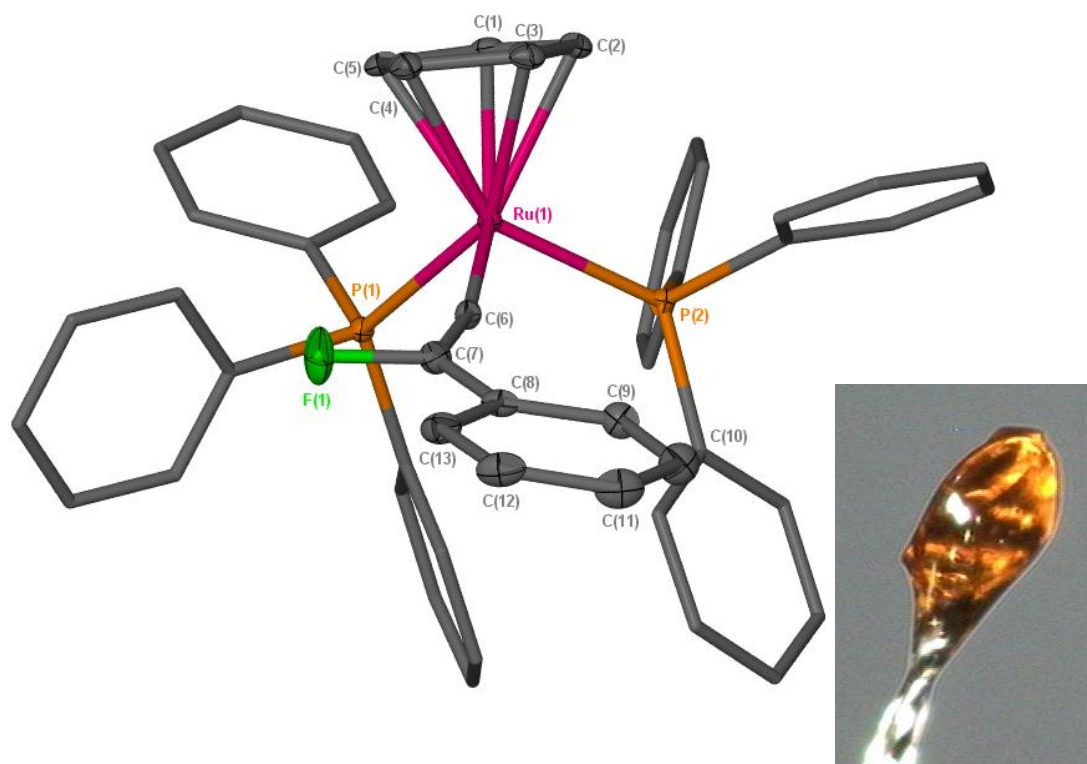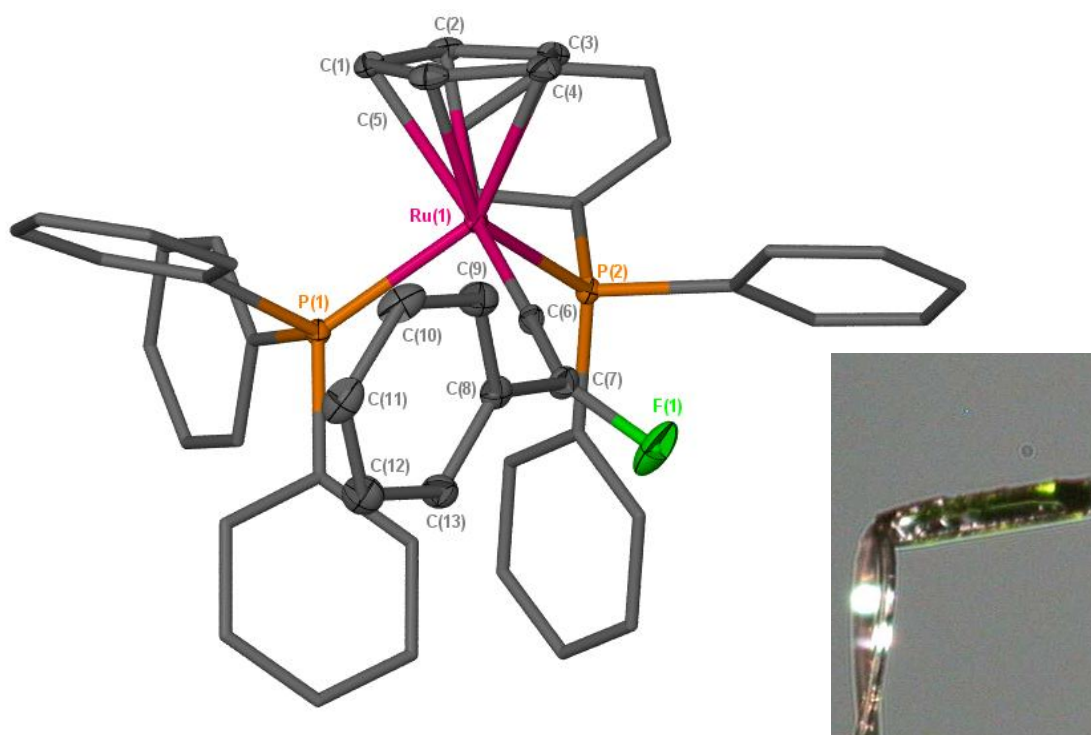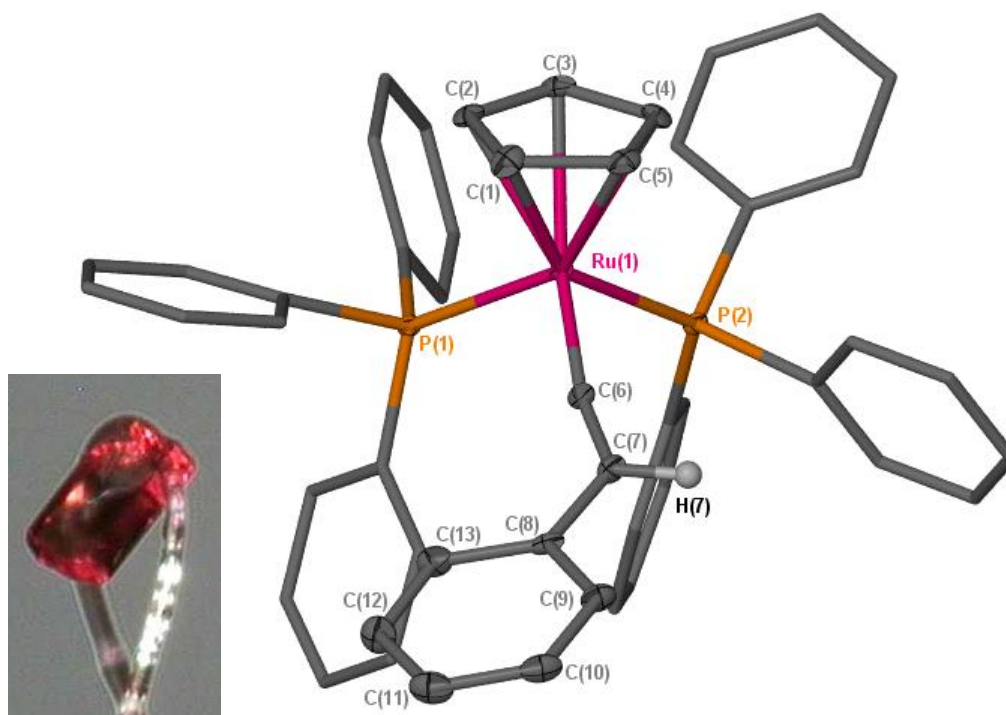
Figure 5.5 X-Seed diagrams of the cations in the two batches of [27^{Ph}]PF$_6$ and [28]PF$_6$. Hydrogen atoms and PF$_6^-$ anions have been omitted for clarity, and where shown the thermal ellipsoids are at a 50 % probability level. Photographs of the crystals are also provided to demonstrate the difference in both colour and shape between the sets.

As shown in Figure **5.3**, in the green crystals the fluorine is oriented away from the cyclopentadienyl ring whereas in the orange crystals it points in the opposite direction. There is also a marked change in geometry between the two isomers of the **[27^{Ph}]$^+$** cation. Key bond lengths and angles of both isomers of **[27^{Ph}]$^+$** (and **[28]$^+$** for comparison) are summarised in Table 5.1.

	Bond Lengths / Å		
	Green [27^{Ph}]⁺	Orange [27^{Ph}]⁺	[28]⁺
P(1) – Ru(1)	2.3355(10)	2.3451(4)	2.3594(11)
P(2) – Ru(1)	2.3526(4)	2.3675(4)	2.3327(10)
Ru(1) – C(6)	1.8385(14)	1.8451(16)	1.850(4)
C(6) – C(7)	1.3168(19)	1.333(2)	1.318(6)
C(7) – C(8)	1.470(2)	1.467(2)	1.474(6)
C(7) – F(1)	1.3626(17)	1.366(2)	-
	Bond Angles / °		
	Green [27^{Ph}]⁺	Orange [27^{Ph}]⁺	[28]⁺
P(1) – Ru(1) – P(2)	102.166(12)	97.466(14)	97.56(4)
P(1) – Ru(1) – C(6)	88.63(4)	91.99(5)	98.89(14)
P(2) – Ru(1) – C(6)	93.18(4)	99.31(5)	91.18(12)
Ru(1) – C(6) – C(7)	172.46(12)	164.16(14)	165.3(4)
C(6) – C(7) – C(8)	121.02(13)	132.51(16)	131.1(4)
C(6) – C(7) – F(1)	121.05(13)	114.77(15)	-
F(1) – C(7) – C(8)	117.72(12)	112.66(14)	-

Table 5.1 Selected bond lengths and angles for orange and green cations of [27^{Ph}]⁺ and [28]⁺ for comparison

The most notable difference between the green and orange polymorphs is the differing geometries of the vinylidene ligands. In the case of the orange crystal, there is a marked deviation from the idealised sp^2-hybridised geometry around the vinylidene β-carbon, C(7), with a C(6) – C(7) – F(1) bond angle of only 114.77(15)°. Instead, the green polymorph exhibits a more typical sp^2-hybridised C(6) – C(7) – F(1) bond angle of 121.06°. The reduced bond angle of the orange crystal allows the fluorine atom to be closer to the metal-bound α-carbon, C(6), of the vinylidene ligand in comparison to the green crystal (carbon-fluorine distances: green crystal 2.333(2) Å; orange crystal 2.273(2) Å). The vinylidene ligand of the orange crystal also exhibits a significant distortion from linearity with a Ru(1) – C(6) – C(7) bond angle of 164.16(14)°, whereas the green polymorph again demonstrates a more idealised bond angle of 172.46(12)°. However, the orientation of the vinylidene ligand in the green crystal is unusual; the preferred geometry for complexes of this type orients the

vinylidene ligand in a perpendicular plane to that formed by the vinylidene α-carbon, the metal atom and the centre of the cyclopentadienyl ring.[278] In this case, the vinylidene ligand is in the same plane as these features, placing the π-system perpendicular to the α-carbon.

However, the bond lengths within the vinylidene ligands, Ru(1) – C(6), C(6) – C(7), C(7) – C(8) and C(7) – F(1), of the two polymorphs are statistically identical; these are also both comparable to those of the protio-vinylidene structure, suggesting that fluorine incorporation has little effect on the bond lengths of the vinylidene ligand.

An examination of the intermolecular contacts within the crystal lattice indicates notable differences in the packing arrangements between the two polymorphic structures. In the green crystal, there is one short contact of 2.663(10) Å between the F(1) of the fluorovinylidene ligand and a proton of a triphenylphosphine ligand in an adjacent molecule. Two phenyl protons of the fluorovinylidene ligand (H(9) and H(10)) interact with fluorine atoms of the PF_6^- anion with short contact distances of 2.5909(11) Å and 2.5253(10) Å respectively, and there are a further four short contact interactions between the phenyl protons of the fluorovinylidene moiety with triphenylphosphine ligands of adjacent complex molecules, ranging between 2.42937(2) and 2.76280(3) Å. A proton of the phenyl moiety, H(9), also interacts with a proton of the dichloromethane of crystallisation with a distance of 2.5820(3) Å. In the orange crystal, the short contacts of the fluorovinylidene ligand within the lattice are different. The F(1) atom of the fluorovinylidene ligand has two short contacts; one to a dichloromethane molecule of crystallisation, Cl(1), of 3.2083(16) Å, and an interaction with a triphenylphosphine ligand of a neighbouring complex, H(22), of 2.4367(14) Å. One phenyl hydrogen atom of the fluorovinylidene moiety interacts with both a cyclopentadienyl ligand of a neighbouring molecule (H(12) – C(5), 2.8567(17) Å) and with a triphenylphosphine ligand, (H(12) – H(30), 2.37031(3) Å). A second hydrogen atom of the fluorovinylidene phenyl group, H(11), has an interaction with a fluorine atom, F(6A), of the PF_6^- anion (2.435(19) Å).

Although the origin of the different colours of the polymorphic crystals cannot be unambiguously determined, numerous potential explanations can be postulated. As discussed above, the orientation of the vinylidene moieties differs between the two complexes, and additional variations can be observed in the short contact interactions between molecules in the crystal lattices. This includes short contact interactions not only of the fluorovinylidene moieties themselves, but also between solvent molecules of

crystallisation, the PF_6^- anions and between the remaining ligands in the complex coordination spheres. Presumably, a combination of these effects is responsible for the dramatic difference in photophysical properties.

5.3.2   UV-visible spectroscopic data for complex [27^{Ph}]PF$_6$

In order to gain further insight into the difference between the orange and green isomeric forms of crystals **[27^{Ph}]PF$_6$,** the UV-visible spectra of the complexes were recorded in both the solid state and in CH_2Cl_2 solution at a concentration of approximately 1 mmol dm^{-3} with a path length of 1 cm, Figure 5.6. The UV-visible spectra in the solid state, (top), were measured using the diffuse reflectance technique, therefore the peaks represent reflectance and the troughs represent the value of maximum absorption, λ_{max}.
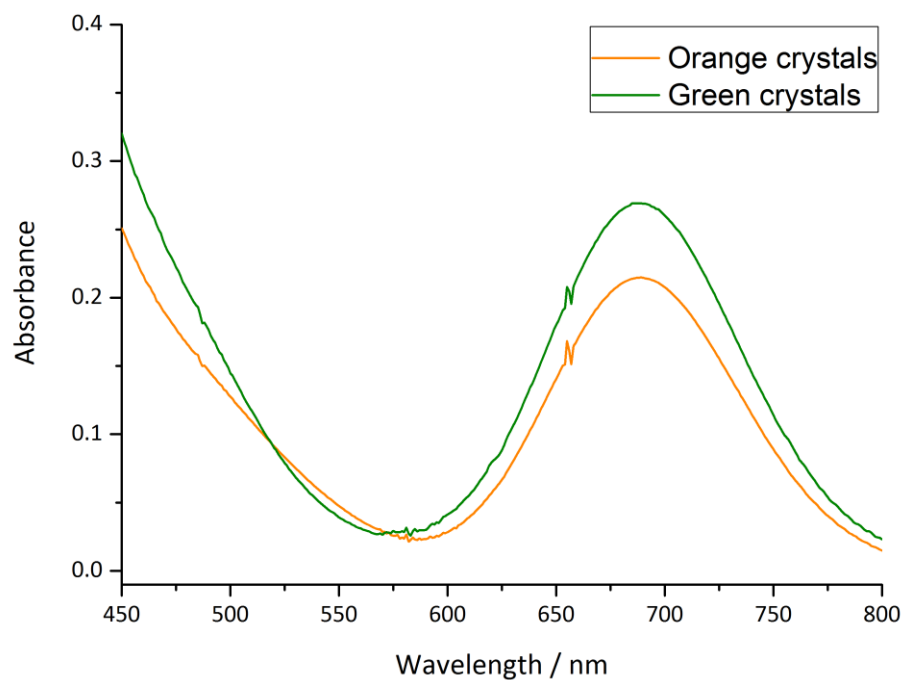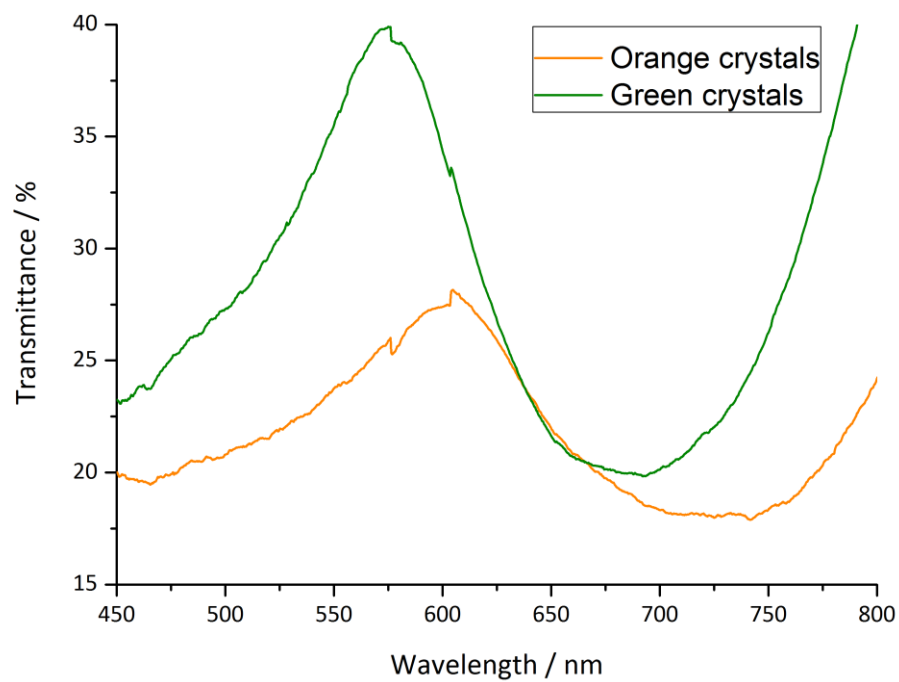
Figure 5.6 UV-visible spectra of the two isomers of [27^{Ph}]PF$_6$ in the solid state using the diffuse reflectance technique (top) and in the solution state in dichloromethane solution (bottom)

The spectra recorded in the solid state showed a clear difference in the position of λ_{max} between the green and orange isomers as expected (green λ_{max} = 692 nm, orange λ_{max} = 742 nm). However, on dissolution of the two batches of crystals in dichloromethane, both solutions appeared dark green in colour. This is evident in Figure 5.3 which shows the very similar λ_{max} values (686 nm for the green crystals and 689 nm for the 'orange' crystals). The molar absorption coefficients were also recorded for each of the batches of crystals and were found to be very similar (green = 2.6 ($\pm$ 0.4) x 10^3 dm^3 mol^{-1} cm^{-1}; orange = 2.1 x 10^3 dm^3 mol^{-1} cm^{-1}). Considering that only one species is detected in the NMR spectra of **[27^{Ph}]PF$_6$** in CD$_2$Cl$_2$, the two crystalline forms must convert to the same species in solution – presumably a time-averaged signal for the different rotameric forms is observed.

A recent paper by Bullock *et al.* reports the crystallisation of an organometallic molybdenum cation as two agostic isomers in the same vessel; one agostomer appeared blue and the other red. The remarkably different electronic spectra were attributed to differences in HOMO and LUMO energies. The β-agostic bonding mode of the phosphine induces a stronger ligand field, leading to a larger HOMO-LUMO gap. Therefore the complex absorbs a lower wavelength and appears red.[281]
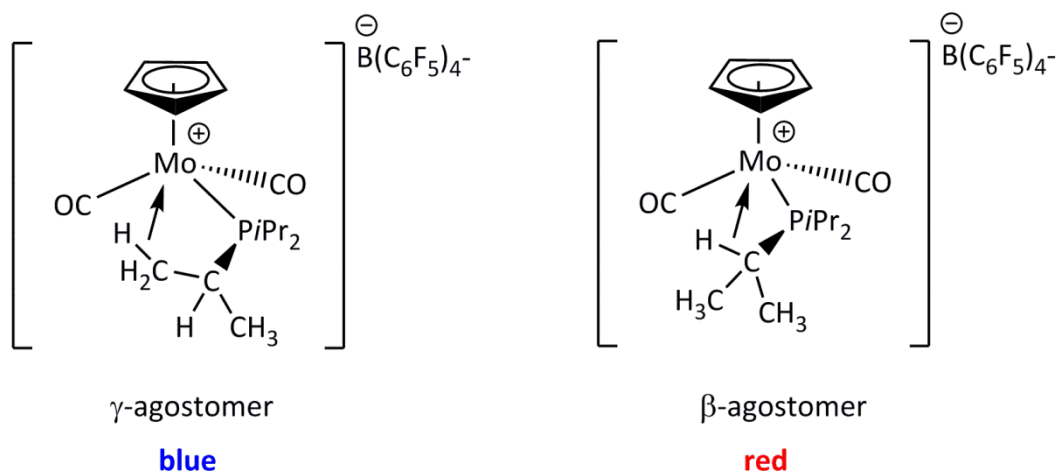
Figure 5.7 β- and γ-agostomers of [Mo(η^5-C$_5$H$_5$)(P*i*Pr$_3$)]B(C$_6$F$_5$)$_4$' 5-*t*

The smaller HOMO-LUMO gap of the γ-agostic leads to the crystal appearing blue. However, in the case of **[27^{Ph}]PF$_6$**, it seems that subtle changes in the structure of the solid state alter the energies of the π to π* transition and therefore affect the photophysical properties.

5.3.3 Investigating the electronic structure of vinylidenes $[Ru(\eta^5\text{-}C_5H_5)(PPh_3)_2(C=C\{R\}R']][X]$

On incorporation of a fluorine atom into a vinylidene ligand, significant effects can be observed in the electronic structure of the complex. These effects are evident in both the $^{13}C\{^1H\}$ NMR spectra and the absorption spectra; with respect to **[28]PF$_6$,** in the $^{13}C\{^1H\}$ NMR data there is a downfield shift in the resonance for the metal-bound carbon atom and in the UV-visible spectrum there is a red-shift (increase in wavelength) of the lowest-energy transition, Table 5.2. In order to investigate this observation, a range of vinylidene complexes were prepared and their absorption and $^{13}C\{^1H\}$ NMR spectra were recorded. Syntheses of all halo-vinylidene complexes were performed by summer student Matthew Skeats. The absorption spectra for all of the complexes were also simulated by Time-Dependent Density Functional theory (TD-DFT) calculations (at the (RI-)PBE0/def2-TZVPP//(RI-)BP86/SV(P) level, 50 singlet excitations considered).

Relevant spectroscopic details are listed in Table 5.2.

Complex	$^{13}C\{^1H\}$ chemical shift $[[Ru]=C=C\{R\}R'$ / ppm	λ_{max} / nm (experimental)	λ_{max} / nm (calculated)
$[27^{Ph}]BF_4$	389.0	691	730
$[27^{CF3}]BF_4$	383.5	684	720
$[27^{OMe}]BF_4$	389.9	698	764
$[28]PF_6$	355.5	524	537
$[38]BF_4$	340.0	488	452
$[39]BF_4$	353.5	615	702
$[40]BF_4$	340.3	627	647
$[41]Br_3$	339.3	626	-
$[42]I_3$	323.6	619	668

R = H	$[27^{Ph}]^+$	
R = CF$_3$	$[27^{CF3}]^+$	
R = OMe	$[27^{OMe}]^+$	

$[28^{Ph}]^+$

R_1 = CF$_3$,	R_2 = H	$[38^{Ph}]^+$
R_1 = Cl,	R_2 = H	$[39^{Ph}]^+$
R_1 = Br,	R_2 = H	$[40^{Ph}]^+$
R_1 = Br,	R_2 = Br	$[41^{Ph}]^+$
R_1 = I,	R_2 = H	$[42^{Ph}]^+$
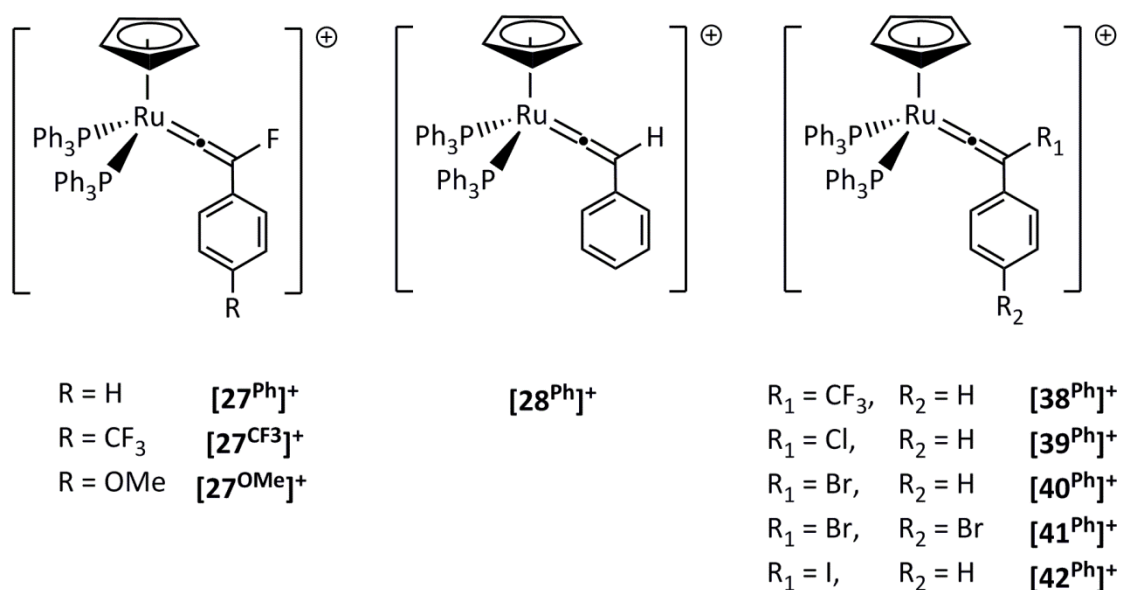
Table 5.2 Summary of $^{13}C\{^1H\}$ NMR data and lowest energy absorption bands of vinylidene complexes. Experimental data were recorded at concentrations of approximately 1 mmol dm^{-3} in CH$_2$Cl$_2$ solution.

Although there are discrepancies between the experimental and calculated λ_{max} values, there is a systematic shift between the two sets of data and on consideration of all experimental and calculated values there is a good correlation between the two. This suggests that the selected computational methodology was appropriate for the calculation on these systems. The correlation between the experimentally measured λ_{max} and calculated λ_{max} values is shown in Figure 5.8.
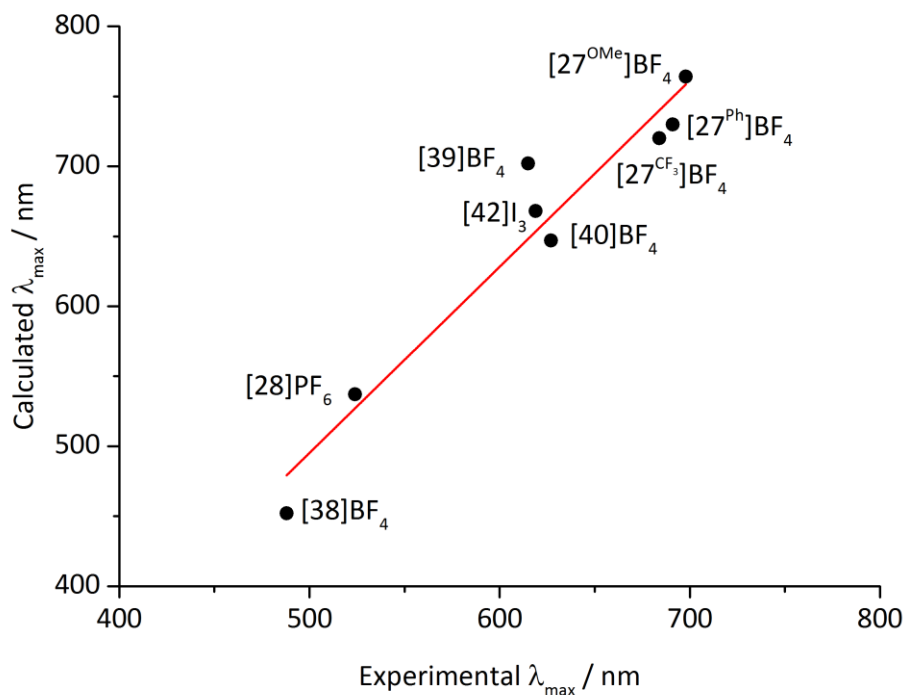
Figure 5.8 Correlation plot of calculated λ$_{max}$ versus experimentally measured λ$_{max}$, R$_2$ = 0.93, y = 1.33x-170

5.3.3.1 TD-DFT calculations of complex [27^{Ph+}]$^+$

With the aid of the TD-DFT calculations, for all halovinylidene complexes studied the lowest energy transition was found to be a π to π^* transition dominated by HOMO $\rightarrow$ LUMO character. The constitutions of the HOMOs and LUMOs in each of the halo-vinylidenes were found to be very similar, Figure 5.9. In the HOMO, the halogen has a lone pair which is antibonding with respect to the π-system of the vinylidene ligand. In turn, the vinylidene π-system is antibonding with respect to a metal-centred orbital. The LUMO shows an interaction of the halogen p-orbital with an orbital based on the metal-bound carbon atom. These interactions should raise the energy of the HOMO and lower the energy of the LUMO, therefore explaining the red-shift observed on halogen functionalisation of the vinylidene ligand, particularly the fluorovinylidene complex **[27^{Ph}]PF$_6$**, when compared to the protio-analogue, **[28]PF$_6$**. The effect of these orbital interactions must also prevail over the lowering of energy of the HOMO which would be expected on incorporation of solely electron withdrawing groups. Therefore mesomeric effects prevail over inductive effects in this case.
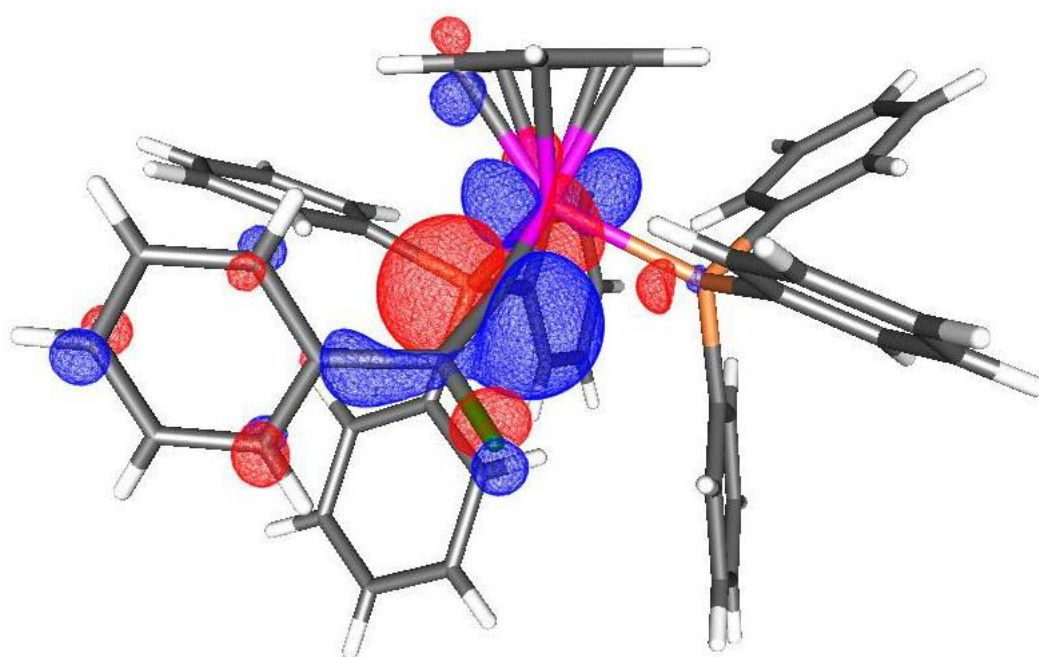
E = -4.794 eV
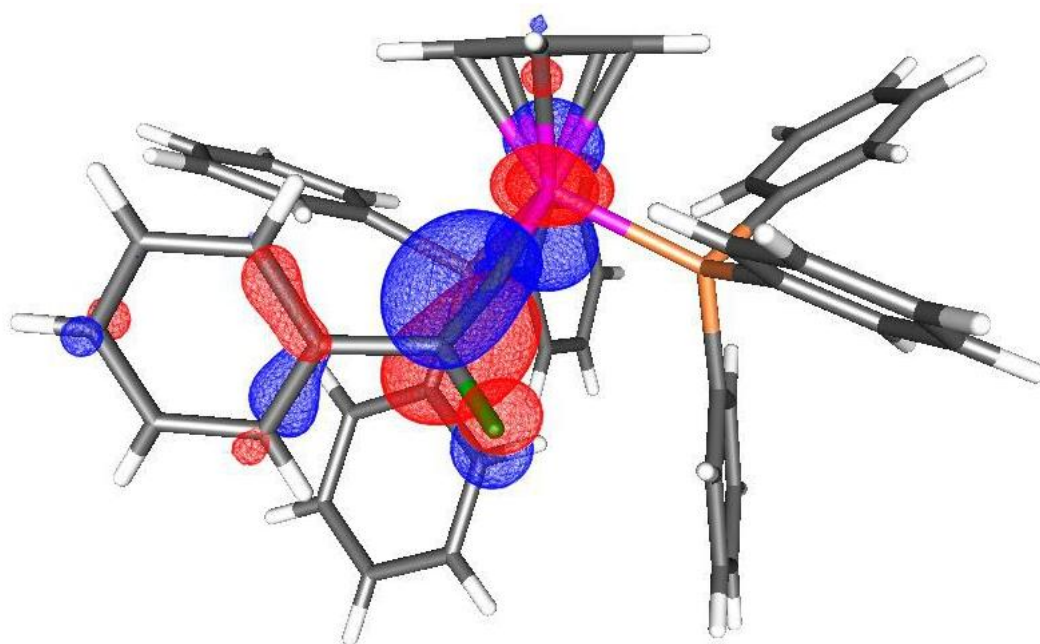
E = -8.451 eV

Figure 5.9 LUMO (top, E = -4.794 eV) and HOMO (bottom, E = -8.451 eV) of [27[Ph]][+] (green crystals)

5.3.3.2   Solvatochromic properties of complex [27^{Ph}]BF$_4$

Both the experimental and calculated λ_{max} data in Table 5.2 indicate that the fluoro-substituted vinylidene complexes, **[27^{R}]BF$_4$**, show the lowest energy transitions in CH$_2$Cl$_2$ solution. In order to further investigate the nature of these transitions, absorption spectra were recorded in a range of solvents of varying polarities. The solvatochromic behaviour of a species in solution is the extent to which the absorption wavelength is affected by solvents of differing polarities, which is due to the interaction between solute and solvent molecules. Therefore, strong solvatochromic behaviour can be observed for transitions which exhibit large changes in dipole moment between two electronic states. The solvatochromic effects on **[27^{Ph}]BF$_4$** are shown in Figure 5.10.
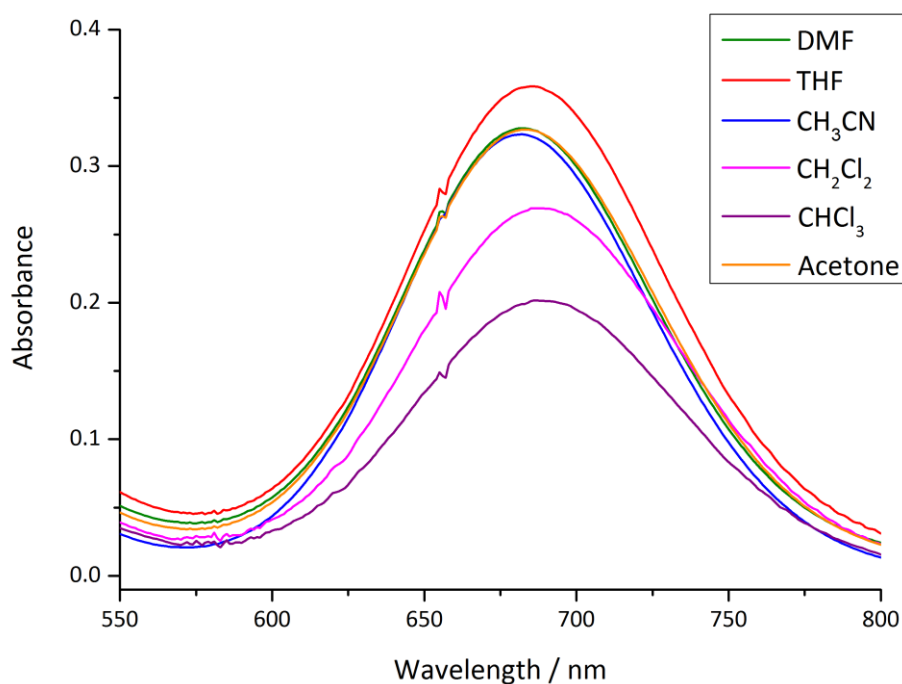
Figure 5.10 Absorption spectra of complex [27^{Ph}]BF$_4$ in DMF, THF, MeCN, CH$_2$Cl$_2$ CHCl$_3$ and acetone
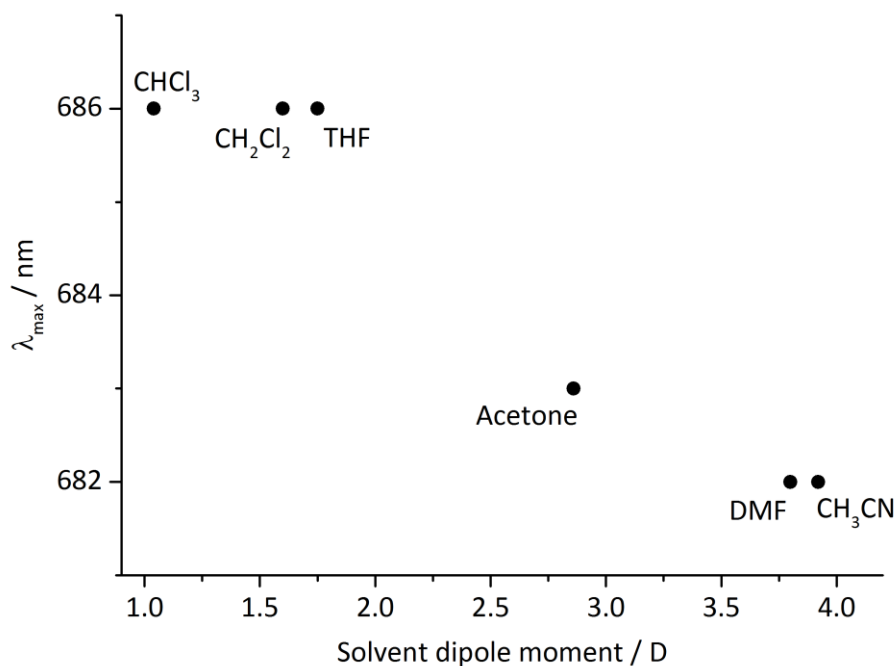
Figure 5.11 Relationship between solvent dipole moment and λ_{max} for [27^{Ph}]BF$_4$

Figure 5.11 shows the relationship between solvent dipole moment and λ_{max}. For **[27^{Ph}]BF$_4$** there is only a very slight solvatochromic behaviour, with more polar solvents such as MeCN and DMF leading to decreases in λ_{max} (682 nm) compared to the least polar solvent, CHCl$_3$ (λ_{max} of 686 nm). This observation suggests an increase in polarity on formation of the excited state which is therefore stabilised more than the ground state in polar solvents.[282] However, as this change is so small (only a 4 nm range) the change in polarity is presumably slight.

5.3.3.3   Comparison of UV-visible spectra for complexes [27^R]X

In order to investigate the effects of electron withdrawing and electron donating groups on the π-π* transition and hence gather more information about its nature, UV-visible absorption spectra were recorded for several fluorinated analogues of **[27^R]BF$_4$,** which contained both electron withdrawing and electron donating substituents. These spectra are shown in Figure 5.12.
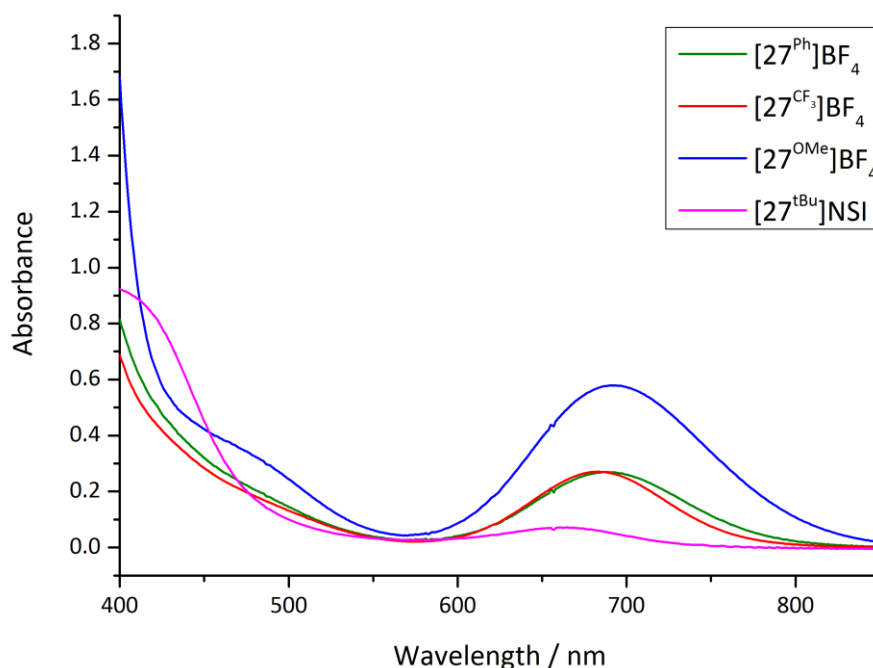
Figure 5.12 Absorption spectra of complexes [27^{Ph}]BF$_4$, [27^{CF3}]BF$_4$, [27^{OMe}]BF$_4$ and [27^{tBu}]NSI

On the introduction of electron donating groups, such as the methoxy group in **[27^{OMe}]BF$_4$**, a bathochromic shift (λ_{max} from 691 nm in **[27^{Ph}]BF$_4$** to 698 nm in **[27^{OMe}]BF$_4$**) was observed, whereas upon the introduction of electron withdrawing substituents, such as the trifluoromethyl- group in **[27^{CF3}]BF$_4$**, an opposite hypochromic shift was noted (to a λ_{max} of 684 nm). The *t*Bu analogue of the complex exhibited a significant hypochromic shift to a shorter wavelength (λ_{max} of 664 nm).

These complexes display the influence of σ- and π- effects on the energy of the π to π^* transition. Good π- donors (such as –OMe) raise the energy of the HOMO and hence lower the energy of the transition, whereas the opposite effect is seen for –I electron withdrawing groups such as the trifluoromethyl moiety in **[27^{CF3}]BF$_4$**.

5.3.3.4 Comparison of UV-visible spectra for complexes protio-, fluoro- and trifluoromethyl- vinylidene complexes

Figure 5.13 illustrates the absorption spectra of fluorovinylidene **[27^{Ph}]BF$_4$** in comparison to protio-vinylidene analogue **[28]PF$_6$** and trifluoromethyl- analogue **[38]BF$_4$**. The latter two complexes cannot engage in mesomeric electronic effects and this significantly influences the position of λ_{max}.
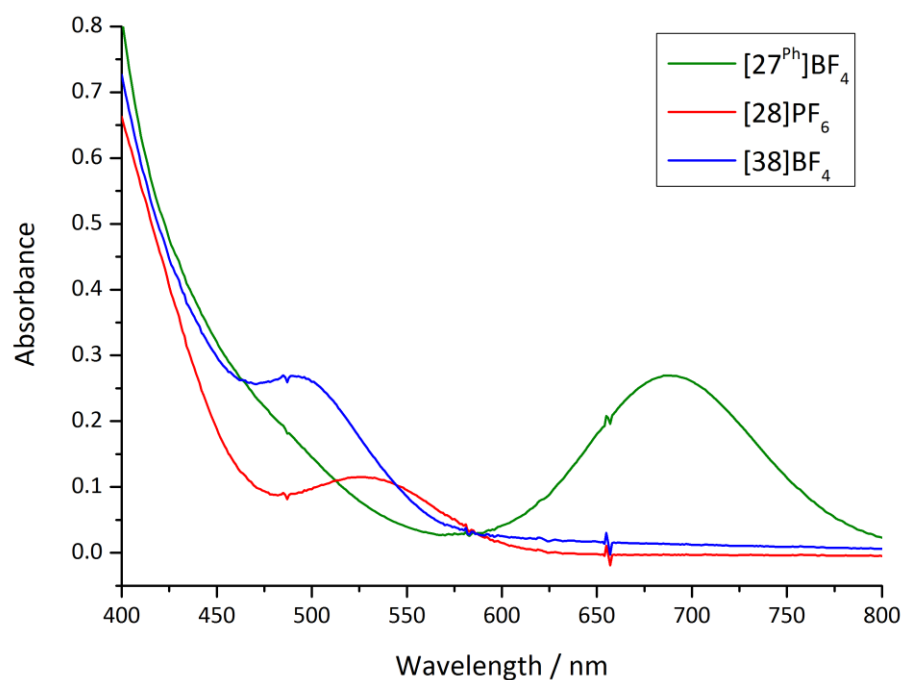
Figure 5.13 Absorption spectra of complexes [27^{Ph}]BF$_4$, [28]PF$_6$ and [38]BF$_4$

Complex **[38]BF$_4$** has the most electron withdrawing (-I) substituent on the vinylidene β-carbon and, correspondingly, the highest energy transition with the lowest λ_{max} (488 nm). This data indicates that the complex has a low-energy HOMO orbital as the trifluoromethyl substituent cannot engage in the π-interactions described in Section 5.3.3.1 and is solely electron withdrawing *via* induction. Protio-vinylidene complex **[28]PF$_6$** can also not engage in these π-orbital interactions and absorbs at a λ_{max} of 524 nm. The higher energy λ_{max} values of both **[28]PF$_6$** and **[38]BF$_4$** explain why these complexes appear red rather than the dark green colour of the fluorinated species.

The balance between σ- and π- effects which is clearly evident in the positions of λ_{max} in the UV-visible spectra can also be observed in the chemical shifts of the vinylidene metal-bound α-carbon in $^{13}C\{^1H\}$ NMR. Complexes **[38]BF$_4$** and **[28]PF$_6$**, which engage solely in inductive effects, have similar chemical shifts (340.0 and 355.5 ppm respectively); the halo-vinylidene complexes, which can participate in mesomeric electronic effects, show a wide chemical shift range of 66 ppm (323.6 – 389.0 ppm).

5.3.3.5   Comparison of UV-visible spectra for the halovinylidene complexes

Finally, the halo-vinylidene complexes were synthesised for comparison with **[27^{Ph}]BF$_4$** and their UV-visible spectra recorded, Figure 5.14.
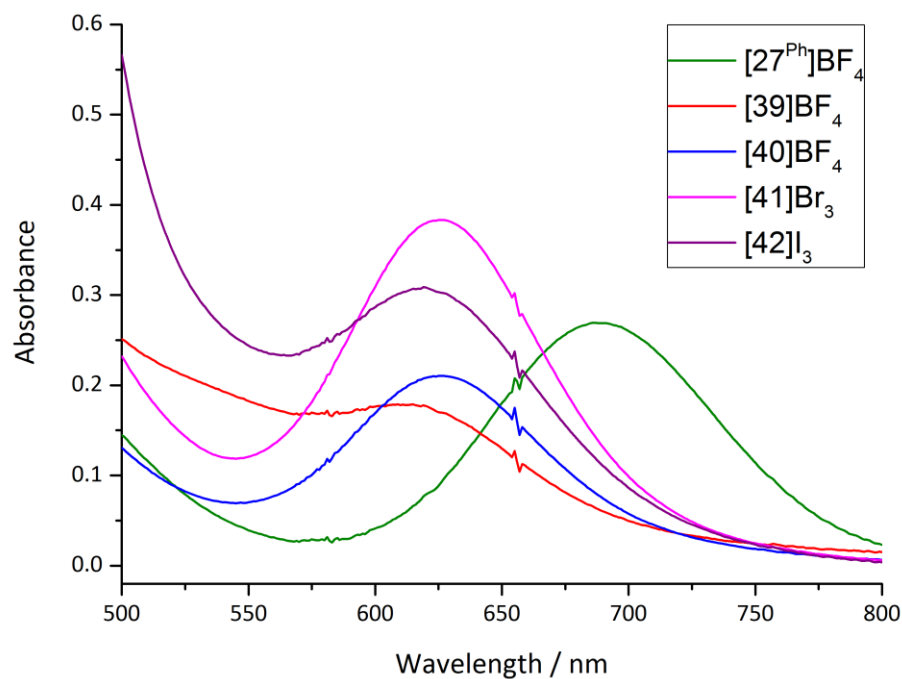
Figure 5.14 Absorption spectra of complexes [27^{Ph}]BF$_{4,}$ [39]BF$_{4,}$ [40]BF$_{4,}$ [41]Br$_3$ and[42]I$_3$

The syntheses of the halovinylidene complexes, with the exception of **[27^{Ph}]BF$_4$,** have been previously reported in the literature. However, **[39]BF$_4$** was synthesised by a new method from the reaction between **[26^{Ph}]** and *N*-chlorosuccinamide, and **[40]BF$_4$** was prepared by the addition of one equivalent of Br$_2$ and NaBF$_4$. This allowed the isolation of the vinylidene complex with a single bromine substituent and a BF$_4^-$ counter-ion, rather than with a second bromine incorporation in the *para*- position of the phenyl ring and as the Br$_3$ salt.[64]

On first inspection of Figure 5.14, it is clear that the fluorovinylidene complex **[27^{Ph}]BF$_4$** has a significantly higher λ_{max} value (691 nm) compared to the other halogenated vinylidene species (615 – 627 nm). This represents a smaller HOMO-LUMO gap in the fluorovinylidene complex **[27^{Ph}]BF$_4$** and therefore a lower energy transition. The electronic differences between the other halovinylidenes when compared to **[27^{Ph}]BF$_4$** are also reflected in the chemical shift values of the metal-bound vinylidene α-carbon resonances. Complex **[27^{Ph}]BF$_4$** resonates remarkably downfield at 389.0 ppm when compared to the others (323.6 – 353.5 ppm). The trend in the resonances of the halogen-substituted vinylidene complexes correlates with their electronegativities. The ligand with the most electron withdrawing substituent (fluorine, **[27^{Ph}]BF$_4$**) has an α-carbon resonance at 389.0 ppm whereas the least electronegative (iodine, **[42]I$_3$**) resonates at 323.6 ppm – a difference of almost 70 ppm. The chemical shifts of the chloro- and bromo-substituted vinylidene ligands follow the trend in electronegativity, resonating at 353.5 ppm and 340.3 ppm respectively. However, the values of λ_{max} do not exactly follow the trend as λ_{max} increases from **[39]$^+$** to **[42]$^+$** to **[40]$^+$** to **[27^{Ph}]$^+$**.

5.4 Reactivity of fluorinated vinylidene complexes

The facile synthesis of fluorinated vinylidene complexes allowed exploration of their reactivity in order to evaluate the effects of fluorine incorporation into the vinylidene moiety. Half-sandwich ruthenium vinylidene complexes, both mono- and di-substituted, are implicated in many stoichiometric and catalytic transformations due to the wide range of reactions in which they participate (see Chapter 1). However, due to the lack of a facile preparation procedure, the reactions of fluorinated vinylidene analogues have not been investigated in any detail. Therefore, the fluorovinylidene complexes **[27^{Ph}]X** and **[30^{Ph}]NSI** were trialled under various reaction conditions in order to explore their behaviour. Comparisons to the mono- and di-substituted vinylidene analogues will be drawn throughout.

5.4.1 Attempted displacement of FC≡CPh

In the case of both mono-[134,283] and di-substituted[71] vinylidene complexes based on the ruthenium half-sandwich structure, heating in MeCN has allowed displacement of the vinylidene moiety as its alkyne tautomer and concomitant coordination of MeCN to the metal centre in order to complete the coordination sphere. An example of this process is shown in Scheme 5.14.
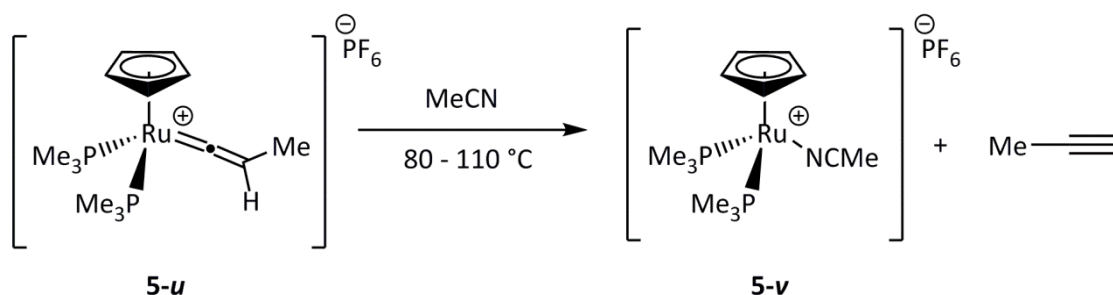
Scheme 5.14 Displacement of vinylidene ligand in 5-*u* as the alkyne tautomer[283]

However, heating a sample of **[27^{Ph}]X** in CD$_3$CN did not result in the formation of [Ru(η^5-C$_5$H$_5$)(PPh$_3$)$_2$(CD$_3$CN)] and FC≡CPh. Instead, after heating the sample at 50 °C for two weeks, the major product of the reaction was **[43]X** (where **X** = BF$_4^-$ or NSI$^-$), containing a coordinated alkene ligand anchored by an orthometallated phosphonium moiety, Scheme 5.15.
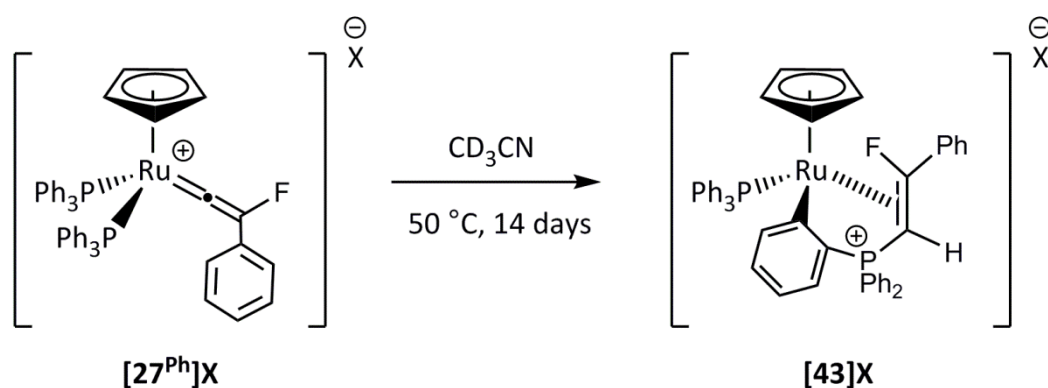
Scheme 5.15 Orthometallation of triphenylphosphine on heating complex [27^{Ph}]X in CD$_3$CN, X = BF$_4^-$ or NSI$^-$

The ^{31}P{^{1}H} NMR spectrum from complex **[43]X** shows two resonances at 46.6 ppm and 42.3 ppm – the first as a doublet of doublets with a $^3J_{PF}$ of 46.8 Hz and a $^3J_{PP}$ of 4.4 Hz, and the latter as a doublet of doublets with a $^3J_{PF}$ of 16.2 Hz and a $^3J_{PP}$ of 4.4 Hz. Resonances in the ^{19}F NMR spectrum (-143.4 ppm, apparent doublet of triplets, $^3J_{PF}$ of 46.8 Hz, $^3J_{HF}$ of 16.9 Hz, $^3J_{PF}$ of 16.2 Hz), the ^{1}H NMR spectrum (4.69 ppm, doublet of doublets, $^3J_{HF}$ of 16.9 Hz, $^2J_{PH}$ of 5.0 Hz, $^3J_{PH}$ of 1.7 Hz) and the ^{13}C{^{1}H} NMR spectrum (113.7, doublet of triplets, $^1J_{CF}$ of 243.0 Hz, $^2J_{CP}$ of 5.6 Hz and 25.9, doublet of doublet of doublets, $^1J_{CP}$ of 75.1 Hz, $^2J_{CF}$ of 7.8 Hz, $^2J_{CP}$ of 2.7 Hz) confirm the presence of the fluorinated alkene. The $^3J_{HF}$ coupling constant of 16.9 Hz for the proton and fluorine substituents on the alkene confirm the *trans-* stereochemistry of these substituents across the double bond.[284] The DFT calculated structures for the *cis-* and *trans-*

isomers indicate that the structure in which the proton and fluorine are *trans-* is energetically favoured by 26 kJ mol^{-1} (Gibbs energies calculated at the (RI-)PBE0-D3/def2-TZVPP//(RI-)BP86/SV(P) level of theory with COSMO solvation in acetonitrile).

On heating **[27^{Ph}] X** in CD$_3$CN at 80 °C, a mixture of organometallic products was formed but on heating at a lower temperature of 50 °C for approximately two weeks, the reaction was relatively selective (~70 % conversion based on ^{31}P{^{1}H} NMR spectroscopy. A related complex to **[43]X** has been reported for PPh$_3$ attack at a protiovinylidene complex, Scheme 5.16.
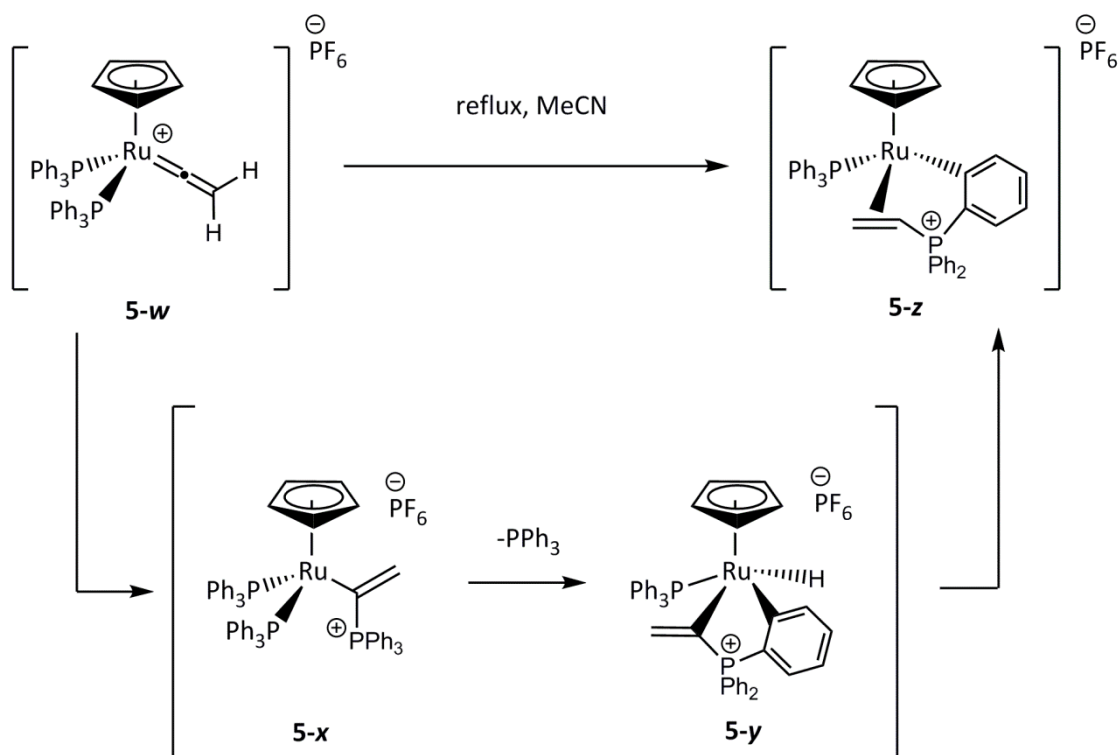
Scheme 5.16 Formation of phosphonium complex 5-*z* *via* attack of triphenylphosphine and subsequent C-H functionalisation

Both the formation of **5-*z***, Scheme 5.16, and **[43]X** can be explained by the following mechanistic proposal. In the first step of the mechanism, the vinylidene ligand would be attacked by free triphenylphosphine at the metal-bound α-carbon in **5-*w*** to form intermediate **5-*x***. The phosphine could be generated internally, by dissociation from the ruthenium centre prior to attack, or externally from another molecule of **5-*w*** (as shown in Scheme 5.16). Dissociation of a triphenylphosphine ligand (either prior to phosphine attack or at this stage) creates an empty coordination site – this allows orthometallation to produce

hydride intermediate **5-y**. Reductive elimination of the hydride to the alkene moiety yields complex **5-z**.[285]

This mechanistic proposal is supported by the fact that the dppe-containing fluorovinylidene complex **[30^{Ph}]NSI** remains unchanged on heating in CD$_3$CN even at 100 °C for two weeks. The bidentate coordination of the dppe prevents initial dissociation of the phosphine which therefore inhibits further reaction. These data confirm that the conversion of the fluorovinylidene to its alkyne form does not proceed under these conditions.

5.4.2 Reactions of fluorovinylidene complexes with pyridine

Many reported applications of ruthenium-vinylidene complexes exploit the electrophilic nature of the metal-bound α-carbon atom, which promotes nucleophilic attack at this position. For example, nucleophilic attack of pyridine at the metal-bound carbon is a crucial process for the C-H activation of pyridine reported in Chapter 3. Therefore, the reactivity between **[27^{Ph}]BF$_4$** and pyridine was investigated in an attempt to prepare fluorinated analogues of 2-substituted *E*-styrylpyridines.

Dissolution of **[27^{Ph}]BF$_4$** in pyridine results in an immediate reaction to form vinyl complex **[44]BF$_4$**, Scheme 5.17. This is accompanied by a rapid colour change from green to orange.
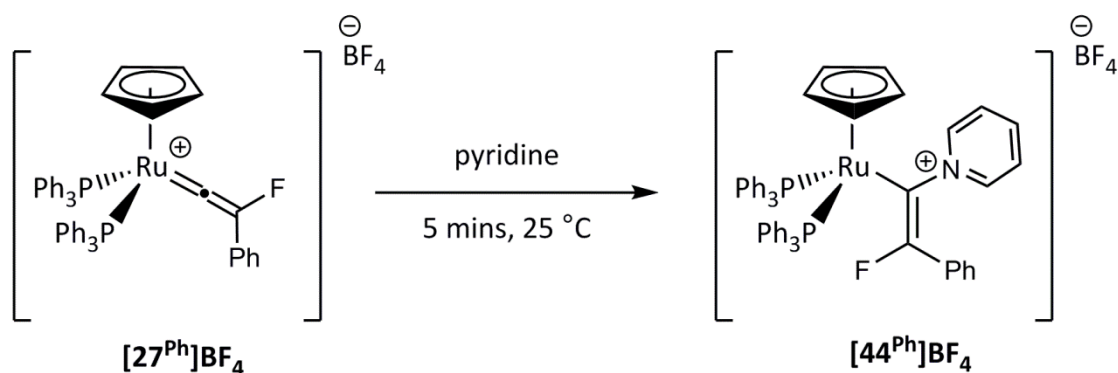
Scheme 5.17 Addition of pyridine to complex [27^{Ph}]BF$_4$

The formation of **[44]BF$_4$** demonstrates that the incorporation of fluorine does not inhibit nucleophilic attack at the vinylidene α-carbon. In CD$_2$Cl$_2$, the ^{19}F NMR spectrum appears as a triplet at -72.8 ppm with a $^4J_{PF}$ coupling constant of 20.3 Hz and the ^{31}P{^{1}H} NMR spectrum exhibited a resonance at 44.0 ppm with a corresponding $^4J_{PF}$ coupling. The ESI-MS also confirmed that a single pyridine molecule had been incorporated. Analogous reactivity is seen on the addition of pyridine to **[30^{Ph}]NSI** to produce the dppe analogue of **[44]BF$_4$**,

[45]NSI. **[45]NSI** exhibits a similar spectroscopic signature in both the ^{19}F and ^{31}P{^{1}H} NMR spectra.

The structure of **[44]BF$_4$** was confirmed by single crystal X-ray diffraction, Figure 5.15, which confirmed that the alkenyl ligand had adopted a *Z*-configuration.
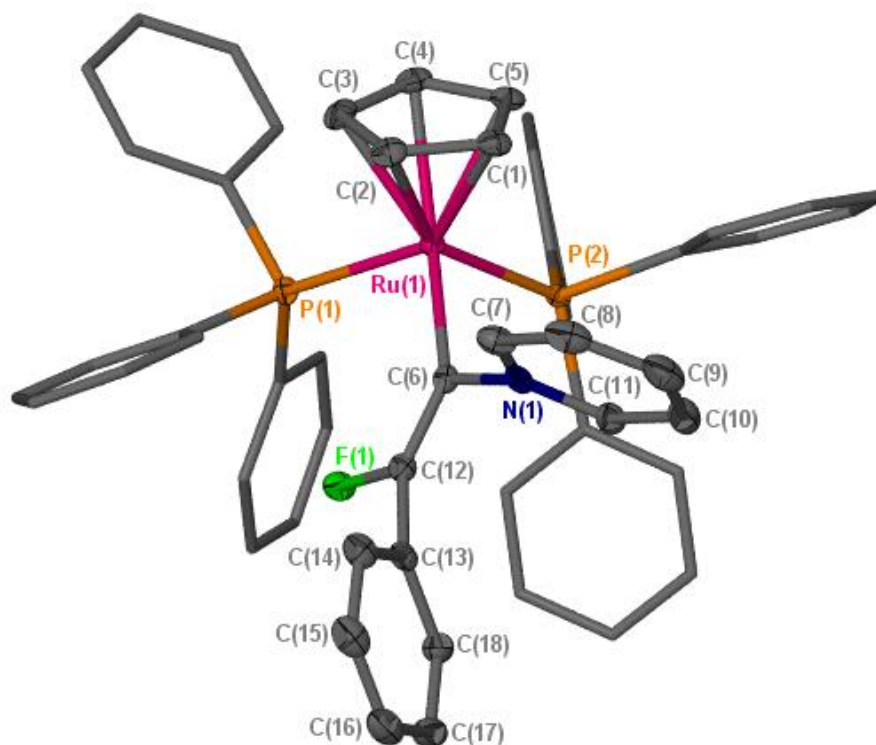
Figure 5.15 X-Seed diagram of the cation from complex [44]BF$_4$. Most hydrogen atoms, a BF$_4^-$ anion and a dichloromethane and diethyl ether of crystallisation have been omitted for clarity, and where shown the thermal ellipsoids are at a 50 % probability level.

[44]BF$_4$ is the fluorinated analogue of a key intermediate proposed in the mechanism of pyridine alkenylation, Chapter 3, and the previous inability to observe this species was attributed to its low intrinsic concentration in solution due to competitive deprotonation of the vinylidene ligand.[45] It seems that the presence of this fluorine atom allows for isolation and characterisation of this complex.

On standing in pyridine solution over a three day period, **[44]BF$_4$** undergoes a further reaction to form **[46]BF$_4$** and free triphenylphosphine, Scheme 5.18.

Scheme 5.18 Formation of complex [46]BF$_4$

Monitoring the reaction by NMR spectroscopy indicated that this reaction proceeds *via* a number of organometallic, phosphorus and fluorine-containing intermediates. The identities of these species are unknown due to their low concentrations in the reaction mixture, but the three most intense intermediates exhibit ^{31}P{^{1}H} resonances at 67.5 (s), 56.1 (s) and 54.1 ppm (d, *J* = 7.9 Hz). In the ^{19}F NMR spectrum of the reaction mixture, resonances were noted at -86.3 (br), -101.1 and -110.0 ppm. In the ^{13}C{^{1}H} NMR spectrum of **[46]BF$_4$**, the metal-bound pyridylidene carbon appeared as a broad signal at 218.0 ppm which is typical for pyridylidene complexes of this type.[63] At 295 K, the ^{1}H NMR spectrum exhibited signs of dynamic behaviour with the presence of a broad feature underneath the aromatic region, proposed to be caused by restricted rotation of the triphenylphosphine ligand. On cooling to 203 K, the aromatic region could be fully resolved and the resonances fully assigned due to the 'frozen' rotation of the phosphorus ligand.

Figure 5.16 Low variable temperature (VT) ^{1}H NMR spectra of complex [46]BF$_4$ (aromatic region only)

The X-ray crystal structure of **[46]BF$_4$**, recorded as its pyridine solvate, confirmed that this species was a novel pyridylidene complex formed by pyridine incorporation into the structure of **[27^{Ph}]BF$_4$**, C-H activation at the *ortho-* position followed by incorporation of a second pyridine molecule and formal loss of HF, Figure 5.17. The Ru(1) − C(6) bond length of 2.011(7) Å confirms the pyridylidene character of the bond and is very similar to those of complex **[20]BF$_4$** and **[21]BF$_4$** discussed in Chapter 4.[63] The dppe analogue of **[44]BF$_4$** (**[45]NSI**) did not undergo C-H activation of the incorporated pyridine, suggesting that loss of a phosphine ligand was important in order to create a free coordination site at the metal centre.
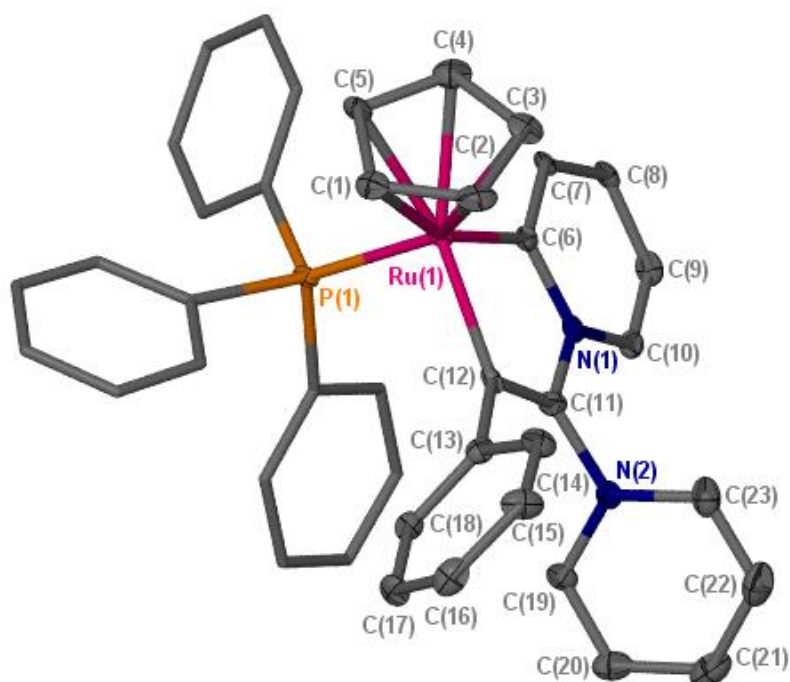
Figure 5.17 X-Seed diagram of the cation from complex [46]BF$_4$. Most hydrogen atoms, a BF$_4^-$ anion and a pyridine of crystallisation have been omitted for clarity, and where shown the thermal ellipsoids are at a 50 % probability level.

The conversion of vinylidene complex **[27^{Ph}]BF$_4$** to pyridylidene species **[46]BF$_4$** has been investigated by a DFT study. Due to changes in molecularity during the proposed reaction pathway, there are significant differences between the Gibbs energies and the zero-point-energy-corrected electronic energies ($E_{SCF+ZPE}$). Gibbs energies will be discussed, although both values at 298.15 K are presented on the potential energy surface (PES), Scheme 5.19. The reference point for the calculations was chosen as **[27^{Ph}]BF$_4$** and two molecules of pyridine, and so all other energies are given relative to these components (which have been set to 0 kJ mol^{-1}). The calculations were performed by Dr Jason Lynam.
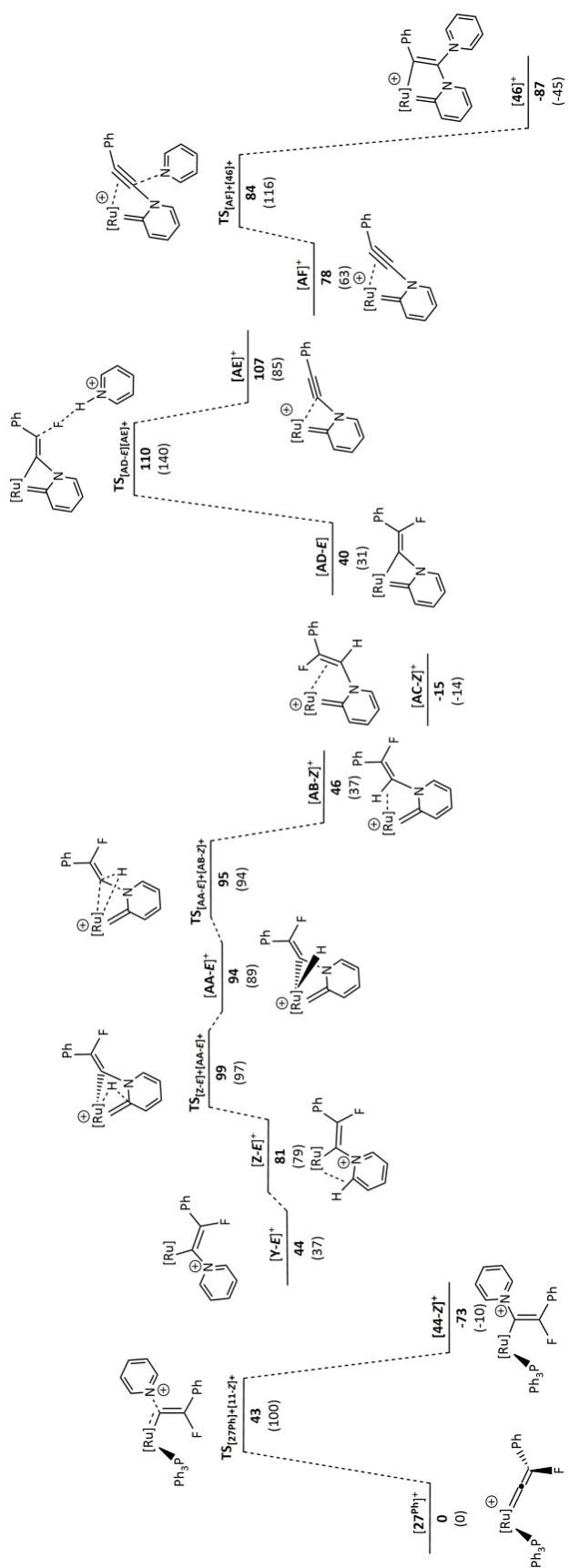
Scheme 5.19 Potential Energy Surface (PES) of the proposed mechanism of formation of [46]$^+$ from [27^{Ph}]$^+$, [Ru] = [Ru(η^5-C$_5$H$_5$)(PPh$_3$)]. $E_{SCF+ZPE}$ energies (top, in bold) and relative Gibbs free energies (bottom, in parentheses) at 298.15 K relative to [27^{Ph}]$^+$ and two molecules of pyridine are shown in kJ mol^{-1}. Calculations are at the (RI-)PBE0-D3/def2-TZVPP//(RI-)BP86/SV(P) level with COSMO solvation in pyridine.

In the first step of the mechanism, a molecule of pyridine attacks at the metal bound α-carbon of the vinylidene ligand in **[27^{Ph}]$^+$** *via* **TS$_{[27Ph]+[44-Z]+}$** to form **[44-Z]$^+$,** Scheme 5.20.
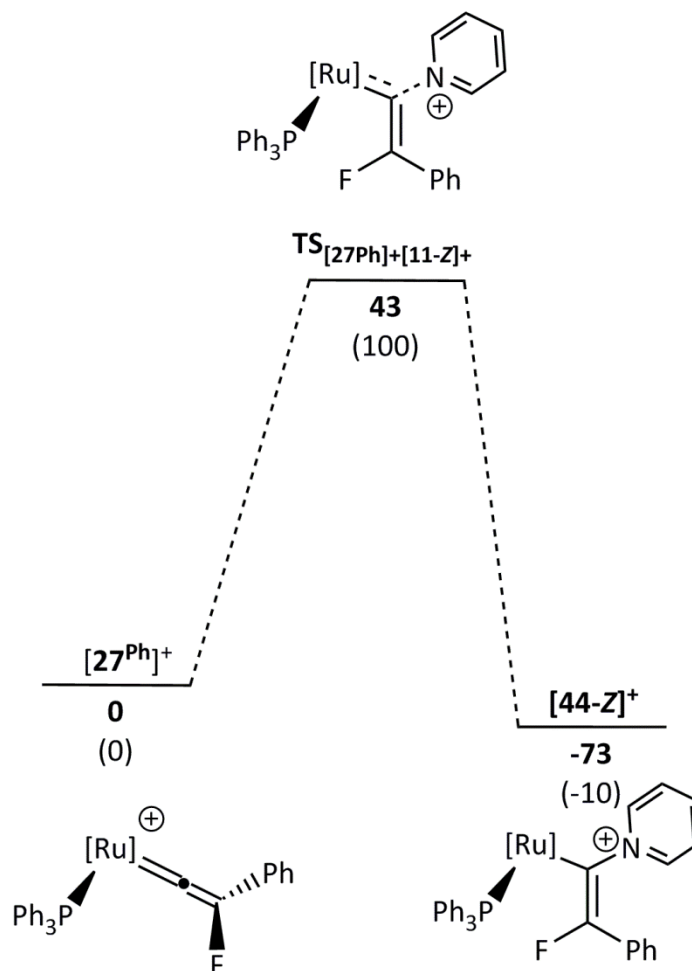
Scheme 5.20 Potential Energy Surface (PES) of pyridine attack at the vinylidene α-carbon in [27^{Ph}]$^+$. $E_{SCF+ZPE}$ energies (top, in bold) and relative Gibbs free energies (bottom, in parentheses) at 298.15 K, at the (RI-)PBE0-D3/def2-TZVPP//(RI-)BP86/SV(P) level with COSMO solvation in pyridine.

This process corresponds to nucleophilic attack at the α-carbon – a well-established process for complexes of this type. The fact that **[44-Z]$^+$** is predicted to have a lower thermodynamic energy than **[27^{Ph}]$^+$**, and **TS$_{[27Ph]+[44-Z]+}$** has a moderate barrier ($\Delta G^\ddagger$ = 100 kJ mol^{-1}) is consistent with the rapid reaction observed on dissolution of **[27^{Ph}]$^+$** in pyridine. The calculations also help to explain the observed stereochemistry. The *E*-isomer of **[44]**, in which the phenyl group points of the alkenyl β-carbon is oriented towards the triphenylphosphine ligand, is

higher energy than both the *Z*-isomer and **[27^Ph]^+** (**[44-*E*]^+** = 65 kJ mol^-1) and the transition state for its formation (**TS_[27Ph]+[44-*E*]+** = 155 kJ mol^-1) is also significantly higher in energy. On examination of the computationally formulated structure, this can be explained by unfavourable steric interactions between the phenyl group of the *E*-isomer and the triphenylphosphine ligand. The DFT optimised structures of intermediates **[44-*E*]^+** and **[44-*Z*]^+** are shown in Figure 5.18.
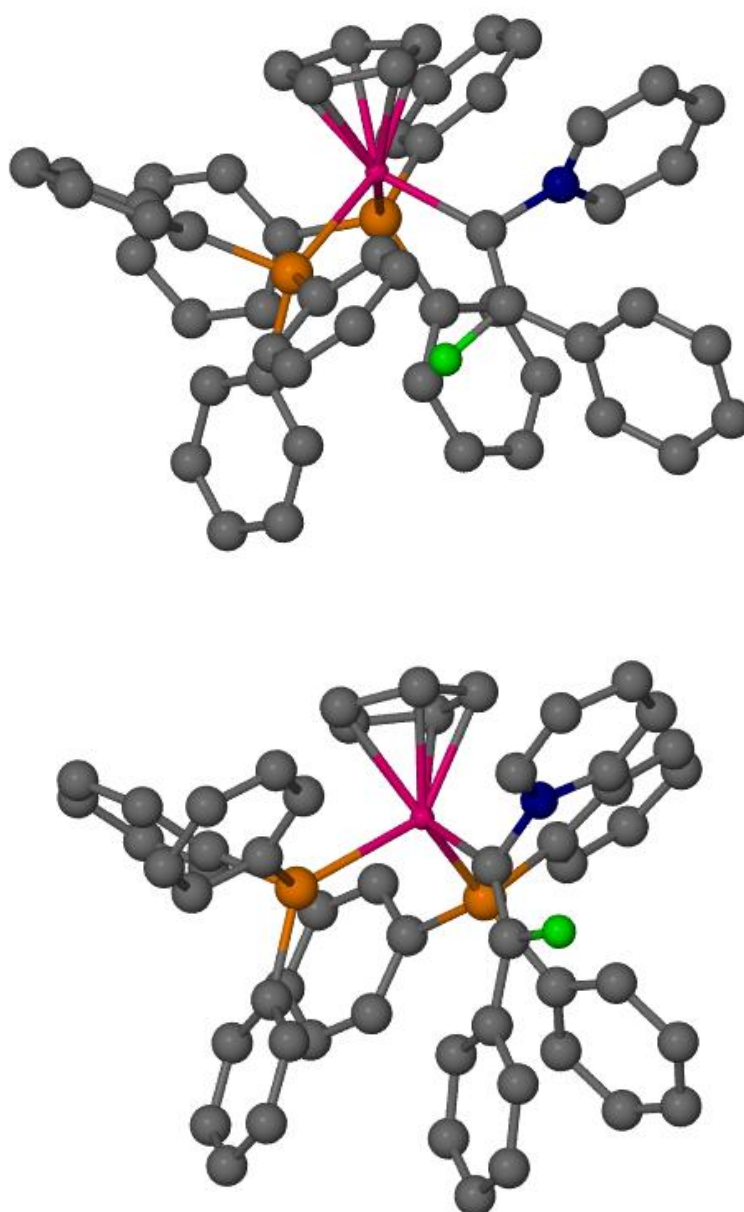
Figure 5.18 DFT optimized structures of [44-*Z*]^+ (top) and [44-*E*]^+ (below) highlighting the unfavourable steric interactions between the phenyl moiety of the vinyl group and the triphenylphosphine ligands in [11-*E*]^+

The subsequent stages of the mechanism, Scheme 5.21, are directly linked to studies of ruthenium-mediated pyridine mono-alkenylation described in Chapter 3.[45]
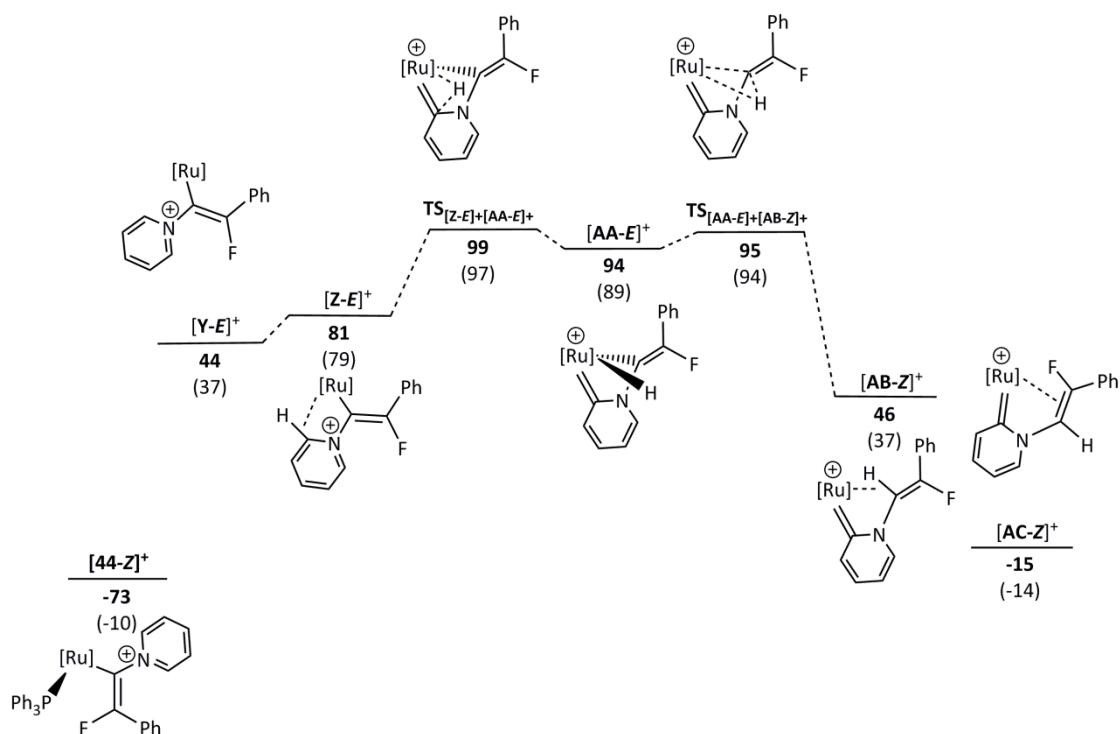
Scheme 5.21 Potential Energy Surface (PES) of triphenylphosphine loss from [44-*Z*]$^+$ and conversion to fluorinated vinyl complex [AC-*Z*]$^+$. $E_{SCF+ZPE}$ energies (top, in bold) and relative Gibbs free energies (bottom, in parentheses) at 298.15 K, at the (RI-)PBE0-D3/def2-TZVPP//(RI-)BP86/SV(P) level with COSMO solvation in pyridine.

Complex **[44-*Z*]$^+$** undergoes loss of a triphenylphosphine ligand to yield **[Y-*E*]$^+$** with an incomplete coordination sphere. This allows for coordination of the *ortho-* C-H bond of the newly incorporated pyridine moiety, **[Z-*E*]$^+$** followed by subsequent C-H activation *via* **TS$_{[Z-E]+[AA-E]+}$** to form pyridylidene-hydride intermediate **[AA-*E*]$^+$** which undergoes a hydride migration to form **[AB-*Z*]$^+$**. Rotation of the alkenyl ligand around the N(pyridylidene)-C(alkenyl) bond allows rearrangement to complex **[AC-*Z*]$^+$** in which the alkenyl group of the ligand coordinates to the ruthenium centre through the carbon-carbon double bond rather than through a carbon-hydrogen agostic interaction. This is a more favourable isomer by 51 kJ mol^{-1}.

From intermediate **[AC-*Z*]$^+$**, a formal elimination of HF must occur to move towards the experimentally observed complex **[46]$^+$**, Scheme 5.22.
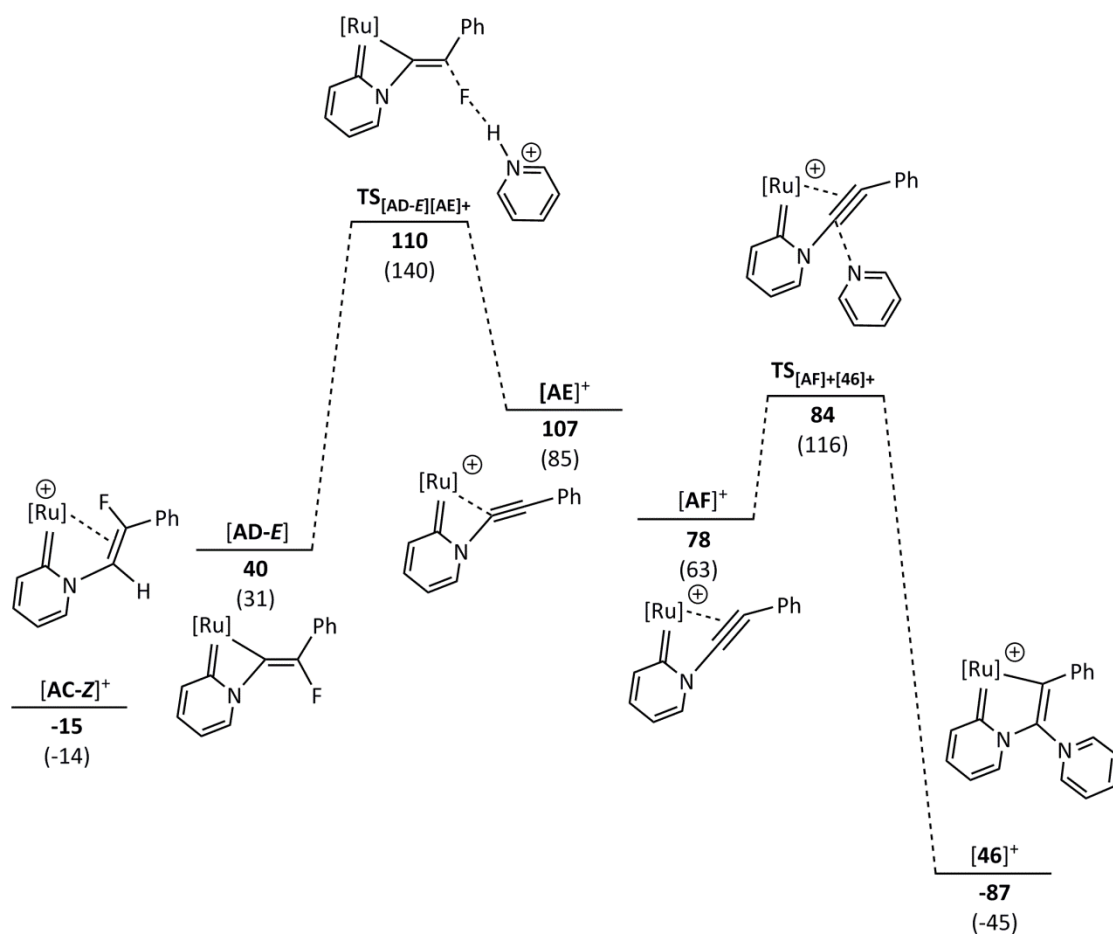
Scheme 5.22 Potential Energy Surface (PES) for the formal elimination of HF from [AC-*Z*]⁺ by pyridinium-mediated defluorination. $E_{SCF+ZPE}$ **energies (top, in bold) and relative Gibbs free energies (bottom, in parentheses) at 298.15 K, at the (RI-)PBE0-D3/def2-TZVPP//(RI-)BP86/SV(P) level with COSMO solvation in pyridine.**

All attempts to model a pyridine-induced E2-type elimination of HF were unsuccessful, suggesting that two discrete steps were necessary. Hence it was proposed that pyridine-mediated deprotonation of the alkenyl complex in **[AC-*Z*]⁺**, or direct deprotonation from **[AA-*E*]⁺**, may occur first to form metallocycle **[AD-*E*]** and $C_5H_5N\text{-}H^+$, followed by defluorination of **[AD-*E*]** mediated by the $C_5H_5N\text{-}H^+$ to form **[AE]⁺**. The newly formed alkyne ligand finds stability on coordination to the ruthenium centre, **[AF]⁺**, and undergoes nucleophilic attack by pyridine *via* **TS[AF]+[46]+** to form the final pyridylidene complex **[46]⁺**. This is the thermodynamic product of the whole PES with an energy of -45 kJ mol⁻¹ relative to **[27^Ph]⁺**.

The defluorination step process, **[AD-*E*]** to **[AE]⁺**, can be modelled from either the *E* or *Z* isomer of **[AD]⁺**, but is far more accessible from the *E*-isomer ($\Delta G^{\ddagger}$ **TS[AD-*E*][AE]+**= + 140 kJ mol⁻¹, $\Delta G^{\ddagger}$ **TS[AD-*Z*][AE]+**= + 173 kJ mol⁻¹). The full *E* and *Z* isomeric pathways are given in Supporting

Information for Chapter 5. There are several possible points of isomer interconversion along the pathway. For example, previous calculations have indicated that vinylidene formation should be possible from intermediates such as **[Y-*E*]⁺**, Scheme 5.23. From **[AG-*E*]⁺**, facile, low energy rotation of the vinylidene ligand can then interchange the *E* and *Z* isomers. Therefore, it is tentatively proposed that at some point following experimentally observed complex **[44-*Z*]⁺**, the system isomerizes and follows the *Z*-isomer pathway.
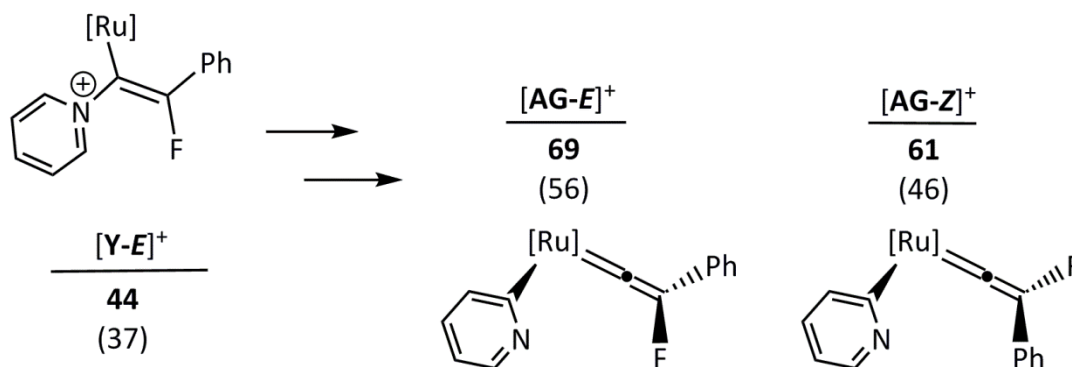
Scheme 5.23 Vinylidene formation from intermediate [Y-*E*]⁺. Calculations at the (RI-)PBE0-D3/def2-TZVPP//(RI-)BP86/SV(P) level with COSMO solvation in pyridine. [Ru] = [Ru(η^5-C₅H₅)(PPh₃)]. $E_{SCF+ZPE}$ (top) and Gibbs energies (bottom) at 298.15 K relative to [27^Ph]⁺ , pyridine and PPh₃.

The mechanistic pathway modeled by the DFT calculations in Scheme 5.19 is consistent with the experimental observations. The initial formation of **[44]BF₄** is rapid, whereas the formation of pyridylidene complex **[46]BF₄** is a second, slower reaction (with barriers of 100 kJ mol⁻¹ and 154 kJ mol⁻¹ respectively). The DFT calculations can also suggest a potential explanation for the exclusive formation of **[46]BF₄** rather than pyridine alkenylation to form **F-14^Ph**, Scheme 5.24, which has been reported for the analogous non-fluorinated system.[45] The key transition state in pyridine alkenylation involves carbon-nitrogen bond cleavage between the pyridylidene nitrogen and the alkenyl alpha carbon, **TS_[AD-*E*][AH-*E*]**, Scheme 5.24, which lies higher in energy than the defluorination pathway, **TS_[AD-*E*][AE]**, by 10 kJ mol⁻¹. This implies that the defluorination pathway is favoured over C-N bond cleavage.
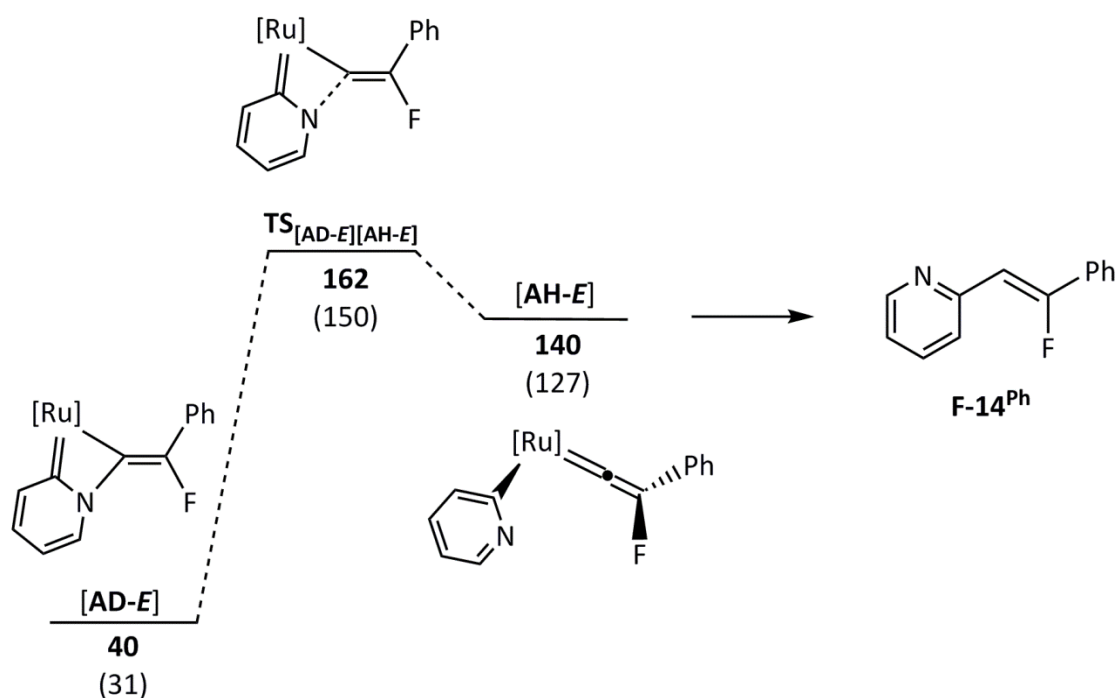
Scheme 5.24 Pyridine alkenylation to form F-14^Ph is through a higher energy transition state than formation of [46]BF_4

In the formation of **[46]BF₄**, carbon-fluorine bond cleavage occurs by pyridinium fluoride abstraction *via* **TS$_{[AD-E][AE]+}$**, Scheme 5.19. A similar carbon-fluorine bond cleavage has been reported by Hughes, in which α-fluoride abstraction from iridium half-sandwich complexes such as **5-aa** leads to cationic carbene-containing species **5-bb**, Scheme 5.25.[286-287] This defluorination technique exploits the low lying carbon-fluorine σ* antibonding orbitals to allow carbon-fluorine bond activation by reduction. In Scheme 5.19, fluoride loss leads to a cationic alkyne complex, **[AF]⁺**; this can then undergo attack by pyridine to form the final product **[46]⁺**.

$R = -F, -CF_3 \text{ or } -C_6F_5$
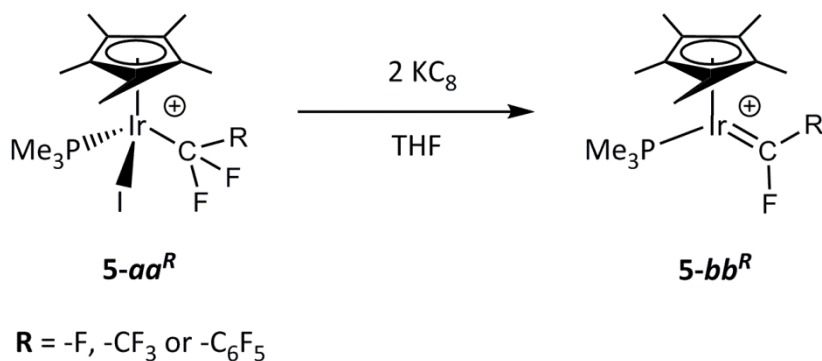
Scheme 5.25 Fluoride abstraction from complex 5-aa by reduction to form fluorinated carbene complex 5-bb

5.4.3 Hydrolysis of fluorovinylidene complexes

The observation that **[27^{Ph}]BF$_4$** undergoes nucleophilic attack by pyridine suggested that the incorporation of fluorine into the structure of the vinylidene ligand did not affect the polarisation of the vinylidene moiety, and allowed retention of the electrophilic α-carbon. Therefore, the complex presumably remained susceptible to attack by a range of nucleophiles and hence its reactivity was explored with a view to producing fluorinated organic molecules.

Ruthenium vinylidene complexes have been studied extensively as catalysts for anti-Markovnikov terminal alkyne hydration, with the key step of the mechanism being the attack of water at the metal bound α-carbon atom as exemplified in Chapter 2.[49,55] Therefore the reactivity of **[27^{Ph}]BF$_4$** was probed by the addition of water to a dichloromethane solution of the complex. Unexpectedly however, in the absence of other additives, the addition of either stoichiometric or excess water to the complex at room temperature did not result in immediate reaction. The addition of a stoichiometric quantity of base, 1,4-diazocyclo[2.2.2]octane (DABCO), in the presence of water (stoichiometric or ten equivalents) resulted in the formation of a mixture of organometallic complexes; the major species could be identified by ^{31}P{^{1}H} NMR spectroscopy as [Ru(η^5-C$_5$H$_5$)(PPh$_3$)$_2$Cl], **[25]**, and [Ru(η^5-C$_5$H$_5$)(PPh$_3$)$_2$(-C≡C{Ph})], **[26^{Ph}]**, Scheme 5.26. The presence of the acetylide complex **[26^{Ph}]** is particularly remarkable as the formation of this species corresponds to a formal loss of 'F$^+$'. The incorporation of chloride into the complex to form **[25]** was also quite unexpected, as no chloride was purposely added to the reaction mixture. The possible sources of chloride could either be from the dichloromethane solvent or from other impurities in the starting material. Monitoring the reactions over a three week period at room temperature showed almost total conversion to the ruthenium-chloride complex, **[25]**. Heating at 50 °C increased the rate of conversion to **[25]** but not the final product distribution.
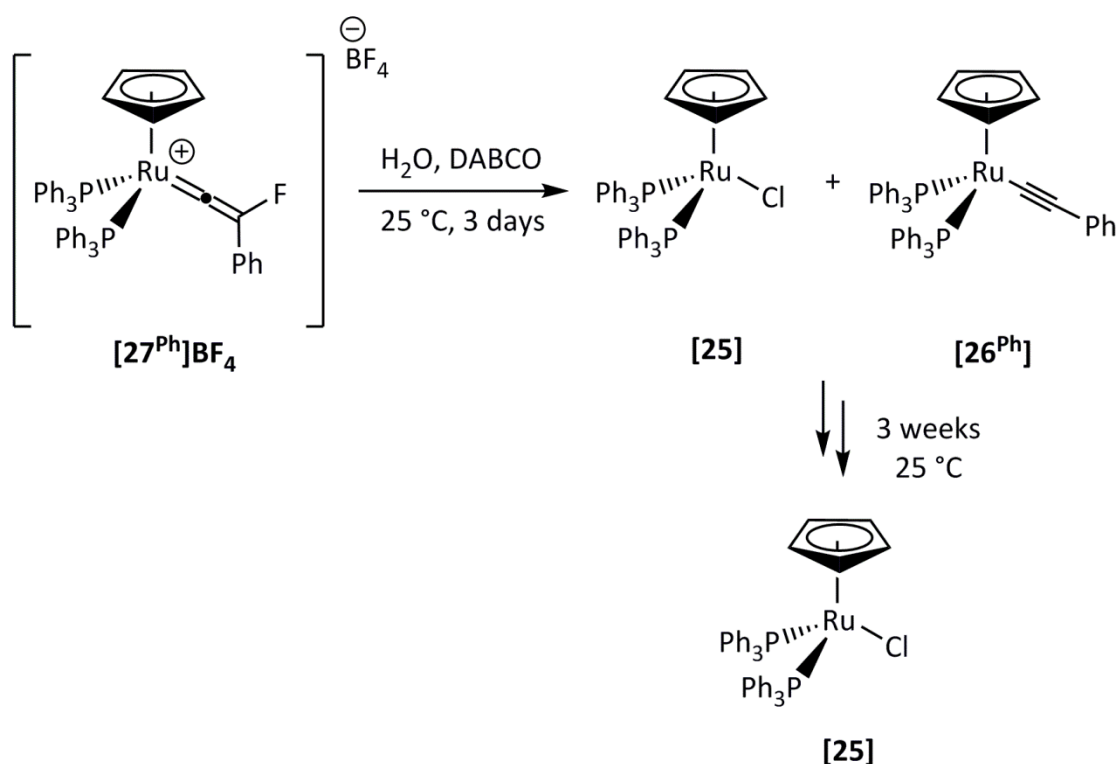
Scheme 5.26 Addition of water and DABCO to complex [27^{Ph}]BF$_4$

This reactivity should be compared with the addition of water to protio-vinylidene complex [28]$^+$ which results in the formation of $[Ru(\eta^5\text{-}C_5H_5)(PPh_3)_2CO]$ and toluene.[113]

In contrast, addition of water in the presence of a chloride additive (introduced as a N^{n}Bu$_4$Cl.H$_2$O) results in selective formation of ruthenium-chloride complex, **[25]**, and an acyl fluoride species, **47**, which is formed from the reaction of water with the vinylidene moiety, Scheme 5.27. The ratio of N^{n}Bu$_4$Cl to H$_2$O was shown to be approximately 1:1 by elemental analysis. Monitoring the reaction by NMR spectroscopy showed that the ruthenium complex **[25]** and **47** were formed at approximately the same rate.
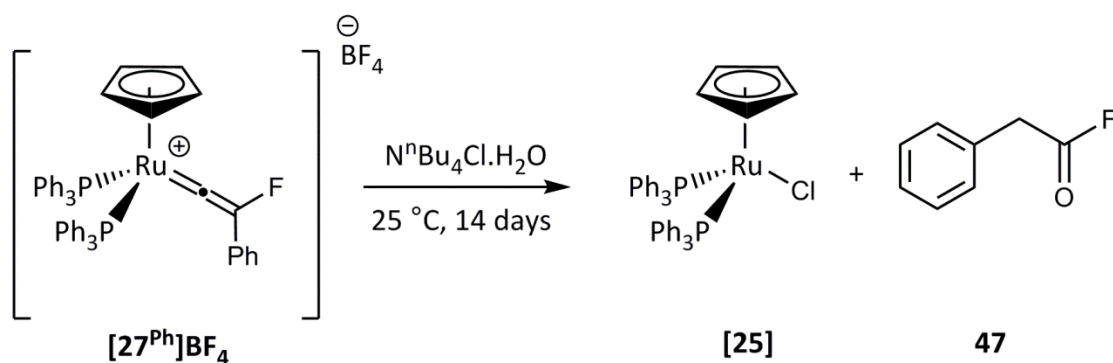
Scheme 5.27 Addition of water (in the form of N^{n}Bu$_4$Cl) to complex [27^{Ph}]BF$_4$

Fluoroacyl compound **47** was identified by characteristic resonances in the NMR spectra; a ^{19}F NMR resonance at 43.7 ppm as a triplet with $^3J_{HF}$ of 1.5 Hz, a doublet at 3.84 ppm in the ^{1}H NMR spectrum with a corresponding $^3J_{HF}$ and resonances in the ^{13}C{^{1}H} NMR spectrum at 39.2 ppm as a doublet with a $^2J_{CF}$ of 54 Hz for the -CH$_2$- protons and at 162.1 ppm as a doublet with a $^1J_{CF}$ of 362 Hz for the -**C**OF carbon. Compound **47** could be isolated as a foul-smelling oil by sublimation but was found to be extremely moisture sensitive. This prevented a yield from being recorded. Acyl fluoride compounds are highly toxic and it is advisable to wash all glassware thoroughly before removal from a fume hood.

On first inspection of Scheme 5.27, the acyl fluoride **47** is a fluorinated analogue of the aldehyde product which might be expected to form from the non-fluorinated vinylidene precursor. However, on closer examination of the vinylidene-mediated mechanism of alkyne hydration, it is evident that a formal fluorine or phenyl migration must have occurred. In the vinylidene precursor, the fluorine atom and phenyl group are attached to the same carbon atom, whereas in the acyl fluoride product **47** they are on different carbon atoms. Attack of water at the vinylidene α-carbon should lead to product **48**, Scheme 5.28. However, no evidence of the expected α-fluoroaldehyde could be observed in the ^{19}F NMR of the reaction mixture.

$$[27^{Ph}]^+ \qquad\qquad 48$$
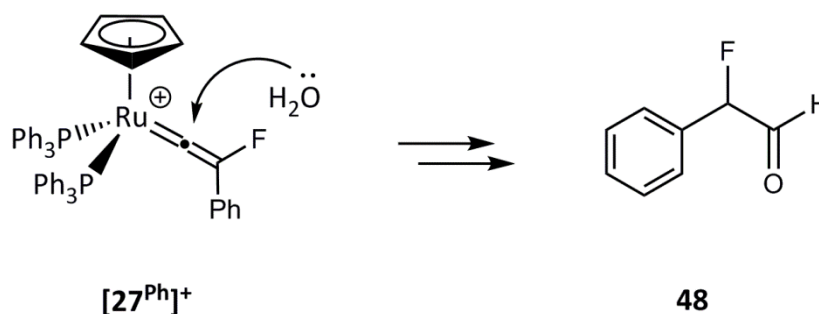
Scheme 5.28 Expected reaction mechanism and α-fluoroaldehyde product, 48, from hydration mediated by complex [27^{Ph}]$^+$

Furthermore, on heating complex **[27^{Ph}]BF$_4$** in CD$_3$CN, no phenyl or fluorine migration to produce FC≡CPh was observed suggesting that these are both high energy processes for this system (however, it should be noted that phenyl migration has been reported previously in disubstituted vinylidene complexes).[71] In order to gain further mechanistic information about this system, the reaction was repeated with ^{13}C-labelled fluorovinylidene, **^{13C}[27^{Ph}]BF$_4$**. This involved the synthesis of the labelled acetylide complex **^{13C}[26^{Ph}]** and subsequent

fluorination. This complex, ^{13C}[27^{Ph}]BF$_4$, was then subjected to identical reaction conditions with N^{n}Bu$_4$Cl, Scheme 5.29.
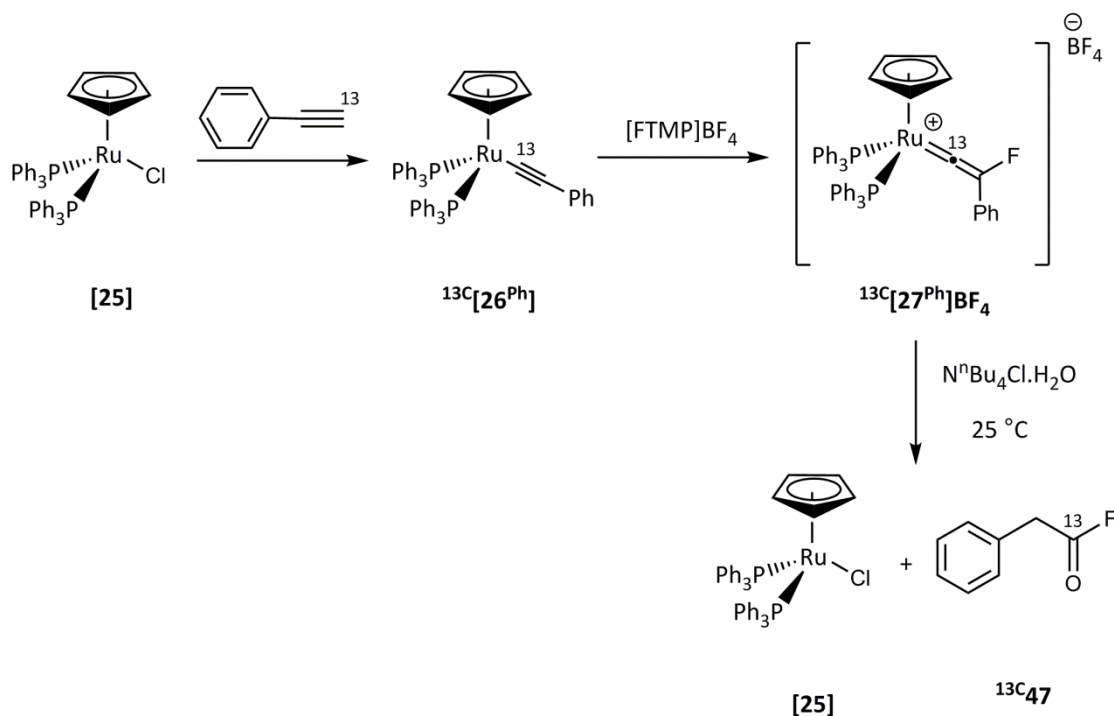
Scheme 5.29 Formation of complex ^{13C}[27^{Ph}]BF$_4$ and subsequent addition of water (in the form of N^{n}Bu$_4$Cl)

Examination of the ^{19}F NMR spectrum demonstrated that the ^{13}C label was exclusively incorporated into the structure of ^{13C}47 as the carbonyl carbon, as the aldehyde carbon and fluorine signal now appeared as doublets with corresponding $^1J_{CF}$ coupling constants of 361.4 Hz. There was no evidence of the labelled carbon in the alternative position (as the -CH$_2$-). Repetition of the hydrolysis reaction with the benzenesulfonimide salt, **[27^{Ph}]NSI**, gave identical reactivity indicating that the source of fluorine in the final acyl fluoride complex originates exclusively from the fluorovinylidene ligand and not from the BF$_4^-$ counter-ion.

Hydrolysis of the dppe-containing complex **[30^{Ph}]NSI** under identical reaction conditions (two equivalents of N^{n}Bu$_4$Cl in dichloromethane solution) was much faster than the triphenylphosphine analogue. Fast formation of [Ru(η^5-C$_5$H$_5$)(dppe)Cl], **[49]**, and the α-fluoroaldehyde **48** was observed at room temperature (63 % conversion to **[49]** was noted within twelve hours and 86 % conversion was observed within 48 hours).Fluoroaldehyde **48** was identified by resonances in the ^{1}H and ^{19}F NMR spectra at 9.72 ppm as a doublet of doublets with a $^3J_{HF}$ of 7.6 Hz and a $^3J_{HH}$ of 0.7 Hz and -191.7 ppm as a doublet of doublets

with a $^2J_{HF}$ of 47.0 Hz and a $^3J_{HF}$ of 7.6 Hz respectively. Over a six day period, the resonances for α-fluoroaldehyde were replaced with those for **47**.
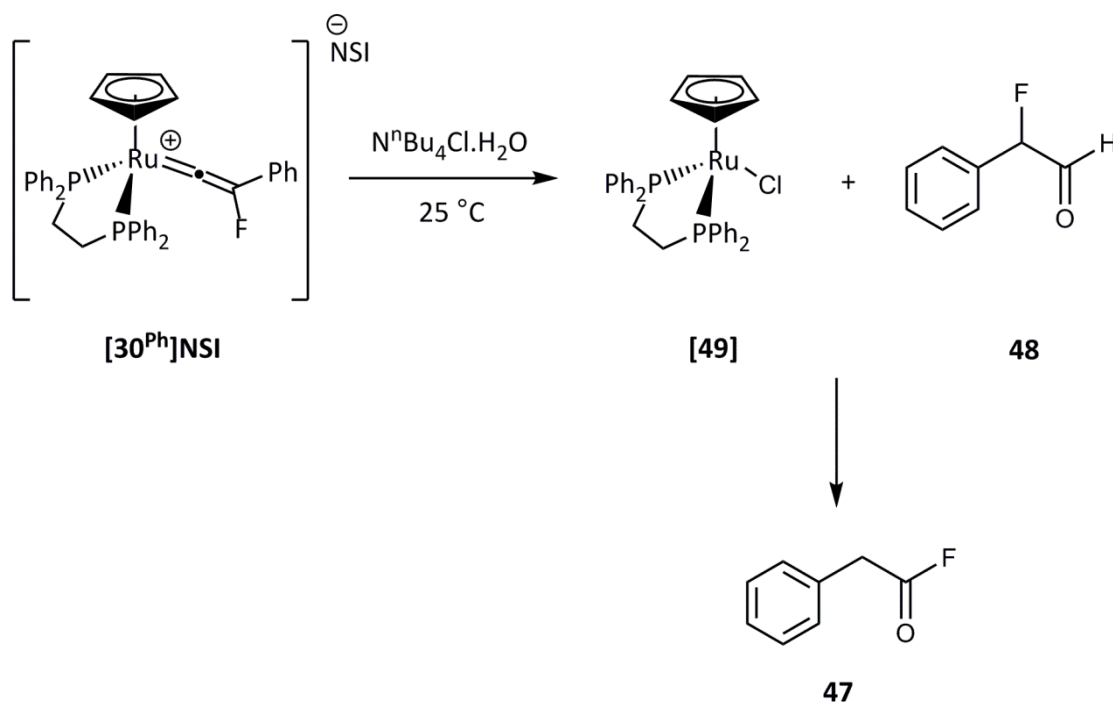
Scheme 5.30 Addition of water (in the form of N^{n}Bu$_4$Cl) to complex [30^{Ph}]NSI

Therefore, it is proposed that initial nucleophilic attack of water at the vinylidene α-carbon leads to the formation of the α-fluoroaldehyde, which subsequently undergoes isomerisation to **47**. According to DFT calculations, the energy of the acyl fluoride is lower in energy than the α-fluoroaldehyde isomer by a significant margin of 97 kJ mol^{-1}, and so the conversion is thermodynamically favoured. Also, aldehydes such as **48** are reported to be very unstable. For example, they are reported to decompose on silica gel and so are often functionalised further from crude reaction mixtures.[288]

5.4.4 Reaction of fluorovinylidenes with fluoride

5.4.4.1 Reaction of complex [27^{Ph}]BF$_4$ with tetramethyl ammonium fluoride, TMAF

As selective carbon-fluorine bond formation can be a challenging area, the reaction of **[27^{Ph}]BF$_4$** was probed with sources of fluoride, F$^-$. Nucleophilic attack of the fluoride ion at the metal-bound vinylidene α-carbon would produce a difluorinated alkenyl complex, increasing the structural complexity of the ligand. Furthermore, selective addition of the fluoride atom to form a single structural isomer of the alkenyl moiety with subsequent liberation from the metal centre could provide a new route to fluorinated alkene compounds.

On the addition of tetramethylammonium fluoride, **TMAF**, to a deuterated tetrahydrofuran (d$_8$-THF) solution of **[27^{Ph}]BF$_4$** at room temperature, no reaction was observed even after several hours. This was thought to be due to the low solubility of the **TMAF** in THF, which could be observed as a white precipitate in the Young's NMR tube. Heating the reaction at 50 °C encouraged the dissolution of **TMAF** and allowed the reaction to proceed.

On observation of the NMR spectra after two hours, a significant amount of **[27^{Ph}]BF$_4$** remained unreacted. However, signals corresponding to the fluorinated alkenyl complex **[50]** could be observed in the reaction mixture, Scheme 5.31. These were particularly diagnostic in the ^{19}F NMR spectra as a doublet at -146.8 ppm with a $^3J_{FF}$ of 113.7 Hz and a doublet of doublets at -72.6 ppm with a corresponding $^3J_{FF}$ and a $^3J_{PF}$ of 32.3 Hz. The $^3J_{FF}$ coupling constant was indicative of a trans-fluoroalkene which often exhibit large couplings (>130 Hz) whereas in a cis-fluoroalkene they are typically be much smaller (<15 Hz). The lack of a second set of resonances indicated that only one isomer was formed with complete stereoselectivity. The ^{31}P{^{1}H} NMR resonance appeared as a doublet of doublets at 52.5 ppm with $^3J_{PF}$ and $^4J_{PF}$ coupling constants of 32.3 and 2.4 Hz respectively. The ^{13}C{^{1}H} NMR spectrum showed distinctive resonances for the alkenyl carbons, the most downfield signal corresponding to the metal bound carbon atom (187.9 ppm, ddt, $^1J_{CF}$ of 296.6 Hz, $^2J_{CF}$ of 90.4 Hz and $^3J_{CP}$ of 18.2 Hz) and the β-carbon was observed at 159.5 ppm (dd, $^1J_{CF}$ of 198.1 Hz and $^2J_{CF}$ of 50.4 Hz).
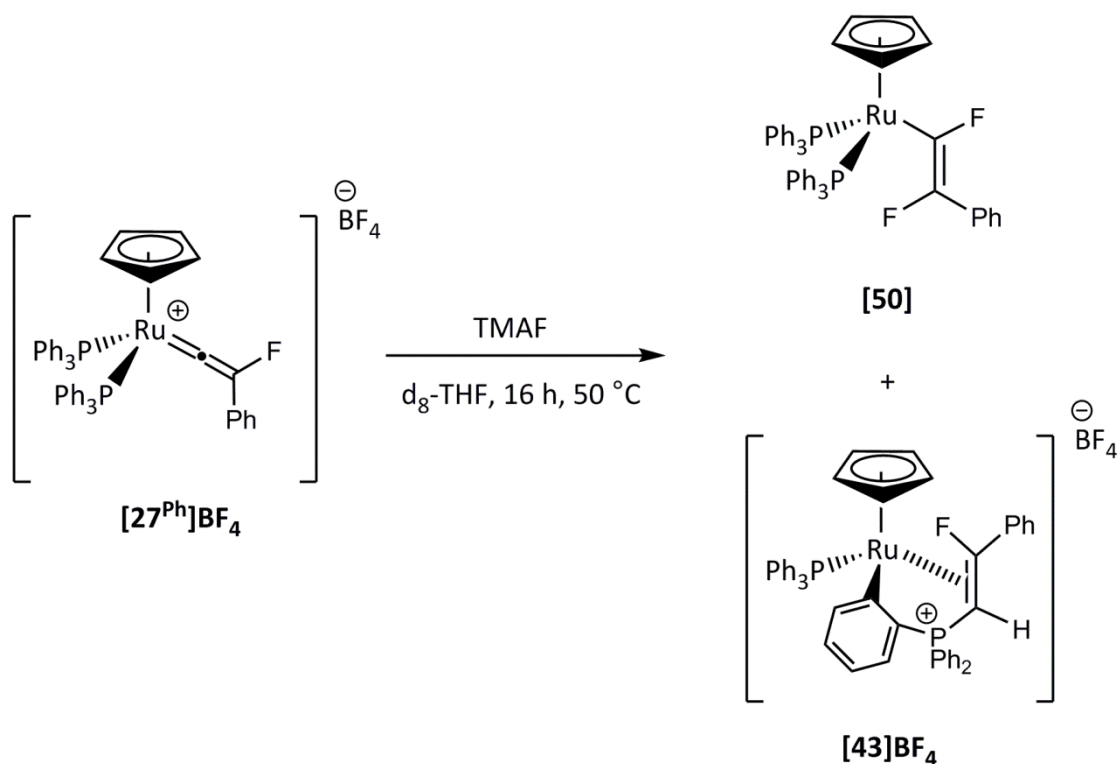
Scheme 5.31 Formation of complex [50]

However, the reaction was not clean and in addition to complex **[50]**, a significant amount of **[43]BF₄** could also be observed in the ^{19}F NMR spectra. On further heating, the signals for **[43]BF₄** became more intense, and a range of other low concentration impurities could also be observed in both the ^{19}F and $^{31}P\{^{1}H\}$ NMR spectra. These could not be identified due to their low concentration. The observation of **[43]BF₄** in the reaction mixture suggests that on heating at 50 °C in THF, the loss of triphenylphosphine and its subsequent attack at the vinylidene α-carbon is more rapid than the attack of fluoride. Presumably, this can be attributed to the low solubility of **TMAF** in the reaction mixture and the lability of triphenylphosphine in THF.

5.4.4.2 Reaction of complex [27^{Ph}]BF₄ with TREAT.HF

In order to overcome the low solubility of the **TMAF** fluoride source, the reaction between **[27^{Ph}]BF₄** and fluoride was repeated using an alternative source of F⁻ - triethylamine trihydrofluoride, **TREAT.HF**. As the ratio of triethylamine to HF is 1:3, one third of an equivalent of **TREAT.HF** was added to a Young's NMR tube containing a solution of **[27^{Ph}]BF₄** in d₈-THF. Although no immediate colour change was observed, NMR spectra were recorded directly on addition. In both the ^{19}F and $^{31}P\{^{1}H\}$ NMR spectra, clear and intense signals were

observed for **[50]** as the major new product, which integrated to 32 % of all the fluorine-containing species in the reaction. 53 % of **[27^Ph]BF₄** remained unreacted. Using the integration of the ^{19}F NMR spectrum, the ratio of **[43]BF₄** to **[50]** in the reaction mixture was 1:5.

The reaction was monitored by NMR spectroscopy but after three days at room temperature showed no significant differences in product distribution. Therefore, another two thirds of an equivalent of **TREAT.HF** was added (with respect to **[27^Ph]BF₄**) and the NMR spectra re-recorded. The spectra showed almost total conversion to **[50]** with no residual **[27^Ph]BF₄** in the reaction mixture. This suggests that only one HF molecule is available for reaction for each molecule of triethylamine, despite the 3:1 stoichiometry of the two components. Small signals could be observed in the ^{31}P{^{1}H} NMR spectrum corresponding to **[43]BF₄** (integration of 10 %), **[26^Ph]** (integration of 8 %) and two unidentified products at 42.6 and 40.0 ppm with integrations of 2 % and 1 % respectively, Scheme 5.32. The presence of **[26^Ph]** was again surprising, and indicated a formal loss of 'F^{+}' from the fluorovinylidene precursor.

Scheme 5.32 Reaction of [27^Ph]BF₄ with TREAT.HF

5.4.4.3 Reaction of complex [30^{Ph}]NSI with TREAT.HF

In order to avoid the formation of **[43]BF$_4$**, the reactivity of fluorovinylidene complexes with fluoride was repeated using dppe-substituted **[30^{Ph}]NSI** in place of the triphenylphosphine complex **[27^{Ph}]BF$_4$**. The use of bidentate dppe in place of monodentate triphenylphosphine avoids dissociation of the phosphine ligand and therefore prevents subsequent formation of complex **[43]X**.

On addition of stoichiometric **TREAT.HF** to a d$_8$-THF solution of **[30^{Ph}]NSI**, a colour change was observed from green to yellow within ten minutes indicating a rapid reaction had occurred. NMR spectra revealed clean conversion to *bis*-fluoroalkenyl complex **[51]**, Scheme 5.33. In the ^{19}F NMR spectrum, signals were observed for the fluorine substituents on the alkenyl ligand at -147.8 ppm as a doublet with a $^3J_{FF}$ of 111.5 Hz and a doublet of triplets at -82.4 ppm with a corresponding $^3J_{FF}$ and a smaller $^3J_{PF}$ of 28.1 Hz. The ^{31}P{^{1}H} NMR spectrum appeared as a doublet of doublet at 94.3 ppm with a $^3J_{PF}$ and $^4J_{PF}$ of 28.1 and 2.6 Hz respectively. In the ^{13}C{^{1}H} NMR spectrum, the metal-bound vinyl carbon resonates at 187.9 ppm with a $^1J_{CF}$ of 296.6 Hz, a $^2J_{CF}$ of 90.4 Hz and a $^3J_{CF}$ of 18.2 Hz, and the β-carbon resonates at 159.5 ppm as a doublet of doublets with a $^1J_{CF}$ of 198.1 Hz and a $^2J_{CF}$ of 50.4 Hz. The ESI-MS indicated a species with an *m/z* of 705.1192 corresponding to the incorporation of a single fluorine atom into the structure of **[30^{Ph}]NSI**. A broad signal at -187.6 ppm could be observed in the ^{19}F NMR spectrum, believed to be due to the presence of fluoride. This could also be linked to a broad signal at 9.4 ppm with a width of approximately 200 Hz in the ^{1}H NMR spectrum which could possibly be due the formation of an adduct, for example, a molecule of HF binding to a fluorine atom in **[51]**.
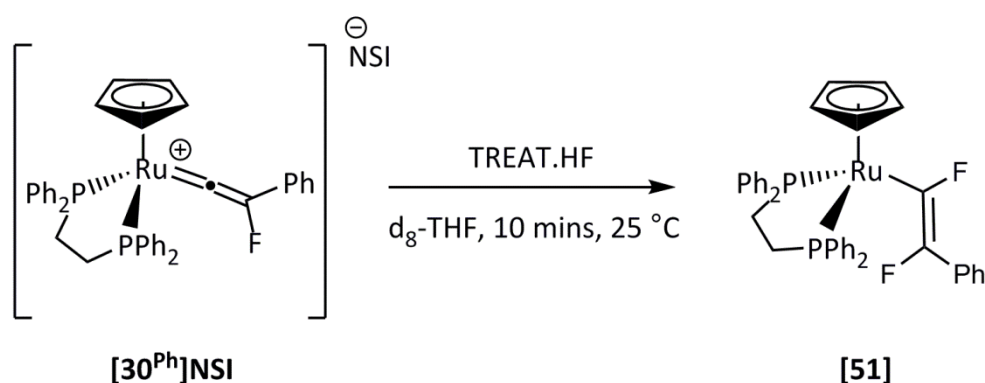
Scheme 5.33 Formation of complex [51]

5.4.5 Reaction of complex [27^{Ph}]BF₄ with diethylamine

The reactivity between **[27^{Ph}]BF₄** and diethylamine was explored in an attempt to liberate an organic, fluorinated molecule from the ruthenium centre. The hypothesis was that diethylamine would act as a nucleophile and attack as demonstrated previously at the electrophilic metal-bound α-carbon of the vinylidene ligand. A subsequent proton migration from the ammonium moiety could protonate the α-carbon of the alkenyl ligand allowing dissociation of the compound, Scheme 5.34.
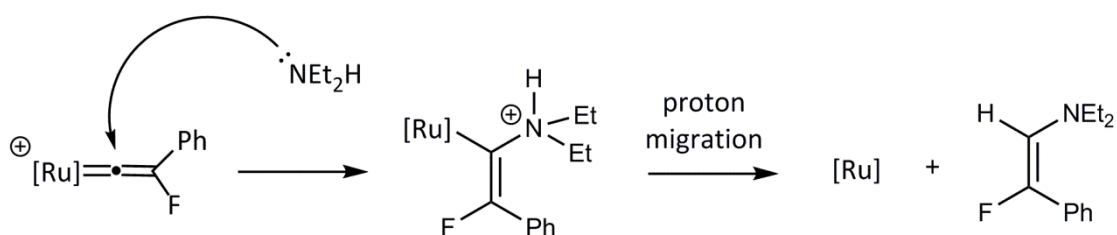
Scheme 5.34 Proposed reactivity of a vinylidene complex with diethylamine, [Ru] = [Ru(η⁵-C₅H₅)(PPh₃)₂]

One equivalent of diethylamine was added to a dichloromethane solution of **[27^{Ph}]BF₄**, and NMR spectra recorded both immediately on addition and after 48 hours indicated that no reaction had occurred. After heating at 50 °C overnight the NMR spectra were recorded again. The ^{19}F NMR spectrum clearly showed the presence of **[43]BF₄** as a doublet of triplets at -144.5 ppm with corresponding coupling constants to those previously observed. This product was also visible in the ^{31}P{^{1}H} NMR spectrum alongside several other organometallic species including the **[27^{Ph}]BF₄** starting material and **[25]**, [Ru(η⁵-C₅H₅)(PPh₃)₂Cl]. Monitoring the reaction by NMR spectroscopy over the course of one week showed a change in the relative rations of these components leading to **[43]BF₄** as the major phosphorus containing species. Neither ESI-MS or EI-MS indicated any traces of liberated organic products, and no characteristic signals were observed by ^{1}H NMR spectroscopy.

5.4.6 Reaction of complex [27^{Ph}]BF₄ with hydrochloric acid

The reaction between **[27^{Ph}]BF₄** and dilute hydrochloric acid was investigated with a view to liberating a fluorinated organic molecule from the metal by protonation. To a Young's NMR tube charged with **[27^{Ph}]BF₄** in CD₂Cl₂ was added one equivalent of 1 mol dm⁻³ hydrochloric acid in ether. No colour change was observed on addition but the NMR spectra indicated that some reaction had occurred within the first hour of addition. Using the integrations of the ^{31}P{^{1}H} NMR spectrum, approximately 80 % of **[27^{Ph}]BF₄** remained unreacted but both the

^{31}P{^{1}H} and ^{19}F NMR spectra showed evidence of **[43]BF$_4$** (approximately 3 % conversion). The ^{31}P{^{1}H} NMR spectrum also showed approximately 6 % conversion to an unidentified pair of seemingly related doublets at 41.3 and 39.3 ppm with a coupling constant of 26.3 Hz, and 9 % conversion to a singlet at 43.9 ppm. In the ^{19}F NMR spectrum, new signals were observed for **[43]BF$_4$** and a doublet at -113.7 ppm with a coupling constant of 4.8 Hz. A corresponding signal could not be observed in the ^{31}P{^{1}H} NMR spectrum suggesting that this coupling was a J_{HF}. In fact, a doublet with a corresponding coupling constant at 5.83 ppm could be seen in the ^{1}H NMR spectrum. These resonances could potentially be assigned to either a fluoroalkene organic product[284] or a ruthenium species such as the fluorocarbene complex, Figure 5.19, which could also explain the singlet signal in the ^{31}P{^{1}H} NMR spectrum at 43.9 ppm.
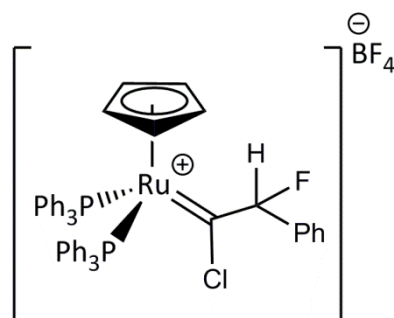
Figure 5.19 Proposed fluorocarbene complex from the reaction of [27^{Ph}]BF$_4$ with HCl, [Ru] = [Ru(η^5-C$_5$H$_5$)(PPh$_3$)$_2$]

The reaction was monitored over the course of three days and showed only subtle changes in the spectra. A second equivalent of acid was supplied but no significant reactivity was observed within several days of addition. Over the course of three weeks, the colour of the reaction mixture changed from green to red and the spectra became very complex, with eight visible peaks in the ^{31}P{^{1}H} NMR spectrum including those for **[43]BF$_4$** and unreacted **[27^{Ph}]BF$_4$**. Interestingly, the signals discussed previously (^{1}H, 5.83 ppm, d, *J* of 4.8 Hz; ^{19}F, -131.7, d, *J* of 48 Hz; [31]P{[1]H}, 43.9 ppm, s) could no longer be observed, suggesting that this organic molecule or ruthenium complex had undergone further reaction or decomposition. The signal in the ^{19}F NMR spectrum showed BF$_4$ decomposition and the ^{1}H NMR spectrum showed evidence of alkyne dimerisation. The ESI-MS indicated the presence of fluorovinylidene complex **[27^{Ph}]BF$_4$** (or an isomer with the same molecular formula), [Ru(η^5-C$_5$H$_5$)(PPh$_3$)$_2$]$^+$ fragments and [Ru(η^5-C$_5$H$_5$)(PPh$_3$)$_2$Cl - H]$^+$.

These complex NMR spectra indicated that the addition of hydrochloric acid to a solution of **[27^{Ph}]BF$_4$** was not an ideal method to liberate organic products from the complex. Even after the addition of two equivalents of acid, some **[27^{Ph}]BF$_4$** could still be observed and a whole range of organometallic products were produced with only tentative evidence of a fluoroalkene product (which was degraded rapidly in the reaction mixture). The degradation of ruthenium complex **[27^{Ph}]BF$_4$** may be explained if the hydrochloric acid solution was wet, in which base the BF$_4^-$ counter-ion may have decomposed to form reactive HF species in solution.

5.5 Mechanistic insight into fluorovinylidene formation

5.5.1 Outer-sphere electrophilic fluorination (OSEF)

Chapter 4 describes the important applications of fluorinated compounds and the wealth of fluorination techniques reported in the literature. In particular, our discovery of the outer-sphere electrophilic fluorination mechanism (OSEF) was highlighted in which both computational and experimental data suggested direct fluorine incorporation into the structure of a ligand at a redox active metal centre, but in the absence of a metal-fluoride intermediate.[63] This process is summarised in Scheme 5.35.
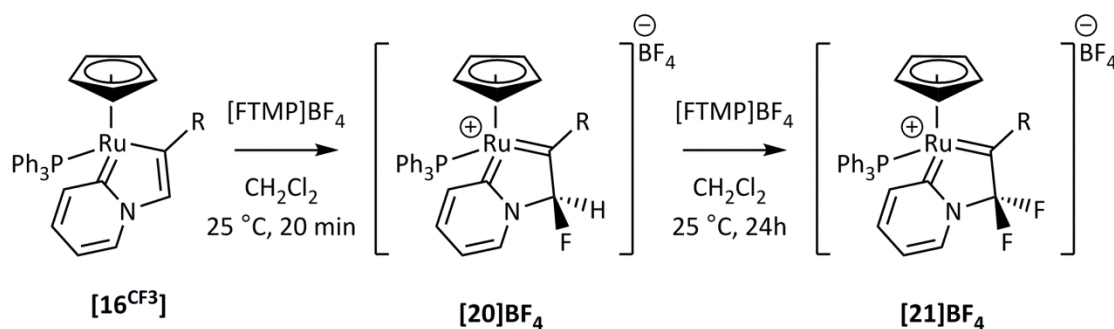
Scheme 5.35 Outer-sphere electrophilic fluorination of ruthenium metallocycle, R = C$_6$H$_4$-4-CF$_3$

Mechanistic evidence suggests that formation of these fluorovinylidene complexes is a second example of this process.

5.5.2 Cold addition of 'F$^+$' to complex [26^{Ph}]

In order to investigate the mechanism of fluorination of complexes **[26^R]**, the addition of **[FTMP]BF$_4$** to ruthenium acetylide complex **[26^{Ph}]** was performed at low temperature and monitored by NMR spectroscopy.

A solution of **[26^{Ph}]** was prepared in CD$_2$Cl$_2$ (20 mg of **[26^{Ph}]** in 0.5 mL of CD$_2$Cl$_2$) in a Young's NMR tube and this was frozen in a flask of liquid nitrogen. The NMR spectrometer was pre-cooled to 195 K and once it had reached a stable temperature, a stoichiometric quantity of **[FTMP]BF$_4$** (6 mg) was introduced to the frozen solution of ruthenium complex. The reaction mixture was then allowed to thaw and rapidly introduced to the NMR spectrometer. The ^{1}H, ^{19}F and ^{31}P{^{1}H} NMR spectra were then recorded at incremental 10 K intervals until complete conversion to **[27^{Ph}]BF$_4$** was observed. Care was taken to ensure that a wide chemical shift range of ^{19}F resonances were recorded (from 200 to -500 ppm) in order to observe any ruthenium fluoride intermediates which typically would be expected between -200 and -450 ppm in the ^{19}F NMR spectra.[256-259] No intermediates of any kind were observed in the spectra, only clean conversion of acetylide **[26^{Ph}]** to fluorovinylidene complex **[27^{Ph}]BF$_4$**.

These low temperature NMR spectra support the absence of ruthenium fluoride intermediates being involved in the fluorination mechanism and therefore suggest an outer-sphere electrophilic fluorination pathway in which the fluorine atom is delivered directly to the ligand in **[26^R]** to form the fluorovinylidene complex **[27^R]X**. This is analogous to the direct fluorination of the ruthenium metallocycle, **[16^{CF3}]**, discussed in Chapter 4. An alternative explanation could be that only low-energy transition states connect any metal-fluoride intermediates to the final fluorovinylidene product, **[27^R]BF$_4$**.

5.6 Conclusions

The electrophilic fluorination of acetylide ligands represents the first synthetic preparation of fluorinated vinylidene complexes *via* a facile, rapid and highly selective carbon fluorine bond formation. This new class of ligands is of value from both a fundamental and synthetic viewpoint. The incorporation of fluorine dramatically affects the electronic properties of vinylidene complexes and these effects have been explored by $^{13}C\{^1H\}$ NMR and UV-visible spectroscopy. It was demonstrated that fluorination decreases the energy of the HOMO-LUMO ($\pi \rightarrow \pi^*$) transition which is responsible for the distinctive green colour of these species.

From a synthetic perspective, vinylidene complexes are widely recognised as key intermediates in a range of catalytic processes, and hence fluorine incorporation into these privileged structures may lead to novel fluorinated products. Therefore these species were trialled in a range of typical vinylidene reactions. Fluorine incorporation did not diminish the electrophilicity of the metal bound α-carbon and therefore reactions with fluoride, pyridine, water and triphenylphosphine were observed. In cases where phosphine loss was possible from the ruthenium centre (from **[27^{Ph}]BF$_4$**), reactions with pyridine led to novel pyridylidene complexes *via* C-H activation and loss of HF. Reactions with water led to the formation of an acyl fluoride compound *via* isomerisation of an α-fluoroaldehyde intermediate.

Future work in this area should focus on two main targets: the liberation of fluorinated organic molecules from the metal centre and the incorporation of fluorovinylidene complexes into a catalytic methodology. Early attempts to dissociate small fluorinated fragments from these complexes using diethylamine or hydrochloric acid have proved unsuccessful, however, reaction of **[27^{Ph}]BF$_4$** in chloride-assisted hydrolysis reactions both cleanly liberates an organic molecule and concomitantly regenerates ruthenium complex **[25]**, [Ru(η^5-C$_5$H$_5$)(PPh$_3$)$_2$Cl] – the initial complex from which these fluorovinylidene species are formed. This indicates the potential applications of these complexes in catalysis.

Chapter 6

Conclusions and future work

6 Conclusions and future work

6.1 Introduction

The experimental and computational studies presented in this thesis cover several areas of ruthenium catalysis including anti-Markovnikov terminal alkyne hydration, pyridine functionalisation and the electrophilic fluorination of pyridylidene and vinylidene ligands. Each of these processes has undergone thorough mechanistic study using NMR spectroscopy, mass spectrometry and DFT calculations. The key findings from each of these studies will be collected in this chapter, with suggestions for future developments of this chemistry.

6.2 Mechanistic insight into anti-Markovnikov terminal alkyne hydration using a self-assembled ruthenium catalyst (Chapter 2)

On the basis of a thorough computational study, a potential mechanism has been proposed for anti-Markovnikov terminal alkyne hydration using the self assembled catalyst, $[Ru(\eta^5\text{-}C_5H_5)(NCMe)(6\text{-}DPPAP)(3\text{-}DPICon)]PF_6$, **[1]PF$_6$**. The proposal is supported by a similar computational study reported by Cooksy *et al*, and experimental evidence from analogous systems of Grotjahn and co-workers.

The regiochemistry of the product was controlled by the involvement of a vinylidene intermediate, and the highly functionalised 6-DPPAP and 3-DPICon ligands promoted three LAPS processes for the interconversion between intermediates; formation of the vinylidene moiety, nucleophilic attack of water at the vinylidene α-carbon and tautomerisation from a hydroxyvinyl to acyl species. These ligand-assisted processes were shown to provide a lower energy pathway for the alkyne to aldehyde transformation. The synergic behaviour between the metal centre and the non-innocent ligand system, both taking an active role in substrate transformation, allow comparison of catalyst **[1]PF$_6$** with one of nature's metalloenzymes.

In combination with the DFT calculations, the reaction was also studied experimentally in an attempt to observe or isolate some important reaction intermediates. On the addition of alkynes (phenylacetylene, 4-ethynyl-α,α,α-trifluorotoluene and 1-nonyne), no reaction with **[1]PF$_6$** was observed at room temperature, even after long reaction times. On heating the reactants at 50 °C over the course of one week, slow but quantitative conversion was observed to complex **[5]PF$_6$** – the formation of which occurs from a formal insertion of the alkyne into the N-H bond of the isoquinolone moiety of the 3-DPICon ligand. Both DFT

calculations and experimental results confirmed that complex **[5]PF$_6$** was not catalytically active and represented a catalyst deactivation product. A potential mechanism was explored computationally, and involves the tautomerisation of the 3-DPICon ligand from the lactam to lactim form to promote nucleophilic attack of the ligand at the vinylidene at the electrophilic α-carbon. The vinylidene intermediate can therefore be considered as a 'branching point' from which either productive catalysis or catalyst deactivation can occur.

According to the DFT calculations, the catalyst deactivation product is both the kinetic and thermodynamic product of this system when compared to the formation of aldehyde and regeneration of the catalyst. **[5]PF$_6$** has a lower energetic span of formation than aldehyde formation (91 kJ mol^{-1} versus 113 kJ mol^{-1}) and a lower thermodynamic energy (-145 kJ mol^{-1} versus -142 kJ mol^{-1}). In reality, although the rate of catalyst deactivation is not enough to prevent aldehyde formation, significant conversion is observed to **[5]PF$_6$** under standard catalytic conditions. Preliminary DFT calculations using alternative solvation parameters have not yet been successful in explaining the experimentally observed results.

Future work on this catalytic system should aim to investigate the origin of the discrepancy between the experimental results and the outcome predicted by DFT. Including explicit solvation in the calculations (strategically placing water molecules into the structure of the intermediates) may help to rationalise the observations, as it is possible that the binding of water to one or more intermediates along the reaction coordinate may alter the energy barriers enough to promote productive catalysis over catalyst deactivation. Alternatively, the structure of the catalyst (most importantly the structure of the phosphine ligands, but potentially the cyclopentadienyl ligand or the metal centre itself) may be modified in order to prevent the formation of **[5]PF$_6$** under catalytic conditions. The substrate scope of the reaction could be investigated by repetition with a range of substituted alkynes (with electron-withdrawing and electron-donating groups, substituents of large and small steric bulk etc).

The main outcome from this study is the deepened understanding of the ligand-assisted processes which participate in the interconversion between intermediates in the alkyne hydration reaction. These principles may be incorporated in the design of future catalysts that promote a range of substrate transformations, in order to lower the energy barriers and allow their operation under milder reaction conditions.

6.3 Investigation of pyridyl-functionalised phosphine ligands in catalysis (Chapter 3)

Pyridine motifs are amongst the most privileged heterocyclic substructures, widely found in pharmaceutical compounds and other natural products. As such, efficient and optimised routes to form these molecules are highly sought after. In 2013, Lynam and Slattery reported an atom-efficient procedure for the catalytic alkenylation of pyridine under mild conditions. However, the reaction showed a marked solvent dependence; in the absence of a basic solvent such a pyridine, the catalyst undergoes deactivation and the reaction can no longer proceed.

Based on the findings of Chapter 2 and the LAPS processes in which highly functionalised ligands (6-DPPAP and 3-DPICon) can participate, two ruthenium complexes were synthesised which contain pyridyl-functionalised phosphine ligands in their coordination spheres, and these complexes were trialled in stoichiometric and catalytic reactions with phenylacetylene and 4-ethynyl-α,α,α-trifluorotoluene. It was anticipated that the pyridine functionality within the ligand could deprotonate the key catalytic intermediate (a ruthenium pyridylidene-hydride complex, **3-z**, Scheme 3.7, Chapter 3) by an intramolecular process, without the requirement of excess pyridine to act as the solvent of the reaction.

Complex **[7b]PF$_6$**, [Ru(η^5-C$_5$H$_5$)(PPh$_2$R)(L)$_2$][PF$_6$] (PPh$_2$R = 2-(1,1-dimethylpropyl)-6-(diphenylphosphino)pyridine) displayed different reactivity with each of the alkynes. In the presence of phenylacetylene, the reaction required two alkyne equivalents to perform a condensation reaction which formed an η^3-butadienyl ligand, **[12b^{Ph}]PF$_6$**. On addition of stoichiometric 4-ethynyl-α,α,α-trifluorotoluene and heating at 50 °C for several hours, complete conversion was observed to a pyridylidene complex, **[13b^{CF3}]PF$_6$**, which was an analogous catalyst deactivation product to that observed with triphenylphosphine in the Lynam and Slattery pyridine alkenylation study.

In the presence of either phenylacetylene or 4-ethynyl-α,α,α-trifluorotoluene, complex **[7c]PF$_6$**, [Ru(η^5-C$_5$H$_5$)(PPh$_2$R)(L)$_2$][PF$_6$] (PPh$_2$R = diphenyl-2-pyridylphosphine), reacted immediately to produce complex **[15c^{Ph}]PF$_6$** or **[15^{CF3}]PF$_6$** respectively. The mechanism of formation was postulated to be initial vinylidene formation at ruthenium, followed by rapid nucleophilic attack of the nitrogen in the pyridine ring of the phosphine ligand at the vinylidene α-carbon. Although not beneficial to optimise catalysis, this result provided

experimental evidence for an important intermediate in the mechanistic route suggested by Lynam and Slattery for pyridine alkenylation, which previously had only been modelled by DFT (complex **3-y**, Scheme 3.7, Chapter 3).

In conclusion, the incorporation of either of the pyridyl-functionalised phosphine ligands did not lead to intramolecular deprotonation of the key catalytic intermediate under stoichiometric conditions, and this was also observed under catalytic conditions. However, the experimental studies instead provided credence to the reaction mechanism suggested previously (*via* complexes **[15c^{Ph}]PF$_6$** and **[15^{CF3}]PF$_6$**), and allowed access to further examples of novel pyridylidene complexes synthesised from non-activated substrates (**[12b^{Ph}]PF$_6$** and **[13b^{CF3}]PF$_6$**). The triphenylphosphine analogues of these complexes were the complexes studied in electrophilic fluorination reactions in Chapter 5.

Future work on this project could include the trial of a wider range of functionalised ligands in the pyridine alkenylation reaction in order to find an alternative for the necessity of excess pyridine in the reaction mixture. For example, other researchers have used imidazolyl-functionalised phosphines and observed that these ligands can involve themselves in intramolecular deprotonation processes such as LAPS.[78] Computational studies using DFT calculations may allow the rational design of a ligand with the correct steric, electronic and conformational properties to engage in deprotonation of the pyridylidene-hydride complex, **3-z** that leads to deactivation.

6.4 Outer-sphere electrophilic fluorination of a ruthenium metallocycle (Chapter 4)

A ruthenium-pyridylidene complex **[16^{CF3}]**, synthesised from non-activated substrates, was observed to undergo electrophilic fluorination selectively at the 3-position of the 1-ruthanaindolizine ring to quantitatively produce a mono-fluorinated metallocycle, **[20]BF$_4$**. The reaction proceeds rapidly under mild conditions (fluorination is complete within twenty minutes of addition of the 'F$^+$' source at 20 °C) and with complete regioselectivity. X-ray diffraction and NOESY NMR experiments indicated that the fluorination also proceeds with complete diastereoselectivity, to produce a single diastereomer in which the fluorine substituent is oriented towards the cyclopentadienyl ligand. This diastereoselectivity can be explained by steric effects, as approach of the fluorinating agent from the 'bottom face' of

[16^{CF3}] is blocked by the bulky triphenylphosphine ligand. The fluorination reaction was tolerant to a range of fluorinating agents including **Selectfluor**, **NFSI** and **[FTMP]BF₄**.

On the addition of two equivalents of **[FTMP]BF₄** to **[16^{CF3}]** (or a second equivalent of **[FTMP]BF₄** to **[20]BF₄**) after 24 hours at 20 °C, quantitative formation of a difluorinated complex was observed, **[21]BF₄**. This corresponds to a net deprotio-difluorination reaction of **[16^{CF3}]**. The ^{19}F NMR spectra indicated that both fluorine atoms were on the same carbon atom due to the characteristic $^2J_{FF}$ of 233.1 Hz observed for each of the fluorine resonances.

Crucially, the fluorinated ligands in **[20]BF₄** and **[21]BF₄** were retained in the coordination sphere of the metal, which allowed the investigation of subsequent metal-mediated reactivity. Upon addition of a base or dissolution in pyridine, **[20]BF₄** was observed to undergo deprotonation at the 3-position of the ruthanaindolizine ring to prepare a fluorinated analogue of the parent 1-ruthanaindolizine starting material, **[22]**. More surprisingly, on dissolution of the difluorinated species in d₅-pyridine, **[21]BF₄,** the same product was observed which corresponds to the formal loss of 'F$^+$'. It was proposed that the formation of **[22]** from **[21]BF₄** is coupled to a hydration process (by reaction with adventitious water in the pyridine solvent) to form an oxygen-containing species, **[24]BF₄** and the release of HF.

Throughout this study, a series of mechanistic data suggested that fluorination was taking place *via* an unprecedented outer-sphere electrophilic fluorination mechanism. No ruthenium fluoride intermediates (or others) were observed spectroscopically during the fluorination of complex **[16^{CF3}]** to form **[20]BF₄,** even during low temperature NMR studies. At temperatures below 245 K, the reaction appeared not to proceed, but by 265 K the fluorination was complete. The absence of ruthenium-fluoride intermediates was surprising based on consideration of related palladium-based chemistry, and suggested that fluorine was either transferred directly to the ligand or that only low-energy transition states connect any potential intermediates to **[20]BF₄**. The reactivity of **[16^{CF3}]** towards H$^+$ was also very different from the reactivity with 'F$^+$'. These results suggested a novel fluorination mechanism was in operation.

Possible fluorination mechanisms were further investigated using DFT studies. Although calculations suggested that formation of a ruthenium-fluoride complex would be thermodynamically favoured over **[16^{CF3}]** and **[FTMP]BF₄** (by 158 and 208 kJ mol^{-1}), the

subsequent high energy barriers to further reaction (between 130 and 204 kJ mol^{-1}) were inconsistent with the complete conversion to **[20]BF$_4$** that was observed at 265 K. The high energy barriers also suggest that any ruthenium-fluoride intermediates would be observed during the low-temperature NMR studies. Furthermore, the kinetic and thermodynamic product from 'F$^+$' migration was calculated to be an experimentally unobserved isomer in which the 2-position of the ruthanaindolizine ring is fluorinated, and not complex **[20]BF$_4$** which was observed experimentally.

Direct fluorination of the 3-position of the ruthanaindolizine ring in **[16^{CF3}]** was also investigated by relaxed PES scans. The reaction pathways for the closed-shell singlet, triplet and singlet diradical states all proceed through low energy barriers (of 58, 27 and 23 kJ mol^{-1} respectively in dichloromethane) which are consistent with the fast conversion to **[20]BF$_4$** observed at low temperatures. Within these possibilities, the open-shell pathways are lower in energy which suggests that a single electron transfer pathway is more probable than the closed-shell route. In either case, the low barriers to fluorination directly at the ligand show significant contrast to those observed *via* a fluoride intermediate and therefore support the proposal of direct ligand fluorination by an outer-sphere mechanism.

In conclusion, the work in this chapter has contributed to the identification of an unprecedented fluorination mechanism termed outer-sphere electrophilic fluorination. Mechanistic studies suggest that the metallocyclic ligand is fluorinated directly with the absence of a fluoride intermediate. This could prove to be a significant addition to the 'toolbox' of fluorination techniques, as carbon-fluorine bonds can be formed with complete regio- and stereoselectivity and under mild conditions.

Future work in this area should attend to the application of this methodology on a wider range of susceptible substrates and metal complexes in order to prepare new carbon-fluorine bonds within the coordination sphere of organometallic complexes. These may prove to be complementary to the carbon-fluorine bonds that are currently attainable using existing fluorination procedures, therefore ultimately allowing the formation of novel fluorinated organic molecules on liberation of the ligands from the metal centre. Due to the relevance of carbon-fluorine bonds in pharmaceutical and agrochemical products, these molecules may have significant applications. Detailed mechanistic work is also required in order to support or disprove the proposed mechanism.

There are many variables that may be modified in order to assess the generality and scope of the outer-sphere electrophilic fluorination mechanism. The general structures which may be susceptible to electrophilic fluorination *via* outer-sphere electrophilic fluorination are highlighted in Figure 6.1, complexes **6-a** to **6-d**. The reactivity reported in this Chapter is based on complex **6-a**, and the work in Chapter 5 is based on an extension of the methodology for complexes such as **6-b**.

metal vinyl complex, **6-a**   metal acetylide complex, **6-b**   metal aryl complexes, **6-c** and **6-d**
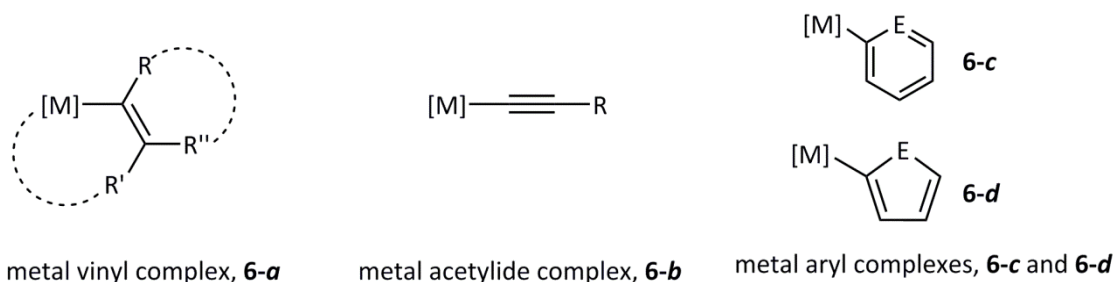
Figure 6.1 General structures of metal complexes which may be susceptible to outer-sphere electrophilic fluorination (R, R' and R'' = H, alkyl-, aryl- or heteroatom-containing functional groups)

The metal centre should be capable of back donation to the ligand, in order to support the vinyl or acetylide moiety pre- and post- fluorination, or it may be redox active in order to stabilise a formal oxidation state change from M^n to $M^{(n+2)}$. Potential metals that fit these criteria include rhenium, iron, osmium, rhodium, palladium, platinum and iridium. The ancillary ligands may also be modified in order to optimise the properties of the complex. The use of an alternative capping ligand which can undergo ring-slipping, for example, an indenyl rather than cyclopentadienyl ligand, may broaden the range of reactions which can be performed at the metal centre. The complex may be an isolated species, such as a stable metal acetylide complex, or be transient and formed during a stoichiometric or catalytic reaction pathway.

The methodology may be suitable for a range of vinyl, acetylide and aryl substrates. Substrates that may be used to form appropriate vinyl complexes are shown in Figure 6.2 (top), and potential aryl complexes are shown in Figure 6.2 (lower).
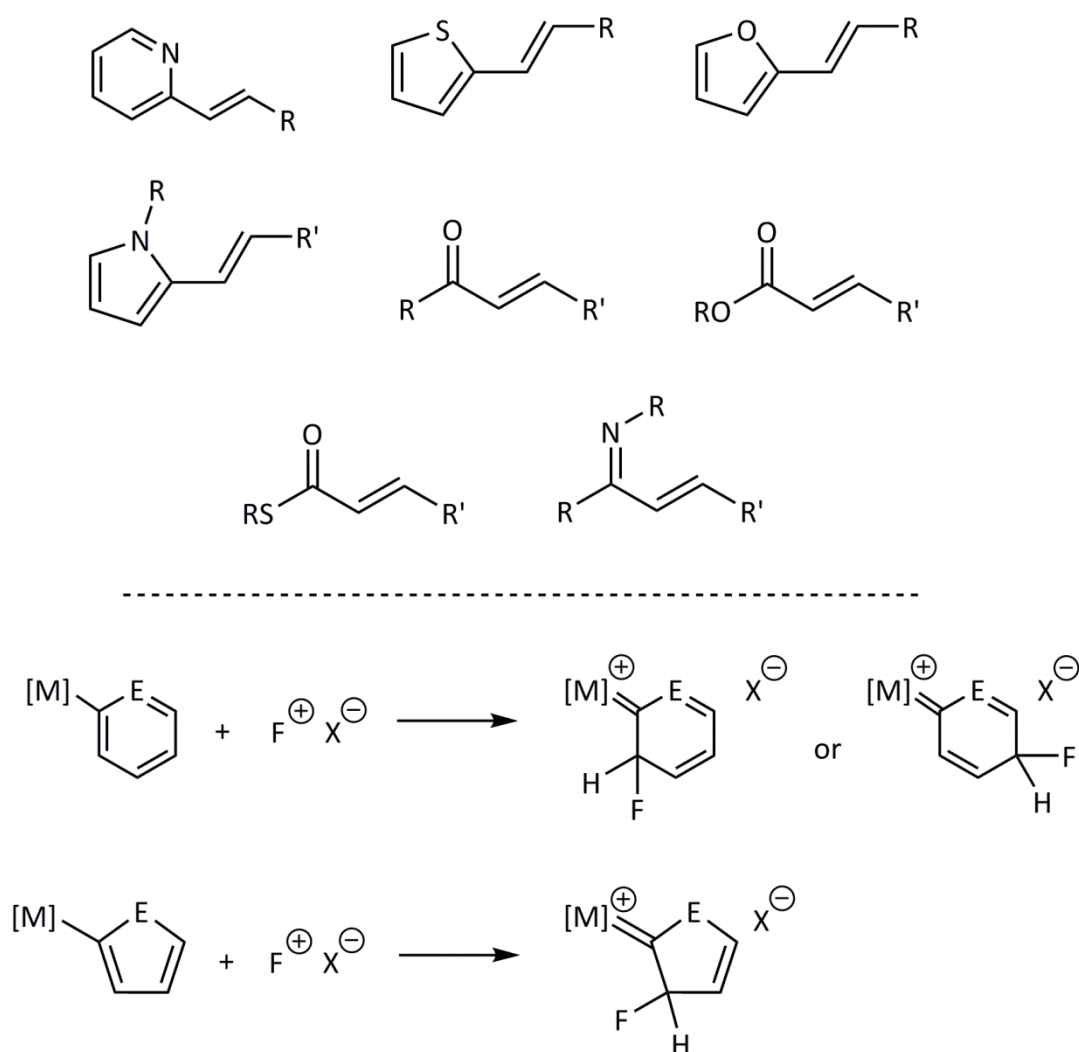
Figure 6.2 Substrates that may be susceptible to electrophilic fluorination (R. R' = H, alkyl-, aryl- or heteroatom-containing functional groups)

By formation of a vinyl ligand at the metal, the complex may undergo similar chemistry to that observed for **[16^CF3]**, which is a cyclic vinyl complex.

A further major area of investigation needed is to obtain experimental evidence in order to support the computationally proposed mechanism. The calculations suggest that fluorination proceeds by a direct addition of fluorine to the ligand in the absence of a fluoride intermediate, and that this transformation most likely occurs by a radical-mediated process. These ideas could be investigated by performing the reaction in an EPR spectrometer at low temperature (in order to observe any radical intermediates) or by using radical trapping agents in order to capture the radicals before further reaction. These methods in some cases can also help to identify the position on which the radical was localised. However, if the

radicals are very short-lived species or the radical recombination is rapid (within the solvent cage) it is unlikely that any intermediates would be observed.

6.5 Synthesis and reactivity of novel fluorovinylidene ligands (Chapter 5)

A range of ruthenium acetylide complexes were prepared as precursors for electrophilic fluorination, which subsequently allowed the formation of fluorinated vinylidene compounds. The synthesis represents the first application of the fluorination procedure reported in Chapter 4 as a methodology to efficiently prepare fluorinated vinylidene ligands *via* a rapid, facile and highly selective procedure, and the synthetic route was shown to be tolerant to a range of alkyne substituents, fluorinating agents and ancillary ligands. The incorporation of a trifluoromethyl substituent was possible using Umemoto's reagent and, serendipitously, the formation of a pyridyl-substituted vinylidene complex was also achieved. Vinylidene ligands are widely recognised as key intermediates in a range of catalytic reaction mechanisms, and therefore the incorporation of fluorine into these structures may provide access to novel, fluorinated metal complexes or, more importantly, new fluorinated organic products which may demonstrate potential applications in pharmaceutical or agrochemical molecules.

In order to investigate the mechanism of formation for these complexes, the addition of **[FTMP][BF$_4$]** to ruthenium acetylide **[26^{Ph}]** was performed at low temperature and monitored by NMR spectroscopy. The ^{1}H, ^{19}F and ^{31}P{^{1}H} spectra did not indicate the presence of any intermediates. Notably, no evidence was obtained for the presence of ruthenium fluoride intermediates (typical ^{19}F chemical shifts between -200 and -450 ppm). These spectra suggest an outer-sphere electrophilic fluorination mechanism analogous to that observed in Chapter 4, in which the fluorine is delivered directly to the acetylide moiety in **[26^{Ph}]** to form the fluorovinylidene ligand.

The fluorovinylidene complexes were extensively characterised, notably by ^{13}C{^{1}H} NMR spectroscopy, single crystal X-ray diffraction and UV-visible spectroscopy. Due to the presence of the highly electron-withdrawing fluorine substituent, the ^{13}C{^{1}H} chemical shifts of the fluorovinylidene α- and β-carbon atoms resonated significantly downfield compared to protio-analogues. Single crystal X-ray diffraction of [Ru(η^5-C$_5$H$_5$)(PPh$_3$)$_2$(C=C{F}Ph)][PF$_6$], **[27^{Ph}]PF$_6$,** revealed two discrete conformational isomers in the solid state (one green, the

other orange) between which the main differences were observed to be the orientation of the vinylidene ligand with respect to the cyclopentadienyl group, and the geometry of the vinylidene moiety. The nature of this discrepancy was investigated by UV-visible spectroscopy in both the solution and solid state.

In order to investigate the electronic effects of varying the β-substituents of a vinylidene ligand, $[Ru]=C=C\{R\}R'$ ($[Ru] = [Ru(\eta^5-C_5H_5)(PPh_3)_2]^+$; R, R' = -H, -Cl, -Br, -I, -F, -CF$_3$, -C$_5$H$_4$N etc) , the electronic structures of a range of vinylidene complexes were studies by UV-visible spectroscopy and TD-DFT calculations. For each of the halogen-functionalised vinylidene complexes, the constitutions of the HOMO and LUMO were found to be very similar but with varying energies depending on the identity of the substituents.

The facile synthesis of the fluorovinylidene complexes allowed an exploration of their reactivity, and comparison of their behaviour with the protio-analogues. Fluorine incorporation did not affect the electrophilic nature of the vinylidene α-carbon and therefore reactivity was observed with fluoride, pyridine, water and triphenylphosphine. Dissolution in pyridine led to the formation of a novel pyridylidene complex formed by pyridine incorporation at the vinylidene α-carbon, C-H activation at the ortho position, incorporation of a second pyridine equivalent and formal loss of HF. The mechanism for this process was investigated by DFT calculations. As vinylidene complexes are also recognised as key intermediates in anti-Markovnikov terminal alkyne hydration (exemplified in Chapter 2), the reactivity of fluorovinylidene complexes with water was probed. Upon the addition of water in the presence of a chloride additive (as $N^nBu_4Cl.H_2O$), the surprising formation of an acyl fluoride complex was observed *via* isomerisation of an α-fluoroaldehyde intermediate.

The two key targets for the future development of this family of fluorovinylidene complexes are clear - the release of fluorinated organic molecules from the ruthenium centre, and the incorporation of fluorovinylidene complexes into a catalytic methodology. Early attempts to dissociate fluorinated fragments (by the addition of diethylamine, hydrochloric acid or heating in a coordinating solvent (acetonitrile)) have unfortunately proved unsuccessful. However, the reaction of fluorovinylidene complexes in chloride-assisted hydrolysis reactions both cleanly liberated an organic molecule and regenerated $[Ru(\eta^5-C_5H_5)(PPh_3)_2Cl]$ – the initial complex from which the fluorovinylidene family of complexes is formed. This indicates the potential of these complexes for catalytic applications. Furthermore, as noted in Section

5.2.3 of Chapter 5, the methodology can be applied to a range of ruthenium complexes including ruthenium half-sandwich complexes with both cyclopentadienyl and pentamethylcyclopentadienyl ligands and [*trans*-RuCl(C≡C{Ph})(dppe)$_2$], which is a promising indication that this fluorination technique may be compatible with a range of organometallic systems. Studies are on-going in the Lynam and Slattery groups in order to investigate the relevance and opportunities for these complexes in future catalytic processes.

Chapter 7

Experimental

7   Experimental

7.1   General considerations for experimental procedures

All experimental procedures were performed under an atmosphere of dinitrogen using standard Schlenk Line and Glove Box techniques. Dichloromethane, pentane, hexane and diethyl ether were purified with the aid of an Innovative Technologies anhydrous solvent engineering system or distilled over sodium (under argon) before use. Pyridine was Acros Organics "Extra Dry" which was stored and handled in a Glove Box. The CD_2Cl_2 and d_5-pyridine used for NMR experiments was dried over CaH_2 and degassed with three freeze-pump-thaw cycles, then used in the glovebox under a nitrogen atmosphere or directly transferred to NMR tubes fitted with PTFE Young's taps. [$RuCl_3.3H_2O$] was purchased from Precious Metals Online. [$Ru(\eta^5\text{-}C_5H_5)(NCMe)_3$]$PF_6$ was supplied by Sigma Aldrich and stored at -20 °C under a nitrogen atmosphere in the glovebox.

NMR spectra were acquired on either a AVIII 300 NB (Operating frequencies; ^{1}H 300.13 MHz, ^{13}C 75.46 MHz, ^{19}F 282.40 MHz), a Jeol ECS400 or ECX400 (Operating frequencies; ^{1}H 399.78 MHz, ^{13}C 100.53 MHz, ^{19}F 376.17 MHz, ^{31}P 162 MHz), a Bruker AVANCE 500 (Operating Frequencies; ^{1}H 500.23 MHz, ^{13}C 125.77 MHz, ^{19}F 470.68 MHz, ^{31}P 202.50 MHz) or a Bruker AVANCE 700 (Operating frequencies; ^{1}H 700.13 MHz, ^{31}P 283.46 MHz, ^{13}C 176.07 MHz). ^{31}P and ^{13}C spectra were recorded with proton decoupling. Assignments were completed with the aid of COSY, DEPT, NOESY, HSQC, HMBC, ^{19}F-^{13}C HMBC and ^{1}H-^{31}P HMQC experiments. NMR experiments were performed in 5 mm NMR tubes fitted with PTFE J. Young's taps typically using ca. 20 mg of the appropriate organometallic complex and 0.55 mL of the appropriate solvent. Mass spectrometry measurements were performed on a either a Bruker micrOTOF MS (ESI) or a Waters GCT Premier Acceleration TOF MS (LIFDI) instrument. IR spectra were acquired on either a Mattson Research Series or Thermo-Nicolet Avatar 370 FTIR spectrometer using CsCl solution cells. Elemental analyses were performed using an Exeter Analytical Inc. CE-440 analyser. Phenylacetylene was supplied by Acros Organics and 4-ethynyl-α,α,α-trifluorotoluene was supplied by Sigma-Aldrich. Both were used as supplied.

UV–visible absorption spectra were measured using an Agilent 8453 spectrometer. Diffuse reflectance spectra were recorded on an Ocean Optics HR2000+ High Resolution Spectrometer with DH-2000-BAL Deuterium/Helium light source (200-1100 nm). A R400-7-UV-Vis reflection probe was used to record diffuse reflectance spectra. Spectra were

recorded in Spectra Suite software using an integration time of 10 seconds, box car smoothing width of 30, and 10 scans to average. Low isolated yields are reported for some experiments, which are due to losses on glassware being more significant in these small scale reactions.

7.2 Complex synthesis and characterisation

7.2.1 Synthesis of [Ru(η^5-C$_5$H$_5$)(6-DPPAP)(3-DPICon)(NCMe)]PF$_6$, [1]PF$_6$
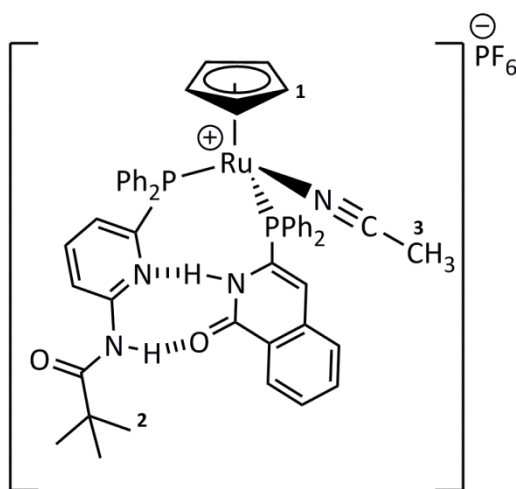
To an oven dried Schlenk tube was added [Ru(η^5-C$_5$H$_5$)(NCMe)$_3$]PF$_6$, **[2]PF$_6$** (100 mg, 230 µM) and 3-DPICon (76 mg, 230 µM, 1 equivalent) in dichloromethane (10 mL). The reaction mixture was allowed to stir for 4 hours before the addition of 6-DPPAP (83 mg, 230 µM, 1 equivalent). The reaction was stirred for a further 4 hours before removal of the solvent under vacuum to yield a yellow powdered solid.

Yield = 158 mg (66 %)

^{1}H NMR (CD$_2$Cl$_2$, 400 MHz, 295 K): δ 1.10 (s, 9H, H$_2$), 1.47 (s, 3H, H$_3$), 4.52 (s, 5H, H$_1$), 6.24 (dd, 1H, J = 7.3 Hz, 1.3 Hz), 6.89 (t, 1H, J = 2.3 Hz), 7.06 (dd, 1H, J = 7.6 Hz, 3.6 Hz), 7.15 (td, 2H, J = 8.0 Hz, 1.8 Hz), 7.22 – 7.38 (m, 10H), 7.42 – 7.57 (m, 11H), 7.63 – 7.76 (m, 2H), 7.82 (dd, 1H, J = 8.4 Hz, 1.8 Hz), 8.14 (d, 1H, J = 8.1 Hz), 10.53 (s, 1H), 12.67 (d, 1H, J = 4.6 Hz)

^{31}P{^{1}H} NMR (CD$_2$Cl$_2$, 162 MHz, 295 K): δ -143.0 (sept, $^1J_{PF}$ = 711 Hz, PF$_6^-$), 46.0 (d, $^2J_{PP}$ = 36.1 Hz), 54.2 (d, $^2J_{PP}$ = 36.1 Hz)

ESI-MS (*m/z*): Expected for C$_{50}$H$_{47}$N$_4$O$_2$P$_2{}^{101.9}$Ru = 899.2226; Observed: 899.2178 [M]$^+$, Error = 3.4 mDa

7.2.2 Characterisation data of [2]PF$_6$ (data taken from literature)[289]
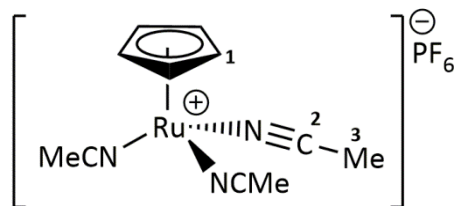
^{1}H NMR (CD$_2$Cl$_2$, 500 MHz, 295 K): δ 2.37 (s, 9H, H$_3$), 4.25 (s, 5H, H$_1$)

^{31}P{^{1}H} NMR (CD$_2$Cl$_2$, 202 MHz, 295 K): δ -143.0 (sept, $^1J_{PF}$ = 711 Hz, PF$_6^-$)

7.2.3 Synthesis of [Ru(η^5-C$_5$H$_5$)(6-DPPAP)$_2$]PF$_6$, [3]PF$_6$
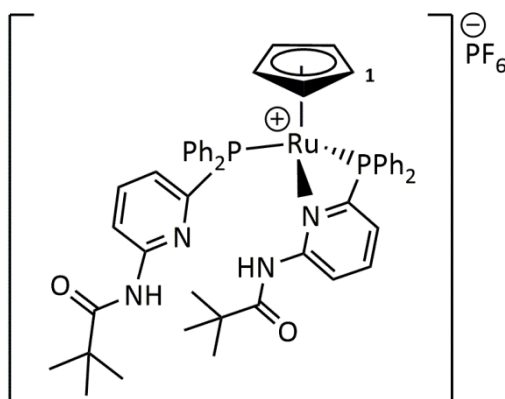
To an oven dried Schlenk tube was added [Ru(η^5-C$_5$H$_5$)(NCMe)$_3$]PF$_6$, **[2]PF$_6$** (100 mg, 230 µM) and 6-DPPAP (167 mg, 460 µM, 2 equivalents) in dichloromethane (10 mL). The reaction mixture was allowed to stir for 4 hours before removal of the solvent under vacuum to yield a yellow solid, which was washed in ether to remove traces of free phosphine.

Yield = 196 mg (82 %)

^{1}H NMR (CD$_2$Cl$_2$, 400 MHz, 295 K): δ 1.07 (s, 9H, *t*Bu), 1.31 (s, 9H, *t*Bu), 4.80 (s, 5H, H$_1$), 6.82 (ddd, 1H, *J* = 7.5 Hz, 4.3 Hz, 0.8 Hz), 7.12 (td, 3H, *J* = 7.8 Hz, 2.3 Hz), 7.16 – 7.29 (m, 4H), 7.30 – 7.51 (m, 15H), 7.66 (s, 1H), 7.78 (s, 1H), 7.88 (m, 1H), 7.99 (d, 1H, *J* = 7.8 Hz), 8.50 (d, 1H, *J* = 8.7 Hz)

^{31}P{^{1}H} NMR (CD$_2$Cl$_2$, 162 MHz, 295 K): δ -143.0 (sept, $^1J_{PF}$ = 711 Hz, PF$_6^-$), -16.6 (d, $^2J_{PP}$ = 36.6 Hz), 48.8 (br)

ESI-MS (*m/z*): Expected for C$_{59}$H$_{51}$N$_4$O$_2$P$_2$$^{101.9}$Ru = 891.2531; Observed: 891.2434 [M]$^+$, Error = 9.7 mDa

7.2.4 Synthesis of [Ru(η^5-C$_5$H$_5$)(3-DPICon)$_2$(NCMe)]PF$_6$, [4]PF$_6$

To an oven dried Schlenk tube was added [Ru(η^5-C$_5$H$_5$)(NCMe)$_3$]PF$_6$, **[2]PF$_6$** (100 mg, 230 μM) and 3-DPICon (152 mg, 460 μM, 2 equivalents) in dichloromethane (10 mL). The reaction mixture was allowed to stir for 4 hours before removal of the solvent under vacuum to yield a yellow solid, which was washed in ether to remove traces of free phosphine.

Yield = 177 mg (76 %)

^{1}H NMR (CD$_2$Cl$_2$, 400 MHz, 295 K): δ 1.59 (s, 3H, H$_2$), 4.56 (s, 5H, H$_1$), 6.63 (t, 2H, J = 2.9 Hz), 7.11 – 7.35 (14H, m), 7.38 – 7.51 (10H, m), 7.59 – 7.67 (m, 2H), 7.70 – 7.77 (m, 2H), 8.29 (d, 2H, J = 8.0 Hz)

^{31}P{^{1}H} NMR (CD$_2$Cl$_2$, 162 MHz, 295 K): δ -143.0 (sept, $^1J_{PF}$ = 711 Hz, PF$_6^-$), 50.4 (s)

ESI-MS (*m/z*): Expected for C$_{49}$H$_{40}$N$_3$O$_2$P$_2$$^{101.9}$Ru = 866.1634; Observed: 866.1600 [M]$^+$, Error = 3.4 mDa
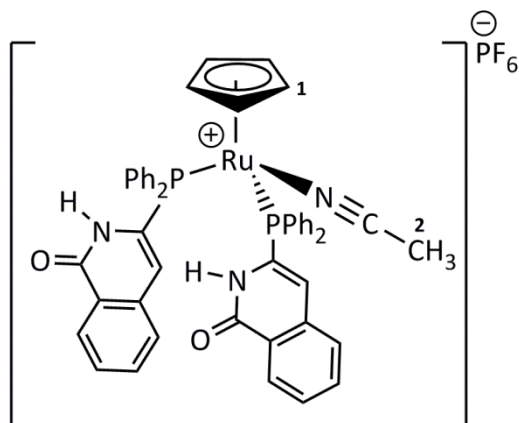
7.2.5 Synthesis of [5^{Ph}]PF$_6$
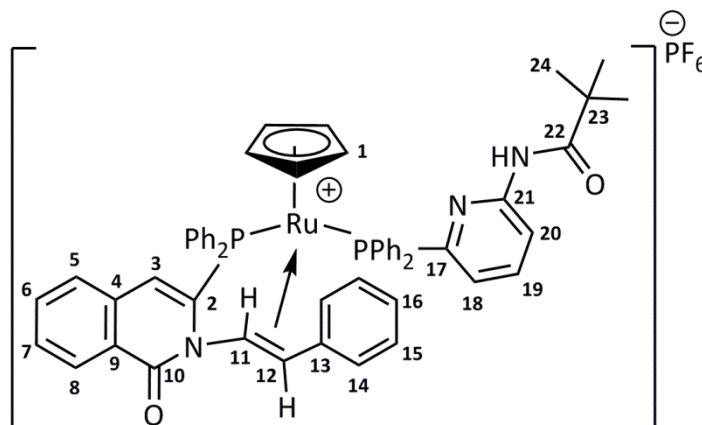
To a Young's NMR tube was added [Ru(η^5-C$_5$H$_5$)(NCMe)$_3$]PF$_6$, **[2]PF$_6$**, (20 mg, 46 μmol) and 3-DPICon (15 mg, 46 μmol, 1 equivalent) in deuterated dichloromethane (0.5 mL). After two hours, 6-DPPAP was added (16 mg, 46 μmol, 1 equivalent) and the reaction was heated at 50 °C for 20 hours (until [Ru(η^5-C$_5$H$_5$)(6-DPPAP)(3-DPICon)(NCMe)]PF$_6$ was the only product in the ^{31}P{^{1}H} NMR spectrum). Phenylacetylene was added (6.3 μL, 138 μmol, 3 equivalents) and the reaction heated at 50 °C for 1 week. 90 % conversion to **[5^{Ph}]PF$_6$** was observed by ^{31}P{^{1}H} NMR spectroscopy.

^{1}H NMR (CD$_2$Cl$_2$, 400 MHz, 295 K): δ 1.20 (s, 9H, H$_{24}$), 5.00 (s, 5H, H$_1$), 6.00 (br, 1H), 6.32 (br, 2H), 6.48 (d, 1H, J = 6.7 Hz), 6.53 (dd, 1H, J = 7.4, 3.5 Hz), 6.65 (br, 2H), 6.97 (dd, 1H J = 9.9, 3.2 Hz, H$_{12}$), 7.00 – 7.10 (m, 4H), 7.21 (m, 4H), 7.27 – 7.40 (m, 4H), 7.43 – 7.46 (d, 1H, J = 7.9 Hz), 7.46 – 7.50 (m, 3H), 7.50 – 7.55 (m, 2H), 7.55 – 7.61 (m, 3H), 7.64 – 7.80 (m, 6H), 8.31 (d, 1H, J = 7.8 Hz), 8.39 (d, 1H, J = 7.1 Hz)

^{13}C{^{1}H} NMR (CD$_2$Cl$_2$, 100 MHz, 295 K): δ 27.4 (s, C$_{24}$), 40.0 (s, C$_{23}$), 62.3 (s, C$_{11}$), 76.4 (d, J = 6.7 Hz, C$_{12}$), 93.2 (s, C$_1$), 110.9 (d, J = 2.9 Hz), 116.1 (s), 124.6 (d, J = 14.5 Hz), 126.0 (s), 127.5 (s), 128.1 (d, J = 8.0 Hz), 128.8 (d, J = 9.2 Hz), 129.1 (d, J = 10.2 Hz), 129.2 (d, J = 6.8 Hz), 130.1 (d, J = 10.9 Hz), 130.3 (d, J = 10.9 Hz), 131.3 (d, J = 2.2 Hz), 131.9 (d, J = 2.6 Hz), 132.3 (d, J = 2.3 Hz), 132.5 (s), 132.6 (d, J = 10.6 Hz), 133.2 (d, J = 11.5 Hz). 133.6 (d, J = 9.2 Hz), 133.7 (s), 134.4 (d, J = 19.6 Hz), 137.0 (d, J = 9.1 Hz), 139.7 (d, J = 5.9 Hz), 141.3 (s), 143.8 (d, $^1J_{CP}$ = 66.3 Hz, C$_{2/17}$), 153.5 (d, J = 18.9 Hz), 156.1 (d, $^1J_{CP}$ = 72.3 Hz, C$_{2/17}$), 163.9 (d, $^3J_{CP}$ = 9.9 Hz, C$_{10}$), 177.1 (s, C$_{22}$)

Residual resonances for free phenylacetylene and acetonitrile have been omitted.

$^{31}P\{^1H\}$ NMR (CD$_2$Cl$_2$, 162 MHz, 295 K): δ -143.0 (sept, $^1J_{PF}$ = 711 Hz, PF$_6^-$), 40.3 (br), 65.5 (d, $^2J_{PP}$ = 32.4 Hz)

ESI-MS (*m/z*): Expected for C$_{56}$H$_{50}$N$_3$O$_2$P$_2$$^{101.9}$Ru = 960.2431; Observed: 960.2372 [M]$^+$, Error = 4.1 mDa

7.2.6 Synthesis of [5^{CF3}]PF$_6$
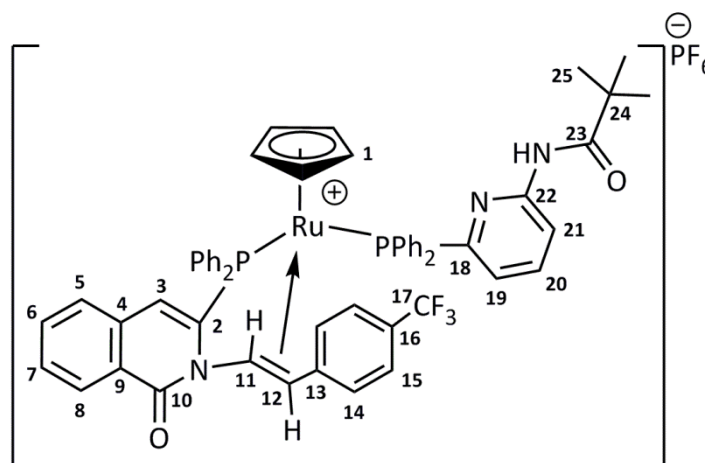
To a Young's NMR tube was added [Ru(η^5-C$_5$H$_5$)(NCMe)$_3$]PF$_6$, **[2]PF$_6$**, (20 mg, 46 μmol) and 3-DPICon (15 mg, 46 μmol, 1 equivalent) in deuterated dichloromethane (0.5 mL). After two hours, 6-DPPAP was added (16 mg, 46 μmol, 1 equivalent) and the reaction heated at 50 °C for 20 hours (until [Ru(η^5-C$_5$H$_5$)(6-DPPAP)(3-DPICon)(NCMe)]PF$_6$ was the only product in the $^{31}P\{^1H\}$ NMR). 4-Ethynyl-α,α,α-trifluorotoluene was added (9.3 μl, 138 μmol, 3 equivalents) and the reaction heated at 50 °C for 1 week. 90 % conversion to **[5^{CF3}]PF$_6$** was observed by $^{31}P\{^1H\}$ NMR spectroscopy. Yellow crystals of **[5^{CF3}]PF$_6$** suitable for single crystal X-ray diffraction were obtained by the slow diffusion of diethyl ether into a dichloromethane solution of the product.

^1H NMR (CD$_2$Cl$_2$, 700 MHz, 290 K): δ 1.17 (s, 9H, H$_{25}$), 4.73 (br, 1H, H$_{11}$), 5.05 (s, 5H, H$_1$), 5.96 (br, 1H), 6.25 (br, 2H), 6.47 (d, 1H, *J* = 6.7 Hz), 6.52 (br, 1H), 6.56–6.71 (br, 2H), 6.93 (br, d, 1H, *J* = 8.4 Hz, H$_{12}$), 6.96–7.12 (m, 4H), 7.18–7.32 (m, 3H), 7.44 (d, 2H, *J* = 7.7 Hz), 7.48–7.53 (br, 3H), 7.57–7.58 (m, 1H), 7.59–7.64 (m, 10H), 7.66 (br, 1H), 7.69–7.78 (m, 5H), 8.29 (d, 1H, *J* = 7.8 Hz), 8.38 (d, 1H, *J* = 6.6 Hz)

$^{13}C\{^1H\}$ NMR (176 MHz, 290 K): δ 26.9 (s, C$_{25}$), 39.6 (s, C$_{24}$), 58.5 (s, C$_{11}$), 76.4 (d, 5.9 Hz, C$_{12}$), 87.6 (s), 93.0 (s, C$_1$), 110.8 (s), 116.0 (s), 123.9 (q, $^1J_{CF}$ = 271 Hz, C$_{17}$), 124.4 (d, *J* = 14.4 Hz), 125.2 (q, $^3J_{CF}$ = 3.8 Hz, C$_{15}$), 125.5 (s, quat.), 125.9 (br, quat.), 127.2 (s), 127.7 (s), 128.5 (d, *J* =

9.2 Hz), 128.8 (d, J = 10.8 Hz), 129.2 (s), 129.8 (d, J = 11.2 Hz), 130.0 (d, J = 10.7 Hz), 130.3 (q, $^2J_{CF}$ = 32.6 Hz, C_{16}), 131.1 (s), 131.7 (s), 131.9 (br, quat.), 132.0 (br), 132.3 (d, J = 10.2 Hz), 132.5 (s), 132.8 (br), 133.2 (br), 133.5 (s), 136.6 (d, J = 8.6 Hz, quat.), 139.4 (br), 143.3 (d, J = 67.6 Hz, $C_{2/18}$), 145.8 (s, C_{22}), 155.9 (d, J = 71.2 Hz, $C_{2/18}$), 163.4 (d, J = 9.8 Hz, C_{10}), 176.8 (s, C_{23})

Residual resonances for free alkyne and acetonitrile have been omitted.

$^{31}P\{^1H\}$ NMR (CD_2Cl_2, 162 MHz, 295 K): δ −143.0 (sept, $^1J_{PF}$ = 711 Hz, PF_6^-), 39.5 (br), 65.1 (d, $^2J_{PP}$ = 31.4 Hz)

^{19}F NMR (CD_2Cl_2, 376 MHz, 295 K): δ −72.7 (PF_6^-), −63.2 (F_{17})

ESI-MS (m/z): Expected for $C_{57}H_{49}N_3O_2P_2{}^{101.9}Ru$ = 1028.2305; Observed: 1028.2245 $[M]^+$, Error = 4.5 mDa

7.2.7 Catalytic anti-Markovnikov hydration of phenylacetylene

To a Young's ampoule was added [Ru(η^5-C_5H_5)(6-DPPAP)(3-DPICon)(MeCN)]PF$_6$, **[1]PF$_6$**, (21 mg, 2 mol %), water (90 mg, 5 mmol), phenylacetylene (109.8 µl, 1 mmol) and deoxygenated acetone (1.6 mL). The ampoule was then sealed under nitrogen and heated under nitrogen for 26 hours at 120 °C. The solvent was removed under vacuum, and NMR spectra recorded.

The ^1H and $^{31}P\{^1H\}$ NMR spectra showed both the **[5^{Ph}]PF$_6$** (deactivation product) and the aldehyde after the reaction.

7.2.8 Catalytic testing of [5^{Ph}]PF$_6$

To a Young's NMR tube was added [Ru(η^5-C_5H_5)(6-DPPAP)(3-DPICon)(MeCN)]PF$_6$, **[1]PF$_6$**, (20 mg, 19 µmol) and phenylacetylene (2 µl, 19 µmol, 1 equivalent) in degassed acetone (1 mL). The reaction was heated at 120 °C for 6 hours until complete conversion to **[5^{Ph}]PF$_6$** was observed. A stoichiometric volume of water was added (0.3 µl, 19 µmol, 1 equivalent) and the reaction mixture heated at 120 °C for 20 hours, with monitoring by high resolution mass spectrometry.

After reaction, the NMR spectra and MS showed no trace of aldehyde.

7.2.9 Synthesis of [Ru(η⁵-C₅H₅)(triphenylphosphine)(NCMe)₂]PF₆, [6a]PF₆
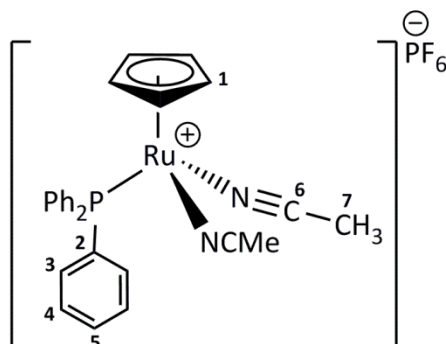
Complex **[6a]PF₆** was synthesised as reported in the literature.[289]

To a solution of [Ru(η⁵-C₅H₅)(NCMe)₃]PF₆, **[2]PF₆**, (96 mg, 0.22 mmol) and dichloromethane (10 mL) was added triphenylphosphine (56 mg, 0.21 mmol, 1 equivalent), and the yellow reaction mixture was stirred (3 hours). The solvent was removed under vacuum and a yellow product was collected.

Yield = 136 mg (96 %)

^{1}H NMR (CD₂Cl₂, 500 MHz, 295 K): δ 2.06 (d, 6H, $^5J_{HP}$ = 1.5 Hz, H₇), 4.44 (s, 5H, H₁), 7.28 – 7.31 (m, 6H, Ph), 7.42 – 7.50 (m, 9H, Ph)

^{31}P{^{1}H} NMR (CD₂Cl₂, 202 MHz, 295 K): δ -143.0 (sept, $^1J_{PF}$ = 711 Hz, PF₆⁻), 52.2 (s, **P**Ph₃)

^{13}C{^{1}H} NMR (CD₂Cl₂, 125 MHz, 295 K): δ 3.97 (s, C₇), 77.3 (d, $^3J_{CP}$ = 2.0 Hz, C₁), 127.5 (C₆), 128.9 (d, $^3J_{CP}$ = 9.9 Hz, C₄), 130.7 (d, $^4J_{CP}$ = 2.3 Hz, C₅), 133.8 (d, $^2J_{CP}$ = 11.1 Hz, C₃), 133.9 (d, $^1J_{CP}$ = 42.5, C₂)

7.2.10 Synthesis of [Ru(η⁵-C₅H₅)(2-(1,1-dimethylpropyl)-6-(diphenylphosphino)-pyridine)(NCMe)₂]PF₆, [6b]PF₆

$7.2.10$ Synthesis of $[Ru(\eta^5\text{-}C_5H_5)(2\text{-}(1,1\text{-dimethylpropyl})\text{-}6\text{-}(diphenylphosphino)\text{-}pyridine)(NCMe)_2]PF_6$, **[6b]PF₆**
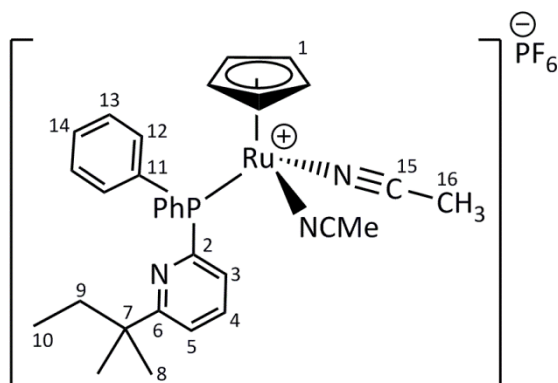
To an oven-dried Schlenk tube was added $[Ru(\eta^5\text{-}C_5H_5)(NCMe)_3]PF_6$, **[2]PF₆** (100 mg, 0.23 mmol), and dichloromethane (10 mL). 2-(1,1-dimethylpropyl)-6-(diphenylphosphino)-pyridine, **b** (77 mg, 0.23 mmol, 1 equivalent) was added dropwise with rapid stirring as a dilute solution in dichloromethane (5 mL) and the reaction mixture stirred for 18 hours. The air sensitive product was dried under vacuum. The excess solvent was removed by filtration and the yellow air-sensitive powder dried under vacuum. Yellow crystals suitable for X-ray diffraction were grown by the slow diffusion of pentane into a dichloromethane solution of the product.

Yield = 162 mg (95 %)

^{1}H NMR (CD₂Cl₂, 400 MHz, 295 K): δ 0.64 (t, 3H, $^3J_{HH}$ = 7.4 Hz, H₁₀), 1.27 (s, 6H, H₈), 1.67 (q, 2H, $^3J_{HH}$ = 7.4 Hz, H₉), 2.08 (d, 6H, $^5J_{HP}$ = 1.3 Hz, H₁₆), 4.43 (s, 5H, H₁), 6.99 (dd, 1H, $^3J_{HH}$ = 7.8 Hz, $^3J_{HP}$ = 3.8 Hz, H₃), 7.31 (dd, 1H, $^3J_{HH}$ = 7.8 Hz, $^5J_{HP}$ = 2.5 Hz, H₅), 7.37 − 7.51 (m, 10H, H₁₂, H₁₃, H₁₄), 7.62 (app. dt, 1H, $^3J_{H3H4}$ = $^3J_{H4H5}$ = 7.8 Hz, $^4J_{HP}$ = 3.8 Hz, H₄)

^{13}C{^{1}H} NMR (CD₂Cl₂, 100 MHz, 295 K): δ 4.1 (s, C₁₆), 9.4 (s, C₁₀), 27.4 (s, C₈), 36.0 (s, C₉), 41.5 (s, C₇), 77.1 (s, C₁), 120.6 (s, C₅), 125.3 (d, $^2J_{CP}$= 22.2 Hz, C₃), 127.3 (s, C₁₅), 128.7 (d, J_{CP} = 9.7 Hz, C₁₂/₁₃), 130.7 (s, C₁₄), 133.9 (d, $^1J_{CP}$ = 42.7 Hz, C₁₁), 134.3 (d, J_{CP} = 11.0 Hz, C₁₂/₁₃), 136.4 (d, $^3J_{CP}$ = 7.2 Hz, C₄), 158.3 (d, $^1J_{CP}$ = 68.0 Hz, C₂), 168.9 (s, C₆)

^{31}P{^{1}H} NMR (CD₂Cl₂, 162 MHz, 295 K): δ -143.0 (sept, $^1J_{PF}$ = 710 Hz, PF₆⁻), 51.4 (s, **P**Ph₂R)

Elemental Analysis: C₃₂H₃₉F₆N₃P₂Ru Calc. / % C 51.24, H 4.85, N 5.78, Found / % C 51.18, H 4.82, N 5.64

IR (CsCl, solution in DCM): 2279 cm^{-1}, 2361 cm^{-1} v(C≡N)

ESI-MS was unsuccessful for this compound, possibly due to the air sensitive nature of **[6b]PF$_6$**.

7.2.11 Synthesis of [Ru(η^5-C$_5$H$_5$)(diphenyl-2-pyridylphosphine)(NCMe)$_2$]PF$_6$, [6c]PF$_6$, and [Ru(η^5-C$_5$H$_5$)(diphenyl-2-pyridylphosphine)(NCMe)]PF$_6$, [9c]PF$_6$

[6c]PF$_6$ **[9c]PF$_6$**

To an oven-dried Schlenk tube was added [Ru(η^5-C$_5$H$_5$)(NCMe)$_3$]PF$_6$, **[2]PF$_6$** (100 mg, 0.23 mmol), and dichloromethane (10 mL). Diphenyl-2-pyridylphosphine, **c** (61 mg, 0.23 mmol, 1 equivalent) was added dropwise with rapid stirring, as a dilute solution in dichloromethane (5 mL) and the reaction mixture stirred for 16 hours. The yellow air sensitive powder was dried under vacuum, to yield a mixture of **[6c]PF$_6$** and **[9c]PF$_6$**, in a ratio of 45:55 (calculated by ^{31}P{^{1}H} NMR spectroscopy). The mixture can be converted to 100 % **[9c]PF$_6$** by the repeated addition of dichloromethane (~2 mL) and solvent removal under vacuum.

Yield (of **[6c]PF$_6$** and **[9c]PF$_6$**) = 153 mg (95 %)

[6c]PF$_6$

Selected ^{1}H NMR (CD$_2$Cl$_2$, 400 MHz, 295 K): δ 2.08 (d, 6H, $^5J_{HP}$ = 1.3 Hz, H$_{12}$), 4.46 (s, 5H, H$_1$), 7.19 (m, 1H, H$_3$), 8.77 (m, 1H, H$_6$)

^{31}P{^{1}H} NMR (CD$_2$Cl$_2$, 162 MHz, 295 K): δ -143.0 (sept, $^1J_{PF}$ = 710 Hz, PF$_6^-$), 52.3 (s, **P**Ph$_2$R)

[9c]PF$_6$
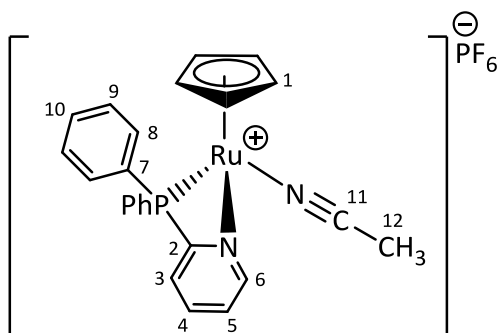
^{1}H NMR (CD$_2$Cl$_2$, 500 MHz, 295 K): δ 2.02 (d, 3H, $^5J_{HP}$ = 1.9 Hz, H$_{12}$), 4.54 (s, 5H, H$_1$), 7.29 (dddd, 1H, $^3J_{HH}$ = 7.8 Hz, $^3J_{HP}$ = 3.8 Hz, $^4J_{HH}$ = 1.4 Hz, $^5J_{HH}$ = 1.0 Hz, H$_3$), 7.40 – 7.72 (m, 11H, H$_5$, P**Ph$_2$**), 7.88 (app. tdd, 1H, $^3J_{H3H4}$ =$^3J_{H4H5}$ = 7.8 Hz, $^4J_{HP}$ = 1.9 Hz, $^4J_{HH}$ = 1.4 Hz, H$_4$), 8.65 (m, 1H, H$_6$)

^{13}C{^{1}H} NMR (CD$_2$Cl$_2$, 125 MHz, 295 K): δ 4.2 (s, C$_{12}$), 73.4 (s, C$_1$), 126.6 (d, J = 35.3 Hz), 127.6 (s, C$_{11}$), 128.0 (d, $^2J_{CP}$= 1.8 Hz, C$_3$), 128.5 (d, $^4J_{CP}$ = 3.1 Hz, C$_5$), 128.9 (d, J = 10.0 Hz), 129.6 (d, J = 10.6 Hz), 131.3 (d, J = 48.5 Hz), 133.9 (d, J = 12.9 Hz), 134.3 (d, J = 11.3 Hz), 137.8 (d, $^3J_{CP}$ = 3.3 Hz, C$_4$), 155.7 (d, $^3J_{CP}$ = 18.5 Hz, C$_6$), 171.0 (d, $^1J_{CP}$ = 49.9 Hz, C$_2$)

^{31}P{^{1}H} NMR (CD$_2$Cl$_2$, 202 MHz, 295 K): δ -143.0 (sept, $^1J_{PF}$ = 710 Hz, PF$_6^-$), 1.6 (s, **P**Ph$_2$R)

ESI-MS was unsuccessful for these compounds, possibly due to their air sensitive nature.

7.2.12 Synthesis of [Ru(η^5-C$_5$H$_5$)(triphenylphosphine)(NC$_5$H$_5$)$_2$]PF$_6$, [7a]PF$_6$
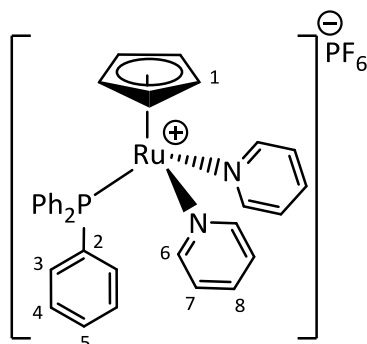
Complex **[7a]PF$_6$** was synthesised as reported in the literature.[289]

To an oven-dried Schlenk tube was added [Ru(η^5-C$_5$H$_5$)(triphenylphosphine)(NCMe)$_2$]PF$_6$, **[6a]PF$_6$** (100 mg, 0.15 mmol) and dichloromethane (10 mL). Pyridine (1.23 mL, 15 mmol, 100 equivalents) was added and the reaction mixture stirred for 18 hours. The reaction mixture was layered with either pentane or hexane to give orange crystals, suitable for X-ray diffraction. The excess solvent was removed by filtration and the air-sensitive product dried under vacuum.

Yield = 88 mg (82 %)

^{1}H NMR (CD$_2$Cl$_2$, 500 MHz, 295 K): δ 4.42 (s, 5H, H$_1$), 7.05 − 7.08 (m, 4H, H$_7$), 7.17 − 7.20 (m, 6H, H$_3$), 7.33 − 7.36 (m, 6H, H$_4$), 7.42 − 7.46 (m, 3H, H$_5$), 7.70 (tt, 2H, $^3J_{HH}$ = 7.6 Hz, $^4J_{HH}$ = 1.5 Hz, H$_8$), 8.29 (m, 4H, H$_6$)

^{31}P{^{1}H} NMR (CD$_2$Cl$_2$, 202 MHz, 295 K): δ -143.0 (sept, $^1J_{PF}$ = 710 Hz, PF$_6^-$), 50.3 (s, **P**Ph$_3$)

^{13}C{^{1}H} NMR (CD$_2$Cl$_2$, 176 MHz, 295 K): δ 78.2 (d, $^2J_{CP}$ = 2.2 Hz, C$_1$), 125.6 (s, C$_7$), 129.1 (d, $^3J_{CP}$ = 9.5 Hz, C$_4$), 130.7 (d, $^4J_{CP}$ = 1.7 Hz, C$_5$), 133.7 (d, $^2J_{CP}$ = 10.9 Hz, C$_3$), 134.2 (d, $^1J_{CP}$ = 39.9 Hz, C$_2$), 137.4 (s, C$_8$), 156.7 (d, $^3J_{CP}$ = 2.5 Hz, C$_6$)

7.2.13 Synthesis of [Ru(η⁵-C₅H₅)(2-(1,1-dimethylpropyl)-6-(diphenylphosphino)-pyridine)(NC₅H₅)₂]PF₆, [7b]PF₆
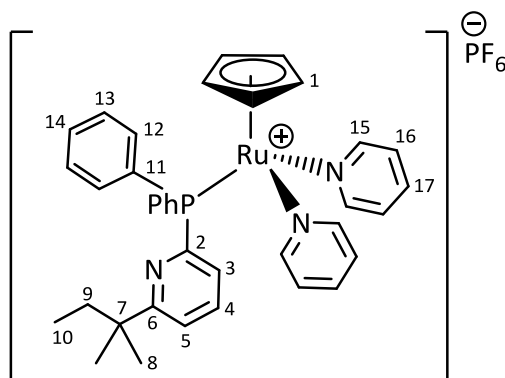
To an oven-dried Schlenk tube was added [Ru(η⁵-C₅H₅)(2-(1,1-dimethylpropyl)-6-(diphenylphosphino)-pyridine)(NCMe)₂]PF₆, **[6b]PF₆** (100 mg, 0.14 mmol) and dichloromethane (10 mL). Pyridine (1.10 mL, 14 mmol, 100 equivalents) was added and the reaction mixture stirred for 18 hours. The solvent was reduced under vacuum, and slow diffusion of pentane into the reaction mixture afforded red crystals of the product, suitable for X-ray diffraction. The excess solvent was removed by filtration and the air-sensitive product dried under vacuum.

Yield = 86 mg (78 %)

^{1}H NMR (CD$_2$Cl$_2$, 700 MHz, 295 K): δ 0.57 (t, 3H, $^{3}J_{HH}$ = 7.9 Hz, H$_{10}$), 1.00 (s, 6H, H$_8$), 1.47 (q, 2H, $^{3}J_{HH}$ = 7.49 Hz, H$_9$), 4.37 (s, 5H, H$_1$), 6.96 (m, 1H, H$_3$), 7.00 (m, 4H, H$_{16}$), 7.26 (m, 5H, H$_{12/13}$, H$_5$), 7.34 (m, 4H, H$_{12/13}$), 7.42 (m, 2H, H$_{14}$), 7.54 (td, 1H, $^{3}J_{HH}$ = 7.8 Hz, $^{4}J_{HP}$ = 3.0 Hz, H$_4$), 7.61 (tt, 2H, $^{3}J_{HH}$ = 7.6 Hz, $^{4}J_{HH}$ = 1.5 Hz, H$_{17}$), 8.55 (m, 4H, H$_{15}$)

^{13}C{^{1}H} NMR (CD$_2$Cl$_2$, 176 MHz, 295 K): δ 9.2 (s, C$_{10}$), 27.2 (s, C$_8$), 35.9 (s, C$_9$), 41.4 (s, C$_7$), 78.2 (d, $^{3}J_{CP}$ = 2.3 Hz, C$_1$), 121.0 (d, $^{4}J_{CP}$ = 1.8 Hz, C$_5$), 125.4 (s, C$_{16}$), 126.5 (d, $^{2}J_{CP}$ = 15.4 Hz, C$_3$), 128.8 (d, J_{CP} = 9.6 Hz, C$_{12/13}$), 130.6 (d, $^{4}J_{CP}$ = 2.1 Hz, C$_{14}$), 134.3 (d, $^{1}J_{CP}$ = 41.2 Hz, C$_{11}$), 134.3 (d, J_{CP} = 11.0 Hz, C$_{12/13}$), 136.8 (d, $^{3}J_{CP}$ = 5.6 Hz, C$_4$), 137.0 (s, C$_{17}$), 157.5 (d, $^{3}J_{CP}$ = 2.6 Hz, C$_{15}$), 157.7 (d, $^{1}J_{CP}$ = 57.4 Hz, C$_2$), 169.7 (d, $^{3}J_{CP}$ = 14.7, C$_6$)

^{31}P{^{1}H} NMR (CD$_2$Cl$_2$, 162 MHz, 295 K): δ -143.0 (sept, $^{1}J_{PF}$ = 710 Hz, PF$_6^-$), 52.2 (s, **P**Ph$_2$R)

ESI-MS (*m/z*): Expected for C$_{37}$H$_{39}$N$_3$P$^{101.9}$Ru = 658.1920; Observed: 658.1913 [M]$^{+}$ (Error = 0.7 mDa). Expected for C$_{32}$H$_{34}$N$_2$P$^{101.9}$Ru = 579.1498; Observed: 579.1505 [M -NC$_5$H$_5$]$^{+}$ (Error = 0.7

mDa). Expected for $C_{27}H_{29}NP^{101.9}Ru$ = 500.1076; Observed: 500.1090 [M - 2(NC$_5$H$_5$)]$^+$ (Error = 0.6 mDa)

Elemental Analysis: $C_{37}H_{39}F_6N_3P_2Ru$ Calc. / % C 55.36, H 4.90, N 5.23, Found / % C 55.04, H 4.78, N 5.10

7.2.14 Synthesis of [Ru(η^5-C$_5$H$_5$)(diphenyl-2-pyridylphosphine)(NC$_5$H$_5$)$_2$]PF$_6$, [7c]PF$_6$, and [Ru(η^5-C$_5$H$_5$)(diphenyl-2-pyridylphosphine)(NC$_5$H$_5$)$_2$]PF$_6$, [10c]PF$_6$

[7c]PF$_6$ **[10c]PF$_6$**
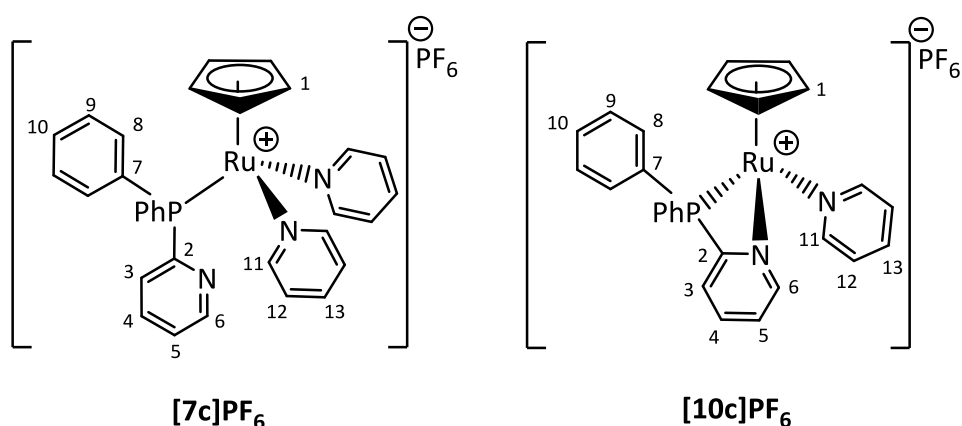
To an oven-dried Schlenk tube was added [Ru(η^5-C$_5$H$_5$)(diphenyl-2-pyridylphosphine)(NCMe)$_2$]PF$_6$, **[6c]PF$_6$,** [Ru(η^5-C$_5$H$_5$)(diphenyl-2-pyridylphosphine)(NCMe)]PF$_6$, **[9c]PF$_6$** (100 mg) and dichloromethane (10 mL). Pyridine (1.85 mL) was added and the reaction mixture stirred for 18 hours. The solvent was reduced under vacuum, and slow diffusion of pentane into the reaction mixture afforded orange crystals of the products, which were a mixture of [Ru(η^5-C$_5$H$_5$)(diphenyl-2-pyridylphosphine)(NC$_5$H$_5$)$_2$]PF$_6$, **[7c]PF$_6$,** and [Ru(η^5-C$_5$H$_5$)(diphenyl-2-pyridylphosphine)(NC$_5$H$_5$)]PF$_6$, **[10c]PF$_6$**. The excess solvent was removed by filtration and the air-sensitive product dried under vacuum.

Yield = 102 mg

Crystals of **[7c]PF$_6$** suitable for X-ray diffraction were grown by the slow diffusion of pentane into a dichloromethane/pyridine solution of the products.

^{1}H NMR (CD$_2$Cl$_2$, 400 MHz, 295 K): δ 4.37 (s, 7H), 4.58 (s, 4H), 6.88 - 7.00 (m, 11H), 7.10 - 7.31 (m, 15H), 7.31 – 7.37 (m, 8H), 7.38 – 7.46 (m, 13H), 7.50 – 7.79 (m, 13H), 7.82 – 7.95 (m, 1H),

8.27 – 8.30 (m, 2H, **[10c]PF$_6$ – H$_{11}$**), 8.35 – 8.39 (m, 1H), 8.52 (d, 6H, $^2J_{HH}$ = 5.1 Hz), 8.58 (d, 2H, $^3J_{HH}$ = 4.1 Hz, free pyridine), 8.92 (d, 1H, $^2J_{HH}$ = 5.1 Hz, **[10c]PF$_6$ - H$_6$**)

^{31}P{^{1}H} NMR (CD$_2$Cl$_2$, 162 MHz, 295 K): δ -143.0 (sept, $^1J_{PF}$ = 710 Hz, PF$_6^-$), 2.8 (s, **[10c]PF$_6$ - P**Ph$_2$R), 52.0 (s, **[7c]PF$_6$ -P**Ph$_2$R)

ESI-MS was unsuccessful for these compounds, possibly due to their air sensitive nature.

7.2.15 Synthesis of [Ru(η^5-C$_5$H$_5$)(2-(1,1-dimethylpropyl)-6-(diphenylphosphino)-pyridine)(NC$_6$H$_7$)(NCMe)]PF$_6$, [8b]PF$_6$
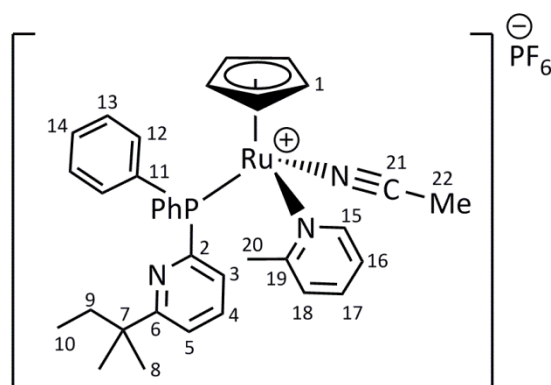
To an oven-dried Schlenk tube was added [Ru(η^5-C$_5$H$_5$)(2-(1,1-dimethylpropyl)-6-(diphenylphosphino)-pyridine)(NCMe)$_2$]PF$_6$, **[6b]PF$_6$** (20 mg, 0.03 mmol) and deuterated dichloromethane (0.5 mL). 2-methylpyridine (272 μL, 3 mmol, 100 equivalents) was added and the reaction mixture stirred for 18 hours. Slow diffusion of pentane into the reaction mixture afforded red crystals of the product, suitable for X-ray diffraction.

^{1}H NMR (CD$_2$Cl$_2$, 400 MHz, 295 K): δ 0.74 (t, 3H, $^3J_{HH}$ = 7.4 Hz, H$_{10}$), 1.34 (s, 3H, H$_8$), 1.36 (s, 3H, H$_8$), 1.77 (m, 2H, H$_9$), 1.96 (d, 3H, $^5J_{HH}$ = 1.7 Hz, H$_{22}$), 2.76 (s, 3H, H$_{20}$), 4.41 (s, 5H, H$_1$), 6.57 – 7.65 (m, 16H), 9.28 (d, 1H, $^3J_{HH}$ = 5.5 Hz, H$_{15}$)

^{31}P{^{1}H} NMR (CD$_2$Cl$_2$, 162 MHz, 295 K): δ -143.0 (sept, $^1J_{PF}$ = 710 Hz, PF$_6^-$), 52.8 (s, **P**Ph$_2$R)

ESI-MS was unsuccessful for this compound, possibly due to the air sensitive nature of **[8b]PF$_6$**.

7.2.16 Synthesis of [Ru(η^5-C$_5$H$_5$) (2-(1,1-dimethylpropyl)-6-(diphenylphosphino)-pyridine)(phenylacetylene)$_2$]PF$_6$, [12b^{Ph}]PF$_6$
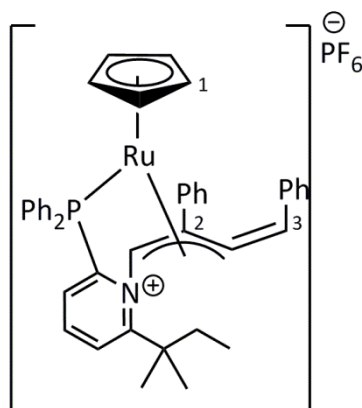
To an oven-dried Young's ampoule was added [Ru(η^5-C$_5$H$_5$)(2-(1,1-dimethylpropyl)-6-(diphenylphosphino)-pyridine)(NC$_5$H$_5$)$_2$]PF$_6$, **[7b]PF$_6$** (121 mg, 0.15 mmol) and phenylacetylene (16.6 µL, 0.15 mmol, 1 equivalent). The reaction mixture was heated at 50 °C for 3 hours and allowed to cool. A second equivalent of phenylacetylene was added (16.6 µL, 0.15 mmol), and the reaction mixture heated again to 50 °C for 3 hours.

Yellow crystals suitable for X-ray diffraction were grown by the slow diffusion of pentane into a dichloromethane/pyridine solution of the product. However, the product was very difficult to purify *via* either crystallisation or washing with pentane or ether. Therefore, selected NMR data is presented.

^{1}H NMR (CD$_2$Cl$_2$, 500 MHz, 295 K): δ 4.93 (s, 5H, H$_1$)

Selected ^{13}C{^{1}H} NMR (CD$_2$Cl$_2$, 125 MHz, 295 K): δ 86.9 (d, $^2J_{PF}$ = 7.2 Hz, C$_2$), 154.4 (d, $^2J_{PF}$ = 14.7 Hz, C$_3$)

^{31}P{^{1}H} NMR (with ^{13}C-labelled phenylacetylene, CD$_2$Cl$_2$, 162 MHz, 298 K): δ -143.0 (sept, $^1J_{PF}$ = 710 Hz, PF$_6^-$), 86.0 (dd, $^2J_{CP}$ = 14.7 Hz, $^2J_{CP}$ = 7.2 Hz, **P**Ph$_2$R)

ESI-MS (*m/z*): Expected for C$_{41}$^{13}C$_2$H$_{41}$NP$^{101.9}$Ru = 706.2082; Observed: 706.2077 [M]$^+$ (Error = 0.5 mDa)

7.2.17 Synthesis of [Ru(η⁵-C₅H₅)(triphenylphosphine)(C₅H₄NCHCH(C₆H₄CF₃)]PF₆, [13^CF3]PF₆
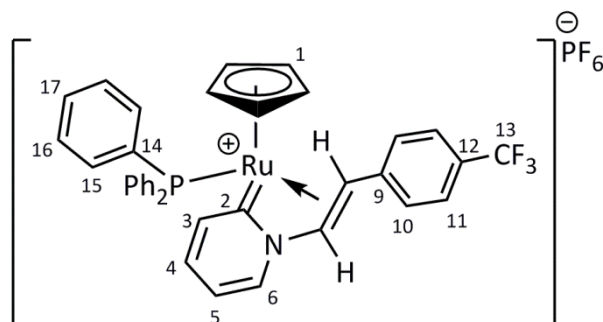
The synthesis was performed using a modified literature procedure.[45]

To an oven-dried ampoule was added [Ru(η⁵-C₅H₅)(PPh₃)(pyr)₂]PF₆, **[7]PF₆** (150 mg, 210 µmol), 4-ethynyl-α,α,α-trifluorotoluene (33 µl, 210 µmol, 1 equivalent) and pyridine (33 µL, 420 µmol, 2 equivalents) in dichloromethane (5mL). The reaction mixture was heated at 50 °C for 16 hours and allowed to cool. The solvent was removed and the brown solid product was washed with pentane (2 x 20 mL).

This product was not purified further and instead was reacted further to form **[16^CF3]** *in situ*. However, the literature reports that further purification is necessary to yield an analytically pure product by the slow diffusion of pentane into the reaction mixture to afford yellow crystals (which can be purified further *via* subsequent crystallisations).

^{31}P{^{1}H} NMR (CD₂Cl₂, 202 MHz, 295 K): -143.0 (sept, $^1J_{PF}$ = 711 Hz, PF₆⁻), 52.9 (s, **P**Ph₃)

7.2.18 Synthesis of [Ru(η^5-C$_5$H$_5$) (2-(1,1-dimethylpropyl)-6-(diphenylphosphino)-pyridine)(C$_5$H$_4$NCHCH(C$_6$H$_4$CF$_3$)]PF$_6$, [13b^{CF3}]PF$_6$
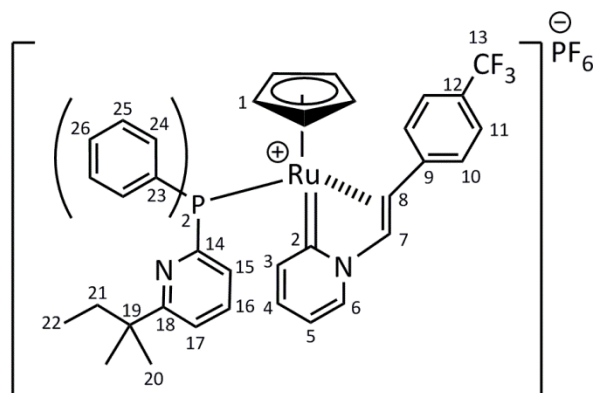
An NMR tube with a PTFE J. Young's tap was charged with [Ru(η^5-C$_5$H$_5$)(2-(1,1-dimethylpropyl)-6-(diphenylphosphino)-pyridine)(NC$_5$H$_5$)$_2$]PF$_6$, **[7b]PF$_6$** (20 mg, 0.025 mmol), deuterated dichloromethane (0.5 mL), 4-ethynyl-α,α,α-trifluorobenzene (4.1 μL, 0.025 mmol, 1 equivalent) and pyridine (4.0 μL, 0.050 mmol, 2 equivalents), and the reaction mixture was heated at 50 °C for 12 hours. Yellow crystals suitable for X-ray diffraction were grown by the slow diffusion of pentane into the reaction mixture.

^{1}H NMR (CD$_2$Cl$_2$, 500 MHz, 295 K): δ 0.52 (t, 3H, $^3J_{HH}$ = 6.5 Hz, H$_{22}$), 0.96 and 1.01 (br, 6H, H$_{20}$), 1.29 (m, 2H, H$_{21}$), 4.98 (s, 5H, H$_1$), 6.63 (br, 2H, H$_{10}$), 6.69 (dd, 1H, $^3J_{HH}$ = 7.7 Hz, $^3J_{HP}$ = 1.6 Hz, H$_7$), 6.80 – 6.95 (m, 4H), 7.08 – 7.62 (m, 16H), 7.82 (d, 1H, $^3J_{HH}$ = 6.1 Hz, H$_6$)

Selected ^{13}C{^{1}H} NMR (CD$_2$Cl$_2$, 125 MHz, 295 K): δ 9.3 (s, C$_{22}$), 27.3 and 27.7 (s, C$_{20}$), 36.3 (s, C$_{21}$), 41.6 (s, C$_{19}$), 55.5 (s, C$_8$), 88.4 (s, C$_1$), 118.0 (s, C$_5$), 121.7 (s, C$_{17}$), 124.7 (q, $^1J_{CF}$ = 271.1 Hz, C$_{13}$), 126.7 (d, $^2J_{CP}$ = 15.6 Hz, C$_{15}$), 127.8 (q, $^2J_{CF}$ = 32.2 Hz, C$_{12}$), 129.3 (q, $^3J_{CF}$ = 5.1 Hz, C$_{11}$), 137.9 (d, $^3J_{CP}$ = 3.4 Hz, C$_3$), 142.4 (s, C$_6$), 145.4 (s, C$_9$), 170.1 (d, $^3J_{CP}$ = 15.4 Hz, C$_{18}$), 180.8 (d, $^2J_{CP}$ = 20.8 Hz, C$_2$)

Due to the overlapping and complex signals of the ^{1}H NMR spectrum at 295 K, the signals in both the ^{1}H and ^{13}C spectra cannot be fully assigned.

^{1}H NMR (CD$_2$Cl$_2$, 700 MHz, 205 K): δ 0.36 (t, 3H, $^3J_{HH}$ = 7.2 Hz, H$_{22}$), 0.80 and 1.00 (br, 6H, H$_{20}$), 1.23 (m, 2H, H$_{21}$), 4.94 (s, 5H, H$_1$), 6.17 (m, 1H, H$_8$), 6.46 (br, 2H, H$_{10}$), 6.67 (d, 1H, $^3J_{HH}$ = 7.0 Hz, H$_7$), 6.80 (m, 3H, H$_5$, P**Ph$_2$**), 6.86 (m, 1H, H$_{15/16/17}$), 7.07 (m, 2H, H$_4$, H$_{15/16/17}$), 7.14 (d, 2H, $^3J_{HH}$ = 7.5 Hz, H$_{11}$), 7.22 (m, 5H, H$_3$, P**Ph$_2$**), 7.43 – 7.56 (m, 5H, H$_{15/16/17}$, PPh$_2$), 7.78 (br, 1H, H$_6$)

^{13}C{^{1}H} NMR (CD$_2$Cl$_2$, 176 MHz, 205 K): δ 8.8 (s, C$_{22}$), 26.6 and 27.1 (C$_{20}$), 36.0 (s, C$_{21}$), 40.9 (s, C$_{19}$), 54.5 (s, C$_7$), 55.9 (d, $^2J_{CP}$ = 3.9 Hz, C$_8$), 87.5 (s, C$_1$), 117.1 (s, C$_5$), 121.0 (s, C$_{15/16/17}$), 124.8 (s, C$_{11}$), 125.5 (s, C$_{10}$), 126.1 (s, C$_{15/16/17}$), 128.9 (d, $^1J_{CP}$ = 51.6 Hz, C$_{23}$), 132.4 (br, P**Ph**$_2$), 134.3 (br, P**Ph**$_2$), 135.7 (s, C$_4$), 136.9 (d, $^3J_{CP}$ = 2.6 Hz, C$_3$), 141.5 (s, C$_6$), 144.8 (s, C$_9$), 154.6 (d, $^1J_{CP}$ = 54.1 Hz, C$_{14}$), 168.7 (d, $^3J_{CP}$ = 14.3 Hz, C$_{18}$), 179.5 (d, $^2J_{CP}$ = 21.1 Hz, C$_2$)

Attempts to locate C$_{12}$ and C$_{13}$ using a range of NMR techniques were unsuccessful. There is also no definitive evidence in the NMR spectra to allow the full assignment of PPh$_2$ and C$_{15}$, C$_{16}$ or C$_{17}$.

^{19}F NMR (CD$_2$Cl$_2$, 376 MHz, 298 K): δ -73.0 (d, $^1J_{PF}$ = 710 Hz, PF$_6^-$), -62.7 (s, F$_{13}$)

^{31}P{^{1}H} NMR (CD$_2$Cl$_2$, 202 MHz, 298 K): δ -143.0 (sept, $^1J_{PF}$ = 710 Hz, PF$_6^-$), 52.0 (s, **P**Ph$_2$R)

ESI-MS (*m/z*): Expected for C$_{41}$H$_{39}$F$_3$N$_2$P$_2{}^{101.9}$Ru = 749.1846; Observed: 749.1818 [M]$^+$ (Error = 2.8mDa)

Elemental Analysis: C$_{41}$H$_{39}$F$_9$N$_2$P$_2$Ru: Calc. / % C 55.10, H 4.40, N 3.13, Found / % C 54.70, H 4.29, N 3.11

7.2.19 Characterisation of 14^{CF3} (data taken from literature)[79]
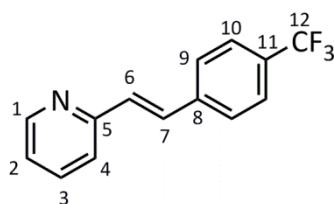
^{1}H NMR (CDCl$_3$, 400 MHz, 295 K): δ 7.19 (m, 1H, H$_2$), 7.24 (d, 1H, $^3J_{HH}$ = 16.3 Hz, H$_{6/7}$), 7.40 (d, 1H, $^3J_{HH}$ = 7.8 Hz, H$_4$), 7.73–7.59 (m, 6H, H$_3$, H$_{6/7}$, H$_9$, H$_{10}$), 8.63 (d, 1H, $^3J_{HH}$ = 4.7 Hz, H$_1$)

^{13}C{^{1}H} NMR (CDCl$_3$, 100 MHz, 295 K): δ 122.8 (s, C$_4$), 122.8 (s, C$_2$), 124.3 (q, $^1J_{CF}$ = 272.2 Hz, C$_{12}$), 125.8 (q, $^4J_{CF}$ = 3.9 Hz, C$_9$), 127.3 (s, C$_{6/7/10}$), 130.1 (q, $^2J_{CF}$ = 32.6, C$_{11}$), 130.3 (s, C$_{6/7}$), 131.3 (s, C$_{6/7/10}$), 136.9 (s, C$_3$), 140.2 (q, $^5J_{CF}$ = 1.6 Hz, C$_8$), 149.9 (s, C$_1$), 155.0 (s, C$_5$)

^{19}F NMR (CDCl$_3$, 376 MHz, 295 K): δ −62.4 (s, F$_{12}$)

7.2.20 Synthesis of [Ru(η^5-C$_5$H$_5$)(diphenyl-2-pyridylphosphine)(NC$_5$H$_5$)(C=CH(C$_6$H$_4$-4-CF$_3$))]PF$_6$, [15c^{CF3}]PF$_6$
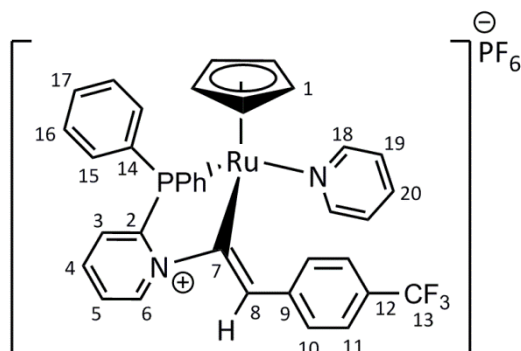
An NMR tube with a PTFE J. Young's tap was charged with [Ru(η^5-C$_5$H$_5$)(diphenyl-2-pyridylphosphine)(NC$_5$H$_5$)$_2$]PF$_6$, **[7c]PF$_6$** and [Ru(η^5-C$_5$H$_5$)(diphenyl-2-pyridylphosphine)(NC$_5$H$_5$)]PF$_6$, **[10c]PF$_6$** (15 mg), deuterated dichloromethane (0.5 mL), and 4-ethynyl-α,α,α-trifluorobenzene (3.5 μL, 0.021 mmol). An immediate colour change was observed on addition of alkyne, from yellow to green/brown. ^{31}P{^{1}H} NMR indicated complete conversion to the product within 18 hours.

Dark red crystals suitable for X-ray diffraction were grown by the slow diffusion of pentane into a dichloromethane/pyridine solution of the product.

^{1}H NMR (CD$_2$Cl$_2$, 500 MHz, 295 K): δ 4.62 (s, 5H, H$_1$), 6.47 (app. t, 2H, $^3J_{HH}$ = 7.04 Hz, H$_{19}$), 7.06 – 7.13 (m, 2H, P**Ph**$_2$), 7.13 – 7.25 (m, 5H, H$_{20}$, P**Ph**$_2$), 7.35 – 7.38 (d, 2H, $^3J_{HH}$ = 8.2 Hz, H$_{10/11}$), 7.43 – 7.51 (m, 4H, P**Ph**$_2$), 7.74 – 7.82 (m, 4H, H$_3$, H$_8$, H$_{10/11}$), 7.94 – 8.00 (m, 3H, H$_5$, H$_{18}$), 8.28 (app. t, 1H, $^3J_{HH}$ = 7.5 Hz, H$_4$), 9.61 (d, 1H, $^3J_{HH}$ = 6.3 Hz, H$_6$)

^{13}C{^{1}H} NMR (CD$_2$Cl$_2$, 125 MHz, 295 K): δ 82.3 (d, $^2J_{CP}$ = 2.1 Hz, C$_1$), 124.7 (q, $^1J_{CF}$ = 270.9 Hz, C$_{13}$), 124.6 (s, C$_{19}$), 124.8 (s, C$_{10/11}$), 128.3 (s, C$_5$), 128.4 (q, $^2J_{CF}$ = 32.2 Hz, C$_{12}$), 128.9 (s, C$_{10/11}$), 129.5 (m, C$_{15/16/17}$), 131.5 (d, $^2J_{CP}$ = 4.6 Hz, C$_3$), 132.6 (d, J_{CP} = 11.2 Hz, C$_{15/16/17}$), 132.8 (s, C$_{15/16/17}$), 135.6 (s, C$_{20}$), 135.7 (d, $^1J_{CP}$ = 48.7 Hz, C$_{14}$), 137.7 (s, C$_8$), 140.4 (d, $^3J_{CP}$ = 7.1 Hz, C$_6$), 142.9 (s, C$_9$), 143.4 (s, C$_4$), 156.8 (s, C$_{18}$), 195.1 (d, $^2J_{CP}$ = 16.4 Hz, C$_7$)

Attempts to locate C$_2$ using a range of NMR techniques were unsuccessful.

^{19}F NMR (CD$_2$Cl$_2$, 376 MHz, 298 K): δ -73.0 (d, $^1J_{PF}$ = 710 Hz, PF$_6^-$), -62.7 (s, F$_{13}$)

^{31}P{^{1}H} NMR (CD$_2$Cl$_2$, 202 MHz, 295 K): δ -143.0 (sept, $^1J_{PF}$ = 710 Hz, PF$_6^-$), 88.7 (s, **P**Ph$_2$R)

Elemental Analysis: $C_{36}H_{29}F_9N_2P_2Ru$ Calc. / % C 52.50, H 3.55, N 3.40, Found / % C 51.83, H 3.57, N 3.20.

ESI-MS (m/z): Expected for $C_{36}H_{29}F_3N_2P^{101.9}Ru$ = 679.1058; Observed: 679.1058 [M]$^+$ (Error = < 0.05 mDa)

7.2.21 Synthesis of [Ru(η^5-C$_5$H$_5$)(diphenyl-2-pyridylphosphine)(pyr)- (C=CH(C$_6$H$_5$))]PF$_6$, [15c^{Ph}]PF$_6$
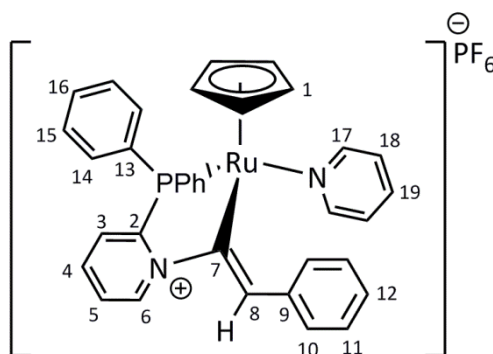
An NMR tube with a PTFE J. Young's tap was charged with [Ru(η^5-C$_5$H$_5$)(diphenyl-2-pyridylphosphine)(NC$_5$H$_5$)]PF$_6$, **[7c]PF$_6$** and [Ru(η^5-C$_5$H$_5$)(diphenyl-2-pyridylphosphine)(NC$_5$H$_5$)$_2$]PF$_6$, **[10c]PF$_6$** (20 mg), deuterated dichloromethane (0.5 mL), and phenylacetylene (3.1 µL, 0.029 mmol). An immediate colour change was observed on addition of alkyne, from yellow to green/brown. ^{31}P{^{1}H} NMR indicated complete conversion to the product within 2 hours.

Dark red crystals suitable for X-ray diffraction were grown by the slow diffusion of pentane into a dichloromethane/pyridine solution of the product.

^{1}H NMR (CD$_2$Cl$_2$, 500 MHz, 295 K): δ 4.58 (s, 5H, H$_1$), 6.49 (app. t, 2H, $^3J_{HH}$ = 6.7 Hz, H$_{18}$), 7.12 – 7.17 (m, 3H, H$_{11}$, H$_{12}$), 7.17 – 7.25 (m, 5H, H$_{19}$, P**Ph$_2$**), 7.36 – 7.46 (m, 4H, P**Ph$_2$**), 7.46 – 7.52 (m, 2H, P**Ph$_2$**), 7.60 (d, 2H, $^3J_{HH}$ = 7.3 Hz, H$_{10}$), 7.72 – 7.79 (m, 2H, H$_3$, H$_8$), 7.92 (app. t, 1H, $^3J_{H4H5}$ = $^3J_{H5H6}$ = 6.5 Hz, H$_5$), 8.02 (d, 2H, $^3J_{HH}$ = 5.5 Hz, H$_{17}$), 8.22 (app. t, 1H, $^3J_{H3H4}$ = $^3J_{H4H5}$ = 7.5 Hz, H$_4$), 9.56 (d, 1H, $^3J_{HH}$ = 6.5 Hz, H$_6$)

^{13}C{^{1}H} NMR (CD$_2$Cl$_2$, 125 MHz, 295 K): δ 82.1 (s, C$_1$), 124.5 (s, C$_{18}$), 127.4 (s, C$_{15/16}$), 128.1 (s, C$_5$), 128.7 (s, C$_9$), 129.1 (s, C$_{10}$), 129.2 (s, C$_{14/15/16}$), 129.4 (d, J_{CP} = 9.1 Hz, C$_{14/15/16}$), 129.5 (d, J_{CP} = 9.8 Hz, H$_{14/15/16}$), 131.3 (d, $^2J_{CP}$ = 13.3 Hz, C$_3$), 132.5 (s, C$_{11/12}$), 135.6 (s, C$_{19}$), 135.9 (d, $^1J_{CP}$ =

48.6 Hz, C_{13}), 139.1 (s, C_8), 140.1 (d, $^3J_{CP}$ = 6.4 Hz, C_6), 142.8 (s, C_4), 156.9 (s, C_{17}), 190.5 (d, $^2J_{CP}$ = 16.6 Hz, C_7)

Attempts to locate C_2 using a range of NMR techniques were unsuccessful.

$^{31}P\{^1H\}$ NMR (CD$_2$Cl$_2$, 202 MHz, 295 K): δ -143.0 (sept, $^1J_{PF}$ = 710 Hz, PF$_6^-$), 88.5 (s, **P**Ph$_2$R)

ESI-MS (*m/z*): Expected for C$_{35}$H$_{30}$N$_2$P$^{101.9}$Ru = 611.1185; Observed: 611.1187 [M]$^+$ (Error = 0.2 mDa)

Elemental Analysis: C$_{35}$H$_{30}$F$_6$N$_2$P$_2$Ru Calc. / % C 55.63, H 4.00, N 3.71, Found / % C 55.90, H 3.92, N 4.27

7.2.22 Synthesis of [Ru(η^5-C$_5$H$_5$)(triphenylphosphine)(C$_5$H$_4$NCHC(C$_6$H$_4$CF$_3$))], [16^{CF3}]
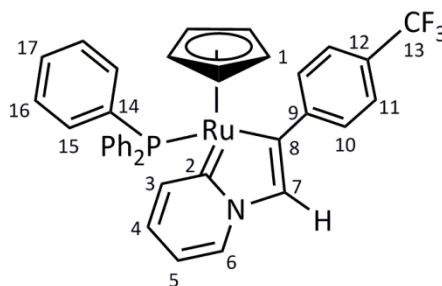
The synthesis was performed using a modified literature procedure.[45,63]

To an oven-dried ampoule was added [Ru(η^5-C$_5$H$_5$)(PPh$_3$)(pyr)$_2$]PF$_6$, **[7]PF$_6$** (150 mg, 210 µmol), 4-ethynyl-α,α,α-trifluorotoluene (33.4 µL, 210 µmol, 1 equivalent) and pyridine (33.1 µL, 420 µmol, 2 equivalents) in dichloromethane (5mL). The reaction mixture was heated at 50 °C for 16 hours and allowed to cool. To the brown solution was added 1,4-diazabicyclo[2.2.2]octane, DABCO (20.7 mg, 190 µmol) and allowed to stir for 16 hours. The solvent was then reduced (approx. 1 mL) and extracted with pentane (approx. 15 mL) by cannula filtration. The solvent was removed under vacuum to give [Ru(η^5-C$_5$H$_5$)(PPh$_3$)(C$_5$H$_4$NCHC{C$_6$H$_4$-4-CF$_3$})], **[16^{CF3}]** as a brown powder.

Yield = 88 mg (62 %)

The spectroscopic data matched that of the literature.[45]

^{1}H NMR (CD$_2$Cl$_2$, 400 MHz, 298 K): δ 4.76 (s, 5H, H$_1$), 6.53 (app. t, 1H, $^3J_{HH}$ = 6.7 Hz, H$_5$), 6.59 (app. t, 1H, $^3J_{HH}$ = 7.6 Hz, H$_4$), 6.98 – 7.08 (m, 6H, H$_{15}$), 7.10 – 7.18 (m, 8H, H$_{10}$, H$_{16}$), 7.24 (t, 3H, $^3J_{HH}$ = 7.2 Hz, H$_{17}$), 7.36 (d, 2H, $^3J_{HH}$ = 8.0 Hz, H$_{11}$), 7.84 (d, 1H, $^3J_{HH}$ = 6.2 Hz, H$_3$), 8.17 (d, 1H, $^3J_{HH}$ = 8.2 Hz, H$_6$)

H$_7$ could not be observed, but has been seen previously using a 700 MHz NMR spectrometer.[45]

^{19}F NMR (CD$_2$Cl$_2$, 295 K, 376 MHz, 298 K): δ -62.0 (s, F$_{13}$)

^{31}P{^{1}H} NMR (CD$_2$Cl$_2$, 162 MHz, 298 K): δ 60.5 (s, **P**Ph$_3$)

7.2.23 Synthesis of [Ru(η^5-C$_5$H$_5$)(2-(1,1-dimethylpropyl)-6-(diphenylphosphino)-pyridine)(C$_5$H$_4$NCHC(C$_6$H$_4$CF$_3$))], [16b^{CF3}]
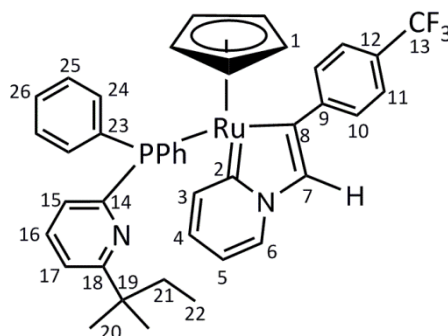
To an oven-dried ampoule was added [Ru(η^5-C$_5$H$_5$)(2-(1,1-dimethylpropyl)-6-(diphenylphosphino)-pyridine)(pyr)$_2$]PF$_6$, **[7b]PF$_6$** (150 mg, 0.19 mmol), 4-ethynyl-α,α,α-trifluorotoluene (30 µl, 0.19 mmol, 1 equivalent) and pyridine (30 µL, 0.37 mmol, 2 equivalents) in dichloromethane (5 mL). The reaction mixture was heated for 16 hours, allowed to cool, and the solvent removed under vacuum. The brown residue was washed with pentane (2 x 10 mL), then redissolved in dichloromethane (10 mL) with 1,4-diazabicyclo[2.2.2]octane, DABCO (21 mg, 0.19 mmol, 1 equivalent) and allowed to stir for 16 hours. The solvent was removed under vacuum, and the residue dried well with consecutive additions of pentane and removal under vacuum. Extraction into pentane gave pure **[16b^{CF3}]** as a brown powder.

Yield = 10 mg (7 %)

^{1}H NMR (CD$_2$Cl$_2$, 500 MHz, 295 K): δ 0.56 (t, 3H, $^3J_{HH}$ = 7.5 Hz, H$_{22}$), 1.18 (s, 6H, H$_{20}$), 1.59 (m, 2H, H$_{21}$), 4.73 (s, 5H, H$_1$), 6.49 (m, 1H, H$_5$), 6.59 (m, 1H, H$_4$), 6.95 – 7.00 (m, 2H, H$_{15}$, H$_7$), 7.02 – 7.08 (m, 4H, 4 of 2H$_{24}$/2H$_{24'}$/2H$_{25}$/2H$_{25'}$), 7.08 – 7.14 (m, 3H, H$_{17}$, 2 of 2H$_{24}$/2H$_{24'}$/2H$_{25}$/2H$_{25'}$), 7.17 – 7.25 (m, 4H, H$_{26}$, H$_{26'}$ and 2 of 2H$_{24}$/2H$_{24'}$/2H$_{25}$/2H$_{25'}$), 7.28 – 7.40 (m, 5H, H$_{16}$, H$_{10}$, H$_{11}$), 7.73 (d, 1H, H$_3$), 8.18 (m, 1H, H$_6$)

^{13}C{^{1}H} NMR (CD$_2$Cl$_2$, 125 MHz, 295 K): δ 9.5 (s, C$_{22}$), 27.6 (s, C$_{20}$), 36.0 (s, C$_{21}$), 41.6 (s, C$_{19}$), 83.2 (s, C$_1$), 113.4 (s, C$_5$), 119.0 (d, $^4J_{CP}$ = 1.6 Hz, C$_{17}$), 124.1 (s, C$_4$), 124.2 (q, $^3J_{CF}$ = 3.8 Hz, C$_{11}$), 125.3 (d, $^2J_{CP}$ = 25.0 Hz, C$_{15}$), 126.2 (q, $^2J_{CF}$ = 31.9 Hz, C$_{12}$), 126.8 (d, J_{CP} = 9.4 Hz, C$_{24}$/C$_{24'}$/C$_{25}$/C$_{25'}$), 127.0 (d, J_{CP} = 9.4 Hz, C$_{24}$/C$_{24'}$/C$_{25}$/C$_{25'}$), 127.6 (s, C$_{10}$), 128.6 (d, $^4J_{CP}$ = 2.0 Hz, C$_{26}$/C$_{26'}$), 128.6 (d, $^4J_{CP}$ = 2.0 Hz, C$_{26}$/C$_{26'}$), 132.4 (s, C$_7$), 134.1 (d, J_{CP} = 10.7 Hz, C$_{24}$/C$_{24'}$/C$_{25}$/C$_{25'}$), 134.3 (d, J_{CP} = 10.7 Hz, C$_{24}$/C$_{24'}$/C$_{25}$/C$_{25'}$), 134.9 (d, $^3J_{CP}$ = 8.5 Hz, C$_{16}$), 136.3 (d, $^1J_{CP}$ = 43.1 Hz,

$C_{23}/C_{23'}$), 136.8 (d, $^1J_{CP}$ = 43.1 Hz, $C_{23}/C_{23'}$), 136.9 (s, C_3), 143.2 (s, C_6), 161.5 (d, $^1J_{CP}$ = 62.2 Hz, C_{14}), 167.6 (d, $^3J_{CP}$ = 12.5 Hz, C_9), 190.5 (d, $^2J_{CP}$ = 12.7 Hz, C_8), 218.7 (d, $^2J_{CP}$ = 14.9 Hz, C_2)

$^{31}P\{^1H\}$ NMR (CD$_2$Cl$_2$, 162 MHz, 295 K): 61.5 (s, **P**Ph$_2$R)

7.2.24 Synthesis of [20]BF$_4$
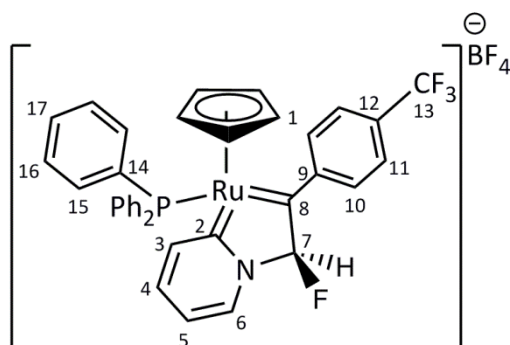
To an oven-dried ampoule was added [Ru(η^5-C$_5$H$_5$)(PPh$_3$)(C$_5$H$_4$NCHC{C$_6$H$_4$-4-CF$_3$})] **[16^{CF3}]**, (20 mg, 30 μmol) and dichloromethane (2 mL).   1-Fluoro-2,4,6-trimethylpyridinium tetrafluoroborate (6.1 mg, 27 μmol, 0.9 equivalents) was added drop wise as a dilute solution in dichloromethane (5 mL). The solution was allowed to stir for *ca.* forty minutes until the colour change from brown to green was deemed complete, and the volume of solvent reduced under vacuum to 0.5 mL. An excess of pentane was added *via* a cannula transfer to produce a green precipitate. This residue was washed with pentane (2 x 10 mL), and dried under vacuum to yield a dark green powder, **[20]BF$_4$**.

Yield = 7 mg (30 %)

Crystals suitable for study by X-ray crystallography were obtained from the slow diffusion of pentane into a dichloromethane solution of **[21]BF$_4$**.

Alternative procedures:

 Fluorination with Selectfluor®: To an oven-dried ampoule was added [Ru(η^5-C$_5$H$_5$)(PPh$_3$)(C$_5$H$_4$NCHC{C$_6$H$_4$-4-CF$_3$})] **[16^{CF3}]** (10 mg, 15 μmol) and dichloromethane (2 mL)., Selectfluor® (5 mg, 15 μmol, 1 equivalent) was added dropwise as a dilute solution in acetonitrile (2mL). The reaction mixture was stirred for *ca.* 60 minutes and then removed under vacuum. The green residue was redissolved in CD$_2$Cl$_2$ (0.5 mL) and NMR spectra recorded.

Fluorination with NFSI: An NMR tube with a PTFE Young's tap was charged with [Ru(η^5-C$_5$H$_5$)(PPh$_3$)(C$_5$H$_4$NCHC{C$_6$H$_4$-4-CF$_3$})]] **[16^{CF3}]** (10 mg, 15 µmol) and NFSI (5 mg, 15 µmol, 1 equivalent) in CD$_2$Cl$_2$ (0.5 mL). NMR spectra were recorded after *ca.* 60 minutes.

^{1}H NMR (CD$_2$Cl$_2$, 500 MHz, 295 K): δ 4.71 (d, 1H, $^2J_{HF}$ = 52.1 Hz, H$_7$), 5.37 (s, 5H, H$_1$), 7.06 (app. t, 1H, $^3J_{HH}$ = 6.8 Hz, H$_5$), 6.12 – 7.19 (m, 6H, P**Ph$_3$**), 7.38 (d, 2H, $^3J_{HH}$ = 8.2 Hz, H$_{10}$), 7.40 – 7.49 (m, 7H, PPh$_3$, H$_4$), 7.49 – 7.56 (m, 3H, H$_{17}$), 7.60 (d, 2H, $^3J_{HH}$ = 8.2 Hz, H$_{11}$), 8.06 – 8.12 (m, 2H, H$_6$, H$_3$)

^{13}C{^{1}H} NMR (CD$_2$Cl$_2$, 125 MHz, 295 K): δ 93.5 (s, C$_1$), 115.9 (d, $^1J_{CF}$ = 219.1 Hz, C$_7$), 120.0 (s, C$_5$), 124.0 (s, C$_{10}$), 124.5 (q, $^1J_{CF}$ = 272.8 Hz, C$_{13}$), 125.8 (q, $^3J_{CF}$ = 3.8 Hz, C$_{11}$), 129.4 (d, J_{CP} = 10.7 Hz, C$_{15/16}$), 131.0 (q, $^2J_{CF}$ = 32.65 Hz, C$_{12}$), 132.0 (d, $^4J_{CP}$ = 2.4 Hz, C$_{17}$), 132.1 (d, $^1J_{CP}$= 51.9 Hz, C$_{14}$), 133.2 (d, J_{CP} = 10.8 Hz, C$_{15/16}$), 135.5 (s, C$_4$), 140.3 (s, C$_3$), 143.4 (d, $^3J_{CF}$ = 1.7 Hz, C$_6$), 211.8 (d, $^2J_{CP}$ = 15.9 Hz, C$_2$), 301.4 (d, $^2J_{CP}$ = 8.1 Hz, C$_8$)

Attempts to locate C$_9$ using a range of NMR techniques were unsuccessful.

^{19}F NMR (CD$_2$Cl$_2$, 471 MHz, 298 K): δ -153.3 (BF$_4^-$), -139.8 (dd, $^2J_{HF}$ = 52.0 Hz, $^4J_{PF}$ = 7.7 Hz, F$_7$), -64.2 (s, F$_{13}$)

^{31}P{^{1}H} NMR (CD$_2$Cl$_2$, 202 MHz, 295 K): δ 47.2 (d, $^4J_{PF}$ = 7.7 Hz, **P**Ph$_3$)

ESI-MS (m/z): Expected for C$_{37}$H$_{29}$F$_4$NP$^{101.9}$Ru = 696.1012; Observed: 696.1023 [M]$^+$ (Error = 1.1 mDa)

Elemental Analysis: C$_{37}$H$_{29}$BF$_8$NPRu Calc. /% C 56.79, H 3.74, N 1.79 Found /% C 56.347, H 3.727, N 1.738

7.2.25 NOESY spectra of [20]BF$_4$

A series of NOESY spectra of **[20]BF$_4$** were recorded with mixing times of 300, 400, 600, 700 and 800 ms. No cross peak was observed between H$_1$ and H$_{11}$, supporting the isomer assignment as shown above. An exemplar NOESY spectrum (mixing time = 600 ms) is shown below. The cross peak between H$_{11}$ (4.71 ppm, d, $^2J_{HF}$ = 52.1 Hz, 1H) and PPh$_3$ (7.12 − 7.19 ppm, m, 6H) further supports the proposed isomer.
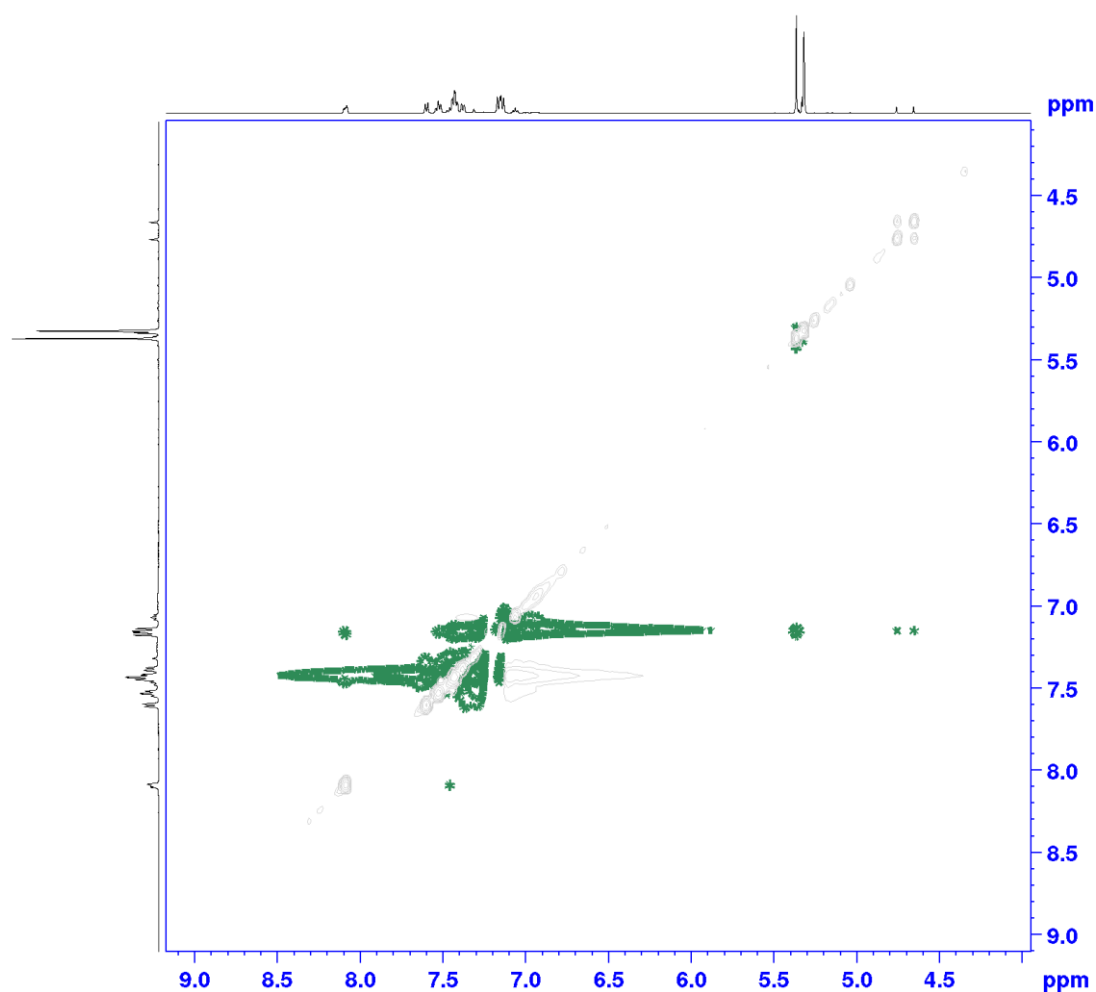
7.2.26 Synthesis of [21]BF$_4$
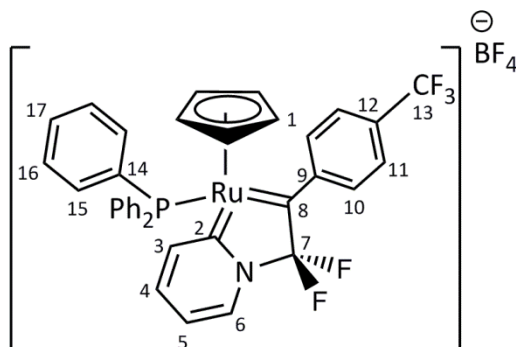
An NMR tube with a PTFE J. Young's tap was charged with $[Ru(\eta^5\text{-}C_5H_5)(PPh_3)(C_5H_4NCHC\{C_6H_4\text{-}4\text{-}CF_3\})]$, **[16^{CF3}]**, (20 mg, 30 μmol) and 1-fluoro-2,4,6-trimethylpyridinium tetrafluoroborate (13.6 mg, 60 μmol, 2 equivalents) in deuterated dichloromethane (0.5 mL). On addition of 1-fluoro-2,4,6-trimethylpyridinium tetrafluoroborate, an immediate colour change was observed from brown to green. The reaction mixture was allowed to stand for 24 hours, and monitored by NMR spectroscopy.

On complete conversion, the reaction mixture was transferred to a Schlenk tube, and an excess of pentane was added *via* a cannula transfer to produce a green precipitate. This residue was washed with further pentane (2 x 10 mL) by cannula filtration, and dried under vacuum to yield a dark green precipitate, **[21]BF$_4$**.

Yield = 9 mg (30 %)

Crystals suitable for study by X-ray crystallography were obtained from the slow diffusion of pentane into a dichloromethane solution of **[21]BF$_4$**.

^{1}H NMR (CD$_2$Cl$_2$, 500 MHz, 295 K): δ 5.35 (s, 5H, H$_1$), 7.07 (app. td, 1H, $^3J_{HH}$ = 6.9 Hz, $^4J_{HH}$ = 1.1 Hz, H$_5$), 7.12 − 7.19 (dd, 6H, $^3J_{HH}$ = 8.2 Hz, $^3J_{HP}$ = 11.9 Hz, H$_{15/16}$), 7.39 (d, 2H, $^3J_{HH}$ = 8.2 Hz, H$_{10}$), 7.43 (app. td, 7H, $^3J_{HH}$ = 7.8 Hz, $^4J_{HP}$ = 2.6 Hz, H$_{15/16}$, H$_4$), 7.46 − 7.55 (m, 5H, H$_{17}$, H$_{11}$), 8.09 (d, 1H, $^3J_{HH}$ = 8.4 Hz, H$_3$), 8.14 (app. d, 1H, $^3J_{HH}$ = 6.7 Hz, H$_6$). Resonances due to residual 2,4,6-trimethylpyridine have been omitted. Integrations are not shown where the 2,4,6-TMP and **[21]BF$_4$** resonances are not clearly defined.

^{13}C{^{1}H} NMR (CD$_2$Cl$_2$, 125 MHz, 295 K): δ 93.0 (s, C$_1$), 123.5* (C$_{13}$) 131.5* (C$_{12}$), 120.9 (s, C$_5$), 125.8 (s, C$_{10}$), 129.6 (d, J_{CP} = 10.7 Hz, C$_{15/16}$), 131.3 (d, $^1J_{CP}$ = 51.5 Hz, C$_{14}$), 132.1 (s, C$_{17}$), 132.3*

(C$_7$), 133.4 (d, J_{CP} = 11.1 Hz, C$_{15/16}$), 137.6 (s, C$_6$), 144.0 (s, C$_3$), 207.6* (C$_2$), 284.5* (C$_8$) (* = resonances located by ^{19}F{^{13}C} two-dimensional correlation spectra)

^{19}F NMR (CD$_2$Cl$_2$, 376 MHz, 295 K): δ -153.0 (BF$_4^-$), -98.3 (d, $^2J_{FF}$ = 233.1 Hz, F$_7$), -79.7 (dd, $^2J_{FF}$ = 233.1 Hz, $^4J_{PF}$ = 6.6 Hz, F$_7$), -66.4 (s, F$_{13}$)

^{31}P{^{1}H} NMR (CD$_2$Cl$_2$, 202 MHz, 295 K): δ 46.1 (d, $^4J_{PF}$ = 6.6 Hz, **P**Ph$_3$)

Attempts to unambiguously assign C$_4$, C$_9$ and C$_{11}$ using a range of NMR techniques, including 2D ^{1}H-^{13}C correlation experiments were unsuccessful.

ESI-MS (m/z): Expected for C$_{37}$H$_{28}$F$_5$NP$^{101.9}$Ru = 714.0927; Observed: 714.0920 [M]$^+$ (Error = 0.7 mDa)

Elemental Analysis: C$_{37}$H$_{28}$BF$_9$NPRu + 1 C$_8$H$_{12}$BF$_4$N ([2,4,6-TMP-H]BF$_4$) Calc. /% C 53.54, H 3.99, N 2.75. Found /% C 53.814, H 4.227, N 3.062

Complex **[21]BF$_4$** could not be isolated cleanly without the presence of one equivalent of [2,4,6-TMP-H]BF$_4$ which is formed during the deprotio-difluorination of metallocycle **[16^{CF3}]**, as both **[21]BF$_4$** and [2,4,6-TMP-H]BF$_4$ crystallise under identical conditions. The mass yield presented above includes the mass of this [2,4,6-TMP-H]BF$_4$, and the percentage yield has been corrected for this.

7.2.27 Synthesis of [Ru(η^5-C$_5$H$_5$)(PPh$_3$)(C$_5$H$_4$NCFC{C$_6$H$_4$-4-CF$_3$})], [22]
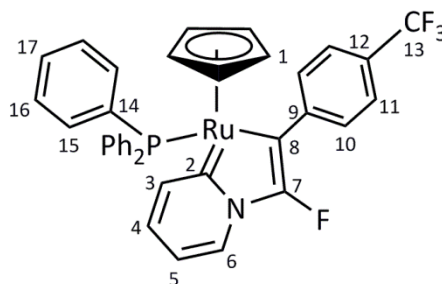
An NMR tube with a PTFE J. Young's tap was charged with [Ru(η^5-C$_5$H$_5$)(PPh$_3$)(C$_5$H$_4$NCF$_2$C{C$_6$H$_4$-4-CF$_3$})]BF$_4$, [21]BF$_4$, (6 mg) dissolved in pyridine-d$_5$ (0.5 mL). The reaction was monitored over 7 days, and produced a mixture of [Ru(η^5-C$_5$H$_5$)(PPh$_3$)(C$_5$H$_4$NCFC{C$_6$H$_4$-4-CF$_3$})], [22], and the oxygen-containing complex, [24]BF$_4$. Complex [22] can also be made independently from the dissolution of [20]BF$_4$ in pyridine. Dissolution in d$_5$-pyridine allows full NMR characterisation to be recorded.

^{1}H NMR (NC$_5$D$_5$, 500 MHz, 295 K): δ 4.95 (s, 5H, H$_1$), 6.58 (td, $^3J_{HH}$ = 6.7 Hz, $^4J_{HH}$ = 1.2 Hz, 1H, H$_5$), 6.68 (m, 1H, H$_4$), 7.21 – 7.26 (m, 6H, H$_{15/16}$), 7.26 – 7.36 (m, 9H, H$_{15/16}$, H$_{17}$), 7.45 - 7.49 (m, 2H, H$_{10}$), 7.54 – 7.59 (m, 2H, H$_{11}$), 7.71 (d, 1H, $^3J_{HH}$ = 6.4 Hz, H$_3$), 8.29 (d, 1H, $^3J_{HH}$ = 8.1 Hz, H$_6$)

^{13}C{^{1}H} NMR (NC$_5$D$_5$, 125 MHz, 295 K): δ 83.9 (s, C$_1$), 113.8 (s, C$_5$), 124.9 (q, $^3J_{CF}$ = 3.8 Hz, C$_{11}$), 126.1 (q, $^1J_{CF}$ = 271.6 Hz, C$_{13}$), 126.3 (s, C$_4$), 126.4 (q, $^2J_{CF}$ = 31.8 Hz, C$_{12}$), 128.4 (d, J_{CP} = 9.4 Hz, C$_{15/16}$), 129.8 (s, C$_{17}$), 129.8 (s, C$_{10}$), 133.9 (d, J_{CP} = 10.8 Hz, C$_{15/16}$), 134.8 (s, C$_3$), 137.2 (d, $^1J_{CP}$ = 41.4 Hz, C$_{14}$), 143.2 (s, C$_6$), 146.9 (br, C$_8$), 153.9 (br, C$_9$), 215.1 (br, C$_2$)

^{19}F NMR (NC$_5$D$_5$, 376 MHz, 295 K): δ -111.7 (s, F$_7$), -63.5 (s, F$_{13}$)

^{31}P{^{1}H} NMR (NC$_5$D$_5$, 202 MHz, 295 K): δ 61.5 (s, **P**Ph$_3$)

ESI-MS (m/z): Expected for C$_{37}$H$_{28}$F$_4$NP$^{101.9}$Ru = 695.0939; Observed: 695.0961 [M]$^+$ (Error = 2.2 mDa)

7.2.28 Characterisation of oxygen-containing complex, [24]BF$_4$
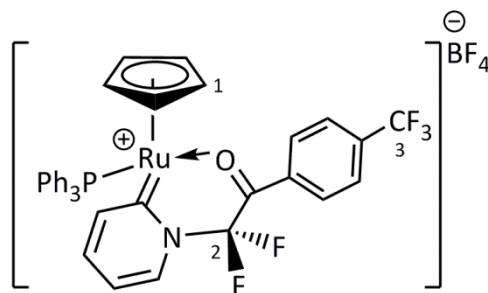
Selected ^{1}H NMR (NC$_5$D$_5$, 500 MHz, 295 K): δ 5.09 (s, 5H, H$_1$)

^{19}F NMR (NC$_5$D$_5$, 471 MHz, 295 K): δ -153.0 (BF$_4^-$), -78.7 (d, $^2J_{FF}$ = 208.5 Hz, F$_2$), -67.6 (d, $^2J_{FF}$ = 208.5 Hz, CF$_2$), -64.5 (s, F$_3$)

^{31}P{^{1}H} NMR (NC$_5$D$_5$, 202 MHz, 295 K): δ 43.2 (s, **P**Ph$_3$)

ESI-MS (m/z): Expected for C$_{37}$H$_{28}$F$_5$NOP$^{101.9}$Ru = 730.0872; Observed: 730.0872 [M]$^+$ (Error <0.05 mDa)

ATR IR (v /cm^{-1}): 528.1 (m), 697.6 (m), 1066.2 (s, C-F stretch), 1090.1 (s, C-F stretch), 1206.5 (m), 1324.4 (m), 1413.0 (w, C=C stretch), 1436.4 (w, C=C stretch), 1458.3 (w, C=C stretch), 1481.1 (w, C=C stretch), 1540.4 (w, C=C stretch), 1640.1 (m, C=O stretch), 2991.0 (w, C-H stretch), 3124.5 (w, C-H stretch), 3184.5 (w, C-H stretch), 3303.9 (w, C-H stretch)

7.2.29 Addition of DABCO to monofluorinated metallocycle, [Ru(η⁵-C₅H₅)(PPh₃)(C₅H₄NCHFC{C₆H₄-4-CF₃})]BF₄, [20]BF₄

An NMR tube with a PTFE J. Young's tap was charged with [Ru(η⁵-C₅H₅)(PPh₃)(C₅H₄NCHFC{C₆H₄-4-CF₃})] BF₄, **[20]BF₄,** (8 mg, 10 µmol) and DABCO (1.1 mg, 10 µmol, 1 equivalent) in deuterated dichloromethane (0.5 mL). A low temperature VT NMR experiment was conducted on the sample, as shown below:
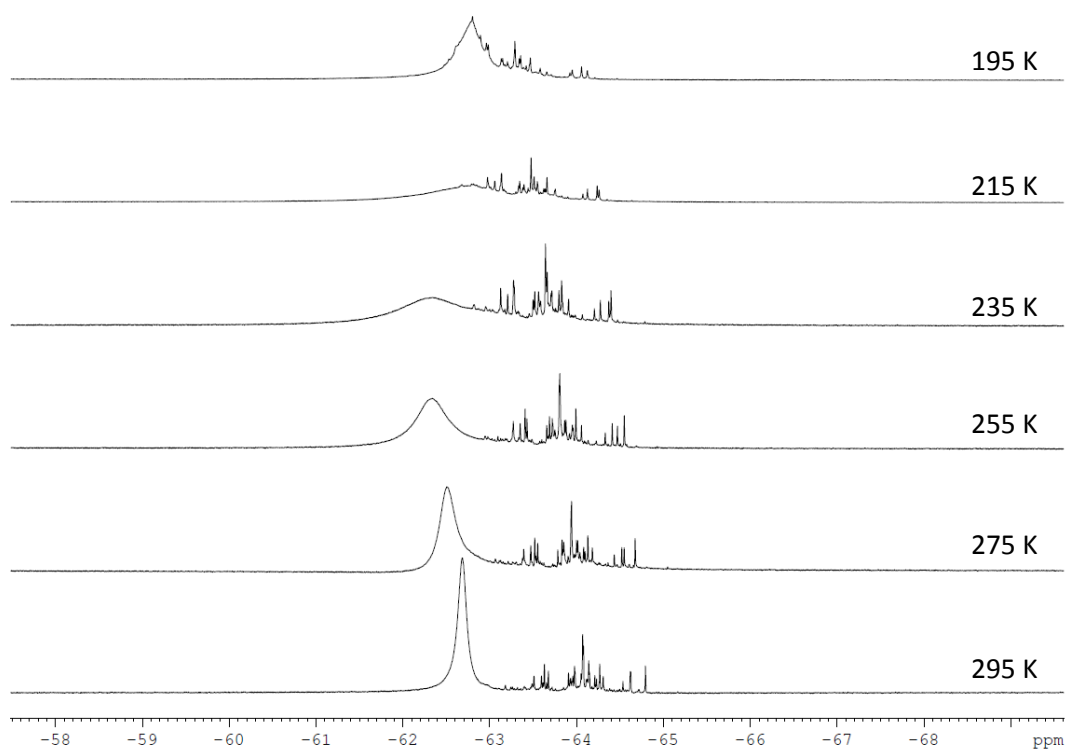
Low variable temperature ^{19}F NMR spectra of **[20]BF₄** and DABCO (CF$_3$ region)
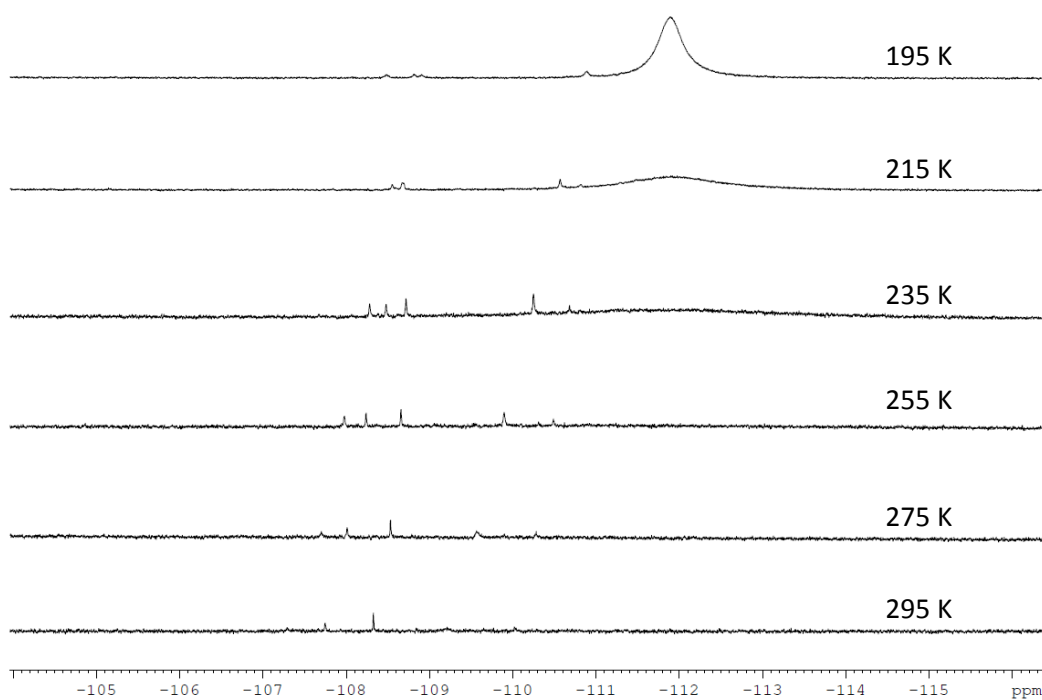
Low variable temperature ^{19}F NMR spectra of **[20]BF$_4$** and DABCO
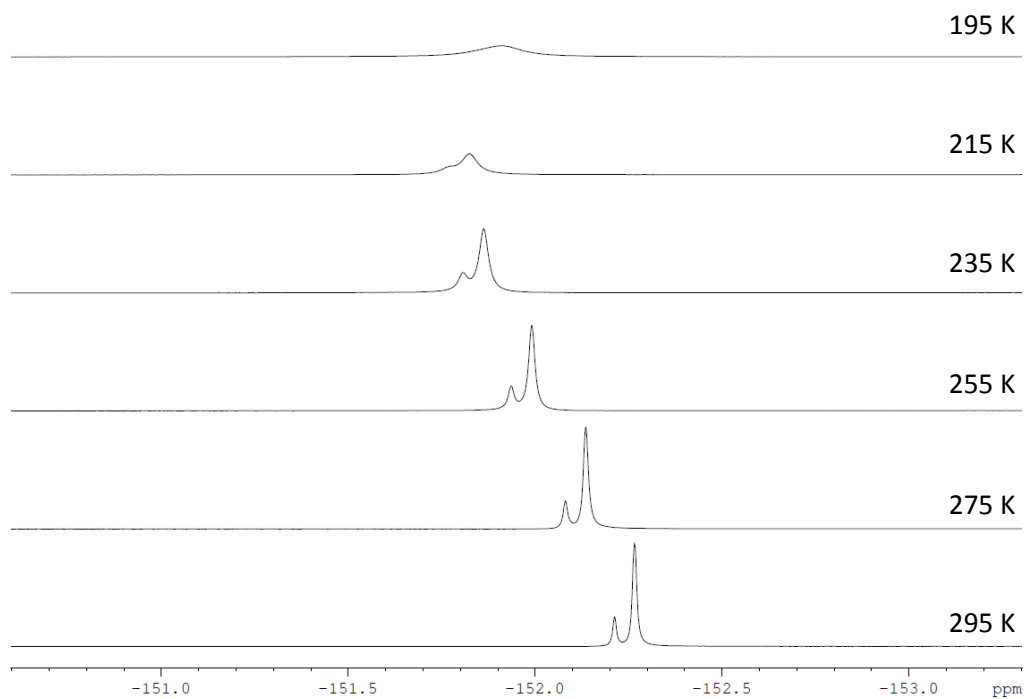
Low variable temperature ^{19}F NMR spectra of **[20]BF$_4$** and DABCO (BF$_4$ region)
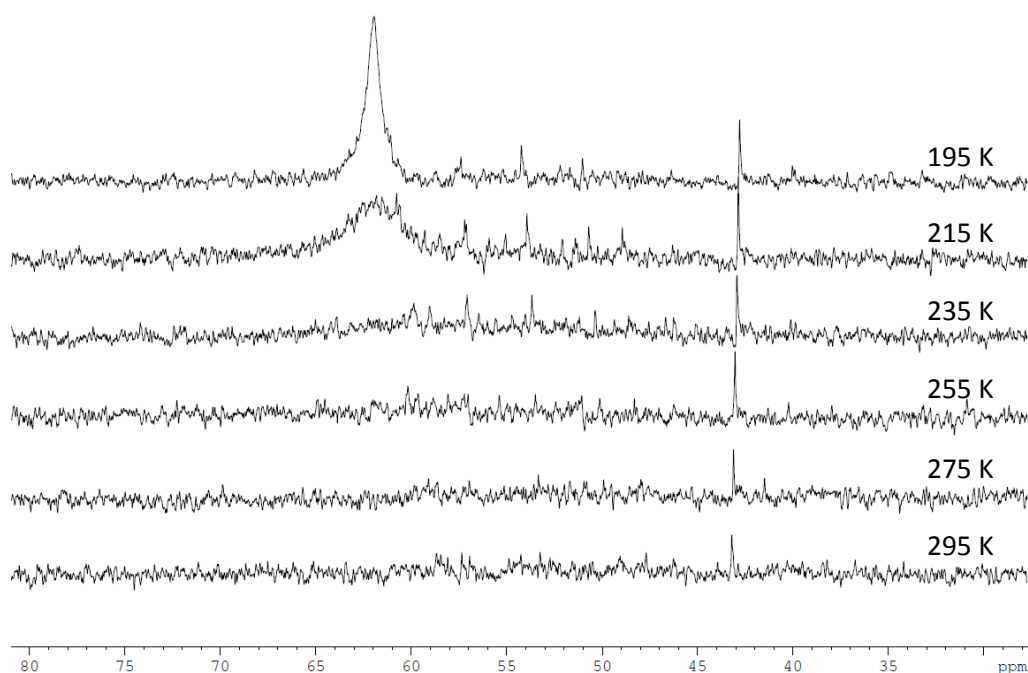
Low variable temperature ^{31}P{^{1}H} NMR spectra of **[20]BF$_4$** and DABCO

7.2.30 Low temperature NMR study of the monofluorination reaction, [16^{CF3}] to [20]BF$_4$

An NMR tube with a PTFE J. Young's tap was charged with [Ru(η^5-C$_5$H$_5$)(PPh$_3$)(C$_5$H$_4$NCHC{C$_6$H$_4$-4-CF$_3$})], **[16^{CF3}]**, (20 mg, 30 μmol) and deuterated dichloromethane (0.5 mL). ^{1}H, ^{19}F and ^{31}P{^{1}H} NMR spectra were recorded. The NMR tube was then cooled in a dry ice/acetone bath and 1-fluoro-2,4,6-trimethylpyridinium tetrafluoroborate (6.7 mg, 30 μmol, 1 equivalent) was added. The NMR spectra were then recorded at a range of temperatures from 195 K to 295 K.

No evidence of any reaction intermediates was observed.

^{31}P{^{1}H} NMR

After the addition of 1-fluoro-2,4,6-trimethylpyridinium tetrafluoroborate (F$^+$), the initial spectra were recorded at 195 K, and evidence for the mono-fluorinated metallocycle **[20]BF$_4$** was obtained at this temperature (^{31}P{^{1}H} NMR: 47.7, br). The integration of this resonance did not increase, relative to [Ru(η^5-C$_5$H$_5$)(PPh$_3$)(C$_5$H$_4$NCHC{C$_6$H$_4$-4-CF$_3$})], **[16^{CF3}]**, on warming the sample to 245 K. This suggests that the initial fluorination occurred on transferring the sample into the NMR spectrometer, during which time it may not have remained at low

temperature. However, by 265 K, the signal for $[Ru(\eta^5-C_5H_5)(PPh_3)(C_5H_4NCHC\{C_6H_4-4-CF_3\})]$, **[16^CF3]**, could no longer be observed, and the dominant species in the reaction mixture was **[20]BF_4**.

During the experiment, as the temperature was increased, the signal for $[Ru(\eta^5-C_5H_5)(PPh_3)(C_5H_4NCHC\{C_6H_4-4-CF_3\})]$, **[16^CF3]**, at around 62 ppm became broader. This could be due to reversible protonation and deprotonation with the solvent, as has been described previously. A small resonance was also observed at around 30.1 ppm, attributed to OPPh_3.

^{19}F NMR

Before the addition of F$^+$, one resonance was observed at -63.3 ppm due to the CF_3 moiety of $[Ru(\eta^5-C_5H_5)(PPh_3)(C_5H_4NCHC\{C_6H_4-4-CF_3\})]$, **[16^CF3]**. ^{19}F NMR spectra were recorded from 245 K onwards. On the addition of F$^+$, the monofluorinated product **[20]BF_4** could be observed at 245 K by the appearance of new resonances at 140.1 ppm (d, $^2J_{HF}$ = 52.0 Hz) and an additional resonance in the -CF_3 region. The resonance for F$^+$ was also visible at 16.3 ppm (s) and -153.6 (BF_4). Spectra recorded at 265 K showed the characteristic resonance for **[20]BF_4** was growing, and by 285 K, two small doublets were visible for the bisfluorinated product **[21]BF_4** (-96.6, d, $^2J_{FF}$ = 233.1 Hz and -78.0 dd, $^2J_{FF}$ = 233.1 Hz, $^4J_{PF}$ = 6.6 Hz).

Broadening of the resonance attributed to the -CF_3 group of **[16^CF3]** was also observed with increasing temperature, in correlation with the broadening of the ^{31}P{^{1}H} NMR resonance associated with this complex. A small resonance was also observed at -220.1 ppm, $^2J_{HF}$ = 47.3 Hz. This has been attributed to 2-monofluoromethyl-4,6-dimethylpyridine formed by deactivation of the 1-fluoro-2,4,6-trimethylpyridinium tetrafluoroborate.

^{1}H NMR

On the addition of F$^+$, 2 sets of resonances were observed for the methyl groups of 2,4,6-trimethylpyridine. These could be due to 2,4,6-TMP, 1-fluoro-2,4,6-TMP or 1-protio-2,4,6-TMP. By 265 K, only one set of resonances were present, suggesting that all of the F$^+$ had been delivered. The cyclopentadienyl resonance for the initial metallocycle $[Ru(\eta^5-C_5H_5)(PPh_3)(C_5H_4NCHC\{C_6H_4-4-CF_3\})]$, **[16^CF3]**, was observed at 4.79 ppm at 195 K, but broadened over time with increasing temperature as was observed in the ^{31}P{^{1}H} and ^{19}F NMR spectra. By 265 K, this Cp resonance was no longer observed and the resonance for the mono-fluorinated **[20]BF_4** species became dominant.

7.2.31 Synthesis of [Ru(η^5-C$_5$H$_5$)(PPh$_3$)Cl], [25]
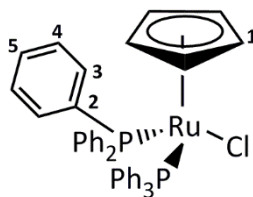
Dicyclopentadiene (50 mL) was cracked to form cyclopentadiene using distillation apparatus. The round bottom flask containing dicyclopentadiene was stirred and heated using a heating mantle, and the temperature at the top of the Vigreux column was maintained at 35 °C in order to prevent transfer of the dimer.

Ethanol (1 L) was degassed in a 2 litre, 2-necked round bottom flask for approximately 60 minutes using a flow of nitrogen. After this time, anti-bumping granules and triphenylphosphine (21 g, 0.08 mol) were added and a reflux condenser was fitted. The mixture was heated to reflux.

RuCl$_3$.3H$_2$O (4.98 g, 0.02 mol) was dissolved in deoxygenated ethanol (approximately 80 mL) under nitrogen. Freshly-distilled cyclopentadiene (10 mL) was added to deoxygenated ethanol (approximately 10 mL) under nitrogen.

Each of these solutions (the RuCl$_3$.3H$_2$O and then the cyclopentadiene) was transferred to the 2-litre round bottom flask containing the triphenylphosphine solution in ethanol *via* cannula transfer. The reaction mixture was heated at reflux for 1 hour. The solution was cooled to room temperature and stored at -20 °C overnight to produce bright red crystals. The crystals were air-stable and therefore were isolated by vacuum filtration in air and washed with ethanol (4 x 25 mL) and diethyl ether (4 x 25 mL). Further batches of crystals could be obtained by reduction of the solvent volume and storing the subsequent solutions in the freezer at -20 °C overnight.

Yield = 11.5 g (79 %)

^{1}H NMR (CD$_2$Cl$_2$, 400 MHz, 295 K): δ 4.10 (s, 5H, H$_1$), 7.15 (app.t, 12H, $^3J_{HH}$ = 7.2 Hz, H$_3$), 7.26 (t, 6H, $^3J_{HH}$ = 7.4 Hz, H$_5$), 7.33 – 7.37 (m, 12H, H$_4$)

^{13}C{^{1}H} NMR (CD$_2$Cl$_2$, 100 MHz, 295 K): δ 81.7 (t, $^2J_{CP}$ = 2.4 Hz, C$_1$), 127.8 (virtual t, sum of J_{CP} = 9.2 Hz, C$_3$), 129.1 (s, C$_5$), 134.1 (virtual t, sum of J_{CP} = 10.2 Hz, C$_4$), 138.8 (m, sum of J_{CP} = 39.7 Hz, C$_2$)

^{31}P{^{1}H} NMR (CD$_2$Cl$_2$, 162 MHz, 295 K): δ 39.5 (s, **P**Ph$_3$)

7.2.32 Synthesis of [Ru(η^5-C$_5$H$_5$)(PPh$_3$)$_2$(-C≡C{Ph})], [26^{Ph}]
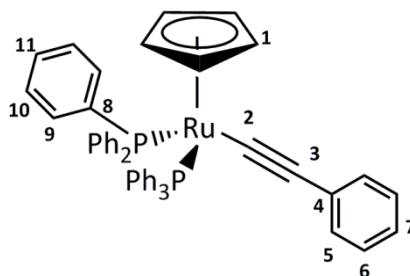
To an oven-dried Schlenk tube was added [Ru(η^5-C$_5$H$_5$)(PPh$_3$)$_2$Cl], **[25]** (250 mg, 0.34 mmol), phenylacetylene (55 µL, 0.5 mmol, 1.5 equivalents) and methanol (15 mL), which was heated under reflux for 30 minutes. The reaction mixture was cannula filtered to remove undissolved starting material. To the red solution was added NaOMe (27 mg, 0.5 mmol, 1.5 equivalents) as a methanol solution (2 mL), to yield a bright yellow precipitate. The solvent was removed by cannula filtration, and the yellow powder dried under vacuum.

Yield = 230 mg (85 %)

The spectroscopic data matched that of the literature.[274]

^{1}H NMR (CD$_2$Cl$_2$, 400 MHz, 295 K): δ 4.34 (s, 5H, H$_1$), 7.08 – 7.09 (m, 17H, ar), 7.23 (t, 6H, $^3J_{HH}$ = 7.4 Hz, H$_{11}$), 7.45 – 7.54 (m, 12H, ar)

^{13}C{^{1}H} NMR (CD$_2$Cl$_2$, 100 MHz, 295 K): δ 85.5 (t, $^3J_{CP}$ = 2.2 Hz, C$_1$), 114.6 (s), 116.9 (broad), 123.3 (s), 127.6 (m), 128.0 (s), 128.8 (s), 130.6 (m), 132.2 (s), 134.1 (m), 139.3 (m, sum of J_{CP} = 41.7 Hz, C$_8$)

^{31}P{^{1}H} NMR (CD$_2$Cl$_2$, 162 MHz, 295 K): δ 50.9 (s, **P**Ph$_3$)

7.2.33 Synthesis of [Ru(η^5-C$_5$H$_5$)(PPh$_3$)$_2$(-C≡C{C$_6$H$_4$-4-CF$_3$})], [26^{CF3}]

To an oven-dried Schlenk tube was added [Ru(η^5-C$_5$H$_5$)(PPh$_3$)$_2$Cl], **[25]** (250 mg, 0.34 mmol), 4-ethynyl-α,α,α-trifluorotoluene (86 μL, 0.5 mmol, 1.5 equivalents) and methanol (15 mL), which was heated under reflux for 30 minutes. The reaction mixture was cannula filtered to remove undissolved starting material. To the red solution was added NaOMe (27 mg, 0.5 mmol, 1.5 equivalents) as a methanol solution (2 mL), to yield a bright yellow precipitate. The solvent was removed by cannula filtration, and the yellow powder dried under vacuum.

Yellow crystals suitable for single crystal X-ray diffraction were obtained from slow evaporation of the solvent from a dichloromethane solution of **[26^{CF3}]**.

Yield = 211 mg (72 %)

^{1}H NMR (CD$_2$Cl$_2$, 500 MHz, 295 K): δ 4.35 (s, 5H, H$_1$), 7.12 (t, 12H, $^3J_{HH}$ = 7.4 Hz, H$_{11}$), 7.16 (d, 2H, $^3J_{HH}$ = 8.3 Hz, H$_5$), 7.24 (t, 6H, $^3J_{HH}$ = 7.4 Hz, H$_{12}$), 7.39 (d, 2H, $^3J_{HH}$ = 8.3 Hz, H$_6$), 7.42 – 7.49 (m, 12H, H$_{10}$)

^{13}C{^{1}H} NMR (CD$_2$Cl$_2$, 125 MHz, 295 K): δ 85.4 (s, C$_1$), 114.3 (s, C$_3$), 123.8 (q, $^2J_{CF}$ = 32.1 Hz, C$_7$), 124.6 (q, $^3J_{CF}$ = 3.7 Hz, C$_6$), 125.0 (q, $^1J_{CF}$ = 270.2 Hz, C$_8$), 125.9 (t, $^2J_{CP}$ = 24.6 Hz, C$_2$), 127.3 (virtual t, sum of J_{CP} = 9.0 Hz, C$_{11}$), 128.6 (s, C$_{12}$), 130.3 (s, C$_5$), 133.7 (virtual t, sum of J_{CP} = 9.7 Hz, C$_{10}$), 134.1 (s, C$_4$), 138.7 (m, sum of J_{CP} = 42.1 Hz, C$_9$)

^{19}F NMR (CD$_2$Cl$_2$, 376 MHz, 295 K): δ -63.3 (s, F$_8$)

^{31}P{^{1}H} NMR (CD$_2$Cl$_2$, 202 MHz, 295 K): δ 51.6 (s, **P**Ph$_3$)

ESI-MS (m/z): Expected for C$_{50}$H$_{40}$F$_3$P$_2$$^{101.9}$Ru = 861.1609; Observed: 861.1600 [M+H]$^+$ (Error = 0.9 mDa)

Elemental Analysis: C$_{50}$H$_{39}$F$_3$P$_2$Ru Calc. /% C 69.84, H 4.57, Found /% C 69.36, H 4.43

7.2.34 Synthesis of [Ru(η^5-C$_5$H$_5$)(PPh$_3$)$_2$(-C≡C{C$_6$H$_4$-4-OMe})], [26^{OMe}]

To an oven-dried Schlenk tube was added [Ru(η^5-C$_5$H$_5$)(PPh$_3$)$_2$Cl], **[25]** (250 mg, 0.34 mmol), 4-ethynylanisole (66 mg, 0.5 mmol, 1.5 equivalents) and methanol (15 mL), which was heated under reflux for 30 minutes. The reaction mixture was cannula filtered to remove undissolved starting material. To the red solution was added NaOMe (27 mg, 0.5 mmol, 1.5 equivalents) as a methanol solution (2 mL), to yield a bright yellow precipitate. The solvent was removed by cannula filtration, and the yellow powder dried under vacuum.

Yield = 218 mg (78 %)

^{1}H NMR (CD$_2$Cl$_2$, 500 MHz, 295 K): δ 3.77 (s, 3H, H$_8$), 4.32 (s, 5H, H$_1$), 6.72 (d, 2H, $^3J_{HH}$ = 8.8 Hz, H$_6$), 7.05 (d, 2H, $^3J_{HH}$ = 8.8 Hz, H$_5$), 7.11 (app. t, 12H, $^3J_{HH}$ = 7.6 Hz, H$_{11}$), 7.22 (t, 6H, $^3J_{HH}$ = 7.4 Hz, H$_{12}$), 7.46-7.54 (m, 12H, H$_{10}$)

^{13}C{^{1}H} NMR (CD$_2$Cl$_2$, 125 MHz, 295 K): δ 55.6 (s, C$_8$), 85.5 (s, C$_1$), 112.1 (t, $^2J_{CP}$ = 24.9 Hz, C$_2$), 113.6 (s, C$_3$), 113.7 (s, C$_6$), 123.9 (s, C$_4$), 127.6 (virtual t, sum of J_{CP} = 9.2 Hz, C$_{10/11}$), 128.8 (s, C$_{12}$), 131.6 (s, C$_5$), 134.2 (virtual t, sum of J_{CP} = 10.4 Hz, C$_{10/11}$), 139.5 (m, sum of J_{CP} = 42.0 Hz, C$_9$), 156.4 (s, C$_7$)

^{31}P{^{1}H} NMR (CD$_2$Cl$_2$, 202 MHz, 295 K): δ 51.6 (s, **P**Ph$_3$)

ESI-MS (m/z): Expected for C$_{50}$H$_{43}$OP$_2$$^{101.9}$Ru = 823.1827; Observed: 823.1841 [M+H]$^+$ (Error = 1.4 mDa)
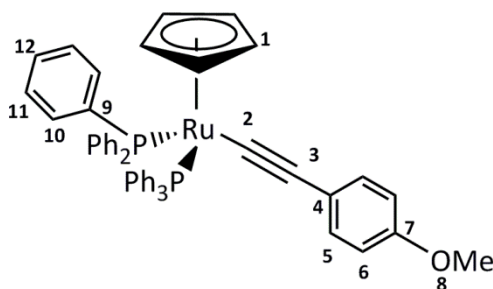
Elemental Analysis: C$_{50}$H$_{42}$OP$_2$Ru Calc. /% C 73.07, H 5.15, Found /% C 72.70, H 5.11

7.2.35 Synthesis of [Ru(η^5-C$_5$H$_5$)(PPh$_3$)$_2$(C=C{F}Ph)]BF$_4$, [27^{Ph}]BF$_4$
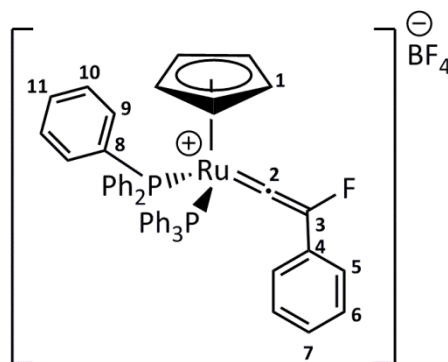
To an oven-dried Schlenk tube was added [Ru(η^5-C$_5$H$_5$)(PPh$_3$)$_2$(-C≡C{Ph})], **[26^{Ph}]** (297 mg, 0.38 mmol) in dichloromethane (15 mL). 1-fluoro-2,4,6-trimethylpyridinium tetrafluoroborate (77.9 mg, 0.34 mmol, 0.9 equivalents) was added, and an immediate colour change was observed from yellow to green. The volume of solvent was reduced under vacuum to approximately 0.5 mL, and a green solid precipitated on the addition of excess diethyl ether. The solvent was then removed by cannula filtration and the dark green solid washed with diethyl ether, then dried under vacuum.

Crystals suitable for single crystal X-ray diffraction were obtained by salt metathesis of **[27^{Ph}]BF$_4$** *via* the addition of twenty equivalents of NaPF$_6$ into a dichloromethane solution. Crystals were subsequently grown by the slow diffusion of pentane into a dichloromethane solution of **[27^{Ph}]PF$_6$**. Two separate batches of crystals were obtained – one green, the other orange.

Yield = 250 mg (82 %)

'One-pot' synthesis of [27^{Ph}]BF$_4$

To an oven-dried Schlenk tube was added [Ru(η^5-C$_5$H$_5$)(PPh$_3$)$_2$Cl], **[26^{Ph}]** (250 mg, 0.34 mmol), phenylacetylene (75 µL, 51 mg, 0.5 mmol, 1.5 equivalents) and methanol (10 mL), which was heated under reflux for 30 minutes. The red solution was filtered and the solvent removed under vacuum. The red solid was redissolved in dichloromethane (10 mL) to which 1-fluoro-2,4,6-trimethylpyridinium tetrafluoroborate (70 mg, 0.31 mmol, 0.9 equivalents) was added as a solid. The solution was stirred for 30 minutes to obtain a green solution which was then reduced under vacuum to approximately 1 mL. A green powder precipitated on the addition

of pentane (*ca.* 10 mL). The solvent was removed by cannula filtration and the precipitate washed with diethyl ether. The green powder was filtered and dried under vacuum.

Yield = 120 mg (47 %)

^{1}H NMR (CD$_2$Cl$_2$, 500 MHz, 295 K): δ 5.45 (s, 5H, H$_1$), 6.98 − 7.05 (m, 14H, H$_{9/10}$, H$_5$), 7.22 − 7.28 (m, 13H, H$_{9/10}$, H$_7$), 7.34 (app. t, 2H, $^{3}J_{HH}$ = 7.6 Hz, H$_6$), 7.40 – 7.46 (t, 6H, $^{3}J_{HH}$ = 7.4 Hz, H$_{11}$)

^{13}C{^{1}H} NMR (CD$_2$Cl$_2$, 125 MHz, 295 K): δ 96.7 (s, C$_1$), 122.3 (s, C$_{5/6}$), 124.3 (s, C$_{5/6}$), 129.1 (s, C$_7$), 129.1 (virtual t, sum of J_{CP} = 10.6 Hz, C$_{9/10}$), 131.6 (s, C$_{11}$), 133.6 (virtual t, sum of J_{CP} = 10.6 Hz, C$_{9/10}$), 139.0 (m, C$_8$), 150.7 (s, C$_4$), 196.7 (d, $^{1}J_{CF}$ = 222.1 Hz, C$_3$), 389.0 (dt, $^{2}J_{CF}$ = 39.3 Hz, $^{2}J_{CP}$ = 16.2 Hz, C$_2$)

^{19}F NMR (CD$_2$Cl$_2$, 376 MHz, 295 K): δ -208.7 (s, F$_3$), -153.7 (BF$_4^-$)

^{31}P{^{1}H} NMR (CD$_2$Cl$_2$, 202 MHz, 295 K): δ 42.1 (s, **P**Ph$_3$)

ESI-MS (m/z): Expected for C$_{49}$H$_{40}$FP$_2$$^{101.9}$Ru = 811.1627; Observed: 811.1656 [M]$^+$ (Error = 2.9 mDa)

Elemental Analysis: C$_{49}$H$_{40}$BF$_5$P$_2$Ru Calc. /% C 65.56, H 4.49, Found /% C 65.32 H 4.74

7.2.36 Synthesis of [Ru(η^5-C$_5$H$_5$)(PPh$_3$)$_2$(C=C{F}C$_6$H$_4$-4-CF$_3$)]BF$_4$, [27^{CF3}]BF$_4$

To an oven-dried Schlenk tube was added [Ru(η^5-C$_5$H$_5$)(PPh$_3$)$_2$(-C≡C{C$_6$H$_4$-4-CF$_3$})], **[26^{CF3}]** (148 mg, 0.17 mmol) in dichloromethane (5 mL). 1-fluoro-2,4,6-trimethylpyridinium tetrafluoroborate (35.2 mg, 0.15 mmol, 0.9 equivalents) was added, and an immediate colour change was observed from yellow to green. The volume of solvent was reduced under vacuum to approximately 0.5 mL, and a green solid precipitated on the addition of excess pentane. The solvent was then removed by cannula filtration and the dark green solid washed with diethyl ether, then dried under vacuum.

Yield = 124 mg (75 %)

^{1}H NMR (CD$_2$Cl$_2$, 500 MHz, 295 K): δ 5.50 (s, 5H, H$_1$), 6.99 – 7.06 (m, 14H, H$_5$, H$_{10/11}$), 7.24 – 7.31 (m, 12H, H$_{10/11}$), 7.44 (t, 6H, $^3J_{HH}$ = 7.31 Hz, H$_{12}$), 7.50 (d, 2H, $^3J_{HH}$ = 8.3 Hz, H$_6$)

^{13}C{^{1}H} NMR (CD$_2$Cl$_2$, 125 MHz, 295 K): δ 96.7 (s, C$_1$), 122.6 (s, C$_5$), 123.9 (q, $^1J_{CF}$ = 270.9 Hz, C$_8$), 125.4 (q, $^3J_{CF}$ = 3.8 Hz, C$_6$), 128.6 (virtual t, sum of J_{CP} = 10.5 Hz, C$_{10/11}$), 129.5 (q, $^2J_{CF}$ = 32.1 Hz, C$_7$), 131.5 (s, C$_{12}$), 132.9 (m, sum of J_{CP} = 52.7 Hz, C$_9$), 133.3 (virtual t, sum of J_{CP} = 10.4 Hz, C$_{10/11}$), 195.5 (d, $^1J_{CF}$ = 221.0 Hz, C$_3$), 383.5 (m, C$_2$). C$_4$ could not be observed.

^{19}F NMR (CD$_2$Cl$_2$, 376 MHz, 295 K): δ -212.1 (s, F$_3$), -153.8 (BF$_4^-$), -64.1 (s, F$_8$)

^{31}P{^{1}H} NMR (CD$_2$Cl$_2$, 202 MHz, 295 K): δ 41.0 (s, **P**Ph$_3$)

ESI-MS (m/z): Expected for C$_{50}$H$_{39}$F$_4$P$_2$$^{101.9}$Ru = 879.1501; Observed: 879.1540 [M]$^+$ (Error = 3.9 mDa)
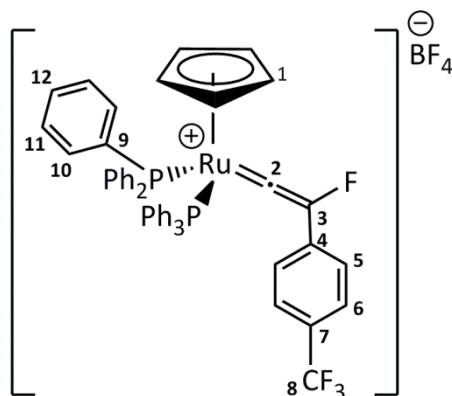
Elemental Analysis: C$_{50}$H$_{39}$BF$_8$P$_2$Ru Calc. /% C 62.19, H 4.07, Found /% C 61.70, H 4.36

7.2.37 Synthesis of [Ru(η^5-C$_5$H$_5$)(PPh$_3$)$_2$(C=C{F}C$_6$H$_4$-4-OMe)]BF$_4$, [27^{OMe}]BF$_4$
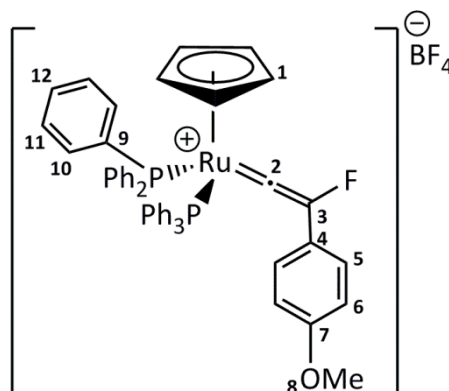
To an oven-dried Schlenk tube was added [Ru(η^5-C$_5$H$_5$)(PPh$_3$)$_2$(-C≡C{C$_6$H$_4$-4-OMe})], **[26^{OMe}]** (183 mg, 0.22 mmol) in dichloromethane (5 mL). 1-fluoro-2,4,6-trimethylpyridinium tetrafluoroborate (45 mg, 0.20 mmol, 0.9 equivalents) was added, and an immediate colour change was observed from yellow to green. The volume of solvent was reduced under vacuum to approximately 0.5 mL, and a green solid precipitated on the addition of excess pentane. The solvent was then removed by cannula filtration and the dark green solid washed with pentane, then dried under vacuum.

Yield = 144 mg (70 %)

^{1}H NMR (CD$_2$Cl$_2$, 500 MHz, 295 K): δ 3.81 (s, 3H, H$_8$), 5.37 (s, 5H, H$_1$), 6.89 – 6.92 (m, 2H, H$_6$), 6.95 – 7.03 (m, 14H, H$_{10}$, H$_5$), 7.23 (app. t, 12H, $^3J_{HH}$ = 8.1 Hz, H$_{11}$), 7.42 (t, 6H, $^3J_{HH}$ = 7.4 Hz, H$_{12}$)

^{13}C{^{1}H} NMR (CD$_2$Cl$_2$, 125 MHz, 295 K): δ 55.4 (s, C$_8$), 96.3 (s, C$_1$), 114.5 (s, C$_6$), 127.0 (s, C$_5$), 128.7 (virtual t, sum of J_{CP} = 10.8 Hz, C$_{10/11}$), 131.2 (s, C$_{12}$), 133.2 (virtual t, sum of J_{CP} = 10.6 Hz. C$_{10/11}$), 133.2 (m, C$_9$), 160.8 (s, C$_7$), 195.6 (d, $^2J_{CF}$ = 225.4 Hz, C$_3$), 389.9 (m, C$_2$)

C$_4$ could not be observed.

^{19}F NMR (CD$_2$Cl$_2$, 376 MHz, 295 K): δ -212.1 (s, F$_3$), -153.8 (BF$_4^-$)

^{31}P{^{1}H} NMR (CD$_2$Cl$_2$, 202 MHz, 295 K): δ 42.8 (s, **P**Ph$_3$)

ESI-MS (m/z): Expected for C$_{50}$H$_{42}$FOP$_2$Ru =841.1733; Observed: 841.1749 [M]$^+$ (Error = 1.6 mDa)

Elemental Analysis: C$_{50}$H$_{42}$BF$_5$OP$_2$Ru Calc. /% C 64.73, H 4.56, Found /% C 64.206, H 4.863

7.2.38 Synthesis of [Ru(η^5-C$_5$H$_5$)(PPh$_3$)$_2$(C=C{H}Ph)]PF$_6$, [28]PF$_6$
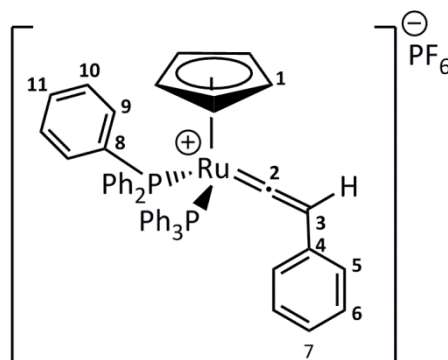
To an oven-dried Schlenk tube was added [Ru(η^5-C$_5$H$_5$)(PPh$_3$)$_2$Cl], **[25]** (250 mg, 0.34 mmol), phenylacetylene (55 µL, 0.5 mmol, 1.5 equivalents), NH$_4$PF$_6$ (169 mg, 1 mmol, 2 equivalents) and methanol (15 mL), which was heated under reflux for 30 minutes. The solution was allowed to cool, filtered and evaporated to dryness. The red residue was extracted with dichloromethane (5 mL) and filtered into stirring diethyl ether (70 mL) to yield a red/orange precipitate

Yield = 212 mg (66 %)

The spectroscopic data matched that of the literature.[274]

^{1}H NMR (CD$_2$Cl$_2$, 400 MHz, 295 K): δ 5.28 (s, 5H, H$_1$), 5.43 (t, 1H, $^4J_{HP}$ = 2.4 Hz, H$_3$), 7.00 − 7.12 (m, 14H, H$_{9/10}$, H$_{5/6}$), 7.16 (tt, 1H, $^3J_{HH}$ = 7.4 Hz, $^4J_{HH}$ = 1.2 Hz, H$_7$), 7.20 − 7.31 (m, 14H, H$_{9/10}$, H$_{5/6}$), 7.43 (t, 6H, $^3J_{HH}$ = 7.4 Hz, H$_{11}$)

^{31}P{^{1}H} NMR (CD$_2$Cl$_2$, 162 MHz, 295 K): δ -143.0 (sept, $^1J_{PF}$ = 710 Hz, PF$_6$), 43.9 (s, **P**Ph$_3$)

7.2.39 Synthesis of [Ru(η⁵-C₅H₅)(dppe)(-C≡C{Ph})], [29]

Step 1: Synthesis of [Ru(η⁵-C₅H₅)(dppe)(C=C{H}Ph)]PF₆
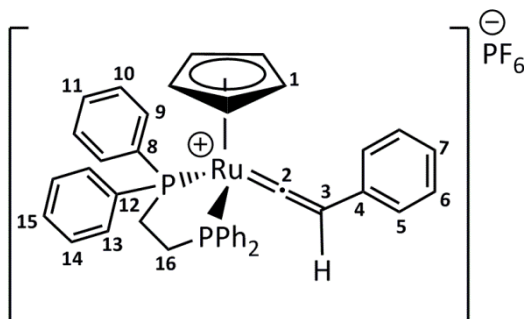
A mixture of [Ru(η⁵-C₅H₅)(dppe)Cl] (156 mg, 0.26 mmol), **[49]** phenylacetylene (27mg, 0.26 mmol) and NH_4PF_6 (82 mg, 0.5 mmol, 2 equivalents) was heated in refluxing methanol (15 mL) for 1 hour. The solvent was allowed to cool and cannula filtered to remove unreacted starting material. The filtrate was then evaporated, the residue extracted in CH_2Cl_2 (10 mL) and the extract filtered into stirring diethyl ether (50 mL). The buff precipitate was collected, washed with Et_2O and dried in vacuo.

Yield = 80 mg (39 %)

^{1}H NMR (CD_2Cl_2, 500 MHz, 295 K): δ 2.69 – 2.88 (m, 2H, $H_{16a/b}$), 2.94 – 3.13 (m, 2H, $H_{16a/b}$), 4.65 (t, 1H, ^4J = 1.4 Hz, H_3), 5.59 (s, 5H, H_1), 6.25 (m, 2H, ar), 6.83 – 6.88 (m, 2H, ar), 6.88 – 6.93 (m, 1H, ar), 7.15 – 7.22 (m, 4H, ar), 7.39 – 7.56 (m, 16H, ar)

^{13}C{^{1}H} NMR (CD_2Cl_2, 125 MHz, 295 K): δ 27.4 (m, C_{16}), 92.4 (s, C_1), 117.9 (s, C_3), 125.9 (s, C_4), 126.0 (s, $C_{5/6}$), 126.8 (s, C_7), 128.9 (s, $C_{5/6}$), 129.6 (m, ar), 131.7 (virtual t, sum of J_{CP} = 10.8 Hz, ar), 132.1 (m, ar), 132.5 (virtual. t, sum of J_{CP} = 10.4 Hz, ar), 134.1 (m, $C_{8/12}$), 135.3 (m, $C_{8/12}$), 353.8 (t, $^2J_{CP}$ = 15.8 Hz, C_2)

^{31}P{^{1}H} NMR (CD_2Cl_2, 202 MHz, 295 K): δ 87.1 (s, **P**Ph₃)

ESI-MS (m/z): Expected for $C_{39}H_{35}P_2{}^{101.9}Ru$ = 667.1262; Observed: 667.1287 [M]$^+$ (Error = 2.5 mDa)

Step 2: Synthesis of [Ru(η^5-C$_5$H$_5$)(dppe)(-C≡C{Ph})], **[29]**
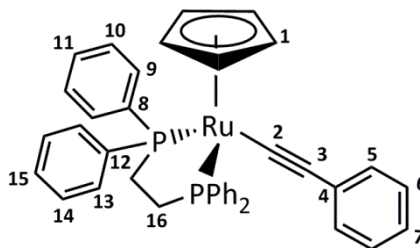
A solution of [Ru(η^5-C$_5$H$_5$)(dppe)(C=C{H}Ph)]PF$_6$ (40 mg, 0.05 mmol) in CH$_2$Cl$_2$ (10 mL) was treated with methanolic KOH (50 mg in 1 mL). The resulting yellow solution was evaporated to dryness, and the residue extracted with CH$_2$Cl$_2$. Hexane was added to the CH$_2$Cl$_2$ extract, and the volume then reduced in vacuo to give a yellow precipitate. This was isolated by cannula filtration and dried under vacuum.

Yield = 20 mg (62 %)

^{1}H NMR (CD$_2$Cl$_2$, 500 MHz, 295 K): δ 2.24 − 2.38 (m, 2H, H$_{16a/b}$), 2.60 − 2.78 (m, 2H, H$_{16a/b}$), 4.80 (s, 5H, H$_1$), 6.35 − 6.39 (m, 2H, H$_5$), 6.77 − 6.82 (m, 1H, H$_7$), 6.85 − 6.91 (m, 2H, H$_6$), 7.23 − 7.34 (m, 10H, ar), 7.40 − 7.48 (m, 6H, ar), 7.88 − 7.95 (m, 4H, ar)

^{13}C{^{1}H} NMR (CD$_2$Cl$_2$, 125 MHz, 295 K): δ 27.7 (m, C$_{16a/b}$), 82.3 (t, J_{CP} = 2.3 Hz, C$_1$), 111.4 (s, C$_3$), 117.2 ($^2J_{CP}$ = 25.9 Hz, C$_2$), 122.8 (s, ar), 127.3 (s, ar), 127.6 (virtual t, sum of J_{CP} = 10.0 Hz, C$_{9/10/13/14}$), 127.9 (virtual t, sum of J_{CP} = 9.0 Hz, C$_{9/10/13/14}$), 128.9 (s, ar), 129.3 (s, ar), 130.0 (s, C$_4$), 130.1 (s, ar), 131.5 (virtual t, sum of J_{CP} = 10.6 Hz, C$_{9/10/13/14}$), 133.8 (virtual t, sum of J_{CP} = 10.4 Hz, C$_{9/10/13/14}$), 137.2 (m, C$_{8/12}$), 142.2 (m, C$_{8/12}$)

^{31}P{^{1}H} NMR (CD$_2$Cl$_2$, 202 MHz, 295 K): δ 86.3 (s, **P**Ph$_3$)

7.2.40 Synthesis of [Ru(η⁵-C₅H₅)(dppe)(C=C{F}Ph)]NSI, [30]NSI
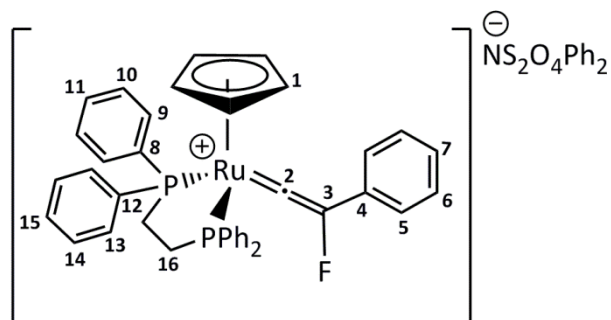
An NMR tube with a PTFE Young's tap was charged with [Ru(η⁵-C₅H₅)(dppe)(-C≡C{Ph})], **[29]** (26 mg, 38 µmol) and NFSI (12 mg, 38 µmol, 1 equivalent) in CD₂Cl₂ (0.5 mL). An immediate colour change was observed from yellow to bright green. Quantitative conversion was observed by ¹H and ³¹P{¹H} NMR spectroscopy and samples were used directly without isolation or further purification.

Crystals suitable for single crystal X-ray diffraction were obtained by salt metathesis of **[30]NSI** *via* the addition of twenty equivalents of NaPF₆ into a dichloromethane solution. Crystals were subsequently grown by the slow diffusion of pentane into a dichloromethane solution of **[30]PF₆**.

¹H NMR (CD₂Cl₂, 500 MHz, 295 K): δ 2.80 – 3.00 (m, 4H, H₁₆), 5.68 (s, 5H, H₁), 6.39 – 6.43 (m, 2H, H₅), 6.96 – 7.04 (m, 3H, H₆/₇), 7.10 – 7.17 (m, 4H, ar), 7.21 – 7.26 (m, 4H, ar), 7.27 – 7.32 (m, 6H, ar), 7.34 – 7.44 (m, 10H, ar), 7.48 – 7.53 (m, 2H, ar), 7.76 – 7.77 (m, 2H, ar), 7.77 – 7.79 (m, 2H, ar)

¹³C{¹H} NMR (CD₂Cl₂, 125 MHz, 295 K): δ 28.2 (m, C₁₆), 94.5 (s, C₁), 122.4 (s, C₅), 126.9 (s, ar), 128.1 (s, C₇), 128.2 (s, ar), 128.8 (s, C₆), 129.2 (virtual t, sum of J_{CP} = 11.0 Hz, C₉/₁₀/₁₃/₁₄), 129.7 (virtual t, sum of J_{CP} = 10.0 Hz, C₉/₁₀/₁₃/₁₄), 130.1 (s, ar), 131.7 (virtual t, sum of J_{CP} = 10.8 Hz, C₉/₁₀/₁₃/₁₄), 132.1 (d, J_{CP} = 4.0 Hz, ar), 132.8 (virtual t, sum of J_{CP} = 11.4 Hz, C₉/₁₀/₁₃/₁₄), 134.2 – 135.3 (m, ar, C₈/₁₂), 146.9 (s, ar), 193.4 (dt, $^1J_{CF}$ = 225.7 Hz, $^3J_{CP}$ = 6.3 Hz, C₃), 385.0 (m, C₂)

³¹P{¹H} NMR (CD₂Cl₂, 202 MHz, 295 K): δ 77.9 (s, **P**Ph₃)

¹⁹F NMR (CD₂Cl₂, 471 MHz, 295 K): δ -210.8 (s, F₃)

ESI-MS (m/z): Expected for C₃₉H₃₄FP₂¹⁰¹·⁹Ru = 685.1168; Observed: 685.1147 [M]⁺ (Error = 2.1 mDa)

7.2.41 Synthesis of [Ru(η^5-C$_5$H$_5$)(PPh$_3$)$_2$(C=C{C$_5$H$_4$N}Ph)]BF$_4$, [37^{Ph}]BF$_4$
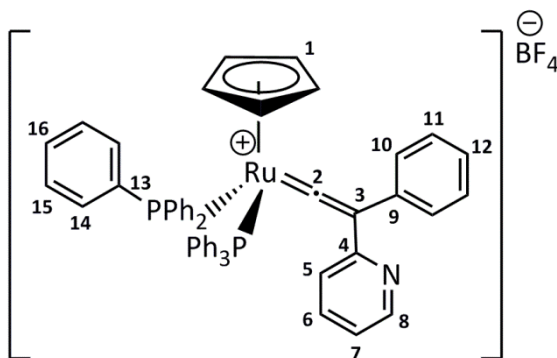
An NMR tube with a PTFE Young's tap was charged with [Ru(η^5-C$_5$H$_5$)(PPh$_3$)$_2$(-C≡C{Ph})] **[26^{Ph}]** (40 mg, 45 µmol) and 1-fluoropyridinium tetrafluoroborate (8 mg, 45 µmol, 1 equivalent) in CD$_2$Cl$_2$ (0.5 mL), and an immediate colour change was observed from yellow to red.

^{1}H NMR (CD$_2$Cl$_2$, 500 MHz, 295 K): δ 5.13 (s, 5H, H$_1$), 6.37 (dt, 1H, $^3J_{HH}$ = 8.0 Hz, $^4J_{HH}$ = 0.9 Hz, pyr) 6.74 – 7.53 (m, 68H, ar), 7.86 (m, 1H, H$_8$)

^{13}C{^{1}H} NMR (CD$_2$Cl$_2$, 125 MHz, 295 K): δ 96.4 (s, C$_1$), 120.5 (s, C$_{5/7}$), 121.5 (s, C$_{5/7}$), 128.6 (virtual t, sum of J_{CP} = 10.8 Hz, C$_{14/15}$), 129.2 (s, C$_{12}$), 130.0 (C$_{10/11}$), 131.3 (s, C$_{16}$), 131.7 (s, C$_{10/11}$), 134.2 (virtual t, sum of J_{CP} = 10.3 Hz, C$_{14/15}$), 136.2 (s, C$_{3/9}$), 136.7 (s, C$_6$), 148.4 (s, C$_8$), 153.9 (s, C$_4$) , 357.5 (t, $^2J_{CP}$ = 16.2 Hz, C$_2$)

Carbons 3, 9 and 13 could not be assigned and may be obscured.

^{31}P{^{1}H} NMR (CD$_2$Cl$_2$, 202 MHz, 295 K): δ 41.5 (s, **P**Ph$_3$)

ESI-MS (m/z): Expected for C$_{54}$H$_{44}$NP$_2$$^{101.9}$Ru = 870.1987; Observed: 870.2024 [M]$^+$ (Error = 3.7 mDa)

All attempts to obtain elemental analysis for **[37^{Ph}]BF$_4$** were unsuccessful due to the presence of several unidentified organometallic species at low concentrations in the reaction mixture which could not be removed by washing with pentane or diethyl ether.

7.2.42 Synthesis of [Ru(η⁵-C₅H₅)(C=C{C₅H₄N}C₆H₄-4-CF₃)(PPh₃)₂]BF₄, [37^{CF3}]BF₄

An NMR tube with a PTFE J. Young's tap was charged with [Ru(η⁵-C₅H₅)(PPh₃)₂(-C≡C{C₆H₄-4-CF₃})] **[26^{CF3}]** (20 mg, 23 μmol) and 1-fluoropyridinium tetrafluoroborate (4 mg, 23 μmol, 1 equivalent) in CD_2Cl_2 (0.5 mL). An immediate colour change was observed from yellow to red.

Red, needle-like crystals were obtained serendipitously from the pentane washings of the reaction mixture.

Yield = 8 mg (34 %)

^{1}H NMR (CD_2Cl_2, 500 MHz, 295 K): δ 5.18 (s, 5H, H_1), 6.37 (dt, 1H, $^3J_{HH}$ = 8.0 Hz, $^4J_{HH}$ = 0.8 Hz, H_5) 6.96 (ddd, 1H, $^3J_{HH}$ = 7.6 Hz, $^3J_{HH}$ = 4.8 Hz, $^4J_{HH}$ = 1.0 Hz, H_7), 7.00 − 7.09 (m, 14H, H_{10}, $H_{15/16}$), 7.18 (m, 12H, $H_{15/16}$), 7.40 (m, 6H, H_{17}), 7.49 (app. td, 1H, $^3J_{HH}$ = 7.8 Hz, $^4J_{HH}$ = 1.6 Hz, H_6), 7.55 (d, 2H, $^3J_{HH}$ = 8.1 Hz, H_{11}), 8.00 (m, 1H, H_8)

^{13}C{^{1}H} NMR (CD_2Cl_2, 125 MHz, 295 K): δ 95.7 (s, C_1), 120.9 (s, C_5), 122.0 (s, C_7), 124.4 (q, $^1J_{CF}$ = 272.7 Hz, C_{13}), 126.7 (q, $^1J_{CF}$ = 3.5 Hz, C_{11}), 128.8 (virtual t, sum of J_{CP} = 10.5 Hz, C_{16}), 131.5 (s, C_{17}), 133.0 (s, C_{10}), 133.8 (m, C_{14}), 134.1 (virtual t, sum of J_{CP} = 10.5 Hz, C_{15}), 135.7 (s, C_3), 137.1 (s, C_6), 148.8 (s, C_8), 153.4 (s, C_4), 354.9 (t, $^2J_{CP}$ = 15.4 Hz, C_2)

Carbons C_9 and C_{12} could not be assigned and may be obscured.

^{19}F NMR (CD_2Cl_2, 376 MHz, 295 K): δ -62.6 (s, F_{13}), -153.0 (BF₄⁻)

^{31}P{^{1}H} NMR (CD_2Cl_2, 202 MHz, 295 K): δ 41.1 (s, **P**Ph₃)

ESI-MS (m/z): Expected for C₅₅H₄₃F₃NP₂$^{101.9}$Ru = 938.1876; Observed: 938.1858 [M]⁺ (Error = 1.8 mDa)

All attempts to obtain elemental analysis for **[37^{CF3}]BF₄** were unsuccessful.

7.2.43 Synthesis of [Ru(η^5-C$_5$H$_5$)(PPh$_3$)$_2$(C=C{CF$_3$}Ph)]BF$_4$, [38^{Ph}]BF$_4$

To an oven-dried ampoule was added [Ru(η^5-C$_5$H$_5$)(PPh$_3$)$_2$(-C≡C{Ph})], **[26^{Ph}]** (190 mg, 0.24 mmol) in dichloromethane (10 mL). 5-(Trifluoromethyl)dibenzothiophenium tetrafluoroborate (73 mg, 22 mmol, 0.9 equivalents) was added, and allowed to stir for 4 hours. The mixture was cannula filtered to remove any residual 5-(trifluoromethyl)dibenzothiophenium tetrafluoroborate, and the volume of solvent was reduced under vacuum to approximately 0.5 mL. A red/orange solid precipitated on the addition of pentane. The solid was isolated by filtration and redissolved in minimum dichloromethane and precipitated with pentane and isolated by filtration a further three times. The solvent was then removed by cannula filtration and the solid dried under vacuum.

Red crystals suitable for X-ray diffraction were grown from the slow diffusion of pentane into a dichloromethane solution of **[38^{Ph}]BF$_4$**.

Yield = 150 mg (66 %)

^{1}H NMR (CD$_2$Cl$_2$, 400 MHz, 295 K): δ 4.74 (s, 5H, H$_1$), 6.80 – 6.84 (m, 2H, H$_5$), 6.84 – 6.92 (m, 12H, H$_{10/11}$), 7.23 –7.31 (td, 12H, $^3J_{HH}$ = 7.8 Hz, $^4J_{HH}$ = 1.6 Hz, H$_{10/11}$), 7.31 – 7.37 (m, 2H, H$_6$), 7.42 (tt, 1H, $^3J_{HH}$ = 7.6 Hz, $^4J_{HH}$ = 1.9 Hz, H$_7$), 7.48 (t, 6H, $^3J_{HH}$ = 7.8 Hz, H$_{12}$)

^{13}C{^{1}H} NMR (CD$_2$Cl$_2$, 125 MHz, 295 K): δ 95.8 (s, C$_1$), 122.1 (q, $^1J_{CF}$ = 272.7 Hz, C$_8$), 123.3 (s, C$_4$), 126.3 (q, $^2J_{CF}$ = 34.8 Hz, C$_3$), 128.7 (virtual t, sum of J_{CP} = 10.6 Hz, C$_{10/11}$), 129.4 (s, C$_6$), 129.8 (s, C$_7$), 131.4 (s, C$_5$), 131.5 (s, C$_{12}$), 133.2 – 132.4 (m, C$_9$), 133.6 (virtual t, sum of J_{CP} = 10.6 Hz, C$_{10/11}$), 340.0 (tq, $^2J_{CP}$ = 15.2 Hz, $^3J_{CF}$ = 3.3 Hz, C$_2$)

^{19}F NMR (CD$_2$Cl$_2$, 376 MHz, 295 K): δ -57.6 (s, F$_8$), -154.1 (BF$_4$)

^{31}P{^{1}H} NMR (CD$_2$Cl$_2$, 202 MHz, 295 K): δ 39.6 (s, **P**Ph$_3$)

ESI-MS (m/z): Expected for $C_{50}H_{40}F_3P_2{}^{101.9}Ru$ = 861.1595; Observed: 861.1611 [M]$^+$ (Error = 1.6 mDa)

Elemental Analysis: $C_{50}H_{40}BF_7P_2Ru$ Calc. /% C 63.37, H 4.25 Found /% C 63.07, H 4.26

7.2.44 Synthesis of [Ru(η^5-C$_5$H$_5$)(PPh$_3$)$_2$(C=C{Cl}Ph)]BF$_4$, [39]BF$_4$

To an oven-dried Schlenk tube was added [Ru(η^5-C$_5$H$_5$)(PPh$_3$)$_2$(-C≡C{Ph})], **[26^{Ph}]** (50 mg, 0.063 mmol) in CH$_2$Cl$_2$ (10 mL). To this solution was added sodium tetrafluoroborate (6.93 mg, 0.063 mmol, 1 equivalent) followed by N-chlorosuccinimide (8.45 mg, 0.063 mmol, 1 equivalent), resulting in a colour change from orange to bright green. After stirring for 1 minute the solution was transferred by cannula filtration to another oven-dried Schlenk tube, and the solvent was removed under vacuum. The residue was washed three times with diethyl ether and dried under vacuum leaving the green solid product.

Yield = 8 mg (14 %)

^{1}H NMR (CD$_2$Cl$_2$, 700 MHz, 295 K): δ 5.31 (s, 5H, H$_1$), 6.97 (t, 12H, $^3J_{HH}$ = 8.9 Hz, H$_{9/10}$), 7.10 (d, 2H, $^3J_{HH}$ = 7.5 Hz, H$_5$), 7.25 (t, 12H, $^3J_{HH}$ = 7.3 Hz, H$_{9/10}$), 7.31 (t, 3H, $^3J_{HH}$ = 7.5 Hz, H$_{6/7}$), 7.43 (t, $^3J_{HH}$ = 7.3 Hz, 6H, H$_{11}$), 7.46 (t, 3H, $^3J_{HH}$ = 7.5 Hz, H$_{6/7}$)

^{13}C{^{1}H} NMR (CD$_2$Cl$_2$, 176 MHz, 295 K): δ 95.9 (s, C$_1$), 127.3 (s, C$_{3/4}$), 128.1 (s, C$_5$), 128.8 (virtual t, sum of J_{CP} = 10.4 Hz, C$_{9/10}$), 129.0 (s, C$_{6/7}$), 131.3 (s, C$_{11}$), 133.0-133.3 (m, sum of J_{CP} = 52.3 Hz, C$_8$), 133.5 (virtual t, sum of J_{CP} = 10.3 Hz, C$_{9/10}$), 133.6 (s, C$_{6/7}$), 139.4 (s, C$_{3/4}$), 353.5 (m, C$_2$)

ESI-MS (m/z): Expected for $C_{49}H_{40}ClP_2{}^{101.9}Ru$ = 827.1332; Observed: 827.1306 [M]$^+$ (Error = 2.6 mDa)

7.2.45 Synthesis of [Ru(η⁵-C₅H₅)(PPh₃)₂(C=C{Br}Ph)]BF₄, [40]BF₄

To an oven-dried Schlenk tube was added [Ru(η⁵-C₅H₅)(PPh₃)₂(-C≡C{Ph})], **[26^Ph]** (50 mg, 0.063 mmol) in dichloromethane (10 mL). To this solution was added sodium tetrafluoroborate (6.93 mg, 0.063 mmol, 1 equivalent) followed by bromine (3.2 µL, 0.063 mmol, 1 equivalent), resulting in a colour change to bright green. After stirring for 1 minute the solution was transferred by cannula filtration into excess pentane producing a green precipitate. The solvent was removed by cannula filtration and the remaining green solid dried under vacuum. This was then extracted with the minimum amount of dichloromethane and recrystallised in excess pentane. The solvent was then removed by cannula filtration and the green solid product dried under vacuum.

Yield = 14 mg (23 %)

^{1}H NMR (CD$_2$Cl$_2$), 500 MHz, 295 K): δ 5.29 (s, 5H, H$_1$), 6.98 (d, 12H, $^3J_{HH}$ = 7.8 Hz, H$_9$), 7.05 (d, 2H, $^3J_{HH}$ = 7.7 Hz, H$_6$), 7.09 (d, 2H, $^3J_{HH}$ = 7.7 Hz, H$_5$), 7.27 (t, 12H, $^3J_{HH}$ = 7.8 Hz, H$_{10}$), 7.30 (t, 1H, $^3J_{HH}$ = 7.1 Hz, H$_7$), 7.45 (t, 6H, $^3J_{HH}$ = 7.2 Hz, H$_{11}$)

^{13}C{^{1}H} NMR (CD$_2$Cl$_2$, 125 MHz, 295 K): δ 95.7 (s, C$_1$), 123.7 (s, C$_{3/4}$), 127.6 (s, C$_{3/4}$), 128.8 (virtual t, sum of J_{CP} = 10.6 Hz, C$_{9/10}$), 129.2 (s, C$_{5/6/7}$), 129.3 (s, C$_{5/6/7}$), 129.4 (s, C$_{5/6/7}$), 131.3 (s, C$_{11}$), 133.0-133.4 (virtual t, sum of J_{CP} = 51.8 Hz, C$_8$), 133.6 (virtual t, sum of J_{CP} = 5.3 Hz, C$_{9/10}$), 340.3 (t, $^2J_{CP}$ = 16.0 Hz, C$_2$)

^{31}P{^{1}H} NMR (CD$_2$Cl$_2$, 202 MHz, 295 K): δ 41.2 (s, **P**Ph$_3$)

ESI-MS (m/z): Expected for C$_{49}$H$_{40}$BrP$_2$$^{101.9}$Ru = 871.0827; Observed: 871.0835 [M]$^+$ (Error = 0.8 mDa)
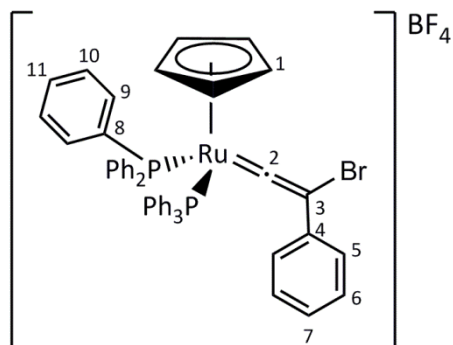
7.2.46 Synthesis of [Ru(η^5-C$_5$H$_5$)(PPh$_3$)$_2$(C=C{Br}C$_6$H$_4$-4-Br)]Br$_3$, [41]Br$_3$[64]
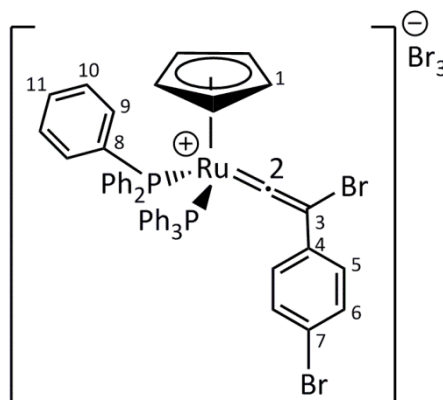
To an oven-dried Schlenk tube was added [Ru(η^5-C$_5$H$_5$)(PPh$_3$)$_2$(-C≡C{Ph})], **[26^{Ph}]** (100 mg, 0.126 mmol) in tetrahydrofuran (10 mL). Bromine (100 μL, 1.89 mmol, 15 equivalents) was added resulting in a colour change from orange to green. After 15 minutes stirring the solvent was removed by vacuum leaving a green solid. This was extracted with the minimum amount of dichloromethane and recrystallised in excess diethyl ether. The solvent was then removed by cannula filtration and the dark green crystals dried under vacuum.

Yield = 47 mg (31 %)

^{1}H NMR (CD$_2$Cl$_2$, 500 MHz, 295 K): δ 5.30 (s, 5H, H$_1$), 6.93 (d, 2H, $^3J_{HH}$ = 7.8 Hz, H$_6$), 6.97 (m, 12H, H$_9$), 7.27 (t, 12H, $^3J_{HH}$ = 6.9 Hz, H$_{10}$), 7.39 (d, 2H, $^3J_{HH}$ = 7.8 Hz, H$_5$), 7.47 (t, 6H, $^3J_{HH}$ = 6.9 Hz, H$_{11}$)

^{13}C{^{1}H} NMR (CD$_2$Cl$_2$, 125 MHz, 295 K): δ 96.1 (s, C$_1$), 123.1 (s, C$_{3/7}$), 123.2 (s, C$_{3/7}$), 126.8 (s, C$_4$), 128.9 (virtual t, sum of J_{CP} = 10.6 Hz, C$_{9/10}$), 130.7 (s, C$_{5/6}$), 131.4 (s, C$_{11}$), 132.3 (s, C$_{5/6}$), 133.1 (virtual t, sum of J_{CP} = 51.8 Hz, C$_8$), 133.6 (virtual t, sum of J_{CP} = 10.6 Hz, C$_{9/10}$), 339.3 (t, $^2J_{CP}$ = 15.9 Hz, C$_2$)

^{31}P{^{1}H} NMR (CD$_2$Cl$_2$, 202 MHz, 295 K): δ 40.9 (s, **P**Ph$_3$)

ESI-MS (m/z): Expected for C$_{49}$H$_{39}$Br$_2$P$_2$$^{101.9}$Ru = 950.9928; Observed: 950.9910 [M]$^+$ (Error = 1.8 mDa). Expected for H$_{49}$C$_{40}$BrP$_2$$^{101.9}$Ru = 871.0832; Observed: 871.0814 [M - Br]$^+$ (Error = 1.8 mDa)

7.2.47 Synthesis of [Ru(η^5-C$_5$H$_5$)(PPh$_3$)$_2$(C=C{I}Ph)]I$_3$, [42]I$_3$[64]
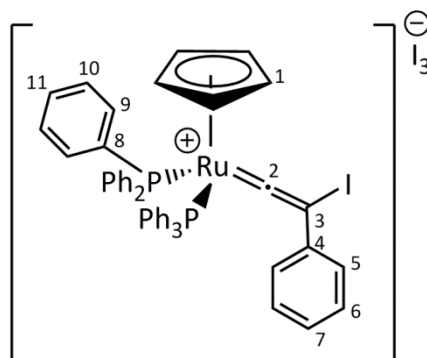
To an oven-dried Schlenk tube was added [Ru(η^5-C$_5$H$_5$)(PPh$_3$)$_2$(-C≡C{Ph})], **[26^{Ph}]** (100 mg, 0.13 mmol) in dichloromethane (10 mL). Iodine (85 mg, 0.34 mmol, 2.7 equivalents) was added resulting in an immediate colour change from orange to dark green. After stirring for 20 minutes the solvent was removed under vacuum leaving a dark green solid.

The dark green solid was extracted with the minimum amount of dichloromethane and recrystallised in excess diethyl ether. The solvent was then removed by cannula filtration and the dark green crystals dried under vacuum.

Yield = 37 mg (29 %)

^{1}H NMR (CD$_2$Cl$_2$, 500 MHz, 295 K): δ 5.23 (s, 5H, H$_1$), 6.96-7.03 (m, 12H, ar), 7.23-7.31 (m, 17H, ar), 7.43-7.50 (m, 6H, ar)

^{13}C{^{1}H} NMR (CD$_2$Cl$_2$, 125 MHz, 295 K): δ 95.2 (s, C$_1$), 128.8 (virtual t, sum of J_{CP} = 10.5 Hz, C$_{9/10}$), 129.0 (s, C$_7$), 129.1 (s, C$_{3/4}$), 129.3 (s, C$_{5/6}$), 130.1 (s, C$_{5/6}$), 131.3 (s, C$_{11}$), 133.0 (s, C$_{3/4}$), 133.0 – 133.6 (m, C$_8$), 133.7 (virtual t, sum of J_{CP} = 10.6 Hz, C$_{9/10}$), 323.6 (t, $^2J_{CP}$ = 16.0 Hz, C$_2$)

^{31}P{^{1}H} NMR (CD$_2$Cl$_2$, 202 MHz, 295 K): δ 40.3 (s, **P**Ph$_3$)

ESI-MS (m/z): Expected for C$_{49}$H$_{40}$IP$_2$$^{101.9}$Ru = 919.0688; Observed: 919.0698 [M]$^+$ (Error = 1.0 mDa)

7.2.48 Synthesis of [43]BF$_4$

An NMR tube with a PTFE J. Young's tap was charged with [Ru(η^5-C$_5$H$_5$)(PPh$_3$)$_2$(C=C{F}Ph)]BF$_4$, **[27^{Ph}]BF$_4$** (20 mg, 0.02 mmol) in d$_3$-acetonitrile (0.5 mL), and heated at 50 °C for around 2 weeks.

A pure sample of **[43]BF$_4$** could not be isolated due to the presence of several unidentified organometallic species which were formed in the reaction mixture and which could not be removed by washing with pentane or diethyl ether. All attempts to form crystals suitable for X-ray diffraction were also unsuccessful.

Selected ^{1}H NMR (CD$_3$CN, 500 MHz, 295 K): δ 4.69 (ddd, 1H, $^3J_{HF}$ = 16.9 Hz, $^2J_{PH}$ = 5.0 Hz, $^3J_{PH}$ = 1.7 Hz, H$_8$), 4.95 (s, 5H, H$_1$)

Selected ^{13}C{^{1}H} NMR (CD$_3$CN, 125 MHz, 295 K): δ 25.9 (ddd, $^1J_{CP}$ = 75.1 Hz, $^2J_{CF}$ = 7.8 Hz, $^2J_{CP}$ = 2.7 Hz, C$_8$), 92.7 (s, C$_1$), 113.7 (dt, $^1J_{CF}$ = 243.0 Hz, $^2J_{CP}$ = 5.6 Hz, C$_9$), 170.9 (dd, $^2J_{CP}$ = 32.6 Hz, $^2J_{CP}$ = 16.6 Hz, C$_2$)

^{19}F NMR (CD$_3$CN, 376 MHz, 295 K): δ -143.4 (app. dt, $^3J_{PF}$ = 48.6 Hz, $^3J_{HF}$ = 16.9 Hz, $^3J_{PF}$ = 16.2 Hz, F$_9$), -153.0 (BF$_4$)

^{31}P{^{1}H} NMR (CD$_3$CN, 202 MHz, 295 K): δ 42.3 (dd, $^3J_{PF}$ = 16.2 Hz, $^3J_{PP}$ = 4.4 Hz), 46.6 (dd, $^3J_{PF}$ = 48.6 Hz, $^3J_{PP}$ = 4.4 Hz)

ESI-MS (m/z): Expected for C$_{49}$H$_{40}$FP$_2$$^{101.9}$Ru = 811.1627; Observed: 811.1637 [M]$^+$ (Error = 1.0 mDa)
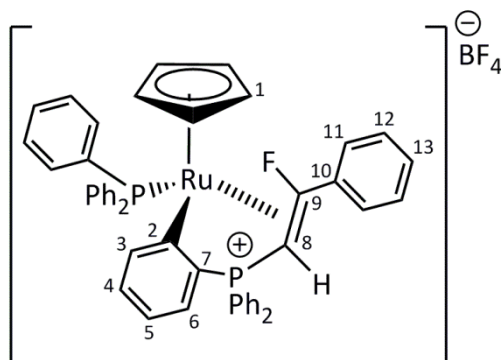
7.2.49 Synthesis of [Ru(η^5-C$_5$H$_5$)(PPh$_3$)$_2$(-C(NC$_5$H$_5$)=C(C$_6$H$_5$)F)]BF$_4$, [44]BF$_4$
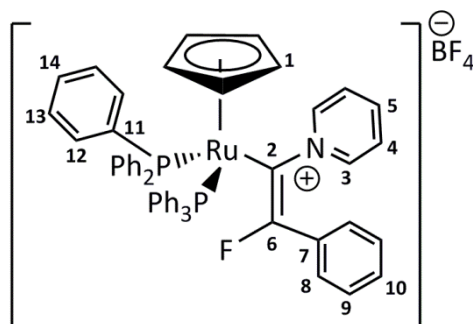
To an oven-dried ampoule was added [Ru(η^5-C$_5$H$_5$)(PPh$_3$)$_2$(C=C{F}Ph)]BF$_4$, **[27^{Ph}]BF$_4$** (65 mg, 7.2 μmol) and pyridine (1 mL), and left to stir for 20 minutes. The reaction mixture was then added *via* a syringe to rapidly stirring diethyl ether (15 mL), to precipitate an orange powder. The solid was isolated by cannula filtration and dried under vacuum.

Orange crystals suitable for X-ray diffraction were obtained on layering a 2:1 pyridine:dichloromethane solution of **[27^{Ph}]BF$_4$** with ether, 15 minutes after [Ru] dissolution.

Yield = 40 mg (57 %)

^{1}H NMR (CD$_2$Cl$_2$, 700 MHz, 275 K): δ 4.16 (s, 5H, H$_1$), 6.32 (d, 2H, $^3J_{HH}$ = 7.6 Hz, H$_8$), 6.97 (app. t, 2H, $^3J_{HH}$ = 7.6 Hz, H$_9$), 7.02 (t, 1H, $^3J_{HH}$ = 7.6 Hz, H$_{10}$), 7.19 (app. t, 12H, $^3J_{HH}$ = 7.4 Hz, H$_{13}$), 7.27 (t, 12H, $^3J_{HH}$ = 7.4 Hz, H$_{12}$), 7.39 (t, 6H, $^3J_{HH}$ = 7.4 Hz, H$_{14}$), 7.61 (app. t, 2H, $^3J_{HH}$ = 7.0 Hz, H$_4$), 8.07 (t, 1H, $^3J_{HH}$ = 7.9 Hz, H$_5$), 8.27 (d, 2H, $^3J_{HH}$ = 5.8 Hz, H$_3$)

^{13}C{^{1}H} NMR (CD$_2$Cl$_2$, 176 MHz, 275 K): δ 84.9 (s, C$_1$), 127.2 (s, C$_4$), 127.8 (s, C$_{8/9}$), 128.1 (virtual t, sum of J_{CP} = 8.6 Hz, C$_{12/13}$), 128.6 (s, C$_{10}$), 128.7 (s, C$_{8/9}$), 129.8 (s, C$_{14}$), 132.3 (d, $^2J_{CF}$ = 32.8 Hz, C$_7$), 134.1 (virtual t, sum of J_{CP} = 8.6 Hz, C$_{12/13}$), 138.5 (virtual t, sum of J_{CP} = 39.7 Hz, C$_{11}$), 142.6 (s, C$_5$), 145.4 (s, C$_3$), 149.6 (dt, $^1J_{CF}$ = 84.8, $^3J_{CP}$ = 17.0 Hz, C$_2$), 164.5 (d, $^1J_{CF}$ = 232.7 Hz, C$_6$)

^{19}F NMR (CD$_2$Cl$_2$, 376 MHz, 295 K): δ -152.3 (BF$_4^-$), -72.8 (t, $^4J_{PF}$ = 20.1 Hz, F$_6$)

^{31}P{^{1}H} NMR (CD$_2$Cl$_2$, 202 MHz, 293 K): δ 44.0 (d, $^4J_{PF}$ = 20.3 Hz, **P**Ph$_3$)

ESI-MS (m/z): Expected for C$_{54}$H$_{45}$FNP$_2$$^{101.9}$Ru = 890.2049; Observed: 890.2039 [M]$^+$ (Error = 1.0 mDa)

All attempts to obtain elemental analysis for **[44]BF$_4$** were unsuccessful.

7.2.50 Synthesis of [Ru(η^5-C$_5$H$_5$)(dppe)(-C(NC$_5$H$_5$)=C(C$_6$H$_5$)F)]NSI, [45]NSI

An NMR tube with a PTFE J. Young's tap was charged with [Ru(η^5-C$_5$H$_5$)(dppe)(C=C{F}Ph)]NSI, **[30]NSI** (15 mg, 23 μmol) and pyridine (1.8 μL, 23 μmol, 1 equivalent) in CD$_2$Cl$_2$ (0.5 mL) and allowed to stand overnight, during which time a colour change was observed from green to red. Quantitative conversion was observed by ^{1}H NMR and ^{31}P{^{1}H} NMR spectroscopy.

^{1}H NMR (CD$_2$Cl$_2$, 500 MHz, 295 K): δ 2.47 − 2.63 (m, 2H, H$_{19a/b}$), 3.00 − 3.19 (m, 2H, H$_{19a/b}$), 4.17 (s, 5H, H$_1$), 5.87 (d, 2H, $^3J_{HH}$ = 8.1 Hz, H$_8$), 6.87 (app.t, 2H, $^3J_{HH}$ = 7.8 Hz, H$_9$), 6.93 − 6.98 (m, 1H, H$_{10}$), 7.23 − 7.29 (m, 9H, ar), 7.29 − 7.33 (m, 2H, ar), 7.36 − 7.41 (m, 6H, ar), 7.48 − 7.59 (m, 7H, H$_4$, ar), 7.75 − 7.82 (m, 8H, ar), 7.84 (d, 2H, $^3J_{HH}$ = 5.9 Hz, H$_3$), 7.94 (tt, 1H, $^3J_{HH}$ = 7.7 Hz, $^4J_{HH}$ = 1.4 Hz, H$_5$)

^{13}C{^{1}H} NMR (CD$_2$Cl$_2$, 125 MHz, 295 K): δ 29.7 (m, C$_{19}$), 85.0 (s, C$_1$), 127.0 (s, C$_{21}$), 127.3 (s, C$_8$), 127.4 (s,ar), 128.2 (s, C$_{22}$), 128.5 (s, C$_9$), 128.7 (virtual t, sum of J_{CP} = 9.6 Hz, C$_{12/13/16/17}$), 129.0 (virtual t, sum of J_{CP} = 10.0 Hz, C$_{12/13/16/17}$), 129.8 (s, C$_{14}$), 130.2 (s, C$_{18}$), 130.3 (s, C$_{23}$), 131.5 (virtual t, sum of J_{CP} = 9.6 Hz, C$_{12/13/16/17}$), 132.5 (virtual t, sum of J_{CP} = 9.6 Hz, C$_{12/13/16/17}$), 137.4 (m, C$_{11/15}$), 142.6 (m, C$_{11/15}$), 142.7 (s, C$_5$), 145.0 (s, C$_3$), 146.7 (s, C$_{20}$), 151.9 (dt, $^2J_{CF}$ = 84.7 Hz, $^2J_{CP}$ = 16.4 Hz, C$_2$), 161.6 (dt, $^1J_{CF}$ = 228.1 Hz, $^3J_{CP}$ = 3.9 Hz, C$_6$)

Carbons 4, 7 and 10 cannot be assigned and may be obscured.

^{31}P{^{1}H} NMR (CD$_2$Cl$_2$, 202 MHz, 295 K): δ 91.1 (d, $^4J_{CF}$ = 14.5 Hz, dppe)

^{19}F NMR (CD$_2$Cl$_2$, 471 MHz, 295 K): δ -82.1 (t, $^4J_{CF}$ = 14.5 Hz, F$_6$)

ESI-MS (m/z): Expected for C$_{44}$H$_{39}$FNP$_2$$^{101.9}$Ru = 764.1580; Observed: 764.1563 [M]$^+$ (Error = 1.7 mDa)
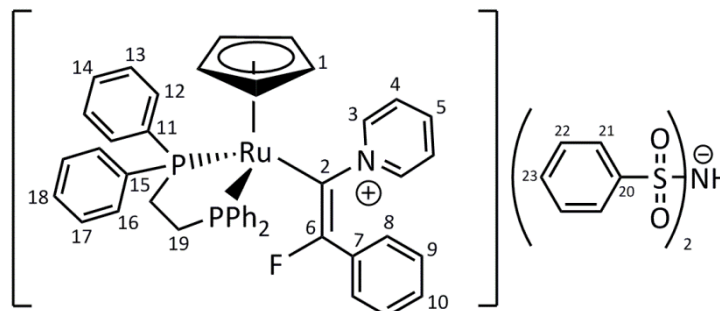
7.2.51 Synthesis of [Ru(η^5-C$_5$H$_5$)(PPh$_3$)((C$_5$H$_4$N)C(C$_5$H$_5$N)=C(C$_6$H$_5$))]BF$_4$, [46]BF$_4$

To an oven-dried ampoule was added [Ru(η^5-C$_5$H$_5$)(PPh$_3$)$_2$(C=C{F}Ph)]BF$_4$, **[27^{Ph}]BF$_4$** (65 mg, 72 µmol) and pyridine (1 mL), which was left to stir for 3 days. The reaction mixture was then layered with pentane. The red crystals, suitable for single crystal X-ray diffraction, were isolated by cannula filtration and dried under vacuum.

Yield = 44 mg (78 %)

^{1}H NMR (CD$_2$Cl$_2$, 500 MHz, 295 K): δ 4.80 (s, 5H, H$_1$), 6.48 (d, 1H, $^3J_{HH}$ = 6.2 Hz, H$_{8/8'}$), 6.64 (dd, 2H, $^3J_{HH}$ = 8.2 Hz, $^4J_{HH}$ = 1.1 Hz, H$_{13}$), 6.79 - 6.88 (m, 2H, H$_4$, H$_5$), 6.99 (tt, 2H, $^3J_{HH}$ = 7.4 Hz, $^4J_{HH}$ = 1.3 Hz, H$_{14}$), 7.08 (t, 4H, $^3J_{HH}$ = 7.4 Hz, H$_{15,}$ $_{19}$) 7.27 (br m, 6H, H$_{17/18}$), 7.39 (m, 7H, H$_{17/18}$, H$_3$), 7.66 (m, 1H, H$_{9/9'}$), 7.93 (m, 1H, H$_{9/9'}$), 8.22 (d, 1H, $^3J_{HH}$ = 8.1 Hz, H$_6$), 8.33 – 8.39 (m, 2H, H$_{8/8'}$, H$_{10}$)

^{13}C{^{1}H} NMR (CD$_2$Cl$_2$, 125 MHz, 295 K): δ 85.1 (s, C$_1$), 115.3 (s, C$_5$), 124.8 (s, C$_{13}$), 125.5 (s, C$_{15}$), 126.2 (s, C$_4$), 128.2 (s, C$_{14}$), 128.3 (s, PPh$_3$), 128.5 (s, C$_{9/9'}$), 129.2 (s, C$_{9/9'}$), 129.9 (s, PPh$_3$), 133.7 (br, PPh$_3$), 134.2 (s, C$_3$), 136.8 (d, $^2J_{CP}$ = 42.2 Hz, C$_{16}$), 144.1 (s, C$_6$), 146.1 (s, C$_{8/8'}$), 146.4 (s, C$_{8/8'}$), 146.8 (s, C$_{10}$), 150.5 (s, C$_{12}$), 199.1 (br, C$_{11}$), 218.0 (br, C$_2$)

^{31}P{^{1}H} NMR (CD$_2$Cl$_2$, 202 MHz, 295 K): δ 60.0 (br, **P**Ph$_3$)

ESI-MS (m/z): Expected for C$_{41}$H$_{25}$D$_9$N$_2$P$^{101.9}$Ru = 696.2063; Observed: 696.2084 [M]$^+$ (Error = 2.1 mDa)

All attempts to obtain elemental analysis for **[46]BF$_4$** were unsuccessful.

7.2.52 Synthesis of phenylacetyl fluoride, 47
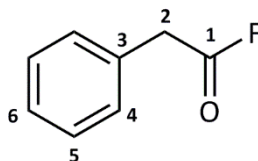
To an oven-dried Schlenk tube was added $[Ru(\eta^5\text{-}C_5H_5)(PPh_3)_2(C=C\{F\}Ph)]BF_4$, **[27^{Ph}]BF$_4$** (230 mg, 0.26 mmol) and NBu_4Cl (142 mg, 0.51 mmol, 2 equivalents) in dichloromethane (10 mL) which was left to stir for one week. The reaction was monitored by NMR spectroscopy. The reaction is also possible using $[Ru(\eta^5\text{-}C_5H_5)(PPh_3)_2(C=C\{F\}Ph)]NSI$, **[27^{Ph}]NSI** and $[Ru(\eta^5\text{-}C_5H_5)(dppe)(C=C\{F\}Ph)]NSI$, **[30]NSI**.

^1H NMR (CD$_2$Cl$_2$, 500 MHz, 295 K): δ 3.66 (d, $^3J_{HF}$ = 1.6 Hz, 2H, H$_2$), 7.25 – 7.37 (m, 5H, Ph)

^{19}F NMR (CD$_2$Cl$_2$, 471 MHz, 295 K): δ 42.5 (t, $^3J_{HF}$ = 1.6 Hz, F$_1$)

7.2.53 Reaction of [Ru(η^5-C$_5$H$_5$)(dppe)(C=C{F}Ph)]NSI, [30]NSI, with 2 equivalents of N^{n}Bu$_4$Cl.H$_2$O
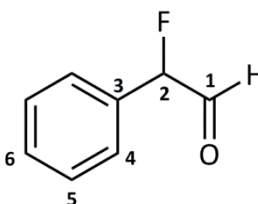
A Young's NMR tube was charged with $[Ru(\eta^5\text{-}C_5H_5)(dppe)(C=C\{F\}Ph)]NSI$, **[30^{Ph}]NSI** (30 mg, 30 μmol) and $NBu_4Cl.H_2O$ (17 mg, 60 μmol, 2 equivalents) in CD$_2$Cl$_2$ (0.5 mL) and monitored by NMR spectroscopy. Immediately on addition of N^nBu_4Cl, conversion of $[Ru(\eta^5\text{-}C_5H_5)(dppe)(C=C\{F\}Ph)]NSI$ to $[Ru(\eta^5\text{-}C_5H_5)(dppe)Cl]$, **[29]**, and α-fluorophenylacetaldehyde (PhCHFCHO, **48**) was observed. α-fluoro-phenylacetaldehyde was identified by comparison of ^{19}F NMR data with literature values.[290]

Selected ^1H NMR (CD$_2$Cl$_2$, 400 MHz, 298 K): δ 9.72 (dd, $^3J_{HF}$ = 7.6 Hz, $^5J_{HH}$ = 0.7 Hz, H$_1$)

^{19}F **NMR** (CD$_2$Cl$_2$, 376 MHz, 298 K): δ -191.7 (dd, $^2J_{HF}$ = 47.0 Hz, $^3J_{HF}$ = 7.6 Hz, F$_1$)

After 6 days, the NMR spectra were recorded again. The dominant organic product was phenylacetyl fluoride, **47.**

7.2.54 Synthesis of [Ru(η^5-C$_5$H$_5$)(dppe)Cl], [49]
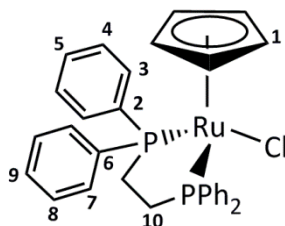
[Ru(η^5-C$_5$H$_5$)(PPh$_3$)$_2$Cl], **[25]** (0.86g, 1.19 mmol) and ethylenebis(diphenylphosphine) (dppe) (0.47 g, 1.19 mmol, 1 equivalent) were added to dry degassed toluene (20 mL) and refluxed under nitrogen for between 24 and 48 hours. The colour of the solution changed from yellow to orange. After this time, the solution was allowed to cool, then concentrated to half the volume and excess hexane added (c.a. 20 mL) to form a yellow precipitate immediately. The solution was left in the freezer overnight to maximise precipitation. The orange powder was then collected by cannula filtration, washed with hexane (3 x 20 mL) and dried in vacuo.

Yield = 0.46 g (65 %)

In some cases, purification *via* an alumina chromatographic column was necessary. Dichloromethane was first used to elute the free PPh$_3$ contaminant from the column, followed by acetone to elute the yellow-orange band of the product.[291]

^{1}H NMR (CD$_2$Cl$_2$, 500 MHz, 295 K): δ 2.36 − 2.51 (m, 2H, H$_{10a/b}$), 2.56 − 2.73 (m, 2H, H$_{10a/b}$), 4.57 (s, 5H, H$_1$), 7.13 − 7.20 (m, 4H, ar), 7.26 − 7.35 (m, 6H, ar), 7.42 − 7.49 (m, 6H, ar), 7.88 − 7.95 (m, 4H, ar)

^{13}C{^{1}H} NMR (CD$_2$Cl$_2$, 125 MHz, 295 K): δ 27.1 (m, C$_{10}$), 79.8 (t, J_{CP} = 2.4 Hz, C$_1$), 128.2 (virtual t, sum of J_{CP} = 9.4 Hz, C$_{3/4/7/8}$), 128.4 (virtual t, sum of J_{CP} = 9.4 Hz, C$_{3/4/7/8}$), 129.4 (s, C$_{5/9}$), 129.9 (s, C$_{5/9}$), 131.7 (virtual t, sum of J_{CP} = 10.6 Hz, C$_{3/4/7/8}$), 134.3 (virtual t, sum of J_{CP} = 10.6 Hz, C$_{3/4/7/8}$)

C$_2$ and C$_6$ could not be observed.

^{31}P{^{1}H} NMR (CD$_2$Cl$_2$, 202 MHz, 295 K): δ 81.8 (s, **P**Ph$_3$)

ESI-MS (m/z): Expected for C$_{31}$H$_{29}$ClNaP$_2$$^{101.9}$Ru = 623.0374; Observed: 623.0392 [M+Na]$^+$ (Error = 1.8 mDa)

7.2.55 Synthesis of (*E*)-[Ru(η^5-C$_5$H$_5$)(PPh$_3$)$_2$(CF=C{F}Ph)], [50]

To an oven-dried ampoule was added [Ru(η^5-C$_5$H$_5$)(PPh$_3$)$_2$(C=C{F}Ph)]BF$_4$, **[27^{Ph}]BF$_4$** (50 mg, 0.56 μmol) and tetramethylammonium fluoride (5.2 mg, 0.56 μmol, 1 equivalent) in dichloromethane (10 mL) which was left to stir for 3 days.

Alternative Procedure: An NMR tube with a PTFE J. Young's tap was charged with [Ru(η^5-C$_5$H$_5$)(PPh$_3$)$_2$(C=C{F}Ph)]BF$_4$, **[27^{Ph}]BF$_4$** (20 mg, 0.02 mmol) and TREAT.HF (triethylamine trihydrofluoride, 10.8 μL, 0.06 mmol) in deuterated tetrahydrofuran (0.5 mL), and the reaction turned from green to yellow. The NMR spectra reported were recorded 5 days after addition. Samples of **[50]** synthesised *via* this route tended to be cleaner and reduce the formation of **[43]BF$_4$**.

^{1}H NMR (C$_4$D$_8$O, 500 MHz, 298 K): δ 4.39 (s, 5H, H$_1$), 6.81 − 7.82 (m, 50H, ar)

^{13}C{^{1}H} NMR (C$_4$D$_8$O, 126 MHz, 298 K): δ 85.8 (d, $^3J_{CF}$ = 1.8 Hz, C$_1$), 124.3 (dd, $^3J_{CF}$ = 10.2 Hz, $^4J_{CF}$ = 8.2 Hz, C$_5$), 127.9 (virtual t, sum of J_{CP} = 9.2 Hz, C$_{9/10}$), 129.0 (s, C$_{6/7}$), 129.2 (s, C$_{11}$), 134.6 (virtual t, sum of J_{CP} = 10.4 Hz, C$_{9/10}$), 139.8 (m, C$_8$), 140.4 (dd, J_{CF} = 20.8 Hz, J_{CF} = 19.3 Hz, C$_4$), 145.7 (dd, $^1J_{CF}$ = 186.7 Hz, $^2J_{CF}$ = 21.3 Hz, C$_3$), 160.8 (dd, $^1J_{CF}$ = 197.3 Hz, $^2J_{CF}$ = 51.7 Hz, C$_2$)

^{19}F NMR (C$_4$D$_8$O, 471 MHz, 298 K): δ -146.8 (d, $^3J_{FF}$ = 113.7 Hz, F$_3$), -72.6 (dt, $^3J_{FF}$ = 113.7 Hz, $^3J_{PF}$ = 32.3 Hz, F$_2$)

^{31}P{^{1}H} NMR (C$_4$D$_8$O, 162 MHz, 298 K): δ 52.5 (dd, $^3J_{PF}$ = 32.3 Hz, $^4J_{PF}$ = 2.4 Hz, **P**Ph$_3$)

All attempts to obtain elemental analysis for **[50]** were unsuccessful due to the presence of low concentration impurities which could not be removed by washing with pentane or diethyl ether. Attempts to crystallise **[50]** were also unsuccessful.

7.2.56 Synthesis of (*E*)-[Ru(η^5-C$_5$H$_5$)(dppe)(CF=C{F}Ph)], [51]

An NMR tube with a PTFE J. Young's tap was charged with [Ru(η^5-C$_5$H$_5$)(dppe)(C=C{F}Ph)]NSI, **[30]NSI** (15 mg, 23 μmol) and TREAT.HF (3.7 μL, 23 μmol, 1 equiv.) in CD$_2$Cl$_2$ (0.5 mL) and allowed to stand for 30 minutes, during which time a colour change was observed from green to yellow. Quantitative conversion of **[30]NSI** to **[51]** was observed by ^{1}H and ^{31}P{^{1}H} NMR spectroscopy.

^{1}H NMR (C$_4$D$_8$O, 500 MHz, 295 K): δ 2.56 – 2.80 (m, 4H, H$_{16}$), 4.65 (s, 5H, H$_1$), 6.75 (tt, 1H, $^3J_{HH}$ = 7.3 Hz, $^4J_{HH}$ = 1.3 Hz, H$_7$), 6.79 – 6.84 (m, 2H, H$_5$), 6.90 (app. t, 2H, $^3J_{HH}$ = 7.6 Hz, H$_6$), 7.20 – 7.32 (m, 16H, dppe), 7.77 – 7.83 (m, 4H, dppe)

^{13}C{^{1}H} NMR (C$_4$D$_8$O, 125 MHz, 295 K): δ 30.1 (m, C$_{16}$), 84.1 (s, C$_1$), 124.0 (t, $^3J_{CF}$ = 22.6 Hz, C$_5$), 124.0 (s, C$_7$), 127.5 (d, $^4J_{CF}$ = 1.9 Hz, C$_6$), 128.1 (virtual t, sum of J_{CP} = 10.4 Hz, C$_{9/10/13/14}$), 128.4 (virtual t, sum of J_{CP} = 9.0 Hz, C$_{9/10/13/14}$), 129.1 (s, C$_{11/15}$), 129.7 (s, C$_{11/15}$), 131.6 (virtual t, sum of J_{CP} = 9.8 Hz, C$_{9/10/13/14}$), 133.9 (virtual t, sum of J_{CP} = 10.7 Hz, C$_{9/10/13/14}$), 134.6 (d, $^2J_{CF}$ = 30.7 Hz, C$_4$), 138.0 (m, C$_{8/12}$), 145.2 (m, C$_{8/12}$), 159.5 (dd, $^1J_{CF}$ = 198.1 Hz, $^2J_{CF}$ = 50.4 Hz, C$_3$), 187.9 (ddt, $^1J_{CF}$ = 296.6 Hz, $^2J_{CF}$ = 90.4 Hz, $^3J_{CP}$ = 18.2 Hz, C$_2$)

^{31}P{^{1}H} NMR (C$_4$D$_8$O, 202 MHz, 295 K): δ 94.3 (dd, $^3J_{PF}$ = 28.1 Hz, $^4J_{PF}$ = 2.6 Hz, dppe)

^{19}F NMR (C$_4$D$_8$O, 471 MHz, 295 K): δ -147.8 (d, $^3J_{FF}$ = 111.5 Hz, F$_3$), -82.4 (dt, $^3J_{FF}$ = 111.5 Hz, $^3J_{PF}$ = 28.1 Hz, F$_2$)

ESI-MS (m/z): Expected for C$_{39}$H$_{34}$F$_2$P$_2$$^{101.9}$Ru = 705.1220; Observed: 705.1192 [M+H]$^+$ (Error = 2.8 mDa)
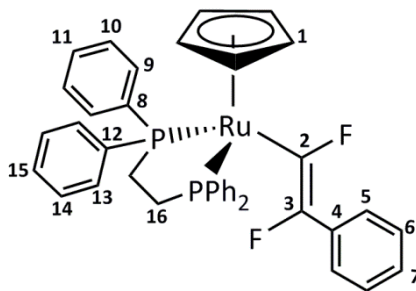
7.3   X-Ray crystallography

7.3.1   Crystallographic details

Diffraction data was collected using an Oxford Diffraction SuperNova diffractometer equipped with a single Molybdenum source using Mo-Ka radiation (0.71073 Å) and an EOS CCD camera. The crystals were cooled with an Oxford Instruments CryoJet typically to 110K. Diffractometer control, data collection, initial unit cell determination, frame integration and unit-cell refinement was carried out with "CrysalisPro".[292]   Face-indexed absorption corrections were applied either using spherical harmonics, implemented in SCALE3 ABSPACK scaling algorithm or analytical numeric absorption correction using a multifaceted crystal model based on expressions derived by Clark and Reid,[293] implemented within "CrysalisPro".[292] OLEX2[294] was used for overall structure solution, refinement and preparation of computer graphics and publication data. Using Olex2, the structure was solved either with the Superflip[295] structure solution program using Charge Flipping or the ShelXS[296] structure solution program using Direct Methods. Refinement was carried out with the ShelXL refinement package using Least Squares minimisation.[296]   All non-hydrogen atoms were refined anisotropically. Unless stated otherwise, hydrogen atoms were placed using a "riding model" and included in the refinement at calculated positions.

Special refinement details - $[5^{CF3}]PF_6$

One phenyl group exhibited disorder and was modelled in two positions of equal occupancy. Equivalent pairs of carbon atoms were constrained to have the same ADP e.g. C30A & C30B. The ADP of 6 carbons in the rings were restrained to be approximately isotropic, namely C30A, C30B, C33A, C33B, C34A, C34B, C35A & C35B.

A dichloromethane was present with occupancy of 0.5 per asymmetric unit; this was also disordered and modelled in two positions with refined occupancies of 0.405:0.095(3). The carbon-chlorine bond lengths were restrained to 1.745 Å. A diethyl ether of crystallisation was also present. This was partially occupied and modelled at 40% occupancy disordered about a centre of inversion. The carbon-carbon and carbon-oxygen bond lengths in this ether were restrained to 1.51 and 1.43 Å respectively. The ADP were restrained to be approximately isotropic (ISOR).

Non-acidic hydrogen atoms were placed using a "riding model" and included in the refinement at calculated positions. The N-H hydrogen was located by difference map after all other atoms had been located and refined.

Special refinement details – **[20]BF₄**

The hydrogen on the same carbon as the fluorine (i.e. H11) was found by difference map and all other hydrogen atoms were calculated.

Special refinement details - **[26^{CF3}]**

The trifluoromethyl group was disordered and modelled in two positions, with refined occupancies of 0.860:0.140(8). The carbon-fluorine and fluorine-fluorine bond distances were restrained to 1.32 Å and 2.12 Å respectively.

Special refinement details – Green **[27^{Ph}]PF₆**

The dichloromethane of crystallization had a disordered chloride atom, which was modelled in two positions with refined occupancies of 0.77:0.23(3).

Special refinement details – Orange **[27^{Ph}]PF₆**

The hexafluorophosphate anion was disordered (rotation about one F-P-F axis), and four fluorine atoms were modelled in two positions with occupancies of 0.957:0.043(3). The fluorine atoms of the minor component were restrained to be approximately isotropic and the distances between them were restrained to be equal. The ADP of opposite pairs of fluorine atoms in the minor component were constrained to be equivalent e.g F4A and F6A. The substituent of the vinylidene beta carbon is either a fluorine or a proton with partial occupancies of 0.885:0.115(5) respectively.

Special refinement details – **[38]BF₄**

The tetrafluoroborate anion was disordered, with three of the fluorines each modelled in two positions with refined occupancies of 0.903:0.097(4). The dichloromethane of crystallisation was also disordered with one of the chlorines modelled in two positions with refined occupancies of 0.663:0.337(3).

Special refinement details – **[44]BF$_4$**

The tetrafluoroborate anion was disordered and modelled in two positions. The occupancies were refined to 0.65:0.35 (4). The boron-fluorine bond lengths were restrained to 1.4 Å and the fluorine-fluorine bond lengths were restrained to 2.285 Å.

Special refinement details – **[46]BF$_4$**

The structure was non-merohedrally twinned and modelled using 2-components. The asymmetric unit contained two complex cations, two tetrafluoroborate anions and a pyridine of crystallisation.

Further crystallographic data can be found in the following tables:

7.3.2 Crystallographic tables

	$[5^{CF3}]PF_6$	$[7b]PF_6$
Identification code	jml1236	jml1306
Empirical formula	$C_{58.3}H_{52}ClF_9N_3O_{2.2}P_3Ru$	$C_{37}H_{39}F_6N_3P_2Ru$
Formula weight	1230.26	802.72
Temperature/K	109.95(10)	110.1(2)
Crystal system	monoclinic	monoclinic
Space group	C2/c	$P2_1/c$
a/Å	23.0193(7)	9.84361(14)
b/Å	15.7635(7)	20.9323(3)
c/Å	31.3450(14)	16.8622(2)
α/°	90	90.00
β/°	101.205(3)	91.3827(12)
γ/°	90	90.00
Volume/Å³	11157.1(8)	3473.42(9)
Z	8	4
ρ_{calc}mg/mm³	1.465	1.535
μ/mm⁻¹	0.491	0.608
F(000)	5019.2	1640.0
Crystal size/mm³	0.181 × 0.1127 × 0.0908	0.1745 × 0.1325 × 0.0594
2Θ range for data collection	5.804 to 56.156°	5.68 to 60.5°
Index ranges	-26 ≤ h ≤ 28, -9 ≤ k ≤ 20, -37 ≤ l ≤ 40	-13 ≤ h ≤ 12, -29 ≤ k ≤ 20, -23 ≤ l ≤ 11
Reflections collected	23119	15605
Independent reflections	11380 [R_{int} = 0.0345, R_{sigma} = 0.0722]	9010[R_{int} = 0.0266]
Data/restraints/parameters	11380/92/775	9010/0/445
Goodness-of-fit on F²	1.090	1.035
Final R indexes [I>=2σ (I)]	R_1 = 0.0639, wR_2 = 0.1192	R_1 = 0.0340, wR_2 = 0.0683
Final R indexes [all data]	R_1 = 0.0996, wR_2 = 0.1336	R_1 = 0.0467, wR_2 = 0.0739
Largest diff. peak/hole eÅ⁻³	0.72/-0.69	0.57/-0.45

	[7c]PF$_6$	[8b]PF$_6$
Identification code	jml1304	jml1305
Empirical formula	C$_{32}$H$_{29}$N$_3$F$_6$P$_2$Ru	C$_{35}$H$_{39}$N$_3$F$_6$P$_2$Ru
Formula weight	732.69	778.70
Temperature/K	110.00(10)	110.00(10)
Crystal system	monoclinic	monoclinic
Space group	Cc	Cc
a/Å	10.57894(12)	30.157(6)
b/Å	16.4524(2)	11.8342(4)
c/Å	17.3336(2)	16.822(3)
α/°	90.00	90.00
β/°	90.2957(11)	144.75(5)
γ/°	90.00	90.00
Volume/Å^3	3016.85(7)	3464.7(10)
Z	4	4
ρ$_{calc}$mg/mm^3	1.613	1.493
μ/mm^{-1}	0.691	0.607
F(000)	1480.0	1592.0
Crystal size/mm^3	0.2243 x 0.1849 x 0.1615	0.2042 × 0.1669 × 0.1457
2Θ range for data collection	6.54 to 64.42°	5.94 to 64.08°
Index ranges	-15 ≤ h ≤ 13, -23 ≤ k ≤ 23, -22 ≤ l ≤ 25	-43 ≤ h ≤ 20, -7 ≤ k ≤ 16, -15 ≤ l ≤ 25
Reflections collected	9128	8662
Independent reflections	6438 [R$_{int}$ = 0.0308]	6498[R$_{int}$ = 0.0226]
Data/restraints/parameters	6438/2/397	6498/39/484
Goodness-of-fit on F^2	1.026	1.060
Final R indexes [I>=2σ (I)]	R$_1$ = 0.0345, wR$_2$ = 0.0832	R$_1$ = 0.0351, wR$_2$ = 0.0857
Final R indexes [all data]	R$_1$ = 0.0370, wR$_2$ = 0.0857	R$_1$ = 0.0383, wR$_2$ = 0.0884
Largest diff. peak/hole / e Å^{-3}	0.94/-0.83	0.72/-0.58

	[12b^{Ph}]PF$_6$	[13b^{CF3}]PF$_6$
Identification code	jml1373	jml1308
Empirical formula	C$_{43}$H$_{41}$F$_6$NP$_2$Ru	C$_{41}$H$_{39}$F$_9$N$_2$P$_2$Ru
Formula weight	848.78	893.75
Temperature/K	110.05(10)	110.00(10)
Crystal system	monoclinic	triclinic
Space group	P2$_1$/c	P-1
a/Å	18.86145(19)	10.9139(4)
b/Å	11.36942(12)	11.4991(4)
c/Å	17.40176(14)	16.8070(6)
α/°	90.00	91.253(3)
β/°	94.9300(8)	105.252(3)
γ/°	90.00	111.126(3)
Volume/Å^3	3717.89(6)	1882.20(11)
Z	4	2
ρ$_{calc}$mg/mm^3	1.516	1.577
μ/mm^{-1}	0.571	0.580
F(000)	1736.0	908.0
Crystal size/mm^3	0.2786 × 0.2103 × 0.1451	0.2039 x 0.122 x 0.0978
2Θ range for data collection	5.62 to 64.44°	5.56 to 64.52°
Index ranges	-27 ≤ h ≤ 26, -13 ≤ k ≤ 16, -25 ≤ l ≤ 25	-16 ≤ h ≤ 11, -16 ≤ k ≤ 17, -23 ≤ l ≤ 24
Reflections collected	29498	21828
Independent reflections	11958[R$_{int}$ = 0.0289]	11902[R$_{int}$ = 0.0255]
Data/restraints/parameters	11958/0/500	11902/0/499
Goodness-of-fit on F^2	1.035	1.035
Final R indexes [I>=2σ (I)]	R$_1$ = 0.0319, wR$_2$ = 0.0688	R$_1$ = 0.0299, wR$_2$ = 0.0670
Final R indexes [all data]	R$_1$ = 0.0404, wR$_2$ = 0.0742	R$_1$ = 0.0363, wR$_2$ = 0.0706
Largest diff. peak/hole / e Å^{-3}	0.54/-0.74	0.57/-0.44

	[15c^{Ph}]PF$_6$	[15c^{CF3}]PF$_6$
Identification code	jml1366	jml1325
Empirical formula	C$_{35.5}$H$_{31}$ClF$_6$N$_2$P$_2$Ru	C$_{147}$H$_{122}$Cl$_6$F$_{36}$N$_8$P$_8$Ru$_4$
Formula weight	798.08	3549.38
Temperature/K	110.05(10)	110.00(10)
Crystal system	orthorhombic	triclinic
Space group	P2$_1$2$_1$2	P-1
a/Å	20.3101(3)	13.5289(5)
b/Å	18.5643(2)	15.7125(7)
c/Å	9.39877(11)	18.1897(9)
α/°	90.00	77.574(4)
β/°	90.00	86.000(4)
γ/°	90.00	70.158(4)
Volume/Å^3	3543.73(8)	3551.9(3)
Z	4	1
ρ$_{calc}$mg/mm^3	1.496	1.659
μ/mm^{-1}	0.668	0.723
F(000)	1612.0	1782.0
Crystal size/mm^3	0.2633 × 0.1080 × 0.0923	0.2305 × 0.0997 × 0.0293
2Θ range for data collection	5.9 to 60°	5.6 to 56°
Index ranges	-22 ≤ h ≤ 28, -26 ≤ k ≤ 23, -6 ≤ l ≤ 13	-16 ≤ h ≤ 17, -19 ≤ k ≤ 20, -23 ≤ l ≤ 22
Reflections collected	12513	28364
Independent reflections	9332[R$_{int}$ = 0.0208]	14463[R$_{int}$ = 0.0286]
Data/restraints/parameters	9332/18/449	14463/136/1070
Goodness-of-fit on F^2	1.049	1.030
Final R indexes [I>=2σ (I)]	R$_1$ = 0.0336, wR$_2$ = 0.0830	R$_1$ = 0.0443, wR$_2$ = 0.1061
Final R indexes [all data]	R$_1$ = 0.0367, wR$_2$ = 0.0850	R$_1$ = 0.0568, wR$_2$ = 0.1154
Largest diff. peak/hole / e Å^{-3}	0.63/-0.74	0.92/-1.26

	[20]BF$_4$	[21]BF$_4$
Identification code	jml1390	jml1376
Empirical formula	C$_{37}$H$_{29}$BF$_8$NPRu	C$_{37}$H$_{28}$BF$_9$NPRu
Formula weight	782.46	800.45
Temperature/K	110.05(10)	110.05(10)
Crystal system	monoclinic	monoclinic
Space group	P2$_1$	Cc
a/Å	9.34095(17)	14.5269(2)
b/Å	17.7554(3)	12.30582(14)
c/Å	9.85967(18)	19.9237(3)
α/°	90.00	90.00
β/°	102.9459(18)	113.8435(17)
γ/°	90.00	90.00
Volume/Å^3	1593.68(5)	3257.69(8)
Z	2	4
ρ$_{calc}$mg/mm^3	1.631	1.632
μ/mm^{-1}	0.619	0.612
F(000)	788.0	1608.0
Crystal size/mm^3	0.1405 × 0.064 × 0.054	0.2484 × 0.1618 × 0.0793
2Θ range for data collection	5.9 to 64.66°	5.56 to 57.6°
Index ranges	-13 ≤ h ≤ 13, -25 ≤ k ≤ 26, -14 ≤ l ≤ 13	-19 ≤ h ≤ 16, -15 ≤ k ≤ 15, -24 ≤ l ≤ 26
Reflections collected	20566	12746
Independent reflections	10120 [R$_{int}$ = 0.0313, R$_{sigma}$ = 0.0467]	6049[R$_{int}$ = 0.0255]
Data/restraints/parameters	10120/1/446	6049/2/451
Goodness-of-fit on F^2	1.035	1.045
Final R indexes [I>=2σ (I)]	R$_1$ = 0.0291, wR$_2$ = 0.0588	R$_1$ = 0.0247, wR$_2$ = 0.0497
Final R indexes [all data]	R$_1$ = 0.0322, wR$_2$ = 0.0606	R$_1$ = 0.0261, wR$_2$ = 0.0510
Largest diff. peak/hole / e Å^{-3}	0.52/-0.45	0.29/-0.28

	[26^{CF3}]	Green - [27^{Ph}]BF$_4$
Identification code	jml1392	jml1411
Empirical formula	C$_{50}$H$_{39}$F$_3$P$_2$Ru	C$_{50}$H$_{42}$Cl$_2$F$_7$P$_3$Ru
Formula weight	859.82	1040.71
Temperature/K	110.00(14)	110.05(10)
Crystal system	monoclinic	orthorhombic
Space group	P2$_1$/c	Pbca
a/Å	16.8756(3)	17.3578(2)
b/Å	15.1925(2)	14.44250(18)
c/Å	17.3468(4)	36.1516(4)
α/°	90	90
β/°	116.921(3)	90
γ/°	90	90
Volume/Å^3	3965.46(16)	9062.86(19)
Z	4	8
ρ$_{calc}$mg/mm^3	1.440	1.525
μ/mm^{-1}	0.526	0.634
F(000)	1760.0	4224.0
Crystal size/mm^3	0.3086 × 0.1372 × 0.1372	0.3612 × 0.0695 × 0.0598
2Θ range for data collection	5.906 to 60.482°	5.586 to 60.844°
Index ranges	-23 ≤ h ≤ 21, -21 ≤ k ≤ 20, -24 ≤ l ≤ 23	-24 ≤ h ≤ 22, -20 ≤ k ≤ 20, -48 ≤ l ≤ 51
Reflections collected	22877	85888
Independent reflections	10476 [R$_{int}$ = 0.0296, R$_{sigma}$ = 0.0420]	12862 [R$_{int}$ = 0.0323, R$_{sigma}$ = 0.0220]
Data/restraints/parameters	10476/12/515	12862/1/578
Goodness-of-fit on F^2	1.052	1.066
Final R indexes [I>=2σ (I)]	R$_1$ = 0.0324, wR$_2$ = 0.0724	R$_1$ = 0.0267, wR$_2$ = 0.0601
Final R indexes [all data]	R$_1$ = 0.0437, wR$_2$ = 0.0781	R$_1$ = 0.0320, wR$_2$ = 0.0628
Largest diff. peak/hole / e Å^{-3}	0.52/-0.49	0.40/-0.49

	Orange - [27^{Ph}]BF$_4$	[28]PF$_6$
Identification code	jml1426	jml1440_twin1_hklf4
Empirical formula	C$_{50}$H$_{42.12}$Cl$_2$F$_{6.88}$P$_3$Ru	C$_{50}$H$_{43}$Cl$_2$F$_{5.98}$P$_3$Ru
Formula weight	1038.64	1022.35
Temperature/K	110.05(10)	110.05(10)
Crystal system	orthorhombic	orthorhombic
Space group	Pbca	Pbca
a/Å	17.5524(3)	17.5817(3)
b/Å	19.8953(4)	19.8417(2)
c/Å	25.3282(5)	25.1626(5)
α/°	90	90
β/°	90	90
γ/°	90	90
Volume/Å^3	8844.9(3)	8778.0(3)
Z	8	8
ρ$_{calc}$mg/mm^3	1.560	1.547
μ/mm^{-1}	0.650	0.650
F(000)	4216.6	4158.3
Crystal size/mm^3	0.3926 × 0.2659 × 0.1639	0.2609 × 0.1318 × 0.053
2Θ range for data collection	5.702 to 64.422	5.654 to 60.082
Index ranges	-19 ≤ h ≤ 25, -28 ≤ k ≤ 24, -28 ≤ l ≤ 36	-24 ≤ h ≤ 15, -27 ≤ k ≤ 14, -29 ≤ l ≤ 35
Reflections collected	33223	22566
Independent reflections	14037 [R$_{int}$ = 0.0297, R$_{sigma}$ = 0.0380]	11833 [R$_{int}$ = 0.1174, R$_{sigma}$ = 0.0884]
Data/restraints/parameters	14037/30/604	11833/145/610
Goodness-of-fit on F^2	1.049	1.071
Final R indexes [I>=2σ (I)]	R$_1$ = 0.0318, wR$_2$ = 0.0730	R$_1$ = 0.0591, wR$_2$ = 0.1653
Final R indexes [all data]	R$_1$ = 0.0444, wR$_2$ = 0.0806	R$_1$ = 0.0929, wR$_2$ = 0.1964
Largest diff. peak/hole / e Å^{-3}	0.62/-0.57	2.05/-3.28

	[37^{CF3}]BF$_4$	[38]BF$_4$
Identification code	jml1461Mo	jml1403
Empirical formula	C$_{55.5}$H$_{44}$BClF$_7$NP$_2$Ru	C$_{51}$H$_{42}$BCl$_2$F$_7$P$_2$Ru
Formula weight	1067.18	1032.56
Temperature/K	110.05(10)	110.05(10)
Crystal system	monoclinic	orthorhombic
Space group	P2$_1$/c	Pbca
a/Å	10.3433(2)	17.8473(4)
b/Å	23.9394(5)	14.6795(3)
c/Å	19.3083(4)	35.2252(16)
α/°	90	90
β/°	98.805(2)	90
γ/°	90	90
Volume/Å^3	4724.64(17)	9228.6(5)
Z	4	8
ρ$_{calc}$mg/mm^3	1.500	1.486
μ/mm^{-1}	0.524	0.589
F(000)	2172.0	4192.0
Crystal size/mm^3	0.3297 × 0.0526 × 0.0173	0.2616 × 0.1943 × 0.1582
2Θ range for data collection	7.01 to 56.022 °	5.822 to 60.072°
Index ranges	-13 ≤ h ≤ 13, -31 ≤ k ≤ 31, -11 ≤ l ≤ 25	-25 ≤ h ≤ 20, -20 ≤ k ≤ 12, -36 ≤ l ≤ 49
Reflections collected	15633	28548
Independent reflections	9356 [R$_{int}$ = 0.0317, R$_{sigma}$ = 0.0680]	13431 [R$_{int}$ = 0.0322, R$_{sigma}$ = 0.0537]
Data/restraints/parameters	9356/54/641	13431/0/597
Goodness-of-fit on F^2	1.034	1.107
Final R indexes [I>=2σ (I)]	R$_1$ = 0.0434, wR$_2$ = 0.0777	R$_1$ = 0.0471, wR$_2$ = 0.0826
Final R indexes [all data]	R$_1$ = 0.0671, wR$_2$ = 0.0862	R$_1$ = 0.0631, wR$_2$ = 0.0896
Largest diff. peak/hole / e Å^{-3}	0.44/-0.41	1.14/-1.02

	[44^{Ph}]BF$_4$	[46^{Ph}]BF$_4$
Identification code	jml1395	jml1396_twin1_hklf4
Empirical formula	C$_{54}$H$_{45}$BF$_5$NP$_2$Ru	C$_{43.5}$H$_{36.5}$BF$_4$N$_{2.5}$PRu
Formula weight	976.73	813.10
Temperature/K	109.8(6)	110.05(10)
Crystal system	triclinic	triclinic
Space group	P-1	P-1
a/Å	11.6304(5)	9.6081(8)
b/Å	13.5851(7)	17.9440(7)
c/Å	15.1453(9)	21.3274(10)
α/°	72.589(5)	99.508(4)
β/°	89.929(4)	101.789(6)
γ/°	79.010(4)	90.366(5)
Volume/Å^3	2237.5(2)	3547.0(4)
Z	2	4
ρ$_{calc}$mg/mm^3	1.450	1.523
μ/mm^{-1}	0.482	0.545
F(000)	1000.0	1660.0
Crystal size/mm^3	0.1731 × 0.1338 × 0.0366	0.4117 × 0.2117 × 0.0261
2Θ range for data collection	6.166 to 63.606°	5.83 to 56.652°
Index ranges	-13 ≤ h ≤ 16, -20 ≤ k ≤ 14, -21 ≤ l ≤ 18	-12 ≤ h ≤ 10, -23 ≤ k ≤ 23, -28 ≤ l ≤ 27
Reflections collected	20403	16538
Independent reflections	13479 [R$_{int}$ = 0.0280, R$_{sigma}$ = 0.0514]	16538 [R$_{sigma}$ = 0.0777]
Data/restraints/parameters	13479/20/614	16538/636/956
Goodness-of-fit on F^2	1.033	0.951
Final R indexes [I>=2σ (I)]	R$_1$ = 0.0355, wR$_2$ = 0.0769	R$_1$ = 0.0560, wR$_2$ = 0.1396
Final R indexes [all data]	R$_1$ = 0.0474, wR$_2$ = 0.0829	R$_1$ = 0.0922, wR$_2$ = 0.1545
Largest diff. peak/hole / e Å^{-3}	0.63/-0.43	1.34/-2.03

7.4 General considerations for computational calculations

Initial optimisations were performed at the (RI-)BP86/SV(P) level, followed by frequency calculations at the same level. Transition states were located by initially performing a constrained minimisation (by freezing internal coordinates that change most during the reaction) of a structure close to the anticipated transition state. This was followed by a frequency calculation to identify the transition vector to follow during a subsequent transition state optimisation. A final frequency calculation was then performed on the optimised transition-state structure. All minima were confirmed as such by the absence of imaginary frequencies and all transition states were identified by the presence of only one imaginary frequency. All transition states were verified as connecting to the expected adjacent minima using the DRC module of TURBOMOLE (using an initial distortion length of 100, 50 cycles and a damping factor of 1). Dynamic reaction coordinate (DRC) calculations aim to follow a classical trajectory from a transition state to the minima on either side of it by moving along its imaginary vibrational mode.[297-298] DRC calculations are similar to, but computationally less expensive than, intrinsic reaction coordinate (IRC) calculations, which attempt to find the minimum energy path (MEP) from the transition state to connecting minima.

Single-point calculations on the (RI-)BP86/SV(P) optimised geometries were performed using the hybrid PBE0 functional and the flexible def2-TZVPP basis set. The (RI-)PBE0/def2-TZVPP SCF energies were corrected for their zero point energies, thermal energies and entropies (obtained from the (RI-)BP86/SV(P)-level frequency calculations). In all calculations, a 28 electron quasi-relativistic ECP replaced the core electrons of Ru. No symmetry constraints were applied during optimisations. All calculations were performed using the TURBOMOLE V6.40 package using the resolution of identity (RI) approximation.[299-307] Solvation effects were modeled using the COSMO module of TURBOMOLE. The pre-optimised gas phase structure were computed in a single-point calculation at the (RI)PBE0/def2-TZVPP level with solvent corrected SCF energies. The dielectric constants used were dichloromethane (8.93 at 298 K), acetone (13.26 at 298 K) and acetonitrile (37.5 at 298 K).[308]

Single-point DFT-D3 corrections (on the (RI-)BP86/SV(P) geometries) have been applied at the PBE0- D3 level using Grimme's DFT-D3 V3.0 Rev 2 program (with BJ-damping)[126-127] and data presented in the main section of the thesis includes this correction. Both DFT-D3 and DFT data can be found in the Supporting Information CD attached to this thesis.

In Chapter 4, single point energy calculations on the previously optimised structures of **[20]BF₄** and **[21]BF₄** were performed using Gaussian 09[309] (at the PBE0/def2-TZVPP level, basis set information was obtained from the EMSL basis set exchange)[310-313] to prepare input for NBO analysis by the NBO 5.9 package.[314] Structures were visualised and modified using Facio,[315] Jmol,[4]33 and gOpenMol.

In Chapter 5, vertical excitation energies were calculated using the ESCF module of TURBOMOLE (full TDDFT) on the (RI-)PBE0/def2-TZVPP optimised structures at the same level of theory. Tight SCF convergence criteria were used in these calculations. 50 singlet excitations were calculated for each state.

Further computational information (including tabulated energetic data, results of NBO calculations, details of structural isomers, naming systems, SCF energies, xyz coordinates and vibrational frequencies) can be found on the attached CD.

Appendix 1 – Energetic Span Model, Kozuch and Shaik [132]

In order to assess the computational findings of the studies presented in Chapter 2, Chapter 4 and Chapter 5 of this thesis, the energetic spans of the potential energy surfaces (PES) have been calculated using the energetic span model proposed by Kozuch and Shaik in 2011 (ES model).

The term 'energetic span, δE' was first proposed by Amatore and Jutand in 1999. According to Arrhenius, starting from the reactive species, C_a, the rate of reaction, r, is:

$$r = [C_a]Ae^{-Ea/RT} \quad \text{where} \quad C_a = \text{the intermediate preceding the transition state}$$

As the concentration of the active species can be defined relative to the lowest energy intermediate, C_o:

$$[C_a] = [C_o]e^{-\Delta E/RT}$$

Therefore:

$$r = [Co]Ae^{-(Ea+\Delta E)/RT}$$

$$E_a + \Delta E = \delta E$$

where the energetic span, δE, is defined as the energy difference between the peak and trough of the PES. However, this equation is only meaningful when the energy of the reaction, ΔG_r, approaches zero. In catalysis, when the reaction completes one full turnover and begins again, the starting point of the next cycle is lower in energy by ΔG_r. This energy difference is taken into account in the Kozuch and Shaik model.

In many catalytic cycles, only one transition state and one intermediate determine the turnover frequency – in the ES model, these are referred to as the TOF-determining transition state, TDTS, and the TOF-determining intermediate, TDI. The energetic span, δE, of the cycle is determined by the energy difference, TDTS - TDI, and the reaction driving force, ΔG_r. If the TDTS appears after the TDI, δE is the energy difference between the two states. If the TDTS appears before the TDI, the reaction driving force must also be added to this value.

These relationships are summarised in the equations below:

$$\delta E = TDTS - TDI \qquad \text{If TDTS appears after TDI}$$

$$\delta E = TDTS - TDI + \Delta G_r \qquad \text{If TDTS appears before TDI}$$

On calculation of δE, the TOF can be calculated using the Arrhenius-Eyring equation using δE as the activation energy of the cycle. The smaller the value of δE, the faster the rate of reaction.

An important point to take from this model is that the TDI and TDTS are not automatically the highest and lowest states, and they do not have to be adjoined as a single step. Neither one reaction step nor one transition state determines the efficiency of the catalyst – rather than rate determining *steps*, it is more appropriate to consider rate determining *states*.

In order to estimate δE using the ES theory, Gibbs energies of the TDTS and TDI should first be calculated. As discussed in Chapter 2, Gibbs energies can be difficult to ascertain computationally due to inaccuracies in corrections of entropy and solvation.[123-125] However, if the TDTS and TDI have the same molecularity, both Gibbs and electronic energies will give similar results.

Appendix 2 – Natural Bond Order (NBO) calculations[316-319]

A natural bond orbital (NBO) calculation is used to determine the distribution of electrons on atoms and in the bonds between them; in basic terms, an NBO calculation aims to generate the Lewis structure which most closely represents the electron density of the molecule.

An NBO calculation can determine:

- The classification of the orbital (as 'bonding', 'non-bonding' or 'antibonding' (a non Lewis NBO)) and the occupancy of each (between 0 and 2 electrons).

- Each bonding orbital is described by the hybridisation of the orbitals which are forming the bond (for example, the C-C bond in ethane would be described as two interacting sp^3 orbitals) and the polarisation of the bond (based on electronegativity of the atoms). This determines the ionic or covalent nature of the bond.

- Interactions between localised orbitals (for example, donation of electron density from filled orbitals and lone pairs to empty orbitals) which can strengthen or weaken the bonds. This is done by calculating all possible interactions and estimating their energetic importance by second order perturbation theory – these interactions are referred to as 'delocalisation' corrections.

- Important resonance structures, which are represented by lists of strong donor and acceptor interactions; Lewis structures do not behave as good models for strongly delocalised systems.

Abbreviations

Å	Angstroms
AMLA	ambiphilic metal ligand activation
app.	apparent
ar	aromatic
au	atomic units
b	broad
Bu	butyl
^{13}C	carbon
$\eta^5\text{-}C_5H_5$	cyclopentadienyl
cm	centimetres
cm^{-1}	wavenumbers
CMD	concerted metalation-deprotonation
COSMO	conductor-like screening model
COSY	correlation spectroscopy
Cy	cyclohexyl
d	doublet
DABCO	1,4-diazabicyclo[2.2.2]octane
dd	doublet of doublets
DEPT	distortionless enhancement by polarisation transfer
DFT	density functional theory
6-DPPAP	6-(diphenylphosphino)-*N*-pivaloyl-2-aminopyridine
dppe	1,2-bis(diphenylphosphino)ethane
3-DPICon	3-diphenylphosphinoisoquinolone
EI	electron impact
eq. or equiv.	equivalents
$E_{SCF+ZPE}$	electronic energy
ESI-MS	electrospray ionisation mass spectrometry
Et	ethyl
Et_2O	diethyl ether
^{19}F	fluorine
FT-IR	fourier transform infrared spectroscopy

[FTMP]$^+$	1-fluoro-2,4,6-trimethylpyridinium
g	grams
h	hours
^{1}H	proton
HMBC	heteronuclear multiple bond correlation
HMQC	heteronuclear multiple quantum coherence
HOMO	highest occupied molecular orbital
[HTMP]$^+$	2,4,6-trimethylpyridinium
Hz	Hertz
Im'	1,4-dimethylimidazol-2-yl
J	coupling constant
K	Kelvin
kJ	kilojoule
L	Ligand
LAPS	ligand-assisted proton shuttle
LLHT	ligand-to-ligand hydrogen transfer
LUMO	lowest unoccupied molecular orbital
m	multiplet
m (prefix)	milli
mDa	milliDalton
Me	methyl
MeCN	acetonitrile
MeOH	methanol
mg	milligram
MHz	megahertz
min	minute
mL	millilitre
mmol	millimole
MO	molecular orbital
mol	mole
m/z	mass/charge
NBO	natural bond order
NFSI	N-fluorobenzenesulfonimide

NHC	*N*-heterocyclic carbene
nm	nanometre
NMR	nuclear magnetic resonance
NOESY	nuclear Overhauser effect
OSEF	outer-sphere electrophilic fluorination
^{31}P	phosphorus
Ph	phenyl
ppm	parts per million
pyr	pyridine
η^5-C$_5$Me$_5$	pentamethylcyclopentadienyl
q	quartet
s	singlet
SCF	self-consistent field
Selectfluor	1-chloromethyl-4-fluoro-1,4-diazoniabicyclo[2.2.2]octane bis(tetrafluoroborate)
SVP	split valence plus polarisation
t	triplet
^{t}Bu	tertiary butyl
td	triplet of doublets
TDTS	turnover determining transition state
TDI	turnover determining intermediate
THF	tetrahydrofuran
TLC	thin-layer chromatography
TMP	2,4,6-trimethylpyridine
TOF	time-of-flight
TS	transition state
tt	triplet of doublets
TZVPP	triple-zeta valence plus polarisation
UV	ultra-violet
Vis	visible
VT	variable temperature
ZPE	zero point energy
°	degrees

°C	degrees Celsius
δ	chemical shift
λ	wavelength
μ (prefix)	micro

References

1. S. D. Pike and A. S. Weller, *Phil. Trans. R. Soc. A,* 2015, **373**, 20140187.
2. J. F. Hartwig, *Nature,* 2008, **455**, 314.
3. K. M. Engle, T.-S. Mei, M. Wasa and J.-Q. Yu, *Acc. Chem. Res.,* 2012, **45**, 788.
4. http://www.nobelprize.org/nobel_prizes/chemistry/laureates/2005/, Accessed 28 February, 2016.
5. http://www.nobelprize.org/nobel_prizes/chemistry/laureates/2010/, Accessed 28 February, 2016.
6. K. Kohler, K. Wussow and A. S. Wirth in *Palladium-Catalyzed Coupling Reactions: Practical Aspects and Future Developments*; Chapter 7; John Wiley & Sons, 2013.
7. A. L. Noffke, A. Habtemariam, A. M. Pizarro and P. J. Sadler, *Chem. Commun.,* 2012, **48**, 5219.
8. R. H. Crabtree in *The Organometallic Chemistry of the Transition Metals*; Chapter 4; Fourth ed.; John Wiley & Sons, 2009.
9. R. H. Crabtree, *J. Organomet. Chem.,* 2005, **690**, 5451.
10. C. A. Tolman, *Chem. Rev.,* 1977, **77**, 313.
11. D. G. Gusev, *Organometallics,* 2009, **28**, 763.
12. B. Breit, *Angew. Chem. Int. Ed.,* 2005, **44**, 6816.
13. G. T. Morgan and H. D. K. Drew, *J. Chem. Soc., Trans.,* 1920, **117**, 1456.
14. P. W. N. M. van Leeuwen, P. C. J. Kamer, J. N. H. Reek and P. Dierkes, *Chem. Rev.,* 2000, **100**, 2741.
15. M. Iwamoto and S. Yuguchi, *J. Org. Chem.,* 1966, **31**, 4290.
16. B. Breit and W. Seiche, *J. Am. Chem. Soc.,* 2003, **125**, 6608.
17. H. Grützmacher, *Angew. Chem. Int. Ed.,* 2008, **47**, 1814.
18. D. B. Grotjahn, *Chem. Eur. J.,* 2005, **11**, 7146.
19. T. E. Creighton in *Proteins: Structures and Molecular Properties*; pages 418 - 434; Macmillan, 1993.
20. A. Radzicka and R. Wolfenden, *J. Am. Chem. Soc.,* 1996, **118**, 6105.
21. R. A. Bryant and D. E. Hansen, *J. Am. Chem. Soc.,* 1996, **118**, 5498.
22. Y. Boutadla, D. L. Davies, S. A. Macgregor and A. I. Poblador-Bahamonde, *Dalton Trans.,* 2009, 5820.
23. D. Lapointe and K. Fagnou, *Chem. Lett.,* 2010, **39**, 1118.
24. D. G. Johnson, J. M. Lynam, J. M. Slattery and C. E. Welby, *Dalton Trans.,* 2010, **39**, 10432.
25. D. Lapointe, T. Markiewicz, C. J. Whipp, A. Toderian and K. Fagnou, *J. Org. Chem.,* 2011, **76**, 749.
26. J. Guihaumé, S. p. Halbert, O. Eisenstein and R. N. Perutz, *Organometallics,* 2011, **31**, 1300.
27. D. B. Grotjahn, C. R. Larsen, J. L. Gustafson, R. Nair and A. Sharma, *J. Am. Chem. Soc.,* 2007, **129**, 9592.
28. G. l. Erdogan and D. B. Grotjahn, *J. Am. Chem. Soc.,* 2009, **131**, 10354.
29. D. Bourissou, O. Guerret, F. P. Gabbaï and G. Bertrand, *Chem. Rev.,* 2000, **100**, 39.
30. P. de Frémont, N. Marion and S. P. Nolan, *Coord. Chem. Rev.,* 2009, **253**, 862.
31. S. F. Vyboishchikov and G. Frenking, *Chem. Eur. J.,* 1998, **4**, 1428.
32. A. F. Hill, W. R. Roper, J. M. Waters and A. H. Wright, *J. Am. Chem. Soc.,* 1983, **105**, 5939.
33. T. E. Taylor and M. B. Hall, *J. Am. Chem. Soc.,* 1984, **106**, 1576.
34. N. C. Baird and K. F. Taylor, *J. Am. Chem. Soc.,* 1978, **100**, 1333.

35. K. K. Irikura, W. A. Goddard and J. L. Beauchamp, *J. Am. Chem. Soc.,* 1992, **114**, 48.
36. B. C. Gilbert, D. Griller and A. S. Nazran, *J. Org. Chem.,* 1985, **50**, 4738.
37. G. Frenking, M. Solà and S. F. Vyboishchikov, *J. Organomet. Chem.,* 2005, **690**, 6178.
38. W. A. Herrmann, *Angew. Chem. Int. Ed.,* 2002, **41**, 1290.
39. A. J. Arduengo, R. L. Harlow and M. Kline, *J. Am. Chem. Soc.,* 1991, **113**, 361.
40. M. N. Hopkinson, C. Richter, M. Schedler and F. Glorius, *Nature,* 2014, **510**, 485.
41. S. Díez-González, N. Marion and S. P. Nolan, *Chem. Rev.,* 2009, **109**, 3612.
42. A. Gautier and F. Cisnetti, *Metallomics,* 2012, **4**, 23.
43. T. Weskamp, W. C. Schattenmann, M. Spiegler and W. A. Herrmann, *Angew. Chem. Int. Ed.,* 1998, **37**, 2490.
44. M. Roselló-Merino, J. Díez and S. Conejero, *Chem. Commun.,* 2010, **46**, 9247.
45. D. G. Johnson, J. M. Lynam, N. S. Mistry, J. M. Slattery, R. J. Thatcher and A. C. Whitwood, *J. Am. Chem. Soc.,* 2012, **135**, 2222.
46. E. Alvarez, S. Conejero, M. Paneque, A. Petronilho, M. L. Poveda, O. Serrano and E. Carmona, *J. Am. Chem. Soc.,* 2006, **128**, 13060.
47. E. Álvarez, S. Conejero, P. Lara, J. A. López, M. Paneque, A. Petronilho, M. L. Poveda, D. del Río, O. Serrano and E. Carmona, *J. Am. Chem. Soc.,* 2007, **129**, 14130.
48. M. Ashworth, R. Daffern and D. L. Hammick, *J. Chem. Soc.,* 1939, 809.
49. C. Bruneau and P. Dixneuf in *Metal Vinylidenes and Allenylidenes in Catalysis: From Reactivity to Applications in Synthesis*; Chapter 1; John Wiley & Sons, 2008.
50. M. I. Bruce, *Chem. Rev.,* 1991, **91**, 197.
51. V. Cadierno, M. P. Gamasa and J. Gimeno, *Coord. Chem. Rev.,* 2004, **248**, 1627.
52. M. C. Puerta and P. Valerga, *Coord. Chem. Rev.,* 1999, **193-195**, 977.
53. F. De Angelis, A. Sgamellotti and N. Re, *Dalton Trans.,* 2004, 3225.
54. B. Solaja, J. Huguet, M. Karpf and A. S. Dreiding, *Tetrahedron,* 1987, **43**, 4875.
55. C. Bruneau and P. H. Dixneuf, *Angew. Chem. Int. Ed.,* 2006, **45**, 2176.
56. B. Breit, U. Gellrich, T. Li, J. M. Lynam, L. M. Milner, N. E. Pridmore, J. M. Slattery and A. C. Whitwood, *Dalton Trans.,* 2014, **43**, 11277.
57. H. Katayama and F. Ozawa, *Coord. Chem. Rev.,* 2004, **248**, 1703.
58. J. M. Lynam, *Chem. Eur. J.,* 2010, **16**, 8238.
59. M. J. Cowley, J. M. Lynam and A. C. Whitwood, *Dalton Trans.,* 2007, 4427.
60. M. J. Cowley, J. M. Lynam and A. C. Whitwood, *J. Organomet. Chem.,* 2010, **695**, 18.
61. O. J. S. Pickup, I. Khazal, E. J. Smith, A. C. Whitwood, J. M. Lynam, K. Bolaky, T. C. King, B. W. Rawe and N. Fey, *Organometallics,* 2014, **33**, 1751.
62. M. I. Bruce and R. C. Wallis, *Aust. J. Chem.,* 1979, **32**, 1471.
63. L. M. Milner, N. E. Pridmore, A. C. Whitwood, J. M. Lynam and J. M. Slattery, *J. Am. Chem. Soc.,* 2015, **137**, 10753.
64. M. I. Bruce, G. A. Koutsantonis, M. J. Liddell and B. K. Nicholson, *J. Organomet. Chem.,* 1987, **320**, 217.
65. H. Berke, G. Huttner, G. Weiler and L. Zsolnai, *J. Organomet. Chem.,* 1981, **219**, 353.
66. P. K. Baker, G. K. Barker, D. S. Gill, M. Green, A. G. Orpen, I. D. Williams and A. J. Welch, *J. Chem. Soc., Dalton Trans.,* 1989, 1321.
67. H. Katayama, K. Onitsuka and F. Ozawa, *Organometallics,* 1996, **15**, 4642.
68. T. Miura and N. Iwasawa, *J. Am. Chem. Soc.,* 2002, **124**, 518.
69. M. J. Shaw, S. W. Bryant and N. Rath, *Eur. J. Inorg. Chem.,* 2007, **2007**, 3943.
70. Y. Ikeda, S. Kodama, N. Tsuchida and Y. Ishii, *Dalton Trans.,* 2015, **44**, 17448.
71. Y. Mutoh, K. Imai, Y. Kimura, Y. Ikeda and Y. Ishii, *Organometallics,* 2011, **30**, 204.
72. Y. Ikeda, T. Yamaguchi, K. Kanao, K. Kimura, S. Kamimura, Y. Mutoh, Y. Tanabe and Y. Ishii, *J. Am. Chem. Soc.,* 2008, **130**, 16856.

73.   Y. Wakatsuki, *J. Organomet. Chem.,* 2004, **689**, 4092.

74.   J. Silvestre and R. Hoffmann, *Helv. Chim. Acta,* 1985, **68**, 1461.

75.   Y. Wakatsuki, N. Koga, H. Yamazaki and K. Morokuma, *J. Am. Chem. Soc.,* 1994, **116**, 8105.

76.   I. de los Ríos, M. J. Tenorio, M. C. Puerta and P. Valerga, *J. Am. Chem. Soc.,* 1997, **119**, 6529.

77.   D. B. Grotjahn, X. Zeng, A. L. Cooksy, W. S. Kassel, A. G. DiPasquale, L. N. Zakharov and A. L. Rheingold, *Organometallics,* 2007, **26**, 3385.

78.   A. J. Arita, J. Cantada, D. B. Grotjahn and A. L. Cooksy, *Organometallics,* 2013, **32**, 6867.

79.   J. M. Lynam, L. M. Milner, N. S. Mistry, J. M. Slattery, S. R. Warrington and A. C. Whitwood, *Dalton Trans.,* 2014, **43**, 4565.

80.   C. Bruneau and P. H. Dixneuf, *Acc. Chem. Res.,* 1998, **32**, 311.

81.   C. Fischmeister and C. Bruneau, *Beilstein J. Org. Chem.,* 2011, **7**, 156.

82.   C. S. Yi and N. Liu, *Organometallics,* 1996, **15**, 3968.

83.   C. Bianchini, M. Peruzzini, F. Zanobini, P. Frediani and A. Albinati, *J. Am. Chem. Soc.,* 1991, **113**, 5453.

84.   Y. Wakatsuki, H. Yamazaki, N. Kumegawa, T. Satoh and J. Y. Satoh, *J. Am. Chem. Soc.,* 1991, **113**, 9604.

85.   S. Mirtschin, A. Slabon-Turski, R. Scopelliti, A. H. Velders and K. Severin, *J. Am. Chem. Soc.,* 2010, **132**, 14004.

86.   J. Gao, S. Rochat, X. Qian and K. Severin, *Chem. Eur. J.,* 2010, **16**, 5013.

87.   M. Yoshizawa, J. K. Klosterman and M. Fujita, *Angew. Chem. Int. Ed.,* 2009, **48**, 3418.

88.   O. Zava, J. Mattsson, B. Therrien and P. J. Dyson, *Chem. Eur. J.,* 2010, **16**, 1428.

89.   E. L. Dias and R. H. Grubbs, *Organometallics,* 1998, **17**, 2758.

90.   J. Soleimannejad, A. Sisson and C. White, *Inorg. Chim. Acta,* 2003, **352**, 121.

91.   V. Cadierno, P. Crochet, S. E. Garcia-Garrido and J. Gimeno, *Dalton Trans.,* 2004, 3635.

92.   A. A. Nazarov, C. G. Hartinger and P. J. Dyson, *J. Organomet. Chem.,* 2014, **751**, 251.

93.   T. S. Morais, T. J. Silva, F. Marques, M. P. Robalo, F. Avecilla, P. J. A. Madeira, P. J. Mendes, I. Santos and M. H. Garcia, *J. Inorg. Biochem.,* 2012, **114**, 65.

94.   V. Moreno, M. Font-Bardia, T. Calvet, J. Lorenzo, F. X. Avilés, M. H. Garcia, T. S. Morais, A. Valente and M. P. Robalo, *J. Inorg. Biochem.,* 2011, **105**, 241.

95.   M. H. Garcia, T. S. Morais, P. Florindo, M. F. M. Piedade, V. Moreno, C. Ciudad and V. Noe, *J. Inorg. Biochem.,* 2009, **103**, 354.

96.   W. M. Motswainyana and P. A. Ajibade, *Adv. Chem.,* 2015, **2015**, 21.

97.   P. Kumar, R. K. Gupta and D. S. Pandey, *Chem. Soc. Rev.,* 2014, **43**, 707.

98.   N. Menashe, E. Salant and Y. Shvo, *J. Organomet. Chem.,* 1996, **514**, 97.

99.   M. Lasa, P. López, C. Cativiela, D. Carmona and L. A. Oro, *J. Mol. Catal. A: Chem.,* 2005, **234**, 129.

100.   E. P. Kündig and F. R. Monnier, *Adv. Synth. Catal.,* 2004, **346**, 901.

101.   C. W. West and D. H. Rich, *Org. Lett.,* 1999, **1**, 1819.

102.   A. J. Pearson and J.-N. Heo, *Tetrahedron Lett.,* 2000, **41**, 5991.

103.   F. Eymery, B. Iorga and P. Savignac, *Synthesis,* 2000, **2000**, 185.

104.   D. Habrant, V. Rauhala and A. M. Koskinen, *Chem. Soc. Rev.,* 2010, **39**, 2007.

105.   R. Chinchilla and C. Nájera, *Chem. Soc. Rev.,* 2011, **40**, 5084.

106.   M. Zeng and S. B. Herzon, *Aldrichim. Acta,* 2014, **47**, 55.

107.   D. B. Grotjahn and D. A. Lev, *J. Am. Chem. Soc.,* 2004, **126**, 12232.

108.   M. S. Newman, *J. Am. Chem. Soc.,* 1953, **75**, 4740.

109.   G. Stork and R. Borch, *J. Am. Chem. Soc.,* 1964, **86**, 935.
110.   K. Imi, K. Imai and K. Utimoto, *Tetrahedron Lett.,* 1987, **28**, 3127.
111.   M. Beller, J. Seayad, A. Tillack and H. Jiao, *Angew. Chem. Int. Ed.,* 2004, **43**, 3368.
112.   M. Tokunaga and Y. Wakatsuki, *Angew. Chem. Int. Ed.,* 1998, **37**, 2867.
113.   M. Bruce and A. Swincer, *Aust. J. Chem.,* 1980, **33**, 1471.
114.   T. Suzuki, M. Tokunaga and Y. Wakatsuki, *Org. Lett.,* 2001, **3**, 735.
115.   D. B. Grotjahn, C. D. Incarvito and A. L. Rheingold, *Angew. Chem. Int. Ed.,* 2001, **40**, 3884.
116.   D. B. Grotjahn, E. J. Kragulj, C. D. Zeinalipour-Yazdi, V. n. Miranda-Soto, D. A. Lev and A. L. Cooksy, *J. Am. Chem. Soc.,* 2008, **130**, 10860.
117.   F. Chevallier and B. Breit, *Angew. Chem. Int. Ed.,* 2006, **45**, 1599.
118.   B. Breit and W. Seiche, *Angew. Chem. Int. Ed.,* 2005, **44**, 1640.
119.   A. W. Kleij and J. N. H. Reek, *Chem. Eur. J.,* 2006, **12**, 4218.
120.   M. Tokunaga, T. Suzuki, N. Koga, T. Fukushima, A. Horiuchi and Y. Wakatsuki, *J. Am. Chem. Soc.,* 2001, **123**, 11917.
121.   A. Labonne, T. Kribber and L. Hintermann, *Org. Lett.,* 2006, **8**, 5853.
122.   T. Kribber, A. Labonne and L. Hintermann, *Synthesis,* 2007, 2809.
123.   L. Rulíšek, K. P. Jensen, K. Lundgren and U. Ryde, *J. Comput. Chem.,* 2006, **27**, 1398.
124.   S. J. Irudayam and R. H. Henchman, *J. Phys. Chem. B,* 2009, **113**, 5871.
125.   U. Ryde, R. A. Mata and S. Grimme, *Dalton Trans.,* 2011, **40**, 11176.
126.   S. Grimme, J. Antony, S. Ehrlich and H. Krieg, *J. Chem. Phys.,* 2010, **132**, 154104.
127.   S. Grimme, S. Ehrlich and L. Goerigk, *J. Comput. Chem.,* 2011, **32**, 1456.
128.   D. G. Johnson, J. M. Lynam, J. M. Slattery and C. E. Welby, *Dalton Trans.,* 2010, **39**, 10432.
129.   B. O. Leung, D. L. Reid, D. A. Armstrong and A. Rauk, *J. Phys. Chem. A,* 2004, **108**, 2720.
130.   D. Ardura, R. López and T. L. Sordo, *J. Phys. Chem. B.,* 2005, **109**, 23618.
131.   P. A. Dub and R. Poli, *J. Mol. Cat. A,* 2010, **324**, 89.
132.   S. Kozuch and S. Shaik, *Acc. Chem. Res.,* 2010, **44**, 101.
133.   J. M. Slattery, J. M. Lynam and N. Fey in *Understanding Organometallic Reaction Mechanisms and Catalysis*; Chapter 3; Wiley-VCH Verlag GmbH & Co. KGaA, 2014.
134.   M. Bassetti, V. Cadierno, J. Gimeno and C. Pasquini, *Organometallics,* 2008, **27**, 5009.
135.   C.-Y. Wei, W.-S. Yu, P.-T. Chou, F.-T. Hung, C.-P. Chang and T.-C. Lin, *J. Phys. Chem. B,* 1998, **102**, 1053.
136.   M. Namazian and M. L. Coote, *J. Chem. Thermodyn.,* 2009, **41**, 1446.
137.   L. Forlani, G. Cristoni, C. Boga, P. E. Todesco, E. Del Vecchio, S. Selva and M. Monari, *Arkivoc,* 2002, **11**, 198.
138.   G. Song, B. Wang, M. Nishiura and Z. Hou, *Chem. Eur. J.,* 2015, **21**, 8394.
139.   A. E. Goetz and N. K. Garg, *Nature Chem.,* 2013, **5**, 54.
140.   M. Schlosser and F. Mongin, *Chem. Soc. Rev.,* 2007, **36**, 1161.
141.   K. S. Kanyiva, Y. Nakao and T. Hiyama, *Angew. Chem. Int. Ed.,* 2007, **46**, 8872.
142.   Y. Nakao, K. S. Kanyiva and T. Hiyama, *J. Am. Chem. Soc.,* 2008, **130**, 2448.
143.   Y. Nakao, Y. Yamada, N. Kashihara and T. Hiyama, *J. Am. Chem. Soc.,* 2010, **132**, 13666.
144.   M. L. Kantam, P. V. Reddy, P. Srinivas and S. Bhargava, *Tetrahedron Lett.,* 2011, **52**, 4490.
145.   S. M. Islam, N. Salam, P. Mondal and A. S. Roy, *J. Mol. Catal. A: Chem.,* 2013, **366**, 321.
146.   K. Karami, M. Ghasemi and N. H. Naeini, *Tetrahedron Lett.,* 2013, **54**, 1352.

147. Z. Ye, F. Chen, F. Luo, W. Wang, B. Lin, X. Jia and J. Cheng, *Synlett,* 2009, **2009**, 2198.
148. J. J. Mousseau, J. A. Bull and A. B. Charette, *Angew. Chem. Int. Ed.,* 2010, **49**, 1115.
149. L. Ilies, S. Asako and E. Nakamura, *J. Am. Chem. Soc.,* 2011, **133**, 7672.
150. M. Kim, J. Kwak and S. Chang, *Angew. Chem. Int. Ed.,* 2009, **48**, 8935.
151. S. C. Söderman and A. L. Schwan, *J. Org. Chem.,* 2012, **77**, 10978.
152. E. Shirakawa, X. Zhang and T. Hayashi, *Angew. Chem. Int. Ed.,* 2011, **50**, 4671.
153. J. A. Labinger and J. E. Bercaw, *Nature,* 2002, **417**, 507.
154. A. D. Ryabov, *Chem. Rev.,* 1990, **90**, 403.
155. R. Tonner, G. Heydenrych and G. Frenking, *Chem. Asian J.,* 2007, **2**, 1555.
156. A. M. Berman, R. G. Bergman and J. A. Ellman, *J. Org. Chem.,* 2010, **75**, 7863.
157. J. C. Lewis, R. G. Bergman and J. A. Ellman, *J. Am. Chem. Soc.,* 2007, **129**, 5332.
158. A. M. Berman, J. C. Lewis, R. G. Bergman and J. A. Ellman, *J. Am. Chem. Soc.,* 2008, **130**, 14926.
159. M. Murakami and S. Hori, *J. Am. Chem. Soc.,* 2003, **125**, 4720.
160. R. H. Fish, H. S. Kim and R. H. Fong, *Organometallics,* 1991, **10**, 770.
161. M. I. Bruce, M. A. Fox, P. J. Low, B. W. Skelton and N. N. Zaitseva, *Dalton Trans.,* 2010, **39**, 3759.
162. C. S. Yi, N. Liu, A. L. Rheingold and L. M. Liable-Sands, *Organometallics,* 1997, **16**, 3910.
163. B. J. Brisdon, R. J. Deeth, A. G. Hodson, C. M. Kemp, M. F. Mahon and K. C. Molloy, *Organometallics,* 1991, **10**, 1107.
164. B. J. Brisdon and R. A. Walton, *Polyhedron,* 1995, **14**, 1259.
165. A. K. Srivastava in *Organic Chemistry Made Simple*; page 6; New Age International Publishers, 2008.
166. K. Müller, C. Faeh and F. Diederich, *Science,* 2007, **317**, 1881.
167. P. Jeschke, *ChemBioChem,* 2004, **5**, 570.
168. S. M. Ametamey, M. Honer and P. A. Schubiger, *Chem. Rev.,* 2008, **108**, 1501.
169. W. R. Dolbier Jr, *J. Fluorine Chem.,* 2005, **126**, 157.
170. T. Liang, C. N. Neumann and T. Ritter, *Angew. Chem., Int. Ed.,* 2013, **52**, 8214.
171. M. Morgenthaler, E. Schweizer, A. Hoffmann-Röder, F. Benini, R. E. Martin, G. Jaeschke, B. Wagner, H. Fischer, S. Bendels, D. Zimmerli, J. Schneider, F. Diederich, M. Kansy and K. Müller, *ChemMedChem,* 2007, **2**, 1100.
172. H.-J. Böhm, D. Banner, S. Bendels, M. Kansy, B. Kuhn, K. Müller, U. Obst-Sander and M. Stahl, *ChemBioChem,* 2004, **5**, 637.
173. W. Zhu, J. Wang, S. Wang, Z. Gu, J. L. Aceña, K. Izawa, H. Liu and V. A. Soloshonok, *J. Fluorine Chem.,* 2014, **167**, 37.
174. D. B. Harper and D. O'Hagan, *Nat. Prod. Rep.,* 1994, **11**, 123.
175. M. G. Campbell and T. Ritter, *Chem. Rev.,* 2015, **115**, 612.
176. T. Furuya, J. E. M. N. Klein and T. Ritter, *Synthesis,* 2010, 1804.
177. R. D. Shannon, *Acta Crystallogr. Sect. A,* 1976, **32**, 751.
178. G. C. Finger and C. W. Kruse, *J. Am. Chem. Soc.,* 1956, **78**, 6034.
179. H. B. Gottlieb, *J. Am. Chem. Soc.,* 1936, **58**, 532.
180. H. Sun and S. G. DiMagno, *Angew. Chem. Int. Ed.,* 2006, **45**, 2720.
181. V. V. Grushin and W. J. Marshall, *Organometallics,* 2008, **27**, 4825.
182. T. Furuya, A. S. Kamlet and T. Ritter, *Nature,* 2011, **473**, 470.
183. V. V. Grushin, *Acc. Chem. Res.,* 2010, **43**, 160.
184. T. Furuya and T. Ritter, *J. Am. Chem. Soc.,* 2008, **130**, 10060.
185. M. Rueda-Becerril, O. Mahé, M. Drouin, M. B. Majewski, J. G. West, M. O. Wolf, G. M. Sammis and J.-F. Paquin, *J. Am. Chem. Soc.,* 2014, **136**, 2637.

186. S. Bloom, J. L. Knippel and T. Lectka, *Chem. Sci.,* 2014, **5**, 1175.
187. S. D. Halperin, H. Fan, S. Chang, R. E. Martin and R. Britton, *Angew. Chem. Int. Ed.,* 2014, **53**, 4690.
188. C. W. Kee, K. F. Chin, M. W. Wong and C.-H. Tan, *Chem. Commun.,* 2014, **50**, 8211.
189. J.-B. Xia, C. Zhu and C. Chen, *J. Am. Chem. Soc.,* 2013, **135**, 17494.
190. J.-B. Xia, C. Zhu and C. Chen, *Chem. Commun.,* 2014, **50**, 11701.
191. D. O'Hagan and H. Deng, *Chem. Rev.,* 2015, **115**, 634.
192. J. Weaver and S. Senaweera, *Tetrahedron,* 2014, **70**, 7413.
193. T. Ahrens, J. Kohlmann, M. Ahrens and T. Braun, *Chem. Rev.,* 2015, **115**, 931.
194. J. H. Clark, *Chem. Rev.,* 1980, **80**, 429.
195. T. Sawamura, K. Takahashi, S. Inagi and T. Fuchigami, *Angew. Chem. Int. Ed.,* 2012, **51**, 4413.
196. S. Manna, J. R. Falck and C. Mioskowski, *Synth. Commun.,* 1985, **15**, 663.
197. C. L. Liotta and H. P. Harris, *J. Am. Chem. Soc.,* 1974, **96**, 2250.
198. W. Navarrini, V. Tortelli, A. Russo and S. Corti, *J. Fluorine Chem.,* 1999, **95**, 27.
199. M. A. Tius, *Tetrahedron,* 1995, **51**, 6605.
200. G. S. Lal, G. P. Pez and R. G. Syvret, *Chem. Rev.,* 1996, **96**, 1737.
201. A. G. Gilicinski, G. P. Pez, R. G. Syvret and G. S. Lal, *J. Fluorine Chem.,* 1992, **59**, 157.
202. T. Furuya, C. A. Kuttruff and T. Ritter, *Curr. Opin. Drug Discovery Dev.,* 2008, **11**, 803.
203. R. E. Banks, *J. Fluorine Chem.,* 1998, **87**, 1.
204. P. T. Nyffeler, S. G. Durón, M. D. Burkart, S. P. Vincent and C.-H. Wong, *Angew. Chem. Int. Ed.,* 2005, **44**, 192.
205. M. J. Adam, B. D. Pate, T. J. Ruth, J. M. Berry and L. D. Hall, *J. Chem. Soc., Chem. Commun.,* 1981, 733.
206. K. P. Butin, Y. M. Kiselev, T. V. Magdesieva and O. A. Reutov, *J. Organomet. Chem.,* 1982, **235**, 127.
207. P. Di Raddo, M. Diksic and D. Jolly, *J. Chem. Soc., Chem. Commun.,* 1984, 159.
208. L. J. Diorazio, D. A. Widdowson and J. M. Clough, *Tetrahedron,* 1992, **48**, 8073.
209. J. DeYoung, H. Kawa and R. J. Lagow, *J. Chem. Soc., Chem. Commun.,* 1992, 811.
210. P. Anbarasan, H. Neumann and M. Beller, *Angew. Chem. Int. Ed.,* 2010, **49**, 2219.
211. T. Furuya, D. Benitez, E. Tkatchouk, A. E. Strom, P. Tang, W. A. Goddard and T. Ritter, *J. Am. Chem. Soc.,* 2010, **132**, 3793.
212. P. Tang, T. Furuya and T. Ritter, *J. Am. Chem. Soc.,* 2010, **132**, 12150.
213. Y. Ye and M. S. Sanford, *J. Am. Chem. Soc.,* 2013, **135**, 4648.
214. J. M. Racowski, J. B. Gary and M. S. Sanford, *Angew. Chem., Int. Ed.,* 2012, **51**, 3414.
215. A. R. Mazzotti, M. G. Campbell, P. Tang, J. M. Murphy and T. Ritter, *J. Am. Chem. Soc.,* 2013, **135**, 14012.
216. V. A. Brunet and D. O'Hagan, *Angew. Chem. Int. Ed.,* 2008, **47**, 1179.
217. K. L. Hull, W. Q. Anani and M. S. Sanford, *J. Am. Chem. Soc.,* 2006, **128**, 7134.
218. X. Wang, T.-S. Mei and J.-Q. Yu, *J. Am. Chem. Soc.,* 2009, **131**, 7520.
219. K. S. L. Chan, M. Wasa, X. Wang and J.-Q. Yu, *Angew. Chem. Int. Ed.,* 2011, **50**, 9081.
220. T. Furuya, H. M. Kaiser and T. Ritter, *Angew. Chem. Int. Ed.,* 2008, **47**, 5993.
221. N. D. Ball and M. S. Sanford, *J. Am. Chem. Soc.,* 2009, **131**, 3796.
222. M. A. Tius and J. K. Kawakami, *Synth. Commun.,* 1992, **22**, 1461.
223. T. Furuya and T. Ritter, *Org. Lett.,* 2009, **11**, 2860.
224. P. Tang and T. Ritter, *Tetrahedron,* 2011, **67**, 4449.
225. T. Furuya, A. E. Strom and T. Ritter, *J. Am. Chem. Soc.,* 2009, **131**, 1662.
226. D. A. Watson, M. Su, G. Teverovskiy, Y. Zhang, J. Garcia-Fortanet, T. Kinzel and S. L. Buchwald, *Science,* 2009, **325**, 1661.

227. M. Álvarez-Corral, M. Muñoz-Dorado and I. Rodríguez-García, *Chem. Rev.,* 2008, **108**, 3174.
228. P. S. Fier, J. Luo and J. F. Hartwig, *J. Am. Chem. Soc.,* 2013, **135**, 2552.
229. T. Noël, T. J. Maimone and S. L. Buchwald, *Angew. Chem. Int. Ed.,* 2011, **50**, 8900.
230. T. J. Maimone, P. J. Milner, T. Kinzel, Y. Zhang, M. K. Takase and S. L. Buchwald, *J. Am. Chem. Soc.,* 2011, **133**, 18106.
231. D. V. Yandulov and N. T. Tran, *J. Am. Chem. Soc.,* 2007, **129**, 1342.
232. H. G. Lee, P. J. Milner and S. L. Buchwald, *J. Am. Chem. Soc.,* 2014, **136**, 3792.
233. P. S. Fier and J. F. Hartwig, *Science,* 2013, **342**, 956.
234. X. Mu and G. Liu, *Org. Chem. Front.,* 2014, **1**, 430.
235. T. Tian, W.-H. Zhong, S. Meng, X.-B. Meng and Z.-J. Li, *J. Org. Chem.,* 2013, **78**, 728.
236. T. Truong, K. Klimovica and O. Daugulis, *J. Am. Chem. Soc.,* 2013, **135**, 9342.
237. E. Lee, J. M. Hooker and T. Ritter, *J. Am. Chem. Soc.,* 2012, **134**, 17456.
238. Y. Ye, S. D. Schimler, P. S. Hanley and M. S. Sanford, *J. Am. Chem. Soc.,* 2013, **135**, 16292.
239. P. M. Pihko, *Angew. Chem. Int. Ed.,* 2006, **45**, 544.
240. T. Hashimoto and K. Maruoka, *Chem. Rev.,* 2007, **107**, 5656.
241. B. Zajc and M. Zupan, *J. Org. Chem.,* 1982, **47**, 573.
242. G. S. Lal, *J. Org. Chem.,* 1993, **58**, 2791.
243. E. Differding and R. W. Lang, *Tetrahedron Lett.,* 1988, **29**, 6087.
244. E. Differding and R. W. Lang, *Helv. Chim. Acta,* 1989, **72**, 1248.
245. D. Cahard, C. Audouard, J.-C. Plaquevent and N. Roques, *Org. Lett.,* 2000, **2**, 3699.
246. N. Shibata, J. Kohno, K. Takai, T. Ishimaru, S. Nakamura, T. Toru and S. Kanemasa, *Angew. Chem., Int. Ed.,* 2005, **44**, 4204.
247. Y. Hamashima, K. Yagi, H. Takano, L. Tamas and M. Sodeoka, *J. Am. Chem. Soc.,* 2002, **124**, 14530.
248. N. Shibata, E. Suzuki and Y. Takeuchi, *J. Am. Chem. Soc.,* 2000, **122**, 10728.
249. A. D. Dilman, P. A. Belyakov, M. I. Struchkova, D. E. Arkhipov, A. A. Korlyukov and V. A. Tartakovsky, *J. Org. Chem.,* 2010, **75**, 5367.
250. S. Qiu, T. Xu, J. Zhou, Y. Guo and G. Liu, *J. Am. Chem. Soc.,* 2010, **132**, 2856.
251. A. W. Kaspi, I. Goldberg and A. Vigalok, *J. Am. Chem. Soc.,* 2010, **132**, 10626.
252. S.-B. Zhao, J. J. Becker and M. R. Gagné, *Organometallics,* 2011, **30**, 3926.
253. N. P. Mankad and F. D. Toste, *Chem. Sci.,* 2012, **3**, 72.
254. K. B. McMurtrey, J. M. Racowski and M. S. Sanford, *Org. Lett.,* 2012, **14**, 4094.
255. W. Liu, X. Huang, M.-J. Cheng, R. J. Nielsen, W. A. Goddard and J. T. Groves, *Science,* 2012, **337**, 1322.
256. K. S. Coleman, J. H. Holloway and E. G. Hope, *J. Chem. Soc., Dalton Trans.,* 1997, 1713.
257. S. A. Brewer, K. S. Coleman, J. Fawcett, J. H. Holloway, E. G. Hope, D. R. Russell and P. G. Watson, *J. Chem. Soc., Dalton Trans.,* 1995, 1073.
258. P. Barthazy, L. Hintermann, R. M. Stoop, M. Wörle, A. Mezzetti and A. Togni, *Helv. Chim. Acta,* 1999, **82**, 2448.
259. S. R. Caskey, M. H. Stewart, Y. J. Ahn, M. J. A. Johnson, J. L. C. Rowsell and J. W. Kampf, *Organometallics,* 2007, **26**, 1912.
260. K. B. Wiberg and P. R. Rablen, *J. Am. Chem. Soc.,* 1993, **115**, 614.
261. K. B. Wiberg, *Acc. Chem. Res.,* 1996, **29**, 229.
262. D. O'Hagan, *Chem. Soc. Rev.,* 2008, **37**, 308.
263. P.-Y. Lien, R.-M. You and W.-P. Hu, *J. Phys. Chem. A,* 2001, **105**, 2391.
264. R. J. Gillespie and E. A. Robinson, *Chem. Soc. Rev.,* 2005, **34**, 396.

265. P. H. S. Owen, M. Headlee, C. Ahmed, *Chemistry for the IB Diploma*; Second Edition ed.; Cambridge University Press, 2015.

266. R. Castro-Rodrigo, M. A. Esteruelas, S. Fuertes, A. M. López, S. Mozo and E. Oñate, *Organometallics,* 2009, **28**, 5941.

267. L. Ciano, N. Fey, C. J. Halliday, J. M. Lynam, L. M. Milner, N. Mistry, N. E. Pridmore, N. S. Townsend and A. C. Whitwood, *Chem. Commun.,* 2015, **51**, 9702.

268. D. J. Anderson, R. McDonald and M. Cowie, *Angew. Chem. Int. Ed.,* 2007, **46**, 3741.

269. M. E. Slaney, D. J. Anderson, M. J. Ferguson, R. McDonald and M. Cowie, *J. Am. Chem. Soc.,* 2010, **132**, 16544.

270. M. E. Slaney, D. J. Anderson, M. J. Ferguson, R. McDonald and M. Cowie, *Organometallics,* 2012, **31**, 2286.

271. M. E. Slaney, M. J. Ferguson, R. McDonald and M. Cowie, *Organometallics,* 2012, **31**, 1384.

272. W. Schulze and K. Seppelt, *Inorg. Chem.,* 1988, **27**, 3872.

273. W. A. Bernett, *J. Org. Chem.,* 1969, **34**, 1772.

274. M. Bruce and R. Wallis, *Aust. J. Chem.,* 1979, **32**, 1471.

275. I. R. Whittall, M. G. Humphrey, D. C. R. Hockless, B. W. Skelton and A. H. White, *Organometallics,* 1995, **14**, 3970.

276. H.-H. Chou, Y.-C. Lin, S.-L. Huang, Y.-H. Liu and Y. Wang, *Organometallics,* 2008, **27**, 5212.

277. M. I. Bruce, M. G. Humphrey, M. R. Snow and E. R. T. Tiekink, *J. Organomet. Chem.,* 1986, **314**, 213.

278. G. Consiglio and F. Morandini, *Inorg. Chim. Acta,* 1987, **127**, 79.

279. M. A. Fox, J. E. Harris, S. Heider, V. Pérez-Gregorio, M. E. Zakrzewska, J. D. Farmer, D. S. Yufit, J. A. K. Howard and P. J. Low, *J. Organomet. Chem.,* 2009, **694**, 2350.

280. S. Purser, P. R. Moore, S. Swallow and V. Gouverneur, *Chem. Soc. Rev.,* 2008, **37**, 320.

281. E. F. van der Eide, P. Yang and R. M. Bullock, *Angew. Chem. Int. Ed.,* 2013, **52**, 10190.

282. M. Zakerhamidi, A. Ghanadzadeh and M. Moghadam, *Chem. Sci. Trans,* 2012, **1**, 1.

283. R. M. Bullock, *J. Chem. Soc., Chem. Commun.,* 1989, 165.

284. W. R. Dolbier in *Guide to Fluorine NMR for Organic Chemists*; Chapter 3; John Wiley & Sons, 2009.

285. K. Onitsuka, M. Nishii, Y. Matsushima and S. Takahashi, *Organometallics,* 2004, **23**, 5630.

286. R. P. Hughes, *Eur. J. Inorg. Chem.,* 2009, **2009**, 4591.

287. R. P. Hughes, R. B. Laritchev, J. Yuan, J. A. Golen, A. N. Rucker and A. L. Rheingold, *J. Am. Chem. Soc.,* 2005, **127**, 15020.

288. D. D. Steiner, N. Mase and C. F. Barbas, *Angew. Chem. Int. Ed.,* 2005, **44**, 3706.

289. N. Mistry, University of York, 2013.

290. S. T. Purrington, N. V. Lazaridis and C. L. Bumgardner, *Tetrahedron Lett.,* 1986, **27**, 2715.

291. P. M. Treichel, D. A. Komar and P. J. Vincenti, *Synth. React. Inorg. Met.-Org. Chem.,* 1984, **14**, 383.

292. CrysalisPro, 1.171.33.36d.

293. R. Clark and J. Reid, *Acta Crystallogr. Sect. A: Found. Crystallogr.,* 1995, **51**, 887.

294. O. V. Dolomanov, L. J. Bourhis, R. J. Gildea, J. A. Howard and H. Puschmann, *J. Appl. Crystallogr.,* 2009, **42**, 339.

295. L. Palatinus and G. Chapuis, *J. Appl. Crystallogr.,* 2007, **40**, 786.

296. G. M. Sheldrick, *Acta Crystallogr. Sect. A: Found. Crystallogr.,* 2008, **64**, 112.

297. J. J. Stewart, L. P. Davis and L. W. Burggraf, *J. Comput. Chem.,* 1987, **8**, 1117.

298. S. Maluendes and M. Dupuis, *J. Chem. Phys.,* 1990, **93**, 5902.

299. P. Császár and P. Pulay, *J. Mol. Struct.,* 1984, **114**, 31.

300. R. Ahlrichs, M. Bär, M. Häser, H. Horn and C. Kölmel, *Chem. Phys. Lett.,* 1989, **162**, 165.

301. K. Eichkorn, O. Treutler, H. Öhm, M. Häser and R. Ahlrichs, *Chem. Phys. Lett.,* 1995, **240**, 283.

302. K. Eichkorn, F. Weigend, O. Treutler and R. Ahlrichs, *Theor. Chem. Acc.,* 1997, **97**, 119.

303. M. von Arnim and R. Ahlrichs, *J. Chem. Phys.,* 1999, **111**, 9183.

304. P. Deglmann and F. Furche, *J. Chem. Phys.,* 2002, **117**, 9535.

305. P. Deglmann, F. Furche and R. Ahlrichs, *Chem. Phys. Lett.,* 2002, **362**, 511.

306. P. Deglmann, K. May, F. Furche and R. Ahlrichs, *Chem. Phys. Lett.,* 2004, **384**, 103.

307. O. Treutler and R. Ahlrichs, *J. Chem. Phys.,* 1995, **102**, 346.

308. W. M. Haynes, *CRC Handbook of Chemistry and Physics*; CRC press, 2014.

309. M. Frisch, G. Trucks, H. Schlegel, G. Scuseria, M. Robb, J. Cheeseman, G. Scalmani, V. Barone, B. Mennucci, G. Petersson, H. Nakatsuji , M. Caricato, X. Li, H. Hratchian, A. Izmaylov, J. Bloino, G. Zheng, J. Sonnenberg, M. Hada, M. Ehara, K. Toyota, R. Fukuda, J. Hasegawa, M. Ishida, T. Nakajima, Y. Honda, O. Kitao, H. Nakai, T. Vreven, J. JA Montgomery, J. Peralta, F. Ogliaro, M. Bearpark, J. Heyd, E. Brothers, K. Kudin, V. Staroverov, T. Keith, R. Kobayashi, J. Normand, K. R. Raghavachari, A, J. Burant, S. Iyengar, J. Tomasi, M. Cossi, N. Rega, J. Millam, M. Klene, J. Knox, J. Cross, V. Bakken, C. Adamo, J. Jaramillo, R. Gomperts, R. Stratmann, O. Yazyev, A. Austin, R. Cammi, C. Pomelli, J. Ochterski, R. Martin, K. Z. Morokuma, VG, G. A. Voth, P. Salvador, J. D. Dannenberg, S, A. Daniels, O. Farkas, J. Foresman, J. Ortiz, J. Cioslowski and D. Fox, *Gaussian, Inc., Wallingford, CT,* 2010.

310. D. Feller, *J. Comput. Chem.,* 1996, **17**, 1571.

311. K. L. Schuchardt, B. T. Didier, T. Elsethagen, L. Sun, V. Gurumoorthi, J. Chase, J. Li and T. L. Windus, *J. Chem. Inf. Model.,* 2007, **47**, 1045.

312. F. Weigend and R. Ahlrichs, *Phys. Chem. Chem. Phys.,* 2005, **7**, 3297.

313. D. Andrae, U. Haussermann, M. Dolg, H. Stoll and H. Preuss, *Theor. Chim. Acta,* 1990, **77**, 123.

314. E. Glendening, J. Badenhoop, A. Reed, J. Carpenter, J. Bohmann, C. Morales and F. Weinhold, *NBO 5.0. Natural Bond Orbital Analysis Program,* Theoretical Chemistry Institute, University of Wisconsin, Madison, WI, 2009

315. M. Suenaga, *J. Comput. Chem. Jpn,,* 2005, **4**, 25.

316. A. E. Reed, L. A. Curtiss and F. Weinhold, *Chem. Rev.,* 1988, **88**, 899.

317. J. Foster and F. Weinhold, *J. Am. Chem. Soc.,* 1980, **102**, 7211.

318. A. E. Reed, R. B. Weinstock and F. Weinhold, *J. Chem. Phys.,* 1985, **83**, 735.

319. A. E. Reed and F. Weinhold, *J. Chem. Phys.,* 1985, **83**, 1736.